ISBN 978-82-471-2576-2 (printed ver.)
ISBN 978-82-471-2577-9 (electronic ver.)
ISSN 1503-8181

Doctoral Thesis
Simen Andreas Ådnøy Ellingsen

Doctoral theses at NTNU, 2011:29

Simen Andreas Ådnøy Ellingsen

# Dispersion forces in Micromechanics

## Casimir and Casimir-Polder forces affected by geometry and non-zero temperature

NTNU
Norwegian University of
Science and Technology

Doctoral theses at NTNU, 2011:29
NTNU

NTNU
Norwegian University of
Science and Technology
Thesis for the degree of
philosophiae doctor
Faculty of Engineering Science and Technology
Department of Energy and Process Engineering

NTNU
Norwegian University of
Science and Technology

Simen Andreas Ådnøy Ellingsen

# Dispersion forces in Micromechanics

Casimir and Casimir-Polder forces affected by geometry and non-zero temperature

Thesis for the degree of philosophiae doctor

Trondheim, January 2011

Norwegian University of
Science and Technology
Faculty of Engineering Science and Technology
Department of Energy and Process Engineering

NTNU
Norwegian University of
Science and Technology

**NTNU**
Norwegian University of Science and Technology

Thesis for the degree of philosophiae doctor

Faculty of Engineering Science and Technology
Department of Energy and Process Engineering



ISBN 978-82-471-2576-2 (printed ver.)
ISBN 978-82-471-2577-9 (electronic ver.)
ISSN 1503-8181

Doctoral Theses at NTNU, 2011:29

Printed by Tapir Uttrykk

# Abstract

The present thesis focuses on several topics within three separate but related branches of the overall field of dispersion forces. The three branches are: temperature corrections to the Casimir force between real materials (Part 1), explicit calculation of Casimir energy in wedge geometries (Part 2), and Casimir-Polder forces on particles out of thermal equilibrium (Part 3).

Part 1 deals primarily with analysis of a previously purported thermodynamic inconsistency in the Casimir-Lifshitz free energy of the interaction of two plane mirrors – violation of the third law of thermodynamics – when the latter's dielectric response is described with dissipative models. It is shown analytically and numerically that the Casimir entropy of the interaction between two metallic mirrors described by the Drude model does tend to zero at zero temperature, provided electronic relaxation does not vanish. The leading order terms at low temperature are found. A similar calculation is carried out for the interaction of semiconductors with small but non-zero DC conductivity. In a generalisation, it is shown that a violation of the third law can only occur for permittivities whose low-frequency behaviour is temperature dependent near zero temperature. A calculation using path integral methods shows that the low temperature behaviour of the interaction of fluctuating Foucault currents in two mirrors of Drude metal is identical to that of the full Casimir-Lifshitz free energy, reasserting a previous finding by Intravaia and Henkel that such fluctuating bulk currents are the physical reason for the anomalous entropy behaviour.

In a related effort, an analysis of the frequency dependence of the Casimir force by Ford is generalised to imperfectly reflecting mirrors. A paradox is pointed out, in that the effects of a perturbation of the reflecting properties of the mirrors in a finite frequency window can be calculated in two ways giving different results. It is concluded that optimistic conclusions reached by Ford based on one of these methods, which seems to allow radically changing and tailoring the Casimir force with engineered materials, can not be realised.

Part 2 presents several explicit calculations of the Casimir energy of different wedge and cylinder geometries. The Casimir energy of a perfectly conducting wedge intercut by a circularly cylindrical arc, either perfectly conducting or (magneto)dielectric, is calculated. The energy is found to include a singular and non-regularisable term due to the corners where the arc meets the wedge, whereas the finite part is an immediate generalisation of the previously known results for a circular cylinder. The energy of a magnetodielectric wedge obeying a criterion of isorefractivity (spatially uniform speed of light) superimposed coaxially on a

perfectly conducting cylindrical shell is calculated. This is the first expression for the energy of a wedge which is not perfectly reflecting. Finally, the energy of the perfectly conducting wedge and arc (and, as a special case, cylinder) is extended to the case of non-zero temperatures. After a regularisation procedure making use of the Chowla-Selberg formula an analytical expression for the temperature-dependent energy at all temperatures is derived, and showed to coincide with previously calculated high-temperature asymptotics by Bordag, Nesterenko and Pirozhenko.

Part 3 considers numerical and analytical studies of the Casimir-Polder forces acting on particles prepared in a given eigenstate (or superposition of such) in an environment which is otherwise at thermal equilibrium. We first consider cold polar molecules outside a metallic halfspace. It is found that the force in the near-zone (non-retarded regime) is much weaker than what would result from a naïve perturbative calculation, and that in the far-zone (retarded regime) the force becomes spatially oscillatory. It is demonstrated how these spatial oscillations may be enhanced in a resonating planar cavity, although for polar molecules the resulting amplitude is still insufficient for observation. A cylindrical cavity, however, can achieve a better enhancement factor. The Casimir-Polder forces on Rydberg atoms near a surface are calculated; because of the very large transition dipole moments of Rydberg transitions, the force is enormous on an atomic scale. We show that the oscillating force on Rydberg atoms can be enhanced into the observable regime by use of a fine-tuned cylindrical cavity. A particle in an eigenstate which is in the non-retarded regime with respect to all its dominant transitions is shown to feel a Casimir-Polder force which is virtually independent of temperature from zero to room temperature and beyond. Both for cold polar molecules and Rydberg atoms, the temperature-independent regime extends to a few and hundreds of micrometers, respectively, and includes the separations generally accessed in experiments.

# Preface

This thesis is submitted in partial fulfilment of the requirements for the degree of Doctor of Philosophy at the Norwegian University of Science and Technology (NTNU). The work included in the thesis is the result of research undertaken between August 2007 and September 2010, under the supervision of Professor Iver H. Brevik.

Apart from a stay of one month at the University of Oklahoma in the spring of 2008, the research has been carried out in Trondheim. Yet, much of the work presented has resulted from international collaboration. The primary collaborators have been Professor Kimball Milton at the Univerity of Oklahoma, and Drs. Stefan Scheel and Stefan Buhmann at Imperial College London. I have visited the London group a number of times, shorter trips made possible by the generous fellowship granted by NTNU. Other academic visits, each of a week's duration, were paid to the University of Potsdam (Dr. Carsten Henkel's group) and the Université de Pierre et Marie Curie in Paris (Drs. Astrid Lambrecht and Serge Reynaud's group).

My fellowship during the project period has been provided by NTNU, the faculty of Engineering Science and Technology. I have received two smaller 'short visit' grants from the European Science Foundation (ESF), via the programme CASIMIR, *www.casimir-network.com*. ESF also sponsored the "CASIMIR-QFEXT Junior Paper Award" which I was fortunate to share with Dr. Jeremy Munday of Harvard University during the QFEXT09 conference in Norman, Oklahoma, September 2009. Further smaller travel grants have been received from Los Alamos National Laboratories and the Max Planck Institute in Dresden.

Simen Andreas Ådnøy Ellingsen
Trondheim, October 2010

# Acknowledgements

No-one can comprehend
what goes on under the sun.
People toil to search it out,
but no one can discover its meaning.
Even if the wise claim they know,
they cannot really comprehend it.
*Eccl.* 8:17

I am nearing the end of a long period of intensive research, the result of which is in your hands. At a time like this one comes to realise that for all the hours I have put into my research, very little progress could have been made without the constant support from my seniors and peers, friends, relatives and colleaugues.

First and foremost on my list of aides is my supervisor, Professor Iver Brevik, whose example, whose wisdom and and whose broad and profound knowledge have been a constant source of inspiration, guidance and practical advice throughout my research. Our collaboration was formed already six years ago when I first set foot in the world of Casimir physics and has continuied fruitfully to this day. It has taken me to many and diverse parts of physics and taught me the value of a broad perspective on physics and the world at large. The gentle and generous way in which he meets everybody sets an example one can but aspire to follow.

It has been a great honour as well as pleasure to have worked with Professor Kimball Milton of the University of Oklahoma. I am particularly thankful for the kind hospitality during my stay in Oklahoma in 2008. Since then, Professor Milton has joined Iver and myself in several projects, and having his formidable knowledge and skill in the team has been very reassuring.

Much the same can be said about another collaborator on my earliest articles for the thesis, Professor Johan S. Høye. His previous work on the Casimir temperature anomaly allowed me to hit the ground running when I first started on that topic, and in our collaborations since have been several and successful.

My other primary collaborators have been Drs. Stefan Scheel and Stefan Buhmann at Imperial College London. A collaboration was first suggested by Stefan B when we met at the Casimir conference in Brazil in 2008, and consequently I popped over to London a little later that year. Since then our collaboration has been productive and very inspiring for me. I was taken to the world of quantum optics (which I had not planned to enter) and found a more applied shade to my research body (which I had been wanting). Our collaboration will

hopefully continue far into the future.

My topic of research has been atypical for the Department of Energy and Process Engineering (EPT) to put it mildly. Yet although my research has been topically different from that of my colleauges, I have always felt at home at EPT. I must thank the Faculty for Engineering Science and Technology for granting a generous PhD Fellowship to a theorist like myself. I furthermore thank the Department for hosting me. Thanks to my bosses as scientific assistant in Fluid Mechanics for seamless co-operation: Professors Lars Sætran, Helge Andersson and Bernhard Müller, Reidar Kristoffersen and Dr. Maria Fernandino. Finally, thanks should go to the administrative staff at the Department who make life so easy for clueless academics like myself. I have only the highest praise for the EPT administration, of whom Gerd Randi, Ingrid, Gunnhild and Anita are the ones I've troubled the most.

Life at the Department would have been dull and dreary if not for my fellow Ph.D. students. My room mate Kristian E. Einarsrud deserves particular mention, for excellent discussions about any thinkable topic, as well as a particularly well functioning co-habitation for three years in room 111. Further thanks to Joris Verschaeve, Claudio Walker, Vagesh Narasimhamurthy, Frode Nygård, Jan Fredrik Helgaker and many more for the fun and the discussions. I cannot forgo the mention of Corridor Cricket, a source of amusement and exercise for the last year and a half. No thanks, however, to the fake tree in the corridor blocking mid-on to mid-wicket and making it dashed hard to score runs on the leg side!

Some will be aware that this is the second time I write the foreword to a Ph.D. thesis. My official and unofficial supervisors for my previous Ph.D. at King's College London, Professor Peter D. Zimmerman and Dr. James Acton were important also in facilitating *this* doctorate in an indirect way. Pete was very understanding of my desire to return to physics, and his blessing made the transition back to Trondheim so much easier. James' ruthless and brilliantly lucid dissection of my thesis chapters every time I popped over to London was was what made it possible to work on two theses simultaneously.

In Oklahoma I met Jef Wagner, K. V. Shajesh and Prachi Parashar. Special thanks must go to Jef and his wife Kristen for taking such good care of me, driving me around Oklahoma and introducing me to a proper southern breakfast, and to Shajesj for getting me to and from the airport in Oklahoma City at ridiculous hours.

Aside from my main collaborators, I have been privileged to work with other experts on a number of smaller projects. All of these have been highly enjoyable and rewarding. Alex Crosse I got to know during my stays at Imperial, and it felt only about time when we finally got both our names on the same paper. Francesco Intravaia and Carsten Henkel were kind enough to invite me for a short stay in Potsdam with them, wich resulted in a paper I've included in the thesis. Carsten and Francesco have a way of thinking about physics which is rather different from my own, and I cannot think of a single research project which has heightened my understanding more than the one I did with them. Finally I must thank Yury Sherkunov who sportingly agreed to team up for the proceedings paper for QFEXT09.

I have had the pleasure and privilege of discussing physics with and get to know a number of young scientists in similar circumstances as my own. Jef, Shajesj, Prachi, Alex, Yury, Stefan B. and Francesco I've already mentioned, but Harald Haakh, Filipe da Rosa,

James Babington, Antoine Carnaguier-Durand, Ines Cavero-Peláez, Elom Abalo, Olesya Gorbunova, Irina Pirozhenko, and Justin Wilson I hadn't before now. Thanks for all good times!

My horizons were severely broadened by Professor Alex Hansen and his Ph.D. students Morten Grøva and Knut S. Gjerden, with whom I co-authored a PRE about density waves in falling sand. Quite some way from the Casimir effect! It all commenced as I took "Computational Physics" for a Ph.D. topic, taught by Prof. Hansen. His model, upon whose analysis our paper expands, was given as topic for the four-day exam, and the conclusions brought forth in the article were conceived in the pangs and woes of those four frenzied days. Dashed spiffing it all was, and a great way to befriend a completely other branch of physics!

Throughout my research I have benefited from discussions with a number of my seniors from around the world. These include in no particular order (and I hope I have not forgotten too many) Dr. Davide Iannuzzi, Prof. Bo Sernelius, Prof. Emilio Elizalde, Prof. Sergei Odintsov, Dr. Guiseppe Bimonte, Prof. Vladimir Nesterenko, Dr. Valery Marachevsky, Prof. Steve Lamoreaux, Dr. Diego Dalvit, Prof. Holger Gies, Dr. Lev Kaplan, Prof. Bo-Sture Skagerstam, Prof. Kåre Olaussen, Dr. Olav Gaute Hellesø, Prof. James Wilkinson, Prof. Thomas Huser, Dr. Per Jakobsen, Prof. Pierre Benech, Prof. Jens Oluf Andersen, Prof. Gert-Ludwig Ingold, Dr. Mauro Antezza, Dr. Michael Bordag, Prof. Klaus Kirsten, Dr. Ricardo Decca, Prof. Umar Mohideen, Prof. Vladimir Mostepanenko, Dr. Giovanni Carugno, Prof. Steven Johnson, Prof. Michael Levin and Prof. Lev Pitaevskii. Particular thanks to Dr. Astrid Lambrecht & Prof. Serge Reynaud who very hospitably invited me to Paris for discussions.

Very special thanks to my erstwhile physics teacher Oddvar Stubø who persuaded me to study physics in the first place. It has made all the difference.

Doing a doctorate, the support of friends and relatives is at least as important as scientific support. So many have been and are important to me in my personal life that I deem it wiser not to attempt to list everyone and risking to inadvertently omit someone. It is my hope that you already know who you are, that I have been able to somehow express how much I value and enjoy our time together. I therefore thank in particular only my parents, who have always supported me on the strange and winding path I have chosen to follow so far in life.

Yet most important of all through these last years has been my dear wife Inger. May we have many days ahead of us, and may I be able to thank and repay you every one of those days for all that you are to me.

And so it was that I became one of the many who toil to search out what goes on under the sun, and I'm not sure I'm any closer to discovering its meaning. But 'pon my word, has it been fun to try! I am ever indebted to Him who died so long ago so that we may live and indulge in such delightful nonsense as this.

Simen Andreas Ådnøy Ellingsen
Trondheim, October 2010

# Thesis contents

## Publications

Papers which are included in the thesis are marked with a superscript letter in square brackets denoting its reference within the thesis (e.g. [a] is Paper [a]). For details of what is included in the thesis and why/why not, see below, page xi.

### Part I: Casimir effect for real materials at non-zero temperature

1. I. Brevik, S. A. Ellingsen and K. A. Milton, *Thermal Corrections to the Casimir Effect*, New Journal of Physics **8** 236 (2006).

2. S. A. Ellingsen, *Casimir attraction in multilayered plane parallel magnetodielectric systems*, Journal of Physics A **40** 1951 (2007).

3. S. A. Ellingsen and I. Brevik, *Casimir force on real materials – the slab and cavity geometry*, Journal of Physics A **40** 3643 (2007).

4[a]. J. S. Høye, I. Brevik, S. A. Ellingsen and J. B. Aarseth, *Analytic and Numerical Verification of the Nernst Theorem for Metals*, Physical Review E **75** 051127 (2007). Reply to Comment: Physical Review E **77** 023102 (2008).

5. I. Brevik, S. A. Ellingsen, J. S. Høye and K. A. Milton, *Analytical and numerical demonstration of how the Drude dispersive model satisfies Nernst's theorem for the Casimir entropy*, Journal of Physics A **41** 164017 (2008).

6[b]. S. A. Ellingsen, *Frequency spectrum of the Casimir force: interpretation and a paradox*, Europhysics Letters **83** 053001 (2008).

7[c]. S. A. Ellingsen, I. Brevik, J. S. Høye and K. A. Milton *Temperature correction to Casimir-Lifshitz free energy at low temperatures: semiconductors*, Physical Review E **78** 021117 (2008).

8[d]. S. A. Ellingsen, *Nernst's heat theorem for Casimir-Lifshitz free energy*, Physical Review E **78** 021120 (2008).

9[e]. S. Å. Ellingsen, *Casimir-Lifshitz pressure and free energy: exploring a simple model* in "The Casimir Effect and Cosmology: A volume in honour of Professor Iver H. Brevik on the occasion of his 70th birthday" edited by S. Odintsov, E. Elizalde and O.G. Gorbunova (Tomsk State Pedagogical University Press, 2008), pp. 45-60 (*arXiv:0811.1427*).

10. I. Brevik and S. A. Ellingsen, *Comment on"Casimir Force Acting on Magneto-dielectric Bodies Embedded in Media"*, Physical Review A **79** 027801 (2009).

11[f]. S. Å. Ellingsen, I. Brevik, J. S. Høye and K. A. Milton *Low temperature Casimir-Lifshitz free energy and entropy: the case of poor conductors*, Journal of Physics: Conference Series **161** 012010 (2009).

12[g]. S. Å. Ellingsen, *The Casimir frequency spectrum: can it be observed?*, Journal of Physics: Conference Series **161** 012011 (2009).

13[h]. F. Intravaia, S. Å. Ellingsen and C. Henkel, *Casimir-Foucault interaction: Free energy and entropy at low temperature*, Physical Review A **82** 032504 (2010).

**Part II: Casimir effect in wedge and cylinder geometry**

14[i]. I. Brevik, S. Å. Ellingsen and K. A. Milton, *Electromagnetic Casimir Effect in a Medium-Filled Wedge*, Physical Review E **79** 041120 (2009).

15[j]. S. Å. Ellingsen, I. Brevik and K. A. Milton, *Electromagnetic Casimir Effect in a Medium-Filled Wedge II*, Physical Review E **80** 021125 (2009).

16[k]. S. Å. Ellingsen, I. Brevik and K. A. Milton, *Casimir effect at nonzero temperature for wedges and cylinders*, Physical Review D **81** 065031 (2010).

17. I. Brevik, S. Å. Ellingsen and K. A. Milton, *Electromagnetic Casimir Effect in Wedge Geometry and the Energy-Momentum Tensor in Media*, International Journal of Modern Physics A **25** 2270 (2010); in "Proceedings of the Ninth Conference on Quantum Field Theory Under the Influence of External Conditions" edited by K. A. Milton and M. Bordag (World Scientific, 2010) pp. 158-167.

18. K. A. Milton, J. Wagner, P. Parashar, I. Cavero-Peláez, I. Brevik and S. Å. Ellingsen, *Multiple Scattering: Dispersion, Temperature Dependence, and Annular Pistons*, To appear in the Proceedings of the Workshop "Cosmology, the Quantum Vacuum and Zeta Functions" (Festschrift for Prof. Emilio Elizalde), Barcelona, March 2010 (*arXiv:1007.3462*).

### Part III: Casimir-Polder effect out of thermal equilibrium

19[l]. S. Å. Ellingsen, S. Y. Buhmann and S. Scheel, *Dynamics of thermal Casimir-Polder forces on polar molecules*, Physical Review A **79** 052903 (2009).

20[m]. S. Å. Ellingsen, S. Y. Buhmann and S. Scheel, *Enhancement of thermal Casimir-Polder potentials of ground-state polar molecules in a planar cavity*, Physical Review A **80** 022901 (2009).

21. S. Å. Ellingsen, Y. Sherkunov, S. Y. Buhmann and S. Scheel, *Casimir-Polder Potential in Thermal Non-Equilibrium* in "Proceedings of the Ninth Conference on Quantum Field Theory Under the Influence of External Conditions" edited by K. A. Milton and M. Bordag (World Scientific, 2010) pp. 168-177 (*arXiv:0910.5608*).

22[n]. S. Å. Ellingsen, S. Y. Buhmann and S. Scheel, *Temperature-independent Casimir-Polder forces despite large thermal photon numbers*, Physical Review Letters **104** 223003 (2010).

23[o]. J. A. Crosse, S. Å. Ellingsen, K. Clements, S. Y. Buhmann and S. Scheel, *Thermal Casimir-Polder shifts in Rydberg atoms near metallic surfaces*, Physical Review A **82** 010901(R) (2010). Erratum *ibid.* **82** 029902(E) (2010).

24[p]. S. Å. Ellingsen, S. Y. Buhmann and S. Scheel, *Casimir-Polder potential and transition rate in resonating cylindrical cavities*, Physical Review A **82** 032516 (2010).

### Other publications: physics

25. I. Brevik and S. Å. Ellingsen, *Transverse radiation force in a tailored optical fiber*, Physical Review A **81** 011806(R) (2010).

26. S. Å. Ellingsen, K. S. Gjerden, M. Grøva and A. Hansen, *Model for density waves in gravity-driven granular flow in narrow pipes*, Physical Review E **81** 061302 (2010).

27. I. Brevik and S. Å. Ellingsen, *Possibility of Measuring the Abraham Force using Whispering Gallery Modes*, Physical Review A **81** 063830 (2010).

28. I. Brevik and S. Å. Ellingsen, *Electromagnetic Momentum Conservation in Media*, Annals of Physics (N.Y.), in press.

### Other publications: social science

29. S. A. Ellingsen, *Safeguards Against Nuclear Terrorism: HEU vs Plutonium*, Defense & Security Analysis **24** 129 (2008)

30. S. A. Ellingsen, *Deliberations of a Nuclear Terrorist: Patience or Opportunism?*, Defense & Security Analysis (to appear December 2010)

### What is included and why

The backbone of the thesis is constituted of articles 7[c], 8[d], 11[f], 15[i], 16[j], 19[l], 20[m], 22[n] and 24[p]. The research presented in these articles represent the majority of my workload during the project period from August 2007 to September 2010. In addition, a further 7 articles (4, 6, 9, 12-14 and 23) are included in this thesis which are either somewhat peripheral to the main themes (6, 9, 12) or the main contribution was made by others (4, 13, 14 and 23).

There are various reasons why the remaining 14 articles in the list are not included in the thesis. Papers 2 and 3 as well as my contribution to article 1 are based mainly on work I did for my Master's thesis, hence that research already formed part of a previous degree. Papers 5, 17, 18, and 21 are conference articles where my contributions are largely covered elsewhere (although article 21 does contain a novel derivation primarily due to Drs. Sherkunov and Buhmann). Paper 10 is a Comment article, and while it contains new calculations it is not natural to include it in a thesis. Papers 25-30 were excluded because they were deemed topically too different from the main research questions.

Note that section V of article [i] is not to be considered part of the thesis.

### My contributions to thesis articles

Of the 16 articles included in the thesis I am the first listed author among several on eight, and for all these I believe it is reasonable to say that I did the majority of the work, both theoretical and numerical, ranging from about half to almost everything. A few of these projects were carried out in constant and close collaboration with co-workers whereas most were characterised by me doing the day-to-day work, with input from and discussions with collaborators at discrete intervals. Of 4 articles I am sole author.

For the remaining 4 articles my contribution was not insubstantial, but less than that of the first author. To article [a] my contribution was the numerics section with all figures, as well as contributions to both appendices. To article [h] I contributed through discussions and doing bits of the analysis as well as writing the first draft. The projects behind articles [i] and [j] were carried out in tandem with Prof. Brevik and myself in main charge of one each. My contribution to [i] was through discussions as well as writing Appendix B. Finally for article [o] I carried out the numerical calculation of the dipole moment part of the potential and prepared figures.

# Chapter 1

# Introduction

The advent of quantum physics brought with it an implication that everything fluctuates. No longer could things be said to be sit at one point in space and time, perfectly still, not even at zero temperture. Even vacuum, which was understood in classical physics as "simply empty space", is neither simple nor empty according to quantum theory. The quantum field theory (QFT) description of vacuum is like a bubbling kettle of particles, antiparticles and field quanta which appear and disappear faster than can be observed. One of the few windows through which quantum fluctuations may be seen is the Casimir effect and its siblings, the van der Waals and Casmir-Polder effects.

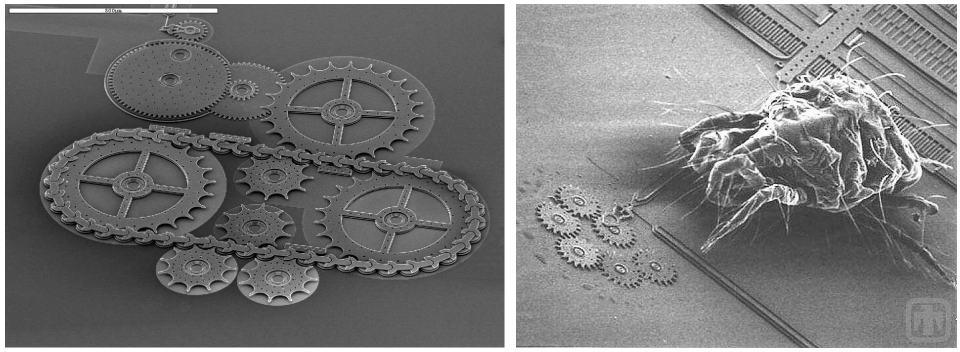

Figure 1.1: Microscopic machinery. Left: a system of microscopic cogs driven by a chain. The white bar in the upper left corner has length 0.5mm. Right: Cogs are dwarfed by a dust mite. Images courtesy of Sandia National Laboratories, *www.sandia.gov*. Systems such as these suffer problems of stiction due to Casimir attraction.

One may not experience quantum fluctuations much in everyday life, and yet these may be said to be the source of a plethora of very diverse phenomena. Some experts believe that 70% of the energy of the universe, the so-called dark energy, is due to vacuum fluctuations, as

supported by recent cosmological data [1, 2]. On the other end of the scale, it is the Casimir effect which makes the gecko's feet sticky, allowing it to walk effortlessly on walls and ceilings [3]. In the microscopic machinery being developed in the rapidly progressing field of nanotechnology (see e.g. figure 1.1), the Casimir effect is a source of trouble, causing moving machine parts to stick to each other [4]. Today, hundreds of papers are published each year about the Casimir effect and related topics as shown in figure 1.2[1].

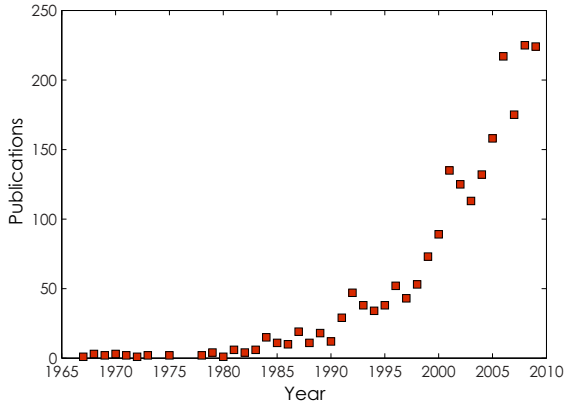


Figure 1.2: Number of publications with Casimir effect and related topics by year.

In this introduction I provide the context for the research presented in this thesis in the form of the 16 scientific articles found in full in the second part. The research articles fall naturally into three categories, all under the common category "dispersion forces", and after a general historical introduction to the overall field, each of the three parts is introduced separately.

## 1.1 A brief history of Casimir effect research

The history of the Casimir effect goes back to the observation of Dutch physicist Johann van der Waals in his 1873 PhD thesis that the equation of state for gases could be much improved with respect to experimental observations by introducing a weak attractive force acting between the atoms and molecules [5]. The force introduced by van der Waals was initially *ad hoc*, and a physical explanation of its origin remained amiss until 1930 when Fritz London, making use of the newly developed quantum theory, showed that it was the effect of fluctuations between the individual charged particles making up the atoms [6]. A short-lived dipole moment is set up by a fluctuation in the electron cloud around one atom,

[1]According to ISI Web of Science, search for topics "Casimir Effect", "Casimir force", "Casimir-Lifshitz", "Casimir-Polder", "retarded van der Waals" and "Casimir energy".

inducing a dipole moment in a nearby atom, and the dipole-dipole force, when averaged over time, gives rise to an attractive force.

Figure 1.3: Hendrik Brugt Gerhard Casimir, 1909-2000

A connection between the London-van der Waals force and the fluctuations of the vacuum itself was made by Hendrik Casimir in 1948. Together with collaborator Dirk Polder he had found an expression for the London-van der Waals force at long distances, where account must be taken for the fact that light travels at a finite speed [7]. A mumbled comment by Niels Bohr spurred Casimir into realising that the interaction could be understood also in terms of fluctuations of the vacuum itself [8]. He went on, therefore, to calculate the potential between two infinite, parallel and perfectly conducting plates separated by a vacuum gap of width $a$. The resulting free energy per unit area, $\mathscr{F}$, and corresponding pressure, $P$, was found as [9] (I use SI units throughout the Introduction)

$$\mathscr{F} = -\frac{\pi^2 \hbar c}{720 a^3}; \qquad P = -\frac{d}{da}\mathscr{F} = -\frac{\pi^2 \hbar c}{240 a^4}. \tag{1.1}$$

Today, in memory of these seminal publications, the following numenclature is established[2]. *London-van der Waals* forces act between two or more atoms or other microscopic particles, *Casimir-Polder* forces act between a particle and a macroscopic body, and *Casimir* forces act between macroscopic bodies. At the fundamental level these are all one and the same phenomenon, measurable forces due to fluctuations of charges and fields, but the distinctions makes sense at least for a theoretician, with reference to which mathematical methods are best suited for calculations. A common name for all these forces is *dispersion forces*.

[2]Although distinctions are often blurred, and terms are sometimes used interchangeably, depending on the background of the researcher.

One of the most important results in the history of the Casimir effect was derived by Lifshitz in 1955 [10] and is today simply referred to as the Lifshitz formula. It expresses the pressure between two parallel plates, the setup considered by Casimir earlier, but now allowing the plates to not be perfect conductors but have general reflection properties[3]

$$\mathcal{F} = \frac{k_\mathrm{B}T}{2\pi} \sum_{\sigma=s,p} {\sum_{m=0}^{\infty}}' \int_0^\infty dq\, q \ln[1 - r_\sigma^+ r_\sigma^- \mathrm{e}^{-2\kappa_0 a}]; \tag{1.2a}$$

$$P = -\frac{k_\mathrm{B}T}{\pi} \sum_{\sigma=s,p} {\sum_{m=0}^{\infty}}' \int_0^\infty dq\, q \kappa_0 \frac{r_\sigma^+ r_\sigma^- \mathrm{e}^{-2\kappa_0 a}}{1 - r_\sigma^+ r_\sigma^- \mathrm{e}^{-2\kappa_0 a}}, \tag{1.2b}$$

where $r_\sigma^\pm(q, \mathrm{i}\zeta_m)$ are the reflection coefficients of the left ($-$) and right ($+$) hand plate for a $\sigma$-polarised wave, and $\zeta_m$ is the $m$th Matsubara frequency, $\zeta_m = 2\pi k_\mathrm{B}T/\hbar$. Here we assume the gap to be vacuum-filled, so $\kappa_0 = \sqrt{\zeta^2/c^2 + q^2}$. If the plates are simply infinitely thick half-spaces of permittivity and permeability $\varepsilon$ and $\mu$ (both relative to their vacuum values), the reflection coefficients take the form

$$r_s(q, \mathrm{i}\zeta) = \frac{\mu\kappa_0 - \kappa_1}{\mu\kappa_0 + \kappa_1}; \;\; r_p(q, \mathrm{i}\zeta) = \frac{\varepsilon\kappa_0 - \kappa_1}{\varepsilon\kappa_0 + \kappa_1} \tag{1.3}$$

where $\kappa_1 = \sqrt{\varepsilon\mu\zeta^2/c^2 + q^2}$.

In the decades after, the Casimir effect remained of a certain theoretical interest, whereas the considerable number of attempts to measure it in experiment were largely inconclusive, the most notable among them perhaps those of Sparnaay [11] and Sabisky and Anderson [12]. Experiments measuring the atom-atom and atom-body forces were more plentiful, and the transition from non-retarded to the retarded regime as predicted by Casimir and Polder was eventually observed directly in 1993 [13].

Of particular interest to the present project are two much cited theoretical papers both appearing in Annals of Physics in 1978, introduced different methods for calculating Casimir forces between bodies of non-trivial geometry today. The first was by French physicists Balian and Duplantier [14] who derived a powerful method of calculating Casimir forces between bodies by making use of the fact that the force has the form of a sum over all multiple scattering paths of light between the bodies [14]. The enormous progress made in recent years on numerical evaluation of Casimir forces between bodies of arbitrary shape and reflecting properties has primarily been made using generalisations of this multiple scattering theory[4]. The second paper was due to Schwinger, DeRaad and Milton [16] who introduced a technique of Green's functions which has enabled analytical calculations of the Casimir force and energy in many geometries later. The two methods, Green's functions and multiple scattering, are equivalent and sometimes employed so that it is not strictly one or the other. In this thesis, Green's functions are made frequent use of (articles [f,l,m,n,o] and [p]), whereas multiple scattering arguments are employed as well, in articles [b,e,g] and [j].

[3] Lifshitz originally assumed purely dielectric half-spaces, later generalised.

[4] It is reasonable to mention that the multiple scattering understanding had been employed in more specialised versions before Balian and Duplantier, e.g. [15].

In contrast to the local method of Green's functions is the method Casimir himself employed [9] for calculation of the global energy shift of fluctuating fields in the presence of boundaries, namely by simply summing up the allowed field solutions (called 'modes') in the presence and absence of these boundaries and taking the difference. A powerful way of performing such calculations by use of Cauchy's integral theorem (the method is often referred to as the 'argument principle') was introduced to Casimir physics in a seminal paper by van Kampen and co-workers in 1968 [17]. Casimir's original method of direct mode summation can only be used in a few simple geometries where the modes are known; we employ this method in articles [i,j] and [k].

The modern era of Casimir effect resarch can be said to have started with its first quantitative measurement, by Lamoreaux in 1997 [18], quickly followed by other impressive experiments [19–25]. The fact that dispersion forces between macroscopic bodies was now within reach of precision experiments lifted this branch of physics, hitherto an almost purely theoretical discipline, into being a focus of interest to a broad range of physicists. Numerous experiments followed, and well over a thousand numerical and theoretical publications.

In the following three sections I will briefly review the backgrouhd for each of the three parts of the thesis. Because emphasis will be on preparing for, informing and illustrating the research presented in the reseach articles included, no attempt is made to cover all aspects of modern Casimir and Casimir-Polder effect research, which has spanned out into a number of sub-fields of which I have worked in three. For a fuller overview, the reader is referred to reviews from various angles, both books [26–28] and articles [29–35]. An up-to-date overview of the questions currently being researched is provided by the Proceedings volumes of two recent conferences [36, 37].

The three next sections contain what is intended to convey a general understanding of the problems analysed in the research articles and an qualitative outline of the methods made use of. I will *not*, however, repeat the numerous conclusions reached in these articles, nor will I reiterate any of the sundry minutiae of the actual implementations, numerical or analytical, of these methods. Such details are all covered in the papers themselves, and a second rendition would not only be a lengthy and rather tedious exercise, but also largely superfluous. I am somewhat prone to prolixity as it is, and will aspire to spare the reader the additional humdrum of avoidable repetition.

## 1.2 Casimir effect at the crossroads: from ideal models to realistic conditions

The "modern era" of Casimir effect research has been marked in particular by the transition from a purely theoretical subject to an experimental and technological discipline. While the theoretical efforts used to be concerned with conceptual questions relating to the nature of the quantum vacuum, a new need arose to provide accurate predictions for the forces measured in experiments. For the Casimir effect this meant that in particular four idealisations which had previously been convenient had to be generalised:

1. *Smooth surfaces to rough surfaces*: Real surfaces are not perfectly smooth. This introduces corrections to results for perfectly smooth surfaces (e.g. [29, 38]).

2. *Plane-Plane to Plane-Sphere geometry*: Although a few experiments have made use of Casimir's original geometry of two parallel plates, replacing one plate by a sphere has proven to be a more workable geometry despite the force between the bodies being weaker in this case [28, 31, 33]. The reason is that it has proven very difficult to keep two planes perfectly parallel. Calculation-wise, however, the sphere-plane geometry is much more difficult, and a large theoretical effort has been put into achieving better analytical and numerical results in this geometry, a work which is still ongoing (e.g. [28, 39, 40]).

3. *Perfect conductors to real materials*: Casimir's calculation [9] assumed perfectly conducting plates, which Lifshitz generalised to material slabs of permittivity $\varepsilon$. The Casimir effect according to Lifshitz theory depends on the dispersive properties of the materials involved at all frequencies, however, and it turns out that inserting fully frequency dependent permittivity and permeabilities into Lifshitz' result is not without complications in certain situations, as will be detailed below.

4. *Zero temperature to finite temperature*: Experiments are typically performed at room temperatures, which introduces corrections. The transition is formally apparently straightforward (in quantum field theory the time dimension becomes compactified at finite temperatures, with period $\hbar/k_{\mathrm{B}}T$) and the expression was written down already by Lifshitz [10].

It soon transpired that, while each of these four transitions in isolation were rather straightforward at least in principle, including two or more corrections at the same time leads to ambiguities. In particular the combination of real materials and non-zero temperature turned out to be controversial, since the two corrections do not commute: it matters which assumption is generalised before the other. I will expand on this in the following.

### 1.2.1 Temperature anomaly for metals

The Casimir effect between metals at non-zero temperature has been a subject of heated debate for a good decade. An ambiguity as to how to take the limit of perfect reflection was recognised early by Scwinger and co-workers [16] and 'solved' by a prescription which was followed for years to follow. The prescription was in essence to set the reflection coefficients entering in Eq. (1.2) to unity prior to further calculation. Thus the original Casimir result was obtained at zero temperatures.

It was a paper by Boström and Sernelius [41] which first pointed out that this prescription was in conflict with application of the most widely employed model for metallic permittivity, the Drude model,

$$\varepsilon(\omega) = 1 - \frac{\omega_{\mathrm{p}}^2}{\omega(\omega + \mathrm{i}\gamma)} \quad \Leftrightarrow \quad \varepsilon(i\zeta) = 1 + \frac{\omega_{\mathrm{p}}^2}{\zeta(\zeta + \gamma)}, \tag{1.4}$$

where $\omega_{\rm p}$ is the metallic plasma frequency and $\gamma$ the relaxation frequency. To see how this happens, consider the $s$ (or TE) reflection coefficient in Eq. (1.3) which features the quantity

$$\kappa_1 = \sqrt{\frac{\varepsilon\zeta^2}{c^2} + q^2} \overset{\zeta\to 0}{\sim} \sqrt{\frac{\omega_{\rm p}^2\zeta}{\gamma c^2} + q^2} \overset{\zeta\to 0}{\to} q \tag{1.5}$$

(we let $\mu = 1$ here and in the following for simplicity), and hence, from Eq. (1.3), $r_s \overset{\zeta\to 0}{\to} \frac{q-q}{q+q} = 0$. In other words the Drude model implies that for the term $m = 0$ in the sums of Eqs. (1.2), there is no contribution from the TE mode.

The vanishing of the TE term has significance at high temperature and/or long interplate separations as one will see when noting that when the arguments of the exponentials in (1.2) are sufficiently large the summands fall off exponentially like[5]

$$\mathrm{e}^{-2\kappa_0 a} \sim \exp\left(-\frac{4\pi m k_{\rm B} T a}{\hbar c}\right) \text{ as } \frac{k_{\rm B} T a}{\hbar c} \to \infty. \tag{1.6}$$

Hence, in the limit $k_{\rm B}Ta/\hbar c \gg 1$, only the term $m = 0$ contributes significantly to the sum, and the Casimir pressure is approximately

$$P \sim -\frac{k_{\rm B}T}{2\pi} \sum_{\sigma=s,p} \int_0^\infty dq q \kappa_0 \left.\frac{r_\sigma^+ r_\sigma^- \mathrm{e}^{-2\kappa_0 a}}{1 - r_\sigma^+ r_\sigma^- \mathrm{e}^{-2\kappa_0 a}}\right|_{\zeta=0}. \tag{1.7}$$

As argued, $r_s(\zeta = 0) = 0$ (at least if the discrete term $m = 0$ is to be interpreted as the *limit* $m \to 0^+$) whereas $r_p$ takes on $q$ dependent values close to unity. All in all the Drude model predicts a force reduced by a factor $\frac{1}{2}$ compared to Casimir's original calculation; a dramatic result! Later calculations have shown that also more detailed, spatially dispersive models give similar results [42, 43]. For the sphere-plane geometry, the factor turns out to be $\frac{2}{3}$ [44].

The Drude prediction was criticicised on two levels, theoretical and experimental. For a more complete review of the debate that ensued, from two different perspectives, see [28] and [45]; here I will merely mention the experimental debate and very briefly account for some of the main theoretical points.

On the experimental side the objection which has been raised is simply that the Drude prediction does not match the experimental data available. First it was found that Lamoreaux's experiment [18] did not favour a metallic model with low-frequency dissipation such as that of Drude, but fitted better with Casimir's original result, which can be approximated by a metallic model without low-frequency dissipation from scattering[6]. Later, experiments by Decca and co-workers [47, 48], claiming extremely high precision down to the 1% level, came to the same conclusion. Still today, no commonly accepted theory explains this apparent discrepancy between theory and experiment.

On the theoretical side, the observation of Boström and Sernelius was soon criticised on thermodynamical grounds [49–52]. The argument, which concerns the vanishing of Casimir

[5] The symbol ~ is used in the sense 'asymptotically'.

[6] Note that Lamoreaux recently attributed this to a systematic correction [46] which, upon inclusion, shifts that experiment in the direction of the Drude result after all.

entropy at zero temperature, has been gradually crystallised through a decade of ensuing debate. The way I myself understand it at the end of all that, it goes as follows[7]. Assume the two slabs of the same metal are truly infinitely large and made of a perfect crystal lattice, completely free of impurities and imperfections which can scatter electrons at zero temperature. In this case the only mechanism to give electronic relaxation is scattering of the free electrons on thermally excited phonons of the material. As temperature decreases, these die away according to the Bloch-Grüneisen formula [53] as

$$\gamma(T) \propto T^5, \quad T \to 0. \tag{1.8}$$

Regarding now the reflection coefficient $r_s$ again, we notice that the two limits $\zeta \to 0$ and $T \to 0$ do not commute:

$$\begin{aligned} &\lim_{T\to 0}\lim_{\zeta\to 0} r_s = 0, \text{ but} \\ &\lim_{\zeta\to 0}\lim_{T\to 0} r_s = \tilde{r}_s = -\chi^2\left(\sqrt{1+\chi^{-2}}-1\right)^2 \neq 0, \end{aligned} \tag{1.9}$$

with $\chi = \frac{c\kappa_0}{\omega_\mathrm{p}}$. Using the Euler-Maclaurin sum formula [54] to calculate the low-frequency behaviour of the free energy (1.2a), one can then show that $\mathscr{F}(T)$ obtains a term linear in $T$:

$$\mathscr{F}(T) = \mathscr{F}_0 + \frac{\omega_\mathrm{p}^2 k_\mathrm{B} T}{4\pi c^2}\int_0^\infty d\chi\chi \ln[1-\tilde{r}_s^2(\chi)e^{-(2a\omega_\mathrm{p}/c)\chi}] + \mathscr{O}[T^2]. \tag{1.10}$$

In other words, the entropy $\mathscr{S} = -\partial_T\mathscr{F}$ is different from zero at $T = 0$, which, it was argued, voilates Nernst's theorem, the third law of thermodynamics.

As mentioned, the dicourse on the violation of the third law has crystallized over time, and the link to the non-commuting limits of frequency and temperature was only arrived at in two independent studies in 2008, of which my article [d] was one, and the other was due to Intravaia and Henkel [55]. The above argument (elaborated in [f]) is the 'end product' after nearly ten years of arguments back and forth, a discourse in which clarity has gradually emerged.

But let us go back in time a little. Starting 2003, Høye, Brevik, Aarseth and Milton published work in support of the Drude description of metals showing that for a realistic metal with imperfections present, entropy does vanish [56, 57]. Their work was supported by the statistical mechanical elaborations of two other groups [58–61]. A further study showed that the low-temperature behaviour of the Casimir free energy between Drude metals is quadratic in $T$ [62], and the two leading order terms of the TE-mode free energy were worked out analytically in article [a].

A highly similar problem was pointed out also for semiconductors which have a small but non-zero conductivity which, for some types of semiconductor, vanishes exponentially as temperature goes to zero, when the conductivity influence on the permittivity is described by

[7] The following is adapted from section 2 of article [f] and shortened.

a Drude-type model [63]. Mathematically the formal violation of the third law of thermodynamics is almost identical to that described for metals above (see [f]), but now concerns the TM rather than TE modes. As a benchmark result, the low $T$ expansion of the free energy also for the TM mode using this discription of conductivity was worked out in article [c].

In recent years, several interesting developements have been made on the theoretical side in an effort to understand the mysterious temperature effect for Drude metals. With respect to the Nernst theorem anomaly, it was pointed out by Bimonte [64] that the interaction of stochastical Johnson noise currents in two wires exhibited the same entropy anomaly, and a little later, Intravaia and Henkel demonstrated that the entropy problem could indeed be attributed to a type of modes corresponding physically to fluctuating overdamped bulk currents, called Foucault currents, within the two materials [65]. In a continuation of that effort, I joined forces with the latter group and we were able to show that the low temperature expansion of the free energy due to these Foucault currents alone is the same as for the entire Casimir-Lifshitz interaction [h]. Other enlightening treatments include the comparison between the Casimir entropy anomaly and that of a Brownian particle, by Ingold and co-workers [66].

I offered some arguments in [d] why the third law of thermodynamics (Nernst's theorem) is probably not a good criterion for choosing how to describe the Casimir interaction at high temperature at all. A main point is, I still believe, that the Nernst theorem is valid at zero temperature. In that regime, simple and local permittivity models such as Drude and Plasma models are not expected to describe real physics anyway because of such effects as the anomalous skin effect or onset of superconductivity, and in any case the reason one needs to distinguish between different models is to correctly describe the Casmir force at *high* temperatures. Indeed, near zero temperature the two models give practically the same Casimir force. An alternative criterion was suggested by Bimonte [67]. He shows that the Bohr-van Leuven theorem of classical statistical mechanics implies that the TE reflection coefficient $r_s$ should tend to zero in the high-temperature limit according to the Drude prediction.

The latest developments on the theory side of temperature debate concern the triple interaction of temperature, real materials and non-flat geometry. A notable step forward was the numerical calculation of Antoine Carnaguier-Durand and co-workers [44, 68]. The sphere + flat plate geometry is what is is typically used in experiments to circumvent issues of retaining parallelity, and is used in all of the most precise measurements of the Casimir force including those of Decca [47, 48] which do not seem to fit with a dissipative description of metals. Noting, however, that both the sphere-plate separation and the sphere radius are the same order of magnitude as the thermal wavelength $\lambda_T = 2\pi\hbar c/k_{\rm B}T$ at room temperature (a few micrometers), it is an appealing thought at a somewhat hand-waving level to think that the smallness of the physical system means temperature effects which would be present for macroscopic plates (and which in that geometry only becomes important only when inter-plate separations $a$ are not much smaller than $\lambda_T$) cannot be "seen" by a microsphere. A brief elaboration of this view was recently published [69]. If Lamoreaux's latest correction [46] to his old experiment [18] and corresponding reanalysis are correct, it might be an indication of such geometry effects: Lamoreaux's spheres are macroscopic (radius in

centimeters) whereas Decca's spheres are much smaller and measure in the tens of microns.

## 1.3 Casimir effect as mathematical physics: the wedge

Before the advent of precise Casimir force experiments [18], the Casimir effect was a subject belonging primarily to mathematical and theoretical physics. A much cited review article from the mid 1980s [70] illustrates this. Its bulk consists of questions such as field quantisation procedures, different boundary conditions, different mathematical routes of evaluation, scalar vs. electromagnetic fields, quarks in gluon bags, and finite temperature. As "applications" the attraction between dielectrics as calculated by Lifshitz is presented. A more recent overview of the theoretical part of Casimir physics is found in Milton's book [26]. A reminder of the quantum field theory roots of the Casimir community is found in the name of the biannual Casimir effect conferences, which still bear the name "Quantum Field Theory Under the Influence of External Boundary Conditions (QFEXT)" [37], although these days you are as likely to hear talks about experimental precision and apparatus as about, say, the vacuum self-energy of $D+1$ dimensional Dirichlet-bounded hyperparaboloids.

Today, a review with the general heading "The Casimir Effect" would be expected to include much more than quantum field theoretical calculations. To forgo the mention of experiments, the various corrections due to system imperfections such as listed above, and the link to applied atomic and colloid physics would be almost unthinkable. Yet, for all the newfound applications of this field of physics which was once a theoretical curiosity, the Casimir effect lives on as a branch mathematical physics as well.

A particular branch of the theoretical side of the Casimir effect has been the striving towards analytical results for the Casimir energy of new geometries. The story of the search to understand the rôle of geometry on the Casimir energy goes back far, probably to Casimir's own stipulation that if the electron could be modelled as a thin shell held together by Casimir attraction but pushed apart by Coloumb forces, the fine-structure constant could be *calculated* [71]. This dream was shattered when Boyer showed in his Ph.D. work that the Casimir stress on a perfectly conducting spherical shell is, modulo some singular but renormalisable terms[8], repulsive [72]. Thus was started the search for more analytical results in new geometries in an attempt to understand how geometry could have such a profound effect on the Casimir energy. This work continues, and as I write it is less than two weeks since the appearence of a paper by Professor Milton's group on cylinders of triangular cross-sections wherein a universal function for the Casimir energy of cylinders of general polygonal cross-sections is proposed [73].

Research on the Casimir effect was sporadic in the first few decades, and results on new geometries were slow in coming. Only in 1981 was the Casimir energy of an infinitely long perfectly conducting circularly cylindrical shell calculated by DeRaad and Milton [74], and the more physical but also much more complicated case of a (magneto)dielectric cylinder has only been treated in relatively recent years [75–82]. A particularly useful kind of "boundary

[8]This has been subject of some controversy, see [26] and references therein.

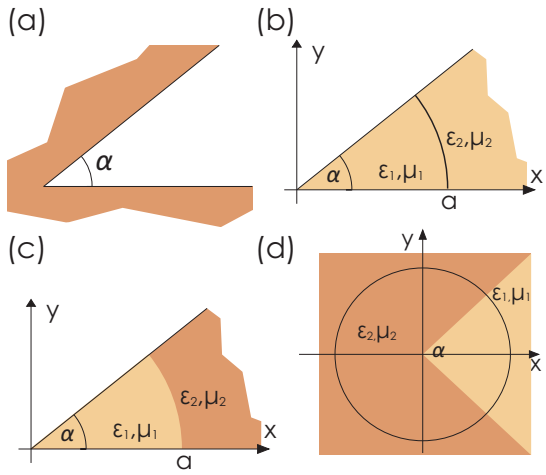


Figure 1.4: Different wedge geometries, (a) the classical perfectly conducting wedge geometry; (b) a material-filled perfectly conducting wedge closed by a perfectly conducting circularly cylindrical arc, considered in article [i]; (c) the perfectly conducting wedge, now with a magnetodielectric arc, considered in article [i]; (d) an isorefractive wedge positioned coaxially in a circularly cylindrical perfectly reflecting shell, the geometry considered in article [j].

conditions" for calculating the Casimir force in various geometries has been the use of $\delta$-function potentials. A host of different geometries have been treated for the scalar field in this formalism via the Klein-Gordon equation which is solved by means of a Green's function (e.g. [26, 30, 83, 84]).

Closely related to the circularly cylindrical geometry is the infinite wedge. The problem was first approached in the late seventies [85, 86]. Since, various embodiments of the wedge have been treated by Brevik and co-workers [87–89] and others [90]. A wedge intercut by a cylindrical shell was considered by Nesterenko and co-workers, first for a semi-cylinder [91], then for arbitrary opening angle [92], and the corresponding local stresses were studied by Saharian [93–95].

It is in light of all this previous research into geometry effects of the Casimir energy that my senior collaborators, Profs. Brevik and Milton, and I contributed another few pieces to the jigsaw in the form of papers [i,j,k]. The first article [i] considers the geometry of a perfectly conducting wedge intercut by a circularly cylindrical arc, either perfectly conducting or magnetodielectric. In the second article [j] the same geometry is chosen, but now letting the wedge be not perfectly conducting but isorefractive, that is, it is magnetodielectric in such a way that the speed of light is the same in all sectors. Finally, in article [k] the results obtained in article [i] are generalised to non-zero temperature.

### 1.3.1 Casimir energy calculated by mode summation

In all these papers, the method of calculation is in essence the same, namely what is called mode summation. The rest of this section contains a sketch of how we calculate Casimir energies at zero and finite temperatures with this method, which is essentially the same as that originally employed by Casimir [9]. I do not strive to be rigorous here, but seek to convey an understanding of the general procedure without involving the nitty-gritty details and subtleties which tend to enter in any real calculation.

According to quantum field theory, the vacuum zero-temperature energy of the fluctuating electromagnetic field is given as

$$\mathscr{E} = \tfrac{1}{2}\hbar \sum_{\varrho} \omega_\varrho = \sum_{\varrho} e(\omega_\varrho) \tag{1.11}$$

where $\omega_\varrho$ are the eigenfrequencies of the field, dependent on a set of quantum numbers $\varrho$, which solves the boundary conditions of the system. At non-zero temperature this expression generalises to [96]

$$\mathscr{E}(T) = k_\mathrm{B} T \sum_{\varrho} \ln\left[2\sinh\frac{\hbar\omega_\varrho}{2k_\mathrm{B}T}\right] = \sum_{\varrho} f_T(\omega_\varrho). \tag{1.12}$$

In principle the sport is now to find what the eigenmodes $\{\varrho\}$ of the geometry are and sum the free energy contribution from all these (infinitely many) modes. In practice, however, doing so explicitly is only feasible for a few very simple geometries. Instead one may employ a very powerful method called the argument principle. The method, introduced to the Casimir world by van Kampen et al. [17] as previously mentioned, requires that a function can be found containing all relevant boundary conditions, such that

$$\mathscr{D}(\omega) = 0 \Leftrightarrow \omega \in \{\omega_\varrho\}. \tag{1.13}$$

The function may have other zeros and poles as well provided these are known and the corresponding spurious solutions can be subsequently subtracted off, but let us assume the function $\mathscr{D}(\omega)$ satisfies (1.13) and is free of other singularities and branch cuts, for simplicity. The energy can then be summed up according to Cauchy's theorem as

$$\mathscr{E}(T) = \sum_{\varrho} f_T(\omega_\varrho) = \frac{1}{2\pi\mathrm{i}} \oint_\Xi \mathrm{d}\omega f_T(\omega) \frac{\mathrm{d}}{\mathrm{d}\omega} \ln \mathscr{D}(\omega) \tag{1.14}$$

where $\Xi$ is a complex integration path encircling all relevant solutions $\omega_\varrho$. In an extension of the simple equations above, the boundary value equation (1.13) can depend on further variables which must be summed over at the end. Typically, the energies (1.11) and (1.12) are infinite and must be regularised by subtracting the corresponding value when the boundaries are removed. This 'empty' system (denoted "$\infty$") has eigenmodes given by $\mathscr{D}_0(\omega) = 0$, and so the regularised, free energy is

$$\mathscr{F}(T) = \left[\sum_{\varrho} - \sum_{\infty}\right] f_T(\omega_\varrho) = \frac{1}{2\pi\mathrm{i}} \oint_\Xi \mathrm{d}\omega f_T(\omega) \frac{\mathrm{d}}{\mathrm{d}\omega} \ln \frac{\mathscr{D}(\omega)}{\mathscr{D}_0(\omega)}. \tag{1.15}$$

This is a sketch of the general route to obtaining the Casimir energy by mode summation.

For the case of a perfectly cylindrical wedge, the solution of the governing electromagnetic equation (the Helmholz equation) can be expanded in partial waves which involve cylindrical Bessel functions and take the general form

$$\mathbf{E},\mathbf{H} = \mathbf{A} \begin{matrix} J_\nu(\kappa\rho) \\ H_\nu^{(1)}(\kappa\rho) \end{matrix} + \mathbf{B} \begin{matrix} J_\nu'(\kappa\rho) \\ H_\nu^{(1)\prime}(\kappa\rho) \end{matrix} \tag{1.16}$$

(for the actual expressions of field components, see [i]) where

$$\kappa(\omega) = \sqrt{k_z^2 - \varepsilon\mu\omega^2}, \tag{1.17}$$

$k_z$ being the wave number along the cylinder axis (**A** and **B** are constants, upper or lower Bessel function chosen according to boundary conditions at $r = 0$ or $r \to \infty$), and $\rho$ is distance from $z$ axis.

For a circularly cylindrical, perfectly reflecting arc of radius $a$ the boundary condition giving the eigenvalues of $\omega$ is

$$\mathscr{D}_{k_z,\nu}(\omega) = 1 - x^2\lambda_\nu^2(x) = 0 \tag{1.18}$$

with

$$\lambda(x) = \frac{\mathrm{d}}{\mathrm{d}x}[I_\nu(x)K_\nu(x)], \quad \text{and} \quad x = \kappa a. \tag{1.19}$$

A somewhat more complicated eigenequation pertains to a magnetodielectric cylindrical arc, see article [i]. After inserting this value into the argument principle, equation (1.15), we finally integrate over $k_z$ and sum over all allowed values of $\nu$.

One quickly finds that the order of the Bessel functions are restricted by the presence of the perfectly conducting wedge to values

$$\nu = mp, \quad p = 2\pi/\alpha, \quad m \in \mathbb{Z}, \tag{1.20}$$

where $\alpha$ is the opening angle of the wedge. After employing the argument principle, the solution must then simply be summed over $m$[9]. The situation is subtler for the diaphanous wedge [j]: there the values of $\nu$ are given not by (1.20) but implicitly, via the eigenequation

$$\sin^2\pi\nu - r^2\sin^2\nu(\pi - \alpha) = 0, \tag{1.21}$$

where

$$r = \frac{\varepsilon_1 - \varepsilon_1}{\varepsilon_2 + \varepsilon_2} = -\frac{\mu_1 - \mu_2}{\mu_1 + \mu_2} \tag{1.22}$$

(since $\epsilon_1\mu_1 = \epsilon_2\mu_2$). In this case it is necessary to use the argument principle twice: once to sum over eigenfrequencies $\omega(\nu)$ and again to sum over the allowed values of $\nu$ for a given $r$.

[9]Note that some subtleties pertain to this sum, see article [i].

### 1.3.2 Generalisation to non-zero temperature

Both articles [i] and [j] operate at zero temperature, in which $f_T(\omega) \to e(\omega) = \frac{1}{2}\hbar\omega$. Nonzero temperatures are typically treated in the expression (1.15) the following way. First, note that the eigenfrequencies of the system typically lie on or slightly below the real frequency axis. Second, note that a contour encircling the *whole* complex frequency plane in a circle at infinity must give zero result presuming (as is physical) $\mathscr{D}(\omega)$ vanishes sufficiently quickly as $|\omega| \to \infty$. Performing a partial integration, we write

$$\frac{1}{2\pi\mathrm{i}}\oint_\infty \mathrm{d}\omega f_T(\omega)\frac{\mathrm{d}}{\mathrm{d}\omega}\ln\frac{\mathscr{D}(\omega)}{\mathscr{D}_0(\omega)} = -\frac{\hbar}{4\pi\mathrm{i}}\oint_\infty \mathrm{d}\omega\coth\frac{\hbar\omega}{2k_\mathrm{B}T}\ln\frac{\mathscr{D}(\omega)}{\mathscr{D}_0(\omega)} = 0. \tag{1.23}$$

The integral (1.23) gets contributions from the zeros of $\mathscr{D}(\omega)$ and $\mathscr{D}_0(\omega)$, and at the poles of the coth function, which are found along the imaginary frequency axis at the Matsubara frequencies

$$\omega = \mathrm{i}\xi_m = \frac{2\pi\mathrm{i}nk_\mathrm{B}T}{\hbar}, \quad n \in \mathbb{Z}, \tag{1.24}$$

hence

$$\frac{\hbar}{4\pi\mathrm{i}}\oint_\infty \mathrm{d}\omega\coth\frac{\hbar\omega}{2k_\mathrm{B}T}\ln\frac{\mathscr{D}(\omega)}{\mathscr{D}_0(\omega)} = -2\mathscr{F}(T) + k_\mathrm{B}T\sum_{n=-\infty}^{\infty}\ln\frac{\mathscr{D}(\mathrm{i}\xi_n)}{\mathscr{D}_0(\mathrm{i}\xi_n)} = 0 \tag{1.25}$$

[the minus sign on $\mathscr{F}_T$ comes from a partial integration like in Eq. (1.23), the factor 2 from equal contributions from eigenfrequencies in the right and left half-plane due to symmetry properties [97]], and hence the free energy can be expressed as a Matsubara sum:

$$\mathscr{F}(T) = \tfrac{1}{2}k_\mathrm{B}T\sum_{n=-\infty}^{\infty}\mathrm{Tr}\ln\frac{\mathscr{D}(\mathrm{i}\xi_n)}{\mathscr{D}_0(\mathrm{i}\xi_n)}. \tag{1.26}$$

I have rather magically applied a trace operator to the last formula to indicate that further summation over other variables (to wit, a sum over $m$ or $\nu$ and an integral over $k_z$ in the wedge case) must also be made, but has been suppressed in this simplified derivation for simplicity. For more rigorous derivations, see papers [i,j]. A useful exposition of such spectral path integral methods in Casimir calculations is also given in article [h].

## 1.4 Casimir-Polder effects out of thermal equilibrium

A number of modern experimental technique have the common trait that they involve detailed manipulation of atoms or nano particles close to surfaces in such a way that the particles are not in thermal equilibrium with their environment. One such area is magnetic trapping of ultracold atoms close to surfaces for a number of experimental uses [98]. Trapping of Bose-Einstein condensates in particular have proven highly useful, for example a the much cited “slow light” experiment by Vestergaard Hau’s group [99], measurement of long-range Casimir-Polder forces [100] as well as possibilities for quantum information processing [101, 102]. Another area is the trapping of cold molecules from molecular beams near surfaces for experimental investigation [103]. This technique has been applied as a sensitive probe of the permanent dipole moment of the electron [104]. A detailed description of

particle-surface interactions for particles out of thermal equilibrium is of importance to the theoretical description of any of these systems.

The above systems may all be said to belong to a category of non-equilibrium systems in which the particles are prepared in a given eigenstate (or superposition of such) whereas the environment is in a state of (approximate) thermal equilibrium at a given temperature. A general theory for such a system was recently presented by by collaborators Buhmann and Scheel [105], as a generalisation of previous work for zero-temperature systems [106]. Buhmann and Scheel's theory generalises a number of previous theoretical efforts on excited atoms, going back at least to Barton's treatments in the 1970s [107–109], and through to recent times [110–112]. The system of a ultra-low temperature Bose-Einstein condensate held outside a substrate at high temperature was considered by Antezza and co-workers [113,114] via a modification of Lifshitz' classic derivation [10]. Another generalisation was recently provided by Sherkunov, who derived the expression for the Casimir-Polder potential between two particles prepared in arbitrary eigenstates, in the presence of an external electric field [115], for example one from thermal radiation. A demonstration of the compatibility of the three non-equilibrium theories of Antezza *et alia*, Buhmann and Scheel, and Sherkunov was provided in the collaborative project resulting in Ref. [116].

I will briefly lay out the essentials of the theory employed in articles [l-p] as an introduction to the research papers found in full text in the second half of the thesis. The specific conclusions from the individual articles are summarised in Chapter 2 and in the papers themselves, and will not generally be repeated in this section, which focuses on the background.

### 1.4.1 Macroscopic Quantum Electrodynamics: Buhmann-Scheel theory

I will briefly account for the main conclusions of the theory due to Buhmann and Scheel [105]. They derive the energy shift of a particle in an arbitrary superposition of its eigenstates in the vicinity of macroscopic bodies held at a temperature $T$. The derivation is made in the dipole approximation via a $\mathbf{d}\cdot\mathbf{E}$ term in the interaction Hamiltonian, and the energy shift is found with perturbation theory to second order (the first order term is zero for parity reasons).

The details of derivation will not be reiterated here, nor will I consider the most general cases of the theory. In the following I restrict attention to a single isotropic particle prepared in a single eigenstate $|n\rangle$ whose transition rates $\Gamma_{kn}$ are small compared to transition frequencies $|\omega_{kn}| = |E_k - E_n|/\hbar$ for all relevant transitions to other states $|k\rangle$ ($E_j$ is energy level of state $|j\rangle$). In this case the potential (energy level shift) of the particle can be written

$$\mathcal{U}_n(\mathbf{r}) = \frac{k_\mathrm{B}T}{\varepsilon_0}\sum_{j=0}^{\infty}{}' \frac{\xi_j^2}{c^2}\alpha_n(\mathrm{i}\xi_j)\mathrm{Tr}\mathbf{G}^{(1)}(\mathbf{r},\mathbf{r};\mathrm{i}\xi_j) + \frac{1}{3\varepsilon_0}\sum_k \frac{\omega_{kn}^2}{c^2}\left\{\Theta(\omega_{kn})n(\omega_{kn}) - \Theta(\omega_{nk})[n(\omega_{nk})+1]\right\}|\mathbf{d}_{kn}|^2\mathrm{Tr}\ \mathrm{Re}\mathbf{G}^{(1)}(\mathbf{r},\mathbf{r};|\omega_{kn}|). \quad (1.27)$$

Here, $\alpha_n(\omega)$ is the particle polarisability of the particle in state $|n\rangle$ (scalar for isotropic parti-

cle)

$$\alpha_n(\mathrm{i}\xi) = \frac{2}{3}\sum_k \frac{\omega_{kn}|\mathbf{d}_{kn}|^2}{\omega_{kn}^2+\xi^2},$$

$\xi_j$ is the $j$th Matsubara frequency $\xi_j = 2j\pi k_\mathrm{B}T/\hbar$, $\mathbf{d}_{kn}$ is the transition dipole moment of the transition $|n\rangle \to |k\rangle$, $\Theta(x)$ is the unit step function, and $\mathbf{G}^{(1)}(\mathbf{r},\mathbf{r}';\omega)$ is the scattering part (excluding direct source field) of the two-point electromagnetic dyadic Green's function of the system, in the reciprocal time domain.

The key observation to make with regard to Eq. (1.27) is that it consists of two terms of fundamentally different nature. The latter term depends on a discrete set of *real* frequencies, whereas the former is a sum of infinitely many equidistant *imaginary* frequencies. We call the latter part the *resonant* contribution, and the Matsubara sum the *non-resonant* contribution. The reasoning behind this numenclature is that the resonant term is due to resonant interaction between the fluctuating thermal EM field and the system's eigenfrequencies $\omega_{kn}$, whereas the Matsubara sum does not resonate with any particular frequency. This can be seen from the relation (Kramers-Kronig)

$$\mathbf{G}^{(1)}(\mathbf{r},\mathbf{r}';\mathrm{i}\xi) = \frac{2}{\pi}\int_0^\infty \frac{\mathrm{d}\omega\omega}{\omega^2+\xi^2}\mathrm{Im}\mathbf{G}^{(1)}(\mathbf{r},\mathbf{r}';\omega) \tag{1.28}$$

which $\mathbf{G}^{(1)}$ must satisfy because it is a generalised susceptibility [97]. Each term of the Matsubara sum therefore corresponds to an integral over all real frequencies, and cannot be made to resonate with any particular frequency.

In the special case where the particle is in thermal equilibrium,

$$|n\rangle \to |T\rangle = \mathcal{Z}^{-1}\sum_k \mathrm{e}^{-E_k/k_\mathrm{B}T}|k\rangle, \tag{1.29}$$

[$\mathcal{Z} = \sum_j \mathrm{e}^{-E_j/k_\mathrm{B}T}$: partition function] one can show [105] that all resonant features vanish from (1.27), which becomes

$$\mathscr{U}_T(\mathbf{r}) = \frac{k_\mathrm{B}T}{\varepsilon_0}\sum_{j=0}^{\infty\,\prime}\frac{\xi_j^2}{c^2}\alpha_T(\mathrm{i}\xi_j)\mathrm{Tr}\mathbf{G}^{(1)}(\mathbf{r},\mathbf{r};\mathrm{i}\xi_j) \tag{1.30}$$

where $\alpha_T(\omega)$ is the polarisability of the thermal state:

$$\alpha_T(\omega) = \mathcal{Z}^{-1}\sum_k \mathrm{e}^{-E_k/k_\mathrm{B}T}\alpha_k(\omega). \tag{1.31}$$

The resonant phenomena due to the second term in (1.27), which we investigate in particular in articles [l,m,p] are therefore strictly thermal non-equilibrium effects.

To obtain an analytical expression for the Casimir-Polder potential in a given geometry within this formalism, one has to find the Green's function (or rather, tensor), which, given the geometrical boundary conditions, solves the Helmholtz equations (I assume the particle be placed in a locally homogeneous medium)

$$\left(\nabla\times\nabla\times\ -\frac{\varepsilon\mu}{c^2}\right)\mathbf{G}(\mathrm{r},\mathrm{r}';\omega) = \mu\delta(\mathrm{r}-\mathrm{r}')\mathbf{I} \tag{1.32}$$

where $\mathbf{I}$ is the $3 \times 3$ unit matrix. The nondimensional permittivity $\varepsilon$ and permeability $\mu$ are in general functions of r and $\omega$. The scattering part $\mathbf{G}^{(1)}$is a homogeneous solution to (1.32) [117]. The dyadic Green's functions of a number of standard geometries have been worked out analytically [119].

In article [l] the Green's function a distance $z$ outside a single plane dielectric half-space of permittivity $\varepsilon_1(\omega)$ is used,

$$\mathbf{G}^{(1)}(\mathbf{r},\mathbf{r};\omega) = \frac{\mathrm{i}}{8\pi}\int_0^\infty \mathrm{d}q\,\frac{q}{\beta}\,e^{2\mathrm{i}\beta z}\Big[\Big(r_s - \frac{\beta^2 c^2}{\omega^2}\,r_p\Big)(\mathbf{e}_x\mathbf{e}_x + \mathbf{e}_y\mathbf{e}_y) + 2\,\frac{q^2c^2}{\omega^2}\,r_p\mathbf{e}_z\mathbf{e}_z\Big], \tag{1.33}$$

with

$$\beta = \sqrt{\omega^2/c^2 - q^2};\;\; \beta_1 = \sqrt{\varepsilon_1(\omega)\omega^2/c^2 - q^2} \tag{1.34}$$

and, as before,

$$r_s = \frac{\beta - \beta_1}{\beta + \beta_1};\;\; r_p = \frac{\varepsilon_1\beta - \beta_1}{\varepsilon_1\beta + \beta_1}. \tag{1.35}$$

For the geometry of a planar cavity only the reflection coefficients are changed to allow for multiple scattering between the walls:

$$r_\sigma \to \frac{r_\sigma^2 e^{2\mathrm{i}\beta a}}{1 - r_\sigma^2 e^{2\mathrm{i}\beta a}};\;\; \sigma = s, p, \tag{1.36}$$

where we assume both walls to be made of the same material for simplicity, and $a$ is the interface-interface separation. For planar multilayers the reflection coefficients can quite readily be generalised further [117, 118].

In article [p] the Green's function for a circularly cylindrical cavity is used, which was worked out by Li et alia some years ago [120]. While far more complicated (for the complete expression, see article [p]) it can be recognised as having the same structure as (1.33) in consisting of propagation factors [analogous to $\exp(\mathrm{i}\beta z)$] and reflection coefficients.

### 1.4.2 Examples: cold polar molecules and Rydberg atoms

Of the various non-equilibrium systems possible, I have participated in the investigation of two examples, namely cold polar molecules and Rydberg atoms held close to surfaces. I will briefly account for some special properties of these systems and how to apply the Buhmann-Scheel theory on them. The full details of these investigations are found in papers [l-p].

Beams of polar molecules can be routinely produced these days [103], and has been made experimental use of as mentioned previously. A large fraction of the molecules in such beams are typically found to be in their ground state; for example the experiment [121] reported a fraction of 90%. A ground state molecule in a room-temperature environment will heat up over time until it reaches a thermal state. The thermalization time is in the order of seconds for such molecules [122]. In principle there is an infinity of excited states to which the molecule can be excited to by absorption of thermal photons, but in practice only a few (typically one or two) of these transitions give a significant contribution to the Casimir-Polder potential.

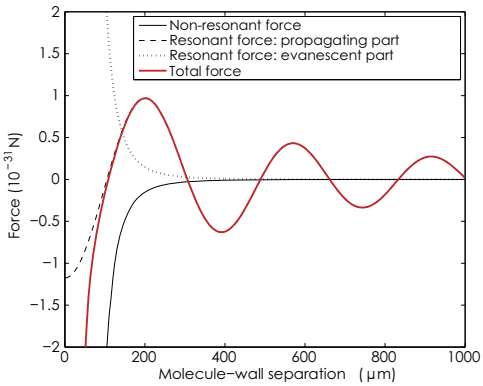


Figure 1.5: Thermal Casimir-Polder force on a ground state LiH molecule outside a gold half-space. Image from article [l].

As an illustration, the different terms of the Casimir-Polder force, Eq. (1.27), on a ground state LiH molecule is shown in figure 1.5: the first term of (1.27) is the non-resonant part, and the second term splits naturally into an evanescent ($q > \omega_{10}/c$) and propagating ($q < \omega_{10}/c$) part, where $\omega_{10}$ is the transition frequency from ground state $|0\rangle$ to first rotational state "$|1\rangle$". For details, see article [l].

For a force or potential term due to a transition of frequency $\omega_{kn}$ I will distinguish between a non-retarded and retarded regime:

$$\begin{array}{ll} z \gg \lambda_{kn} & \text{retarded} \\ z \ll \lambda_{kn} & \text{non-retarded} \end{array} \quad ; \quad \lambda_{kn} = \frac{2\pi c}{|\omega_{kn}|}. \tag{1.37}$$

For the transition from ground-state to the first rotational states[10], the transition wavelength is $\lambda_{01} \approx 14\mu$m.

**How many transitions to include in the $k$-sum?**

How many transition levels must be included depends on whether the separations involved are retarded or non-retarded (as well as on the required numerical precision, of course). As long as the particle is in the non-retarded regime with respect to all significant transitions, the fully thermal Casimir-Polder force turns out to be *independent of temperature* and given by the simple formula (see article [n])

$$\mathscr{U}_{kn} \overset{z \ll \lambda_{kn}}{=} -\frac{|\mathbf{d}_{nk}|^2}{48\pi\varepsilon_0 z^3}, \tag{1.38}$$

[10]There is a threefold degeneration due to magnetic quantum number $m = 0, \pm 1$ [l].

where $\mathcal{U}_n = \sum_k \mathcal{U}_{kn}$. In this regime the monotonous non-resonant and resonant evanescent terms dominate, and almost cancel each other out. Hence, the potential contribution from different transitions scales strictly with the transition dipole moments squared.

In the retarded regime far from the plate, shown in figure 1.5, the resonant propagating part dominates, and is oscillating in sign. As the molecule thermalizes, these oscillations gradually die out [l]. Asymptotically far from the wall (assumed to be metal) the potential is now [l]:

$$\mathcal{U}_{kn} \overset{z\gg\lambda_{kn}}{\sim} -\frac{|\mathbf{d}_{nk}|^2}{12\pi\varepsilon_0 z}\frac{\omega_{kn}^2}{c^2}\{\Theta(\omega_{kn})n(\omega_{kn}) - \Theta(\omega_{nk})[n(\omega_{nk})+1]\}\cos(2|\omega_{kn}|z/c). \tag{1.39}$$

In this regime, therefore, the contribution from a given transition is estimated from

$$\mathcal{U}_{kn} \overset{z\gg\lambda_{kn}}{\propto} |\mathbf{d}_{nk}|^2\omega_{kn}^2 n(\omega_{kn}) \tag{1.40}$$

which depends both on the dipole moment matrix elements, the transition frequency and, importantly, on temperature[11].

### Enhancing oscillations in retarded regime

The fact that the Casimir-Polder potential becomes spatially oscillating in the retarded regime means there is in principle a possibility for trapping and guiding particles for as long as the particle stays in the ground state. However, the corresponding potential depth outside a half-space is in the order of $10^{-2}$ Hz, probably too shallow to even be measurable and certainly not useful for guiding purposes.

A scheme to geometrically enhance these oscillations using a planar cavity was investigated in article [m]. Unfortunately, the enhancement factor scales with the logarithm of the $Q$ factor of the cavity, limiting the enhancement potential to about one order of magnitude, which is not enough.

A similar investigation for a cylindrical cavity was undertaken in article [p]. That geometry is a more promising candidate, as one might expect since such a cavity confines the electromagnetic modes in two rather than one spatial dimension. Still, the enhancement factor is only in the hundreds, and still insufficient for trapping molecules. A better candidate, thus is, as I consider next, Rydberg atoms.

### Rydberg atoms: a promising set-up

Rydberg atoms are atoms excited to very high principal quantum numbers. These atoms are thus strongly out of thermal equilibrium, since their thermal state at room temperature is essentially the atomic ground state. Such highly excited atoms have the following properties which make them ideal candidates for observing the thermal non-equilibrium forces described above:

[11] A similar expression for the potential maximum in a planar cavity reported in article [m] has prefactor $\omega_{kn}^3$ instead. This is because (roughly) $z \to j\lambda_{kn}$, $j \in \mathbb{N}$, because the cavity is tuned to an integer number of wavelenghts in that article.

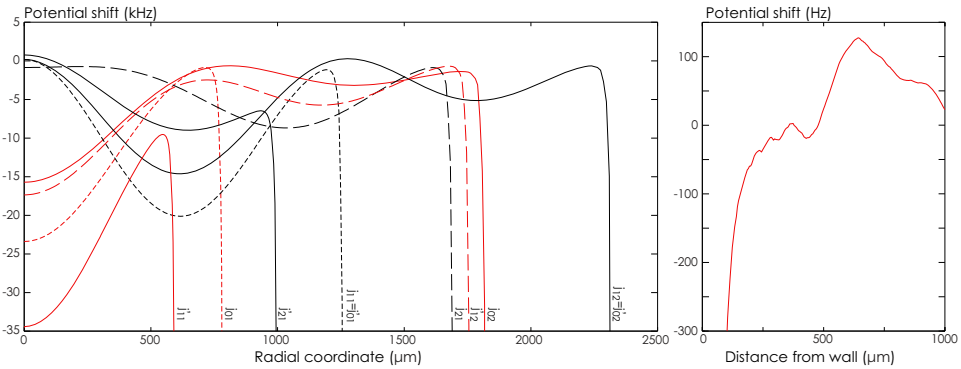


Figure 1.6: Left: Enhanced Casimir-Polder potential on a Rb atom in state $|32s_{1/2}\rangle$ for different resonant radii (for details, see article [p]). Right: same potential, outside a half-space.

- Their large physical size means they have enormous transition dipole moments which increase rapidly with $n$: $|\mathbf{d}|^2 \propto n^4$.
- At large $n$ the atomic energy levels lie close together, and the energy differences between nearby levels (such as constitute the dominating transitions) are small compared to thermal energies: $E_n \ll k_B T$. Thus, the thermal photon numbers $n(\omega_{kn})$ are large.
- Long transition wavelengths (typically hundreds of μm) mean the atoms remain in the non-retarded regime at all experimentally useful separations. This implies that the dipole force is given by the simple formula (1.38), and the Casimir-Polder force is independent of temperature except at extremely large distances.
- Although large cylinder radii are required in order to resonate with the dominating Rydberg transitions (approx a millimeter), the enormous atomic dipole moment means the resulting force can be boosted into the measurable regime (see article [p]).
- Rydberg states have long lifetimes on an atomic scale; micro- to milliseconds.

I include a few results as demonstrations of the favourable properties of Rydberg atoms for Casimir-Polder investigations. The potential felt by a Rb atom prepared in the low-lying Rydberg state $|32s_{1/2}\rangle$ in a cylindrical gold cavity made to resonate with the transition to $|31p_{3/2}\rangle$ is shown in figure 1.6. Because of the small energy difference and correspondingly long wavelength of the transition, the resonating radii are macroscopic, measured in millimeters. Still the potential (and correspondingly, atomic energy level shift) at the center of the cavity can be enhanced to tens of kHz.

Close to a wall, the atomic energy level shift is naturally far greater, as shown in figure 1.7 for three different Rydberg states of Rb. Because of the large physical size of the

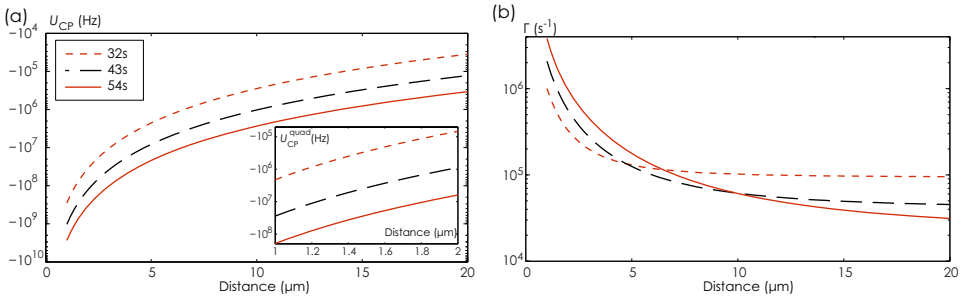


Figure 1.7: Three different Rydberg states of Rb near a gold half space. (a) potential, inset: quadrupole correction to potential; (b) total transition rate. Figure adapted from article [o] (erratum).

atom, corrections to the dipole approximation become noticeable, with quadrupole shifts of the energy ranging in the hundreds of MHz at a micrometer's separation.

# Chapter 2

# Summary of thesis articles

For journal references of the below articles, see list at the end of the Bibliography below.

## 2.1 Part 1

### Article [a]

**Analytic and Numerical Verification of the Nernst Theorem for Metals**
This article builds on and extends previous calculations by Høye, Brevik, Aarseth and Milton in connection with the purported entropy anomaly of the Casimir effect between Drude metals. The Casimir-Lifshitz entropy and (Helmholtz) free energy between two metals described by the Drude model is analyzed in detail both analytically and numberically to obtain the leading order terms as temperature vanishes. Analytical expressions for the two leading order free energy terms are found, proportional to $T^2$ and $T^{5/2}$, respectively, and a detailed numerical analysis is performed to ascertain the correctness of these two terms.

### Article [b]

**Frequency spectrum of the Casimir force: interpretation and a paradox**
This article was inspired by an article by Ford many years previously [123] in which the "frequency spectrum" of the Casimir force was analysed between perfectly conducting plates. I show that his result can be extended analytically when the plates are described by a simple transparency model, and that the discontinuous spectrum Ford found becomes smooth for imperfect reflectivity. A paradox is observed when comparing two methods of calculating correction to the Casimir effect due to a material transpareny frequency window.

### Article [c]

**Temperature correction to Casimir-Lifshitz free energy at low temperatures: semiconductors**
In this article the low temperature thermal correction to Casimir-Lifshitz free energy is considered in a similar fashion as article [a], but this time with respect to another purported entropy anomaly, between semiconductors with a small but nonzero conductivity, whose permittivity is described by a Drude model. By a lengthy calculation we derive the first few terms for both TE and TM polarisations and support the calculation by numerical analysis.

### Article [d]

**Nernst's heat theorem for Casimir-Lifshitz free energy**
In this article I analyse the formal violation of the third law of thermodynamics (Nernst's theorem), but unlike articles [a,c] the analysis is made at real rather than imaginary frequencies. The entropy problems, which appear for temperature dependent permittivity functions, are identified as originating from non-commutation of the limits of zero frequency and temperature. The general insight obtained is thus that no entropy anomaly can occur between materials whose leading order frequency term is temperature-constant near zero temperature. A similar conclusion was reached independently in [55].

### Article [e]

**Casimir-Lifshitz pressure and free energy: exploring a simple model**
This article, written for the Festschrift in honour of Professor Brevik, derives a series of results for the Casimir effect between materials described by a simple "constant reflection" model, which I first introduced in article [b]. By use of polylogarithmic functions, closed expressions for the Casimir pressure and free energy are obtained, as well as the full asymptotic low temperature expansion of the free energy. It is shown how the known temperature expansion for perfect conductors can be regained as a limit. Finally a speculative consideration of a generalised force on reflectivity is discussed in connection with the thermal discussion in the Casimir community. A simple calculation indicates that even if such a force exists, it would only provide a minute correction to experiments.

### Article [f]

**Low temperature Casimir-Lifshitz free energy and entropy: the case of poor conductors**
This conference article partly overlaps with articles [c,d], but has some new contributions in its sections 2 and 3. Section 2 lays out the insights in article [d] in a succinct and analytical form, and simple analytical formulae are produced relating non-commuting limits of temperature and frequency to residual entropy at zero temperature. Section 3 lays out in detail the method of obtaining low-temperature expansions from Matsubara-sum free energy expressions used in [c]. While implicit in [c,d], the ideas behind these methods had been

further crystallised since their publication, and the proceedings format allowed for them to be presented again with greater clarity and generality.

### Article [g]

**The Casimir frequency spectrum: can it be observed?**
This article reviews and extends article [b]. A new calculation is included, assuming the permittivity of two plates to be made transparent over an infinitesimal frequency band, and analysing the effect on the Casimir attraction due to this by two methods under the criterion that the perturbation obeys criteria of causality and the 'f-sum rule'. It is found that even in this case, the paradox remains.

### Article [h]

**Casimir-Foucault interaction: Free energy and entropy at low temperature**
This article compares the low frequency expansions found in articles [a, f] for the Casimir interaction between two Drude metal plates to that of the free energy stemming from the interaction of coupled Foucault currents alone. It had previously been shown [65] that the peculiar now-temperature behaviour could be attributed to these currents. The two free energies are found to be identical for good metals to the two leading low-temperature terms. Moreover, a simpler and more elegant method for obtaining low temperature expansions by means of complex frequency contour integrals is developed which readily reproduces the results of article [a].

## 2.2 Part 2

### Article [i]

**Electromagnetic Casimir Effect in a Medium-Filled Wedge**
The Casimir energy of a perfectly conducting wedge closed by a circular arc is calculated when the arc is either perfectly conducting or dielectric. After regularisation, the results are found to be closely analogous to previously obtained results for perfectly conducting or dielectric cylinders, except for a singular and non-regularisable term pertaining to the sharp corners where the arc meets the wedge. The singular term is shown to be finite when the wedge is assumed to be transparent at high-frequencies.

### Article [j]

**Electromagnetic Casimir Effect in a Medium-Filled Wedge II**
Like in article [i], the Casimir energy of a wedge geometry is calculated also here, but this time for a transparent wedge closed by a perfectly reflecting cylindrical shell. For calculability, the wedge is assumed to be isorefractive (diaphanous). This was the first time the Casimir energy of wedge described by electromagnetic and imperfectly reflecting boundaries

had been calculated. The singular term found in [i] is argued to be absent because of coupling of solutions in the two wedge sectors. A very significant effort went into the numerical part of the article which involves nested infinite integrals of modified Bessel functions of imaginary order, with respect to both order and argument.

### Article [k]

**Casimir effect at nonzero temperature for wedges and cylinders**
This article provides an extension of the results of article [i] for nonzero temperatures. The full temperatue behaviour of the Casimir energy for wedges and cylinders had not been found before, only the high-temperature asymptotics for a cylinder were known [124]. As is typical for such calculations, the energy expression is formally divergent, but a regularsation procedure was found using the Chowla-Selberg formula. Finally, high temperature asymptotics are derived and shown to be consistent with previous publications.

## 2.3 Part 3

### Article [l]

**Dynamics of thermal Casimir-Polder forces on polar molecules**
This article was the result of the first project with the Stefans at Imperial College. We applied their recently derived theory [105] to the case of cold polar molecules near a gold surface. We observe that the thermal Casimir-Polder force is oscillating in the far-zone due to thermal non-equilibrium, and study the dynamics of the polar molecule as it heats up. A “naïve calculation" of the force on such molecules using equilibrium theory and ground state polarizability is shown to be wrong by up to three orders of magnitude.

### Article [m]

**Enhancement of thermal Casimir-Polder potentials of ground-state polar molecules in a planar cavity**
Picking up on the oscillations of the thermal Casimir-Polder force observed in article [l], we investigate a possible scheme to enhance the oscillatory behaviour by use of a fine-tuned planar cavity of good reflectors. The scheme is shown to work, but the resulting enhancement turns out to scale with the logarithm of the cavity $Q$-factor, strongly limiting the potentiality of such a scheme. The various dependencies of the potential depth obtainable are laid out.

### Article [n]

**Temperature-independent Casimir-Polder forces despite large thermal photon numbers**
We show in this article that the Casimir-Polder potential on a particle in an eigenstate can be independent of the temperature of the surrounding system from zero temperature up to room

temperature and beyond, provided the particle is much closer to the surface than the wavelength of the dominating intraparticle transitions. Many cold polar molecules fall in this category for separations up to several micrometers (as do Rydberg atoms, although these were not considered in this article), whereas ground state atoms, in contrast, show a linear dependence on temperature at typical separations.

### Article [o]

**Thermal Casimir-Polder shifts in Rydberg atoms near metallic surfaces**
The Casimir-Polder force on Rydberg atoms is calculated close to a metallic surface. Due to the enormous dipole moment associated with Rydberg atom transitions, the Casimir-Polder force is enormous on an atomic scale. The quadrupole correction to the force is of significant at small separations due to the large physical size of the atom. Rydberg atoms exhibit the temperature independence derived in article [n] even for large particle-surface distances, up to hundreds of micrometers.

### Article [p]

**Casimir-Polder potential and transition rate in resonating cylindrical cavities**
The same enhancement scheme as in article [m] is investigated, but replacing the planar cavity by a cylindrical geometry which allows mode confinement in two spatial dimensions rather than one. We show that the enhancement factor is considerably improved compared to the planar case. When using atoms in low-lying Rydberg states inside a cylindrical cavity of fine-tuned radius, potential oscillations of tens of kiloherz can be obtained on the central axis, within the region of observability of modern experiments. An extensive analytical as well as numerical analysis is undertaken.

# Bibliography


[1] S. Weinberg, Rev. Mod. Phys. **61**, 1 (1989).
[2] E. Komatsu *et al. arXiv:1001.4538* (2010).
[3] K. Autumn *et. al.*, Proc. Natl. Acad. Sci. **99**, 12252 (2002).
[4] e.g. E. Buks and M. L. Roukes, Europhys. Lett. **54**, 220 (2001).
[5] J. D. van der Waals, *Over de Continueïteit van den Gas- en Vloeistoftoestand*, PhD thesis, Leiden 1873.
[6] F. London, Zeitschr. Phys. **63**, 245 (1930).
[7] H. B. G. Casimir and D. Polder, Phys. Rev. **73**, 360 (1948).
[8] H. B. G. Casimir, in *The Casimir effect 50 Years Later*, edited by M. Bordag, World Scientific 1999, p. 3.
[9] H. B. G. Casimir, Proc. Kon. Ned. Akad. Wetensch. **51**, 793 (1948).
[10] E. M. Lifshitz, Zh. Eksp. Teor. Fiz. **29**, 94 (1955) [Sov. Phys. JETP **2**, 73 (1956)].
[11] M. Y. Sparnaay, Physica **24**, 751 (1958).
[12] E. S. Sabisky and C. H. Anderson, Phys. Rev. A **7**, 790 (1973).
[13] C. I. Sukenik, M. G. Boshier, D. Cho, V. Sandoghdar and E. A. Hinds, Phys. Rev. Lett. **70**, 560 (1993).
[14] R. Balian and B. Duplantier, Ann. Phys. **112**, 165 (1978).
[15] M. J. Renne, Physica **56**, 125 (1971).
[16] J. Schwinger, L. L. DeRaad, Jr., and K. A. Milton, Ann. Phys. (N.Y.) **115**, 1 (1978).
[17] N. G. van Kampen, B. R. A. Nijboer, and K. Schram, Phys. Lett. A **26**, 307 (1968).
[18] S. K. Lamoreaux, Phys. Rev. Lett. **78**, 5 (1997).
[19] U. Mohideen and A. Roy, Phys. Rev. Lett. **81**, 4549 (1998).
[20] A. Roy, C.-Y. Lin, and U. Mohideen, Phys. Rev. D **60**, 111101(R) (1999).
[21] B. W. Harris, F. Chen, and U. Mohideen, Phys. Rev. A **62**, 052109 (2000).
[22] T. Ederth, Phys. Rev. A **62**, 062104 (2000).
[23] H. B. Chan, V. A. Aksyuk, R. N. Kleiman, D. J. Bishop, and F. Capasso, Phys. Rev. Lett. **87**, 211801 (2001).
[24] H. B. Chan, V. A. Aksyuk, R. N. Kleiman, D. J. Bishop, and F. Capasso, Science **291**, 1941 (2001).
[25] G. Bressi, G. Carugno, R. Onofrio, and G. Ruoso, Phys. Rev. Lett. **88**, 041804 (2002).
[26] K. A. Milton, *The Casimir Effect: Physical Manifestations of Zero Point Energy* (World Scientific, 2001).
[27] V. A. Parsegian, *Van der Waals Forces: A Handbook for Biologiests, Chemists, Engineers, and Physicists* (Cambridge University Press, 2006).
[28] M. Bordag, G.L. Klimchitskaya, U. Mohideen, and V.M. Mostepanenko, *Advances in the Casimir Effect*, (Oxford University Press, 2009).
[29] M. Bordag, U. Mohideen, and V. M. Mostepanenko, Phys. Rep. **353**, 1 (2001).
[30] K. A. Milton, J. Phys. A: Math. Gen. **37**, R209 (2004).
[31] S. K. Lamoreaux, Rep. Prog. Phys. **68**, 201 (2005).
[32] S. Y. Buhmann and D.-G. Welsch, Prog. Quantum Electron. **31**, 51 (2007).

[33] F. Capasso, J. N. Munday, D. Iannuzzi, and H. B. Chan, IEEE J. Selec. Top. Quant. Electron. **13**, 400 (2007).
[34] S. Scheel and S. Y. Buhmann, Acta Phys. Slov. **58**, 675 (2008).
[35] G. L. Klimchitskaya, U. Mohideen and V. M. Mostepanenko, Rev. Mod. Phys. **81**, 1827 (2009).
[36] G. Barton *et al.* (eds.), *International Workshop "60 Years of the Casimir Effect"*, Brasilia, Brazil, June 2008, J. Phys.: Conf. Proc. **161** (2009).
[37] K. A. Milton and M. Bordag (eds.), *Proceedings of the Ninth Conference on Quantum Field Theory under the Influence of External Conditions (QFEXT09)*, Norman, Oklahoma, September 2009, (World Scientific, 2010).
[38] A. Lambrecht, P. A. Maia Neto and S. Reynaud, New J. Phys. **8**, 243 (2006).
[39] M. Bordag and V. Nikolaev, Phys. Rev. D **81**, 065011 (2010).
[40] M. Bordag and I. Pirozhenko, Phys. Rev. D **81**, 085023 (2010).
[41] M. Boström and B. E. Sernelius, Phys. Rev. Lett. **84**, 4757 (2000).
[42] V. B. Svetovoy and R. Esquivel, Phys. Rev. E **72**, 036113 (2005).
[43] B. E. Sernelius, Phys. Rev. B **71**, 235114 (2005).
[44] A. Canaguier-Durand, P. A. Maia Neto, A. Lambrecht, and S. Reynaud, Phys. Rev. Lett. **104**, 040403 (2010).
[45] I. Brevik S. A. Ellingsen and K. A. Milton, New J. Phys. **8**, 236 (2006).
[46] S. K. Lamoreaux, Phys. Rev. A, **82**, 024102 (2010).
[47] R. S. Decca, D. López, E. Fischbach, G. L. Klimchitskaya, D. E. Krause, and V. M. Mostepanenko, Ann. Phys. **318**, 37 (2006).
[48] R. S. Decca, D. López, E. Fischbach, G. L. Klimchitskaya, D. E. Krause, and V. M. Mostepanenko, Phys. Rev. D **75**, 077101 (2007).
[49] G. L. Klimchitskaya and V. M. Mostepanenko, Phys. Rev. A **63**, 062108 (2001).
[50] V. B. Bezerra, G. L. Klimchitskaya, and V. M. Mostepanenko, Phys. Rev. A **65**, 052113 (2002).
[51] F. Chen, G. L. Klimchitskaya, U. Mohideen, and V. M. Mostepanenko, Phys. Rev. Lett. **90**, 160404 (2003).
[52] V. B. Bezerra, G. L. Klimchitskaya, V. M. Mostepanenko, and C. Romero, Phys. Rev. A **69**, 022119 (2004).
[53] e.g. E. U. Condon and H. Odishaw (eds.) *Handbook of Physics* (McGraw-Hill, 1967), equation 6.12.
[54] e.g. M. Abramowitz and I. A. Stegun *Handbook of Mathematical Functions* (New York: Dover, 1964), p. 806.
[55] F. Intravaia and C. Henkel, J. Phys. A **41**, 164018 (2008).
[56] J. S. Høye, I. Brevik, J. B. Aarseth, and K. A. Milton, Phys. Rev. E **67**, 056116 (2003).
[57] I. Brevik, J. B. Aarseth, J. S. Høye, and K. A. Milton, Phys. Rev. E **71**, 056101 (2005).
[58] B. Jancovici and L. Šamaj, J. Stat. Mech. P08006 (2004).
[59] B. Jancovici and L. Šamaj, Europhys. Lett. **72**, 35 (2005).
[60] P. R. Buenzli and Ph. D. Martin, Europhys. Lett. **72**, 42 (2005).
[61] P. R. Buenzli and Ph. D. Martin, Phys. Rev. E **77**, 011114 (2008).
[62] I. Brevik, J. B. Aarseth, J. S. Høye, and K. A. Milton, in *Quantum Field Theory under the Influence of External Conditions (QFEXT03)*, K. A. Milton (ed.) (Rinton Press, 2004), p. 54.
[63] B. Geyer, G. L. Klimchitskaya, and V. M. Mostepanenko, Phys. Rev. D **72**, 085009 (2005)
[64] G. Bimonte, New J. Phys. **9**, 281 (2007).
[65] F. Intravaia and C. Henkel, Phys. Rev. Lett. **103**, 130405 (2009).
[66] G.-L. Ingold, A. Lambrecht, and S. Reynaud, Phys. Rev. E **80**, 041113 (2009).
[67] G. Bimonte, Phys. Rev. A **79**, 042107 (2009).
[68] A. Canaguier-Durand, P. A. Maia Neto, A. Lambrecht, and S. Reynaud, Phys. Rev. A **82**, 012511 (2010).
[69] V. A. Yampol'skii, S. Savel'ev, Z. A. Maizelis, S. S. Apostolov, and F. Nori, Phys. Rev. A **82**, 032511 (2010).
[70] G. Plunien, B. Müller, and W. Greiner, Phys. Rep. **134**, 87 (1986).

[71] H. B. G. Casimir, Physica **19**, 846 (1956).
[72] T. H. Boyer, Phys. Rev. **174**, 1764 (1968).
[73] E. K. Abalo, K. A. Milton, and L. Kaplan, *arXiv:1008.4778 (hep-th)*
[74] L. L. DeRaad, Jr. and K. A. Milton, Ann. Phys. **186**, 229 (1981).
[75] I. Brevik and G. H. Nyland, Ann. Phys. **230**, 321 (1994).
[76] P. Gosdzinsky and A. Romeo, Phys. Lett. B **441**, 265 (1998).
[77] K. A. Milton, A. V. Nesterenko and V. V. Nesterenko, Phys. Rev. D **59**, 105009 (1999).
[78] G. Lambiase, V. V. Nesterenko and M. Bordag, J. Math. Phys. **40**, 6254 (1999).
[79] I. Cavero-Peláez and K. A. Milton, Ann. Phys. **320**, 108 (2005).
[80] A. Romeo and K. A. Milton, Phys. Lett. B **621**, 309 (2005).
[81] I. Brevik and A. Romeo, Phys. Scripta **76**, 48 (2007).
[82] I. Cavero-Peláez, K. A. Milton and K. Kirsten, J. Phys. A **40**, 3607 (2007)
[83] K. A. Milton, J. Phys.: Conf. Series **161**, 012001 (2009).
[84] K. A. Milton, P. Parashar, J. Wagner, and I. Cavero-Pelaez, J. Vac. Sci. Technol. B **28**, C4A8 (2010).
[85] J. S. Dowker and G. Kennedy, J. Phys. A **11**, 895 (1978)
[86] D. Deutsch and P. Candelas, Phys. Rev. D **20**, 3063 (1979)
[87] I. Brevik and M. Lygren, Ann. Phys. **251**, 157 (1996)
[88] I. Brevik, M. Lygren and V. Marachevsky, Ann. Phys. **267**, 134 (1998)
[89] I. Brevik, K. Pettersen, Ann. Phys. **291**, 267 (2001)
[90] V. V. Nesterenko, G. Lambiase and G. Scarpetta, Ann. Phys. **298**, 403 (2002)
[91] V. V. Nesterenko, G. Lambiase and G. Scarpetta, J. Math. Phys. **42**, 1974 (2001)
[92] V. V. Nesterenko, I. G. Pirozhenko and J. Dittrich, Class. Quantum Grav. **20**, 431 (2003)
[93] A. H. Rezaeian and A. A. Saharian, Clas. Quant. Grav. **19**, 3625 (2002)
[94] A. A. Saharian, Eur. Phys. J. C **52**, 721 (2007)
[95] A. A. Saharian, in *The Casimir Effect and Cosmology*, S. Odintsov et al. (eds.) (Tomsk State Pedagogical University Press, 2008), p.87, .
[96] e.g. Y. S. Barash and V. L. Ginzburg, Usp. Fiz. Nauk. **116**, 5 (1975) [Sov. Phys. Usp. **18**, 305 (1975)].
[97] L. D. Landau and E. M. Lifshitz *Statistical Physics Part 1* 3rd ed. (Elsevier Butterworth-Heinemann, 1980), §123.
[98] J. Fortágh and C. Zimmermann, Rev. Mod. Phys. **79**, 235 (2007).
[99] N. S. Ginsberg, S. R. Garner, and L. Vestergaard Hau, Nature **445**, 623 (2007).
[100] J. M. Obrecht, R. J. Wild, M. Antezza, L. P. Pitaevskii, S. Stringari, and E. A. Cornell, Phys. Rev. Lett. **98**, 063201 (2007).
[101] G. Birkl and J. Fortágh, Laser & Photon. Rev. **1**, 12 (2007).
[102] M. Saffman, T. G. Walker, and K. Mølmer, Rev. Mod. Phys. **82**, 2313 (2010).
[103] S. Y. T. van de Meerakker, H. L. Bethlem, and G. Meijer, Nature Physics **4**, 595 (2008).
[104] J. J. Hudson, B. E. Sauer, M. R. Tarbutt, and E. A. Hinds, Phys. Rev. Lett. **89**, 023003 (2002).
[105] S. Y. Buhmann and S. Scheel, Phys. Rev. Lett. **100**, 253201 (2008).
[106] S. Y. Buhmann, H. T. Dung, L. Knöll, and D.-G. Welsch, Phys. Rev. A **70** 052117 (2004).
[107] G. Barton, Proc. R. Soc. London A **320**, 251 (1970).
[108] G. Barton, Proc. R. Soc. London A **367**, 117 (1979).
[109] G. Barton, Proc. R. Soc. London A **410**, 141 (1987).
[110] W. Jhe, Phys. Rev. A **43**, 5795 (1991).
[111] W. Jhe, Phys. Rev. A **44**, 5932 (1991).
[112] M.-P. Gorza and M. Ducloy, Eur. Phys. J. D **40**, 343 (2006).
[113] M. Antezza, L. P. Pitaevskii, and S. Stringari, Phys. Rev. Lett. **95**, 113202 (2005).
[114] M. Antezza, L. P. Pitaevskii, S. Stringari, and V. B. Svetovoy, Phys. Rev. A **77**, 022901 (2008).
[115] Y. Sherkunov, Phys. Rev. A **79**, 032101 (2009).
[116] S. Å. Ellingsen, Y. Sherkunov, S. Y. Buhmann, and S. Scheel, in *Proceedings of QFEXT09*, Ref. [37], pp. 168-177.
[117] M. S. Tomaš, Phys. Rev. A **51**, 2545 (1995).

[118] M. S. Tomaš, Phys. Rev. A **81**, 044104 (2010).
[119] C.-T. Tai, *Dyadic Green Functions in Electromagnetic Theory*, 2nd ed. (IEEE Press, 1994).
[120] L.-W. Li, M.-S. Leong, T.-S. Yeo, and P.-S. Kooi, J. Electromag. Waves. App. **14**, 961 (2000).
[121] S. K. Tokunaga, J. O. Stack, J. J. Hudson, B. E. Sauer, E. A. Hinds, and M. R. Tarbutt, J. Chem. Phys. **126**, 124314 (2007).
[122] S. Y. Buhmann, M. R. Tarbutt, S. Scheel, and E. A. Hinds, Phys. Rev. A **78**, 052901 (2008).
[123] L. H. Ford, Phys. Rev. A, **48** 2962 (1993).
[124] M. Bordag, V. V. Nesterenko, and I. Pirozhenko, Phys. Rev. D **65**, 045011 (2002).

### Thesis articles

[ a ] J. S. Høye, I. Brevik, S. A. Ellingsen, and J. B. Aarseth, Phys. Rev. E **75**, 051127 (2007). c.f. also Comment *ibid.* **77**, 023101 (2008) and Reply.
[ b ] S. A. Ellingsen, Europhys. Lett. **82**, 53001 (2008).
[ c ] S. A. Ellingsen, I. Brevik, J. S. Høye and K. A. Milton, Phys. Rev. E **78**, 021117 (2008).
[ d ] S. A. Ellingsen, Phys. Rev. E **78**, 021120 (2008).
[ e ] S. A. Ellingsen, in *The Casimir Effect and Cosmology*, S. Odintsov et al. (eds.) (Tomsk State Pedagogical University Press, 2008), p. 45.
[ f ] S. Å. Ellingsen, I. Brevik, J. S. Høye and K. A. Milton, J. Phys.: Conf. Series **161**, 012010 (2009).
[ g ] S. Å. Ellingsen, J. Phys.: Conf. Series **161**, 012011 (2009).
[ h ] F. Intravaia, S. Å. Ellingsen, and C. Henkel, Phys. Rev. A **82**, 032504 (2010).
[ i ] I. Brevik, S. Å. Ellingsen, and K. A. Milton, Phys. Rev. E **79**, 041120 (2009).
[ j ] S. Å. Ellingsen, I. Brevik, and K. A. Milton, Phys. Rev. E **80**, 021125 (2009).
[ k ] S. Å. Ellingsen, I. Brevik, and K. A. Milton, Phys. Rev. D **81**, 065031 (2010).
[ l ] S. Å. Ellingsen, S. Y. Buhmann, and S. Scheel, Phys. Rev. A **79**, 052903 (2009).
[ m ] S. Å. Ellingsen, S. Y. Buhmann, and S. Scheel, Phys. Rev. A **80**, 022901 (2009).
[ n ] S. Å. Ellingsen, S. Y. Buhmann, and S. Scheel, Phys. Rev. Lett. **104**, 223003 (2010).
[ o ] J. A. Crosse, S. Å. Ellingsen, K. Clements, S. Y. Buhmann, and S. Scheel, Phys. Rev. A **80**, 022901(R) (2010).
[ p ] S. Å. Ellingsen, S. Y. Buhmann, and S. Scheel, Phys. Rev. A **82**, 032516 (2010).

# Research articles in full text

# Part I

## Casimir effect for real materials at non-zero temperatures

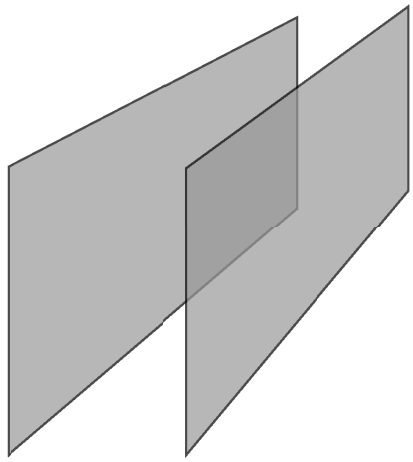

# Article [a]

***Analytical and numerical verification of the Nernst theorem for metals***

J.S. Høye, I. Brevik, S.A. Ellingsen, J.B. Aarseth

Physical Review E 75, 051127 (2007)

# Analytical and numerical verification of the Nernst theorem for metals

Johan S. Høye*
*Department of Physics, Norwegian University of Science and Technology, N-7491 Trondheim, Norway*

Iver Brevik†
*Department of Energy and Process Engineering, Norwegian University of Science and Technology, N-7491 Trondheim, Norway*

Simen A. Ellingsen‡
*Department of War Studies, King's College London, Strand, London WC2R 2LS, United Kingdom*

Jan B. Aarseth§
*Department of Structural Engineering, Norwegian University of Science and Technology, N-7491 Trondheim, Norway*

(Received 17 March 2007; published 31 May 2007)

In view of the current discussion on the subject, an effort is made to show very accurately both analytically and numerically how the Drude dispersion model gives consistent results for the Casimir free energy at low temperatures. Specifically, for the free energy near $T=0$ we find the leading term proportional to $T^2$ and the next-to-leading term proportional to $T^{5/2}$. These terms give rise to zero Casimir entropy as $T\to 0$ and are thus in accordance with Nernst's theorem.

DOI: 10.1103/PhysRevE.75.051127 PACS number(s): 05.30.−d, 42.50.Nn, 12.20.Ds, 65.40.Gr

## I. INTRODUCTION

In recent years there has been a lively discussion about the thermodynamic consistency of the expression for the Casimir pressure at finite temperature $T$. The problem gets accentuated at low values of $T$, where one has to satisfy the Nernst theorem saying that $S=-\partial F/\partial T$ goes to zero as $T\to 0$. (Here $S$ is the entropy and $F$ the free energy, both referring to unit plate area.) What we shall consider in the following is the standard Casimir configuration, implying two semi-infinite homogeneous metallic media separated by a vacuum gap of width $a$. We take the two media to be identical and assume that they are nonmagnetic with a frequency-dependent relative permittivity $\varepsilon(\omega)$. Spatial dispersion is neglected. The two surfaces lying at $z=0$ and $z=a$ are assumed to be perfectly planar and to be of infinite extent.

A central ingredient in the discussion of the thermodynamic consistency of calculated results for the Casimir attractive force between real materials is the form of a dispersion relation used as input in the conventional Lifshitz formula. A very useful dispersion relation—the one that in our opinion is by far the most preferable one among simple dispersion relations for real systems at arbitrary frequencies—is the Drude expression

$$\varepsilon(i\zeta) = 1 + \frac{\omega_p^2}{\zeta(\zeta+\nu)}. \tag{1}$$

Here $\omega=i\zeta$, $\omega_p$ is the plasma frequency, and $\nu$ is the relaxation frequency (we use the same notation as in Ref. [1]). The plasma wavelength is $\lambda_p=2\pi c/\omega_p$. For gold, the substance that we shall focus on in the following, we use

$$\omega_p = 9.03 \text{ eV}, \quad \nu = 34.5 \text{ meV}, \quad \lambda_p = 137.4 \text{ nm}. \tag{2}$$

In Ref. [1], we employed the values $\omega_p=9.0$ eV and $\nu=35$ meV, which amounts roughly to a difference on the 1% level. The exact determination of Drude parameters is a nontrivial matter as discussed in [2]. Using a slightly different set of Drude parameters will shift our numerical results slightly, but does not alter any of our conclusions.

When comparing with experimental values it turns out that the Drude relation fits optical data very accurately for $\zeta<2\times 10^{15}$ rad/s [3,4]. In this connection we should bear in mind the following fact (cf. also the discussion in Ref. [5]): There exist no measurements of the permittivity at very low frequencies. What is available is a series of measurements of the imaginary part $\varepsilon''(\omega)$ of the complex permittivity $\varepsilon(\omega)=\varepsilon'(\omega)+i\varepsilon''(\omega)$. The Kramers-Kronig relations then permit us to calculate the real part $\varepsilon'(\omega)$, and thus the complete $\varepsilon(\omega)$ is known. Permittivity data kindly supplied by Astrid Lambrecht cover a very large frequency region, from $1.5\times 10^{11}$ rad/s to $1.5\times 10^{18}$ rad/s. From these data, the relaxation frequency $\nu$ can be derived. As mentioned, from comparison with experimental data it turns out that $\nu$ can be taken to be constant to a good accuracy, up to about $\zeta=2\times 10^{15}$ rad/s. For low frequencies the Drude relation yields the proper extrapolation down to $\zeta=0$.

A word of caution is called for, as regards the circumstance that permittivity measurements are done at *room temperature* in practice. The frequency $\nu$ is in principle temperature dependent, and we do not know the value of $\nu(T=0)$ very accurately. It might seem natural here to invoke the Bloch-Grüneisen formula for the temperature dependence of the electrical resistivity (cf. [6] or also the discussion in Ref. [1]). From this, a form for $\nu=\nu(T)$ can in principle be found.

*Electronic address: johan.hoye@phys.ntnu.no
†Electronic address: iver.h.brevik@ntnu.no
‡Electronic address: simen.ellingsen@kcl.ac.uk
§Electronic address: jan.b.aarseth@mtf.ntnu.no

 

According to the formula, the value of $\nu$ should go to *zero* as $T \to 0$. However, in practice this is not true. There are always impurities present, which make the value of $\nu$ finite at $T=0$ [7]. The Bloch-Grüneisen formula, thus, is not followed in this limit. Mathematically, the important point is that

$$\zeta^2[\varepsilon(i\zeta) - 1] \to 0 \quad \text{as } \zeta \to 0. \tag{3}$$

This relation ensures that the zero-frequency TE mode does not contribute to the Casimir force at all, as discussed in detail in Ref. [1]. Strictly, the Drude parameters of Eq. (2) are valid at room temperature, and $\nu$ will take significantly smaller values for low temperatures. This affects our numerical results quantitatively, but not qualitatively; as long as $\nu$ is nonzero, the TE part of the free energy vanishes at zero frequency which is the central point.

The recent series of works on the Casimir effect by the present group of authors [1,5,8–13]—built upon the Lifshitz formula and the measured values of $\varepsilon(\omega)$ in combination with the Drude relation—have nowhere been found to run into conflict with basic thermodynamic principles. And there are other papers in agreement with ours: for instance, Jancovici and Šamaj [14] and Buenzli and Martin [15] considered the Casimir force between two plates in the high-temperature limit. They found the linear dependence in $T$ for the Casimir force to be reduced by a factor of 2 from the behavior of an *ideal* metal, this being a signal of the vanishing influence from the zero-frequency TE mode. (The first observation of the vanishing influence from this particular mode was made by Boström and Sernelius [16].) Further support is found in the paper of Sernelius [17], who calculates the Casimir force taking spatial dispersion into account as well. It is found that at high temperatures and/or at large separations the force is reduced by the same factor of 2 compared with the ideal-metal (IM) result.

There is no universal agreement on these issues, however. In a series of recent papers—cf., for instance, Refs. [18–22]—it is argued that the Drude dispersion relation runs into trouble explaining recent experiments and, moreover, comes into conflict with the Nernst theorem. These authors favor, instead of the Drude relation, the plasma relation

$$\varepsilon(i\zeta) = 1 + \frac{\omega_p^2}{\zeta^2}, \tag{4}$$

which corresponds to setting $\nu=0$ in Eq. (1). [It should be noted that expression (4) does *not* satisfy condition (3).]

An argument of the latter references is that omission of a zero-frequency TE mode would add a term linear in $T$ to the free energy. This would violate the Nernst theorem as it would give a nonzero contribution to the entropy at $T=0$. However, this argument is based upon use of the IM model where $\varepsilon=\infty$ for all $\zeta$ or use of the plasma model (4) where no relaxation is present. With $\nu>0$ the term in question is still linear away from $T=0$, but the precise behavior as $T \to 0$ has been less obvious. As argued in Ref. [1], the straight line should bend to become horizontal at $T=0$. This was not verified in utmost detail, however; the numerical results of Ref. [1] did not go sufficiently close to $T=0$ to show the behavior very distinctly, and the previous discussion and disagreement about violation of the Nernst theorem has accordingly continued. The main purpose of the present work is to investigate the issue more closely: we will show in detail, both analytically and numerically, how the Casimir energy behaves close to $T=0$ and by that show how it is consistent with the Nernst theorem.

We shall not go into a study of experimental aspects in this paper. Rather, the objections referred to above make it mandatory to reconsider the thermodynamics associated with the Drude relation anew, which brings us to the central theme of this paper. We will aim at showing, via a combination of analytical and numerical methods, how the basic theory sketched above (essentially the Drude theory) satisfies the Nernst theorem to a very high accuracy. We consider this point to be important; a simple physical model of course cannot be permitted to run into conflict with thermodynamics.

In the next section we show analytically, by using the Euler-Maclaurin formula, that the dominant contribution to the free Casimir energy $F$ near $T=0$ is proportional to $T^2$. We evaluate both this term and the leading correction term, which is proportional to $T^{5/2}$. This implies that the entropy $S=-\partial F/\partial T$ tends to zero as $T \to 0$, in accordance with the Nernst theorem. In Sec. III we calculate $F$ numerically and find agreement with the previous analytical result to a very high degree of accuracy. The results are illustrated in various figures. Thus, we can conclude that the Drude ansatz does not run into conflict with thermodynamics at all.

Readers interested in recent reviews on the Casimir effect may consult Milton's book[1] [23] and several review articles [24–27]. A great deal of recent information can also be found in special issues of J. Phys. A [28] and New J. Phys. [29].

As mentioned above, we shall not be concerned with a comparison between theory and experiment in the present paper. We mention, though, the recent experiment of Obrecht *et al.* [30], which seems to report the first accurate measurement of thermal Casimir effects. The experiment is important, but it lies outside the scope of the present investigation since it deals with nonuniformly heated systems.

Finally, we mention the special variant of the thermal Casimir problem consisting in studying, instead of a metal, a *semiconductor* endowed with a small but finite conductivity at zero frequency [31,32]. According to the authors of these references, this situation implies an interchange of the roles of the TE and TM modes, as compared with the case of a metal. Namely, within an idealized approach, they find that the TM reflection coefficient gets a discontinuity at $\zeta=0$, implying in turn an apparent conflict with the Nernst theorem. The problem is interesting, and we hope to return to it in a later paper.

## II. ANALYTICAL APPROACH: CASIMIR FREE ENERGY NEAR $T=0$ FOR REAL METALS

As mentioned, we use the same notation as in Ref. [1]. We will evaluate the leading $T$ dependence of the Casimir free

[1]It may be mentioned for completeness that this book from 2001 was written from the standpoint of the "classical" IM model.

energy near $T=0$ for metals using the Drude relation (1),

$$\varepsilon(i\zeta)-1=\frac{\omega_p^2}{\zeta(\zeta+\nu)}\approx\frac{D}{\zeta},\quad \zeta\ll\nu, \tag{5}$$

with $D=\omega_p^2/\nu$. The free energy is given by expression (3.4a) in [1] as

$$\beta F=\frac{1}{2\pi}{\sum_{m=0}^{\infty}}'\int_{\zeta/c}^{\infty}[\ln(1-\lambda^{\mathrm{TM}})+\ln(1-\lambda^{\mathrm{TE}})]q\,dq, \tag{6}$$

where $\beta=1/kT$ and

$$\lambda^{\mathrm{TM}}=Ae^{-2qa},$$

$$\lambda^{\mathrm{TE}}=Be^{-2qa}.$$

The prime on the summation sign means that the case $m=0$ is taken with half weight. The coefficients $A$ and $B$ are the squared Fresnel reflection coefficients for the two media and are given by

$$A=\left(\frac{s-\epsilon p}{s+\epsilon p}\right)^2,\quad B=\left(\frac{s-p}{s+p}\right)^2, \tag{7}$$

with

$$s=\sqrt{\varepsilon-1+p^2},\quad p=\frac{qc}{\zeta}.$$

Here $a$ is the plate separation, $\varepsilon$ the relative permittivity, $c$ the velocity of light in vacuum, and $\zeta$ the Matsubara frequency given by

$$\zeta=\frac{2\pi k}{\hbar}mT. \tag{8}$$

Note that the quantities $A$, $B$, $s$, $p$, and $\zeta$ all depend upon the summation variable $m$. (Units $c=\hbar=k=1$ are not used.) The term of interest is the TE mode, since this is the term that gives rise to the controversy about the Nernst theorem.

With the small-$\zeta$ dependence of Eq. (5) the $B$ has a scaling form such that it can be expressed in terms of one variable. So by introducing a new variable $x$ to replace $q$ the $\zeta$ dependence can be removed fully:

$$x^2=\frac{q^2c^2}{(\varepsilon-1)\zeta^2}\approx\frac{q^2c^2}{D\zeta},\quad \zeta\ll\nu. \tag{9}$$

With this we have

$$B=\left(\frac{\sqrt{1+x^2}-x}{\sqrt{1+x^2}+x}\right)^2=(\sqrt{1+x^2}-x)^4, \tag{10}$$

and the TE free energy expression can be written as

$$\beta F^{TE}=C{\sum_{m=0}^{\infty}}'g(m), \tag{11}$$

with

$$g(m)=m\int_{x_0}^{\infty}x\ln(1-Be^{-y})dx, \tag{12}$$

where

$$C=\frac{D}{c^2\hbar\beta}=\frac{\omega_p^2}{c^2\hbar\nu\beta},\quad y=2qa=2\frac{a}{c}\sqrt{D\zeta}x,\quad x_0=\sqrt{\frac{\zeta}{D}}. \tag{13}$$

The small-$T$ behavior can now be obtained by use of the Euler-Maclaurin summation formula

$${\sum_{n=0}^{\infty}}'g(n)=\int_0^{\infty}g(u)du-\frac{1}{12}g'(0)+\frac{1}{720}g'''(0)-\cdots. \tag{14}$$

One easily sees that

$$g'(0)=\int_0^{\infty}x\ln(1-B)dx. \tag{15}$$

This integral can be performed analytically. First introduce a new variable $x=\sinh t$ with $dx=\cosh t dt$:

$$\begin{aligned}g'(0)&=\int_0^{\infty}\sinh t\cosh t\ln(1-e^{-4t})\,dt\\&=\frac{1}{4}\int_0^{\infty}(e^{2t}-e^{-2t})\ln(1-e^{-4t})dt.\end{aligned} \tag{16}$$

Next we substitute $e^{-2t}=u$ for which $-2e^{-2t}dt=du$ and use partial integration to obtain

$$\begin{aligned}g'(0)&=-\frac{1}{8}\int_0^1\left(1-\frac{1}{u^2}\right)\ln(1-u^2)du\\&=-\frac{1}{8}\left\{\frac{1}{u}[(1+u)^2\ln(1+u)+(1-u)^2\ln(1-u)]-2u\right\}_0^1\\&=-\frac{1}{4}(2\ln 2-1)\approx-0.09657.\end{aligned} \tag{17}$$

At $T=0$ the free energy is determined by the integral in Eq. (14) (besides the contribution from the TM mode). For small $T\to 0$ the deviation from the $T=0$ value is thus ($\beta=1/kT$)

$$\Delta F^{TE}=\frac{C}{\beta}\left[-\frac{1}{12}g'(0)\right]=\frac{C}{48\beta}(2\ln 2-1). \tag{18}$$

This result was presented by Milton at the QFEXT03 Workshop and is given as Eq. (22) in Ref. [8] or Eq. (4.9) in Ref. [11].

It can be noted that $\Delta F^{TE}$ is independent of the plate separation $a$ and can thus be valid only sufficiently close to $T=0$ for a given $a$ such that $\Delta F^{TE}\ll F^{TE}\sim\hbar c/a^3$. Evaluation of the next term as given by the result (30) below verifies this. The leading term of $\Delta F^{TE}$ dominates its next term only when the dimensionless quantity $aC^{1/2}\ll 1$ or $a^2kT\ll\hbar\nu c^2/\omega_p^2$. A consequence of this is that for increasing $a$ the temperature interval where Eq. (18) is valid decreases rapidly, and $\Delta F^{TE}$ becomes more and more negligible compared to $F^{TE}$ since then $\Delta F^{TE}\sim C/\beta=\omega_p^2(kT)^2/(c^2\hbar\nu)\ll c^2\hbar\nu/(\omega_p^2a^4)$. (Thus in the present case $\Delta F^{TE}\ll F^{TE}$ provided $a>c\nu/\omega_p^2\approx 0.1$ nm with $a^2kT\ll\hbar\nu c^2/\omega_p^2$ fulfilled.) In the limit $a\to\infty$ the IM ($\varepsilon$

$=\infty$), but now with the linear term included, is recovered. But the latter does not violate the Nernst theorem as long as $a$ is finite, and for $a=\infty$ there is no Casimir free energy anyway.[2]

Inserting the value for $g'(0)$ and the values $\hbar\omega_p = 9.03$ eV and $\hbar\nu = 34.5$ meV for Au we find with $C$ given by Eqs. (13) ($\hbar = 1.0545\times10^{-34}$ J s, $k = 1.381\times10^{-23}$ J/K, $c = 2.998\times10^{8}$ m/s)

$$\Delta F^{TE} = C_1 T^2 \quad \text{with } C_1 \approx 5.81\times10^{-13}\ \text{J/(m}^2\,\text{K}^2\text{)}. \tag{19}$$

It turns out that Eq. (18) holds only very close to $T=0$ (i.e., $T \ll 0.01$ K), but there will be a leading correction that we can obtain with good accuracy. Expanding $g(m)$ in powers of $m$ one notes that half-integer powers will occur. Thus, formula (14) is not quite valid as $g'''(0)$ and higher-order derivatives will diverge. However, this problem can be avoided since the formula can be applied to summation starting at $m=p$ ($p=1,2,3,\ldots$). Thus, we have

$$\begin{aligned}\sum_{n=0}^{\infty} g(n) &= \sum_{n=0}^{p-1} g(n) + \int_p^{\infty} g(u)du + \frac{1}{2}g(p) - \frac{1}{12}g'(p) \\ &\quad + \frac{1}{720}g'''(p) + \cdots \\ &= \int_0^{\infty} g(u)du + S - \frac{1}{12}g'(p) + \frac{1}{720}g'''(p) + \cdots,\end{aligned} \tag{20}$$

where

$$S = \sum_{n=0}^{p-1} g(n) + \frac{1}{2}g(p) - \int_0^p g(u)du. \tag{21}$$

For a power term $g_\sigma(m)=m^\sigma$ (for small $m$) we have

$$g'_\sigma(p) = \sigma p^{\sigma-1}, \quad g'''_\sigma(p) = \sigma(\sigma-1)(\sigma-2)p^{\sigma-3}, \quad \int_0^p g_\sigma(u)du = \frac{1}{1+\sigma}p^{\sigma+1}. \tag{22}$$

With the choice $p=1$ we get

$$S = S_\sigma(1) = \frac{1}{2} - \frac{1}{1+\sigma}. \tag{23}$$

One may note that $S_1(1)=0$ as should be expected. The power of key interest here will be $\sigma=3/2$ by which $S_\sigma = 1/10$, and thus

$$\Delta S_\sigma(1) \equiv S_\sigma(1) - \frac{1}{12}g'_\sigma(1) + \frac{1}{720}g'''_\sigma(1) \approx -0.02552 \approx -0.204\frac{1}{12}g'_\sigma(1). \tag{24}$$

When other terms are neglected the error can be estimated from the next term in the series (provided the sums of higher-order terms converge):

$$\frac{1}{30240}g^{(V)}_\sigma(1) = \frac{-1}{30240}\frac{3}{2}\left(\frac{1}{2}\right)\left(\frac{-1}{2}\right)\left(\frac{-3}{2}\right)\left(\frac{-5}{2}\right) \approx 4.65\times10^{-5}, \tag{25}$$

which is only about 0.2% of the value (24). For increasing values of $p$ the error goes further down rapidly. [Instead of the result (24), $p=2$ yields $\approx -0.02549$.] Thus, Eq. (24) with $p=1$ is a good estimate for the sum of interest.

With $g(m)$ given by Eq. (12) we can expand to leading order in $m$ or $y(\propto T^{1/2})$. To this leading order the limit of integration $x_0(\propto T^{1/2})$ can be put equal to zero since the integrand vanishes for $x=0$. We find

$$g(m) = mg'(0) + myI + \cdots. \tag{26}$$

Now, from Eqs. (8) and (13),

$$y = 2a\sqrt{2\pi C}xm^{1/2}, \tag{27}$$

with $C$ given by Eq. (13). Thus the derivative becomes

$$g'(m) = g'(0) + 3a\sqrt{2\pi C}Im^{1/2} + \cdots, \tag{28}$$

where $g'(0)$ is given by Eq. (17) and [with substitution $x=\sinh t$ as in Eq. (16)]

$$I = \int_0^{\infty} \frac{x^2 B}{1-B}dx = \frac{1}{8}\int_0^{\infty}(e^{-t} - e^{-3t})dt = \frac{1}{12}. \tag{29}$$

Now we will use Eq. (21) for the most simple case $m=p=1$ for which $S_\sigma(1)$ is given by Eq. (23), and with exponent $\sigma$ equal to 1 and 3/2 for the two separate terms in Eq. (26) the corresponding values of $S_\sigma(1)$ are 0 and 1/10, respectively. Thus, with Eqs. (24) and (28) we have $12\Delta S_1(1) = -g'_1(0) = -g'(0)$ and $12\Delta S_{3/2}(1) = -0.204 g'_{3/2}(1) = -0.204\times 3a\sqrt{2\pi C}I$. So with Eq. (18) the change in free energy becomes

$$\begin{aligned}\Delta F^{TE} &= \frac{C}{\beta}[\Delta S_1(1) + \Delta S_{3/2}(1) + \cdots] \\ &= \frac{C}{\beta}\left[-\frac{1}{12}g'(0)\right]\left[1 - 0.204\cdot\frac{3a\sqrt{2\pi C}}{-12g'(0)} + \cdots\right],\end{aligned} \tag{30}$$

which gives the small-$T$ correction to the result (18). Again inserting the previous values for $\omega_p$ and $\nu$ we obtain with plate separation $a=1000$ nm:

$$\Delta F^{TE} = C_1 T^2[1 - C_2 T^{1/2} + \cdots] \quad \text{with } C_2 \approx 3.03\ \text{K}^{-1/2}. \tag{31}$$

[2]It may be noted that for $a/(\hbar c\beta) \ll 1$ an $a$-independent contribution to the free energy was found also in the "classical" Casimir theory for metals at low temperature. See Eq. (3.38) in Ref. [23] or Eq. (3.24) in Ref. [1].

This result can only be valid for very small $T$ as it otherwise becomes negative already for $T$ slightly larger than 0.1 K. To avoid this one may instead write

$$\Delta F_{th}^{TE} = \frac{C_1 T^2}{1 + C_2 T^{1/2}} \tag{32}$$

as the theoretical or analytical result for $\Delta F^{TE}$ for small $T$. This Padé approximant form [which is equivalent to Eq. (31) with respect to the first two terms] turns out to be convenient for comparison with numerical evaluations. If the corresponding numerical result for $\Delta F^{TE}$ is $\Delta F_{num}^{TE}$, one can evaluate the ratio

$$R = \frac{\Delta F_{th}^{TE} - \Delta F_{num}^{TE}}{\Delta F_{th}^{TE}} \tag{33}$$

and consider the limit $T \to 0$ for which the limiting value should be $R=0$ (cf. more details in Appendix B).

## III. NUMERICAL CALCULATION OF FREE ENERGY AT LOW TEMPERATURES

We have calculated the free energy $F^{TE}$ as a function of temperature given by Eq. (6) for two gold half-spaces separated by a vacuum gap of width $a=1.0$ $\mu$m. This would be a typical experimental situation where the influence from the finite temperature is large, about a 15% increase in the magnitude of the Casimir free energy [1] and a corresponding decrease of the Casimir force according to our theory with no contribution from the TE mode at zero frequency. The calculations use the permittivity data for gold, received from Astrid Lambrecht as mentioned. At $T=0$ the free energy is calculated numerically as a double integral rather than a sum of integrals using a two-dimensional version of Simpson's method.

The vanishing of the zero-frequency mode is intimately connected with the behavior of the reflection coefficient $B$ at vanishing frequency. According to the Drude model [or any model satisfying (3)] the TE mode reflection coefficient tends to zero as $\zeta \to 0$. To illuminate this point, we have plotted $A$ and $B$ as a function of imaginary frequency and transverse momentum, $k_\perp$, for an interface between gold and vacuum in Fig. 1. In part (c) of this figure, we clearly see how $B$ vanishes smoothly when $\zeta \to 0$ for $k_\perp \neq 0$ consistent with Maxwell's equations of electrodynamics. However, the coefficient $A$ in Fig. 1(a) for the TM mode equals 1 for all $k_\perp$ as $\zeta \to 0$, as is also the case for all $\zeta$ for an ideal metal. In the latter limit we also have $B \to 1$, but for $\zeta=0$, $B$ remains zero.

For ideal or nonideal metals it is well known that the temperature correction for the TM mode behaves as $T^4$. Thus, it does not add to the $T^2$ and $T^{5/2}$ terms that we find from the TE mode.

By direct numerical integration and lengthy summations independent of the analytic derivations made in Sec. II, we obtain the free energy numerically. Figure 2 shows the free energy versus temperature up to 800 K, while the inset shows details of the parabolic shape close to $T=0$. First of all the figure shows the controversial decrease of the magnitude of the Casimir free energy and thus also the related decrease

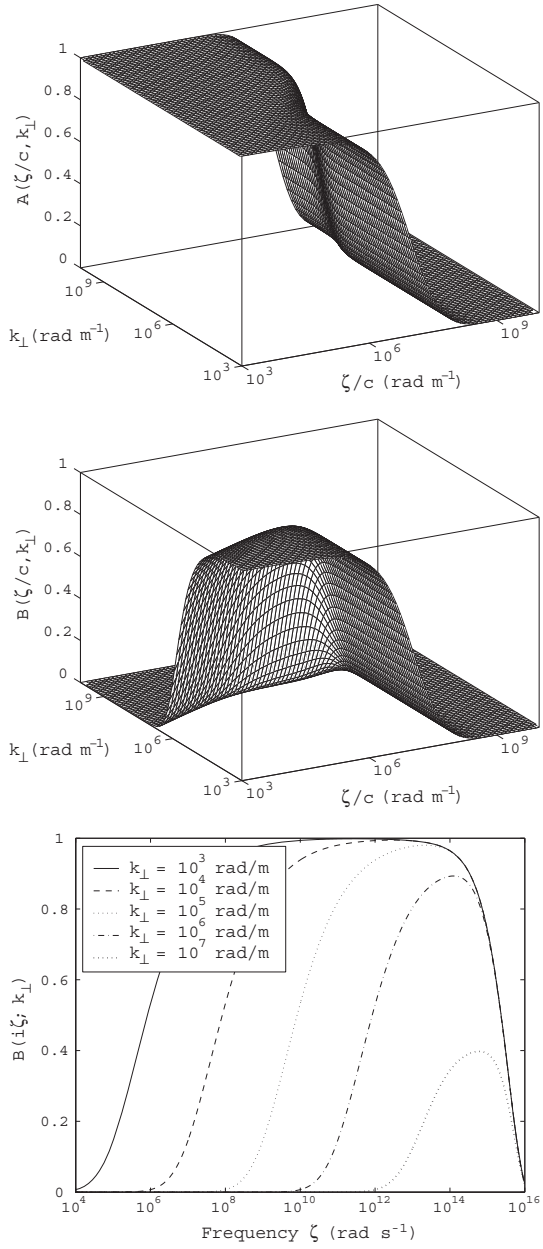


FIG. 1. Squared reflection coefficients $A$ and $B$ of the metal interfaces as defined in Eq. (7) for the TM and TE modes, as a function of $\zeta/c$ and the transverse momentum $k_\perp$. (a) $A$ for the TM mode, (b) $B$ for the TE mode, and (c) $B$ for $k_\perp$ and $\zeta$ close to zero.

of the Casimir force up to a certain temperature. Second, the inset shows that the tangent of the curve is horizontal at $T=0$ as predicted. This implies that the entropy due to the Casimir force is indeed zero at $T=0$. Thus the Nernst theorem is not violated when using the realistic Drude dispersion

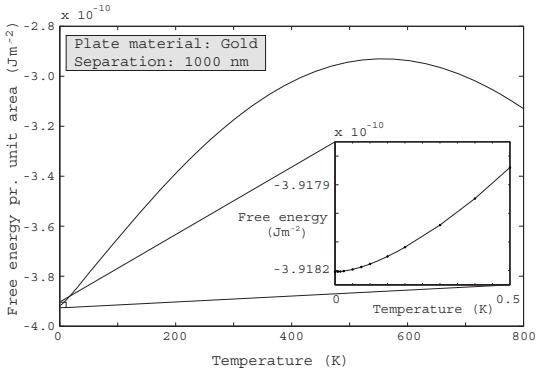


FIG. 2. Numerical evaluation of the free energy (6) between two gold half-spaces as a function of temperature. The inset gives details for low $T$.

model. In contrast, it would be violated if a TE term were added for $\zeta=0$. This conclusion, as mentioned above, is clearly in contrast to that presented in various earlier works [18–22]. The reader should note that the dependence of $\nu$ on temperature has been neglected in Fig. 2.

Now there are always some uncertainties connected with numerical calculations. Also the analytic derivation has some uncertainties, e.g., concerning proper use of the Euler-Maclaurin formula, and concerning convergence and neglect of higher-order terms. In Fig. 3 we have therefore made a more accurate and much more sensitive test of the behavior near $T=0$ comparing the analytic result with the numerical one, by plotting the ratio $R$ defined in Eq. (33). We see that $R$ when extrapolated approaches zero linearly with a finite slope (when taking the curvature of the plot into account). Thus, with high accuracy we find full agreement concerning the $T^2$ and $T^{5/2}$ terms in the free energy and their coefficients $C_1$ and $C_2$. As the number of terms to be summed numerically increases rapidly when $T=0$ is approached, our evaluations were terminated at $T=0.008$ K. The extrapolated value $R=0$ for $T=0$ means that the coefficient $C_1$ is correct while the finite slope means that $C_2$ is correct too within numerical uncertainties. Also if a more dominant power were present, $R$ would diverge at $T=0$. The finite slope of $R$ at $T=0$ means that the next term in $\Delta F^{TE}$ is of higher order (see also Appendix B for details).

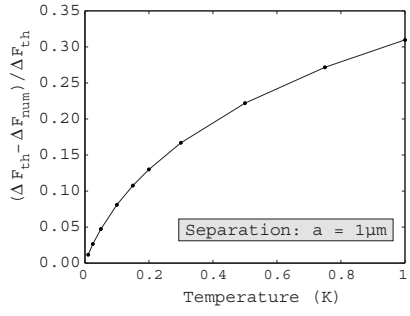


FIG. 3. Plot of the ratio $R$ defined in Eq. (33).


## ACKNOWLEDGMENTS

We thank Astrid Lambrecht for providing accurate dispersive data for gold, and we thank Kimball A. Milton for valuable comments.


## APPENDIX A: ALTERNATIVE DERIVATION BY EXPANSION OF $g(m)$

As a variant of the analytic approach, let us show how the essential dependence of the free energy $F^{TE}$ on $T$ near $T=0$ also can be recovered by making use of complex integration. We begin with the TE expression

$$\beta F^{TE} = C \sum_{m=0}^{\infty}{}' m \int_{x_0}^{\infty} x \ln(1 - Be^{-\alpha x}) dx, \tag{A1}$$

where

$$C = \frac{\omega_p^2}{\beta\hbar\nu c^2}, \quad \alpha = 2a\sqrt{2\pi C m}. \tag{A2}$$

The essential step now is to expand the logarithm to the first term,

$$\beta F^{TE} = -C \sum_{m=1}^{\infty} m \int_{0}^{\infty} xBe^{-\alpha x} dx \tag{A3}$$

[$m=0$ does not contribute to the sum (A1)], where we have also replaced the lower limit $x_0$ by zero. We next use the formula [34]

$$e^{-\alpha x} = \frac{1}{2\pi i} \int_{c-i\infty}^{c+i\infty} ds (\alpha x)^{-s} \Gamma(s), \quad c > 0, \tag{A4}$$

where $\Gamma(s)$ is the gamma function. The summation over $m$ is easily done,

$$\sum_{m=1}^{\infty} m^{1-s/2} = \zeta\left(\frac{s}{2} - 1\right). \tag{A5}$$

Here $\zeta$ is the Riemann zeta function, defined by the analytic continuation of

$$\zeta(s) = \frac{1}{\Gamma(s)} \int_0^{\infty} \frac{t^{s-1}}{e^t - 1} dt \tag{A6}$$

for $\mathrm{Re}(s) < 1$ [33]. As is known, $\zeta(s)$ is one-valued everywhere except for $s=1$, where it has a single pole with residue 1. As $\Gamma(s)$ has simple poles at $s=-n$ with residue $(-1)^n/n!$, $n=0,1,2,\ldots$, we get, by taking $c>4$ and closing the contour of integral (A4) as a large semicircle on the left,

$$\beta F^{TE} = -C \int_0^{\infty} Bx \left[ \frac{\Gamma(4)}{(2ax)^4} \frac{1}{(2\pi C)^2} + \zeta(-1) - 2ax\sqrt{2\pi C}\zeta\left(-\frac{3}{2}\right) + \cdots \right] dx. \tag{A7}$$

The first term in Eq. (A7) diverges, the reason being that we have replaced the lower limit $x_0$ by zero. This term is inde-

pendent of $T$ and can thus be omitted in the present context. Thus using $\zeta(-1)=-1/12$, $\zeta(-3/2)=-0.025485$, together with the integrals $\int_0^\infty Bx dx=1/12$ and $\int_0^\infty Bx^2 dx=8/105$, gives the temperature-dependent free energy to first order in $B$.

However, this is easily extended to arbitrary order in $B$ by expansion of the integrand in Eq. (A1) since $(Be^{-\alpha x})^n = B^n\left[1-\alpha n x+\frac{1}{2}(\alpha n x)^2+\cdots\right]$. Thus, by summation $xB \to x\Sigma_{n=1}^\infty B^n/n=-x\ln(1-B)$ and $x(Bx)\to x\Sigma_{n=1}^\infty (nB^n/n)x = x^2B/(1-B)$. By this the above integrals become those of Eqs. (15) and (29), and for the temperature-dependent part of the free energy we thus get

$$\Delta F^{TE} = -\frac{C}{\beta}\left[-g'(0)\zeta(-1)-2a\sqrt{2\pi C}I\zeta\left(-\frac{3}{2}\right)+\cdots\right] = \frac{C}{\beta}\left[-\frac{1}{12}g'(0)\right]\left[1-8\zeta\left(-\frac{3}{2}\right)\frac{3a\sqrt{2\pi C}}{-12g'(0)}+\cdots\right], \tag{A8}$$

fully consistent with the result (30). Note that $\zeta(-3/2)$ is close to the approximate value (24) and even closer to the more accurate value (25). Thus, we have reason to consider $\zeta(-3/2)$ to be the exact result for the Euler-Maclaurin expansion performed in Sec. II.

## APPENDIX B: REMARKS ON THE QUANTITY *R*

Let us explain in some more detail the interpretation of the quantity $R$, defined in Eq. (33). This quantity gives the relative difference between the temperature-dependent theoretical free energy $\Delta F_{th}^{TE}$, having the form (32), and the temperature-dependent numerical free energy $\Delta F_{num}^{TE}$ calculated from Eq. (6). (As mentioned in Sec. III, the TM mode behaves as $T^4$ and is thus negligible near $T=0$.)

Let us assume that $\Delta F_{th}^{TE}$ has the same form (32) as before, with coefficients $C_1$ and $C_2$, and that $\Delta F_{num}^{TE}$ has the form

$$\Delta F_{num}^{TE} = D_1(T^2 - D_2T^{5/2} + D_3T^3 + \cdots), \tag{B1}$$

with calculated values for the coefficients $D_1$, $D_2$, and $D_3$. Then,

$$R = \frac{\Delta F_{th}^{TE} - \Delta F_{num}^{TE}}{\Delta F_{th}^{TE}} = \frac{C_1-D_1}{C_1} + \frac{D_1}{C_1}(D_2-C_2)T^{1/2} + \frac{D_1}{C_1}(C_2D_2-D_3)T + \cdots .$$

If $C_1=D_1$ and $C_2=D_2$, we see that $R$ is zero at $T=0$ and is linear in $T$ for low $T$. From Fig. 3 we see that the fit is perfect insofar as it may be determined from the graph. A constant term would have caused a nonzero value at $T=0$, and a nonzero $T^{1/2}$ term would have caused a vertical slope near $T=0$. None of these effects are perceivable within the numerical accuracy, from which we must conclude that $C_1$ and $C_2$ are correct within the numerical accuracy.


[1] J. S. Høye, I. Brevik, J. B. Aarseth, and K. A. Milton, Phys. Rev. E **67**, 056116 (2003).
[2] I. Pirozhenko, A. Lambrecht, and V. B. Svetovoy, New J. Phys. **8**, 238 (2006).
[3] A. Lambrecht and S. Reynaud, Eur. Phys. J. D **8**, 309 (2000).
[4] A. Lambrecht and S. Reynaud, Phys. Rev. Lett. **84**, 5672 (2000).
[5] I. Brevik and J. B. Aarseth, J. Phys. A **39**, 6187 (2006).
[6] *Handbook of Physics*, 2nd ed., edited by E. U. Condon and H. Odishaw (McGraw-Hill, New York, 1967), Eq. (6.12).
[7] Khoshenevisan, W. P. Pratt, Jr., P. A. Schroeder, and S. D. Steenwyk, Phys. Rev. B **19**, 3873 (1979).
[8] I. Brevik, J. B. Aarseth, J. S. Høye, and K. A. Milton, in *Quantum Field Theory under the Influence of External Conditions*, edited by K. A. Milton (Rinton Press, Princeton, NJ, 2004), p. 54.
[9] I. Brevik, J. B. Aarseth, J. S. Høye, and K. A. Milton, Phys. Rev. E **71**, 056101 (2005).
[10] J. S. Høye, I. Brevik, J. B. Aarseth, and K. A. Milton, J. Phys. A **39**, 6031 (2006).
[11] I. Brevik, S. A. Ellingsen, and K. A. Milton, New J. Phys. **8**, 236 (2006).
[12] S. A. Ellingsen, J. Phys. A **40**, 1951 (2007).
[13] S. A. Ellingsen and I. Brevik, J. Phys. A **40**, 3643 (2007).
[14] B. Jancovici and L. Šamaj, Europhys. Lett. **72**, 35 (2005).
[15] P. R. Buenzli and Ph. A. Martin, Europhys. Lett. **72**, 42 (2005).
[16] M. Boström and Bo E. Sernelius, Phys. Rev. Lett. **84**, 4757 (2000).
[17] Bo E. Sernelius, J. Phys. A **39**, 6741 (2006).
[18] V. B. Bezerra, G. L. Klimchitskaya, V. M. Mostepanenko, and C. Romero, Phys. Rev. A **69**, 022119 (2004).
[19] R. S. Decca, D. López, E. Fischbach, G. L. Klimchitskaya, D. E. Krause, and V. M. Mostepanenko, Ann. Phys. (N.Y.) **318**, 37 (2005).
[20] V. B. Bezerra, R. S. Decca, E. Fischbach, B. Geyer, G. L. Klimchitskaya, D. E. Krause, D. López, V. M. Mostepanenko, and C. Romero, Phys. Rev. E **73**, 028101 (2006).
[21] V. M. Mostepanenko, V. B. Bezerra, R. Decca, B. Geyer, E. Fischbach, G. L. Klimchitskaya, D. E. Krause, D. López, and C. Romeo, J. Phys. A **39**, 6589 (2006).
[22] V. M. Mostepanenko, e-print arXiv:quant-ph/0702061; G. L. Klimchitskaya, U. Mohideen, and V. M. Mostepanenko, J. Phys. A **40**, F339 (2007).
[23] K. A. Milton, *The Casimir Effect: Physical Manifestation of Zero-Point Energy* (World Scientific, Singapore, 2001).
[24] M. Bordag, U. Mohideen, and V. M. Mostepanenko, Phys. Rep. **353**, 1 (2001).
[25] K. A. Milton, J. Phys. A **37**, R209 (2004).
[26] V. V. Nesterenko, G. Lambiase, and G. Scarpetta, Riv. Nuovo Cimento **27** No. 6, 1 (2004).
[27] S. K. Lamoreaux, Rep. Prog. Phys. **68**, 201 (2005).
[28] J. Phys. A **39**, No. 21 (2006) [special issue: papers presented at the 7th Workshop on Quantum Field Theory under the In-

fluence of External Conditions (QFEXT05), Barcelona, Spain, 2005].
[29] New J. Phys. **8**, No. 236 (2006) (focus issue on Casimir forces).
[30] J. M. Obrecht, R. J. Wild, M. Antezza, L. P. Pitaevskii, S. Stringari, and E. A. Cornell, Phys. Rev. Lett. **98**, 063201 (2007).
[31] B. Geyer, G. L. Klimchitskaya, and V. M. Mostepanenko, Phys. Rev. D **72**, 085009 (2005).
[32] G. L. Klimchitskaya, B. Geyer, and V. M. Mostepanenko, J. Phys. A **39**, 6495 (2006).
[33] E. Elizalde, S. D. Odintsov, A. Romeo, A. A. Bytsenko, and S. Zerbini, *Zeta Regularization Techniques with Aplications* (World Scientific, Singapore, 1994).
[34] E. T. Whittaker and G. N. Watson, *A Course of Modern Analysis* (Cambridge University Press, Cambridge, England, 1962) p. 280.

# Article [b]

***Frequency spectrum of the Casimir force: Interpretation and a paradox***

S.A. Ellingsen

Europhysics Letters **82**, 53001 (2008)

A Letters Journal Exploring the Frontiers of Physics

June 2008

EPL, **82** (2008) 53001 www.epljournal.org
doi: 10.1209/0295-5075/82/53001

# Frequency spectrum of the Casimir force: Interpretation and a paradox

S. A. Ellingsen[(a)]

*Department of Energy and Process Engineering, Norwegian University of Science and Technology N-7491 Trondheim, Norway*

received 4 January 2008; accepted in final form 16 April 2008
published online 28 May 2008

PACS 34.20.-b – Interatomic and intermolecular potentials and forces, potential energy surfaces for collisions
PACS 12.20.-m – Quantum electrodynamics
PACS 03.70.+k – Theory of quantized fields

**Abstract** – The frequency spectrum of the Casimir force between two plates separated by vacuum as it appears in the Lifshitz formalism is reexamined and generalised as compared to previous works to allow for imperfectly reflecting plates. As previously reported by Ford (*Phys. Rev. A*, **48** (1993) 2962), the highly oscillatory nature of the frequency dependence of the Casimir force points to possibilities for very large and indeed negative Casimir forces if the frequency-dependent dielectric response, $\epsilon(\omega)$, of the materials could be tuned. A paradox occurs, however, because an alternative calculation of the effect of a perturbation of $\epsilon(\omega)$ involving a Wick rotation to imaginary frequencies indicates only very modest effects. A recent experiment appears to convincingly rule out the reality of Ford's optimistic predictions, although given the enormous technological promise of such frequency effects, further theoretical and experimental study is called for.



In an interesting paper [1], Ford analysed the frequency spectrum of the Casimir pressure as it appears when read directly out of Lifshitz' celebrated formula [2]. His calculations extended a previous study of the spectrum of the Casimir effect for a massless scalar field [3] and subsequent analysis of the electromagnetic vacuum stress tensor by Hacyan *et al.* [4]. In [1], the classical Casimir set-up is considered, where two perfectly reflecting metal plates of infinite transverse size are separated by a vacuum-filled gap of width $a$. For this system, the pressure between the plates was found by Casimir [5] to be

$$P_C(a) = -\frac{\hbar c \pi^2}{240 a^4}. \tag{1}$$

Ford's puzzling finding was that if the pressure is expressed as an integral over all frequencies of the zero-point oscillations of the electromagnetic field in the cavity, the integrand is wildly oscillating and discontinuous as a function of frequency and the integral a sum of almost exactly cancelling positive and negative contributions, each of which far larger in magnitude than the measurable pressure itself. By a suitable cutoff procedure, however, the integral is calculable and the result correct. Similar considerations were later performed for a sphere and plate set-up [6,7] and the electromagnetic stress tensor in a cavity [8]. An extension of Ford's work on two ideally conducting plates was recently presented by Lang [9].

The unruly behaviour of the Casimir force as a function of real frequencies was recently treated for numerical purposes [10] and the same oscillatory behaviour was found. As a consequence these latter authors like most before performed the Wick rotation to imaginary time (and imaginary frequencies), which is permitted when the permittivity is assumed causal. As expressed for imaginary frequencies, the Lifshitz expression is much more well behaved and rather than complex and strongly oscillating, the frequency integrand is real, nicely peaked and exponentially decreasing at high imaginary frequency. The importance of good optical data for the precise calculation of Casimir forces has been emphasised in a number of recent efforts [11–14], but these have all employed a Wick rotated formalism.

Ford suggested that if the frequency response of the plate materials could be tuned, for example if a material could be found which is transparent for all but a small band of frequencies in which it was a good

[(a)]E-mail: simen.a.ellingsen@ntnu.no

reflector, Casimir forces much larger than that between perfect conductors could be observed and by changing the reflection band the force could be changed from attractive to repulsive. Despite the potentially enormous technological potential of such tuning for applications in microengineering and nanotechnology, the issue of the physical interpretation of the frequency spectrum of the Casimir force has remained largely unaddressed.

A relevant experiment was recently performed by Iannuzzi, Lisanti and Capasso at Harvard [15] in which the Casimir force was measured in the same configuration with a good and poor reflector, respectively. The material used was a so-called hydrogen-switchable mirror which can be switched from mirror to transparent at optical frequencies by introducing hydrogen. At frequencies in the IR and UV parts of the spectrum, reflection is presumed by the authors of [15] to be approximately unchanged. This is the inverse of the situation suggested by Ford, and based on [1] large effects should be expected. Iannuzzi *et al.* observed no change of the force in the two cases, however.

The paradox is theoretical as well as experimental: Assume that the permittivity of one or both of the plates in a standard two-plate set-up [5] is changed in a band of frequencies. The effect on the force of this perturbation may, one may think, be calculated in two different ways. Either Lifshitz' expression for the force is integrated over the relevant band of *real* frequencies and the difference taken. Alternatively, the new, perturbed permittivity is rotated to imaginary frequencies using the Kramers-Kronig relations and the force calculated as an integral (assuming zero temperature) over imaginary Matsubara frequencies. The numerical results obtained in the two ways, however, appear to differ greatly.

In the following, Ford's calculations are generalised to imperfectly reflecting plates represented by an effective reflection coefficient. While the same oscillatory behaviour is found, the integrand is no longer discontinuous. In the limit of perfect reflection, Casimir's result is once more obtained. Thereafter the paradox is elaborated and compared to the recent experiment by Iannuzzi *et al.*

**Casimir force and frequency spectrum with constant reflection coefficients.** – The expression for the Casimir pressure was given by Lifshitz as an integral over (real) frequencies and the variable $p$ by [2]

$$P_T(a) = -\frac{\hbar}{2\pi^2 c^3}\Re\mathrm{e}\int_0^\infty \mathrm{d}\omega\omega^3\int_C \mathrm{d}pp^2\coth\left(\frac{\hbar\omega}{2k_\mathrm{B}T}\right) \times\sum_{\sigma=\mathrm{TE}}^{\mathrm{TM}}\frac{r_\sigma^2\exp(2ip\omega a/c)}{1-r_\sigma^2\exp(2ip\omega a/c)}, \tag{2}$$

where the variable $p$ relates to the transverse wave vector $\mathbf{k}_\perp$ as

$$p=\frac{ic}{\omega}\sqrt{\mathbf{k}_\perp^2-\omega^2/c^2}$$

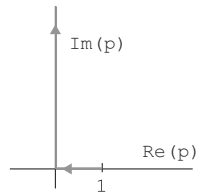


Fig. 1: The integration contour in (2).

and the contour of integration $C$, shown in fig. 1, runs from 1 to 0 along the real axis and thence along the imaginary axis to $+i\infty$. We have assumed both plates equal in (2) but all results in the following may be generalised to different media 1 and 2 by letting $r^2\to r_1r_2$. It is easy to show that the former part of the integral covers all modes which propagate in vacuum, that is when $\omega>|\mathbf{k}_\perp|c$, and the latter covers all evanescent modes $\omega<|\mathbf{k}_\perp|c$ which vanish exponentially away from the surfaces.

In the first part of the analysis we shall consider complex reflection coefficients which are constant with respect to $\omega$ and $p$, but in principle dependent on the separation $a$. We will assume zero temperature throughout so that the coth function in (2) is set to 1.

To denote the frequency dependence we use the notation

$$P=\int_0^\infty \mathrm{d}\omega P_\omega=\int_0^\infty \mathrm{d}\omega\sum_{\sigma=\mathrm{TE}}^{\mathrm{TM}}P_{\omega\sigma}.$$

Let us assume now that the reflection coefficient $r_\sigma$ is a constant quantity with respect to $\omega$ and $p$ which we allow to be complex for generality.

Consider first the propagating part of (2). The $p$ integral may now be evaluated explicitly. Consider one of the modes and suppress the index $\sigma$ for now to find

$$\begin{aligned}\Re\mathrm{e}\int_1^0\frac{\mathrm{d}p\cdot p^2r^2e^{2ip\omega a/c}}{1-r^2e^{2ip\omega a/c}}&=\Re\mathrm{e}\sum_{n=1}^\infty\frac{\partial^2}{\partial\gamma_n^2}\frac{r^{2n}}{i\gamma_n}(e^{i\gamma_n}-1)\\&=\Re\mathrm{e}\sum_{n=1}^\infty r^{2n}\left[\frac{ie^{in\xi}}{n\xi}-\frac{2e^{in\xi}}{n^2\xi^2}-\frac{2i}{n^3\xi^3}(e^{in\xi}-1)\right],\end{aligned}$$

where $\gamma=n\xi$ and $\xi=2\omega a/c$. We now introduce the polylogarithmic function whose $m$-th order is defined,

$$\mathrm{Li}_m(z)=\sum_{n=1}^\infty\frac{z^n}{n^m}.$$

Then we may write the pressure contribution from propagating waves (PW) $P_{\omega\sigma}^{\mathrm{PW}}$ as

$$\begin{aligned}P_{\omega\sigma}^{\mathrm{PW}}=\frac{-\hbar}{16\pi^2a^3}&\left[-\xi^2\Im\mathrm{m}\mathrm{Li}_1(r_\sigma^2e^{i\xi})-2\xi\Re\mathrm{e}\mathrm{Li}_2(r_\sigma^2e^{i\xi})\right.\\&\left.+2\Im\mathrm{m}\mathrm{Li}_3(r_\sigma^2e^{i\xi})-2\Im\mathrm{m}\mathrm{Li}_3(r_\sigma^2)\right].\end{aligned}\tag{3}$$

When $r_\sigma$ are real, there is no evanescent contribution to the pressure as we will see. We have plotted the

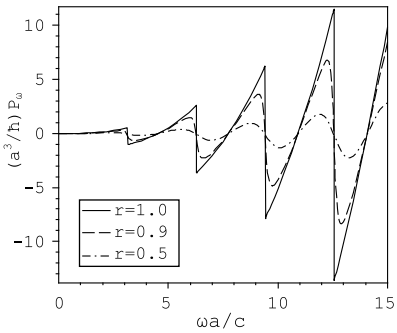


Fig. 2: Plot of (3) normalised by $a^3/\hbar$ as a function of $\omega a/c$ for different real values of $r$. This figure generalises fig. 2 of [1].

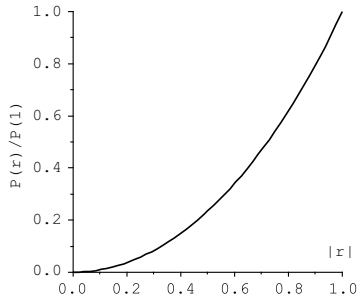


Fig. 3: The Casimir pressure for non-unitary real reflection coefficient (assumed equal for TE and TM) plotted relative to Casimir's result (1).

integrand (3) as a function of $\xi$ for various real values of the effective reflection coefficient $r$ in fig. 2 (assumed equal for TE and TM for simplicity). In the limit $r=1$ one obtains the discontinuous behaviour reported by Ford. Equation (3) thus generalises Ford's calculation; indeed fig. 2 is formatted so as to ease comparison with fig. 2 of [1].

We can go on to calculate the force for constant reflection coefficients. The analysis so far only required $r_\sigma$ to be independent of $p$; one could define some $p$-averaged $r_\sigma(\omega)$ and plot it the way we have in fig. 2. By assuming $r$ independent of $\omega$ as well, however, we are able to evaluate the $\omega$ integral explicitly. We substitue $\omega$ by $\xi$ in the integral and write $u_\sigma \equiv r_\sigma^2 \exp(i\xi)$ for short.

For a $\xi$-independent $r_\sigma$ one may show from the recursion property [16]

$$\int_0^z \mathrm{d}t \frac{\mathrm{Li}_n(t)}{t} = \mathrm{Li}_{n+1}(z)$$

that the following relations are fulfilled:

$$\Im\mathrm{m}\int_0^\xi \mathrm{d}\xi' \mathrm{Li}_{2n-1}(r_\sigma^2 e^{i\xi'}) = -\Re\mathrm{e}\mathrm{Li}_{2n}(r_\sigma^2 e^{i\xi}),$$
$$\Re\mathrm{e}\int_0^\xi \mathrm{d}\xi' \mathrm{Li}_{2n}(r_\sigma^2 e^{i\xi'}) = \Im\mathrm{m}\mathrm{Li}_{2n+1}(r_\sigma^2 e^{i\xi}).$$

The integrand as given by (3) is a wildly oscillating function of $\xi$ as fig. 2 indicates. For definiteness, let $r \to r\exp(-\delta\xi)$, where $\delta$ is a small real quantity which we will take to zero in the end. The same procedure was followed by Ford [1] and reflects the physical fact that all materials become transparent at very high frequencies. By moderately lengthy but straightforward partial integrations of (3) with respect to $\xi$ one may then obtain for constant and real reflection coefficients

$$P_\sigma^{\mathrm{PW}} = \frac{-\hbar c}{16\pi^2 a^4}\left[\frac{1}{2}\xi^2 \Re\mathrm{e}\mathrm{Li}_2 u_\sigma - 2\xi\Im\mathrm{m}\mathrm{Li}_3 u_\sigma \right.$$
$$\left. -3\Re\mathrm{e}\mathrm{Li}_4 u_\sigma - \frac{1}{2}\xi\Im\mathrm{m}\mathrm{Li}_3 r_\sigma^2\right]_{\xi=0}^{\infty}. \qquad (4)$$

With the normalising factor $\exp(-\delta\xi)$ in all reflection coefficients the $\infty$ limit is zero as physically expected. In the limit $\xi = 0$, $u_\sigma \to r_\sigma^2$ and only the term with no factor $\xi$ remains:

$$P_\sigma^{\mathrm{PW}} = -\frac{3\hbar c}{16\pi^2 a^4}\Re\mathrm{e}\mathrm{Li}_4 r_\sigma^2.$$

Secondly we consider the part of the pressure from evanescent waves (EW). The same way as above we evaluate the $p$ integral as follows:

$$\Re\mathrm{e}\int_0^{i\infty} \frac{\mathrm{d}p\cdot p^2}{r_\sigma^{-2}e^{-2ipwa/c}-1} = \Im\mathrm{m}\int_0^\infty \frac{\mathrm{d}q\cdot q^2}{r_\sigma^{-2}e^{2qwa/c}-1}$$
$$= \frac{2}{\xi^3}\Im\mathrm{m}\mathrm{Li}_3(r_\sigma^2), \qquad (5)$$

where $p = iq$. Clearly if $r_\sigma$ is real as in a non-dissipative medium, there is no evanescent contribution. Moreover, one notices that that the evanescent contribution is exactly cancelled by the last term of (3) above. Using the same normalisation as before the evanescent part accumulates to zero. Note that we could have let the normalisation $\exp(-\delta\xi)$ pertain to the exponential factor $\exp(i\xi)$ in the integration (4) since the remaining divergent term is exactly cancelled by evanescent contributions.

Hence the final result is obtained when $r_\sigma$ is constant:

$$P(a,r) = -\frac{3\hbar c}{16\pi^2 a^4}\sum_{\sigma=\mathrm{TE}}^{\mathrm{TM}} \Re\mathrm{e}\mathrm{Li}_4(r_\sigma^2). \qquad (6)$$

In the limit of perfect reflection, $r_\sigma \to 1$, the summation over $\sigma$ gives a factor 2, and with $\mathrm{Li}_4(1) = \zeta(4) = \pi^4/90$ we get Casimir's result (1). $P(a,r)$ is plotted in fig. 3 relative to the case for ideal reflection.

In exactly the same manner we could find the Casimir free energy for real and constant reflection coefficients to be given as

$$\mathscr{F}(a,r) = -\frac{\hbar c}{16\pi^2 a^3}\sum_{\sigma=\mathrm{TE}}^{\mathrm{TM}} \Re\mathrm{e}\mathrm{Li}_4(r_\sigma^2). \qquad (7)$$

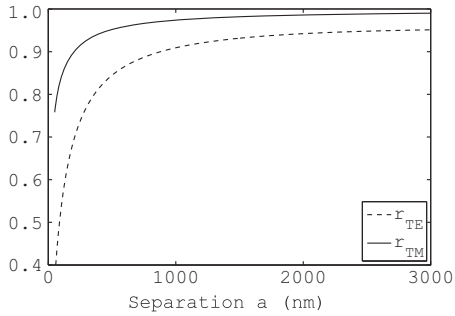


Fig. 4: $r_\sigma(a)$ for gold as computed from numerically calculated force using (8).

Again Casimir's result is obtained in the limit $r_\sigma = 1$. Some caution should be excerted here since the function $\mathrm{Li}_4(z)$ has a branch cut along the real axis from $z = 1$ to $\infty$ across which its imaginary part is discontinuous. Its real part, however, is continuous everywhere [16].

**Physical significance: naïve approach.** – Physically, reflection coefficients are far from constant with respect to frequency and transverse momentum, but the above analysis using constant reflection coefficients can be thought of as an averaging process in which the constant $r_\sigma$ is defined as the value which, when replacing the realistic $r_\sigma(\omega, p)$, does not change the value of the integral (2). Such an interpretation requires $r_\sigma$ to depend on $a$ as well.

Using the calculated Casimir pressure between gold plates where realistic data from [17] are employed (the calculation was previously presented in [18]), we can calculate the effective reflection coefficients $r_\sigma(a)$ by

$$r_\sigma = \left[\mathrm{Li}_4^{-1}\left\{-\frac{16\pi^2 a^4}{3\hbar c} P_\sigma^{\mathrm{num}}(a)\right\}\right]^{1/2}, \qquad (8)$$

where $P_{\mathrm{num}}$ are the calculated data, and $\mathrm{Li}_m^{-1}$ is the inverse polylogarithm of order $m$. By use of the series reversion functionality of analytic software the inverse polylogarithm is simple to calculate numerically. We plot the effective reflection coefficient in fig. 4.

Ford [1] (and later Lang [9]) appears to argue that the frequency spectrum shown in fig. 2 resembles the real spectrum, with the modification that the oscillations will be dampened and finally vanish at high frequencies. He concludes from this that since the oscillations themselves are much larger than the final force (which is the remainder of large fluctuations which cancel each other almost exactly), much larger and even repulsive Casimir forces could be obtained if media could be found which were good reflectors only in a range of frequencies.

Such a simple physical interpretation of the frequency spectrum is not unproblematic, however. For comparison with a more physically realistic system we have plotted the frequency spectrum obtained by plugging tabulated optical data for gold from Palik's book [17] directly into (2) and integrating over transverse momentum numerically (the separation is 100 nm; the integrand is now a function of $\omega$ and $a$ individually, not only their product), as well as the same integrand as obtained when using the simple plasma model, $\epsilon(\omega) = 1 - \omega_p^2/\omega^2$ with plasma frequency for gold $\omega_p = 9\,\mathrm{eV}$. Although the force predicted by either model at zero temperature is found to be very similar in magnitude when calculated by way of Wick rotation[1], the frequency spectrum clearly differs greatly.

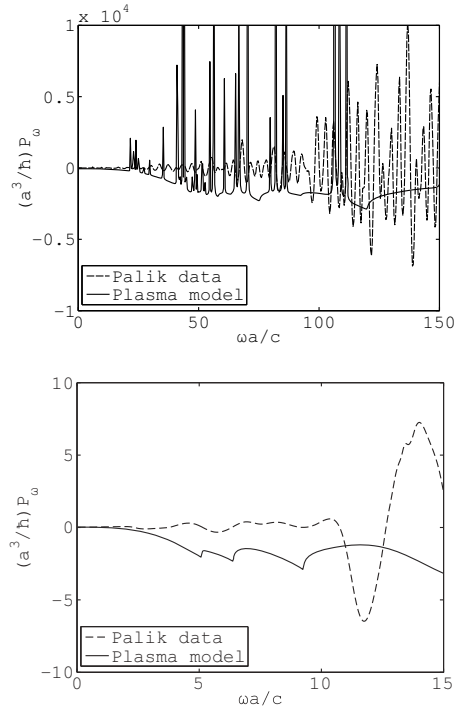


Fig. 5: The frequency spectrum of the Casimir pressure calculated using real data for gold and the plasma model, respectively. We have used $a = 100\,\mathrm{nm}$. The bottom graph is a zoom of the above.

While a useful generalisation, the formalism of mean reflection coefficients should be used with care since its substitution renders the integrand of (4) void of physical meaning other than giving the correct value per definition after integration: $\omega$ simply becomes a dummy variable. If Ford's result can be seen as a limiting case of the same procedure, this would indicate that the spectrum depicted in fig. 2, while interesting, may not represent physics.

Nonetheless, the key feature of the integrands of figs. 2 and 5, the presence of large oscillations, is a hallmark of all these graphs. These fluctuations should be physically observable as noted by several authors. As we will see,

[1] Disregarding the disputed behaviour of the TE mode near zero frequency [18].

however, indications are that while experimental confirmation of the Casimir force as calculated using Wick rotation is plentiful (see [19] for a review), calculation by straightforward integration over real frequencies seems at odds with a recent experiment. This is paradoxical since the two methods are typically presented as equivalent.

**The paradox and an experiment.** – Assume that the permittivity of two metallic planes in a Casimir cavity is perturbed in such a way that it is made transparent in a band of frequencies but is still a good reflector outside this band (with reflectivity dying off at high frequencies). The effect on the force from this perturbation may be calculated in two different ways and the results are different.

Exactly such a situation was probed experimentally by Iannuzzi *et al.* [15]. The force between two metallic plates (in reality a sphere and a plane) was measured, one of which was a hydrogen-switchable mirror (HSM). A good mirror in its as-deposited state, the HSM becomes transparent in the visible region once in a hydrogen-rich atmosphere. According to the authors of [15] the switching of the mirror corresponded roughly to setting the material reflectivity to zero over a wavelength range 0.2–2.5 $\mu$m, corresponding to $\omega$ between about $\omega_1 = 7.5 \cdot 10^{14}1/\mathrm{s}$ and $\omega_2 = 9.4 \cdot 10^{15}1/\mathrm{s}$. At a precision of 10%–15% (measured roughly from fig. 4 in [15]) the group was unable to detect any difference in the force with the mirror switched on and off, respectively.

We will estimate the effect of the transparency window using two different methods (an idealised version of such a material was considered in [9]). Assume first that the boundaries of the transparent window, between frequencies $\omega_1$ and $\omega_2$, are sharp so that for a complex permittivity $\epsilon = \epsilon' + i\epsilon'' \equiv 1 + \chi$,

$$\chi(\omega) \to \chi(\omega)[1 - \theta(\omega - \omega_1)\theta(\omega_2 - \omega)],$$

where $\theta$ is the unit step function. Using, as in [15], the Drude model with data for gold, $\epsilon(\omega) = 1 - \omega_p^2/(\omega^2 + i\omega\nu)$ with $\omega_p = 9\,\mathrm{eV}$ and $\nu = 35\,\mathrm{meV}$, the change in the permittivity at imaginary frequencies is found as $\epsilon(i\zeta) \to \epsilon(i\zeta) - \Delta\epsilon(i\zeta)$ by use of the Kramers-Kronig relation

$$\begin{aligned}\Delta\epsilon(i\zeta) &= \frac{2}{\pi}\int_{\omega_1}^{\omega_2} \frac{\mathrm{d}\omega\epsilon''(\omega)}{\omega^2 + \zeta^2} \\ &= \frac{\omega_p^2}{\zeta^2 - \nu^2}\frac{2}{\pi}\left[\arctan\frac{\omega_2}{\nu} - \arctan\frac{\omega_2}{\nu} \right. \\ &\quad \left. - \frac{\nu}{\zeta}\left(\arctan\frac{\omega_2}{\zeta} - \arctan\frac{\omega_1}{\zeta}\right)\right],\end{aligned}$$

the use of which ensures that the perturbation obeys causality. $\Delta\epsilon(i\zeta)$ makes for a correction to $\epsilon(i\zeta)$ on the level of 1%–4% and a corresponding correction to the force which would be unobservable at the precision of the experiment [15]. The latter authors use precisely this argument to explain their negative result.

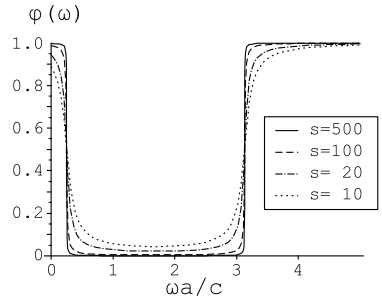


Fig. 6: $\varphi(\omega)$ for $\Delta = 1$ with different $s$ values.

Now let us calculate the correction by instead inserting a modified $\epsilon(\omega)$ into (2) where for a single interface

$$r_{\mathrm{TE}} = \frac{p - \sqrt{p^2 + \epsilon - 1}}{p + \sqrt{p^2 + \epsilon - 1}}; \quad r_{\mathrm{TM}} = \frac{\epsilon p - \sqrt{p^2 + \epsilon - 1}}{\epsilon p + \sqrt{p^2 + \epsilon - 1}},$$

and instead of the step functions we model the transparent window using a function which allows smooth boundaries. Let $\chi(\omega) \to \chi(\omega)\varphi(\omega; \Delta, s)$ with

$$\varphi(\omega) = 1 - \frac{\Delta}{\pi}\left[\arctan\frac{s(\omega - \omega_1)}{c/a} + \arctan\frac{s(\omega_2 - \omega)}{c/a}\right]. \quad (9)$$

Here the parameter $\Delta \in [0, 1]$ is the relative reduction in the window and $s$ determines the sharpness of the edges with $s = \infty$ giving unit step behaviour. The function $\varphi$ is plotted in fig. 6 for $\Delta = 1$ and different values of $s$.

We now calculate the change in the force by simply inserting this modified $\epsilon(\omega)$ into (2) and integrate over $p$ and a sufficiently large frequency range, then taking the difference. We use the Drude and plasma model, respectively with parameters for gold to model $\epsilon$ (the data of [17] contain too few points to use without extensive extrapolation). In the experiment of [15] only one of the plates was gold, yet the calculations are so rough that the difference does not matter here. The fact that in this estimation both reflection coefficients vanish in the transparency window whilst in the experiment only one did so, makes for a slight overestimation of the effect for smooth window edges, whilst it makes no difference when edges are sharp since the force only depends on the product of the reflection coefficients of the two materials. Note, furthermore, that the erratic behaviour of the integrand makes the numerical accuracy of integration somewhat rough, and also that in the modelling of the transparency band no effort has been made to ensure that causality is satisfied. Thus, the estimate is accurate only to an order of magnitude.

The results for different values of $\Delta$ and $s$ at separation $a = 100\,\mathrm{nm}$ are shown in fig. 7. Note that the absolute pressure between parallel gold plates at $T = 0$ is approximately 6 Pa (*e.g.* [18]) and that the difference between using Drude and plasma models is negligible here. Clearly

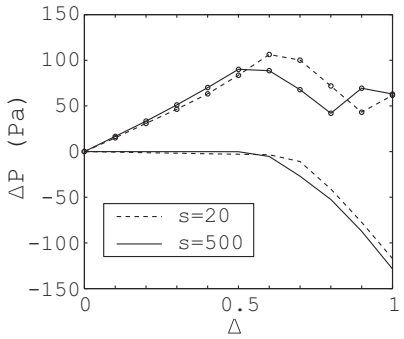


Fig. 7: Force difference with and without a transparent window using direct frequency calculation. Circles: Drude model, no circles: plasma model.

the corrections at $\Delta$ close to 1 are much too large, more than 10 times the force itself. The smoothness of the edges has no obvious effect. Only the plasma model with sharp boundaries and $\Delta < 0.5$ could fall within the experimental accuracy of [15], yet it seems highly likely that the relatively small corrections at low $\Delta$ and high $s$ for the plasma model are due to chance, especially since the more realitic Drude model gives corrections which are enormous and also, counterintuitively, positive. Such large corrections would be in keeping with Ford's predictions, but seem clearly ruled out by experiment.

**Conclusions.** – We have revisited the question of the frequency spectrum of the Casimir force, generalising Ford's result [1] to the case of subunitary reflection coefficients. While this smooths out the frequency spectrum as given by the real-frequency Lifshitz formula integrand, the integrand is still wildly oscillating. This result is used to calculate the Casimir force, and free energy for constant, "effective", reflection coefficients, a new result to the author's knowledge.

While the effective reflection coefficient may be a useful model, there is little reason to believe the resulting frequency spectrum to represent physics. A more realistic spectrum using physical models for the permittivity of materials is still highly irregular and, taken at face value, indicates that large and even repulsive Casimir forces could be attainable by tuning the dielectric response of materials used. An alternative means of calculation, paradoxically, gives a different pessimistic result, and the large effects seemingly implied by the wildly behaved frequency spectrum will seem to be excluded by a recent experiment by Ianuzzi *et alia*.

With the possibility of technological applications of the Casimir force, however, there is reason to strive for a better understanding of the physical interpretation of the frequency spectrum of the Casimir force as well as make further experimental efforts to settle this issue. An experiment similar to [15] accompanied by a careful measurement of the dielectric response of the actual sample used over a large frequency region would be a straightforward possibility, and a more sensitive measurement of the force might also be able to measure the actual difference in pressure.

It appears that the straightforward interpretation of the Casimir frequency spectrum as the integrand of the Lifshitz force formula at real frequencies is not valid, yet given the modesty of the efforts presented herein further investigation is warranted. Furthermore, the paradox presented herein pends a satisfactory resolution, hopefully to appear in the future.

* * *

The author thanks I. Pirozhenko for supplying the data from [17] in electronic format and acknowledges highly useful suggestions from an anonymous referee.

REFERENCES

[1] Ford L. H., *Phys. Rev. A*, **48** (1993) 2962.
[2] Lifshitz E. M., *Zh. Eksp. Teor. Fiz.*, **29** (1954) 94 (*Sov. Phys. JETP*, **2** (1956) 73); Landau L. D. and Lifshitz E.M., *Electrodynamics of Continuous Media* (Pergamon Press, New York) 1960, Chapt. XIII.
[3] Ford L. H., *Phys. Rev. D*, **38** (1988) 528.
[4] Hacyan S., Jáuregui R., Soto F. and Villareal C., *J. Phys. A*, **23** (1990) 2401.
[5] Casimir H. B. G., *Proc. K. Ned. Akad. Wet.*, **60** (1948) 793.
[6] Ford L. H., *Phys. Rev. A*, **58** (1998) 4279.
[7] Sopova V. and Ford L. H., *Phys. Rev. A*, **70** (2004) 062109.
[8] Ford L. H., *Int. J. Theor. Phys.*, **46** (2007) 2218.
[9] Lang A. S. I. D., *J. Math. Phys.*, **46** (2005) 102105.
[10] Rodriguez A., Ibanescu M., Iannuzzi D., Joannopoulos J. D. and Johnson S. G., *Phys. Rev. A*, **76** (2007) 032106.
[11] Lambrecht A. and Reynaud S., *Eur. Phys. J. D*, **8** (2000) 309.
[12] Pirozhenko I., Lambrecht A. and Svetovoy V. B., *New J. Phys.*, **8** (2006) 238.
[13] Pirozhenko I. and Lambrecht A., *Phys. Rev. A*, **77** (2008) 013811.
[14] Svetovoy V. B., van Zwol P. J., Palasantzas G. and De Hosson J. Th. M., *Phys. Rev. B*, **77** (2008) 035439.
[15] Iannuzzi D., Lisanti M. and Capasso F., *Proc. Natl. Acad. Sci. U.S.A.*, **101** (2004) 4019.
[16] Kölbig K. S., Mignaco J. A. and Remiddi E., *BIT*, **10** (1970) 38.
[17] Palik E. D. (Editor), *Handbook of Optical Constants of Solids* (Academic Press, New York) 1995.
[18] Brevik I., Ellingsen S. A. and Milton K. A., *New J. Phys.*, **8** (2006) 236.
[19] Milton K. A., *J. Phys. A*, **37** (2004) R209.

# Article [c]

***Temperature correction to Casimir-Lifshitz free energy at low temperatures: Semiconductors***

S.A. Ellingsen, I. Brevik, J.S. Høye, K.A. Milton

Physical Review E **78**, 021117 (2008)

# Temperature correction to Casimir-Lifshitz free energy at low temperatures: Semiconductors

Simen A. Ellingsen* and Iver Brevik†
*Department of Energy and Process Engineering, Norwegian University of Science and Technology, N-7491 Trondheim, Norway*

Johan S. Høye‡
*Department of Physics, Norwegian University of Science and Technology, N-7491 Trondheim, Norway*

Kimball A. Milton§
*Oklahoma Center for High Energy Physics and Department of Physics and Astronomy, The University of Oklahoma, Norman, Oklahoma 73019, USA*

(Received 20 May 2008; published 15 August 2008)

The Casimir force and free energy at low temperatures have been the subject of focus for some time. We calculate the temperature correction to the Casimir-Lifshitz free energy between two parallel plates made of dielectric material possessing a constant conductivity at low temperatures, described through a Drude-type dielectric function. For the transverse magnetic (TM) mode such a calculation is made. A further calculation for the case of the TE mode is thereafter presented which extends and generalizes previous work for metals. A numerical study is undertaken to verify the correctness of the analytic results.

DOI: 10.1103/PhysRevE.78.021117 PACS number(s): 72.20.−i, 11.10.Wx, 42.50.Lc, 78.20.Ci

## INTRODUCTION

There has been an explosion of interest in the Casimir effect [1], generalized to dielectrics by Lifshitz [2], since the modern experiments began with Lamoreaux in 1997 [3]. The zero-temperature Casimir-Lifshitz theory seems to have been confirmed to 1% accuracy over a range from 100 nm to a micrometer [4–12].

However, there has been a continuing controversy over the temperature dependence of this effect. The prescription given in Ref. [13] was seriously questioned by Boström and Sernelius [14] who pointed out that necessarily the transverse electric reflection coefficient at zero frequency must vanish for metals. This discontinuity predicted a linear temperature term at low temperatures, resulting in about a 15% correction to the result found by Lamoreaux. Lamoreaux believes that his experiment could not be in error to this extent [15]. More heatedly, Mostepanenko and collaborators have insisted that this behavior is inconsistent with thermodynamics (the Nernst heat theorem) because it would predict, for an ideal metal, that the free energy has a linear temperature term at low temperature, and hence that the entropy would not vanish at zero temperature [16]. Moreover, they assert that the precision Purdue experiments rule out the linear temperature term in the low-temperature expansion [12].

The issue is as yet unresolved, and is summarized in recent reviews [17,18]. We will not add further to the discussion of this controversy here. Rather, the purpose of this paper is to examine another purported temperature anomaly. In several recent papers [19–22] Geyer, Klimchitskaya, and Mostepanenko have claimed that in real dielectrics, which possess a very small, but nonzero conductivity which vanishes at $T=0$, a similar discontinuity in the transverse magnetic reflection coefficient occurs, which would lead to a similar violation of the Nernst theorem. The same applies to semiconductors whose conductivity vanishes as temperature drops to zero. The solution according to these authors, as in the TE case for good conductors, is to prescribe the effect away. We argue, however, that such a solution is physically unsatisfactory.

In Sec. I, we will review and clarify their argument for a standard Drude-type permittivity model for a weakly conducting material. We thereafter work out the leading-order temperature corrections to the free energy in the cases where the media are assumed to have a finite but small residual conductivity at $T=0$, as is implied when a Drude model is employed for taking the conductivity into account. This is a new result to the best of our knowledge (a similar calculation for materials with zero conductivity was undertaken in Ref. [19]). While this calculation does not solve the thermal anomaly brought forth in Refs. [19–21] and reviewed in Sec. I, it serves to further illuminate the mathematical behavior of the free energy of poor conductors at very low temperatures when different models for the dielectric response of the materials are employed. A similar calculation is subsequently performed for the TE mode, which extends that of Ref. [23] in several ways: We allow for the conductivity to be small; we work out one further order of the temperature correction to the free energy; and we allow, for generality, the permittivity to have a finite dielectric constant term in addition to the Drude-type dielectric response due to free charges.

A word about units. For our theoretical calculations, it is most convenient to use Gaussian electromagnetic units, as well as natural space-time units: $\hbar=c=k_B=1$. However, for final results, which could be experimentally observed, we use Système International (International System of Units) (SI) units. The mapping between units is very simply carried out by dimensional considerations, using the unit conversion factor $\hbar c=1.97\times10^{-5}$ eV cm. The conductivity transforma-

*simen.a.ellingsen@ntnu.no
†iver.h.brevik@ntnu.no
‡johan.hoye@phys.ntnu.no
§milton@nhn.ou.edu

 

tion between Gaussian and SI units is the simple replacement $4\pi\sigma=\sigma^{\mathrm{SI}}/\epsilon_0$, where $\epsilon_0=8.85\times10^{-12}$ F/m is the absolute permittivity of the vacuum and the notation $\sigma^{\mathrm{SI}}$ is used to explicate that SI units are used.

## I. TEMPERATURE ANOMALY FOR SEMICONDUCTORS

Here is a simple way to understand the argument of Ref. [19]. Suppose we model a dielectric with some small conductivity by the permittivity function

$$\varepsilon(i\zeta)=1+\frac{\bar{\varepsilon}-1}{1+\zeta^2/\omega_0^2}+\frac{4\pi\sigma}{\zeta}. \tag{1.1}$$

The essential point is that as $\zeta\to0$, $\varepsilon\to\bar{\varepsilon}$ if $\sigma=0$, otherwise $\varepsilon\to\infty$. The Casimir (Lifshitz) free energy between two half spaces, separated by a distance $a$, assumed to be of the same material for simplicity, is given by

$$F=\frac{T}{2\pi}{\sum_{m=0}^{\infty}}'\int_{\zeta_m}^{\infty}d\kappa\kappa[\ln(1-r_{\mathrm{TM}}^2e^{-2\kappa a})+\ln(1-r_{\mathrm{TE}}^2e^{-2\kappa a})]. \tag{1.2}$$

Here $\kappa$, $r_{\mathrm{TE}}$, and $r_{\mathrm{TM}}$ are functions of the discrete Matsubara frequencies $\zeta_m=2\pi mT$; $\kappa^2=k_\perp^2+\zeta^2$ with $\mathbf{k}_\perp$ the transverse wave vector, directed parallel to the surfaces. As is conventional, the prime on the summation mark implies the $m=0$ term be taken with half weight. We need to examine the behavior of the reflection coefficients in the small $\zeta$ limit. These are

$$r_{\mathrm{TE}}=\frac{\kappa-\sqrt{\kappa^2+\zeta^2(\varepsilon-1)}}{\kappa+\sqrt{\kappa^2+\zeta^2(\varepsilon-1)}}, \tag{1.3}$$

$$r_{\mathrm{TM}}=\frac{\varepsilon\kappa-\sqrt{\kappa^2+\zeta^2(\varepsilon-1)}}{\varepsilon\kappa+\sqrt{\kappa^2+\zeta^2(\varepsilon-1)}}, \tag{1.4}$$

where $\varepsilon=\varepsilon(i\zeta)$. For the case of an ideal metal, it was $r^{\mathrm{TE}}$ which was discontinuous:

$$r_{\mathrm{TE}}(\zeta=0)=0,\quad \lim_{\zeta\to0}r_{\mathrm{TE}}=-1, \tag{1.5}$$

so this gave a linear temperature term when the sum over Matsubara frequencies is converted to an integral according to the Euler-Maclaurin formula, for example (Ref. [19] uses the Abel-Plana formula, but that is equivalent).

For a dielectric the TE reflection coefficient is continuous and vanishes as $\zeta\to0$, but if there is a small (but not zero) conductivity which vanishes with $T$ linearly or faster, the TM coefficient exhibits a discontinuity at $\zeta=0$ as we now explain. When the conductivity is small we can assume there exists a temperature so that the $m=1$ Matsubara frequency, $\zeta_1=2\pi T$, satisfies the inequality

$$0<4\pi\sigma\ll\zeta_1\ll\omega_0, \tag{1.6}$$

in which case

$$r_{\mathrm{TM}}(i\zeta=0)=1,\quad r_{\mathrm{TM}}(i\zeta_1)=\frac{\bar{\varepsilon}-1}{\bar{\varepsilon}+1}. \tag{1.7}$$

Typical values of $\omega_0$ are in the optical or near IR frequency regions, so Eq. (1.6) will hold at room temperature for many semiconductors. If now $\sigma$ goes to zero as $T\to0$ linearly or faster, Eq. (1.6) continues to hold true all the way to zero temperature where Eq. (1.7) becomes a true discontinuity,

$$r_{\mathrm{TM}}(i\zeta=0)=1,\quad \lim_{\zeta\to0}r_{\mathrm{TM}}(i\zeta)=\frac{\bar{\varepsilon}-1}{\bar{\varepsilon}+1}. \tag{1.8}$$

Clearly if $\sigma$ reaches some residual value $>0$, Eq. (1.6) will not hold near zero temperature. Likewise the discontinuity disappears should $\sigma$ be exactly zero in a temperature region of finite width including $T=0$.

As in the metal case, Eq. (1.8) gives rise to a linear temperature term in the pressure and the free energy (see, e.g., Ref. [17] and references therein for details). Let $f_m$ be the summand of Eq. (1.2) or a similar expression for the Casimir pressure. Since $f_m$ is discontinuous at $m=0$, we must replace it by a continuous function,

$${\sum_{m=0}^{\infty}}'f_m=\frac{1}{2}f_0+\sum_{m=1}^{\infty}f_m=\frac{1}{2}(f_0-\tilde{f}_0)+{\sum_{m=0}^{\infty}}'\tilde{f}_m, \tag{1.9}$$

where $\tilde{f}_m$ is continuous,

$$\tilde{f}_m=\begin{cases}\tilde{f}_0 & =\lim_{m\to0}f_m, \quad m=0,\\ \tilde{f}_m & =f_m, \qquad m\neq0,\end{cases} \tag{1.10}$$

so that the Euler-Maclaurin summation formula can be applied to the sum over $\tilde{f}_m$. Then the first term in the third form in Eq. (1.9) gives rise to a free-energy contribution which is a linear function of $T$. Defining the shorthand notation

$$A_0=\left(\frac{\bar{\varepsilon}-1}{\bar{\varepsilon}+1}\right)^2, \tag{1.11}$$

that linear term is

$$\begin{aligned}F^{\mathrm{TM}}&=\frac{T}{4\pi}\int_0^{\infty}d\kappa\kappa[\ln(1-A_0e^{-2\kappa a})-\ln(1-e^{-2\kappa a})]\\&=\frac{T}{4\pi}\sum_{n=1}^{\infty}\frac{1}{n}[A_0^n-1]\int_0^{\infty}d\kappa\kappa e^{-2n\kappa a}\\&=\frac{T}{16\pi a^2}[\mathrm{Li}_3(A_0)-\zeta(3)],\end{aligned} \tag{1.12}$$

where the polylogarithmic function is

$$\mathrm{Li}_n(\xi)=\sum_{k=1}^{\infty}\frac{\xi^k}{k^n}. \tag{1.13}$$

Note that the linear term vanishes for $\bar{\varepsilon}\to\infty$ as is clear from noting the relation to the Riemann $\zeta$ function,

$$\mathrm{Li}_n(1)=\zeta(n). \tag{1.14}$$

Thus at zero temperature, the entropy is nonzero,

$$S = -\left(\frac{\partial F}{\partial T}\right)_V = -\frac{1}{16\pi a^2}[\mathrm{Li}_3(A_0) - \zeta(3)], \qquad (1.15)$$

which, if physical, is a violation of the Nernst heat theorem, or the third law of thermodynamics, which states that the entropy of a system must vanish at zero temperature.

## II. GENERAL FORMALISM

For reference throughout the next sections we will go though the formalism of determining the leading temperature corrections to the Casimir (Lifshitz) free energy by use of the Euler-Maclaurin formula, a procedure often employed previously.

Considering one polarization mode at a time, the free energy for the $q$ mode ($q$=TM,TE) is written in the form

$$F_q = f(a,T)\sum_{m=0}^{\infty}{}' g(m), \qquad (2.1)$$

where we have pulled out a convenient prefactor.

When $T \to 0$ the Matsubara sum becomes an integral, so the temperature correction to the free energy, given by

$$\Delta F_q = f(a,T)\left[\sum_{m=0}^{\infty}{}' - \int_0^\infty dm\right] g(m), \qquad (2.2)$$

can be determined by use of the Euler-Maclaurin formula. For the summands of the Lifshitz formula, the higher derivatives of $g(m)$ are singular near $m=0$. When this is the case the Euler-Maclaurin formula can be applied to the sum starting at $m=1$ (or a higher value of $m$) instead, whereby

$$\begin{aligned}\tilde{\Gamma} &\equiv \left[\sum_{m=0}^{\infty}{}' - \int_0^\infty dm\right] g(m) \\ &= \frac{1}{2}g(0) - \int_0^1 g(m)dm + \frac{1}{2}g(1) - \sum_{k=1}^{\infty}\frac{B_{2k}}{(2k)!}g^{(2k-1)}(1) \\ &= \frac{1}{2}g(0) - \int_0^1 g(m)dm + \frac{1}{2}g(1) - \frac{1}{12}g'(1) + \frac{1}{720}g'''(1) \\ &\quad - \cdots, \end{aligned} \qquad (2.3)$$

where $B_n$ are the Bernoulli numbers,

$$B_2 = \frac{1}{6}; \quad B_4 = -\frac{1}{30}; \quad B_6 = \frac{1}{42}; \quad \ldots, \qquad (2.4)$$

using the convention of [24] Sec. 23.2. (Two remarks are called for here: We have assumed that $g$ and all its derivatives vanish at infinity, and we have converted this formula into one which is commonly asymptotic because we have omitted the remainder term which is present when only a finite number of derivatives terms are retained. Thus we are considering only the leading terms in an asymptotic expansion for small $T$.)

As mentioned above, $g(m)$ is not analytic at $m=0$. It can be written in the asymptotic form for small $m$

$$g(m) \sim c_0 + c_1 m + c_{3/2} m^{3/2} + c_{2l} m^2 \ln m + c_2 m^2 + \cdots, \qquad (2.5)$$

$$m \to 0.$$

The terms needed for the right-hand side of Eq. (2.3) are now

$$g(0) = c_0, \qquad (2.6a)$$

$$g(1) = c_0 + c_1 + c_2 + c_{3/2} + \cdots, \qquad (2.6b)$$

$$g'(1) = c_1 + c_{2l} + 2c_2 + \frac{3}{2}c_{3/2} + \cdots, \qquad (2.6c)$$

$$g'''(1) = 2c_{2l} - \frac{3}{8}c_{3/2} + \cdots, \qquad (2.6d)$$

$$\int_0^1 dm g(m) = c_0 + \frac{1}{2}c_1 - \frac{1}{9}c_{2l} + \frac{1}{3}c_2 + \frac{2}{5}c_{3/2} + \cdots. \qquad (2.6e)$$

When inserted into Eq. (2.3) the terms involving $c_0$ and $c_2$ cancel and one is left with

$$\tilde{\Gamma} \approx -\frac{c_1}{12} + \frac{11c_{2l}}{360} - \frac{49}{1920}c_{3/2} + \cdots. \qquad (2.7)$$

Here the term due to $c_1$ is exact, whereas the terms with $c_{2l}$ and $c_{3/2}$ receive contributions from all higher derivatives in the Euler-Maclaurin formula, and to obtain exact expressions for the coefficients, all such terms must be kept, as we now show.

Retaining the higher derivative terms in the Euler-Maclaurin formula one finds by using

$$\phi_{2n} = \left.\frac{d^{2n-1}}{dm^{2n-1}}m^{3/2}\right|_{m=1} = -\frac{3(4n-7)!}{2^{4n-5}(2n-4)!}, \quad n \geqslant 2, \qquad (2.8a)$$

and

$$\psi_{2n} = \left.\frac{d^{2n-1}}{dm^{2n-1}}m^2 \ln m\right|_{m=1} = 2(2n-4)!, \quad n \geqslant 2, \qquad (2.8b)$$

that the temperature correction to free energy is

$$\Delta F_q = f(a,T)\tilde{\Gamma}, \qquad (2.9)$$

where with Eq. (2.3),

$$\tilde{\Gamma} = -\frac{c_1}{12} + \Psi c_{2l} + \Phi c_{3/2} + \cdots, \qquad (2.10)$$

with the coefficients

$$\Psi = \frac{1}{9} - \frac{B_2}{2} - \sum_{n=2}^{\infty}\frac{B_{2n}\psi_{2n}}{(2n)!}, \qquad (2.11a)$$

$$\Phi = \frac{1}{2} - \frac{2}{5} - \frac{3B_2}{4} - \sum_{n=2}^{\infty} \frac{B_{2n}\phi_{2n}}{(2n)!}. \tag{2.11b}$$

These series are formally divergent as is typical for perturbation series near singularities. Indeed, they arise from the asymptotic Euler-Maclaurin formula (2.3). For example, $\Phi$ can be recognized as a special case of the expansion of the Riemann $\zeta$ function in terms of Bernoulli numbers, Eq. 23.2.3 of Ref. [24] with an infinite number of terms retained in the sum, and the remainder omitted. A meaningful value can nonetheless be assigned to them through Borel summation as detailed in the Appendix. Numerically, the mathematical software Maple computes the numerical values by means of a Levin $u$ transform to

$$\Psi = 0.03044845705840\ldots, \tag{2.12a}$$

$$\Phi = -0.0254852018898\ldots. \tag{2.12b}$$

By either numerical or analytical correspondence we thus recognize that

$$\Phi = \zeta\left(-\frac{3}{2}\right), \tag{2.13a}$$

$$\Psi = \frac{\zeta(3)}{4\pi^2}, \tag{2.13b}$$

where $\zeta$ is the Riemann $\zeta$ function.

When Eq. (1.1) is used in the Lifshitz formalism with constant and finite $\sigma$ and $\bar{\varepsilon} > 1$ in Secs. III and IV, we will find that the terms of $F$ stemming from $c_1$, $c_{3/2}$, and $c_{2l}$ are proportional to $T^2$, $T^{5/2}$, and $T^3$, respectively. Higher-order terms of $g(m)$ will likewise give higher-order temperature corrections.

## III. TM MODE, RESIDUAL CONDUCTIVITY

In the following sections we will work out the low-temperature behavior of corrections to the free energy under the assumption that a Drude-type dielectric function (1.1) may be used, and that $\sigma$ is finite and constant with respect to $\zeta$ and $T$ for small $T$ and $\zeta$. As argued in Ref. [25], when $\sigma$ is finite close to zero temperature Nernst's theorem will be satisfied. Here we will calculate explicitly the low-temperature behavior of the free energy for the TM mode.

Conventionally, semiconductors are found within the broad interval of conductivity $\sigma^{\mathrm{SI}}$ in SI units $10^{-5}\ (\Omega\,\mathrm{m})^{-1} < \sigma^{\mathrm{SI}} < 10^{5}\ (\Omega\,\mathrm{m})^{-1}$, that is

$$10^{6}\ \mathrm{s}^{-1} < \sigma^{\mathrm{SI}}/\epsilon_0 < 10^{16}\ \mathrm{s}^{-1}. \tag{3.1}$$

For numerical purposes we will use the intermediate value $\sigma^{\mathrm{SI}}/\epsilon_0 = 10^{12}\ \mathrm{s}^{-1}$, which is large enough not to hamper numerical verification unnecessarily, but small enough to distinguish the material in question from a good metal. The frequency corresponding to $\sigma^{\mathrm{SI}}/\epsilon_0$ for a metal is $\omega_p^2/\nu$, where $\omega_p$ is the plasma frequency and $\nu$ the relaxation frequency. For gold at room temperature $\omega_p^2/\nu$ has the approximate value $3.5 \times 10^{22}\ \mathrm{s}^{-1}$.

Returning to Gaussian units, we consider the TM mode and introduce the shorthand notation

$$t = \frac{\zeta_1}{4\pi\sigma} = \frac{2\pi T}{4\pi\sigma} = \frac{2\pi k_{\mathrm{B}} T}{\hbar(\sigma^{\mathrm{SI}}/\epsilon_0)} \tag{3.2}$$

and the symbol

$$\mu = mt. \tag{3.3}$$

If $4\pi\sigma = 10^{12}\ \mathrm{s}^{-1}$ as assumed above,

$$t \approx 0.83T, \tag{3.4}$$

with $T$ in Kelvin.

The free energy is given by Eq. (1.2), for which we now consider only the TM term,

$$F^{\mathrm{TM}} = \frac{T}{2\pi}{\sum_{m=0}^{\infty}}' \int_{\zeta}^{\infty} d\kappa\kappa \ln(1 - Ae^{-2\kappa a}), \tag{3.5}$$

where the reflection coefficient squared is

$$A \equiv r_{\mathrm{TM}}^2 = \left(\frac{\varepsilon - \sqrt{1 + (\varepsilon - 1)(\zeta/\kappa)^2}}{\varepsilon + \sqrt{1 + (\varepsilon - 1)(\zeta/\kappa)^2}}\right)^2. \tag{3.6}$$

Here and henceforth the index $m$ on Matsubara frequencies $\zeta_m$ and quantities dependent on it will frequently be suppressed.

The temperature corrections to the free energy at low temperatures are dominated by small frequencies, so we can assume as an approximation that the middle term of Eq. (1.1) is simply equal to $\bar{\varepsilon} - 1$ and write

$$\varepsilon(i\zeta) \approx \bar{\varepsilon} + \frac{4\pi\sigma}{\zeta} = \bar{\varepsilon} + \frac{1}{\mu}. \tag{3.7}$$

We define the dimensionless quantity

$$\alpha = 2a(4\pi\sigma) = \frac{2a}{c}(\sigma^{\mathrm{SI}}/\epsilon_0), \tag{3.8}$$

where $a$ is the distance between the semiconductor plates. For the value $4\pi\sigma \approx 10^{12}\ \mathrm{s}^{-1}$ or smaller, $\alpha$ is a small quantity, which we use to define a criterion for the smallness of the conductivity in the remainder of this paper,

$$\alpha \ll 1. \tag{3.9}$$

For $a = 1\ \mu$m and $\sigma$ as above, as used for numerical purposes later, $\alpha$ has a value of about $6.7 \times 10^{-3}$, so this criterion is well satisfied.

By defining the variable $x$,

$$x = 2\kappa a = \frac{\kappa\alpha}{4\pi\sigma} = \frac{\kappa\alpha\mu}{\zeta}, \tag{3.10}$$

$A$ can be written

$$A = \left(\frac{1 + \bar{\varepsilon}\mu - \mu\sqrt{1 + [1 + (\bar{\varepsilon} - 1)\mu]\alpha^2\mu/x^2}}{1 + \bar{\varepsilon}\mu + \mu\sqrt{1 + [1 + (\bar{\varepsilon} - 1)\mu]\alpha^2\mu/x^2}}\right)^2, \tag{3.11}$$

and the integral (3.5) with the use of Eq. (3.2) and $\zeta = 2\pi mT$ becomes

$$F^{\mathrm{TM}} \equiv \frac{(4\pi\sigma)^3 t}{4\pi^2\alpha^2} {\sum_{m=0}^{\infty}}' g(m), \tag{3.12}$$

where

$$g(m) = \int_{\alpha\mu}^{\infty} dx x \ln(1 - Ae^{-x}). \tag{3.13}$$

We wish now to extract explicitly the temperature dependence of the integrals $g(m)$ in Eq. (3.13). The procedure we choose is to expand Eq. (3.13) to leading order in the small parameter $\alpha$, and then expand the resulting term in powers of $m$ to obtain the form (2.5).

The first term in the Taylor expansion of the logarithm in powers of $\alpha$ is

$$\ln(1 - Ae^{-x}) = -\mathrm{Li}_1(A_\mu e^{-x}) + O(\alpha^2) \tag{3.14}$$

where we use the polylogarithmic function defined in Eq. (1.13) and define the quantity

$$A_\mu = \left(\frac{1 + (\bar{\varepsilon} - 1)\mu}{1 + (\bar{\varepsilon} + 1)\mu}\right)^2. \tag{3.15}$$

For integral $s \leqslant 1$ the polylogarithm $\mathrm{Li}_s(y)$ can be expressed by elementary functions, specifically

$$\mathrm{Li}_1(y) = -\ln(1 - y); \quad \mathrm{Li}_0(y) = \frac{y}{1 - y};$$

$$\mathrm{Li}_{-1} = \frac{y}{(1 - y)^2}. \tag{3.16}$$

The summand $g(m)$ thus has the form

$$g(m) = -\int_{\alpha\mu}^{\infty} dx x \,\mathrm{Li}_1(A_\mu e^{-x}) + O(\alpha^2). \tag{3.17}$$

Now we will expand $g(m)$ in powers of $m$. It is easy to show from Eq. (1.13) that

$$\int dy \,\mathrm{Li}_n(Ce^{-\beta y}) = -\frac{1}{\beta}\mathrm{Li}_{n+1}(Ce^{-\beta y}); \tag{3.18}$$

from which by partial integration

$$g(m) = -\alpha\mu \,\mathrm{Li}_2(A_\mu e^{-\alpha\mu}) - \mathrm{Li}_3(A_\mu e^{-\alpha\mu}) + O(\alpha^2). \tag{3.19}$$

We now use the property

$$\mathrm{Li}_n(Ce^{-y}) = \sum_{l=0}^{\infty} \frac{(-y)^l}{l!}\mathrm{Li}_{n-l}(C) \tag{3.20}$$

for $|C| < 1$ to expand the polylogarithms in powers of $\alpha\mu$. The terms containing $\mathrm{Li}_2$ then cancel and we are left with

$$g(m) = -\mathrm{Li}_3(A_\mu) + \frac{1}{2}\alpha^2\mu^2\mathrm{Li}_1(A_\mu) + O(\alpha^2) \tag{3.21}$$

with $A_\mu$ given by Eq. (3.15). Henceforth we shall denote the first two terms of the expansion (3.21) $g_I(m)$ and $g_{II}(m)$. The remaining $O(\alpha^2)$ term comes from the error in Eq. (3.14). As before we are going to truncate the expansion in $\alpha$ at leading order, but will evaluate the explicit correction $\sim\alpha^2$ to Eq. (3.21) later as a measure of the error. We thus have the simple expression

$$g_I(m) = -\mathrm{Li}_3(A_\mu). \tag{3.22}$$

We will next expand Eq. (3.22) in $\mu$. $\mathrm{Li}_3(A_\mu)$ does not have a Taylor expansion near $m=0$ (where $A_0=1$) because its second derivative is singular here. Using

$$\frac{\mathrm{d}}{\mathrm{d}y}\mathrm{Li}_n(y) = \frac{1}{y}\mathrm{Li}_{n-1}(y), \tag{3.23}$$

we differentiate Eq. (3.22) to find

$$g_I'(m) = \frac{4t\,\mathrm{Li}_2(A_\mu)}{[1 + (\bar{\varepsilon} + 1)\mu][1 + (\bar{\varepsilon} - 1)\mu]}. \tag{3.24}$$

We can use the identity [26]

$$\mathrm{Li}_2(z) + \mathrm{Li}_2(1 - z) = \frac{\pi^2}{6} - \ln(z)\ln(1 - z), \tag{3.25}$$

which is easily verified by differentiation, use of Eq. (1.13), and $\mathrm{Li}_2(1) = \pi^2/6$. Furthermore, $\mathrm{Li}_2(1 - A_\mu)$ has a simple Taylor expansion around $A_\mu = 1$,

$$\mathrm{Li}_2(1 - A_\mu) = 4\mu - 4(\bar{\varepsilon} + 1)\mu^2 + \cdots \tag{3.26}$$

and

$$\frac{4}{[1 + (\bar{\varepsilon} + 1)\mu][1 + (\bar{\varepsilon} - 1)\mu]} = 4 - 8\bar{\varepsilon}\mu + \cdots, \tag{3.27}$$

whereby we find

$$g_I'(m) = \frac{2\pi^2 t}{3} - 4mt^2\left(\frac{\bar{\varepsilon}\pi^2}{3} + 4\right) + 16mt^2 \ln 4\mu + \cdots, \tag{3.28}$$

where the next term of the series is of order $t^3$.

Comparing with Eq. (2.5) we recognize the coefficients

$$c_1 = \frac{2\pi^2 t}{3}, \quad c_{2l} = 8t^2, \tag{3.29}$$

which we insert into Eq. (2.10) to find

$$\left[{\sum_{m=0}^{\infty}}' - \int_0^{\infty} dm\right] g_I(m) = -\frac{\pi^2 t}{18} + 8\Psi t^2. \tag{3.30}$$

We thus obtain the approximate correction to the free energy for small $t$,

$$\Delta F_I^{\mathrm{TM}} = \frac{(4\pi\sigma)^3 t}{4\pi^2\alpha^2}\left[{\sum_{m=0}^{\infty}}' - \int_0^{\infty} dm\right] g_I(m)$$

$$\approx -\frac{(4\pi\sigma)^3}{72\pi^2\alpha^2} t^2[\pi^2 - 144\Psi t] \tag{3.31}$$

in terms of our reduced units $t$ and $\alpha$. In SI units, inserting Eq. (2.13b),

$$\Delta F_I^{\mathrm{TM}} = -\frac{\pi^2 (k_B T)^2}{72\hbar(\sigma^{\mathrm{SI}}/\epsilon_0)a^2} + \frac{\zeta(3)(k_B T)^3}{\pi[\hbar(\sigma^{\mathrm{SI}}/\epsilon_0)a]^2}$$
$$= -\frac{\pi^2 (k_B T)^2}{72\hbar(\sigma^{\mathrm{SI}}/\epsilon_0)a^2}\left(1 - \frac{72\zeta(3)k_B T}{\pi^3 \hbar \sigma^{\mathrm{SI}}/\epsilon_0}\right). \quad (3.32)$$

### A. Correction due to subleading terms of Eq. (3.21)

Twice in the above we truncated the expressions at leading order in the parameter $\alpha$, in Eq. (3.14) and Eq. (3.21). As an indication of the magnitude of the error we will calculate the next order in $\alpha$ of Eq. (3.21) while a similar calculation for Eq. (3.14) is more troublesome due to singularities and beyond the scope of the present effort. The correction $\propto \alpha^2$ of Eq. (3.21) was

$$\Delta g(m) = \frac{1}{2}\alpha^2 m^2 t^2 \mathrm{Li}_1(A_\mu) + O(\alpha^3 t^3). \quad (3.33)$$

We will only consider the first term, since the next terms give temperature corrections $\propto T^4$ and higher. We Taylor expand as before in powers of $\mu$,

$$\mathrm{Li}_1(A_\mu) = -\ln(4t) - \ln m + (\bar{\varepsilon} + 2)\mu + O(\mu^2), \quad (3.34)$$

from which the leading correction from $\Delta g_l(m)$, is found from Eq. (2.10) to order $T^3$ to which only the term $\propto m^2 \ln m$ contributes,

$$\delta F^{\mathrm{TM}} = \frac{(4\pi\sigma)^3 t}{4\pi^2\alpha^2}\delta\tilde{\Gamma} \approx \frac{(4\pi\sigma)^3 \Psi t^3}{8\pi^2}. \quad (3.35)$$

Being $\alpha$ independent, the correction (3.35) is much smaller than the leading term (3.31) for small $\alpha$. In SI units,

$$\delta F^{\mathrm{TM}} = \frac{\zeta(3)(k_B T)^3}{4\pi\hbar^2 c^2} + O(T^4). \quad (3.36)$$

The relative magnitude of this term compared to the $T^3$ term of Eq. (3.32) is with our numerical data

$$\frac{(\sigma^{\mathrm{SI}}/\epsilon_0)^2 a^2}{4c^2} \approx 2.8 \times 10^{-6}. \quad (3.37)$$

The correction from the truncation of Eq. (3.14) is likely to be of similar size and therefore much smaller than the accuracy of the numerical investigation.

### B. Numerical investigation of TM mode result

The numerical investigation in Fig. 1(a) employs Eq. (1.1) with $\sigma^{\mathrm{SI}}/\epsilon_0 = 10^{12}\ \mathrm{s}^{-1}$, $\bar{\varepsilon} = 11.67$, and $\omega_0 = 8\times 10^{15}\ \mathrm{s}^{-1}$ as appropriate for Si [27]. While the analytical expression fits well for $T < 0.1$ K, corrections $\sim T^4$ become important beyond this point. The two leading orders in temperature corrections were shown to be independent of $\bar{\varepsilon}$ to leading order in $\alpha$, but the $T^4$ correction (not calculated analytically herein) depends heavily on this value. A qualitative measure of this effect is given in Fig. 1(b) where we have used $\bar{\varepsilon} = 1$, cetera paribus. In all plots the curves are given by Eq. (3.32) with and without inclusion of its second term.

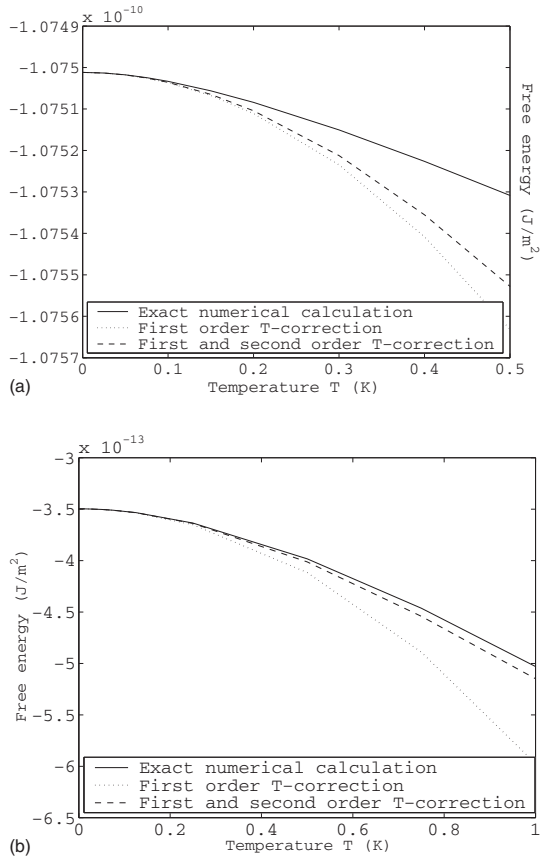


FIG. 1. $F^{\mathrm{TM}}$ and its approximation with (a) $\bar{\varepsilon} = 11.67$ and (b) $\bar{\varepsilon} = 1$. Correction curves, calculated from Eq. (3.31), are shifted to match the numerical calculations at $T = 0$ in each graph.

It is noteworthy that, as seen from Fig. 1, while the $\zeta^{-1}$ term of Eq. (1.1) gives the dominant temperature correction for small $T$, nearly all (99.7% with our data) of the free energy at $T = 0$ is due to the $\bar{\varepsilon}$ term.

While the fit pictured in Fig. 1 is indicative, a much more sensitive confirmation of the accuracy of the theoretical results is provided by considering the quantity

$$R = \frac{\Delta F_{\mathrm{th}} - \Delta F_{\mathrm{num}}}{\Delta F_{\mathrm{th}}}, \quad (3.38)$$

where $\Delta F_{\mathrm{num}}$ is the direct numerical calculation and $\Delta F_{\mathrm{th}}$ is the theoretical result to next-to-leading order, in the form (3.31). An analysis exactly similar to this was performed in Ref. [23]; the reader may refer to that paper for further details.

We have found that $\Delta F_{\mathrm{th}}$ is of the form

$$\Delta F_{\mathrm{th}} = -CT^2(1 - C_1 T) \quad (3.39)$$

and assume $\Delta F_{\mathrm{num}}$ to be of the form

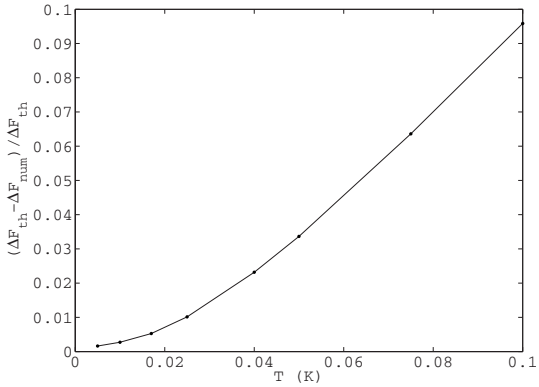


FIG. 2. The quantity $R$ defined in Eq. (3.38) plotted for the TM result (3.31) and numerical calculations.

$$\Delta F_{\text{num}} = -DT^2(1 - D_1T + D_2T^2 + \cdots), \tag{3.40}$$

from which one finds

$$R = \frac{C-D}{C} - \frac{D}{C}(C_1 - D_1)T - \frac{D}{C}[D_2 + C_1(C_1 - D_1)]T^2 + \cdots . \tag{3.41}$$

In the special case where $C=D$ and $C_1=D_1$, this becomes

$$R = -D_2T^2 + O(T^3) \tag{3.42}$$

which is zero in the limit $T=0$ and has zero slope in this limit. The zero-temperature limit of $R$ and its slope thus provide measures of the accuracy of the theoretical results: if the $T^2$ coefficient is correct, $R$ should approach zero as $T\to 0$, and if the $T^3$ coefficient is correct, the slope of $R(T)$ should vanish in this limit as well. We have not taken the corrections (3.36) into account in the plotting of Fig. 2.

We have undertaken a numerical study of the behavior close to zero temperature, resulting in the graph of $R$ shown in Fig. 2. Due to the vanishing denominator of Eq. (3.38), the analysis is extremely sensitive to numerical errors as the zero temperature limit is approached. From the figure it seems clear that the errors in the two coefficients are small enough to confirm the correctness of Eq. (3.31), although some caution must be exerted due to the numerical volatility of $R$. Comparing Fig. 2 to Eq. (3.42) it is clear that $D_2<0$ which implies that the coefficient of the $T^4$ term of the free energy be positive, which conforms with the corrections in Fig. 1 not accounted for to order $T^3$.

## IV. TE MODE, RESIDUAL CONDUCTIVITY

For the TE mode the dominant temperature correction to the free energy comes from the last term of Eq. (1.1). The permittivity (1.1), which can be approximated as Eq. (3.7), is similar, but not identical, to that for a Drude metal, considered in Refs. [23,28]. There, instead of Eq. (3.7) the permittivity was assumed to be

$$\varepsilon_{\text{metal}} = 1 + \frac{\omega_p^2}{\zeta(\zeta+\nu)} \approx 1 + \frac{\omega_p^2}{\nu\zeta}. \tag{4.1}$$

The principal difference is that the constant term $\bar{\varepsilon}$ is assumed to be significant here and kept general. Since for small $\zeta$ the term $\sim\zeta^{-1}$ dominates the constant term, an approximation to the low-temperature behavior of the dielectric would be expected to be found by the same analysis as that of Refs. [23,28] but with the substitution

$$\frac{\omega_p^2}{\nu} \to 4\pi\sigma. \tag{4.2}$$

For typical semiconductors, $4\pi\sigma$ is smaller than $\omega_p^2/\nu$ for a good metal by many orders of magnitude. For this reason, since the free energy at zero temperature is of the same order of magnitude for the metals and semiconductors for the same separation, the relative temperature corrections for the TE mode are expected to be much smaller than for a metal. Thus, there is reason to investigate whether the effects of $\bar{\varepsilon}>1$, while negligible for a metal, could be important for small $\sigma$. In some dielectric materials, as is well known, $\bar{\varepsilon}$ can exceed unity by as much as two orders of magnitude, and a more careful analysis is therefore justified. The procedure is the same as above, and an extension of that found in Ref. [23], to which the reader may turn for further detail.

It was found in Refs. [23,28] that for $T\to 0$, and $\bar{\varepsilon}=1$,

$$\Delta F_{\text{TE}} = C_2T^2 - C_{5/2}T^{5/2} + \cdots, \tag{4.3}$$

where

$$C_2 = \frac{(4\pi\sigma)}{48}(2\ln 2 - 1), \tag{4.4a}$$

$$C_{5/2} = \frac{\sqrt{2\pi}}{6}\zeta(-3/2)(4\pi\sigma)^{3/2}a. \tag{4.4b}$$

Here $\zeta(y)$ is the Riemann $\zeta$ function (for this closed form of $C_{5/2}$, see Appendix A of Ref. [23]).

For the numerical values indicated this gives the SI values

$$C_2 = 1.618\,571\,9\times 10^{-19}\frac{\text{J}}{\text{K m}^2}\left(\frac{\sigma^{\text{SI}}/\epsilon_0}{10^{12}\ \text{s}^{-1}}\right), \tag{4.5a}$$

$$C_{5/2} = 2.584\,437\,3\times 10^{-22}\frac{\text{J}}{\text{K}^{5/2}\,\text{m}^2}\left(\frac{a}{1\ \mu\text{m}}\right)\left(\frac{\sigma^{\text{SI}}/\epsilon_0}{10^{12}\ \text{s}^{-1}}\right)^{3/2}. \tag{4.5b}$$

Thus the TE temperature correction is expected to be positive and in the order of magnitude of $10^{-19}\ \text{J/m}^2$ at $T=1$ K.

The numerical calculations shown in Fig. 3 were complicated by the fact that the thermal corrections are many orders of magnitude smaller than the free energy at zero temperature, making a graph of the quantity $R$ similar to Fig. 2 unfeasible within the assumption of $\alpha\ll 1$. We show here, however, that assuming $\bar{\varepsilon}>1$ does not change the theoretically predicted thermal correction to the free energy to order $T^3$, and therefore merely refer to Ref. [23] for further numerical support of the theoretical result.

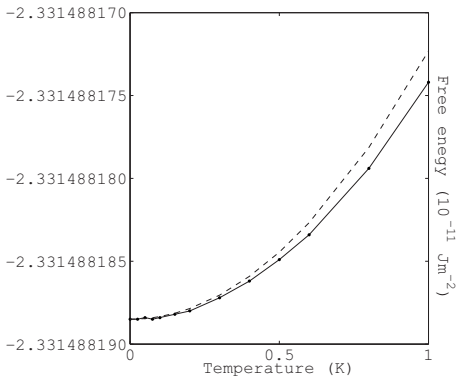


FIG. 3. Temperature dependence of the free energy for TE at 1 micron separation. The solid line is an exact numerical calculation including all terms of Eq. (1.1) with $\bar{\varepsilon}=11.66$ and $\omega_0=8.0\times10^{15}$ s$^{-1}$, the dashed line is the parabolic temperature correction (4.3). The term $\propto T^{5/2}$ is too small to be visible in the graph.

### A. More general treatment of the TE mode

Let us treat the TE mode temperature correction to the free energy more carefully. Starting with the expression (1.2) we perform the substitution

$$x=\frac{\kappa}{\zeta\sqrt{\varepsilon(i\zeta)-1}}=\frac{\kappa\mu}{\chi\zeta} \tag{4.6}$$

where we define the recurring quantity

$$\chi=\sqrt{\mu+(\bar{\varepsilon}-1)\mu^2}. \tag{4.7}$$

Then the free energy may be written

$$F^{\mathrm{TE}}=\frac{(4\pi\sigma)^3 t}{4\pi^2}{\sum_{m=0}^{\infty}}' g(m) \tag{4.8a}$$

with

$$g(m)=\chi^2\int_{\mu/\chi}^{\infty} dx x\ln(1-Be^{-\alpha\chi x}). \tag{4.8b}$$

The squared reflection coefficient given by Eq. (1.3) now depends only on $x$,

$$B=(x-\sqrt{x^2+1})^4. \tag{4.9}$$

We expand the integrand of $g(m)$,

$$\ln(1-Be^{-\alpha\chi x})=\ln(1-B)+\frac{\alpha\chi x B}{1-B}+\cdots. \tag{4.10}$$

Note that this is as far as we can expand this way, since the next term of the $\alpha$ expansion gives a divergent contribution (an alternative method which avoids some divergences but is somewhat more cumbersome is the method employed in Appendix A of Ref. [23] where the corrections are calculated without the use of the Euler-Maclaurin formula).

Consider the first terms of the expansion (4.10) [we dub the terms of $g(m)$ from the expansion $g_I(m), g_{II}(m),\ldots$],

$$g_I(m)=\chi^2\int_{\mu/\chi}^{\infty} dx x\ln[1-(x-\sqrt{x^2+1})^4]. \tag{4.11}$$

This integral can be evaluated explicitly (a similar integral was evaluated in Ref. [23] where the lower limit was approximated as zero). Perform the substitution $x=\sinh u$. Then we may write

$$g_I(m)=\frac{\chi^2}{4}\int_{u_0}^{\infty} du(e^{2u}-e^{-2u})\ln(1-e^{-4u}) \tag{4.12a}$$

with

$$u_0=\operatorname{arsinh}\frac{\mu}{\chi}=\frac{1}{2}\ln\left(\frac{\sqrt{\bar{\varepsilon}\mu+1}+\sqrt{\mu}}{\sqrt{\bar{\varepsilon}\mu+1}-\sqrt{\mu}}\right). \tag{4.12b}$$

With the substitution $y=e^{-2u}$,

$$g_I(m)=\frac{\chi^2}{8}\int_0^{y_0} dy(y^{-2}-1)\ln(1-y^2), \tag{4.13a}$$

where

$$y_0=e^{-2u_0}=\frac{\sqrt{\bar{\varepsilon}\mu+1}-\sqrt{\mu}}{\sqrt{\bar{\varepsilon}\mu+1}+\sqrt{\mu}}$$
$$=1-2\sqrt{\mu}+2\mu+(\bar{\varepsilon}-2)\mu^{3/2}+\cdots. \tag{4.13b}$$

The integral is straightforward to evaluate and the result is

$$g_I(m)=-\frac{\chi^2}{8}\left[\left(\frac{1}{y_0}+y_0\right)\ln(1-y_0^2)-2y_0+2\ln\frac{1+y_0}{1-y_0}\right]. \tag{4.14}$$

We expand this in powers of $\mu$ and find that the terms $\propto\mu^{3/2}$ cancel, consistent with the small-$x$ dependence of the integrand of $g_I(m)$. We are left with

$$g_I(m)=-\frac{\mu}{4}(2\ln2-1)-\frac{\mu^2}{4}[\ln4\mu+\bar{\varepsilon}(2\ln2-1)]$$
$$+\frac{2}{3}\mu^{5/2}+O(\mu^3). \tag{4.15}$$

Comparing with Eq. (2.5) we see

$$c_1=-\frac{t}{4}(2\ln2-1)\ \text{and}\ c_{2l}=-\frac{t^2}{4}, \tag{4.16}$$

while the dependence on $\bar{\varepsilon}$ only enters in the $c_2$ term $\sim m^2$ which does not contribute to the Euler-Maclaurin formula. The temperature correction to first order in $\alpha$ is thus

$$\Delta F_I^{\mathrm{TE}}\approx\frac{(4\pi\sigma)^3 t^2}{4\pi^2}\left[\frac{2\ln2-1}{48}-\frac{\Psi t}{4}\right]. \tag{4.17}$$

We see that the leading term conforms with Eq. (4.3) when Eq. (4.4a) is inserted. The first term beyond those calculated is proportional to $T^{7/2}$ according to Eq. (4.15). In SI units with (2.13b),

$$\Delta F_I^{\mathrm{TE}}\approx\frac{\sigma^{\mathrm{SI}}(k_{\mathrm{B}}T)^2}{48\varepsilon_0\hbar c^2}(2\ln2-1)-\frac{\zeta(3)(k_{\mathrm{B}}T)^3}{8\pi\hbar^2c^2}. \tag{4.18}$$

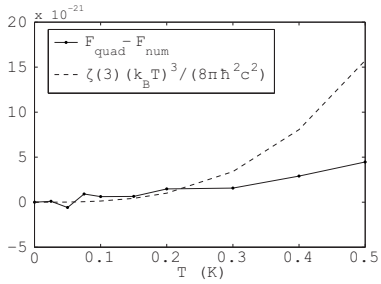


FIG. 4. The difference between the numerically calculated free energy and the quadratic $T$ term of Eq. (4.18) (equal to the difference between the graphs in Fig. 3) plotted against the absolute value of the $T^3$ term of Eq. (4.18).

The $T^3$ term of Eq. (4.18) has the same form as that found for ideal metals in the limit $aT \ll 1$ [29,30]. A similar term is present in Eq. (3.36). [Note that the $T^3$ correction for the TM mode is not fully accounted for therein.] A numerical comparison of this term with the difference between the graphs in Fig. 3 is shown in Fig. 4. It shows that the $T^3$ coefficient in Eq. (4.18) is the right order of magnitude, but the numerical precision is not sufficient to draw definite conclusions about its accuracy at this time.

### B. First-order correction to expansion (4.10)

The first-order correction term in Eq. (4.10) is easily calculated with a similar scheme. We have

$$g_{II}(m) = \alpha\chi^3 \int_{\mu/\chi}^{\infty} dx \frac{x^2 B}{1-B} = \frac{\alpha\chi^3}{4} \int_{\mu/\chi}^{\infty} dx \frac{x(x-\sqrt{x^2+1})^2}{\sqrt{x^2+1}}. \tag{4.19}$$

The procedure for solving this integral is as before. Substitute $x = \sinh u$ to obtain with a little shuffling

$$g_{II}(m) = \frac{\alpha\chi^3}{8} \int_{u_0}^{\infty} du e^{-u}(1-e^{-2u}). \tag{4.20}$$

With the substitution $z = e^{-u}$ this becomes very simple,

$$g_{II}(m) = -\frac{\alpha\chi^3}{8} \int_{z_0}^{0} dz(1-z^2) = \frac{\alpha\chi^3}{8}\left(z_0 - \frac{z_0^3}{3}\right) \tag{4.21}$$

with

$$z_0 = e^{-u_0} = \left(\frac{\sqrt{\bar{\varepsilon}\mu+1}-\sqrt{\mu}}{\sqrt{\bar{\varepsilon}\mu+1}+\sqrt{\mu}}\right)^{1/2}$$

$$= 1 - \sqrt{\mu} + \frac{\mu}{2} + \frac{1}{2}(\bar{\varepsilon}-1)\mu^{3/2} + \cdots. \tag{4.22}$$

Thus we find the $\mu$ expansion of $g_{II}(m)$,

$$g_{II}(m) = \frac{\alpha}{8}\left(\frac{2}{3}\mu^{3/2} - (2-\bar{\varepsilon})\mu^{5/2} + \cdots\right). \tag{4.23}$$

Hence, with Eqs. (2.10) and (4.8a),

$$\Delta F_{II}^{\mathrm{TE}} = \frac{(4\pi\sigma)^3\alpha}{48\pi^2}\Phi t^{5/2} + O(t^{7/2}), \tag{4.24a}$$

or in SI units with $\Phi = \zeta(-\frac{3}{2})$,

$$\Delta F_{II}^{\mathrm{TE}} = \frac{\sqrt{2\pi}\zeta\left(-\frac{3}{2}\right)a(\sigma^{\mathrm{SI}}/\epsilon_0)^{3/2}}{6\hbar^{3/2}}(k_B T)^{5/2} + \cdots. \tag{4.24b}$$

Comparison with Eq. (4.4b) shows full agreement with the result for metals ($\bar{\varepsilon}=1$).

It is worth noting that while the next-to-leading temperature correction is of order $T^{5/2}$, the term $\propto T^3$ in Eq. (4.18) dominates it with respect to $\alpha$. Thus in the small $\sigma$ limit the $T^{5/2}$ dependency becomes all but imperceptible.

## CONCLUSIONS

We have worked out the two leading terms of the temperature correction to the Casimir-Lifshitz free energy at low temperatures between poor conductors obeying a Drude-type dispersion relation. We have assumed that the materials have a small residual conductivity (compared to the reciprocal of the interplate separation) which is finite and constant with respect to temperature and frequency near $T=0$.

The calculation for the TM mode complements that of Ref. [19] where the temperature correction for free energy between two dielectrics of zero conductivity was calculated. Both the TE and TM free energy temperature corrections are quadratic to leading order. To the extent of our computations, the TM mode has integer powers of $T$ beyond the leading, whereas the TE mode has both integer and half-integer powers. The temperature anomaly reviewed in Sec. I occurs when the transition from finite to zero conductivity happens at exactly $T=0$, and while the analysis presented here does not resolve the anomaly, it is of interest to know the low-temperature behavior of the free energy in each of the two cases.

Note furthermore that the effects of the static dielectric permittivity $\bar{\varepsilon}$ only enters to order $T^4$ for the TM mode and order $T^{7/2}$ for the TE mode. The fact that the coefficient of the term $T^{7/2}$ appears to depend on $\bar{\varepsilon}$ is noteworthy since only integer powers of $T$ were reported in Ref. [19], although seeing as we have not calculated the coefficient here it is possible that cancellations occur.

Our calculations are delicate since they rely on the relative smallness of different parameters simultaneously. We have assumed the parameter $t$ (essentially temperature $T$ divided by conductivity $\sigma$) small while at the same time letting $\sigma$ be small compared to the inverse of the separation $a$. This is the reason why the leading order temperature corrections in Eq. (3.31) appear to diverge as $\sigma$ vanishes. On a deeper level these subtleties stem from noncommuting limits in the Lifshitz formalism which are the cause of anomalies such as that reviewed in Sec. I. Another curious property both of the present calculations and those of Geyer, Klimchitskaya, and Mostepanenko [19] is that the free energy corrections of order in $T$ just beyond what we have considered here appear to

diverge as $\bar{\varepsilon}\to\infty$, as indicated for example by Eqs. (3.34) and (4.23). This limit would *a priori* be expected to yield the ideal metal limit. Such phenomena should be addressed in future studies in the effort to achieve full understanding of the low-temperature behavior of the Casmir force and free energy.

The asymptotics of the Lifshitz formula as frequency and temperature approach zero are fraught with inherent subtleties both mathematical and physical. While the method employed herein is highly useful for its simplicity and transparency, it has limitations because the functions involved are not analytic in the limits considered and noninteger powers and logarithms enter. Physically we have assumed herein a model which may represent certain physical systems, but avoids the temperature behavior which leads to the anomaly reviewed in Sec. I. It also neglects effects which may be of importance, such as spatial dispersion, a subject which has been extensively investigated over the years [31–34]. A theoretical effort to attempt to describe the screening effects and dielectric response of the vanishing density of free charges in insulators near zero temperature involving all important physical effects will likely be required in the future and will hopefully provide the resolution of the anomaly for dielectrics.

## ACKNOWLEDGMENTS

K.A.M.'s research is supported in part by a grant from the US National Science Foundation (Grant No. PHY-0554926) and by a grant from the US Department of Energy (Grant No. DE-FG02-04ER41305). S.A.E. acknowledges the University of Oklahoma for its hospitality while working on this project. We have benefited from discussions and suggestions from Emilio Elizalde, Klaus Kirsten, and Jef Wagner.

## APPENDIX: BOREL SUMMATION

The Borel sum of the divergent series $\Sigma_{n=0}^{\infty}a_n$ exists (Ref. [35], Sec. 8.2) if the function

$$\phi(x)=\sum_{n=0}^{\infty}\frac{a_n x^n}{n!} \tag{A1}$$

is convergent for sufficiently small $x$ and the integral

$$\mathcal{B}(x)=\int_0^{\infty}dt e^{-t}\phi(xt) \tag{A2}$$

exists. Then the Borel sum is $\Sigma_{n=0}^{\infty}a_n=\mathcal{B}(1)$. Consider the quantity $\Psi$ defined in Eq. (2.11a) and consider the term

$$\tilde{\Psi}=\sum_{n=2}^{\infty}\frac{B_{2n}(2n-4)!}{(2n)!}=\sum_{n=4}^{\infty}\frac{B_n(n-4)!}{n!} \tag{A3}$$

(the latter equality follows from $B_{2n+1}=0$, $n=1,2,\ldots$). Letting $a_{n-4}=B_n(n-4)!/n!$ we obtain

$$\phi(x)=\sum_{n=0}^{\infty}\frac{B_{n+4}x^n}{(n+4)!}=\frac{1}{x^4}\left[\frac{x}{e^x-1}-1+\frac{x}{2}-\frac{x^2}{12}\right], \tag{A4}$$

where the identity $\Sigma_{n=0}^{\infty}B_n x^n/n!=x/(e^x-1)$ was used. The Borel sum

$$\tilde{\Psi}=\mathcal{B}(1)=\int_0^{\infty}\frac{dte^{-t}}{t^4}\left[\frac{t}{e^t-1}-1+\frac{t}{2}-\frac{t^2}{12}\right] \tag{A5}$$

is now possible to evaluate analytically (the divergence in the lower limit is illusory because the expression in brackets is of order $t^4$) to find the desired value as $\Psi=1/36-2\tilde{\Psi}=\zeta(3)/(4\pi^2)$. A similar numerical procedure using Eqs. (A1) and (A2) will give the value of $\Phi$, which as noted in the text has a well-known asymptotic expression.

An alternative and equivalent approach which is most often simpler is to sum each term of the expansion of $g(m)$ in Eq. (2.5) directly (disregarding the zero temperature contribution) and obtain finite values of the terms of the temperature expansion by means of $\zeta$ regularization [36]. Such a procedure immediately yields $\Phi=\zeta(-\frac{3}{2})$ by the definition of the $\zeta$ function as the analytic continuation of $\zeta(s)=\Sigma_{m=1}^{\infty}m^{-s}$. Likewise the value of $\Psi$ can easily be found by comparison with the asymptotic series expansion of the derivative of $\zeta(s)$

$$\zeta'(s)=-\sum_{n=1}^{\infty}n^{-s}\ln n, \tag{A6}$$

whereby $\Psi=-\zeta'(-2)=\zeta(3)/4\pi^2$. The same reasoning also yields the coefficient of the $c_1$ term of Eq. (2.10) directly as $\zeta(-1)=-1/12$. We thank Emilio Elizalde for alerting us to this point.

[1] H. B. G. Casimir, Proc. K. Ned. Akad. Wet. **51**, 793 (1948).
[2] E. M. Lifshitz, Zh. Eksp. Teor. Fiz. **29**, 94 (1956).
[3] S. K. Lamoreaux, Phys. Rev. Lett. **78**, 5 (1997).
[4] U. Mohideen and A. Roy, Phys. Rev. Lett. **81**, 4549 (1998).
[5] A. Roy, C.-Y. Lin, and U. Mohideen, Phys. Rev. D **60**, 111101(R) (1999).
[6] B. W. Harris, F. Chen, and U. Mohideen, Phys. Rev. A **62**, 052109 (2000).
[7] T. Ederth, Phys. Rev. A **62**, 062104 (2000).
[8] F. Chen, U. Mohideen, G. L. Klimchitskaya, and V. M. Mostepanenko, Phys. Rev. Lett. **88**, 101801 (2002).
[9] H. B. Chan, V. A. Aksyuk, R. N. Kleiman, D. J. Bishop, and F. Capasso, Phys. Rev. Lett. **87**, 211801 (2001); Science **291**, 1941 (2001).
[10] G. Bressi, G. Carugno, R. Onofrio, and G. Ruoso, Phys. Rev. Lett. **88**, 041804 (2002).
[11] V. B. Bezerra, R. S. Decca, E. Fischbach, B. Geyer, G. L. Klimchitskaya, D. E. Krause, D. López, V. M. Mostepanenko, and C. Romero, Phys. Rev. E **73**, 028101 (2006).
[12] R. S. Decca, D. López, E. Fischbach, G. L. Klimchitskaya, D. E. Krause, and V. M. Mostepanenko, Ann. Phys. (N.Y.) **318**, 37 (2005).
[13] J. Schwinger, L. L. DeRaad, Jr., and K. A. Milton, Ann. Phys. (N.Y.) **115**, 1 (1978).

[14] M. Boström and Bo E. Sernelius, Phys. Rev. Lett. **84**, 4757 (2000).
[15] S. K. Lamoreaux, Phys. Today **60**(2), 40 (2007).
[16] G. L. Klimchitskaya and V. M. Mostepanenko, Phys. Rev. A **63**, 062108 (2001).
[17] I. Brevik, S. A. Ellingsen, and K. A. Milton, New J. Phys. **8**, 236 (2006).
[18] G. L. Klimchitskaya and V. M. Mostepanenko, Contemp. Phys. **47**, 131 (2006).
[19] B. Geyer, G. L. Klimchitskaya, and V. M. Mostepanenko, Phys. Rev. D **72**, 085009 (2005).
[20] G. L. Klimchitskaya, B. Geyer, and V. M. Mostepanenko, J. Phys. A **39**, 6495 (2006).
[21] B. Geyer, G. L. Klimchitskaya, and V. M. Mostepanenko, Int. J. Mod. Phys. A **21**, 5007 (2006).
[22] G. L. Klimchitskaya and B. Geyer, J. Phys. A **41**, 164014 (2008).
[23] J. S. Høye, I. Brevik, S. A. Ellingsen, and J. B. Aarseth, Phys. Rev. E **75**, 051127 (2007).
[24] M. Abramowitz and I. A. Stegun, *Handbook of Mathematical Functions* (Dover, New York, 1964).
[25] S. A. Ellingsen, e-print arXiv:quant-ph/0710.1015, Phys. Rev. E (to be published); F. Intravaia and C. Henkel, J. Phys. A **41**, 164018 (2008).
[26] L. Lewin, in *Structural Properties of Polylogarithms*, edited by L. Lewin (American Mathematical Society, Providence, 1991).
[27] F. Chen, G. L. Klimchitskaya, V. M. Mostepanenko, and U. Mohideen, Phys. Rev. B **76**, 035338 (2007).
[28] I. Brevik, S. A. Ellingsen, J. S. Høye, and K. A. Milton, J. Phys. A **41**, 164017 (2008).
[29] J. S. Høye, I. Brevik, J. B. Aarseth, and K. A. Milton, Phys. Rev. E **67**, 056116 (2003), Sec. III.
[30] K. A. Milton, *The Casimir Effect: Physical Manifestations of the Zero-Point Energy* (World Scientific, Singapore, 2001), p. 56.
[31] G. Barton, Rep. Prog. Phys. **42**, 963 (1979).
[32] Bo E. Sernelius, Phys. Rev. B **71**, 235114 (2005).
[33] V. B. Svetovoy and R. Esquivel, J. Phys. A **39**, 6777 (2006).
[34] R. Esquivel-Sirvent, C. Villarreal, W. L. Mochán, A. M. Contreras-Reyes, and V. B. Svetovoy, J. Phys. A **39**, 6323 (2006).
[35] C. M. Bender and S. A. Orszag, *Advanced Mathematical Methods for Scientists and Engineers* (Springer, New York, 1999).
[36] E. Elizalde, S. D. Odintsov, A. Romeo, A. A. Bytsenko, and S. Zerbini, *Zeta Regularization Techniques with Applications* (World Scientific, Singapore, 1994).

# Article [d]

***Nernst's heat theorem for Casimir-Lifshitz free energy***

S.A. Ellingsen

Physical Review E **78**, 021120 (2008)

# Nernst's heat theorem for Casimir-Lifshitz free energy

Simen A. Ellingsen*
*Department of Energy and Process Engineering, Norwegian University of Science and Technology, N-7491 Trondheim, Norway*
(Received 4 October 2007; revised manuscript received 5 May 2008; published 18 August 2008)

Consideration of the Lifshitz expression for the Casimir free energy on the real frequency axis rather than the imaginary Matsubara frequencies as is customary sheds light on the ongoing debate regarding the thermodynamical consistency of this theory in combination with common permittivity models. It is argued that when permittivity is temperature independent over a temperature interval including zero temperature, a cavity made of causal material with continuous dispersion properties separated by vacuum cannot violate Nernst's theorem (the third law of thermodynamics). The purported violation of this theorem pertains to divergencies in the double limit in which frequency and temperature vanish simultaneously. While any model should abide by the laws of thermodynamics within its range of applicability, we emphasize that the Nernst heat theorem is a relevant criterion for choosing among candidate theories only when these theories are fully applicable at zero temperature and frequency.

DOI: 10.1103/PhysRevE.78.021120 PACS number(s): 05.30.−d, 12.20.Ds, 42.50.Nn, 65.40.G−

## INTRODUCTION

Since Boström and Sernelius first predicted the existence of large thermal corrections to the Casimir force in 2000 [1], controversies over the thermal behavior of this effect, which in its most typical embodiment may be seen as the attraction between macroscopic objects due to zero-point fluctuations of the quantum vacuum, have been extensively covered in the published literature. The use of the Drude model to describe dielectric permittivity employed in [1] was soon criticized on thermodynamical grounds [2]. The reason was that in the case of a perfect crystal lattice, when all dissipation is due to scattering of electrons on thermal phonons, the Casimir free energy as calculated with the Lifshitz formula appears to violate Nernst's heat theorem which states that entropy should vanish as $T\rightarrow 0$. The Drude model was defended by other authors [3–5] who argued that, since the Drude model offers a better description of impure metals, and since real metal samples always have impurities, the Drude model must be employed. It was shown in [6] and recently in a more extensive treatment [7] that the free energy with Drude permittivity is quadratic in $T$ for small temperatures when impurities are present. No consensus has yet been reached on the important physical question of why Casimir force predictions for the perfect lattice model, important in solid state physics, differ significantly from those pertaining to real metals with a very small but nonzero concentration of imperfections.

Recently, a somewhat analogous problem was brought forth for dielectrics with a small conductivity for finite $T$ which vanishes at $T=0$ [8]. While the purported violation in the case of Drude metals referred to the transverse electric (TE) mode, this time the bother appears to be a discontinuity in the transverse magnetic (TM) Fresnel reflection coefficient giving rise to nonzero entropy at zero temperature. The problem was recently argued to extend to insulators and intrinsic and lightly doped semiconductors as well as Mott-Hubbard semiconductors, and indeed the permittivity contribution from Debye rotation of molecular dipoles [9].

According to the argument presented herein both the Drude model and the dielectric permittivity model with conductivity included belong to a group of permittivities which cannot violate Nernst's theorem when permittivity can be regarded as temperature invariant in a range of temperatures near and including $T=0$. While the present paper does not aspire to solve the physical question of how to take into account the presence of a small conductivity in dielectrics when substituted into the Lifshitz formula, it seeks to illuminate the ever recurring question of thermodynamical consistency. It has previously been shown [10] by use of the Euler-Maclaurin (or equivalently Abel-Plana) formula that, for Fresnel reflection coefficients which are continuous functions of *imaginary* frequencies in the limit $T\rightarrow 0$, Nernst's theorem is satisfied. An exploration of Casimir entropy in the formalism of surface modes was undertaken independently of this work by Intravaia and Henkel [11] whose conclusions accord with ours. By a method of summation of the eigenmodes of the vacuum between two plates they demonstrate that Nernst's theorem can be broken between metal plates only for temperature-dependent relaxation such as in a perfect and infinitely large metal lattice.

This paper demonstrates a similar result using the real frequency Lifshitz formalism between plates of a generic nonmagnetic material whose permittivity satisfies a small set of criteria. The real frequency formalism is more complicated and less elegant, but with the advantage of a more direct physical interpretation. Finally, a discussion of the physical implications of the mathematical limits involved is given. In particular, we emphasize the importance of assessing when Nernst's theorem, which concerns zero temperature, can be used to inform finite-temperature physics.

## I. FREE ENERGY AND ENTROPY AT REAL FREQUENCIES

The Lifshitz expression [12] for the free energy per unit transverse area between two identical dielectric plates separated by vacuum is in general of the form

*simen.a.ellingsen@ntnu.no

 

$$\mathcal{F}(a,T) = \int_0^\infty d\omega \coth\left(\frac{\omega}{2\omega_T}\right)\mathrm{Im}\{\phi(\omega,T)\}, \tag{1}$$

where $\omega_T \equiv k_B T/\hbar$ and $\phi(\omega,T)$ is the zero-temperature integrand

$$\phi(\omega,T) = \frac{\hbar}{4\pi^2}\int_0^\infty dk_\perp k_\perp \sum_{q=\mathrm{TE}}^{\mathrm{TM}} \ln D_q(\omega, c\mathbf{k}_\perp, T), \tag{2}$$

wherein

$$D_q \equiv 1 - r_q^2 \exp(-2\kappa_0 a), \tag{3a}$$

$$r_{\mathrm{TE}} = \frac{\kappa_0 - \kappa}{\kappa_0 + \kappa}, \quad r_{\mathrm{TM}} = \frac{\epsilon\kappa_0 - \kappa}{\epsilon\kappa_0 + \kappa}. \tag{3b}$$

We have assumed $\mu=1$ everywhere for simplicity, $\epsilon$ is the permittivity of the dielectric relative to vacuum, and

$$\kappa_0 = (k_\perp^2 - \omega^2/c^2)^{1/2}, \quad \kappa = (k_\perp^2 - \epsilon\omega^2/c^2)^{1/2}. \tag{4}$$

We assume that $\epsilon$ does not depend on transverse momentum, thus neglecting any nonlocal effects and furthermore that it is a generalized susceptibility and obeys causality, which implies in particular that [13] (1) $\epsilon(-\omega^*)=\epsilon^*(\omega)$; (2) $|\mathrm{Im}\{\epsilon(\omega)\}|>0$ on the entire real frequency axis except at $\omega=0$ where it may be undefined. In general $\epsilon$ is also temperature dependent, making for the temperature dependence of $\phi(\omega,T)$. The complex conjugate is denoted with an asterisk and we will consider only real frequencies henceforth. One might furthermore impose the physically reasonable demand that (3) $\epsilon(\omega)$ is continuous and $|\epsilon(\omega)|<\infty$ for all real frequencies except possibly $\omega=0$.

The function $\phi$ obeys the symmetry property $\phi(-\omega)=\phi^*(\omega)$ for real frequencies,[1] hence the real part of $\phi(\omega)$ is even with respect to $\omega$ while its imaginary part is odd. This allows us to write $\mathcal{F}$ in a form that makes the mathematical discussion in the following somewhat more transparent. Since both $\mathrm{Im}\phi$ and $\coth(\omega/2\omega_T)$ are odd functions of $\omega$, the integrand of (1) is even and we can let the $\omega$ integral run from $-\infty$ to $\infty$ and divide by 2. Adding the real part of $\phi$ by substituting $\mathrm{Im}\phi \to \phi/i$ will make no difference, since it makes for an odd integrand term which vanishes under symmetrical integration, so

$$\mathcal{F}(a,T) = \frac{1}{2i}\int_{-\infty}^\infty d\omega \coth\left(\frac{\omega}{2\omega_T}\right)\phi(\omega,T) \tag{5}$$

is equivalent to (1).

Assume for the moment that $\epsilon$, and hence $\phi$, is invariant with temperature over at least a finite range of small temperatures including $T=0$. In this case the temperature dependence of $\mathcal{F}(T)$ can be treated very simply when $T$ is in this range, since the $T$ dependence now resides only in the factor $\coth(\omega/2\omega_T)$. From thermodynamics the Casimir entropy in the cavity, $S$, is given as

$$S = -\frac{\partial}{\partial T}\mathcal{F}(T), \tag{6}$$

so if one were able to interchange integration and differentiation with respect to $T$, one could write

$$S = -\frac{1}{2i}\int_{-\infty}^\infty d\omega\, \phi(\omega)\frac{d}{dT}\coth\left(\frac{\omega}{2\omega_T}\right)$$
$$= -\frac{\hbar}{ik_B T^2}\int_{-\infty}^\infty d\omega\, \phi(\omega)\frac{\omega\exp(\omega/\omega_T)}{[\exp(\omega/\omega_T)-1]^2}. \tag{7}$$

For any finite $\omega$ the integrand of (7) vanishes extremely fast, as $\exp(-\hbar|\omega|/k_B T)$, when $T\to 0$. This demonstrates the finding of Torgerson and Lamoreaux [14] that temperature corrections are important only for frequencies below $\omega_T$, which is a very low frequency even at room temperature ($\sim 10^{13}$ rad/s). At $\omega=0$ (and finite $T$) the rightmost fraction in (7) has a simple pole, yet only the imaginary part of $\phi(\omega)$ contributes to (7), which is zero here since $\mathrm{Im}\{\phi\}$ is an odd function of $\omega$, removing this pole. Thus, in the limit $T\to 0$, entropy vanishes as it should and the third law of thermodynamics is obeyed (there are subtleties pertaining to the TM mode as will be discussed in the following).

Two questions arise from this consideration, Under what circumstances may differentiation be interchanged with integration? And what happens if one or more parameters of $\epsilon(\omega)$ are temperature dependent all the way down to zero temperature?

## II. TEMPERATURE-INDEPENDENT $\epsilon(\omega)$

We will treat the first question first. Leibnitz' integral rule for improper integrals,

$$\frac{d}{dy}\int_{x_0}^\infty dx\, f(x,y) = \int_{x_0}^\infty dx \frac{d}{dy} f(x,y), \tag{8}$$

is always valid when ([15] §4.44) (i) $f(x,y)$ and $df(x,y)/dy$ are both continuous on $x\in[x_0,\infty\rangle$ and the relevant interval of values of $y$; (ii) the integral on the left exists; and (iii) the integral on the right converges uniformly. The generalization to integrals with both limits infinite is trivial.

To make our considerations more concrete, let us concentrate on some permittivity models which are in common use:

$$\epsilon(\omega) = 1 - \frac{\omega_p^2}{\omega(\omega + i\nu)}, \tag{9}$$

$$\epsilon(\omega) = 1 + \frac{\epsilon_\infty - 1}{1 - \omega^2/\omega_0^2 - i\gamma\omega/\omega_0^2} + \frac{i\sigma}{\epsilon_0\omega}, \tag{10}$$

of which the former is the Drude model for metals, and the latter describes a semiconductor. Here $\omega_p$ is the plasma frequency, $\nu$ the relaxation frequency, $\epsilon_0$ the vacuum permittivity, and $\epsilon_\infty$, $\gamma$, and $\omega_0$ material parameters. $\sigma$ is the dc conductivity of the semiconductor. Some common models which obey criterion 1 but not 2 are

[1] This is easily argued: Because $\epsilon$ satisfies this relation by assumption, so, one finds, does $D_q$. The logarithm of a complex function is infinitely degenerate, and for $\ln D_q$ to give meaning we should interpret it as its principal value, $\ln D_q \equiv \ln|D_q| + i\,\mathrm{Arg} D_q$, which incidentally also satisfies $\ln D_q(-\omega)=[\ln D_q(\omega)]^*$.

$$\epsilon(\omega) = 1 - \frac{\omega_p^2}{\omega^2}, \tag{11}$$

$$\epsilon(\omega) = 1 + \frac{\epsilon_\infty - 1}{1 - \omega^2/\omega_0^2}, \tag{12}$$

the plasma model[2] for metals and a model of dielectrics with $\delta$ function dissipation at $\omega=\omega_0$ [17]. Notice that (9) and (10) obey criteria 1–3.

### A. Propagating and evanescent waves

One notices that we seem to run into trouble with the continuity criterion at $|\omega|=ck_\perp$, where $\kappa_0=0$, since, when regarded as a double integral, (5) seems at first glance to imply integration *across* the lines $\omega=\pm ck_\perp$, which would cause trouble with continuity: one sees from (3a) that $D_q=0$ for $\kappa_0=0$; hence the real part of $\ln D_q$ is undefined and the imaginary part turns out to be discontinuous as these lines are crossed.

The problem can be avoided, however. Let us define $\beta=k_\perp c/\omega$ for short. For positive frequencies, $\beta=1$ is the limit in which the electromagnetic fields in the cavity travel parallel to the plates and become evanescent in vacuum as the $\beta=1$ barrier is crossed, a limit whose discontinuous properties are physically obvious: the waves just on the propagating side ($ck_\perp$ just smaller than $\omega$) travel through the system just gracing the surfaces, while the fields on the evanescent side stay *on* the surfaces; they are qualitatively different phenomena and the transition from one to the other can be expected to be discontinuous.[3] Negative frequencies have no direct physical meaning; hence the terms "propagating" and "evanescent" must be understood in a mathematical sense here, defined by $|\beta|<1$ and $|\beta|>1$, respectively.

In the original Lifshitz paper [12], the $\mathbf{k}_\perp$ integral is split automatically into propagating and evanescent parts by substituting $p=i\kappa_0 c/\omega$. Propagating contributions correspond to integrating $p$ from 1 to 0 and evanescent to an integral from $i0$ to $i\infty$, thus avoiding the problem. We notice furthermore that the issues related to $|\beta|=1$ occur for *any* choice of $\epsilon(\omega)$ and hence can have nothing to do with the problems with Nernst's theorem, which all concern particular permittivity models.

### B. Continuity

In the classical treatment by Casimir, the vacuum energy shift was found by summing over the cavity modes of the system [18], a method developed further by van Kampen *et al.* by use of the so-called generalized argument principle [19] and elaborated by Barash and Ginzburg [20]. The normal modes of the cavity solve the characteristic equation of the set of electromagnetic boundary conditions which reduce to the equation $D_q=0$. At these frequencies $\varphi(\omega)$ would have poles which would cause trouble with continuity.

With permittivity models such as (9) and (10) where dissipation is included [i.e., $\epsilon(\omega)$ has a nonzero imaginary part], $D(\omega,k_\perp)=0$ has no real-frequency solutions[4] except possibly $\omega=0$ since $r_q\neq 1$ everywhere. The same is the case with (12) if an imaginary term is inserted in the denominator as in (10) (otherwise $|r_q|=1$ at $\omega=\omega_0$). The real-valued permittivities as given in (11) and (12) cause $r_{\mathrm{TM}}$ to diverge where $\epsilon\kappa_0+\kappa=0$, however, in transgression of the continuity criterion. We conclude that the continuity of $\phi(\omega)$ is ensured for all $\omega\neq 0$ so long as $r_q^2$ is finite, continuous and $\neq 1$, sufficient criteria for which are that $\epsilon(\omega)$ satisfies criteria 1–3.

What remains is the point $\omega=0$. *A priori*, this is the interesting limit, since when $T$ is very small, the coth function in (5) differs from unity only very close to zero frequency. As is well known, reflection coefficients are occasionally ill defined in the limit where $\omega$ and $ck_\perp$ both approach zero, as is the case for the Drude model TE reflection coefficient, for example. $r_q^2$ is always *bounded*, however, so the integrand of $\phi(\omega)$ approaches zero in this limit due to the factor $k_\perp$ stemming from the isotropic infinitesimal $d^2k_\perp=2\pi k_\perp dk_\perp$ for any $\beta\neq 1$. Hence $\phi(\omega)$ is continuous for all $\omega$ if $\epsilon(\omega)$ obeys criterion 3.

A more serious problem is caused by the simple poles of $\coth(\omega/2\omega_T)$ and its $T$ derivative at $\omega=0$. As argued previously, the imaginary part of $\phi(\omega)$ is zero at $\omega=0$, so the integrand of (7) does not diverge, but is in some cases finite in this limit. For sufficiently small $\omega$ and finite $\sigma$, (9) and (10) both have the form $\epsilon\sim A+iB/\omega$ where $A$ and $B$ are constants, while if $\sigma=0$ (10) instead has the form $\epsilon\sim A+iB\omega$. In both cases the imaginary part of $r_{\mathrm{TE}}^2$ falls off quickly, as $\omega^3$ and $\omega^5$, respectively, but when $A\neq 1$, $\mathrm{Im}\{r_{\mathrm{TM}}^2\}$ decreases only linearly. One easily verifies that, with respect to $\omega$, $\mathrm{Im}\{\phi(\omega)\}\propto\mathrm{Im}\{r_q^2(\omega)\}$ to leading order; hence the TM mode term of $\phi(\omega)$ is proportional to $\omega$ in the above mentioned cases.

To see how this is troublesome, consider the functions

$$H(x,t) = x\frac{e^{x/2t}+e^{-x/2t}}{e^{x/2t}-e^{-x/2t}}, \tag{13}$$

$$I(x,t) = \frac{x^2 e^{x/t}}{t^2(e^{x/t}-1)^2}, \tag{14}$$

which are essentially (up to a constant factor) the integrands of (5) and (7), respectively, when $\phi(\omega)\propto\omega$; here $x$ and $t$ are suitably nondimensionalized frequency and temperature, respectively, so that $\omega/\omega_T=x/t$. Notice that $\partial H/\partial t=2I$. Equations (13) and (14) are plotted in Fig. 1 for $x$ and $t$. If we define $H(0,0)$ to be its limiting value 0, the integrand of (5) is continuous for all $\omega$ and $T$ as we hoped, but its $T$ derivative [essentially $I(x,t)$] is not. As $T\to 0$, the integrand of (7) becomes a spike of finite height and zero width. The integral past this spike is clearly zero (so the entropy would be zero as concluded above), but we run into trouble with the continuity condition. Were the limit $T\to 0$ to be taken prior to

[2] A generalized, causal form of the plasma model was recently proposed [16].

[3] Due to the nonzero imaginary part of $\epsilon$ there are no similar problems for $\kappa$ near $ck_\perp=|\omega|\sqrt{\mathrm{Re}\{\epsilon(\omega)\}}$.

[4] Sernelius has recently shown how the normal mode interpretation may still be applied [21].

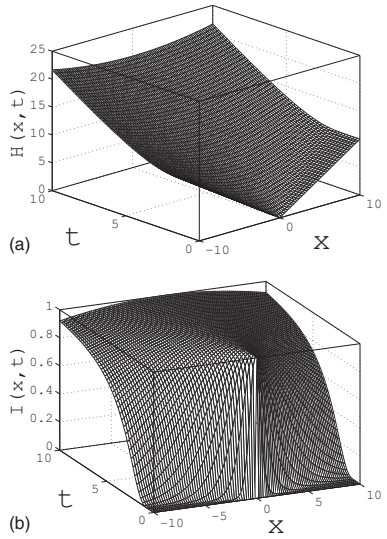


FIG. 1. Equations (13) and (14) as functions of $x$ and $t$. The functions $H$ and $I$ are essentially the integrands of (5) and (7) when $\phi(\omega) \propto \omega$.

integration, $I(0,0)$ would be zero instead, and $I$ would be continuous with respect to $x$ but discontinuous with respect to $t$.

Physically it does not matter whether $I(0,0)$ is 1, 0, or something in between, since the contribution from this single point is zero in either case. Hence this one point should not matter. Formally we could state this by excluding the point $\omega=0$ from the $\omega$ integrals (5) and (7). Furthermore it is well known that the notion that *every* $\epsilon(\omega)$ in the form $A+iB\omega$ or $A+iB/\omega$ would violate Nernst's theorem is incorrect; on the contrary, we argue that so long as $A$ and $B$ are temperature independent, none of these will. Using an analytical software such as MAPLE, it is quick to check that integration of $H(x,t)$ with respect to $x$ followed by differentiation with respect to $t$ gives the same result as when the order of the operations is reversed. While this argument is not rigorous it should convince the reader that the continuity issues at zero temperature and frequency can be avoided since this point is of no physical significance.

A formally similar problem emerges when the permittivity is temperature dependent all the way down to zero temperature, as we will see, and in the latter case the singularity at zero temperature and frequencies *does* appear to give a physical contribution and cannot be ignored.

### C. Uniform convergence

An improper integral (8) is said to converge uniformly ([15] §4.42) if $\forall\ \varepsilon>0$ there exists a number $a_0>0$ independent of $T$ such that for all $a,a' \geqslant a_0$,

$$\left| \int_a^{a'} dx\, f(x,T) \right| < \varepsilon.$$

Let us briefly analyze the behavior of $\ln D_q(\omega,k_\perp)$ as $|\omega|$ and $k_\perp$ approach infinity. The existence of the free energy integral (5) itself is well known; hence we need but check explicitly whether the integral (7) converges uniformly along different directions in the $\omega, ck_\perp$ plane; clearly, if the double integral over $\omega$ and $k_\perp$ converges uniformly, the $\omega$ integral (7) does so as well.

As argued, we consider propagating and evanescent contributions separately, in which case uniform convergence is straightforward to check. Reflection coefficients fall off rapidly as $|\omega|\to\infty$ (e.g., for the Drude model the real and imaginary parts of $r_q^2$ fall off as $\omega^{-4}$ and $\omega^{-5}$, respectively) and for $|\beta|>1$, $\kappa_0$ is real and positive so the integrand furthermore decreases exponentially. The factor $\exp(-2\kappa_0 a)$ is oscillatory for $|\beta|<1$, but the Dirichlet integral $\int_0^\infty dx \sin x/x$ is known to be uniformly convergent, and our integrand converges more quickly than this. It is easy to check that this also holds as $|\beta|\to 0$ and $|\beta|\to\infty$.

The splitting of (2) into propagating and evanescent parts may be done by integrating each part of the plane and taking the relevant limit to $ck_\perp \to |\omega|$ in the end. Convergence problems are then avoided for the imaginary part of $\ln D_q$ in (7); reflection coefficients fall off rapidly and further help is provided by the factor

$$\frac{\exp(\omega/\omega_T)}{(\exp(\omega/\omega_T)-1)^2} \approx \exp(-|\omega|/\omega_T), \quad |\omega| \gg \omega_T.$$

The rate of convergence due to this factor depends on $T$ and hence apparently cannot be used to demonstrate uniformity. We are interested only in low temperatures, however, so, by defining a finite upper temperature limit $\tilde{T}$ above which the formalism is not valid, $a_0$ can be made $T$ independent (dependent on $\tilde{T}$ only). The fact that the convergence of this factor alone is not uniform for infinite temperature is unproblematic, of course.

Thus we conclude that Nernst's theorem is satisfied for $T$-independent $\epsilon(\omega)$ satisfying 1–3. The violation of Nernst's theorem in temperature-dependent cases, as we shall see, can be understood as a direct consequence of violating the continuity criterion of Leibnitz' rule for improper integrals.

## III. TEMPERATURE-DEPENDENT PERMITTIVITY

In many models used in solid state physics, $\epsilon$ is temperature dependent for all temperatures, and herein lies the source of much of the controversy over what is the correct theory of the Casimir force between plates of real materials. The reader should note that the above theory only requires that permittivity be temperature independent for a finite temperature interval *close to zero* temperature. Rather than rigorously generalizing all of the above, suffice it here to discuss how the introduction of temperature-dependent permittivity illuminates the entropy problems that emerge and hints at possible resolutions. In the following we will think physically in terms of positive frequencies, bearing in mind that negative frequencies exert mathematically equivalent behavior through the symmetry criterion 1.

The models which have caused bother so far are the TE mode of (5) using the Drude model (9) when $\nu(T)\to 0$ as $T\to 0$ (perfect lattice, no impurities) and the TM mode for

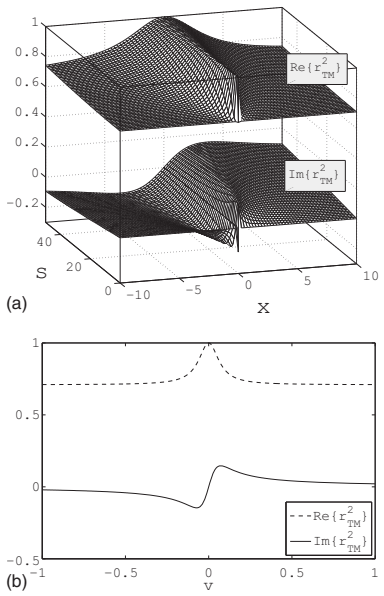


FIG. 2. Real and imaginary parts of $r_{\mathrm{TM}}^2$ with (10) for $\omega, \sqrt{\omega\gamma} \ll k_\perp c$, $\omega_0$ and $\omega \sim \sigma/\epsilon_0$ as simplified in (15) with $\epsilon_\infty = 11.66$, as function of (a) independent $x$ and $s$ and (b) $v = x/s$.

dielectrics (10) with $\sigma(T) \to 0$. The two different cases share many common traits, so analyzing one of them in detail will suffice as illustration. Since the Drude model has already been treated in numerous efforts by both sides of the dispute (e.g., [2,5]), we choose the dielectric for the discussion below.

As should be clear by now, the troubles with entropy emerge for small frequencies at low temperatures. Let us from now on consider the only interesting frequency range in which $\omega^2, \gamma\omega \ll k_\perp^2 c^2, \omega_0^2$, but making no assumptions about the relative magnitude of $\omega$ and $\sigma/\epsilon_0$. Physically this corresponds to bringing $\omega$ and $T$ close enough to the limit so that for all quantities that depend on their absolute values separately they may be replaced by zero, and only quantities that depend on their relative values, specifically the TM reflection coefficient, remains in question. In this case $r_{\mathrm{TM}}$ with (10) inserted simplifies to

$$r_{\mathrm{TM}} \approx \frac{(i\omega\epsilon_0/\sigma)(\epsilon_\infty - 1) - 1}{(i\omega\epsilon_0/\sigma)(\epsilon_\infty + 1) - 1} = \frac{iv(\epsilon_\infty - 1) - 1}{iv(\epsilon_\infty + 1) - 1}, \qquad (15)$$

where $v \equiv \omega\epsilon_0/\sigma \equiv x/s$ where $x$ and $s$ are again suitably nondimensionalized variables proportional to $\omega$ and $\sigma$, respectively. We have plotted the real and imaginary parts of the squared reflection coefficients as shown in Fig. 2 for illustration, using $\epsilon_\infty = 11.66$ as reported for Si in [22].

We find that $\mathrm{Re}\{r_{\mathrm{TM}}^2\}$ is $r_0^2 \equiv (\epsilon_\infty - 1)^2/(\epsilon_\infty + 1)^2 \approx 0.71$ except for $x \ll s$ ($v \approx 0$) where it is unitary. Likewise $\mathrm{Im}\{r_{\mathrm{TM}}^2\}$ for small $s$ is approximately zero for the most part but increases to an extremum for small $|v|$ and thence decreases linearly through 0 at $v = 0$, the same linear behavior that led to $\mathrm{Im}\{\phi(\omega)\} \propto \omega$ and the discontinuity of Fig. 1 in the TM case before, which we argued was not essential. This time, however, there are *additional* discontinuities as $s \to 0$ (equivalent to $\sigma \to 0$). In particular, $\mathrm{Im}\{r_{\mathrm{TM}}^2\}$ (which contributes to the integrals) is 0 everywhere except at $x = 0$ where it can take any value between its maximum and minimum ($\approx \pm 0.079$ for $\epsilon_\infty = 11.66$).

Now remember that the imaginary part of the squared reflection coefficient shown in Fig. 2 is to be multiplied with either the coth factor or its $T$ derivative, both of which diverge as $T/\omega$ as $\omega \to 0$. The result is an exceedingly volatile behavior of the integrands of (5) and (7) near zero frequency and temperature, and the limit where both are zero can take any value between $-\infty$ and $\infty$ depending on the way the limit is taken. This contrasts the bounded discontinuity shown in Fig. 1 in the temperature-independent case.

Furthermore, when $\epsilon$ contains temperature-dependent parameters, the entropy (7) will have an additional term

$$\frac{\hbar}{8\pi^2 i} \int_{-\infty}^{\infty} d\omega \sum_{q=\mathrm{TE}}^{\mathrm{TM}} \frac{e^{-2\kappa_0 a} \coth(\omega/2\omega_T)}{1 - r_q^2 e^{-2\kappa_0 a}} \frac{\partial(r_q^2)}{\partial T}. \qquad (16)$$

Additional entropy problems stem from this term. From (15) one finds with a little algebra that

$$\frac{\partial}{\partial T}(r_{\mathrm{TM}}^2) = -4iv \frac{iv(\epsilon_\infty - 1) - 1}{[iv(\epsilon_\infty + 1) - 1]^3} \frac{1}{\sigma} \frac{\partial\sigma}{\partial T}. \qquad (17)$$

Assuming conductivity at low temperatures to behave as $\sigma_0 \exp(-T_0/T)$ with $\sigma_0$ a constant (see below),

$$\frac{1}{\sigma} \frac{\partial\sigma}{\partial T} = \frac{T_0}{T^2}.$$

When $\omega \neq 0$ this inverse quadratic temperature dependence is no problem since (17) varies as $v^{-1} \propto \sigma$, so the term (16) is zero by a good measure when $T = 0$. The limit $\omega \to 0$ may be taken so that $v$ has a finite value, however, in which case the derivative (17) diverges as $T^{-2}$. This corresponds to $r_{\mathrm{TM}}^2$ making a sudden jump from 1 to $r_0^2$ at $T = 0$ for $\omega = 0$. The term $\partial(r_q^2)/\partial T$ at $T = 0$ is thus zero for all frequencies except $\omega = 0$, where it is infinite. We can no longer argue that this one point does not contribute to the physical quantity $S$, and while the purported zero-temperature entropy may be difficult to calculate in this way (it is straightforward to calculate it in the imaginary frequency framework), it seems likely that the entropy obtains a finite value assuming the formalism may be taken at face value.

### A. Findings of the mathematical analysis

An important realization is thus that a violation of the third law of thermodynamics is predicted in the present framework when $\epsilon(\omega)$ changes the power of its leading order term with respect to $\omega$ at *exactly* zero temperature. When $\epsilon(\omega)$ changes from $\propto\omega^{-2}$ to $\propto\omega^{-1}$, a violation occurs in the TE mode; when the change is from $\propto\omega^{-1}$ to $\propto\omega^0$, the TM mode gives the zero-temperature entropy contribution.

The bottom line is that, when viewed in the framework of real frequencies, all apparent zero-temperature entropy anomalies stem from divergencies of the Lifshitz integrand in the double limit $T\to 0$ and $\omega\to 0$. The reader should note that in this author's understanding, this result does not contradict the findings of either [1,3–7] or [2,8,9]. The last of these references also notes a formal violation of Nernst's theorem due to rotation of permanent ionic dipole moments in the materials. In light of the above, we may conclude that the latter effect is only problematic in media where the rotational degree of freedom of the ions vanishes with temperature in such a manner that its resonant frequency is finite at $T>0$ and zero at $T=0$. This anomaly needs to be studied further in the future.

### B. Physical discussion of thermodynamical anomalies

In this section we will undertake a brief physical discussion of the mathematical results in the previous sections, reviewing the temperature debate for metals and semiconductors in light of the above analysis. Models used when studying the physics of real systems are founded on assumptions which we may categorize as modeling idealizations and approximations in the description of the behavior of these models, and there may be a need to distinguish between these in the present context. A relevant modeling idealization, for example, is that a metal sample has infinitely large dimensions and a perfect crystal lattice structure. Much of science is founded on such ideal models and corrections to them. A relevant approximation in this context is the use of simple dielectric functions such as (9)–(12) which in particular assume that the media in question have local dielectric response (i.e., they depend only on frequency, not momentum $\mathbf{k}$). Even for idealized systems, such approximations typically have limitations.

An ideal model which can in principle be realized (notwithstanding its infeasibility in practice) cannot be allowed to violate the laws of nature, thermodynamics in particular. An approximation, on the other hand, will typically have a finite range of applicability, and cannot be expected to behave correctly outside this range. Given that the limits $T=0$ and $\omega=0$ are in some ways extreme cases, it is especially important to investigate the latter point in relation to the purported problems with the third law of thermodynamics. Specifically, if an approximation which works well at room temperature does not hold for $T=0$ one cannot conclude from a formal violation of Nernst's theorem that it cannot be used *within* its applicability range.

The much investigated temperature anomaly for metals is a good example of the above, and we will review it briefly for illustration. For a perfect and infinitely large metal lattice, the relaxation $\nu(T)$ is due to electron-phonon interactions only and follows the Bloch-Grüneisen formula (see Appendix D of [3]), according to which $\nu$ vanishes as $T^5$ as temperature tends to zero, leading to the above reported anomalies. It has been pointed out that no real metal sample is ever perfect [3] nor infinitely large,[5] so relaxation does not vanish in real systems. There is now consensus that for impure metals the Drude relation does not lead to thermodynamic inconsistencies.

However, the theoretical problem is thereby only halfway solved, because as pointed out [2] the fulfilment of the laws of nature cannot hinge upon the presence of imperfections: the ideal system should accord with thermodynamics as well. The solution according to the authors of [2] is to remove the relaxation from the Drude model and, more recently, introduce dissipation instead through a generalized plasma model [16], unfortunately at the expense of ignoring the manifest presence of relaxation at room temperature. Experiments seem to confirm the predictions from such a procedure and rule out those implied by the use of the Drude model (9) (e.g., [23]) but the theory has not been universally accepted.

While the ideal crystal lattice, when treated in all detail, should certainly be found to abide by Nernst's theorem, the approximation that its dielectric response is well described by the local formalism has been questioned for temperatures approaching $T=0$. Svetovoy and Esquivel [26] and Sernelius [27] conclude independently that at low temperatures nonlocal effects (the anomalous skin effect) dominate, and the local models are no longer reliable. Their analyses accounting for spatially dispersive effects reveal that, within the approximations made in [26,27] Nernst's theorem is satisfied independently of the presence of imperfections, as it should be. The spatial dispersion approach was criticized [28] on several accounts with reference to a treatment by Barash and Ginzburg many years ago [29] (see also [30]). The paradox remains that such a careful procedure (albeit not free of approximations) does not accord with available experimental data. Commendable efforts at a resolution include the recent exploits by Bimonte [31].

While mathematically analogous to the metal case, the temperature anomaly for semiconductors is physically different. Here the problem is not related to idealized models (the conductivity of insulators truly does vanish at zero $T$), but approximations only.

One can argue intuitively that the approximate model (10) probably cannot be taken at face value when conductivity is very small since it implies that even an infinitesimal conductivity should give rise to large thermal corrections in the Lifshitz formalism, contrary to physical intuition. For insulators, by definition, conductivity vanishes at $T=0$, and for many such materials the conductivity even at room temperature is so small it would be expected to make for a minor perturbation only.[6] If (10) is a poor approximation at low frequencies as $\sigma$ vanishes, its violating thermodynamic laws in this case may not be too worrisome.

A recent experiment [22] measured the force between a substrate of the semiconductor silicon and a gold sphere. The

[5]The conductivity of very pure metals at low temperatures is found experimentally to be sample size dependent [24] so even assuming perfectly pure metal, $\nu$ still reaches a finite value when its Bloch-Grüneisen mean free path becomes comparable to the sample dimensions.

[6]For an introduction to different types of semiconductors, see Chap. 1 of [25].

semiconductor was excited into a metallic state by a pulsed laser and it was concluded that while the model (10) was a good representation in the metallic state, the inclusion of the $\sigma$ term when the material was in the poorly conducting state was excluded at 95% confidence. This conclusion may not be surprising in light of the above argument, which indicates that a Drude-type permittivity model overestimates the effect of a small conductivity in the Lifshitz formalism. If so, it is likely that the experimental result might be explained without reference to the Nernst theorem, which concerns physics far removed from laboratory conditions.

Attempts at a more careful description of the effect of a small density of free charges were recently made by Pitaevskii [32] and by Dalvit and Lamoreaux [33], based on the effects of Debye-Hückel screening from free charges in mean field theory. The resulting expressions do not fit experimental data well [34], and it is possible that a more detailed screening model is needed.

## CONCLUSION

While the Lifshitz formalism at real frequencies is much more complicated than the imaginary frequency equivalent normally considered, the consideration of quantities with direct physical interpretations sheds added light on the problem of nonvanishing Lifshitz entropy at zero temperature. We have argued that Nernst's heat theorem is not violated for any causal and continuous (except at $\omega=0$) $\epsilon(\omega)$ which is independent of $T$ near $T=0$. This accords with the findings of Intravaia and Henkel [11] using a different approach. More generally, this holds for dielectric plates whose squared Fresnel TE and TM reflection coefficients are continuous for all $\omega$ and $T$ and nonunitary except at $\omega=0$. It follows from this that the entropy anomalies previously reported pertain to the persistence of the permittivity's temperature variance all the way to zero temperature and are consequences of divergencies in the Lifshitz formalism in the double limit $\omega\to 0$ and $T\to 0$.

When considering physical consistency in such limits as a means to distinguish between candidate theories, particular care must be taken. We emphasize that approximations can be judged only based on their performance within their domain of applicability. Specifically, approximations which are invalid at $T=0$ cannot be expected to be well behaved in this limit, and hence cannot be rejected for causing violation of Nernst's theorem, which concerns zero temperature only. It is therefore important to verify carefully that approximate physical models probed by invoking Nernst's theorem are valid in this case. We finally argue that a recent experiment using an optically excited semiconductor can probably be explained without reference to the Nernst theorem by accounting for the presence of free charges more carefully than by the use of local Drude-type models.

## ACKNOWLEDGMENTS

The author thanks Professor Iver Brevik, Professor Kimball Milton, and Dr. Francesco Intravaia for discussions and useful comments. Further thanks to Professor Vladimir Mostepanenko for many useful remarks on the manuscript and for kindly allowing a preview of [9].

[1] M. Boström and B. E. Sernelius, Phys. Rev. Lett. **84**, 4757 (2000).
[2] G. L. Klimchitskaya and V. M. Mostepanenko, Phys. Rev. A **63**, 062108 (2001); V. B. Bezerra, G. L. Klimchitskaya, and V. M. Mostepanenko, *ibid.* **65**, 052113 (2002); F. Chen, G. L. Klimchitskaya, U. Mohideen, and V. M. Mostepanenko, Phys. Rev. Lett. **90**, 160404 (2003); V. B. Bezerra, G. L. Klimchitskaya, V. M. Mostepanenko, and C. Romero, Phys. Rev. A **69**, 022119 (2004).
[3] J. S. Høye, I. Brevik, J. B. Aarseth, and K. A. Milton, Phys. Rev. E **67**, 056116 (2003).
[4] M. Boström and B. E. Sernelius, Physica A **339**, 53 (2004).
[5] I. Brevik, J. B. Aarseth, J. S. Høye, and K. A. Milton, Phys. Rev. E **71**, 056101 (2005); J. S. Høye, I. Brevik, J. B. Aarseth, and K. A. Milton, J. Phys. A **39**, 6031 (2006); I. Brevik and J. B. Aarseth, *ibid.* **39**, 6187 (2006); I. Brevik, S. A. Ellingsen, and K. A. Milton, New J. Phys. **8**, 236 (2006).
[6] I. Brevik, J. B. Aarseth, J. S. Høye, and K. A. Milton, in *Quantum Field Theory under the Influence of External Conditions (QFEXT03)*, edited by K. A. Milton (Rinton Press, Princeton, NJ, 2004), p. 54.
[7] J. S. Høye, I. Brevik, S. A. Ellingsen, and J. B. Aarseth, Phys. Rev. E **75**, 051127 (2007).
[8] B. Geyer, G. L. Klimchitskaya, and V. M. Mostepanenko, Phys. Rev. D **72**, 085009 (2005); J. Phys. A **39**, 6495 (2006); Int. J. Mod. Phys. A **21**, 5007 (2006).
[9] G. L. Klimchitskaya and B. Geyer, J. Phys. A **41**, 164032 (2008).
[10] For example, K. A. Milton, J. Phys. A **37**, R209 (2004).
[11] F. Intravaia and C. Henkel, J. Phys. A **41**, 164018 (2008).
[12] E. M. Lifshitz, Zh. Eksp. Teor. Fiz. **29**, 94 (1955) [Sov. Phys. JETP **2**, 73 (1956)].
[13] L. D. Landau and E. M. Lifshitz, *Statistical Physics Part 1*, 3rd ed. (Butterworth-Heinemann, Oxford, 1980), Sec. 123.
[14] J. R. Torgerson and S. K. Lamoreaux, Phys. Rev. E **70**, 047102 (2004).
[15] E. T. Whittaker and G. N. Watson, *A Course of Modern Analysis*, 4th ed. (Cambridge University Press, Cambridge, U.K., 1962).
[16] B. Geyer, G. L. Klimchitskaya, and V. M. Mostepanenko, J. Phys. A **40**, 13485 (2007).
[17] B. E. Sernelius, *Surface Modes in Physics* (Wiley-VCH, Berlin, 2001), Chap. 2.
[18] H. B. G. Casimir, Proc. K. Ned. Akad. Wet. **50**, 793 (1948).
[19] N. G. van Kampen, B. R. A. Nijboer, and K. Schram, Phys. Lett. **26A**, 307 (1968).
[20] Y. S. Barash and V. L. Ginzburg, Usp. Fiz. Nauk **143**, 345 (1984) [Sov. Phys. Usp. **27**, 467 (1984)].
[21] B. E. Sernelius, Phys. Rev. B **74**, 233103 (2006).
[22] F. Chen, G. L. Klimchitskaya, V. M. Mostepanenko, and U.

Mohideen, Phys. Rev. B **76**, 035338 (2007).
[23] R. S. Decca, D. Lopez, E. Fischbach, G. L. Klimchitskaya, D. E. Krause, and V. M. Mostepanenko, Phys. Rev. D **75**, 077101 (2007), and references therein.
[24] G. Burns, *Solid State Physics*, Int. ed. (Academic Press, London, 1985), Chap. 9.
[25] F. Gebhard, *The Mott Metal-Insulator Transition* (Springer, Berlin, 1997).
[26] V. B. Svetovoy and R. Esquivel, Phys. Rev. E **72**, 036113 (2005).
[27] B. E. Sernelius, Phys. Rev. B **71**, 235114 (2005).
[28] G. L. Klimchitskaya and V. M. Mostepanenko, Phys. Rev. B **75**, 036101 (2007).
[29] Yu. S. Barash and V. L. Ginzburg, Usp. Fiz. Nauk **116**, 5 (1975) [Sov. Phys. Usp. **18**, 305 (1975)].
[30] V. M. Agranovich and V. L. Ginzburg, *Spatial Dispersion in Crystal Optics and the Theory of Excitons* (Interscience Publishers, London, 1966).
[31] G. Bimonte, New J. Phys. **9**, 281 (2007).
[32] L. P. Pitaevskii, e-print arXiv:0801.0656.
[33] D. A. R. Dalvit and S. K. Lamoreaux, e-print arXiv:0805.1676.
[34] G. L. Klimchitskaya, V. M. Mostepanenko, and U. Mohideen, e-print arXiv:0802.2698.

# Article [e]

***Casimir-Lifshitz pressure and free energy: exploring a simple model***

S.A. Ellingsen

in "The Casimir Effect and Cosmology: A volume in honour of Professor Iver H. Brevik on the occasion of his 70th birthday"
(Tomsk State Pedagogical University Press, 2008), pp. 45-60.

# Casimir Lifshitz pressure and free energy: exploring a simple model

**Simen A. Ådnøy Ellingsen**[1]
*Department of Energy and Process Engineering, Norwegian University of Science and Technology, N-7491 Trondheim, Norway*

**Abstract**

The Casimir effect, the dispersion force attracting neutral objects to each other, may be understood in terms of multiple scattering of light between the interacting bodies. We explore the simple model in which the bodies are assumed to possess reflection coefficients independent of the energy and angle of incidence of an impinging field and show how much information can be extracted within the geometry of two parallel plates. The full thermal behaviour of the model is found and we discuss how non-analytic behaviour emerges in the combined limits of zero temperature and perfect reflection. Finally we discuss the possibility of a generalised force conjugate to the reflection coefficients of the interacting materials and how, if the materials involved were susceptible to changing their reflective properties, this would tend to enhance the Casimir attraction. The dependence of thi correction on separation is studied for the constant reflection model, indicating that the effect may be negligible under most experimental circumstances [2].

## 1 Introduction

The Casimir effect was first reported in 1948 [1] as an attractive force between parallel mirrors due to the zero point fluctuations of the electromagnetic field in vacuum. Casimir calculated the formally infinite quantum energy associated with the eigenmodes $n$ of the field between the plates, $\frac{\hbar}{2}\sum_n \omega_n$, subtracted the corresponding energy of free space (infinte plate separation) and obtained after some regularisation the simple result

$$P_C^0 = -\frac{\hbar c \pi^2}{240 a^4}; \quad \mathcal{F}_C^0 = -\frac{\hbar c \pi^2}{720 a^3} \tag{1}$$

where $P_{\mathrm{C}}$ and $\mathcal{F}_{\mathrm{C}}$ are the Casimir pressure and free energy per unit plate area respectively and $a$ is the separation between the plates. Here and henceforth a superscript 0 refers to zero temperature. A negative pressure here corresponds to an attractive force. Naturally,

[1]E-mail: simen.a.ellingsen@ntnu.no

[2]This article is **dedicated to 70th aniversary of Professor Iver Brevik**

the relation between pressure and free energy is $P(a) = -\partial\mathcal{F}(a)/\partial a$. In the following we will employ natural units $\hbar = k_{\mathrm{B}} = c = 1$.

In the following section we give a brief review of the understanding of Casimir interactions as a multiple scattering or reflection phenomenon. The remainder of the paper is the beginnings of an exploration of a simple model, first employed in [2] to the author's knowledge. The model is one in which the interacting bodies scatter electromagnetic fields with reflection coefficients $|r| \leq 1$ which are modelled as invariant with respect to the energy and direction of the wave. We do not venture beyond the planar geometry herein, but show that certain closed form solutions exist in this case, and how the model enables simple extraction of key information.

We review in section 3 the derivation of closed form expressions for the Casimir force and free energy in the constant reflection model and in section 4 how this model was used to generalise the frequency spectrum of the Casimir energy to imperfect reflection. In sections 5 through 6 we thereafter calculate the full temperature behaviour of the Casimir-Lifshitz pressure and free energy within the model and demonstrate how one encounters non-analytic behaviour in the limit of perfect reflection, reminiscent of the still ongoing debate over the temperature corrections to the Casimir force. Finally in section 7 we consider the possibility that the Casimir free energy could exhibit a generalised force on the reflective properties of the materials involved, thereby increasing its own magnitude. We lay out the basic theory of such a possibility, not hitherto reported to the author's knowledge, and use the constant reflection model to extract information about how the corresponding correction to Casimir attraction scales with temperature and separation.

## 2 A brief review of the multiple scattering understanding of Casimir interactions

The beauty and simplicity of Casimir's results (1) stems from the assumption of perfectly conducting plates, that is, the metal plates are perfect mirrors at all frequencies of the electromagnetic field. Drawing on the theory of fluctuations due to Rytov [3], Lifshitz made an important generalisation of Casimir's results to the case of two half-spaces with frequency dependent permittivities $\epsilon_1(\omega)$ and $\epsilon_2(\omega)$ [4] (Lifshitz moreover assumed the slabs be immersed in a third medium which we assume to be vacuum here for simplicity). The calculation was rather involved and the result at zero temperature was found to be:

$$P^0 = -\frac{1}{2\pi^2}\int_0^\infty d\zeta \int_\zeta^\infty d\kappa\kappa^2 \sum_{\sigma=s,p} \frac{r_\sigma^{(1)} r_\sigma^{(2)} e^{-2\kappa a}}{1 - r_\sigma^{(1)} r_\sigma^{(2)} e^{-2\kappa a}} \tag{2a}$$

$$\mathcal{F}^0 = \frac{1}{4\pi^2}\int_0^\infty d\zeta \int_\zeta^\infty d\kappa\kappa \sum_{\sigma=s,p} \ln\left[1 - r_\sigma^{(1)} r_\sigma^{(2)} e^{-2\kappa a}\right] \tag{2b}$$

where the quantities $r_\sigma^{(i)}$ pertaining to medium $i$ are

$$r_s^{(i)} = \frac{\kappa - \kappa_i}{\kappa + \kappa_i}; \quad r_p^{(i)} = \frac{\epsilon_i(i\zeta)\kappa - \kappa_i}{\epsilon_i(i\zeta)\kappa + \kappa_i} \tag{3}$$

and $\kappa_i = \kappa_i(\kappa, i\zeta) = \sqrt{\kappa^2 + [\epsilon_i(i\zeta) - 1]\zeta^2}$.

By noting that $i\kappa = k_z$, $\hat{z}$ being the axis normal to the plates one may recognise $r_s^{(i)}$ and $r_p^{(i)}$ as the standard Fresnel reflection coefficients of a single interface for the TE and

TM polarisation respectively, as well known from classical optics. Thus the Casimir-Lifshitz force (2a) does not depend directly on the bulk properties of the materials of the slabs as is ostensible from the original Lifshitz derivation, but only on the reflection properties of the *surfaces* of the material half-spaces. Kats [5] may have been the first to point this out explicitly in 1977, and the point has been given widespread attemtion more recently [6, 7, 8, 9]. It is a simple exercise to show that inserting $(r_\sigma^{(i)})^2 = 1, \quad \forall i, \sigma$ into (2a) and (2b) yields the Casimir limits (1).

The trait that the Casimir-Lifshitz pressure (2a) is a function of reflection properties only is a tell-tale that the effect may be thought of as the result of multiple scattering of light between boundaries. Another hint is the recognition of the fraction in (2a)

$$\frac{r_\sigma^{(1)} r_\sigma^{(2)} e^{-2\kappa a}}{1 - r_\sigma^{(1)} r_\sigma^{(2)} e^{-2\kappa a}} = \sum_{k=1}^{\infty} \left( r_\sigma^{(1)} r_\sigma^{(2)} e^{2ik_z a} \right)^k \tag{4}$$

as a sum of contributions from waves which are reflected off both interfaces $k$ times before returning to whence it originated.

This implies that the Casimir interaction between much more general materials than bulk dielectrics (as considered by Lifshitz) may be calculated, if one is able to obtain an expression for the reflection properties of the surfaces involved and how light is transmitted between the bodies. This fact was used, among other things, to calculate the effect of spatial dispersion [5, 10, 11, 12] and interaction between (magneto)dielectric multilayers [13, 14, 15, 16, 17] based on Green's function methods [18]. Some further considerations were given in [19].

In recent years, the understanding of Casimir problems in terms of multiple scattering has become widespread and makes way for what is presently perhaps the most powerful techniques for calculating Casimir energies in non-trivial geometries. Within such a general scattering formalism the Lifshitz formula (2b) may be seen as a special case of the much more general formula

$$\mathcal{F}^0 = \int_0^\infty \frac{d\zeta}{2\pi} \mathrm{Tr} \ \ln \left[ 1 - \mathbb{T}_1 \mathbb{G}_{12}^0 \mathbb{T}_2 \mathbb{G}_{21}^0 \right] \tag{5}$$

where $\mathbb{T}_i$ is the T-matrices (operators) of two arbitrary interacting bodies and $\mathbb{G}_{ij}^0$ is a vacuum propagator (Green's function) from object $i$ to object $j$. The energy expression (5) was recently dubbed the TGTG formula and is written here as derived in [20, 21], but the use of less general embodiments of essentially the same multiple scattering technique goes back at least to the 1970s [22, 23]. The recent acceleration of progress towards understanding the role of geometry in Casimir interactions has brought much attention to this technique in recent years (e.g. [24, 25, 26, 27, 28]; for a review see [29] and the introduction to [27]).

To see somewhat roughly how the Casimir-Lifshitz free energy (2b) is a special case of (5) let the propagators be simply that of a plane wave along the $\hat{z}$ direction over a distance $a$, $\mathbb{G}^0 \to \exp(ik_z a)$ and let the T matrices represent specular scattering at the surfaces, $\mathbb{T}_i \to \mathrm{diag}(r_s^{(i)}, r_p^{(i)})$. Take the trace operation in (5) to include an integral over the transverse momentum $\mathbf{k}_\perp$ plane (isotropic due to rotational symmetry) and one obtains (2b) with minimal manipulation. See e.g. [30] for details.

For reasons of simplicity much of the recent research on geometry effects has been made for the massless scalar field satisfying the Klein-Gordon equation rather than the vectorial electromagnetic field. Historically, Dirichlet and Neumann boundary conditions have been employed together with path integral methods of quantum field theory to mimic the two electromagnetic polarisations (note that the sum of the Dirichlet and Neumann scalar solutions of the wave equation only reproduces the ideally conducting electromagnetic case in

special geometries where the electromagnetic modes decouple, such as the original Casimir geometry).

In order to model semi-transparent bodies in this formalism, the introduction of delta-function potentials into the Klein-Gordon equation has been common (see review in [30]). A delta potential $V(\mathbf{r}) = \lambda\delta^3(f(\mathbf{r}))$ models a body whose surface solves $f(\mathbf{r}) = 0$ and where the coupling constant $\lambda$ determines the "transparency". Dirichlet boundary conditions are regained in the strong coupling limit $\lambda \to \infty$, and it has turned out that several non-trivial geometries are exactly solvable to linear order in $\lambda$ in the weak coupling case $\lambda \ll 1$ [26, 27].

The model of constant reflection coefficients is a somewhat similar idea and constitutes another model of semi-transparency where some physicality is traded for mathematical manageability.

## 3 Closed form expression using polylogarithms

It is straightforward to obtain a closed form expression for the Casimir pressure and energy in the constant reflection model. The mathematical formalism which enters is that of polylogarithmic functions. The $\nu$th order polylogarithm of $x$ is defined as

$$\mathrm{Li}_\nu(x) = \sum_{k=1}^{\infty} \frac{x^k}{k^\nu}. \tag{6}$$

It is related to the Riemann zeta functions (as is obvious for $\nu > 1$) by $\mathrm{Li}_\nu(1) = \zeta(\nu)$ and obeys the recursion relation $(d/dx)\mathrm{Li}_\nu(x) = (1/x)\mathrm{Li}_{\nu-1}(x)$, which in particular implies that for $|\Re\mathrm{e}A| < 1$

$$\int dx \mathrm{Li}_\nu(Ae^{-bx}) = -\frac{1}{b}\mathrm{Li}_{\nu+1}(Ae^{-bx}) + C \tag{7}$$

where $A, b, C$ are constants. We recognise the polylogarithms which enter into (2a) and (2b),

$$\mathrm{Li}_1(x) = -\ln(1-x); \quad \mathrm{Li}_0(x) = \frac{x}{1-x}. \tag{8}$$

The polylogarithms of interest herein are all of real and integer order.

In the Wick rotated formalism in Euclidean space where the time axis is imaginary, it follows from the general properties of causal response functions that the reflection coefficients are necessarily real quantities [31]. Now, assuming the reflection coefficients are constants with respect to $\kappa$ and $\zeta$ the integrals are easily solved with partial integration using (7) and yields for the pressure and free energy at zero temperature, respectively[3],

$$P^0 = -\frac{3}{16\pi^2 a^4} \sum_{\sigma=p,s} \mathrm{Li}_4(r_\sigma^{(1)} r_\sigma^{(2)}); \tag{9}$$

$$\mathcal{F}^0 = -\frac{1}{16\pi^2 a^3} \sum_{\sigma=p,s} \mathrm{Li}_4(r_\sigma^{(1)} r_\sigma^{(2)}). \tag{10}$$

In the ideal limit $|r_\sigma| \to 1$, $\mathrm{Li}_4(r_\sigma^{(1)} r_\sigma^{(2)}) \to \zeta(4) = \pi^4/90$ and Casimir's results (1) are regained. The Casimir pressure as a function of the squared reflection coefficient $r^2$ (assuming both materials equal and the same coefficient for both polarisations) is plotted in figure 1. A similar graph for the free energy would obviously be exactly identical.

[3] If the calculation is performed for real frequencies, reflection coefficients are generally complex and the real part of the $\mathrm{Li}_4$ functions should be taken [2].

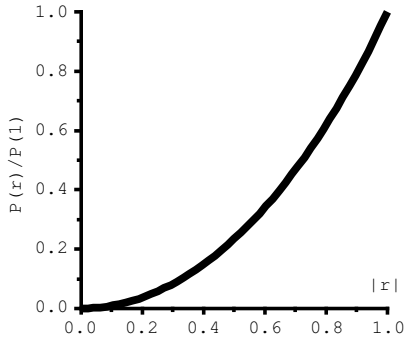


Figure 1: Casimir pressure as a function of a constant reflection coefficient relative to the ideal conductor Casimir result. Materials are assumed similar and the reflection coefficient equal for both polarisations for simplicity.

# 4 Real-frequency spectrum

The model of constant reflections was introduced in [2] in order to slightly generalise considerations of the real-frequency spectrum of the Casimir force due to Ford [32]. He showed from quantisation of the vacuum how the Lifshitz frequency integrand is equal to the vacuum energy spectrum, which in the case of perfect mirrors studied by Ford turns out to be an oscillating function of frequency with discontinuities at $\omega = n\pi/a,\ n \in \mathbb{N}$. The Lifshitz pressure formula for real frequencies at zero temperatures reads [4]

$$P^0(a) = -\frac{1}{2\pi^2}\Re\mathrm{e}\int_0^\infty d\omega\omega^3 \int_\Gamma dpp^2 \times \sum_{\sigma=s,p} \frac{r_\sigma^2 \exp(2ip\omega a)}{1 - r_\sigma^2 \exp(2ip\omega a)} \tag{11}$$

where the Lifshitz variable $p$ is the positive real part root of $p = \sqrt{1-(\mathbf{k}_\perp/\omega)^2}$. In the following we will assume the materials equal for simplicity; the generalisation to different reflectivity is $r_\sigma^2 \to r_\sigma^{(1)} r_\sigma^{(2)}$. Replacing an isotropic integral over all $\mathbf{k}_\perp$ the integration contour $\Gamma$ therefore runs from 1 to 0 (propagating modes) and thence to $i\infty$ (evanescent modes).

By assuming reflection coefficients to be constant with $|\Re\mathrm{e}\{r_\sigma^2\}| \leq 1$, the frequency spectrum can be found. Defining

$$P^0 = \int_0^\infty d\omega \sum_{\sigma=s,p} P^0_{\omega,\sigma} \tag{12}$$

one finds the spectrum

$$P^0_{\omega,\sigma} = \frac{-1}{16\pi^2 a^3}\left[-\xi^2 \Im\mathrm{m}\mathrm{Li}_1(r_\sigma^2 e^{i\xi}) - 2\xi\Re\mathrm{e}\mathrm{Li}_2(r_\sigma^2 e^{i\xi}) + 2\Im\mathrm{m}\mathrm{Li}_3(r_\sigma^2 e^{i\xi})\right] \tag{13}$$

where we have defined the shorthand dimensionless quantity $\xi = 2\omega a$. The spectrum (13) is plotted for a few different $r_\sigma$ in figure 2. Note how the discontinuous behaviour seen in the ideal case $r_\sigma^2 = 1$, which stems from the term

$$\Im\mathrm{m}\mathrm{Li}_1(e^{i\xi}) = \arctan\left(\frac{\sin\xi}{1-\cos\xi}\right) \tag{14}$$

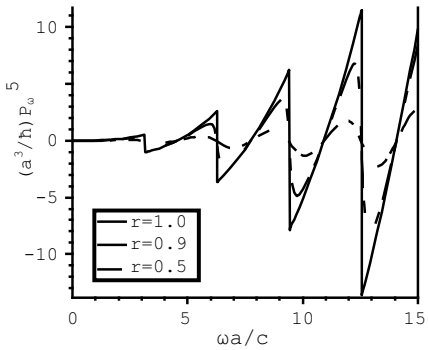


Figure 2: Casimir-Lifshitz frequency spectrum for real constant reflection coefficients. This figure generalises figure 2 of [32].

becomes smooth for $r_\sigma^2 < 1$. This is one example of how the Lifshitz formulae exhibit non-analytic behaviour in the perfectly reflecting limit, a fact which is closely related to the ongoing dispute about the temperature correction to the Casimir force as explained in the following.

# 5 Thermal behaviour

We start by generalising the closed form result (10) to include finite temperature corrections. It is easiest to work within the imaginary frequency formalism. When going to finite temperature the real frequency integrand of (11) and the corresponding free energy expression receives an additional factor $\coth(\omega/2T)$ from the Bose-Einstein distribution. By use of Cauchy's theorem the real frequency integral can be written as a sum over the poles of this factor at $\omega/2T = m\pi i,\ m \in \mathbb{N}$. Thus the Lifshitz formula for free energy of polarisation mode $\sigma$ (letting $\mathcal{F} = \mathcal{F}_p + \mathcal{F}_s$) at temperature $T$ is

$$\mathcal{F}_\sigma^T = \frac{T}{2\pi} {\sum_{m=0}^{\infty}}' \int_{\zeta_m}^{\infty} d\kappa\kappa \ln(1 - r_\sigma^2 e^{-2\kappa a}) \tag{15a}$$

$$= -\frac{T}{8\pi a^2} {\sum_{m=0}^{\infty}}' \left[2a\zeta_m \mathrm{Li}_2(r_\sigma^2 e^{-2\zeta_m a}) + \mathrm{Li}_3(r_\sigma^2 e^{-2\zeta_m a})\right] \tag{15b}$$

where $\zeta_m = 2\pi m T$ are the Matsubara frequencies and the prime on the sum means the $m = 0$ term is taken with half weight. In the last form we use that $\ln(1-x) = -\mathrm{Li}_1(x)$, and partial integration by use of (7).

In the high temperature limit $2\zeta_1 a \gg 1$ the $m = 0$ term dominates (other terms are exponentially small) and we immediately obtain the free energy in this limit:

$$\mathcal{F}_\sigma^T \sim -\frac{T}{16\pi a^2}\mathrm{Li}_3(r_\sigma^2);\quad \zeta_1 a \gg 1, \tag{16}$$

in accordance with the well known high-temperature free energy between ideal plates, $\mathcal{F}_C \approx -\zeta(3)T/(8\pi a^2)$ known at least since the 1960s [33].

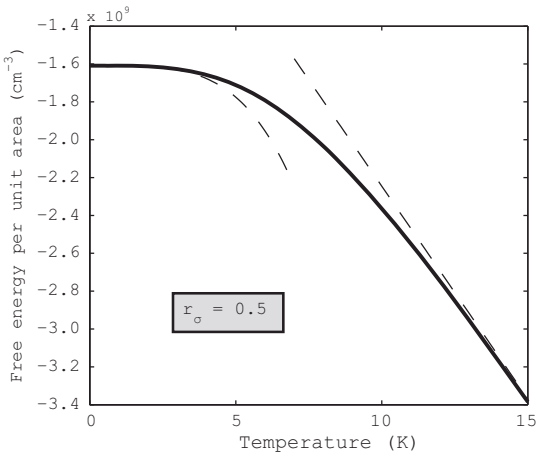


Figure 3: Casimir-Lifshitz free energy as a function of temperature for $r_\sigma = 1/2$ and the high and low temperature asymptotics, (16) and (18) respectively.

By using the definition (6) and changing the order of summation, (15b) can be written

$$\mathcal{F}_\sigma^T = \frac{-T}{16\pi a^2} \sum_{k=1}^{\infty} \frac{r_\sigma^{2k}}{k^3} \left[ \frac{\zeta_k a}{\sinh^2(\zeta_k a)} + \coth(\zeta_k a) \right] \tag{17}$$

This is a generalisation of equation (3.12) of [34], which is for ideal conductors. One may note that the expression between the square brackets equals the Wronskian $\mathcal{W}(\coth x, x)$ with $x = \zeta_k a$. For numerical purposes (17) is useful for having a summand which converges geometrically and consists of standard functions only.

We go on to find the asymptotic behaviour for small $T$. When $aT$ is small and $r_\sigma^2 < 1$ only small values of the quantity $\zeta_k a$ are of importance to the sum (17) because for a given $r_\sigma$ the temperature may be chosen so small that the sum has converged due to the factor $r_\sigma^{2k}$ before $\zeta_k a$ becomes of order unity. Then a Laurent expansion

$$x \sinh^{-2}(x) + \coth(x) = 2x^{-1} + 2x^3/45 + ...$$

gives the low temperature expansion assuming $r_\sigma^2 < 1$:

$$\begin{aligned} \mathcal{F}_\sigma^T \sim & -\frac{1}{16\pi^2 a^3} \mathrm{Li}_4(r_\sigma^2) - \frac{\pi^2 a T^4}{45} \frac{r_\sigma^2}{1 - r_\sigma^2} \\ & + \mathcal{O}(T^6); \quad T \to 0 \end{aligned} \tag{18}$$

where we use $\mathrm{Li}_0(x) = x/(1-x)$. The thermal behaviour of $\mathcal{F}_\sigma$ is plotted in figure 3 together with the high and low temperature asymptotics.

One may note a couple of peculiar traits about this low-temperature behaviour. Firstly, all finite temperature coefficients are singular in the ideal limit $r_\sigma^2 \to 1$; there are only even order terms, and the temperature correction of order $T^{2n}$ diverges as $(1 - r_\sigma^2)^{3-n}$ for $n \geq 2$ as we will show below. This is an indication that $\mathcal{F}_\sigma^T$ is not analytic in the double limit where $T$ vanishes and $r_\sigma^2 \to 1$.

Secondly, note the contrast with the corresponding ideal result $r_\sigma^2 = 1$ derived in [34, 35],

$$\frac{1}{2}\mathcal{F}_C^T \sim -\frac{\pi^2}{1440a^3} - \frac{\zeta(3)T^3}{4\pi} + \frac{\pi^2 a T^4}{90} + ...; \quad T \to 0. \tag{19}$$

where further corrections are exponentially small (see also [36]). Mathematically the change of sign and coefficient of the $T^4$ term from (18) to (19) can be naïvely explained by

$$\frac{r_\sigma^2}{1-r_\sigma^2} = \mathrm{Li}_0(r_\sigma^2) \overset{r_\sigma^2 \to 1}{\longrightarrow} \zeta(0) = -\frac{1}{2}, \tag{20}$$

yet there appears a hitherto unseen term $\propto T^3$ which is independent of $a$ and therefore does not contribute to the Casimir pressure.

Mathematically, the reason for this fundamental change of temperature behaviour at $r_\sigma^2 = 1$ is due to the fact that the summand of (15a) becomes a non-analytical function of $m$ at $m = 0$ when $r_\sigma^2 = 1$, but is analytical whenever $r_\sigma^2 < 1$. It was demonstrated in [37] that a term $\propto T^3$ in the low temperature expansion of $\mathcal{F}$ appears when the summand of (15a) contains a term proportional to $m^2 \ln(m)$.

Before elaborating this further, we will work out the full asymptotic series expansion of $\mathcal{F}$ in powers of $T$ by use of the method developed in [37]. We define the function $g_\sigma(\mu)$

$$\mathcal{F}_\sigma^T \equiv -\frac{T}{8\pi a^2} {\sum_{m=0}^{\infty}}' g_\sigma(\mu) \tag{21}$$

where $\mu = mT$ and $g_\sigma(\mu)$ is the expression inside the square brackets of (15b). When $g_\sigma(\mu)$ is analytical at $\mu = 0$, $g_\sigma$ can be written as a Taylor series $g_\sigma(\mu) = \sum_{k=0}^{\infty} c_k^\sigma \mu^k$. By zeta regularisation the temperature correction $\Delta\mathcal{F}_\sigma(T) = \mathcal{F}_\sigma^T - \mathcal{F}_\sigma^0$ can be written[37]

$$\begin{aligned}\Delta\mathcal{F}_\sigma(T) &\sim -\frac{1}{8\pi a^2}\sum_{k=1}^{\infty} c_{2k-1}^\sigma \zeta(1-2k) T^{2k} \\ &= \frac{1}{8\pi a^2}\sum_{k=1}^{\infty} c_{2k-1}^\sigma \frac{B_{2k}}{2k} T^{2k}; \quad T \to 0,\end{aligned} \tag{22}$$

where $B_n$ are the Bernoulli numbers as defined in [38]. Only odd orders of $\mu$ from the Taylor expansion contribute since $\zeta(-2k) = 0$; $k \in \mathbb{N}$, thus there are only even orders of $T$.

Since

$$\left(\frac{d}{dx}\right)^k \mathrm{Li}_n(Ae^{-bx}) = (-b)^k \mathrm{Li}_{n-k}(Ae^{-bx})$$

and since for $\Re\mathrm{e}A < 1$,

$$\mathrm{Li}_{-k}(A) \propto (1-A)^{-(k+1)}, \quad k \geq 0,$$

it is clear that the summand of (15a) is analytic if and only if $r_\sigma^2 < 1$, since the higher derivatives of the $\mathrm{Li}_3$ term become divergent at $m = 0$. The asymptotic series on the form (22) is therefore valid for all $r_\sigma^2 < 1$ but not in the perfectly reflecting limit.

When $r_\sigma^2 < 1$ it is obvious that

$$\mathrm{Li}_n(r_\sigma^2 e^{-\alpha}) = \sum_{l=0}^{\infty} \frac{(-\alpha)^l}{l!} \mathrm{Li}_{n-l}(r_\sigma^2),$$

which automatically gives the Taylor expansion of $g_\sigma(\mu)$. Inserted into $g_\sigma(\mu)$ from (15b) we find

$$g_\sigma(\mu) = \mathrm{Li}_3(r_\sigma^2) - \sum_{k=1}^{\infty} \frac{k-1}{k!}(-4\pi a\mu)^k \mathrm{Li}_{3-k}(r_\sigma^2). \tag{23}$$

It is thus clear that $c_1^\sigma = 0$, in accordance with (18) where the lowest correction to zero temperature was found to be $T^4$. With (22) the full temperature expansion to arbitrary order is thus

$$\mathcal{F}_\sigma^T = \frac{1}{16\pi^2 a^3} \sum_{k=0}^{\infty} \frac{(k-1)B_{2k}}{(2k)!} \mathrm{Li}_{4-2k}(r_\sigma^2)(4\pi a T)^{2k}. \tag{24}$$

One may easily verify that this generalises (18), noting that $\mathrm{Li}_0(x) = x/(1-x)$. One may show that this series has zero convergence radius, that is, it does not converge for any finite $T$.

# 6 Asymptotic temperature expansion for perfect conductors revisited

The fact that the naïve transition (20) yields the correct $T^4$ term for ideal conductors leads one to speculate that the even-power terms of the asymptotic $T$-series for ideal conductors may be given by simply letting $\mathrm{Li}_{4-2k}(r_\sigma^2) \to \zeta(4-2k)$ in (24). Since the Riemann zeta function with even negative integer arguments is zero, this would if so truncate the series beyond order $T^4$. This does not explain the appearence of the $T^3$ term in (19), however, and does not preclude the emergence of other additional terms of higher non-even order.

The answer is readily found using the above mentioned method developed in [37]. From (15b) and (21) we see that for ideal conductors

$$g_\sigma(\mu) = \tau \mathrm{Li}_2(e^{-\tau}) + \mathrm{Li}_3(e^{-\tau}) \tag{25}$$

where we have defined the shorthand $\tau = 4\pi a\mu$. The asymptotic behaviour of $\mathrm{Li}_n(e^{-\tau})$ for small $\tau$ was found by Robinson [39] who studied the function[4]

$$\phi(s,\tau) = \frac{1}{\Gamma(s)} \int_0^\infty dx \frac{x^{s-1}}{e^{x+\tau}-1} = \mathrm{Li}_s(e^{-\tau}).$$

For integer $s = n$ the Robinson formula is

$$\begin{aligned} \mathrm{Li}_n(e^{-\tau}) =& \frac{(-\tau)^{n-1}}{(n-1)!} \left[ \sum_{k=1}^{n-1} \frac{1}{k} - \ln(\tau) \right] \\ &+ \sum_{\substack{k=0 \\ k \neq n-1}}^{\infty} \frac{\zeta(n-k)}{k!}(-\tau)^k \end{aligned} \tag{26}$$

which gives

$$\begin{aligned} g_\sigma(\mu) =& \zeta(3) - \frac{\tau^2}{4} + \frac{1}{2}\tau^2 \ln(\tau) \\ &- \sum_{k=3}^{\infty} \frac{k-1}{k!} \zeta(3-k)(-\tau)^k. \end{aligned} \tag{27}$$

[4] For this integral representation of the polylogarithm see e.g. [40] equation (2.4).

It is shown in [37] that, as defined in (21), a term in $g_\sigma(\mu)$ of the form $c_{2l}^\sigma \mu^2 \ln \mu$ gives a term in the free energy

$$\mathcal{F}_{2l} = -\frac{1}{8\pi a^2}\frac{\zeta(3)}{4\pi^2} c_{2l}^\sigma T^3.$$

From (27) one recognises $c_{2l}^\sigma = 8\pi^2 a^2$, wherewith the $T^3$ term of (19) is regained.

Terms of $g_\sigma(\mu)$ which are constant or proportional to $\mu^2$ give no contribution to the temperature correction to free energy and a comparison of (23) and (27) to order $\mu^3$ and higher shows that for all orders of $T$ above cubic the expansion of $\mathcal{F}_C^T$ is the same as (24) with $\mathrm{Li}_{2-2k}(r_\sigma^2) \to \zeta(2-2k) = -\frac{1}{2}, 0, 0, ...$ for $k = 1, 2, 3, ...$ Thus the series is terminated at fourth order and the expansion (19) is in fact the full temperature behaviour modulo exponentially small corrections:

$$\mathcal{F}_C^T \sim -\frac{\pi^2}{720a^3} - \frac{\zeta(3)T^3}{2\pi} + \frac{\pi^2 a T^4}{45}; T \to 0. \tag{28}$$

This result was found by different methods in [34, 35, 36] and is consistent with Mehra's early considerations [33].

### 6.1 Relation to the temperature debate

In connection with an ongoing debate concerning the temperature correction to the Casimir force, a point which has been raised is that the application of certain reflectivity models lead to apparent inconsistencies with the third law of thermodynamics, the Nernst heat theorem (c.f. [41] and references therein), that is, entropy does not vanish with vanishing temperature as it should. It was recently concluded that these formal violations of Nernst's theorem stem from non-analytical behaviour in the combined limit of zero frequency (where reflection coefficients approach unity for metal models) and zero temperature [42, 43]. Indeed, violation can only occur due to particular types of non-analyticities causing abrupt change of reflectivity at the point $\omega = T = 0$ [44]. The nonzero entropy at zero temperature would then stem from the fact that the summand of the free energy sum such as (15a) became discontinuous at $m = 0$.

The transition from imperfect to perfect reflection in the previous paragraph is reminiscent of the anomalous entropy at some level. In [42, 43, 44] the situation is one in which the reflection coefficients and thus the free energy summand is discontinuous when frequency and temperature are taken continuously to zero. Here the second temperature *derivative* of the free energy integrand (15a) is discontinuous (indeed divergent) as reflection coefficient and temperature are taken continuously to zero. The former discontinuity leads to a change in free energy leading temperature dependence from quadratic to linear, the linear dependence which implies nonzero entropy at zero temperature since $S = -\partial\mathcal{F}/\partial T$. The $r_\sigma \to 1$ transition considered above changes the temperature correction from quartic to cubic. No anomalous entropy at $T = 0$ stems from this transition, yet its mathematical dynamics are very similar.

## 7 A generalised force on reflectivity?

We conclude with a few remarks on the possibility of a generalised force whose generalised coordinate is the reflectivity of one of the materials. In most calculations of Casimir forces between real materials the material is treated as inert and it is assumed that its reflection properties do not change due to the Casimir interaction across the gap. One could remark, however, that were it possible, the system could lower its free energy by increasing its reflectivity. Such a mechanism was in fact suggested as a possible explanation of the energetics of

the high temperature superconducting transition in which a ceramic multilayer can decrease its total free energy by becoming superconducting, thus a better reflector [45].

In the following a few notes are made on this possibility. A determination of the question of whether such an effect could be measurable is only possible subsequent to calculating the material's free energy as a functional of its reflection coefficients and determining to which extent variation of reflectivity is a degree of freedom. This is complicated task we shall not pursue herein.

One is reminded at this point of the previously mentioned dispute over the thermal dependence of the Casimir effect between real materials (reviews include [46, 41]). Puzzlingly, recent high accuracy experiments which have measured the Casimir force between good metals ([47] and references therein) report a measured Casimir pressure significantly larger than that predicted by several theoretical groups [34, 46, 48, 49].

Our calculations indicate that the Casimir self-enhancing effect is negligible under most circumstances yet it might be worth investigating it further taking into account specific material characteristics for a quantitative treatment. Here we shall content ourselves with laying out the very basic theory and using the constant reflection model as a tool to extract the dependence on temperature and separation in two limits.

Consider the Lifshitz free energy on yet another form,

$$\begin{aligned}\mathcal{F}_\sigma^T[r_\sigma^{(1)}, r_\sigma^{(2)}] =& \frac{1}{2i}\int_{-\infty}^{\infty}\frac{d\omega}{2\pi}\coth\frac{\omega}{2T} \\ &\times\int\frac{d^2k_\perp}{(2\pi)^2}\ln(1-r_\sigma^{(1)}r_\sigma^{(2)}e^{-2\kappa a})\end{aligned} \tag{29}$$

with $\kappa=\sqrt{\mathbf{k}_\perp^2-\omega^2}$ with $\Re\mathrm{e}\{\kappa\}>0$ and reflection coefficients functions of $\mathbf{k}_\perp$ and $\zeta$. In the special case of a single interface between vacuum and a dielectric, $r_\sigma^{(i)}$ take the form (3). Note that the integrand of (29) is complex but only the imaginary part contributes due to symmetry properties so that the expression as a whole is real (see e.g. [43]). The logarithm is understood as its principal value.

The total free energy of the system per unit transverse area should be well approximated by

$$\mathcal{F}_\sigma^{\mathrm{tot}} = \mathcal{F}_\sigma^{(1)}[r_\sigma^{(1)}] + \mathcal{F}_\sigma^{(2)}[r_\sigma^{(2)}] + \mathcal{F}_\sigma^{\mathrm{L}}[r_\sigma^{(1)}, r_\sigma^{(2)}]$$

where the first two terms on the right hand side pertain to the two media on either side of the gap and the last term is the Lifsthiz free energy, now with a superscript L for distinction (we assume finite temperature throughout this section except as explicated). We define the generalised force acting on material $i$:

$$\begin{aligned}\Phi_\sigma^{(i)}(\omega,\mathbf{k}_\perp) =& -\frac{\delta\mathcal{F}_\sigma^{\mathrm{L}}[r_\sigma^{(i)}, r_\sigma^{(j)}]}{\delta r_\sigma^{(i)}(\mathbf{k}_\perp,\omega)} \\ =& \frac{1}{2i}\coth\left(\frac{\omega}{2T}\right)\frac{r_\sigma^{(j)}e^{-2\kappa a}}{1-r_\sigma^{(i)}r_\sigma^{(j)}e^{-2\kappa a}}\end{aligned} \tag{30}$$

where $i,j=1,2$; $i\neq j$ and $\delta/\delta r_\sigma^{(i)}$ denotes the functional derivative. The dependence of reflection coefficients on $\omega$ and $\mathbf{k}_\perp$ has been suppressed on the right hand side. The generalised force can take either sign but always acts so as to increase the attraction between the plates, an observation which is self evident from the fact that the negative Casimir-Lifshitz free energy (15a) increases in magnitude with increasing reflectivity [5].

[5] One may note that if one were to have a dielectric and a magnetic material, repulsion can in principle be effectuated. In this case $\Phi_\sigma$ acts to decrease repulsion.

A given material $i$ will have a generalised susceptibility which determines its ability to alter its reflective properties in response to $\Phi_\sigma$,

$$\chi_\sigma^{(i)}(\omega,\omega',\mathbf{k}_\perp,\mathbf{k}'_\perp) = \frac{\delta r_\sigma^{(i)}(\omega,\mathbf{k}_\perp)}{\delta\Phi_\sigma^{(i)}(\omega',\mathbf{k}'_\perp)} \tag{31}$$

$$= \left[\frac{\delta^2\mathcal{F}_\sigma^{(i)}[r_\sigma^{(i)}]}{\delta r_\sigma^{(i)}(\omega,\mathbf{k}_\perp)\delta r_\sigma^{(i)}(\omega',\mathbf{k}'_\perp)}\right]^{-1} \tag{32}$$

and a Taylor expansion in $\Phi_\sigma$ gives

$$\Delta r_\sigma^{(i)}(\omega,\mathbf{k}_\perp) = \int_{-\infty}^{\infty}\frac{d\omega'}{2\pi}\int\frac{d^2k'_\perp}{(2\pi)^2}\chi_\sigma^{(i)}(\omega,\omega',\mathbf{k}_\perp,\mathbf{k}'_\perp) \times \Phi_\sigma^{(i)}(\omega',\mathbf{k}'_\perp) + ...$$

At finite temperature we may close the $\omega'$ integral path around the upper half complex plane and invoke the Cauchy theorem. Since $\chi_\sigma^{(i)}(\cdots)$ does not have any singularities in the upper $\omega'$ plane [31], the integral over $\omega'$ then gives a sum over the poles of $\coth(\omega'/2T)$, and by letting $\omega \to i\zeta$ we obtain

$$\Delta r_\sigma^{(i)}(i\zeta,\mathbf{k}_\perp) = T\sum_{m=0}^{\infty}{}'\int\frac{d^2k'_\perp}{(2\pi)^2}\chi_\sigma^{(i)}(i\zeta,i\zeta_m,\mathbf{k}_\perp,\mathbf{k}'_\perp) \times \Phi_\sigma^{(i)}(i\zeta_m,\mathbf{k}'_\perp) + ... \tag{33}$$

where

$$\Phi_\sigma^{(i)}(i\zeta,\mathbf{k}_\perp) = \frac{r_\sigma^{(j)}(i\zeta,\mathbf{k}_\perp)e^{-2\kappa a}}{1-r_\sigma^{(i)}(i\zeta,\mathbf{k}_\perp)r_\sigma^{(j)}(i\zeta,\mathbf{k}_\perp)e^{-2\kappa a}}. \tag{34}$$

On the imaginary frequency axis all quantities in (33) and (34) are real.

Since $\chi_\sigma^{(i)}(\cdots)$ depends on $r_\sigma^{(i)}$ and $\Phi_\sigma^{(i)}$ depends on both reflection coefficients, quation (33) defines a set of integral equations for the new reflection coefficients. Note that $\Phi_\sigma^{(i)}$ always has the same sign as $r_\sigma^{(i)}$ and increases in magnitude with increasing $|r_\sigma^{(i)}|$, so equation (33) implies that given time, $|r_\sigma^{(i)}|$ will flow to ever higher values until the fixed point

$$\chi_\sigma^{(i)}(i\zeta,i\zeta,\mathbf{k}_\perp,\mathbf{k}_\perp) = 0 \tag{35}$$

is reached for both materials. If one is able to calculate $\chi_\sigma^{(i)}(\cdots)$ for a given $r_\sigma^{(i)}$, (33) with (34) may be invoked iteratively for a simple numerical scheme to obtain the new reflection coefficients.

An approximation of the change in reflectivity is provided by use of (33) using the 'first order' estimate

$$\Phi_{\sigma,0}^{(i)} = \frac{r_{\sigma,0}^{(j)}e^{-2\kappa a}}{1-r_{\sigma,0}^{(i)}r_{\sigma,0}^{(j)}e^{-2\kappa a}} \tag{36}$$

where $r_{\sigma,0}^{(i)}$ are the reflection coefficients without any Casimir interaction, which satisfy $\delta\mathcal{F}_\sigma^{(i)}/\delta r$ 0. To first order in $\Delta r$ the change in Lifshitz free energy is

$$\Delta\mathcal{F}_\sigma^{\mathrm{L}} = -T\sum_{m=0}^{\infty}{}'\int\frac{d^2k_\perp}{(2\pi)^2}\left(\frac{\Delta r_\sigma^{(1)}}{r_{\sigma,0}^{(1)}}+\frac{\Delta r_\sigma^{(2)}}{r_{\sigma,0}^{(2)}}\right) \times \frac{r_{\sigma,0}^{(1)}r_{\sigma,0}^{(2)}e^{-2\kappa a}}{1-r_{\sigma,0}^{(1)}r_{\sigma,0}^{(2)}e^{-2\kappa a}}. \tag{37}$$

which, upon comparison with (36) gives the 'one-loop' approximation

$$\Delta\mathcal{F}_\sigma^{\rm L} \approx -T^2 \sum_{m,m'=0}^{\infty}{}' \int \frac{d^2k_\perp}{(2\pi)^2}\frac{d^2k'_\perp}{(2\pi)^2} \sum_{i=1,2} \Phi^{(i)}_{\sigma,0}(i\zeta_m,\mathbf{k}_\perp)\chi^{(i)}_\sigma(i\zeta_m,i\zeta_{m'},\mathbf{k}_\perp,\mathbf{k}'_\perp)\Phi^{(i)}_{\sigma,0}(i\zeta_{m'},\mathbf{k}'_\perp). \tag{38}$$

It is understood that $\chi^{(i)}_\sigma(\cdots)$ is evaluated assuming unperturbed reflection.

### 7.1 Constant reflection model

Assuming constant reflection coefficients as before it is easy to see that $\Phi_\sigma$ scales with distance like $\mathcal{F}_\sigma$:

$$\begin{aligned}\Phi^{(i)}_\sigma &= T\sum_{m=0}^{\infty}{}' \int \frac{d^2k'_\perp}{(2\pi)^2}\Phi^{(i)}_\sigma(i\zeta_m,\mathbf{k}_\perp) = -\frac{\partial\mathcal{F}_\sigma}{\partial r^{(i)}_\sigma} \\ &\sim \begin{cases} (16\pi^2a^3r^{(i)}_\sigma)^{-1}{\rm Li}_3(r^{(1)}_\sigma r^{(2)}_\sigma), & T\to 0 \\ T(16\pi a^2 r^{(i)}_\sigma)^{-1}{\rm Li}_2(r^{(1)}_\sigma r^{(2)}_\sigma), & aT\gg 1 \end{cases}\end{aligned} \tag{39}$$

where only the last form is specific to the constant reflection model.

The one-loop correction (38) now simplifies to

$$\begin{aligned}\Delta\mathcal{F}_\sigma^{\rm L} \approx &-\frac{T^2}{4\pi^2}\sum_{m,m'=0}^{\infty}{}'\int_{\zeta_m}^{\infty} d\kappa\kappa \int_{\zeta_{m'}}^{\infty} d\kappa'\kappa' \\ &\times \sum_{i=1,2}\Phi^{(i)}_{\sigma,0}(\kappa)\chi^{(i)}_\sigma(\kappa,\kappa')\Phi^{(i)}_{\sigma,0}(\kappa').\end{aligned}$$

The dependence of $\chi^{(i)}_\sigma$ on $\kappa,\kappa'$ is of course unknown, but it is in the spirit of our simple model to assume it constant with respect to these arguments (dependent on $r^{(1)}_\sigma$ and $r^{(2)}_\sigma$ only) as a first approximation so as to extract some information as to how the corrections to Casimir force and free energy depend on distance. In this model the simple result is

$$\Delta\mathcal{F}_\sigma^{\rm L} \approx -\chi^{(i)}_\sigma\left[\Phi^{(i)}_\sigma\right]^2 \propto \begin{cases} a^{-6}, & T=0 \\ T^2a^{-4}, & aT\gg 1 \end{cases} \tag{40}$$

with $\Phi^{(i)}_\sigma$ from (39).

The indication is thus that the change in the Casimir pressure will fall off as $a^{-7}$ and $a^{-5}$ in the two regimes respectively, much faster than the Casimir pressure, which falls off as $a^{-4}$ and $a^{-3}$ respectively. Although tentative and subject to restrictive assumptions, the above calculation indicates that the effect of the generalised force on reflectivity is likely to be negligible under most circumstances. It is notable, however, that the effect increases as $T^2$ in the high $aT$ limit, whereas the Casimir force is a linear function of temperature in this regime.

## Conclusions

We have reviewed how the Casimir effect can be thought of as a multiple scattering phenomenon, an observation which inspires the use of a simple model in which the reflection coefficients of interacting bodies (the relative amplitude of reflected vs. incoming field) are

assumed to be independent of the direction and energy of the field. We review how this simple model yields some closed form results in the planar geometry famoyusly considered by Casimir and Lifshitz, and how much important information may be extracted with relatively simple methods within the confines of the model.

We review how the frequency spectrum of the Casimir effect is generalised from perfect reflection and becomes analytic and continuous upon introducing non-unity reflection coefficients. The full asymptotic behaviour of the Casimir-Lifshitz free energy in powers of temperature is found, and it is demonstrated how the transition to the perfectly reflecting case is not smooth. This is another demonstration of the non-analytic behaviour of the Lifshitz formalism in the double limit of zero temperature and perfect reflection which has given rise to debate over the thermodynamic consistency of various reflection models in connection with the temperature behaviour of the Casimir force.

We finally discuss the idea of a generalised "Casimir" force conjugate to the reflection coefficients of the interacting bodies. If there exist mechanisms by which the materials involved could be susceptible to changing their reflective properties, the generalised force initiates a back reaction effect by which the reflection coefficients tend towards their maximal available values, increasing the Casimir interaction. The indication is, however, that the effect would be small and fall off faster with interplate separation than the Casimir force itself.

## Acknowledgements

I wish to express my gratitude to Professor Iver Brevik who opened my eyes to the Casimir universe, whose formidable insight into many and diverse areas of physics is a constant source inspiration, and without whose careful supervision and assiduous support I could not have come this far. Further thanks go to Professor Kimball A. Milton for many useful comments on this manuscript.

## References

[1] H. B. G. Casimir, Proc. Kon. Ned. Akad. Wetensch. **51**, 793 (1948).

[2] S. A. Ellingsen, Europhys. Lett. **82**, 53001 (2008)

[3] S. M. Rytov, *Theory of Electric Fluctuations and Thermal Radiation* (Academy of Sciences Press, Moscow, Russia, 1953), English translation 1959 ed.

[4] E. M. Lifshitz, Zh. Eksp. Teor. Fiz. **29**, 94 (1955) [Sov. Phys. JETP **2**, 73 (1956)]

[5] E. I. Kats, Zh. Eksp. Teor. Fiz. **73**, 212 (1977) [Sov. Phys. JETP **46**, 109 (1977)]

[6] M. T. Jaekel and S. Reynaud, J. Phys. I **1**, 1395 (1991)

[7] A. Lambrecht, M. T. Jaekel and S. Reynaud, Phys. Lett. A **225** 188 (1997)

[8] C. Genet, A. Lambrecht and S. Reynaud, Phys. Rev. A **67**, 043811 (2003)

[9] A. Lambrecht, P. A. Maia Neto and S. Reynaud, New J. Phys. **8** 243 (2006)

[10] R. Esquivel, C. Villareal and W. Luis Mochán, Phys. Rev. A **68**, 052103 (2003)

[11] V. B. Svetovoy and R. Esquivel, Phys. Rev. E **72**, 036113 (2005)

[12] B. E. Sernelius, Phys. Rev. B **71**, 235114 (2005)

[13] M. S. Tomaš, Phys. Rev. A **66**, 052103 (2002)

[14] C. Raabe, L. Knöll and D.-G. Welsch, Phys. Rev. A **68**, 033810 (2003)

[15] M. S. Tomaš, Phys. Lett. A **342**, 381 (2005)

[16] C. Henkel, K. Joulain, Europhys. Lett **72**, 929 (2005)

[17] S. A. Ellingsen, J. Phys. A **40**, 1951 (2007)

[18] M. S. Tomaš, Phys. Rev. A **51**, 2545 (1995)

[19] S. A. Ellingsen and I. Brevik, J. Phys. A **40**, 3643 (2007)

[20] O. Kenneth and I. Klich, Phys. Rev. Lett. **97**, 160401 (2006)

[21] O. Kenneth and I. Klich, Preprint: quanth-ph/0707.4017 (2007)

[22] M. J. Renne, Physica **56** 125 (1971)

[23] R. Balian and B. Duplantier, Ann. Phys. **104**, 300 (1977); ibid. **112**, 165 (1978)

[24] M. Bordag, Phys. Rev. D **73**, 125018 (2006)

[25] T. Emig, N. Graham, R. L. Jaffe and M. Kardar, Phys. Rev. Lett **99**, 170403 (2007)

[26] K. A. Milton and J. Wagner, Phys. Rev. D **77**, 045005 (2008)

[27] K. A. Milton and J. Wagner, J. Phys. A **41**, 155402 (2008)

[28] K. A. Milton, P. Parashar and J. Wagner, Phys. Rev. Lett. (to appear), Preprint: hep-th/0806.2880 (2008)

[29] K. A. Milton, Invited opening talk at "60 years of Casimir effect", Brasilia, June 2008. Preprint: hep-th/0809.2564 (2008)

[30] K. A. Milton, J. Phys. A: Math. Gen. **37**, R209 (2004)

[31] L. D. Landau and E. M. Lifshitz *Statistical Physics Part 1* 3rd ed. (Amsterdam: Elsevier Butterworth-Heinemann, 1980) §123

[32] L. H. Ford, Phys. Rev. A **48**, 2962 (1993)

[33] J. Mehra, Physica **37** 145 (1967)

[34] J. S. Høye, I. Brevik, J. B. Aarseth, and K. A. Milton, Phys. Rev. E, **67**, 056116 (2003)

[35] L. S. Brown and G. J. Maclay, Phys. Rev. **184**, 1272 (1969)

[36] K. A. Milton *The Casimir Effect: Physical Manifestations of the Zero-Point Energy* (World Scientific, Singapore, 2001) §3.2.1

[37] S. A. Ellingsen, I. Brevik, J. S. Høye and K. A. Milton, Phys. Rev. E **78**, 021117 (2008)

[38] M. Abramowitz and I. A. Stegun *Handbook of Mathematical Functions* (New York: Dover, 1964)

[39] J. E. Robinson, Phys. Rev. **83** 678 (1951)

[40] K. S. Kölbig, J. A. Mignaco and E. Remiddi, BIT **10**, 38 (1970)

[41] G. L. Klimchitskaya and V. M. Mostepanenko, Contemp. Phys. **47**, 131 (2006)

[42] F. Intravaia and C. Henkel, J. Phys. A **41**, 164018 (2008)

[43] S. A. Ellingsen, Phys. Rev. E **78**, 021120 (2008)

[44] S. A. Å. Ellingsen, I. Brevik, J. S. Høye and K. A. Milton, Contribution to Proceedings of "60 years of Casimir effect", Brasilia, June 2008. Preprint: hep-th/0809.0763 (2008)

[45] A. Kempf, J. Phys. A **41** 164038 (2008)

[46] I. Brevik, S. A. Ellingsen and K. A. Milton, New J. Phys. **8**, 236 (2006)

[47] V. B. Bezerra et al., Phys. Rev. E **73**, 028101 (2006).

[48] M. Boström and Bo E. Sernelius, Phys. Rev. Lett. **84**, 4757 (2000); Physica A **339**, 53 (2004)

[49] P. R. Buenzli and Ph. A. Martin, Phys. Rev. E **77**, 011114 (2008)

# Article [f]

***Low temperature Casimir-Lifshitz free energy and entropy: the case of poor conductors***

S.Å. Ellingsen, I. Brevik, J.S. Høye, K.A. Milton

Journal of Physics: Conference Series **161**, 012010 (2009)

Journal of Physics: Conference Series **161** (2009) 012010 doi:10.1088/1742-6596/161/1/012010

# Low temperature Casimir-Lifshitz free energy and entropy: the case of poor conductors

**Simen Ådnøy Ellingsen[1], Iver Brevik[1], Johan S. Høye[2], Kimball A Milton[3]**

[1]Department of Energy and Process Engineering, Norwegian University of Science and Technology, N-7491 Trondheim, Norway
[2]Department of Physics, Norwegian University of Science and Technology, N-7491 Trondheim, Norway
[3]Oklahoma Center for High Energy Physics and Department of Physics and Astronomy, The University of Oklahoma, Norman, OK 73019, USA

E-mail: simen.a.ellingsen@ntnu.no

**Abstract.** The controversy concerning the temperature correction to the Casimir force has been ongoing for almost a decade with no view to a solution and has recently been extended to include semiconducting materials. We review some theoretical aspects of formal violations of Nernst's heat theorem in the context of Casimir Lifshitz thermodynamics and the role of the exponent of the leading term of the dielectric permittivity with respect to imaginary frequency. A general formalism for calculating the temperature corrections to free energy at low temperatures is developed for systems which do not exhibit such anomalies, and the low temperature behaviour of the free energy in a gap between half-spaces of poorly conducting materials modelled with a Drude type permittivity is calculated.

## 1. Introduction

The Casimir force [1], once merely a theoretical curiosity, is becoming the center of widespread attention in the wake of rapid developments in microtechnology. The enormous experimental progress made over the last decade towards accurately measuring this force [2–14] has created the need to calculate the Casimir force with high accuracy in realistic settings, taking into account such effects as material optical properties, surface roughness and geometry effects. Reviews of recent progress include [15–17].

It was realised quite early that an ambiguity existed as to the interpretation of Lifshitz' formula [18] for the Casimir attraction between dielectric half-spaces: when describing an ideal metal by taking the permittivity to infinity, different results were obtained at finite temperatures depending on the way the limit was taken. The ambiguity was originally sidestepped by prescription [19] and re-examined only much later by Boström and Sernelius [20] who concluded that due to the finite relaxation time of conduction electrons in a metal the transverse electric (TE) reflection coefficient of a metal-vacuum interface must vanish in the zero frequency limit, contrary to Casimir's ideal metal approximation in which reflection coefficients are set to unity at all energies. This was further supported by another study by Høye et al. [21]. For finite temperatures this vanishing of the TE zero frequency reflection coefficient leads to a prediction of a relatively large reduction of the Casimir force between metal plates at finite temperature, up

 

to 15% at 300K. The Boström-Sernelius analysis was opposed on thermodynamical grounds for violating Nernst's theorem (the third law of thermodynamics) which states that a nondegenerate system must have zero entropy at zero temperature [22]. Moreover it was concluded that the series of high accuracy experiments at Purdue exclude the thermal correction predicted by the theory in which the TE zero frequency mode does not contribute [11, 13]. The debate is summarised in recent reviews [23, 24].

Recently an analogous ambiguity in the Lifshitz formalism was brought up for the case of semiconductors [25–28]. A formal violation of Nernst's theorem is once again the difficulty, this time due to discontinuous behaviour in the transverse magnetic (TM) reflection coefficient, whose value in the limit of zero frequency depends intimitely on the way the small density of conducting electrons in semiconducting materials at finite temperatures are taken into account.

However, we do not expect such formal violations of Nernst's theorem stemming from the mathematical subtleties of the Lifshitz formula to have implications for the physics of the problem. In [21] it was concluded that on physical grounds, no TE zero mode should be present for real metals, and recently a quantum statistical mechanical treatment came to the same result [29]. For semiconductors, earlier statistical mechanical analyses by Jancovici and Šamaj [30, 31] and by Buenzli and Martin [32] for ionic systems are of interest. What is found is that the effective separation between the plates increases as twice the ionic shielding length, which implies a non-local behaviour of the dielectric function. This increase in effective separation also means that the ionic contribution to reflectivity vanishes with vanishing ionic concentration. The results of refs. [30–32] are restricted to ionic systems, but in the high temperature (classical) limit they recover the ideal metal result corresponding to no TE zero mode.

Several others have also developed non-local approaches to the problem of Lifshitz theory for poor conductors, notably Pitaevskii [33], Lamoreaux and Dalvit [34, 35], Esquivel [36] and most recently Svetovoy [37]. Also some these have not gone without objections [38–42]. We restrict ourselves to local permittivity models in the present effort.

## 2. Formal violations of Nernst's heat theorem; general theory

The Lifshitz formula expresses the Casimir free energy between parallel surfaces described by polarisation specific reflection coefficients $r_q$ where $q \in \{p, s\}$ is the polarisation (assuming specular reflection and no coupling between $p$ and $s$ modes). For simplicity we shall assume the surfaces to be identical in the following, in which case the Casimir free energy at temperature $T$ reads

$$\mathcal{F}(a) = \frac{T}{2\pi}{\sum_{m=0}^{\infty}}' \int_{\zeta_m}^{\infty} \mathrm{d}\kappa\kappa \sum_{q=p,s} \ln(1 - r_q^2 \mathrm{e}^{-2\kappa a}) \tag{1}$$

wherein $a$ is the plate separation, $p, s$ denotes TM and TE polarisations respectively, and $\mathrm{i}\zeta_m$ are the (imaginary) Matsubara frequencies so that $\zeta_m = 2\pi m T$. As conventional, the prime on the summation mark signifies that the $m = 0$ term be taken with half weight. We will be using natural units $k_\mathrm{B} = \hbar = c = 1$ throughout. Henceforth we will frequently omit the subscript $m$ on $\zeta_m$ and the various quantities depending on it. The integral in (1) is over all transverse momenta $\mathbf{k}_\perp$ of the field ($\perp$ denotes a direction parallel to the surfaces) and the substitution $\kappa^2 = \mathbf{k}_\perp^2 + \zeta^2$ has been made.

In the case where the interfaces are between vacuum and a half-space made of dielectric material, the Fresnel reflection coefficients read

$$r_s = \frac{\kappa - \tilde{\kappa}}{\kappa + \tilde{\kappa}}; \quad r_p = \frac{\varepsilon\kappa - \tilde{\kappa}}{\varepsilon\kappa + \tilde{\kappa}}; \quad \tilde{\kappa} \equiv \sqrt{\kappa^2 + \zeta^2(\varepsilon - 1)}. \tag{2}$$

Here $\varepsilon = \varepsilon(\mathrm{i}\zeta)$ denotes the dielectric permittivity relative to vacuum.

It is straightforward to verify that the values of $r_q$ in the limit $\zeta \to 0$ depend on the leading exponent of $\varepsilon(\mathrm{i}\zeta)$ as this limit is approached. For materials with mobile charges, models of the permittivity will typically diverge in the zero frequency limit, whereas that of a pure dielectric isolator reaches a finite value, $\lim_{\zeta\to 0}\varepsilon(\mathrm{i}\zeta) = \bar{\epsilon}$. Assuming $\varepsilon(\mathrm{i}\zeta) \sim (\zeta/\tilde{\omega})^{\lambda}$ ($\tilde{\omega}$ is a constant) as $\zeta \to 0$, one readily obtains the limits arrayed in table 1 in which

$$\tilde{r}_s(\kappa) = -\frac{\kappa^2}{\tilde{\omega}^2}\left(\sqrt{1+\frac{\tilde{\omega}^2}{\kappa^2}}-1\right)^2 \leq 0. \tag{3}$$

| $\lambda$ | $r_s$ | $r_p$ |
|---|---|---|
| 0 | 0 | $\frac{\bar{\epsilon}-1}{\bar{\epsilon}+1}$ |
| $-1$ | 0 | 1 |
| $-2$ | $\tilde{r}_s(\kappa)$ | 1 |
| $< -2$ | $-1$ | 1 |

**Table 1.** Values of $r_q(\mathrm{i}\zeta \to 0, \kappa)$ for different exponents $\lambda$.

The model permittivities which cause formal violation of Nernst's theorem have the common trait that the exponent $\lambda$ takes one value at all finite temperatures which changes abruptly at exactly $T = 0$. A general treatment demonstrates that such temperature dependence is necessary in order for a formal violation of the theorem to occur [43, 44] as we will briefly explain.

An example is the application of a Drude model to describe the dielectric response of an infinitely large and perfectly pure metal lattice, for which $\varepsilon(\mathrm{i}\zeta)$ is modelled as

$$\varepsilon(\mathrm{i}\zeta) = 1 + \frac{\omega_{\mathrm{p}}^2}{\zeta[\zeta+\nu(T)]}. \tag{4}$$

For a real metal sample of finite size, $\nu(T)$ reaches a nonzero value at zero temperature due to electron scattering on boundaries, impurities and imperfections, and $\lambda = -1$ for all temperatures. In this case entropy vanishes in the zero temperature limit as it should [45,46]. In a perfect lattice of infinite size, however, electron relaxation is solely due to scattering on thermal phonons, so that $\nu \sim T^5$ as $T \to 0$. Thus $\lambda$ changes from $-1$ to $-2$ at $T = 0$, making $r_s$ jump discontinuously from zero to a finite value as seen in table 1. Clearly $\tilde{\omega} = \omega_{\mathrm{p}}$ in (3) in the case $\lambda = -2$.

Another example is the semiconductor whose conductivity vanishes as a function of $T$. If a Drude model is used to model the permittivity of such a material,

$$\varepsilon(\mathrm{i}\zeta) = 1 + \frac{\bar{\epsilon}-1}{1+\zeta^2/\omega_0^2} + \frac{4\pi\sigma(T)}{\zeta}, \tag{5}$$

a formal violation occurs when $\sigma(T)$ vanishes at exactly $T = 0$. In this case $\lambda = -1$ at all $T$ until absolute zero, where it skips to $\lambda = 0$ and the magnitude of $r_p$ jumps discontinuously.

Let

$$\lim_{\zeta\to 0} r_q = R_q(\kappa;\lambda) \tag{6}$$

as tabulated (note that apart from the $\lambda = -2$ $s$-mode, $R_q$ is independent of $\kappa$). It can be shown that when reflection coefficients jump discontinuously at $\zeta = 0$, the free energy obtains a term linear in temperature equal to the difference of the $m = 0$ terms of (1) as obtained with the two zero-frequency reflection coefficients respectively. If the leading $\zeta$ exponent of $\varepsilon$ changes

from $\lambda_1$ to $\lambda_2$ at exactly $T = 0$, therefore, it leads to a residual entropy $\mathcal{S} = -\partial\mathcal{F}/\partial T$ at zero temperature

$$\mathcal{S}_{\lambda_1\to\lambda_2} = \frac{1}{4\pi}\sum_{q=p,s}\int_0^\infty \mathrm{d}\kappa\kappa \ln\frac{1-R_q^2(\kappa;\lambda_2)\mathrm{e}^{-2\kappa a}}{1-R_q^2(\kappa;\lambda_1)\mathrm{e}^{-2\kappa a}}. \tag{7}$$

In particular, when $R_q(\kappa;\lambda_1) = R_q(\lambda_1)$ and $R_q(\kappa;\lambda_2) = R_q(\lambda_2)$ one may use the relation

$$\int_0^\infty \mathrm{d}\kappa\kappa \ln[1-R^2\mathrm{e}^{-2\kappa a}] = -\frac{1}{4a^2}\mathrm{Li}_3(R^2) \tag{8}$$

where $\mathrm{Li}_n(x)$ is the $n$th order polylogarithmic function

$$\mathrm{Li}_n(x) = \sum_{l=1}^\infty \frac{x^l}{l^n} \tag{9}$$

to write

$$\mathcal{S}_{\lambda_1\to\lambda_2} = \frac{1}{16\pi a^2}\sum_{q=p,s}\left\{\mathrm{Li}_3[R_q^2(\lambda_1)] - \mathrm{Li}_3[R_q^2(\lambda_2)]\right\}. \tag{10}$$

In the particular cases of Drude modelled metals and semiconductors discussed above it follows immediately from table 1 and Eqs. (7) and (10) that, respectively,

$$\mathcal{S}_{-1\to-2} = \frac{1}{4\pi}\int_0^\infty \mathrm{d}\kappa\kappa \ln[1-\tilde{r}_s^2(\kappa)\mathrm{e}^{-2\kappa a}]; \qquad \text{(metals)} \tag{11a}$$

$$\mathcal{S}_{-1\to0} = \frac{1}{16\pi a^2}\left\{\zeta(3) - \mathrm{Li}_3[R_p^2(0)]\right\} \qquad \text{(semiconductors)} \tag{11b}$$

where $R_p(0) = (\bar{\epsilon}-1)/(\bar{\epsilon}+1)$ and where we have used $\mathrm{Li}_n(1) = \zeta(n)$, the Riemann zeta function. These two exponent transitions are those which come into play for metals and dielectrics respectively, or more precisely, upon plugging a Drude-type permittivity model with vanishing $\nu(T)$ or $\sigma(T)$ into the Lifshitz formula and extrapolating to zero temperature. Other exponent transitions, naturally, would give other zero point entropy expressions.

Note that by letting $\tilde{\omega}\to\infty$ in (3) so that $\tilde{r}_s(\kappa)\to-1$, the entropy (11a) becomes

$$\mathcal{S}_{-1\to-2} \overset{\tilde{\omega}\to\infty}{\longrightarrow} -\frac{\zeta(3)}{16\pi a^2}, \tag{12}$$

which is the well known result for the so-called modified ideal metal model obtained by this procedure [21].

## 3. Free energy temperature correction for poor Drude conductor

The model for the conductivity we will be studying in the following is assumed not to depend on $T$ within a finite range of temperatures including $T = 0$, in which case it is clear from the above that Nernst's theorem will be satisfied. While the consideration of such a model cannot resolve such anomalies as reported in the previous section, it is nonetheless useful to establish benchmark results in various models within the Lifshitz formalism which exhibits very nontrivial behaviour in the joint limit of zero temperature and frequency $\zeta$.

We consider a semiconductor modelled by a Drude type permittivity such as (5), but where we assume $\sigma$ to be constant within a finite range of low temperatures including $T = 0$ (the case $\sigma = 0$ was worked out in [25]). A more detailed treatment of this model may be found in [47].

The method used is to note that $\mathcal{F}(a,T)$ depends on $T$ only through the prefactor $T$ and the Matsubara frequencies $\zeta_m = 2\pi m T$, so we may write the free energy (1) on the form[1]

$$\mathcal{F} = T \sum_{q=p,s} f_q(a) {\sum_{m=0}^{\infty}}' g(\mu) \tag{13}$$

where the function $f_q(a)$ is a convenient prefactor and we use the shorthand notation $\mu \equiv mt$ where $t = T/T_0$ is a dimensionless rescaled temperature to be defined in Eq. (18) below.

In the limit $T = 0$ the sum becomes an integral, and we are interested in the difference between sum and integral, which may be found from the Euler-Maclaurin formula. It turns out $g(\mu)$ is not analytical at $m = 0$ so it is necessary to start the sum at $m = 1$ (or a higher value), writing

$$\begin{aligned}\tilde{\Gamma} &\equiv \left[{\sum_{m=0}^{\infty}}' - \int_0^\infty \mathrm{d}m\right] g(mt) = \frac{1}{2}g(0) - \int_0^1 g(mt)\mathrm{d}m + \frac{1}{2}g(t) - \sum_{k=1}^{\infty} \frac{B_{2k}}{(2k)!} g^{(2k-1)}(t) \\ &= \frac{1}{2}g(0) - \int_0^1 g(mt)\mathrm{d}m + \frac{1}{2}g(t) - \frac{1}{12}g'(t) + \frac{1}{720}g'''(t) - \ldots .\end{aligned} \tag{14}$$

Since the correction terms in (14) are evaluated at $m = 1$ and we are considering small $T$, we may choose $T_0 \gg T$ so that $\mu \ll 1$. We anticipate that when expanded for small $\mu$, the function $g(\mu)$ is of the form

$$g(\mu) \sim c_0 + c_1\mu + c_{\frac{3}{2}}\mu^{\frac{3}{2}} + c_{2l}\mu^2 \ln(\mu) + c_2\mu^2 + c_3\mu^3 + ..., \quad \mu \to 0 \tag{15}$$

Upon insertion into (14) one finds that the $c_0$ and $c_2$ terms do not contribute. Terms of integer powers of $\mu$ are determined by a finite number of terms in the series (14), but for the terms containing logarithms or half-integer powers every term contributes. The series obtained is asymptotic but a meaningful value may nonetheless be assigned to all terms of (15) by defining the series by Borel summation[2] or zeta regularisation. The result for polarisation mode $q = p, s$ is [47]

$$\Delta\mathcal{F}_q = T f_q(a) \tilde{\Gamma}_q = T f_q(a) \left[ -\frac{c_1}{12}t + \zeta(-\tfrac{3}{2})c_{\frac{3}{2}}t^{\frac{3}{2}} + \frac{\zeta(3)c_{2l}}{4\pi^2}t^2 + \frac{c_3}{120}t^3 + ... \right]_q \tag{16}$$

giving terms proportional to respectively $T^2, T^{\frac{5}{2}}, T^3$ and $T^4$. It is understood that the coefficients $c_1$ through $c_3$ are polarisation mode specific. We shall content ourselves with expanding free energy to order $T^3$ in the present paper.

Equation (16) effectively reduces the problem to one of determining the expansion coefficients of Eq. (15). This task is still not trivial, however, and we consider only the "intermediate asymptotic" region in which conductivity is very small compared to inverse separation but much greater than temperature

$$T \ll 4\pi\sigma \ll \frac{1}{a}. \tag{17}$$

It is convenient now to define $T_0 = 2\sigma$, that is

$$t = \frac{T}{T_0} \equiv \frac{\zeta_1}{4\pi\sigma} = \frac{2\pi T}{4\pi\sigma}. \tag{18}$$

[1] Note that this convention differs sightly from that of [47].
[2] See appendix of [47]

Assumption (17) ensures that $t \ll 1$. The frequency which enters into (14) is $\zeta_1 \sim T \ll \sigma$, so $\varepsilon(\mathrm{i}\zeta)$ simplifies to

$$\varepsilon = \bar{\epsilon} + \frac{1}{\mu} \tag{19}$$

We will consider the $p$ and $s$ modes individually in the following.

## 4. The TM mode

The TM mode expression for Casimir Lifshitz free energy exhibits highly nontrivial behaviour near zero temperature. To simplify matters we note from (17) that the quantity

$$\alpha \equiv 2a(4\pi\sigma) \tag{20}$$

obeys $\alpha \ll 1$. We will determine free energy corrections perturbatively in powers of $\alpha$ in order to obtain analytical results for the coefficients in (15).

Substituting the integration variable

$$x = 2\kappa a = \frac{\kappa\alpha\mu}{\zeta} \tag{21}$$

the TM free energy may be written

$$\mathcal{F}_p = \frac{(4\pi\sigma)^3 t}{4\pi^2\alpha^2}{\sum_{m=0}^{\infty}}' \left\{ \int_{\alpha\mu}^{\infty} \mathrm{d}x x \ln(1 - r_p^2 \mathrm{e}^{-x}) \right\} \equiv \frac{(4\pi\sigma)^3 t}{4\pi^2\alpha^2}{\sum_{m=0}^{\infty}}' g_p(m) \tag{22}$$

where $g_p(m)$ is now chosen to be the expression within the curly braces. To leading order in $\alpha$ one finds

$$\ln(1 - r_p^2 \mathrm{e}^{-x}) = \ln(1 - A_\mu \mathrm{e}^{-x}) + \mathcal{O}(\alpha^2); \tag{23a}$$

$$A_\mu \equiv \left( \frac{1 + (\bar{\epsilon} - 1)\mu}{1 + (\bar{\epsilon} + 1)\mu} \right)^2. \tag{23b}$$

With the reflection squared coefficient now a constant with respect to $x$ the integral in (22) can be solved explicitly and expansion in $\mu$ as in (15) yields the coefficients $c_1$ and $c_{2l}$ to leading order in $\alpha$ as simply [47]

$$c_1 = \frac{2\pi^2}{3}; \quad c_{2l} = 8 \tag{24}$$

and with (16) the low temperature correction to free energy is to leading order in $\alpha$ in terms of $T$ and $\sigma$ reads:

$$\Delta\mathcal{F}_p = -\frac{\pi^2 T^2}{72(4\pi\sigma)a^2} + \frac{\zeta(3)T^3}{\pi(4\pi\sigma)^2 a^2}. \tag{25}$$

An examination shows that the correction to this result is approximately a factor $\alpha^2$ smaller as anticipated.

## 5. The TE mode

A similar procedure is performed for the $s$ (or TE) mode. With the substitution

$$x = \frac{\kappa}{\zeta\sqrt{\varepsilon(i\zeta) - 1}} = \frac{\kappa\mu}{\chi\zeta}; \quad \chi \equiv \sqrt{\mu + (\bar{\epsilon} - 1)\mu^2}, \tag{26}$$

the TE term of the free energy (1) may be written

$$\mathcal{F}_s = \frac{(4\pi\sigma)^3 t}{4\pi^2} {\sum_{m=0}^{\infty}}' \left\{ \chi^2 \int_{\mu/\chi}^{\infty} \mathrm{d}x x \ln(1 - r_s^2 \mathrm{e}^{-\alpha\chi x}) \right\} = \frac{(4\pi\sigma)^3 t}{4\pi^2} {\sum_{m=0}^{\infty}}' g_s(m). \tag{27}$$

Again $g_s(m)$ is defined as the expression between the curly braces and in the new variables the squared reflection coefficient reads

$$r_s^2(x) = (\sqrt{x^2+1} - x)^4. \tag{28}$$

Expanding the logarithm of (27) to linear order in $\alpha$,

$$\ln(1 - r_s^2 \mathrm{e}^{-\alpha\chi x}) = \ln(1 - r_s^2) + \frac{\alpha\chi x r_s^2}{1 - r_s^2} + \mathcal{O}(\alpha^2) \tag{29}$$

allows us to determine the temperature corrections for these orders of $\alpha$. Both terms on the right hand side of (29) give integrals over $x$ which are explicitly solvable, and subsequent expansions in powers of $\mu$ give the coefficients

$$c_1 = -\frac{1}{4}(2\ln 2 - 1); \quad c_{2l} = -\frac{1}{4}; \quad c_{\frac{3}{2}} = \frac{\alpha}{12}. \tag{30}$$

Clearly $c_{\frac{3}{2}} \ll c_1, c_{2l}$, being of linear order in $\alpha$. The temperature corrections for the TE mode thus read

$$\Delta\mathcal{F}_s = \frac{(4\pi\sigma)T^2}{48}(2\ln 2 - 1) + \frac{1}{6}\sqrt{2\pi}\zeta(-\tfrac{3}{2})a(4\pi\sigma)^{\frac{3}{2}}T^{\frac{5}{2}} - \frac{\zeta(3)T^3}{8\pi} + \mathcal{O}(T^{\frac{7}{2}}). \tag{31}$$

This result is in fact in perfect agreement with that obtained for Drude metals [45] but includes one more order. Thus the concordance implies that a further expansion in $\alpha$ would only yield corrections of higher orders in temperatures, and that for the case of the TE mode the expansion in $\alpha$ was not essential for obtaining this result. Eq. (31) is therefore valid also when $\alpha$ is not small, as is the case for a good conductor.

Notably the temperature corrections are independent of $\bar{\epsilon}$ to order $T^3$ for both polarisations and only enters in higher orders, an insight not included in [45].

## 6. Numerical verification of results

The final results (25) and (31) have been checked numerically to verify their correctness [47]. A plot of the theoretical correction (25) compared to a direct numerical calculation of the free energy is provided in figure 1.

A much more sensitive test is provided by the quantity

$$R_p = \frac{\Delta\mathcal{F}_p^{\mathrm{th}} - \Delta\mathcal{F}_p^{\mathrm{num}}}{\Delta\mathcal{F}_p^{\mathrm{th}}} \tag{32}$$

where $\Delta\mathcal{F}_p^{\mathrm{th}}$ is the theoretically predicted free energy correction (25) and $\Delta\mathcal{F}_p^{\mathrm{num}}$ is that found by direct numerical calculation. The data used for calculation are (in SI units) $a = 1000\mathrm{nm}$, $\sigma^{\mathrm{SI}}/\epsilon_0 = 10^{12}\mathrm{s}^{-1}$, $\bar{\epsilon} = 11.66$ and $\omega_0 = 8 \cdot 10^{15}\mathrm{s}^{-1}$.

We have found that $\Delta\mathcal{F}_p^{\mathrm{th}}$ is of the form $\Delta\mathcal{F}_p^{\mathrm{th}} = -CT^2(1 - C_1 T)$ and assume $\Delta\mathcal{F}_p^{\mathrm{th}}$ to have the expansion

$$\Delta\mathcal{F}_p^{\mathrm{num}} = -DT^2(1 - D_1 T + D_2 T^2 + \dots), \tag{33}$$

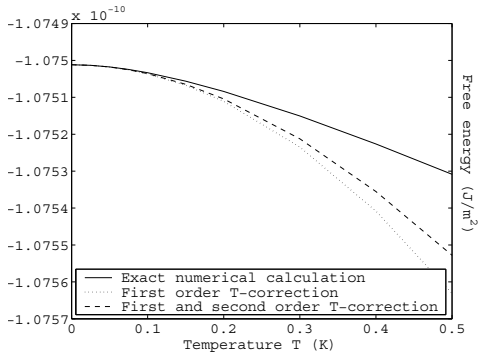


**Figure 1.** Free energy $\mathcal{F}_p$ calculated using direct numerical calculation and the theoretical correction (25) shifted to coincide with the numerical result at $T = 0$.

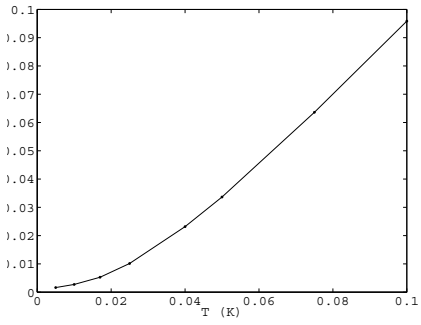


**Figure 2.** Plot of the quantity $R$ from Eq. (32).

which predicts the following expansion for $R$:

$$R = \frac{C-D}{C} - \frac{D}{C}(C_1 - D_1)T - \frac{D}{C}[D_2 + C_1(C_1 - D_1)]T^2 + \dots. \tag{34}$$

In the special case where $C = D$ and $C_1 = D_1$, this becomes

$$R = -D_2 T^2 + \mathcal{O}(T^3). \tag{35}$$

Thus if the coefficient $C$ is incorrect $R$ would not converge to 0 at $T = 0$, and an incorrect $C_1$ would show as a linear behaviour at small temperatures. None of these effects are perceptible in the figure, demonstrating that the corrections to (25) are small as predicted.

A similar high precision check of the result for the $s$ mode (31) was not possible with these numerical parameter values because the correction relative to the free energy at zero temperature is extremely small, of order $10^{-9}$ at 1K. The correctness of the terms proportional to $T^2$ and $T^{\frac{5}{2}}$ was however thoroughly verified for a good conductor in [45]. The term $\propto T^3$ is numerically elusive because while requiring very high accuracy for verification when $\alpha \ll 1$, it is completely dominated by other terms for good conductors. A comparison of a direct numerical calculation with the prediction (31) to order $T^2$ in figure 3 reveals that the difference between these graphs, plotted in figure 4, is in the same order of magnitude as the $T^3$ term in (31), while the term proportional to $T^{\frac{5}{2}}$ is too small to be visible at this level.

## 7. Conclusions

We have reviewed the theory of formal violations of Nernst's heat theorem emphasising the way such a formal violation can only occur when the leading order behaviour of $\varepsilon(\mathrm{i}\zeta)$ with respect to $\zeta$ undergoes a discontinuous change at exactly $T = 0$. Such apparent problems with the Lifshitz formalism occur when the double limit where $T$ and $\zeta$ are both taken to zero is not unique and depends intimately on the exact way in which a material's dielectric (and, in general, magnetic) response is modelled in this limit. As a general remark, Nernst's theorem concerns zero temperature only, and it is not *a priori* clear that one can simply extrapolate between these two very different temperatures and use a result at one temperature to draw conclusions at another. In particular, if a system behaves essentially different at $T = 0$ than

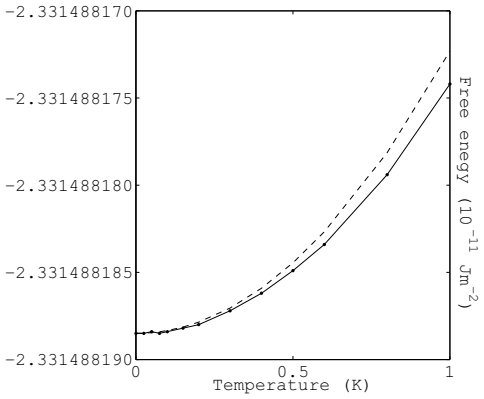


**Figure 3.** Free energy $\mathcal{F}_s$ calculated using direct numerical calculation and the theoretical correction (31) to order $T^2$ shifted to coincide with the numerical result at $T = 0$.

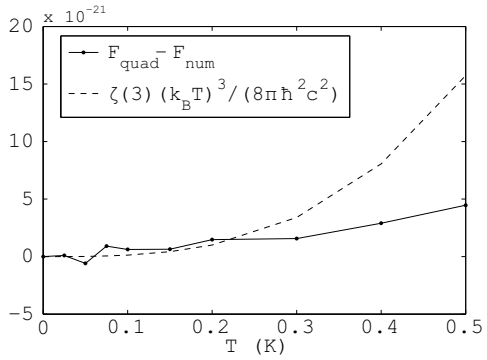


**Figure 4.** The difference between the graphs in figure 3 plotted against the $T^3$ term of (31).

at room temperature, a formal violation of Nernst's theorem by extrapolation is not necessarily worrisome. The results obtained complement those found in the case of zero conductivity in [25] and generalise TE mode calculations for Drude metals in [45].

Using a Drude type model to describe a poor conductor whose conductivity stays finite at zero temperature we establish the low temperature corrections to Casimir Lifshitz free energy between two identical half-spaces separated by vacuum. As modelled, both TE and TM modes exhibit a quadratic temperature behaviour at low temperatures.

## References

[1] Casimir H B G 1948 *Proc. Kon. Ned. Akad. Wetensch.* **51** 793
[2] Lamoreaux S K 1997 *Phys. Rev. Lett.* **87** 5
[3] Mohideen U and A. Roy A 1998 *Phys. Rev. Lett.* **81** 4549
[4] Roy A, Lin C-Y, and Mohideen U 1999 *Phys. Rev. D* **60** 111101(R)
[5] Harris B W, Chen F, and Mohideen U 2000 *Phys. Rev. A* **62** 052109
[6] Ederth T 2000 *Phys. Rev. A* **62** 062104
[7] Chan H B et al. 2001 *Phys. Rev. Lett.* **87** 211801; 2001 *Science* **291** 1941
[8] Chen F, Mohideen U, Klimchitskaya G L, and Mostepanenko V M 2002 *Phys. Rev. Lett.* **88** 101801
[9] Bressi G, Carugno G, Onofrio R, and Ruoso G 2002 *Phys. Rev. Lett.* **88** 041804
[10] D. Iannuzzi, M. Lisanti and F. Capasso, Proc. Natl. Acad. Sci. USA **101** 4019 (2004)
[11] Decca R S et al. 2005 *Ann. Phys. (N.Y.)* **318** 37
[12] M. Lisanti, D. Iannuzzi and F. Capasso, Proc. Natl. Acad. Sci. USA **102** 11989 (2005)
[13] Bezerra V B et al. 2006 *Phys. Rev. E* **73** 028101
[14] Chen F, Klimchitskaya G L, Mostepanenko V M, and Mohideen U 2007 *Phys. Rev. B* **76** 035338
[15] Milton K A 2004 *J. Phys. A: Math. Gen.* **37** R209
[16] Buhmann S Y and Welsch D-G 2007 *Prog. Quantum Electron.* **31** 51
[17] Capasso F, Munday J N, Iannuzzi D and Chan H B 2007 *IEEE J. Selec. Top. Quant. Electron.* **13** 400
[18] Lifshitz E M 1955 *Zh. Eksp. Teor. Fiz.* **29** 94
[19] Schwinger J, DeRaad Jr. L L, and Milton K A 1978 *Ann. Phys. (N.Y.)* **115** 1
[20] Boström M and Sernelius B E 2000 *Phys. Rev. Lett.* **84** 4757
[21] Høye J S, Brevik I, Aarseth J B, and Milton K A 2003 *Phys. Rev. E* **67** 056116
[22] Klimchitskaya G L and Mostepanenko V M 2001 *Phys. Rev. A* **63** 062108
[23] Brevik I, Ellingsen S A and Milton K A 2006 *New J. Phys.* **8** 236
[24] Klimchitskaya G L and Mostepanenko V M 2006 *Comtemp. Phys.* **47** 131

[25] Geyer B, Klimchitskaya G L, and Mostepanenko V M 2005 *Phys. Rev. D* **72** 085009
[26] Klimchitskaya G L, Geyer B, and Mostepanenko V M 2006 *J. Phys. A: Math. Gen.* **39** 6495
[27] Geyer B, Klimchitskaya G L, and Mostepanenko V M 2006 *Int. J. Mod. Phys. A* **21** 5007
[28] Klimchitskaya G L and Geyer B 2008 *J. Phys. A: Math. Theor.* **41** 164014
[29] Buenzli P R and Martin Ph A 2008 *Phys. Rev. E* **77** 011114
[30] Jancovici B and Šamaj L 2004 *J. Stat. Mech.* P08006
[31] Jancovici B and Šamaj L 2005 *Europhys. Lett.* **72** 35
[32] Buenzli P R and Martin Ph A 2005 *Europhys. Lett.* **72** 42
[33] Pitaevskii L P 2008 *Phys. Rev. Lett* **101** 163202
[34] Lamoreaux S K 2008 *Preprint* quant-ph:0801.1283
[35] Dalvit D A R and Lamoreaux S K 2008 *Preprint* quant-ph:0805.1676
[36] Esquivel-Sirvent R 2008 *Phys. Rev. A* **77** 042107
[37] Svetovoy V B 2008 *Phys. Rev. Lett.* **101** 163603
[38] Klimchitskaya G L, Mohideen U and Mostepanenko V M 2008 *J. Phys. A* **41** 432001
[39] Decca R S et al. 2008 *Preprint* quant-ph:0803.4247
[40] Geyer B, Klimchitskaya G L, Mohideen U and Mostepanenko 2008 *Preprint* quant-ph:0810.3243
[41] Decca R S et al. 2008 *Preprint* quant-ph:0810.3244
[42] Klimchitskaya G L, Mohideen U and Mostepanenko 2008 *Preprint* cond-mat:0810.3247
[43] Ellingsen S A 2008 *Phys. Rev. E* **78** 021120
[44] Intravaia F and Henkel C 2008 *J. Phys. A: Math. Theor.* **41** 164018
[45] Høye J S, Brevik I, Ellingsen S A, and Aarseth J B, 2007 *Phys. Rev. E* **75** 051127
[46] Brevik I, Ellingsen S A, Høye J S, and Milton K A 2008 *J.Phys. A: Math. Theor.* **41** 164017
[47] Ellingsen S A, Brevik I, Høye J S, and Milton K A 2008 *Phys. Rev. E* **78** 021117

# Article [g]

***The Casimir frequency spectrum: can it be observed?***

S.Å. Ellingsen

Journal of Physics: Conference Series **161**, 012011 (2009)

Journal of Physics: Conference Series **161** (2009) 012011 doi:10.1088/1742-6596/161/1/012011

# The Casimir frequency spectrum: can it be observed?

**Simen Ådnøy Ellingsen**

Department of Energy and Process Engineering, Norwegian University of Science and Technology, N-7491 Trondheim, Norway

E-mail: simen.a.ellingsen@ntnu.no

**Abstract.** The frequency spectrum of the Casimir force between real materials is studied with a view to assess possible ways of by which its dramatic oscillatory behaviour might be observed. Two simple attempts are made in which a model material is perturbed so as to become semitransparent in a band of frequencies. It is found that the real frequency formalism of the Casimir Lifshitz force is extremely volatile upon manipulations of optical properties and produces nonsensical results when extreme care is not taken to ensure the physicality of all perturbations, whereas the imaginary frequency formalism is highly robust and behaves well even under unphysical manipulations. The indication is thus that the general physical requirements of response functions preclude the observation of the frequency spectrum.

## 1. Introduction

The dependence of the Casimir force on the frequency dependent dielectric response of materials has long been an issue of intense research and at times a source of controversy. Casimir's original calculation of the fluctuation induced attraction between parallel plates assumed ideal conductors, perfectly reflecting at all field energies [1], and was generalised by Lifshitz a few years later [2] to materials of arbitrary frequency dependent dielectric response. The Lifshitz formula has since come to be recognised as a special case of a much more general formalism of multiple scattering [3, 4], yet while much progress has been made in research on the Casimir effect between more general bodies, the role of the inclusion of material dispersion properties in the simple two-plate geometry is still imperfectly understood. This has been most clearly demonstrated in the long ongoing disagreement over the thermal behaviour of the Casimir force and free energy (e.g. [5, 6] and references therein), a controversy centered in essence on the exact optical properties of materials at very low frequencies.

Upon incorporating the dispersive properties of materials, the expression for the total Casimir attraction between objects must necessarily include an integral over all frequencies of the electromagnetic field. Since all real materials obey the laws of causality it is possible [7] to shift the integral from the real to the positive imaginary frequency axis, which for the purposes of calculation is most often preferable. While the integrand along the imaginary frequency axis will typically be nicely peaked and exponentially decaying at high frequencies and therefore well suited for numerical evaluation, the real-frequency integrand is the direct opposite. Ford and others investigated the real-frequency spectrum of the Casimir force some time ago and showed how it is wildly oscillating, with the area under one oscillation peak of the frequency integrand much greater than the measurable Casimir force itself [8–10].

Formally, thus, the Casimir effect appears to emerge as the sum of an alternating series of very

 

large and almost exactly canceling contributions. This inspired the suggestions that the optical properties of materials may be tuned so as to produce a Casimir force of desired magnitude and even sign [10, 11]. A handful of efforts have since elaborated this prospect [12–15], while an analysis by Genet and co-workers concluded that due to general restrictions of causality and analyticity such possibilities could not be realised [16].

Recently, the interpretation of an experiment by Iannuzzi and co-workers [17] was revisited in light of the considerations of the frequency spectrum of the Casimir force [18]. The experiment measured the Casimir attraction between so-called hydrogen switchable mirrors (HSMs). A HSM is a material which is a good metallic reflector in its as-deposited state but becomes transparent in the visible frequency range upon placement in a hydrogen rich atmosphere. While the reflection properties of the HSM are quite drastically different in the two states, the group was unable to detect a significant change in the Casimir attraction from one atmosphere to the other at a precision in the order of 15%. At face value this negative result seems at odds with the predictions of Ford, yet an alternative calculation of the effects of such a change of reflectivity indicates that the expected effects on the force might indeed be rather modest. A more careful analysis was made in [19].

In the following the recent analysis on the effect of perturbations of optical properties on the real frequency axis is reviewed and extended.

## 2. Frequency spectrum of the Casimir Lifshitz force

The frequency spectrum of Casimir interactions may be taken from the Lifshitz formula for real frequencies or worked out on more general grounds from the stress tensor operator of the quantised electromagnetic field. The Lifshitz formula in the form most useful for this purpose reads [2] (zero temperature is assumed henceforth)

$$P(a) = -\frac{1}{2\pi^2}\Re\mathrm{e}\int_0^\infty \mathrm{d}\omega\omega^3\int_C \mathrm{d}pp^2\sum_{\sigma=s,p}\frac{r_\sigma^2\exp(2\mathrm{i}p\omega a)}{1-r_\sigma^2\exp(2\mathrm{i}p\omega a)}. \tag{1}$$

Here $P(a)$ is the Casimir pressure between the parallel plates separated by a distance $a$ where the minus sign signifies an attractive force. Natural units $\hbar = c = k_\mathrm{B} = 1$ are used throughout. $\omega$ is the real-valued frequency and the integral over the Lifshitz variable $p = \sqrt{(\mathbf{k}_\perp/\omega)^2 - 1}$ (physically the sum over all momentum components parallel to the surfaces) runs from 1 to 0 covering the propagating part of the spectrum, and thence to $\mathrm{i}\infty$ summing up all evanescent field contributions.

The frequency spectrum $P_\omega(a)$ is simply defined as

$$P(a) = \int_0^\infty \mathrm{d}\omega P_\omega(a) = \int_0^\infty \mathrm{d}\omega\sum_{\sigma=s,p} P_{\omega,\sigma}(a). \tag{2}$$

This spectrum in fact equals that derived by Ford with a more fundamental procedure [8, 10]. With the special modelling assumption that reflection coefficients are constant with respect to $\mathbf{k}_\perp$ the $p$-integral (1) may be solved explicitly by use of the polylogarithmic function

$$\mathrm{Li}_n(x) = \sum_{k=1}^\infty \frac{x^k}{k^n} \tag{3}$$

which obeys the useful recursion relation ($A$ and $K$ are constants)

$$\int \mathrm{d}y\mathrm{Li}_n(A\mathrm{e}^{\eta y}) = \frac{1}{\eta}\mathrm{Li}_{n+1}(A\mathrm{e}^{\eta y}) + K \tag{4}$$

to yield the following frequency spectrum

$$P_\omega(a;\{r_\sigma\}) = \frac{-1}{16\pi^2 a^3}\sum_{\sigma=s,p}\left[-\xi^2\Im\mathrm{m}\mathrm{Li}_1(r_\sigma^2 e^{\mathrm{i}\xi}) - 2\xi\Re\mathrm{e}\mathrm{Li}_2(r_\sigma^2 e^{\mathrm{i}\xi}) + 2\Im\mathrm{m}\mathrm{Li}_3(r_\sigma^2 e^{\mathrm{i}\xi})\right] \quad (5)$$

where the shorthand dimensionless quantity $\xi = 2\omega a$ is introduced. The spectrum (5) is plotted in figure 1 assuming $r_\sigma$ are also constant with respect to frequency.

When the latter assumption is made, the frequency integral is explicitly solvable and the Casimir zero temperature pressure is found as

$$P(a,\{r_\sigma\}) = -\frac{3}{16\pi^2 a^4}\sum_{\sigma=p,s}\Re\mathrm{e}\mathrm{Li}_4(r_\sigma^2). \quad (6)$$

Casimir's result $P_\mathrm{C}(a) = -\pi^2/(240a^4)$ is regained by inserting $r_p^2 = r_s^2 = 1$ and $\mathrm{Li}_4(1) = \zeta(4) = \pi^4/90$. Exactly the same treatment starting from the Lifshitz formula for the zero temperature free energy rather than pressure yields

$$\mathscr{F}(a,\{r_\sigma\},T=0) = -\frac{1}{16\pi^2 a^3}\sum_{\sigma=p,s}\Re\mathrm{e}\mathrm{Li}_4(r_\sigma^2) \quad (7)$$

which again simplifies trivially to Casimir's result in the limit $r_\sigma = 1$.

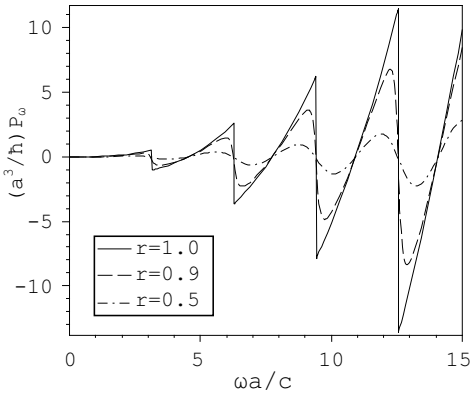


**Figure 1.** The frequency spectrum (5) normalised by $a^{-3}$ for different (constant) values of $r_\sigma = r$, assumed equal for both polarisations.

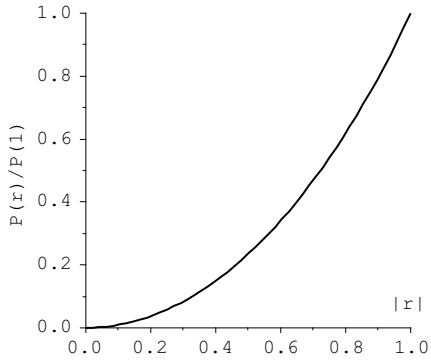


**Figure 2.** Casimir pressure (6) as function of constant reflection coefficient $r$, normalised by the ideal conductor limit $P_\mathrm{C}(a) = -\pi^2/(240a^4)$.

### 3. Frequency spectrum with real materials

When more realistic material properties are employed, the frequency spectrum of the Casimir force is no longer as regular as that shown in figure 1, but shares the property of wild oscillation of increasing amplitude throughout the frequency range in which optical data are typically available. Given an explicit expression of reflection coefficients as functions of frequency and transverse momentum, it is straightforward to calculate and plot the frequency spectrum, as shown in figure 3. In these calculations the permittivity function for gold is used, represented

by, respectively, the simple plasma model $\epsilon(\omega) = 1 - \omega_{\rm p}^2/\omega^2$ with $\omega_{\rm p} = 9.0$eV and interpolation of experimental optical data tabulated in [20]. The graphs share the trait of large oscillations which make them unsuitable for most numerical purposes. It is notable, however, that the two spectra are radically different even though a calculation of the total Casimir force by the standard method of rotating the integral onto the imaginary frequency axis gives almost identical results whether the plasma model or the corresponding data set from [20] is used.

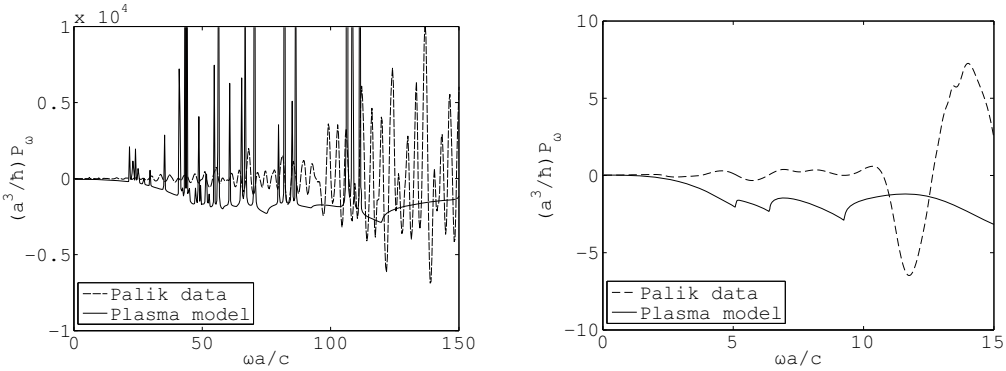


**Figure 3.** Numerically calculated frequency spectrum using repectively data from [20] and the plasma model, $\epsilon(\omega) = 1 - \omega_{\rm p}^2/\omega^2$. Note that the spectrum is now a function of $a$ and $\omega$ individually, not only their product; $a = 100$nm is used in the figure.

The striking nature of these spectra naturally raises the question whether or not such giant oscillations could be observable, and, if so, might even be used for experimental or technological purposes as proposed in previous publications. On purely qualitative grounds one may conclude from the extreme difference between the graphs in figure 3 that if observation of such a spectrum were indeed possible, quantitative predictions cannot be made using simple models such as the plasma or Drude model (the latter produces a spectrum reminiscent of that of the plasma model in figure 3 with a greater number of sharp peaks), and the direct use of extremely accurate optical data would be required.

## 4. Effects of a band perturbation of reflectivity

As figure 3 shows clearly, due to its highly oscillating nature the real frequency formalism is not very helpful for calculating the absolute Casimir force [21]. One may think, however, that it could nonetheless be fruitful for calculating a *change* of optical properties which was limited to a small interval of frequencies, in which case an integral might not need to span the entire frequency axis.

The experiment described above in which HSMs were used for the measurement of Casimir forces would seem a natural candidate for the use of a real-frequency formalism. Upon hydrogenation of the HSM, the material became transparent in the visible frequency range whereas the optical properties in the infrared and ultraviolet remained largely unchanged. The authors of [17, 19] propose a rough model for the description of the alteration of reflectivity in which the metallic permittivity of the mirror in the as-deposited state is "switched off" at $\omega_1 \approx 7.5 \cdot 10^{14}$rad/s and "on" again at $\omega_2 \approx 9.4 \cdot 10^{15}$rad/s. That is, $\epsilon(\omega) = 1 + 4\pi\chi(\omega) \longrightarrow \tilde{\epsilon}(\omega) = 1 + 4\pi\tilde{\chi}(\omega)$ where

$$\tilde{\chi}(\omega) = \chi(\omega)[1 - \theta(\omega - \omega_1)\theta(\omega_2 - \omega)]. \tag{8}$$

Here $\theta(x)$ is the unit step function. In fact the transition alters the properties at all frequencies to some extent [19], but as a first approximation one might expect that the "off/on" model would give at least an idea of the magnitude of the effect.

Using the formalism of imaginary frequencies, the effect of such an "off/on" model can be calculated by integration over the imaginary part of $\epsilon(\omega)$ in the relevant Kramers-Kronig relation. Using as an example the Drude model,

$$\epsilon(\omega) = 1 - \frac{\omega_{\rm p}^2}{\omega(\omega + {\rm i}\nu)}, \tag{9}$$

with $\nu$ being the electronic relaxation frequency (for gold $\nu = 35$meV is often used [22]), one may readily calculate the correction $\epsilon({\rm i}\zeta) \to \epsilon({\rm i}\zeta) - \Delta\epsilon({\rm i}\zeta)$ explicitly as

$$\begin{aligned}\Delta\epsilon({\rm i}\zeta) &= \frac{2}{\pi}\int_0^\infty \frac{{\rm d}\omega\omega[\epsilon''(\omega) - \tilde{\epsilon}''(\omega)]}{\omega^2+\zeta^2} = \frac{2}{\pi}\int_{\omega_1}^{\omega_2} \frac{{\rm d}\omega\omega\epsilon''(\omega)}{\omega^2+\zeta^2} \\ &= \frac{\omega_p^2}{\zeta^2-\nu^2}\frac{2}{\pi}\left[\arctan\frac{\nu\Delta\omega}{\nu^2+\omega_1\omega_2} - \frac{\nu}{\zeta}\arctan\frac{\zeta\Delta\omega}{\zeta^2+\omega_1\omega_2}\right]\end{aligned} \tag{10}$$

with $\Delta\omega = \omega_2 - \omega_1$. Here the real and imaginary parts of $\epsilon(\omega)$ are denoted with a single and double prime respectively. For moderate values of of $\Delta\omega$ this gives only a relatively small contribution to $\epsilon({\rm i}\zeta)$, on the level of a few percent for the values of $\omega_1$ and $\omega_2$ mentioned, and the consequences for the pressure would be unobservable at the precision of the experiment [17], in line with the negative conclusion of that paper. The "off/on" model is appealing as a first approach due to its simplicity and intuitiveness and when applied this way provides a very simple qualitative explanation of the effects of the introduction of a transparency window.

Using the real-frequency spectrum directly, however, gives very different results. The change in the force is calculated by subtracting a band of frequencies from the spectrum plotted in figure 3. To avoid possible troubles stemming from cutting the spectrum off sharply, an envelope function is used,

$$\varphi(\omega) = 1 - \frac{\Delta}{\pi}\{\arctan[sa(\omega-\omega_1)] + \arctan[sa(\omega_2-\omega)]\}, \tag{11}$$

so that $\epsilon(\omega) \to 1 + 4\pi\chi(\omega)\varphi(\omega)$. The parameter $\Delta \in [0,1]$ is the relative reduction of $\epsilon(\omega)$ in the band and $s$ determines the smoothness of the edges. The limit $s \to \infty$ giving the unit step behaviour of (8) [18]. A numerical integration over a sufficiently large frequency integral around $\Delta\omega$ with and without $\varphi(\omega)$ yields a rough prediction of the change in the force, which is plotted in figure 4. Clearly the change found this way is absurdly large and, counterintuitively, has opposite sign whether the Drude or plasma model is employed. At separation $a = 100$nm as used in this calculation, the absolute Casimir pressure between ideally conducting parallel plates is approximately 13Pa, shown as a grey band in the figure for scale. It is immediately clear that a simple "off/on" model such as this is not compatible with direct real frequency calculation.

## 5. Causal perturbation on narrow frequency band

For all its intuitive appeal, the "off/on" model, even in its smooth form (11) is not very realistic and suffers from problems which could give rise to the dramatic failure when applied on the real frequency axis. The sharp edges of the frequency band initially employed violate conditions of continuity and analyticity, but the indication is that this is not important since the introduction of smooth boundaries through the envelope function $\varphi(\omega)$ makes for only qualitative adjustments of the results.

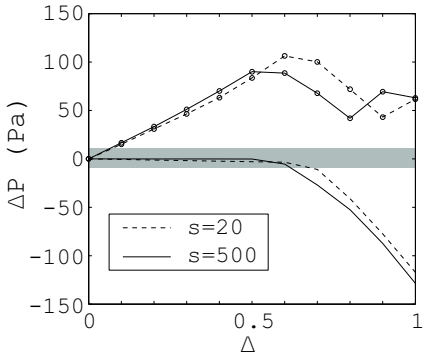


**Figure 4.** Numerically calculated change in the force based on an integral over a band of frequencies of the spectra using respectively the Drude model (circles) and plasma model (no circles). The grey band shows the range $\pm P_{\rm C}(a)$, the absolute Casimir force between ideal conductors.

More serious is the fact that the way the transparency band is calculated on the real axis does not adhere to requirements of causality, in particular, that $\epsilon(\omega)$ fulfils the Kramers-Kronig relations. In the following an investigation is made of the feasibility of using real-frequency calculation for the assessment of the effect of a narrow-band perturbation of $\epsilon(\omega)$ in a way so that (12) and the so-called f-sum rule are obeyed.

It is a standard procedure in the study of the optical properties of materials to model the absorption spectrum $\epsilon''(\omega)$ of the material and work out $\epsilon'(\omega)$ based on this using

$$\epsilon'(\omega) = 1 + \frac{2}{\pi}\mathscr{P}\int_0^\infty \mathrm{d}\xi \frac{\xi\epsilon''(\xi)}{\xi^2-\omega^2}. \tag{12}$$

Likewise, $\epsilon(\mathrm{i}\zeta)$ is calculated using the corresponding Kramers Kronig relation (10). Remarkably informative and useful information about different classes of materials can be extracted from very simple models [23]. This provides motivation to regard the consequences of perturbing $\epsilon''(\omega)$ in a causal way.

The perturbation in the dissipation function is modelled in the following way[1]:

$$\epsilon''(\omega) \to \tilde{\epsilon}''(\omega) = \epsilon''(\omega)[(1+\eta) - \Delta\cdot\theta(\omega-\omega_0)\theta(\omega_0+\delta\omega-\omega)], \quad \omega \geq 0 \tag{13}$$

that is, $\epsilon''$ is approximately unchanged everywhere except in a small frequency band at $\omega_0$ of width $\delta\omega$ in which dissipation is reduced by a constant quantity $\Delta$. The small parameter $\eta$ has the same sign as $\Delta$ and is introduced because the imaginary part of the permittivity must satisfy the f-sum rule (e.g. [24]):

$$\int_0^\infty \mathrm{d}\omega\omega\epsilon''(\omega) = \text{const.} = \frac{\pi}{2}\sum_\alpha \frac{4\pi\aleph_\alpha q_\alpha^2}{m_\alpha^*} \equiv \frac{\pi}{2}\Omega_{\rm p}^2 \tag{14}$$

where sum is over the types of particles, $\alpha$, causing dissipation, characterised by number density $\aleph_\alpha$, charge $q_\alpha$ and effective mass $m_\alpha^*$. When dissipation is due to conduction electrons only, $\Omega_{\rm p} = \omega_{\rm p}$ as in the Drude and plasma models. Insisting that (14) be satisfied both before and after the perturbation implies

$$\eta = \frac{2}{\pi}\frac{\Delta}{\Omega_{\rm p}^2}\int_{\delta\omega}\mathrm{d}\omega\omega\epsilon''(\omega) \approx \frac{2\Delta}{\pi}\frac{\omega_0}{\Omega_{\rm p}^2}\epsilon''(\omega_0)\delta\omega \tag{15}$$

[1] Causality requires that the perturbation is an odd function of $\omega$, but only positive frequencies are considered here.

where $\int_{\delta\omega} \mathrm{d}\omega$ denotes integration from $\omega_0$ to $\omega_0+\delta\omega$ and the latter form is true when $\delta\omega$ is small compared to all other frequency scales. Assuming $\delta\omega$ small implies that $\eta \ll 1$.

To keep the considerations a little more concrete, consider the special case of the Drude model (9), for which $\eta$ becomes:

$$\eta_{\mathrm{D}} = \frac{2}{\pi}\Delta \cdot \arctan\left(\frac{\nu\cdot\delta\omega}{\nu^2+\omega_0(\omega_0+\delta\omega)}\right) \approx \frac{2\Delta}{\pi}\frac{\nu\cdot\delta\omega}{\nu^2+\omega_0^2}. \tag{16}$$

The perturbed real part $\tilde{\epsilon}'(\omega)$ now follows from (12)

$$\tilde{\epsilon}'(\omega) = 1 + \frac{2}{\pi}\mathscr{P}\left\{(1+\eta)\int_0^\infty \mathrm{d}\xi - \Delta\int_{\delta\omega}\mathrm{d}\xi\right\}\frac{\xi\epsilon''(\xi)}{\xi^2-\omega^2}$$

which gives, to linear order in $\delta\omega$ or $\eta$, the change in $\epsilon'(\omega)$

$$\delta\epsilon'(\omega) \equiv \tilde{\epsilon}'(\omega) - \epsilon'(\omega) \approx \eta\left[\epsilon'(\omega) - 1 - \frac{\Omega_{\mathrm{p}}^2}{\omega_0^2-\omega^2}\right] \tag{17}$$

where (15) was used. The case of the Drude model gives

$$\delta\epsilon'_{\mathrm{D}}(\omega) = -\eta_{\mathrm{D}}\frac{\omega_{\mathrm{p}}^2(\omega_0^2+\nu^2)}{(\omega^2+\nu^2)(\omega_0^2-\omega^2)}. \tag{18}$$

In the same fashion, inserting (13) into the corresponding Kramers-Kronig integral for imaginary argument, (10), yields to linear order in $\eta$

$$\delta\epsilon(\mathrm{i}\zeta) \equiv \tilde{\epsilon}(\mathrm{i}\zeta) - \epsilon(\mathrm{i}\zeta) \approx \eta\left[\epsilon(\mathrm{i}\zeta) - 1 - \frac{\Omega_{\mathrm{p}}^2}{\omega_0^2+\zeta^2}\right]. \tag{19}$$

The important difference between (17) and (19) is that while $\delta\epsilon(\mathrm{i}\zeta) \ll \epsilon(\mathrm{i}\zeta)$ over the entire imaginary frequency axis, the perturbation $\delta\epsilon'(\omega)$ grows large close to its pole at $\omega_0$. While the perturbation (13) is negligible when calculated for imaginary frequencies, thus, it may be worth taking a closer look at what happens in the real frequency setting, equation (1).

The permittivity $\epsilon(\omega)$ for a Casimir cavity of two dielectric half-spaces (assumed to be made of the same material for simplicity) enters into the Lifshitz formula through the Fresnel reflection coefficients

$$r_s = \frac{p-s}{p+s}; \quad r_p = \frac{\epsilon p - s}{\epsilon p + s} \tag{20}$$

where $s \equiv \sqrt{p^2+\epsilon-1}$. The reflection coefficients stay approximately unchanged by $\delta\epsilon'$ except when $\omega$ is in the neighbourhood of $\omega_0$ where $\tilde{\epsilon}'(\omega)$ becomes dominated by the otherwise negligible correction $\delta\epsilon'$. Here, thus, $\tilde{s} \sim \sqrt{\delta\epsilon'(\omega)}$ and $\tilde{s}$ therefore rises towards $+\infty$, skips to $+\mathrm{i}\infty$ and decreases quickly thence to its unperturbed value once more. The effect for $r_p$ and $r_s$ is, roughly, that over a frequency interval of order $\delta\omega$ near $\omega_0$ they rise to unity and return to their unperturbed value once more. Since $\delta\omega$ is assumed smaller than all other frequency scales involved, all other quantities can be seen as approximately constant over this interval from which it follows that the change in Casimir pressure from (1) behaves as

$$\delta P(a) \sim \delta\omega \cdot P_{\omega_0}(a;\{r_\sigma\})|_{r_s=r_p=1} \tag{21}$$

where $P_{\omega_0}(a;\{r_\sigma\})$ is the discontinuous spectrum function (5) at $\omega=\omega_0$ taken with unity reflection coefficients just as worked out by Ford [10] and shown in figure 1.

The result (21) is again counterintuitive in that it depends sensitively on the frequency $\omega_0$ and could be either positive or negative depending on the quantity $\omega_0 a$. Indeed the spectrum $P_{\omega_0}(a)|_{r_\sigma=1}$ is discontinous at $\omega_0 a = n\pi,\ n \in \mathbb{N}$, meaning $\delta P$ would make a leap were $\omega_0 a$ to be shifted slightly past such a value, e.g. by changing the separation slightly close to $a = n\pi/\omega_0$.

In conclusion it seemes that the fact that the perturbation is made causal by use of (12) and made to fulfil the f-sum rule (14) does not in itself salvage the apparent paradox that a calculation using the real frequency integral yields apparently nonsensical results while a calculation along the imaginary axis appears robust. If the perturbation $\Delta\epsilon''(\omega)$ fulfilled all the requirements of analyticity and causality and were taken into account by an integral (12) spanning the entire positive frequency axis, the real-frequency and imaginary frequency formalisms must necessarily give the same results. The observation of the vast fluctuations of the Casimir frequency spectrum, however, requires that access be somehow gained to finite intervals of the spectrum, and although a somewhat coarse analysis, the above considerations strongly indicate a pessimistic conclusion with regards to the feasibility of such an enterprise.

## 6. Conclusions and outlook

The frequency spectrum of the Casimir force between real materials is studied with a view to assess whether it may be possible to observe the dramatic oscillatory behaviour of the real frequency Casimir energy spectrum. A generalisation of Ford's result for ideal conductors [10] to a model of constant subunity reflection coefficients reveals a smoothening of the spectrum, but the oscillatory behaviour remains unchanged.

Upon inserting more realistic optical data for real materials, the frequency spectra obtain an even more wild and erratic behaviour. Observation of the dependence on real frequencies requires that access be somehow gained to finite intervals of real frequencies as opposed to the absolute force itself, which dependes only on the integral over all frequencies.

Two simple attempts are made to investigate the question whether a perturbation of the optical properties of materials which is restricted to a finite band of real frequencies could reveal a way to observe the large oscillations described. These have not been concerned with whether and when such perturbations may be made in practice, but have focussed on a problem of theoretical nature which occurs upon attempting to calculate the effects of such perturbations on the Casimir force: the predictions are radically different whether it is performed using the real frequency or imaginary frequency formulation of the Lifshitz formula. This paradox was first reported in [18].

In the first and coarsest approach the materials involved are assumed to be made transparent in a band of frequencies but remain unchanged outside this band. At a qualitative level this mimics the situation created in a recent experiment by Iannuzzi and co-workers [17] in which a hydrogen-switchable mirror is used which becomes transparent in the optical region upon hydrogenation. Using an imaginary time formalism the change in the force predicted is quite modest, in accordance with the experiment, whereas an exclusion of a part of the *real* frequency axis leads to nonsensical predictions of enormous amplitude and apparently arbitrary sign.

In a second attempt the perturbation is made in the imaginary part of permittivity $\epsilon(\omega)$ over a very small frequency range and causality is ensured by the invocation of the Kramers Kronig relations to calculate $\epsilon$ for imaginary frequencies and the real part of $\epsilon$ for real frequencies. Again a real frequency calculation reveals highly counterintuitive results whereas the imaginary frequency calculation appears reasonable in sign and magnitude and in accordance with intuition.

It is clear that the real frequency formalism of the Casimir Lifshitz force is very volatile upon manipulations of optical properties whereas the imaginary frequency formalism is robust and behaves well even with permittivities violating criteria of analyticity and causality. While it may be shown that the two formalisms must yield the same result for measurable quantities when the entire frequency integral is evaluated, both attempts to access the dependency on a

finite frequency band made herein have yielded very different results in the two formalisms, of which there are good reasons to believe the result in the imaginary frequency domain to be the physical one. While this study is far from exhaustive, it indicates that the peculiar real-frequency spectrum of the Casimir force is not observable.

**Acknowledgements**
The author thanks Professor Victor Dodonov and the rest of the organising team for hosting such an excellent conference in Brasilia. In the endeavours reported above I have benefited from discussions with professor Bo E. Sernelius.

**References**

[1] Casimir H B G 1948 *Proc. K. Ned. Akad. Wet.* **60** 793
[2] Lifshitz E M 1955 *Zh. Eksp. Teor. Fiz.* **29** 94 [1956 *Sov. Phys. JETP* **2** 73]
[3] Lambrecht A, Maia Neto P A and Reynaud S 2006 *New J. Phys.* **8** 243
[4] Klich I 2008 Contribution to this volume.
[5] Brevik I, Ellingsen S A, and Milton K A 2006 *New J. Phys.* **8** 236
[6] Geyer B and Klimchitskaya G L 2008 *J. Phys. A* **41** 164032
[7] Landau L D and Lifshitz E M 1980 *Statistical Physics* Pt. 1, 3rd ed. (Amsterdam: Elsevier Butterworth-Heinemann) §123
[8] Ford L H 1988 *Phys. Rev. D* **38** 528
[9] Hacyan S, Jáuregui R, Soto F, and Villareal C 1990 *J. Phys. A* **23** 2401
[10] Ford L H 1993 *Phys. Rev. A* **48** 2962
[11] Iacopini E 1993 *Phys. Rev. A* **48** 129
[12] Ford L H 1998 *Phys. Rev. A* **58** 4279
[13] Sopova V and Ford L H 2004 *Phys. Rev. A* **70** 062109
[14] Lang A S I D 2005 *J. Math. Phys.* **46** 102105
[15] Ford L H 2007 *Int. J. Theor. Phys.* **46** 2218
[16] Genet C, Lambrecht A, and Reynaud S 2003 *Phys. Rev. A* **67** 043811
[17] Iannuzzi D, Lisanti M and Capasso F 2004 *Proc. Natl. Acad. Sci. U.S.A.* **101** 4019
[18] Ellingsen S A 2008 *Europhys. Lett.* **82** 53001
[19] de Man S and Iannuzzi D 2006 *New J. Phys.* **8** 235
[20] Palik E D (ed) 1995 *Handbook of Optical Constants of Solids* (New York: Academic Press)
[21] Rodriguez A, Ibanescu M, Iannuzzi D, Joannopoulos J D, and Johnson S G 2007 *Phys. Rev. A* **76** 032106
[22] Lambrecht A and Reynaud S 2000 *Eur. Phys. J. D* **8** 309
[23] Sernelius B E 2001 *Surface Modes in Physics* (Berlin: Wiley-VCH) Ch. 2
[24] Peiponen K-E, Vartiainen E M, and Asakura T 1999 *Dispersion, Complex Analysis and Optical Spectroscopy* (Berlin: Springer) Ch. 6

# Article [h]

***Casimir-Foucault interaction: Free energy and entropy at low temperature***

F. Intravaia, S.Å. Ellingsen, C. Henkel

Physical Review A **82**, 032504 (2010)

# Casimir-Foucault interaction: Free energy and entropy at low temperature

Francesco Intravaia
*Theoretical Division, MS B213, Los Alamos National Laboratory, Los Alamos, New Mexico 87545, USA*

Simen Å. Ellingsen
*Department of Energy and Process Engineering, Norwegian University of Science and Technology, N-7491 Trondheim, Norway*

Carsten Henkel
*Institut für Physik und Astronomie, Universität Potsdam, Karl-Liebknecht-Strasse 24/25, D-14476 Potsdam, Germany*
(Received 3 May 2010; published 13 September 2010)

It was recently found that thermodynamic anomalies which arise in the Casimir effect between metals described by the Drude model can be attributed to the interaction of fluctuating Foucault (or eddy) currents [F. Intravaia and C. Henkel, Phys. Rev. Lett. **103**, 130405 (2009).] We focus on the transverse electric (TE) polarization, where the anomalies occur, and show explicitly that the two leading terms of the low-temperature correction to the Casimir free energy of interaction between two plates are identical to those pertaining to the Foucault current interaction alone, up to a correction which is very small for good metals. Moreover, a mode density along real frequencies is introduced, showing that the TE contribution to the Casimir free energy, as given by the Lifshitz theory, separates in a natural manner into contributions from eddy currents and propagating cavity modes, respectively. The latter have long been known to be of little importance to the low-temperature Casimir anomalies. This convincingly demonstrates that eddy current modes are responsible for the large temperature correction to the Casimir effect between Drude metals, predicted by the Lifshitz theory, but not observed in experiments.

DOI: 10.1103/PhysRevA.82.032504 PACS number(s): 31.30.jh, 11.10.Wx, 05.40.−a, 42.50.Lc

## I. INTRODUCTION

For a decade the finite-temperature correction to the Casimir force [1] between parallel metal plates has been a topic of intense investigation and debate. Describing the metals by a standard Drude model,

$$\varepsilon(\omega) = 1 - \frac{\Omega^2}{\omega(\omega + i\gamma)}, \tag{1.1}$$

where $\Omega$ is the plasma frequency and where the relaxation frequency $\gamma$ does not vanish at $T = 0$, the Lifshitz theory implies that the temperature dependence is considerably different from perfect reflectors [2]: a significant thermal contribution is predicted already at distances shorter than the Wien wavelength $\hbar c/(2\pi k_B T)$, on the one hand, and there is a difference of a factor of $\frac{1}{2}$ in the large-distance limit, on the other. This strong difference arises because one polarization [transverse electric (TE)] gives a vanishing contribution at large distance. Puzzlingly, such a large temperature dependence is not found in recent precision experiments at Purdue [3]. For reviews of the thermal debate around the Casimir effect, cf. Refs. [4,5] and references therein.

The thermodynamics of the Casimir effect has been of particular interest in this context. For metals described by Eq. (1.1), the Gibbs-Helmholtz free energy of the Casimir interaction is nonmonotonic as a function of temperature, leading to a negative Casimir entropy in a large temperature range [4]. Moreover, if $\gamma$ vanishes faster than linearly as the temperature $T \to 0$, the Casimir entropy remains nonzero in this limit; this was argued to violate Nernst's theorem, the third law of thermodynamics [6,7].

Recently two of the present authors investigated the contribution to the Casimir force from Johnson-Nyquist noise, focusing on specific solutions of the Maxwell equations for the two-plate setup, namely, purely dissipative (i.e., overdamped) modes which are physically Foucault current or "eddy current" modes [8]. (A related investigation with a simplified model is found in Bimonte [9].) These modes have pure imaginary frequencies and are transverse, and their dynamics is described by a diffusion equation. The diffusion constant is given by $D = \gamma\lambda^2$, where $\gamma$ is the dissipation rate of the metal and $\lambda \equiv c/\Omega$ is the plasma penetration depth, with $\Omega$ being the corresponding plasma frequency. The electromagnetic field associated with these currents is evanescent in vacuum; that is, it exponentially decays with the distance from the surface of the metal. It was shown that the eddy current contribution alone accounts for the apparently anomalous thermodynamics of the Casimir effect [8]. More specifically, the nonvanishing entropy that appears when first $\gamma \to 0$ and then $T \to 0$ (taken in this order and assumed to be independent parameters) is due to an infinite degeneracy of quasistatic Foucault current states, a glasslike situation for which the Nernst theorem does not apply [10]. The situation is closely analogous to that of a free particle coupled to a heat bath [11], which is essentially in its high-temperature limit for any nonzero temperature when no damping is present, and for which the Nernst theorem is satisfied for a fixed friction rate [12].

The apparent thermodynamical anomaly of the Casimir interaction is investigated in detail in Refs. [13–15]. It is now established that, for nonvanishing dissipation rates, the Lifshitz theory gives a low-temperature expansion of the TE Casimir free energy between two Drude metals in the form [11,15–19]

$$\Delta F_{\mathrm{CL}}(T) = f_{\mathrm{CL}}^{(2)} T^2 + f_{\mathrm{CL}}^{(5/2)} T^{5/2} + \cdots, \tag{1.2}$$

where the free energies are split into

$$F(T) = F_0 + \Delta F(T), \tag{1.3}$$

 

$F_0$ being the zero temperature value. The derivation of these results in Refs. [17–19], starting from a Matsubara sum, is quite tricky (see Sec. 3 of Ref. [15]). They were confirmed independently using a scattering approach by Ingold and collaborators [11].

In this article we go one step further in showing how the behavior of the TE contribution to the Casimir effect between good Drude metals is dictated entirely by the contribution from Foucault current modes. We introduce a free energy of interaction between Foucault current modes in two Drude plates and find it to have the same form at low temperatures:

$$\Delta F_D(T) = f_D^{(2)} T^2 + f_D^{(5/2)} T^{5/2} + \cdots . \tag{1.4}$$

We use throughout the subscript $D$ to denote the eddy current (or diffusive modes) contribution to the Casimir interaction. We are able to calculate the coefficients $f_D^{(2)}$ and $f_D^{(5/2)}$ and, quite remarkably, find

$$f_D^{(2)} = f_{\mathrm{CL}}^{(2)} + O\big((\gamma/\Omega)^2\big); \tag{1.5a}$$

$$f_D^{(5/2)} = f_{\mathrm{CL}}^{(5/2)}. \tag{1.5b}$$

The calculations are based on an analysis of the zeros and branch cuts of the dispersion function for the Casimir energy, similar to previous work based on the argument principle [10,20,21]. This mode assignment permits us to identify a density of states (DOS) for both the Foucault-current interaction and the full electromagnetic Casimir interaction within the Lifshitz theory. This method reveals a close relationship between the two interactions and yields the results (1.5) in a fairly simple way, including the correction term to $f^{(2)}$ of order $\gamma^2/\Omega^2$ which we calculate in the limit of good conductors.

The low-temperature expansion is valid on a temperature scale lower than

$$k_B T \ll \frac{\hbar D}{L^2} = \frac{\hbar \gamma c^2}{\Omega^2 L^2}, \tag{1.6}$$

where $D$ is the diffusion coefficient of Foucault currents [22] and $L$ the distance between the plates. This scale ("Thouless energy" [23]) has been identified in previous work [14,24,25] and emerges naturally when spatially diffusive modes in two half-spaces are coupled by electromagnetic fields across a gap of width $L$ [8]. It corresponds to a temperature around 20 K for $L = 100$ nm and the conductivity of gold at room temperature. We refer frequently to this parameter in the following.

The mode analysis we perform is similar in spirit to previous work [26–28] where the role of surface plasmon modes and their contribution to the Casimir interaction were examined. Surface plasmons and eddy currents have in common being associated with evanescent electromagnetic fields in vacuum. However, they are connected with two physically distinct phenomena. Conversely to eddy current modes, surface plasmons appear only in the transverse magnetic (TM) polarization and are associated with oscillations of the charge density at the vacuum-metal interface. In the following we focus on good conductors, where the thermal anomalies occur only in the TE polarization, and therefore surface plasmon contributions do not appear in our analysis.

The article is structured as follows: In Sec. II, we introduce a general scheme for calculating the low-temperature expansion of the Gibbs-Helmholtz free energy from DOS functions and recapitulate the DOS for the Casimir-Lifshitz and Foucault current interactions, respectively. We use a method of contour integration to derive a relation between the DOS of the two types of interaction. This provides an intuitive tool for calculating the desired expansion coefficients $f^{(2)}$ and $f^{(5/2)}$ in Sec. III, first to leading order in the small parameter $\gamma/\Omega$ and then the correction term. Various mathematical results are collected in the appendices.

Throughout the calculation we assume the material be described by Eq. (1.1) and let $\hbar = k_B = 1$. We use the terms eddy current and Foucault current interchangably.

## II. MODE DENSITIES

### A. Introduction

The Gibbs-Helmholtz free energy $F$ for a system with a continuous distribution of bosonic normal modes is related to the DOS $\rho(\omega)$ (modes per angular frequency) by the relation

$$\begin{aligned}\Delta F(T) &= T\int_0^\infty d\omega \rho(\omega)\ln(1-e^{-\omega/T}) \\ &= \int_0^\infty d\omega \frac{\mathcal{M}(\omega)}{e^{\omega/T}-1},\end{aligned} \tag{2.1}$$

where $\mathcal{M}(\omega)$ is the integrated mode density:

$$\rho(\omega) = -\partial_\omega \mathcal{M}(\omega). \tag{2.2}$$

[We fix the integration constant with $\mathcal{M}(0) = 0$.] The mode density $\rho(\omega)$ (per angular frequency) specifies the physical system. (Note the difference in the density of states per unit energy introduced in Ref. [29].) In the low-temperature limit, the exponential confines the integrand to small values of $\omega$, and we can expand $\mathcal{M}(\omega)$ in powers of $\omega$ (see also Ref. [30]). Integrating termwise, each power $\omega^\nu$ of the expansion yields a contribution $\sim T^{\nu+1}$ according to

$$\int_0^\infty \frac{d\omega\, \omega^\nu}{e^{\omega/T}-1} = \Gamma(\nu+1)\zeta(\nu+1)T^{\nu+1}. \tag{2.3}$$

This method is the real-frequency analog of the method laid out in Ref. [15] and used in Ref. [18] where Matsubara sums were expanded at low temperatures. The exponential cutoff from the temperature dependence makes the procedure considerably more straightforward here, since standard methods of asymptotic expansion are applicable.

For the two-plate geometry, $F$ is a free energy per area and also depends on their separation $L$, with the corresponding pressure given by $p = -\partial F/\partial L$. The low-frequency expansion of the mode density $\mathcal{M}_D(\omega)$ for the diffusive modes is found to be of the form

$$\mathcal{M}_D(\omega) \approx \left[ m_D^{(1)} \frac{\omega}{D} + m_D^{(3/2)} L \left(\frac{\omega}{D}\right)^{3/2} \ldots \right], \tag{2.4}$$

where the inverse diffusion constant $1/D$ conveniently provides the physical units and the Thouless frequency $D/L^2$ gives the relevant frequency scale. The coefficients $m_D^{(1)}$ and $m_D^{(3/2)}$ are dimensionless, the first of which relates quite obviously to the static value of the mode density [see (2.2)]:

$$\rho_D(0) = -\frac{m_D^{(1)}}{D}. \tag{2.5}$$

Applying the identities (2.3), we get the desired free energy expansion:

$$\Delta F_D(T) = \zeta(2)\frac{m_D^{(1)}}{D}T^2 + \frac{\sqrt{\pi}\,\zeta\left(\frac{5}{2}\right)}{2} m_D^{(3/2)}\frac{T^{5/2}L}{D^{3/2}} + O(T^3), \tag{2.6}$$

where $\zeta(2) = \pi^2/6$ and $\zeta(\frac{5}{2}) \approx 1.341\,49$. As we calculate in Sec. III below,

$$m_D^{(1)} \approx \frac{2\ln 2 - 1}{8\pi^2} + \frac{\lambda(\gamma/\Omega)^2}{4\pi^2(L+2\lambda)}; \tag{2.7a}$$

$$m_D^{(3/2)} = -\frac{\sqrt{2}}{24\pi^2}, \tag{2.7b}$$

where an expansion for good conductors ($\gamma \ll \Omega$) has been performed, with corrections to $m_D^{(1)}$ appearing at the order $O^2(\gamma/\Omega)$. The plasma penetration depth is defined as $\lambda = c/\Omega$. Note that the limit $L \to \infty$ cannot be applied here, since it conflicts with the small parameter $TL^2/D$ in the expansion [Eq. (1.6)]; this is why the scaling with $L$ in the third term on the right-hand side of of Eq. (2.6) is not unphysical. In the limit $L \to 0$, $\Delta F_D$ is nonzero and finite: this can be attributed to the change in the bulk self-energy of the electromagnetic excitations of the metallic medium, as a pair of surfaces is introduced (the "cleavage energy" discussed by Barton [31]). The surfaces introduce boundary conditions for the fluctuating electromagnetic modes (eddy currents in this case), leading to a change in energy per area with respect to a uniform bulk medium.

We identify in the two following sections the mode densities $\rho_{\rm CL}(\omega)$ and $\rho_D(\omega)$ that determine, respectively, the free energy due to all modes and due to diffusive modes. The former quantity is calculated within the Lifshitz theory for the Casimir effect [32].

### B. All modes: Lifshitz mode density

Let us recall that the mode density $\rho_{\rm CL}(\omega)$ counts how the mode number at a given frequency $\omega$ for two half-spaces at separation $L$ differs from the situation of two plates at infinite distance. The Lifshitz formula for the Casimir free energy [33] can be written in the form of Eq. (2.1) so that the following form of the mode density can be written as

$$\rho_{\rm CL}(\omega) = -\mathrm{Im}\,\partial_\omega \mathcal{D}(z = \omega + i0). \tag{2.8}$$

Here and henceforth, let $z$ denote a complex frequency. The "dispersion function" $\mathcal{D}(z)$ is given by the integral

$$\mathcal{D}(z) \equiv \sum_{\sigma=\mathrm{p,s}} \mathcal{D}^\sigma = \sum_{\sigma=\mathrm{p,s}} \int_0^\infty \frac{kdk}{2\pi^2} \ln\left[1 - r_\sigma^2(\kappa,z)\, e^{-2\kappa L}\right], \tag{2.9}$$

Here, $\kappa = \sqrt{k^2 - z^2/c^2}$, $\sigma$ is a polarization index, and $L$ is the cavity width. In the following, we only consider the $s$ (or TE) polarization and drop the polarization label. The reflection coefficient becomes [using the Drude dielectric function (1.1)]

$$r(\kappa,z) = r_{\rm s}(\kappa,z) = \frac{\kappa - \sqrt{\kappa^2 + \kappa_\gamma^2(z)}}{\kappa + \sqrt{\kappa^2 + \kappa_\gamma^2(z)}}; \tag{2.10a}$$

$$\kappa_\gamma(z) = \frac{\Omega}{c}\sqrt{\frac{z}{z + i\gamma}}. \tag{2.10b}$$

All square roots are chosen here with positive real parts; this implies in particular that $\mathrm{Im}\,\kappa \geqslant 0$ and $\mathrm{Im}\sqrt{\kappa^2 + \kappa_\gamma^2(z)} \geqslant 0$ for $z$ in the upper half plane.

### C. Eddy current modes

The dispersion function $\mathcal{D}(z)$ is analytic in the upper half plane. When it is analytically continued, singularities appear on the real axis and in the lower half plane: branch points where the argument of the logarithm in Eq. (2.9) vanishes, and branch cuts from the square roots involved in the reflection coefficients (see Fig. 1). These singularities are related to the electromagnetic resonance frequencies of the two-plate setup that determine the Lifshitz free energy from the argument principle [10,13,21]. They also provide a physically motivated way to isolate the contribution of a particular class of modes to the Casimir interaction.

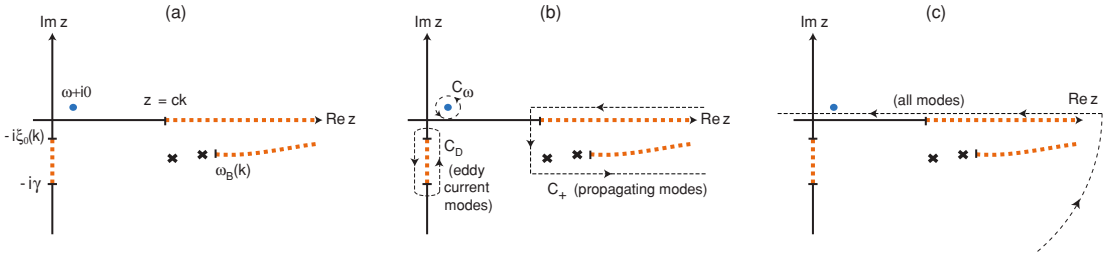


FIG. 1. (Color online) (a) Complex eigenfrequencies in the parallel plate geometry, for a fixed wave vector $k$ (not to scale). The thick dotted lines show branch cuts (three-dimensional mode continuum) and crosses mark poles (discrete frequencies). The circular dot is a pole of the first factor in Eq. (2.18). The pole structure is symmetric with respect to the imaginary axis, according to Eq. (2.19). The frequency $\omega_{\rm B}(k)$ marks the transition from discrete cavity modes to a continuum of bulk modes (see Ref. [27] for details). (b) Integration path: $C_D$ around the eddy current continuum, $C_\omega$ around the pole at $z = \omega + i0$, $C_+$ around cavity and propagating modes. The corresponding paths in the left half plane are denoted $C_{-\omega}$ and $C_-$, respectively. (c) Integration path that encircles all modes, as relevant for the Lifshitz theory. Closing this contour in the upper half plane, one gets the residue from the pole $z = \omega + i0$ in the upper half plane.

The eddy current (diffusive) modes, for fixed $k$, are identified as a branch cut of $\mathcal{D}(z)$ along the negative imaginary frequency axis (see Fig. 1), $z=-i\xi_0\cdots-i\gamma$ [$\xi_0=\xi_0(k)$ is defined below]. This branch cut is an example of a dispersion function that is not real on the imaginary frequency axis, in distinction from the familiar behavior in the upper half plane. Indeed, one can confirm from the macroscopic Maxwell equations that purely imaginary eigenfrequencies appear in a planar cavity of two half spaces described by the Drude dielectric function [22]. As is well known in scattering theory (see, e.g., Ref. [21,34]), the branch cut can be interpreted as a dense coalescence of discrete modes, and the relevant quantity is a mode density given by

$$\mu_D(\xi)=-\mathrm{Im}\,\partial_\xi\mathcal{D}(z=-i\xi+0),\quad 0\leqslant\xi\leqslant\gamma. \tag{2.11}$$

The dispersion function is evaluated here to the right of the branch cut. Continuing analytically from the upper half plane, we find that $\kappa$ is mainly real, while $\kappa_\gamma(-i\xi+0)=-ik_\gamma(\xi)$ becomes mainly imaginary with

$$k_\gamma(\xi)=\frac{\Omega}{c}\sqrt{\frac{\xi}{\gamma-\xi}}. \tag{2.12}$$

As a consequence, $[\kappa^2-k_\gamma^2(\xi)]^{1/2}$ moves to the (negative) imaginary axis if $\kappa$ is small enough; more precisely, we require

$$0\leqslant\kappa\leqslant k_\gamma(\xi). \tag{2.13}$$

This is equivalent to

$$\xi_0(k)\leqslant\xi\leqslant\gamma, \tag{2.14}$$

where the lower bound $\xi_0(k)$ solves

$$(\gamma-\xi_0)(c^2k^2+\xi_0^2)=\Omega^2\xi_0. \tag{2.15}$$

We note the limiting behavior $\xi_0(k)\approx Dk^2$ as $k\to0$, where $D$ is the diffusion coefficient of Eq. (1.6). In the range (2.14), the reflection coefficient becomes the unitary number,

$$r(\kappa,-i\xi+0)=\frac{\kappa+i\sqrt{k_\gamma^2(\xi)-\kappa^2}}{\kappa-i\sqrt{k_\gamma^2(\xi)-\kappa^2}}, \tag{2.16}$$

where the sign of the square root applies on the right side of the branch cut and follows by carefully evaluating the imaginary parts of $\kappa$ and $k_\gamma(\xi)$. For imaginary frequencies outside the range (2.14), the reflection coefficient is real ($-1<r_s<0$), and the eddy current mode density (2.11) vanishes.

After integrating over $k$, one gets a mode density, $\mu_D(\xi)$, that is nonzero in the range $0\leqslant\xi\leqslant\gamma$. Finally, the density for eddy current modes $\rho_D(\omega)$ at real frequencies is defined by associating with each overdamped mode $z=-i\xi$ a Lorentzian spectrum centered at zero frequency whose width is $\sim\mathrm{Im}\,z$. Referring to Ref. [8] for details, we get

$$\rho_D(\omega)=\int_0^\gamma\frac{d\xi}{\pi}\frac{\xi}{\xi^2+\omega^2}\mu_D(\xi). \tag{2.17}$$

### D. Contour integral representation

In this section we derive a contour integral represention for the mode densities of the full Casimir-Lifshitz interaction and of the eddy current contribution. This demonstrates a simple relation between $\rho_{\mathrm{CL}}(\omega)$ and $\rho_D(\omega)$. We thus prepare the low-frequency analysis we perform in Sec. III focusing on the particular case of a good Drude conductor (i.e., $\gamma\ll\Omega$).

It is easy to see from the sign flip of the root involving $\kappa_\gamma(\xi)$ in Eq. (2.10) that the dispersion function $\mathcal{D}(z)$ jumps and changes into its complex conjugate across the branch cut $z=0\cdots-i\gamma$. This jump defines the eddy current DOS in Eq. (2.11). The latter can thus be written as a contour integral in the complex plane,

$$\rho_D(\omega)=-\oint_{C_D}\frac{dz}{2\pi}\frac{z}{z^2-\omega^2}\partial_z\mathcal{D}(z), \tag{2.18}$$

where the path $C_D$ encircles the cut on the negative imaginary axis in the positive sense as shown in Fig. 1(b). Now, shifting the contour toward infinity, we encounter the poles at $z=\pm\omega$ from Eq. (2.18) and other singularities (poles and branch cuts) of $\partial_z\mathcal{D}(z)$. The behavior of the exponential $e^{-2\kappa L}$ for $|z|\to\infty$ makes $\mathcal{D}(z)$ vanish at infinity. Hence we conclude that the integral around $C_D$ is equal to the negative residues of the poles $z=\pm\omega$ minus integrals over the contours $C_\pm$ in Fig. 1(b) that encircle the singularities near the left and right half of the real axis. We use here the link between the dispersion function and the response (or Green) function of the two-plate cavity [20,21] that entails the symmetry relation

$$\mathcal{D}(-z^*)=\mathcal{D}^*(z)\,. \tag{2.19}$$

As a consequence, complex mode frequencies and branch cuts appear in pairs on opposite sides of the imaginary axis. (In Fig. 1, only the right half is shown.)

The residues at the poles are easily calculated from the contours $C_{\pm\omega}$ in Fig. 1(b):

$$\begin{aligned}\oint_{C_\omega+C_{-\omega}}\frac{dz}{2\pi}\frac{z}{z^2-\omega^2}\partial_z\mathcal{D}(z)&=\frac{i}{2}\left[\partial_z\mathcal{D}(\omega)+\partial_z\mathcal{D}(-\omega)\right]\\&=-\mathrm{Im}\,\partial_\omega\mathcal{D}(\omega)=\rho_{\mathrm{CL}}(\omega).\end{aligned} \tag{2.20}$$

We thus recover the mode density for the Lifshitz theory as one term in the eddy current DOS. This is actually not surprising, since $\rho_{\mathrm{CL}}(\omega)$ can be written as a contour integral similar to Eq. (2.18), but evaluated along a contour just above the real axis [Fig. 1(c)] and closed at infinity in the lower half plane. This contour encircles all singularities of the dispersion function as it should, since the Lifshitz theory accounts for all modes. If this contour is shifted through infinity into the upper half plane, only the two residues calculated in Eq. (2.20) contribute since the dispersion function is analytic inside the contour.

In conclusion, we can write the following splitting of the mode density for the Casimir effect:

$$\rho_{\mathrm{CL}}(\omega)=\rho_D(\omega)+\rho_\pm(\omega), \tag{2.21}$$

where the last term gives the contribution of modes near the real axis [contour $C_+$ in Fig. 1(b), and corresponding $C_-$ in the left half plane]. By continuity with the limiting case $\gamma\to0$, we can identify the latter modes with propagating modes in the vacuum cavity, in the bulk, or with electromagnetic surface modes (for example, surface plasmons that appear in the TM polarization). We see in the next section that for nonzero, but small $\gamma\ll\Omega$, the mode density $\rho_\pm(\omega)$ becomes small at low

frequencies ($\omega < D/L^2, \gamma, c/L$), so that in this range, the full electromagnetic DOS $\rho_{\rm CL}(\omega)$ nearly coincides with the eddy current DOS $\rho_D(\omega)$.

## III. LOW-FREQUENCY EXPANSION

We calculate now the small $\omega$ expansion of the density of states for eddy current modes. According to Eq. (2.21), we start with the full Casimir-Lifshitz interaction and discuss then the differences between the two. We begin with a general estimate of the scaling for good conductors.

### A. Scaling for weak damping

The analysis in the complex plane, as illustrated in Fig. 1, suggests that the density of diffusive modes is concentrated in a range $\sim\gamma$ near zero frequency. Anticipating from the analysis below a total number of $\sim 1/L^2$ modes per unit area, one gets for $\gamma \to 0$ a scaling $\rho_D(\omega) \approx 1/(\gamma L^2)\theta(\omega/\gamma, L/\lambda)$, where the frequency appears in the function $\theta$ only in the dimensionless form $\omega/\gamma$ (and similarly for the distance $L/\lambda \equiv \Omega L/c$). A different behavior emerges for propagating modes (inside the contour $C_+$ in Fig. 1): they move onto the real axis for small $\gamma$ and contribute to $\rho_\pm(\omega)$ in the range $\omega \sim c/L, \Omega$. Their contribution at much lower frequencies that interests us here is proportional to their imaginary part and therefore scales linearly with $\gamma$. This observation provides us with a simple rule to identify the respective contributions of eddy current and propagating modes in the full (Lifshitz) mode density (Sec. III B). Note that we consider here the case of a fixed (temperature-independent) scattering rate $\gamma$.

Some further corroboration of these rough estimates is desirable. Let us consider for the simplicity of argument that the dispersion function $\partial_z \mathcal{D}(z)$ has only discrete poles $\omega_n(k)$ in the lower half plane, labeled by the momentum quantum number $k$. This can be achieved by enclosing the system in a finite box [13,21]. One recovers the branch cuts by taking the box size to infinity [34]. From the symmetry relation (2.19), the poles occur either on the imaginary axis (as for diffusive modes) or pairwise in the lower left and right quadrants (as for propagating modes). The two terms $\rho_D(\omega)$ and $\rho_\pm(\omega)$ collect these poles, respectively.

We make the replacement $d\xi\, \mu_D(\xi) \mapsto d^2k/(2\pi)^2 \sum_{n\in\text{eddy}}$ and find that the DOS for diffusive modes $\rho_D(\omega)$ can be written in the following scaling form:

$$\rho_D(\omega) = \frac{1}{\gamma} \int \frac{kdk}{2\pi^2} \Bigg[ \sum_{n\in\text{eddy}} \frac{\xi_n(k)/\gamma}{(\omega/\gamma)^2 + (\xi_n(k)/\gamma)^2} \Bigg]_{L\to\infty}^{L},$$

where the limit of the mode branches for two separate plates ($L \to \infty$) is subtracted. We have already seen that the mode frequencies satisfy $\xi_n(k) \leqslant \gamma$. As a consequence, the integral tends toward a finite limit as $\gamma \to 0$, $\rho_D(\omega)$ depends only on the scaled frequency $\omega/\gamma$ and is proportional to the scaling factor $1/\gamma$. This implies in particular that the integral over the diffusive mode density can give a nonzero contribution even as $\gamma \to 0$. We confirm these results in Eq. (3.9).

The density of propagating modes $\rho_\pm(\omega)$ shows a different scaling with $\gamma$. With the same rewriting, the contours $C_+$ and $C_-$ collect the modes away from the imaginary axis and lead to the representation

$$\begin{aligned}\rho_\pm(\omega) &= -\oint_{C_+ + C_-} \frac{dz}{2\pi} \frac{z}{z^2-\omega^2} \partial_z \mathcal{D}(z) \\ &= -\int_0^\infty \frac{kdk}{2\pi^2} \text{Im} \Bigg[ \sum_{n\in\text{prop}} \frac{\omega_n(k)}{\omega^2 - \omega_n^2(k)} \Bigg]_{L\to\infty}^{L}, \end{aligned} \tag{3.1}$$

where in the second line we represent the modes by the poles in the lower right quadrant. Now, the imaginary part of the eigenfrequency $\omega_n(k)$ is negative and, for a small Drude scattering rate, of the order $\gamma$. A typical scale for its real part, on the other hand, is the lowest cavity eigenfrequency $c/L$ or the plasma frequency $\Omega$. Although we do not need them here, recall that the surface plasmon modes appear at $\approx \Omega/\sqrt{2} - i\gamma/2$ for $k \gg \Omega/c$ [35]. For an estimate of $\rho_\pm(\omega)$, we focus on frequencies $\omega$ much smaller than the real part, $\omega \ll c/L, \Omega$ and take $1/L$ to estimate the relevant wave vectors. This gives

$$\omega \to 0: \quad \rho_\pm(\omega) \sim O\left(\frac{\gamma}{\Omega^2 L^2}\right) \cdots O\left(\frac{\gamma}{c^2}\right), \tag{3.2}$$

as we confirm in Eq. (3.17) below. This small "tail" of the mode density near zero frequency can be understood from the broadening of the discrete modes due to damping (a $\delta$ peak becomes similar to a Lorentzian; see also Ref. [29]). In particular, it vanishes in the limit $\gamma \to 0$, where $\rho_\pm(\omega)$ goes over into the mode density of the plasma model which scales proportional to $\omega^2$.

To summarize this estimate, we expect from Eq. (2.21) that, as $\gamma \to 0$, the low-frequency mode density for the Casimir-Foucault interaction and for the full Casimir interaction coincide in order $1/\gamma$, with a small difference of $\sim\gamma$ arising from propagating modes. These contributions are calculated in the following sections. We are thus able to check our approach against the free-energy expansion of Refs. [17,18].

### B. Lowest order: Lifshitz theory

Let us calculate the coefficients $m_D^{(1)}$ and $m_D^{(3/2)}$ defined in Eq. (2.4), starting with the leading order in the small parameter $\gamma/\Omega$, which, as we have just seen, is provided by the full Lifshitz theory. It is convenient to work with the integrated mode density which from Eq. (2.8) we can write as

$$\mathcal{M}_{\rm CL}(\omega) = \text{Im}\, \mathcal{D}(\omega + i0). \tag{3.3}$$

We therefore start by analyzing in detail the behavior of $\mathcal{D}(z)$ in the complex frequency range of $|z| \ll \gamma$.

The $k$ integral in Eq. (2.9) is rewritten in terms of a real variable, $y > 0$, defined by $\kappa = y\kappa_\gamma(z)$. This is equivalent to a shift of the integration path in the complex $\kappa$ plane along a more convenient direction: one still has convergence from the exponential $\exp(-2\kappa L)$ because $\text{Re}\, \kappa_\gamma(z) > 0$ (keeping clear of the branch cut for $z$ on the negative imaginary axis). The reflection coefficient (2.10) becomes real along this direction and independent of $z$:

$$r(y) = \frac{y - \sqrt{y^2+1}}{y + \sqrt{y^2+1}} = \frac{1}{(y+\sqrt{y^2+1})^2}. \tag{3.4}$$

We get

$$\mathcal{D}(z) = \kappa_\gamma^2(z) \int_{\chi(z)}^{\infty} \frac{y dy}{2\pi^2} \ln[1 - r^2(y)\, e^{-2y\kappa_\gamma(z)L}], \tag{3.5}$$

where the lower limit is given by the complex number

$$\chi(z) = -\frac{iz}{c\kappa_\gamma(z)} = -\frac{iz}{\Omega}\sqrt{\frac{z+i\gamma}{z}}. \tag{3.6}$$

For $|z| < \gamma$, we have $|\chi(z)| \leqslant \sqrt{2}(\gamma/\Omega) \ll 1$ for a good conductor, and to leading order, we can replace the lower limit in Eq. (3.5) by zero. This defines $\mathcal{D}_0(z)$, and via Eq. (3.3), $\mathcal{M}_{\mathrm{CL},0}(\omega)$. We write $\mathcal{M}_{\mathrm{CL},\gamma}(\omega)$ for the error [i.e., the integral from 0 to $\chi(z)$] and calculate it in Eq. (3.10).

By inspection, $\mathcal{D}_0(z)$ depends on $z$ only via the function $\kappa_\gamma(z)$ that can be written as

$$\kappa_\gamma(z) = \kappa_1(z/\gamma) = \frac{\Omega}{c}\sqrt{\frac{z/\gamma}{z/\gamma + i}}, \tag{3.7}$$

involving the scaled quantity $z/\gamma$. From the reflection coefficient $r(y)$, the relevant integration domain is $0 \leqslant y \lesssim 1$. We can therefore expand the exponential in Eq. (3.5) provided $\kappa_1(z/\gamma)L \ll 1$. This yields the condition $(|z|/\xi_L)^{1/2} \ll 1$, where $\xi_L$ is the Thouless frequency introduced in Eq. (1.6). Expanding to the first order in this small parameter, we get ($D$ is the diffusion coefficient)

$$\mathcal{D}_0(z) \approx \frac{z}{iD}\int_0^\infty \frac{y dy}{2\pi^2} \ln[1 - r^2(y)] + \frac{z}{iD}\left(\frac{z}{i\xi_L}\right)^{1/2} \int_0^\infty \frac{y^2 dy}{2\pi^2} \frac{2r^2(y)}{1 - r^2(y)} + O^2(z/\xi_L), \tag{3.8}$$

where powers $z$ and $z^{3/2}$ have appeared. The integrals can be solved exactly (see Appendix A), and we get from Eq. (3.3) the following approximation of the Lifshitz integrated DOS:

$$\mathcal{M}_{\mathrm{CL},0}(\omega) \approx \frac{2\ln 2 - 1}{8\pi^2}\frac{\omega}{D} - \frac{L\sqrt{2}}{24\pi^2}\left(\frac{\omega}{D}\right)^{3/2}, \tag{3.9}$$

valid for $\omega \ll \xi_L, \gamma$. This proves the first term in Eqs. (2.7). It is clear from this calculation [a power series in $(\omega/\xi_L)^{1/2}$] that these results cannot be applied for $\gamma \to 0$ at fixed $\omega > 0$. In other words, the limits $\gamma \to 0$ and $\omega \to 0$ do not commute. For a discussion, see Refs. [13,14].

Calculate now the small correction $\mathcal{M}_{\mathrm{CL},\gamma}(\omega)$ from the lower integration limit in Eq. (3.5). This arises between the boundaries $y = 0$ and $y = \chi(z)$. Recall that in the limit $\gamma \ll \Omega$ we have $|\chi(z)| \ll 1$ and expand the integrand for $y \ll 1$. This gives

$$\mathcal{M}_{\mathrm{CL},\gamma}(\omega) \approx -\mathrm{Im}\,\kappa_\gamma^2(z)\int_0^{\chi(z)} \frac{y dy}{2\pi^2} \ln[2y(2 + \kappa_\gamma(z)L)] \approx -\frac{1}{16\pi}\frac{\omega^2}{c^2}, \tag{3.10}$$

one-half the mode density for the so-called plasma model where $\gamma = 0$ is taken from the outset. Notably, this term gives a contribution to the free energy proportional to $T^3$, which exactly coincides with the expression given in Refs. [15,18]. Note that the term scaling with Eq. (3.2) has not appeared in the full (Lifshitz) mode density. We outline an interpretation in Sec. IV.

### C. Eddy current modes

We now address the density of eddy current modes alone that involves according to Eq. (2.17) an integral along the branch cut of $\mathcal{D}(z)$ on the imaginary axis. It is again convenient to work out the integrated mode density $\mathcal{M}_D(\omega)$. A partial integration leads to the integral representation

$$\mathcal{M}_D(\omega) = -\int_0^\gamma \frac{d\xi}{\pi}\frac{\omega}{\xi^2 + \omega^2} M_D(\xi), \tag{3.11}$$

where $M_D(\xi)$ is the integrated mode density along the branch cut. By changing the momentum variable from $k$ to $\kappa$, this function can be written as

$$M_D(\xi) = -\int_{\xi/c}^{k_\gamma(\xi)} \frac{\kappa d\kappa}{2\pi^2} \mathrm{Im}\,\ln[1 - r^2(\kappa, -i\xi)\, e^{-2\kappa L}], \tag{3.12}$$

where the integrand is zero above the upper integration limit $k_\gamma(\xi)$ that was defined in Eq. (2.12).

The limiting behavior of this expression for a good conductor can be worked out similar to Eq. (3.5). Writing the integral in terms of $x = \xi/\gamma$, we see that $\mathcal{M}_D(\omega)$ [Eq. (3.11)] depends on the scaled frequency $\omega/\gamma$. The upper integration limit takes a form similar to Eq. (3.7),

$$k_\gamma(\xi) = k_1(x) = \frac{\Omega}{c}\sqrt{\frac{x}{1-x}}, \tag{3.13}$$

while the lower one, $\xi/c = x\gamma/c$, can be taken as small compared to the typical values $\kappa \sim 1/L$ and $\kappa \sim k_1(x)$ that appear in the integrand.

This motivates again a splitting of $M_D(\xi)$ into two terms: a first one where the lower boundary in Eq. (3.12) is taken as zero, and a correction, similar to what we did after Eq. (3.5). The two terms produce a split of the mode density (3.11) into

$$\mathcal{M}_{D,0}(\omega) + \mathcal{M}_{D,\gamma}(\omega), \tag{3.14a}$$

where the first term can be written as

$$\mathcal{M}_{D,0}(\omega) = \int_0^1 \frac{dx}{\pi}\frac{\omega/\gamma}{x^2 + (\omega/\gamma)^2} \times \int_0^{k_1(x)} \frac{\kappa d\kappa}{2\pi^2} \mathrm{Im}\,\ln[1 - r^2(\kappa, -ix\gamma)\, e^{-2\kappa L}]. \tag{3.14b}$$

Here, we have succeeded in removing from the integrand all dependence on $\gamma$, except for the frequency scaling. The second term, $\mathcal{M}_{D,\gamma}(\omega)$, is discussed in Sec. III D, Eq. (3.17). This term is related to the correction proportional to $\gamma$ identified in Sec. III A, the only difference being that we are dealing here with integrated mode densities. The expression $\mathcal{M}_{D,0}(\omega)$ [Eq. (3.14b)] is nonzero in the limit $\gamma \to 0$, except for the appearance of the scaled frequency $\omega/\gamma$. Therefore, this term corresponds to the (differential) mode density scaling with $1/\gamma$ of Sec. III A. Since we know from Eq. (2.21) that the leading orders for $\gamma \to 0$ coincide for the diffusive modes and the

Lifshitz theory, we can conclude

$$\mathcal{M}_{D,0}(\omega) = \mathcal{M}_{\mathrm{CL},0}(\omega), \tag{3.15}$$

provided the frequency $\omega$ is below the range where other (propagating) modes appear that are not contained in $\mathcal{M}_D(\omega)$. The identity (3.15) is checked by a direct calculation in Appendix B.

### D. Damping correction of eddy current modes

We now show that one gets for good conductors the second term, of relative order $(\gamma/\Omega)^2$, in the coefficient $m_D^{(1)}$ [Eq. (2.7a)]. It arises from the correction $\mathcal{M}_{D,\gamma}(\omega)$ to the diffusive mode density. It is interesting that this shows a scaling of $\sim\gamma\omega$, in distinction from the correction in the Lifshitz theory, Eq. (3.10).

The second term in Eq. (3.14a), $\mathcal{M}_{D,\gamma}(\omega)$, is of the same form as Eq. (3.14b), with the upper limit $k_1(x)$ replaced by $\gamma x/c$. For good conductors, the upper integration limit $\kappa \leqslant \gamma x/c$ is small compared to the scale $k_1(x)$ [Eq. (3.13)] that appears in the reflection coefficient. The argument of the exponential is small if we take $\gamma \ll c/L$. Expanding both quantities for small $\kappa$, we get

$$\mathcal{M}_{D,\gamma}(\omega) \approx \int_0^1 \frac{dx}{\pi}\frac{\omega/\gamma}{x^2+(\omega/\gamma)^2} \times \int_0^{\gamma x/c}\frac{\kappa d\kappa}{2\pi^2}\mathrm{Im}\,\ln[2\kappa(L+2i/k_1(x))]. \tag{3.16}$$

The imaginary part does not depend on $\kappa$, and the integration gives a factor of $\frac{1}{2}(\gamma x/c)^2$. At this stage, we can take the low-frequency limit ($\omega \ll \gamma$) and are left with

$$\mathcal{M}_{D,\gamma}(\omega) \approx \frac{\omega\gamma}{4\pi^2c^2}\int_0^1\frac{dx}{\pi}\arctan\left(\frac{2\lambda}{L}\sqrt{\frac{1-x}{x}}\right) = \frac{\omega}{D}\frac{\gamma^2}{4\pi^2\Omega^2}\frac{\lambda}{2\lambda+L}, \tag{3.17}$$

where $\lambda = c/\Omega$ is the plasma wavelength. This yields the correction to $m_D^{(1)}$ appearing in Eq. (2.7a). We have checked that $\mathcal{M}_{D,\gamma}(\omega)$ does not contain, at the next order, the fractional power $\omega^{3/2}$, as found for $\mathcal{M}_{D,0}(\omega)$.

We suggest the following interpretation for this correction: it is related to the mutual influence of the two types of modes, overdamped and propagating waves. To wit, as the two slabs approach each other, the different mode frequencies cannot shift independently because, taken all together, they have to satisfy a sum rule quoted in Ref. [13]:

$$\int d^2k\left[\sum_{\text{all modes}}\mathrm{Im}\,\omega_n(k)\right]_{L\to\infty}^{L} = 0, \tag{3.18}$$

where the notation assumes that branch cut continua have been discretized (see Sec. III A). The eddy current modes play a crucial role in satisfying this sum rule. Indeed, any modification in the imaginary part of the propagating (cavity and bulk) modes due to a change of the distance $L$ (i.e., the propagating modes leave the continuum above the plasma frequency and become discrete cavity modes as the distance $L$ is increased) is simultaneously balanced by a shift in the diffusive mode density on the imaginary axis that extends down to $-i\gamma$.

Due to the sum rule (3.18), the small correction for eddy currents appears also, with the opposite sign, in the propagating modes. For this reason, the Lifshitz mode density does not contain this term [see Eq. (3.9)], and its next-order correction, Eq. (3.10), is independent of the damping rate $\gamma$.

## IV. DISCUSSION AND CONCLUSIONS

We have calculated the low-temperature behavior of the interaction between two parallel half-spaces across a gap of width $L$ due to low-frequency Johnson noise in the bulk of the conducting medium, in particular eddy or Foucault currents that are coupled to TE-polarized electromagnetic fields. The interaction is calculated in orders $T^2$ and $T^{5/2}$ and is compared to the Casimir free energy within the Lifshitz theory for Drude metals. A striking result is uncovered: the low-temperature correction to the Casimir effect between parallel slabs of good Drude conductors is dictated entirely by the contribution from eddy currents, as demonstrated by the two leading-order correction terms as $T \to 0$. This adds a further piece of support to the findings of Ref. [8], where the unusual physics of the thermal Casimir effect between Drude conductors is attributed to the interaction between eddy currents.

Within our approach, we find small differences in the free energy that are of the second order in the ratio scattering rate to plasma frequency, $\gamma/\Omega$ [Eq. (2.7a)]. This correction reflects the mutual influence between the modes that are constrained by a sum rule, Eq. (3.18). Note the curious fact that this makes $\Delta F_D$ depend on $L$ already at order $T^2$, different from $\Delta F_{\mathrm{CL}}$. Therefore the eddy current interaction makes a tiny contribution to the pressure ($p = -\partial F/\partial L$) quadratic in temperature. However this is exactly canceled by a corresponding contribution from propagating modes and the resulting Casimir pressure is proportional to $T^{5/2}$ to leading order, as Eq. (3.9) shows.

Let us finally emphasize the analysis of the singularities of the Lifshitz dispersion function that we performed in the complex plane. This picture identifies in a natural way the mode frequencies of the system, even in the presence of dissipation, and justifies a natural splitting of the free energy in contributions of specific types of modes. We gained in particular the insight that the mode density for the full Casimir-Lifshitz interaction is simply the sum of eddy current modes and of propagating cavity and bulk modes. The second contribution becomes small at low frequencies, weak damping, and not too large distances because the complex mode frequencies are located sufficiently far away from the origin. This provides a deeper understanding of why propagating modes are of little relevance to the temperature dependence of the Casimir-Lifshitz interaction between Drude metals. Indeed, this dependence was previously found to originate primarily in low-frequency evanescent modes [24,25].

## ACKNOWLEDGMENTS

We have benefited from discussions with Gert-Ludwig Ingold. We also thank G. L. Klimchitskaya and V. M. Mostepanenko for constructive comments. Support from the

European Science Foundation (ESF) within the Research Networking Programme "New Trends and Applications of the Casimir Effect" is gratefully acknowledged. F.I. acknowledges partial financial support by the Humboldt foundation and LANL.

## APPENDIX A: INTEGRALS FOR LIFSHITZ THEORY

The integrals in Eq. (3.8) can be evaluated with the substitution $y = \sinh t$. This simplifies the reflection coefficient (3.4) into $r(y) = -e^{-2t}$. Hence

$$\int_0^\infty dy\; y \ln[1 - r^2(y)] = \int_0^\infty dt \frac{\sinh 2t}{2} \ln(1 - e^{-4t}). \tag{A1}$$

Expanding the logarithm, integrating term by term, and evaluating the sum, we get

$$\int_0^\infty \frac{\sinh 2t}{2} \ln(1 - e^{-4t}) = -\frac{2\ln 2 - 1}{4}. \tag{A2}$$

For the second integral in Eq. (3.8), the same substitution gives

$$\int_0^\infty dy \frac{2y^2 r^2(y)}{1 - r^2(y)} = \int_0^\infty dt \frac{\sinh t\; e^{-2t}}{2} = \frac{1}{6}. \tag{A3}$$

## APPENDIX B: INTEGRALS FOR EDDY CURRENTS

We prove here Eq. (3.15): the low-frequency mode densities for eddy currents, $\mathcal{M}_{D,0}(\omega)$, and for all modes, $\mathcal{M}_{\mathrm{CL},0}(\omega)$, coincide to leading order in $\gamma$.

Consider Eq. (3.14b) for the eddy current mode density. We want to write this as a contour integral, similar to Eq. (2.18), around the eddy current branch cut $C_D$ in Fig. 1. Note first that the Im can be pulled in front of the $\kappa$ integral and that integral can be extended from $k_1(x)$ to $\infty$. This is possible without changing the value of the integral if $\kappa$ is taken just below the real axis, the reflection coefficient (2.16) getting real and smaller than unity in modulus. Hence, the logarithm is real, and this part of the integration range does not make any contribution to the imaginary part.

The contour integral in the variable $z = -i\gamma x \pm 0$ finally takes a form similar to that in Sec. II D:

$$\mathcal{M}_{D,0}(\omega) = -\oint_{C_D} \frac{dz}{2\pi} \frac{\omega}{\omega^2 - z^2} \mathcal{D}_{D,0}(z), \tag{B1}$$

where $\mathcal{D}_{D,0}(z)$ is the integral

$$\mathcal{D}_{D,0}(z) = \int_0^\infty \frac{\kappa d\kappa}{2\pi^2} \ln[1 - r^2(\kappa, z)\, e^{-2\kappa L}], \tag{B2}$$

and the reflection coefficient is given by Eq. (2.10). Note that, to the right of the branch cut, $k_1(x) = i\kappa_\gamma(z)$.

The variable change $\kappa = y\kappa_\gamma(z)$ with $y \geqslant 0$ now shows that the function $\mathcal{D}_{D,0}(z)$ is indeed identical to the small-$\gamma$ approximation to the Lifshitz dispersion function, $\mathcal{D}_0(z)$, defined by setting the lower integration limit in Eq. (3.5) to zero. Note that this actually shifts the integration path in the lower right quadrant of the complex $\kappa$ plane: from $\mathrm{Re}\,\kappa_\gamma(z) > 0$, convergence at $y \to \infty$ is secured. The reflection coefficient $r(y)$ [Eq. (3.4)] is analytic and of modulus smaller than unity in this quadrant; hence the logarithm encounters no branch points.

We still have to evaluate the integral (B1) and do this with the same technique as in Sec. II D. Pulling the contour $C_D$ to infinity, one encounters simple poles at $z = \pm\omega$. In the present case, we can argue that the function $\mathcal{D}_0(z)$ is analytic in the right half plane and by the symmetry relation (2.19) also in the left half plane: this is due to the way the integration variable $y$ keeps the wave vector $\kappa$ clear of the branch cuts that are located inside the contours $C_\pm$ (Fig. 1). Indeed, across these cuts either $\kappa$ or $\sqrt{\kappa^2 + \kappa_\gamma^2(z)}$ are purely imaginary and jump in sign. This never happens along the path parametrized as $\kappa = y\kappa_\gamma(z)$, as can be checked easily. Indeed, if $z$ is in the right half plane, $\kappa$ remains in the lower right quadrant, excluding the real and imaginary axes.

As a consequence of $\mathcal{D}_0(z)$ being analytic in the left and right half planes, the integral (B1) is given by the pole contributions $\mathcal{D}_0(\pm\omega)$ only. Referring to Eq. (3.3), we thus get the desired link to the approximated Lifshitz mode density

$$\mathcal{M}_{D,0}(\omega) = \mathrm{Im}\,\mathcal{D}_0(\omega) = \mathcal{M}_{\mathrm{CL},0}(\omega), \tag{B3}$$

which is Eq. (3.15).

[1] H. B. G. Casimir, Proc. K. Ned. Akad. Wet. **51**, 793 (1948).
[2] M. Boström and B. E. Sernelius, Phys. Rev. Lett. **84**, 4757 (2000).
[3] R. S. Decca, D. López, E. Fischbach, G. L. Klimchitskaya, D. E. Krause, and V. M. Mostepanenko, Phys. Rev. D **75**, 077101 (2007).
[4] I. Brevik, S. A. Ellingsen, and K. A. Milton, New J. Phys. **8**, 236 (2006).
[5] M. Bordag, G. L. Klimchitskaya, U. Mohideen, and V. M. Mostepanenko, *Advances in the Casimir Effect* (Oxford University Press, Oxford, 2009).
[6] V. B. Bezerra, G. L. Klimchitskaya, and V. M. Mostepanenko, Phys. Rev. A **66**, 062112 (2002).
[7] V. B. Bezerra, G. L. Klimchitskaya, V. M. Mostepanenko, and C. Romero, Phys. Rev. A **69**, 022119 (2004).
[8] F. Intravaia and C. Henkel, Phys. Rev. Lett. **103**, 130405 (2009).
[9] G. Bimonte, New J. Phys. **9**, 281 (2007).
[10] F. Intravaia and C. Henkel, in *Proceedings of Quantum Field Theory under the Influence of External Boundary Conditions (Norman, OK, September 2009)*, edited by K. A. Milton and M. Bordag (World Scientific, Singapore, 2010).
[11] G.-L. Ingold, A. Lambrecht, and S. Reynaud, Phys. Rev. E **80**, 041113 (2009).
[12] P. Hänggi and G.-L. Ingold, Acta Phys. Pol. B **37**, 1537 (2006).
[13] F. Intravaia and C. Henkel, J. Phys. A **41**, 164018 (2008).
[14] S. A. Ellingsen, Phys. Rev. E **78**, 021120 (2008).

[15] S. A. Ellingsen, I. Brevik, J. S. Høye, and K. A. Milton, J. Phys. Conf. Series **161**, 012010 (2009).
[16] I. Brevik, J. B. Aarseth, J. S. Høye, and K. A. Milton, in *Quantum Field Theory under the Influence of External Conditions*, edited by K. A. Milton (Rinton Press, Princeton, NJ, 2004), p. 54.
[17] J. S. Høye, I. Brevik, S. A. Ellingsen, and J. B. Aarseth, Phys. Rev. E **75**, 051127 (2007); G. L. Klimchitskaya and V. M. Mostepanenko, *ibid.* **77**, 023101 (2008); J. S. Hoye, I. Brevik, S. A. Ellingsen, and J. B. Aarseth, *ibid.* **77**, 023102 (2008).
[18] S. A. Ellingsen, I. Brevik, J. S. Høye, and K. A. Milton, Phys. Rev. E **78**, 021117 (2008).
[19] I. Brevik, S. A. Ellingsen, J. S. Høye, and K. A. Milton, J. Phys. A **41**, 164017 (2008).
[20] B. Davies, Chem. Phys. Lett. **16**, 388 (1972).
[21] K. Schram, Phys. Lett. A **43**, 282 (1973).
[22] J. D. Jackson, *Classical Electrodynamics*, 2nd ed. (Wiley & Sons, New York, 1975).
[23] D. J. Thouless, Phys. Rev. Lett. **39**, 1167 (1977).
[24] J. R. Torgerson and S. K. Lamoreaux, Phys. Rev. E **70**, 047102 (2004).
[25] V. B. Svetovoy, Phys. Rev. A **76**, 062102 (2007).
[26] F. Intravaia and A. Lambrecht, Phys. Rev. Lett. **94**, 110404 (2005).
[27] F. Intravaia, C. Henkel, and A. Lambrecht, Phys. Rev. A **76**, 033820 (2007).
[28] H. Haakh, F. Intravaia, and C. Henkel, Phys. Rev. A **82**, 012507 (2010).
[29] A. Hanke and W. Zwerger, Phys. Rev. E **52**, 6875 (1995).
[30] G. W. Ford and R. F. O'Connell, Phys. E **29**, 82 (2005).
[31] G. Barton, Rep. Prog. Phys. **42**, 963 (1979).
[32] E. M. Lifshitz, Sov. Phys. JETP **2**, 73 (1956) [Zh. Eksp. Teor. Fiz. USSR **29**, 94 (1955)].
[33] V. A. Parsegian, *Van der Waals Forces—A Handbook for Biologists, Chemists, Engineers, and Physicists* (Cambridge University Press, New York, 2006).
[34] V. V. Nesterenko, J. Phys. A **39**, 6609 (2006).
[35] H. Raether, *Surface Plasmons on Smooth and Rough Surfaces and on Gratings*, Vol. 111 of Springer Tracts in Modern Physics (Springer, Berlin/Heidelberg, 1988).

# Part II

## Casimir effect in wedge and cylinder geometry

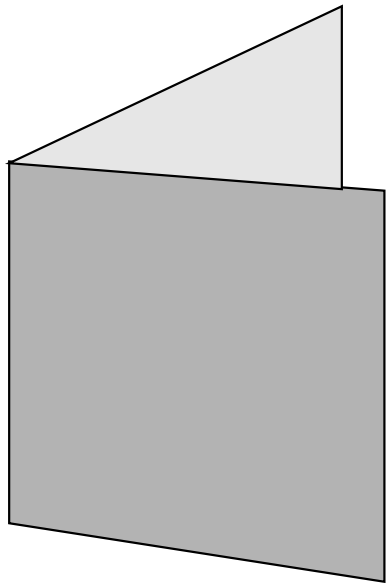

# Article [i]

***Electrodynamic Casimir effect in a medium-filled wedge***

I. Brevik, S.Å. Ellingsen, K.A. Milton

Physical Review E **79**, 041120 (2009)

# Electrodynamic Casimir effect in a medium-filled wedge

Iver Brevik* and Simen Å. Ellingsen†
*Department of Energy and Process Engineering, Norwegian University of Science and Technology, N-7491 Trondheim, Norway*

Kimball A. Milton‡
*Oklahoma Center for High Energy Physics and Homer L. Dodge Department of Physics and Astronomy, The University of Oklahoma, Norman, Oklahoma 73019, USA*

(Received 27 January 2009; revised manuscript received 6 March 2009; published 13 April 2009)

We re-examine the electrodynamic Casimir effect in a wedge defined by two perfect conductors making dihedral angle $\alpha=\pi/p$. This system is analogous to the system defined by a cosmic string. We consider the wedge region as filled with an azimuthally symmetric material, with permittivity and permeability $\varepsilon_1$, $\mu_1$ for distance from the axis $r<a$, and $\varepsilon_2$, $\mu_2$ for $r>a$. The results are closely related to those for a circular-cylindrical geometry, but with noninteger azimuthal quantum number $mp$. Apart from a zero-mode divergence, which may be removed by choosing periodic boundary conditions on the wedge, and may be made finite if dispersion is included, we obtain finite results for the free energy corresponding to changes in $a$ for the case when the speed of light is the same inside and outside the radius $a$, and for weak coupling, $|\varepsilon_1-\varepsilon_2|\ll 1$, for purely dielectric media. We also consider the radiation produced by the sudden appearance of an infinite cosmic string, situated along the cusp line of the pre-existing wedge.

DOI: 10.1103/PhysRevE.79.041120 PACS number(s): 05.30.−d, 42.50.Pq, 42.50.Lc, 11.10.Gh

## I. INTRODUCTION

Quantum field theory in the wedge geometry continues to attract interest, especially in connection with the Casimir effect. Usually it is assumed that the interior region of the wedge is a vacuum, and that the two plane surfaces $\theta=0$ and $\theta=\alpha$ ($\alpha$ denotes the opening angle) are perfectly conducting. The coordinate system is conventionally oriented such that the $z$ axis coincides with the singularity axis, i.e., the intersection line for the planes. For an introduction to the wedge model one may consult the book of Mostepanenko and Trunov [1].

The Casimir energy and stress in a wedge geometry was approached already in the 1970s [2,3]. Since that time, various embodiments of the wedge with perfectly conducting walls have been treated by Brevik and co-workers [4–6] and others [7]. More recently a wedge intercut by a cylindrical shell was considered by Nesterenko and collaborators, first for a semicircular wedge [8], then for arbitrary dihedral angle [9]. Local Casimir stresses were examined by Saharian and co-workers [10–12]. Rosa and collaborators studied the interaction of an atom with a wedge [13,14], the situation under which the closely related Casimir-Polder force was investigated by Sukenik *et al.* some years ago [15]. That interaction was first worked out by Barton [16].

One reason for the interest in the wedge geometry is the similarity with the formalism encountered in Casimir theory of systems having circular symmetry. This applies to the case of a perfectly conducting circular boundary [17–20], as well as to the case of a dielectric circular boundary [21–25]. Another reason for studying the wedge is the analogy—at least in a formal sense—with the theory of a cosmic string (cf., for instance, Ref. [26] or [4]). Let us briefly elaborate on the last-mentioned point. The line element outside a cosmic string is, in standard notation,

$$ds^2 = -dt^2 + dr^2 + (1-4GM)^2 r^2 d\theta^2 + dz^2, \tag{1.1}$$

where $G$ is the gravitational constant and $M$ the string mass per unit length. This is the geometry of locally flat space, with a deficit angle $\Phi=8\pi GM$ being removed. Let us introduce the symbols $\beta$ and $p$ by

$$\beta = (1-4GM)^{-1} = (1-\Phi/2\pi)^{-1}, \tag{1.2a}$$

$$p = \pi/\alpha. \tag{1.2b}$$

Now comparing the electromagnetic energy-momentum tensor outside the string [27]

$$\langle T_{\mu\nu}\rangle = \frac{1}{720\pi^2 r^4}(\beta^2+11)(\beta^2-1)\mathrm{diag}(1,-3,1,1) \tag{1.3}$$

with the electromagnetic energy-momentum in the wedge [2–4]

$$\langle T_{\mu\nu}\rangle = \frac{1}{720\pi^2 r^4}\left(\frac{\pi^2}{\alpha^2}+11\right)\left(\frac{\pi^2}{\alpha^2}-1\right)\mathrm{diag}(1,-3,1,1), \tag{1.4}$$

we see that $\beta$ corresponds to $p$. Hence the deficit angle $\Phi$ corresponds to $2\pi-2\alpha$. We shall return to this analogy later. Note that the stress tensor diverges at $r=0$, which makes the definition of a total Casimir energy in these configurations problematic. (Possible solutions to this problem were offered by Khusnutdinov and Bordag [28].)

A particular variant of the wedge model occurs if we introduce a cylindrical boundary of radius $a$ in the cavity. The

*iver.h.brevik@ntnu.no
†simen.a.ellingsen@ntnu.no
‡milton@nhn.ou.edu

 

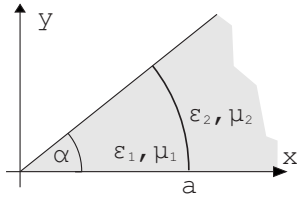


FIG. 1. The geometry considered in Secs. II and III. There is a cylindrical perfectly conducting shell at radius $a$. In these sections the indices of refraction are equal, $n^2=\epsilon_1\mu_1=\epsilon_2\mu_2$.

situation is sketched in Fig. 1. This model has been studied in particular by Nesterenko *et al.* and by Saharian *et al.*; cf. Refs. [8–12] with a wealth of further references therein. (For example, the fermionic situation for the circular case was discussed by Bezzera de Mello *et al.* [29].) The model can be looked upon as being intermediate between that of a conventional wedge, and an optical fiber. And that brings us to the main theme of the present paper, namely to study the situation of Fig. 1 in the presence of a dielectric medium, both in the interior $r<a$ as well as in the exterior, $r>a$. We designate the two regions by indices 1 and 2. Thus in the interior the refractive index is $n_1=\sqrt{\epsilon_1\mu_1}$ with $\epsilon_1$ and $\mu_1$ being the permittivity and the permeability, whereas in the exterior we have analogously $n_2=\sqrt{\epsilon_2\mu_2}$. We take all material quantities $\epsilon_1,\mu_1$ and $\epsilon_2,\mu_2$ to be constant and nondispersive. The special case when the circular boundary is perfectly conducting is included in the general situation when there is simply a dielectric/diamagnetic boundary. The plane surfaces $\theta=0$ and $\theta=\alpha$ are taken to be perfectly conducting, as usual.

We begin in Sec. II by considering the Fourier decomposition of the TE and TM modes when the circular boundary is perfectly conducting. This is the simplest case. Then we move on to give an expression for the Casimir energy. The case of a dielectric/diamagnetic boundary is considered thereafter (Fig. 2). The results for the wedge are in general divergent, not because of the divergence associated with the apex of the wedge, which does not contribute to the outward stress on the circular arc, but because of the corners where the arc meets the sides of the wedge. This divergence may be isolated in the azimuthal zero modes, independent of the angular coordinates. We propose isolation and removal of this divergence; alternatively, if the perfectly conducting boundaries at $\theta=0,\alpha$ are replaced by periodic boundary conditions, these divergences disappear. When either of these devices are employed, we obtain numerical results for the resulting finite

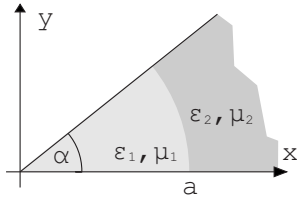


FIG. 2. The wedge with a dielectric/diamagnetic boundary at $r=a$. In Sec. IV we will allow $n_1\neq n_2$.

Casimir energy, referring to the boundary between the two regions, $r<a$ and $r>a$, both for weak and strong coupling. Finally, we exploit the analogy with a cosmic string to calculate, via the Bogoliubov transformation, the production of electromagnetic energy associated with a "sudden" creation of the full wedge situation, as compared with the initial case of a single-medium-filled wedge.

## II. ZERO-POINT ENERGY IN THE INTERIOR REGION—PERFECTLY CONDUCTING ARC

As mentioned, we consider an isotropic and homogeneous medium with permittivity $\epsilon_1$ and permeability $\mu_1$ enclosed within a wedge region limited by the conducting plane surfaces $\theta=0$ and $\theta=\alpha$ ($\leq 2\pi$). In an $xy$ plane, the cusp is situated at the origin. We use cylindrical coordinates $(r,\theta,z)$. We employ Heaviside-Lorentz units, and put $\hbar$ and $c$ equal to unity.

Assume, to begin with, that the wedge is closed by a perfectly conducting singular arc at $r=a$. We write down the fundamental modes for stationary electromagnetic modes in the interior wedge, by invoking the expansions given in Ref. [30],

$$E_r=\sum_{m=1}^{\infty}\left[-\frac{2k}{\lambda_1}J'_{mp}(\lambda_1 r)a_m^i-\frac{2i\mu_1\omega mp}{\lambda_1^2 r}J_{mp}(\lambda_1 r)b_m^i\right]\times F_0\sin mp\theta, \tag{2.1a}$$

$$E_\theta=-\sum_{m=0}^{\infty}\left[\frac{2kmp}{\lambda_1^2 r}J_{mp}(\lambda_1 r)a_m^i+\frac{2i\mu_1\omega}{\lambda_1}J'_{mp}(\lambda_1 r)b_m^i\right]\times F_0\cos mp\theta, \tag{2.1b}$$

$$E_z=2i\sum_{m=1}^{\infty}J_{mp}(\lambda_1 r)a_m^i F_0\sin mp\theta, \tag{2.1c}$$

$$H_r=\sum_{m=0}^{\infty}\left[\frac{2mp\epsilon_1\omega}{\lambda_1^2 r}J_{mp}(\lambda_1 r)a_m^i+\frac{2ik}{\lambda_1}J'_{mp}(\lambda_1 r)b_m^i\right]F_0\cos mp\theta, \tag{2.1d}$$

$$H_\theta=-\sum_{m=1}^{\infty}\left[\frac{2\epsilon_1\omega}{\lambda_1}J'_{mp}(\lambda_1 r)a_m^i+\frac{2ikmp}{\lambda_1^2 r}J_{mp}(\lambda_1 r)b_m^i\right]\times F_0\sin mp\theta, \tag{2.1e}$$

$$H_z=2\sum_{m=0}^{\infty}J_{mp}(\lambda_1 r)b_m^i F_0\cos mp\theta. \tag{2.1f}$$

Here $k$ is the axial wave number and $\lambda_1$ is the transverse wave number given by

$$\lambda_1^2=n_1^2\omega^2-k^2. \tag{2.2}$$

The $J_{mp}$'s are ordinary Bessel functions of order $mp$, which are finite at the origin for $mp\geq 0$, for $p$ nonintegral, while

$$F_0 = \exp(ikz - i\omega t) \tag{2.3}$$

is the $m=0$ version of the more general quantity $F_m=\exp(imp\theta+ikz-i\omega t)$. Expressions (2.1a), (2.1b), (2.1c), (2.1d), (2.1e), and (2.1f) satisfy the electromagnetic boundary conditions on the surfaces $\theta=0$ and $\theta=\alpha$ automatically, for arbitrary values of the coefficients $a_m$ and $b_m$. The $i$ superscript on the coefficient refers to the interior region. The $a_m$ modes and the $b_m$ modes are independent of each other.

Because of the closure of the region at $r=a$ the problem becomes an eigenvalue problem. Only discrete values of the transverse wave number $\lambda_1$ can occur. Let us distinguish between the two kinds of modes:

(i) TM polarization (the $a_m^i$ modes), which correspond to

$$J_{mp}(\lambda_1 a) = 0. \tag{2.4}$$

We denote the roots by $j_{mp,s}$, where $s=1,2,3\ldots$. For a given value of the axial wave number $k$ the energy eigenvalues are accordingly

$$\omega_{msk}^{\mathrm{TM}} = \frac{1}{n_1 a}\sqrt{j_{mp,s}^2 + k^2 a^2}, \quad m \geq 1, s \geq 1. \tag{2.5}$$

(ii) TE polarization (the $b_m^i$ modes), which correspond to zeroes of $J'_{mp}$,

$$\omega_{msk}^{\mathrm{TE}} = \frac{1}{n_1 a}\sqrt{(j'_{mp,s})^2 + k^2 a^2}, \quad m \geq 0, s \geq 1. \tag{2.6}$$

The interior zero-point energy per unit length is

$$\mathcal{E}^{\mathrm{int}} = \frac{1}{2}\int_{-\infty}^{\infty}\frac{dk}{2\pi}\sum_{s=1}^{\infty}\left[\omega_{0sk}^{\mathrm{TE}} + \sum_{m=1}^{\infty}(\omega_{msk}^{\mathrm{TM}} + \omega_{msk}^{\mathrm{TE}})\right]. \tag{2.7}$$

We here include the zero-point energy associated with the azimuthally symmetric TE mode, although there is no such TM mode.

To simplify the formalism somewhat, we introduce the symbol $\mathcal{E}_m^{\mathrm{int}}$,

$$\mathcal{E}_m^{\mathrm{int}} = \frac{1}{2}\int_{-\infty}^{\infty}\frac{dk}{2\pi}\sum_{s=1}^{\infty}(\omega_{msk}^{\mathrm{TM}} + \omega_{msk}^{\mathrm{TE}}). \tag{2.8}$$

For $m=0$ only the TE mode is to be included. We now make use of the argument principle. Any meromorphic function $g(\omega)$ of a complex variable $\omega$ satisfies the equation

$$\frac{1}{2\pi i}\oint \omega\frac{d}{d\omega}\ln g(\omega)d\omega = \sum \omega_{\mathrm{zeros}} - \sum \omega_{\mathrm{poles}}, \tag{2.9}$$

where $\omega_{\mathrm{zeros}}$ are the zeros and $\omega_{\mathrm{poles}}$ the poles of $g(\omega)$ lying inside the integration contour. The contour is chosen to be a large semicircle in the right half-plane with radius $R$, closed by a straight line along the imaginary $z$ axis from $\omega=iR$ to $\omega=-iR$. A general advantage of this method is that the multiplicities of zeros as well as for poles are automatically taken care of.

In the present case it is evident that $g(\omega)$ can be chosen as the product of $J_{mp}$ and $J'_{mp}$. There are no poles involved, and the contribution of the large semicircle goes to zero when $R\to\infty$. Thus we obtain

$$\mathcal{E}_m^{\mathrm{int}} = \frac{1}{2}\frac{1}{2\pi i}\int_{-\infty}^{\infty}\frac{dk}{2\pi}\int_{i\infty}^{-i\infty}d\omega\omega\times\frac{d}{d\omega}\ln[J_{mp}(\lambda_1 a)J'_{mp}(\lambda_1 a)]. \tag{2.10}$$

In the second integral, $k$ and $\omega$ are to be regarded as independent variables in $\lambda_1=\lambda_1(k,\omega)$. We now introduce the imaginary frequency $\zeta$ via $\omega\to i\zeta$, whereby

$$\lambda_1 = \sqrt{n_1^2\omega^2 - k^2} \to \sqrt{-(n_1^2\zeta^2 + k^2)} \equiv i\kappa_1. \tag{2.11}$$

We thus encounter Bessel functions of imaginary arguments, $J_{mp}(ix)$, with $x=\kappa_1 a$, $m\geq 0$. Introducing the modified Bessel function $I_\nu(x)$ via $J_\nu(ix)=i^\nu I_\nu(x)$ for arbitrary order $\nu$ we get

$$\mathcal{E}_m^{\mathrm{int}} = -\frac{1}{2}\frac{1}{2\pi}\int_{-\infty}^{\infty}\frac{dk}{2\pi}\int_{-\infty}^{\infty}d\zeta\zeta\frac{d}{d\zeta}\ln[I_{mp}(x)I'_{mp}(x)]. \tag{2.12}$$

Here we rewrite the derivative as $d/d\zeta=(n_1^2a^2\zeta/x)d/dx$, and take into account the symmetry properties $\int_{-\infty}^{\infty}dk\to 2\int_0^{\infty}dk$, $\int_{-\infty}^{\infty}d\zeta\to 2\int_0^{\infty}d\zeta$ to get

$$\mathcal{E}_m^{\mathrm{int}} = -\frac{n_1^2a^2}{2\pi^2}\int_0^{\infty}dk\int_0^{\infty}\frac{\zeta^2 d\zeta}{x}\times\frac{d}{dx}\ln[I_{mp}(x)I'_{mp}(x)]. \tag{2.13}$$

In the plane spanned by the axes $n_1\zeta$ and $k$ we may introduce polar coordinates $X$ and $Y$

$$X = n_1\zeta = \kappa_1\cos\theta, \tag{2.14a}$$

$$Y = k = \kappa_1\sin\theta, \tag{2.14b}$$

fulfilling the relation $X^2+Y^2=\kappa_1^2$. The area element in the $XY$ plane becomes $\kappa_1 d\kappa_1 d\theta = n_1 d\zeta dk$. The integration of the polar angle over the first quadrant then becomes simple, $\int_0^{\pi/2}\cos^2\theta d\theta=\pi/4$, and we get

$$\begin{aligned}\mathcal{E}_m^{\mathrm{int}} &= -\frac{1}{8\pi n_1 a^2}\int_0^{\infty}dx x^2\frac{d}{dx}[I_{mp}(x)I'_{mp}(x)] \\ &= -\frac{1}{8\pi n_1 a^2}\int_0^{\infty}dx x^2\left[\frac{I'_{mp}(x)}{I_{mp}(x)} + \frac{I''_{mp}(x)}{I'_{mp}(x)}\right].\end{aligned} \tag{2.15}$$

Going back to Eq. (2.7) we can thus write the interior zero-point energy as

$$\begin{aligned}\mathcal{E}^{\mathrm{int}} = -\frac{1}{8\pi n_1 a^2}\Bigg\{&\sum_{m=1}^{\infty}\int_0^{\infty}x^2 dx\left[\frac{I'_{mp}(x)}{I_{mp}(x)} + \frac{I''_{mp}(x)}{I'_{mp}(x)}\right] \\ &+ \int_0^{\infty}dx x^2\frac{I''_0(x)}{I'_0(x)}\Bigg\},\end{aligned} \tag{2.16}$$

where the last term represents the TE $m=0$ mode. No regularization procedure has been applied at this stage.

## III. EXTERIOR REGION INCLUDED, ASSUMING PERFECTLY CONDUCTING CIRCULAR ARC

We now include the exterior region $r\geq a$, still assuming the circular arc at $r=a$ to be perfectly conducting.

A choice has to be made for what kind of medium to fill the space $r>a$. One possible choice might be to assume a vacuum on the outside. Another natural choice would be to take the exterior medium to be identical to the interior one. We will in this section allow for a generalization of the last option, namely, to assume that the exterior space is filled with a medium with arbitrary constants $\epsilon_2$ and $\mu_2$, but with the restriction that their product is the same as in the interior,

$$\epsilon_2\mu_2 = \epsilon_1\mu_1 = n^2. \tag{3.1}$$

We will refer to this situation as "diaphanous." This condition implying the constancy of light everywhere has under several occasions turned out to be convenient mathematically, for instance in connection with the Casimir theory for dielectric balls [31–37], and in the Casimir theory for the relativistic piecewise uniform string [38–42] (a review is given in Ref. [43]). In the latter case, the velocity of light is to be replaced with the velocity of sound. Condition (3.1) means in the present problem that $\lambda$ takes the same value on the outside as on the inside (assuming $k$ to take the same values on the two sides). The principal advantage of this assumption, which is not easily satisfied in nature, is that in simple cases Casimir self-energies will turn out then to be finite.

In the exterior region $r>a$ we have the expansions, keeping the formalism at first quite general,

$$E_r = \sum_{m=1}^{\infty}\left[-\frac{2k}{\lambda_2}H_{mp}^{(1)\prime}(\lambda_2 r)a_m^e - \frac{2i\mu_2\omega mp}{\lambda_2^2 r}H_{mp}^{(1)}(\lambda_2 r)b_m^e\right] \times F_0 \sin mp\theta, \tag{3.2a}$$

$$E_\theta = -\sum_{m=0}^{\infty}\left[\frac{2kmp}{\lambda_2^2 r}H_{mp}^{(1)}(\lambda_2 r)a_m^e + \frac{2i\mu_2\omega}{\lambda_2}H_{mp}^{(1)\prime}(\lambda_2 r)b_m^e\right] \times F_0 \cos mp\theta, \tag{3.2b}$$

$$E_z = 2i\sum_{m=1}^{\infty} H_{mp}^{(1)}(\lambda_2 r)a_m^e F_0 \sin mp\theta, \tag{3.2c}$$

$$H_r = \sum_{m=0}^{\infty}\left[\frac{2mp\epsilon_2\omega}{\lambda_2^2 r}H_{mp}^{(1)}(\lambda_2 r)a_m^e + \frac{2ik}{\lambda_2}H_{mp}^{(1)\prime}(\lambda_2 r)b_m^e\right] \times F_0 \cos mp\theta, \tag{3.2d}$$

$$H_\theta = -\sum_{m=1}^{\infty}\left[\frac{2\epsilon_2\omega}{\lambda_2}H_{mp}^{(1)\prime}(\lambda_2 r)a_m^e + \frac{2ikmp}{\lambda_2^2 r}H_{mp}^{(1)}(\lambda_2 r)b_m^e\right] \times F_0 \sin mp\theta, \tag{3.2e}$$

$$H_z = 2\sum_{m=0}^{\infty} H_{mp}^{(1)}(\lambda_2 r)b_m^e F_0 \cos mp\theta. \tag{3.2f}$$

As before, $F_0$ is given by Eq. (2.3). The presence of the Hankel function of the first kind, $H_{mp}^{(1)}$, ensures proper behavior (outgoing waves) at infinity. The $e$ superscript refers to exterior modes.

Let us now take into account condition (3.1), implying $\lambda_1=\lambda_2\equiv\lambda$, and consider the boundary conditions. For the TM polarization (the $a_m^e$ modes) we get

$$H_{mp}^{(1)}(\lambda a) = 0, \quad m \geq 1, \tag{3.3}$$

whereas for the TE polarization (the $b_m^e$ modes),

$$H_{mp}^{(1)\prime}(\lambda a) = 0, \quad m \geq 0. \tag{3.4}$$

The roots of these eigenvalue equations are complex—nevertheless, the argument principle may be applied as has been explained in detail in many places [17,44,45]. We can now calculate the exterior zero-point energy $\mathcal{E}^{\text{ext}}$ in the same way as above. The modified Bessel function $K_\nu$ is introduced via $H_\nu^{(1)}(ix)=(2/\pi)i^{-(\nu+1)}K_\nu(x)$. For the total zero-point energy/length $\mathcal{E}=\mathcal{E}^{\text{int}}+\mathcal{E}^{\text{ext}}$ we obtain

$$\mathcal{E} = -\frac{1}{8\pi a^2}\left\{\sum_{m=1}^{\infty}\int_0^\infty x^2dx\left[\frac{I_{mp}'(x)}{I_{mp}(x)} + \frac{I_{mp}''(x)}{I_{mp}'(x)} + \frac{K_{mp}'(x)}{K_{mp}(x)} + \frac{K_{mp}''(x)}{K_{mp}'(x)}\right] + \int_0^\infty x^2dx\left[\frac{I_0''(x)}{I_0'(x)} + \frac{K_0''(x)}{K_0'(x)}\right]\right\}. \tag{3.5}$$

We now must face up to the fact that our result contains an irremovable divergence, associated with the nonzero $a_2$ heat kernel coefficient found by Nesterenko *et al.* [8,9]. This occurs precisely because of the $m=0$ terms in Eq. (3.5). If we were to write that expression as

$$\mathcal{E} = -\frac{1}{8\pi a^2}\left\{{\sum_{m=0}^{\infty}}'\int_0^\infty x^2dx\left[\frac{I_{mp}'(x)}{I_{mp}(x)} + \frac{I_{mp}''(x)}{I_{mp}'(x)} + \frac{K_{mp}'(x)}{K_{mp}(x)} + \frac{K_{mp}''(x)}{K_{mp}'(x)}\right] - \frac{1}{2}\int_0^\infty x^2dx\frac{d}{dx}\ln\left(\frac{I_0(x)}{I_0'(x)}\frac{K_0(x)}{K_0'(x)}\right)\right\} = \tilde{\mathcal{E}} + \hat{\mathcal{E}}, \tag{3.6}$$

where the prime on the summation sign means that the $m=0$ terms are counted with half weight, we see in the following that the summation, $\tilde{\mathcal{E}}$, may now be rendered finite (see Appendix A), but the residual correction, $\hat{\mathcal{E}}$, is divergent.

It is instructive to break up this residual zero-mode contribution into its Dirichlet (TM) and Neumann (TE) parts. The former involves, asymptotically for large $x$

$$I_0(x)K_0(x) \sim \frac{1}{2x}\left[1 + \frac{1}{8x^2} + O\left(\frac{1}{x^4}\right)\right], \tag{3.7a}$$

while the latter requires

$$I_0'(x)K_0'(x) \sim -\frac{1}{2x}\left[1 - \frac{3}{8x^2} + O\left(\frac{1}{x^4}\right)\right]. \tag{3.7b}$$

Then the two contributions to the residual zero-mode terms are

$$-\frac{1}{2}\int_0^\infty dx x^{2-s}\frac{d}{dx}\ln[I_0(x)K_0(x)] \sim \frac{1}{2}\int_0^\infty dx x^{2-s}\left(\frac{1}{x} + \frac{1}{4x^3} + \ldots\right), \tag{3.8a}$$

$$\frac{1}{2}\int_0^\infty dx x^{2-s}\frac{d}{dx}\ln[I_0'(x)K_0'(x)] \sim \frac{1}{2}\int_0^\infty dx x^{2-s}\left(-\frac{1}{x}+\frac{3}{4x^3}+\ldots\right), \tag{3.8b}$$

so the $1/x$ terms cancel between the two modes (alternatively those terms may be removed by contact terms, as we will see in the following), but the subleading $1/x^3$ terms constitute an irremovable logarithmic divergence. Here, we have indicated an analytic regularization by taking $s$ to zero through positive values, which corresponds to the following divergent terms as $s\to 0$:

$$-\frac{1}{2}\int_0^\infty dx x^{2-s}\frac{d}{dx}\ln I_0(x)K_0(x) \sim \frac{1}{8s}, \tag{3.9a}$$

$$\frac{1}{2}\int_0^\infty dx x^{2-s}\frac{d}{dx}\ln I_0'(x)K_0'(x) \sim \frac{3}{8s}. \tag{3.9b}$$

These precisely correspond to the two mode contributions, adding up to $1/2s$, found by Nesterenko *et al.* [8].

This zero-mode divergence is due to the sharp corners where the arc meets the wedge. We will proceed by setting this term aside, and computing the balance of the Casimir free energy. We note there is a closely related problem which Nesterenko *et al.* [9] dubbed a cone. That is, we identify the two wedge boundaries at $\theta=0$ and $\alpha$, and impose periodic boundary conditions there. This means that we may take the angular function in the mode sums to be $e^{imp\theta}$, where $m$ may be either positive or negative, and where now $p=2\pi/\alpha$. Now all modes, including the zero modes ($m=0$) contribute equally, and the summation on $m$ becomes

$$\sum_{m=-\infty}^{\infty} = 2\sum_{m=0}^{\infty}{}' \tag{3.10}$$

with the zero modes both having 1/2 weight in the latter form. (For the radial function in the interior we can only use $I_{|\nu|}$ in order that the solution be finite at the origin.) Thus we get precisely $2\tilde{\mathcal{E}}$ [Eq. (3.6)] without the residual zero-mode term $\hat{\mathcal{E}}$, and we have eliminated the irremovable logarithmic divergence. This is because the sharp corners, where the arc meets the wedge, have been removed because there is no wedge boundary. So if the reader prefers, he or she may regard the rest of the discussion in this and the following section to refer to this situation, which will introduce an additional factor of two into the Casimir free energy, and with the restriction $p\geq 1$, where $p=1$ corresponds to the circular cylinder first considered in Ref. [17].

So in any case disregarding in the following the residual zero-mode pieces $\hat{\mathcal{E}}$, we consider now the regularization of the $\Sigma'_{m=0}{}^{\infty}$ terms in Eq. (3.6), $\tilde{\mathcal{E}}$, which, in order to be a Casimir energy, ought to be given in such a form that it reduces to zero in the limit when $a\to\infty$. This will eliminate the divergence associated with the apex, which is not relevant to the force on the circular arc. It is easy to satisfy this requirement by observing that for large values of $x$, and for general $\nu$, we can approximate

$$I_\nu(x)\sim\frac{1}{\sqrt{2\pi x}}e^x, \quad K_\nu(x)\sim\sqrt{\frac{\pi}{2x}}e^{-x}, \quad x\to\infty, \tag{3.11}$$

implying that $I_\nu'\sim I_\nu$ and $K_\nu'\sim -K_\nu$. Accordingly,

$$\frac{d}{dx}\ln(-I_\nu K_\nu I_\nu' K_\nu') \sim 2\frac{d}{dx}\ln(I_\nu K_\nu)\sim -\frac{2}{x} \tag{3.12}$$

to leading order in $x$. This term is to be subtracted off from the integrand in Eq. (3.5). The Casimir energy for the wedge becomes then

$$\tilde{\mathcal{E}} = -\frac{1}{8\pi n a^2}\sum_{m=0}^{\infty}{}'\int_0^\infty x^2 dx\left[\frac{I_{mp}'(x)}{I_{mp}(x)}+\frac{I_{mp}''(x)}{I_{mp}'(x)}+\frac{K_{mp}'(x)}{K_{mp}(x)} + \frac{K_{mp}''(x)}{K_{mp}'(x)}+\frac{2}{x}\right]. \tag{3.13}$$

We may here perform a partial integration (the boundary terms at $x=0$ and $x=\infty$ do not contribute),

$$\tilde{\mathcal{E}} = \frac{1}{4\pi n a^2}\sum_{m=0}^{\infty}{}'\int_0^\infty x dx \times \ln[-4x^2 I_{mp}(x)I_{mp}'(x)K_{mp}(x)K_{mp}'(x)]. \tag{3.14}$$

It is helpful to introduce a quantity $\lambda_\nu(x)$ for arbitrary order $\nu$,

$$\lambda_\nu(x) = [I_\nu(x)K_\nu(x)]', \tag{3.15}$$

and to take into account the Wronskian $W\{I_\nu,K_\nu\}=-1/x$. From this we calculate the following useful relationship:

$$-4x^2 I_\nu(x)I_\nu'(x)K_\nu(x)K_\nu'(x) = 1-x^2\lambda_\nu^2(x), \tag{3.16}$$

and so end up with the following convenient form for the Casimir energy,

$$\tilde{\mathcal{E}} = \frac{1}{4\pi n a^2}\sum_{m=0}^{\infty}{}'\int_0^\infty x dx\,\ln[1-x^2\lambda_{mp}^2(x)]. \tag{3.17}$$

This is thus the boundary-induced contribution to the zero-point energy. If the boundary $r=a$ were removed and either the interior or the exterior medium were chosen to fill the whole wedge region, we would get $\tilde{\mathcal{E}}=0$. This is a property relying on condition (3.1) above. The temperature is assumed to be zero.

Although the leading behavior of the Bessel functions has been subtracted in Eq. (3.17), it is still not in general finite. We will see in the following section how a finite self-energy may be extracted from this formula. For now, we observe that this is a generalization of the standard formal result for a conducting circular cylinder, which is obtained from this result in the special case $p=1$ [17]. (The overall $1/n$ comes from an elementary scaling argument [46].) When $p=1$ expression (3.17) is one-half that for a conducting circular cyl-

inder. Referring to the perfectly conducting wedge boundaries, we see that the Casimir energy for periodic boundary conditions, with period $2\pi$, is twice the Casimir energy for a perfectly conducting boundary condition imposed on the $\theta$ interval of $\pi$, a result obvious from the replacement of $e^{im\theta}$ for $m$ of either sign in the former case by $\sin m\theta$ or $\cos m\theta$, $m \geq 0$, in the latter. This general observation, which is the theorem stated in Eq. (2.49) of Ref. [47] (see also Ref. [48]) will allow us to obtain numerical results rather immediately. For the periodic boundary-condition situation, which eliminates the zero-mode problem, $p=1$ is exactly the circular cylinder problem, and there is no additional factor of 1/2.

## IV. DIELECTRIC BOUNDARY AT $r=a$

Assume now that the perfectly conducting arc at $r=a$ is removed and replaced by a dielectric boundary, wherewith the interior and exterior regions become coupled via electromagnetic boundary conditions at $r=a$. As before, we assume that the plane surfaces $\theta=0$ and $\theta=\alpha$ are perfectly conducting for all values of $r$. (Alternatively, we may impose periodic boundary conditions there.)

We shall assume in the following that the media are arbitrary, with real and constant parameters $\epsilon_1, \mu_1$ in the interior and $\epsilon_2, \mu_2$ in the exterior, without any restriction imposed on their product. This will, however, result in general in a divergent Casimir self-energy.

Let $\lambda_2$ be the transverse wave number in the exterior region,

$$\lambda_2^2 = n_2^2\omega^2 - k^2, \tag{4.1}$$

with $n_2^2 = \epsilon_2\mu_2$. The basic expansions are Eqs. (2.1a), (2.1b), (2.1c), (2.1d), (2.1e), and (2.1f) in the interior and Eqs. (3.2a), (3.2b), (3.2c), (3.2d), (3.2e), and (3.2f) in the exterior.

As for the boundary conditions at $r=a$, only the tangential field components have to be taken into account. From the continuity of $E_z$ and $H_z$ we get, respectively,

$$J_{mp}(u)a_m^i = H_{mp}^{(1)}(v)a_m^e \tag{4.2}$$

and

$$J_{mp}(u)b_m^i = H_{mp}^{(1)}(v)b_m^e, \tag{4.3}$$

where we have defined

$$u = \lambda_1 a, \quad v = \lambda_2 a. \tag{4.4}$$

From the component $E_\theta$ we get

$$\frac{kmp}{u^2}J_{mp}(u)a_m^i + \frac{i\mu_1\omega}{u}J'_{mp}(u)b_m^i = \frac{kmp}{v^2}H_{mp}^{(1)}(v)a_m^e + \frac{i\mu_2\omega}{v}H_{mp}^{(1)\prime}(v)b_m^e, \tag{4.5}$$

and from the component $H_\theta$,

$$\frac{i\epsilon_1\omega}{u}J'_{mp}(u)a_m^i - \frac{kmp}{u^2}J_{mp}(u)b_m^i = \frac{i\epsilon_2\omega}{v}H_{mp}^{(1)\prime}(v)a_m^e - \frac{kmp}{v^2}H_{mp}^{(1)}(v)b_m^e. \tag{4.6}$$

The two last equations mean that a superposition of the TM and TE waves is in general necessary to satisfy the boundary conditions. The exception is the axially symmetric case $m=0$. The condition for solution of the set of linear equations is that the system determinant vanishes. Observing the relation

$$u^2 - v^2 = (n_1^2 - n_2^2)\omega^2 a^2 \tag{4.7}$$

which follows from Eqs. (4.1) and (4.4), we obtain after some manipulations the condition

$$\left[\frac{\mu_1}{u}\frac{J'_{mp}(u)}{J_{mp}(u)} - \frac{\mu_2}{v}\frac{H_{mp}^{(1)\prime}(v)}{H_{mp}^{(1)}(v)}\right]\left[\frac{\epsilon_1\omega^2}{u}\frac{J'_{mp}(u)}{J_{mp}(u)} - \frac{\epsilon_2\omega^2}{v}\frac{H_{mp}^{(1)\prime}(v)}{H_{mp}^{(1)}(v)}\right] = m^2p^2k^2\left(\frac{1}{v^2} - \frac{1}{u^2}\right)^2. \tag{4.8}$$

This is essentially the same transcendental eigenvalue equation as found for a step-index optical fiber (cf., for instance, Ref. [30] or [49]). In transmission problems, one is usually interested in calculating the discrete values of the propagation constant $k$, assuming that the waveguide is fed with some frequency $\omega$. Here our intention is different, namely, to calculate the discrete values of $\omega$ on the basis of an input value for the continuous axial wave vector $k$. As we noted in Sec. III, this dispersion relation generalizes that for a circular cylinder, the special case $p=1$.

It may be noted that the roots of Eq. (4.8) are both real and complex. Application of the argument principle to such a problem is discussed in Ref. [50].

### A. $n_1 = n_2$

The TE and TM modes decouple in the special case when $n_1 = \sqrt{\epsilon_1\mu_1} = n_2 = \sqrt{\epsilon_2\mu_2}$. In this case, dispersion relation (4.8) reduces to $\Delta\tilde{\Delta}=0$, where $\Delta$ and $\tilde{\Delta}$ are the two factors on the left-hand side of Eq. (4.8), and then using the Wronskian, we find after Euclidean rotation, $\omega \to i\zeta$,

$$\Delta\tilde{\Delta} = \frac{(\epsilon_1+\epsilon_2)}{4c^2\epsilon_1\epsilon_2}\frac{1-\xi^2x^2(I_{mp}K_{mp})'^2}{x^2I_{mp}^2(x)K_{mp}^2(x)}, \tag{4.9}$$

where $x=\kappa a$, $c=1/n$, and the reflection coefficient (for either polarization)

$$\xi = \frac{\epsilon_2-\epsilon_1}{\epsilon_2+\epsilon_1}. \tag{4.10}$$

We conclude that the formula for the (zero-mode subtracted) Casimir energy is

$$\tilde{\mathcal{E}} = \frac{1}{2}\frac{1}{2\pi i}\int_{-\infty}^{\infty}\frac{dk}{2\pi}\sum_{m=0}^{\infty}{}'\int_{i\infty}^{-i\infty}d\omega\omega\frac{d}{d\omega}\ln g_m(x), \tag{4.11}$$

where

$$g_m(x) = 1 - \xi^2 x^2 \lambda_{mp}^2, \tag{4.12}$$

where $\lambda_{mp}$ is given by Eq. (3.15). Here, we have again subtracted off the terms that would be present if either medium filled the entire wedge. [The divergence structure of the zero-mode term subtracted from Eq. (4.11) is analyzed in Appendix B.] Again cavalierly integrating by parts, we obtain, using the change of variables (2.14),

$$\widetilde{\mathcal{E}} = \frac{1}{4\pi n a^2} {\sum_{m=0}^{\infty}}' \int_0^\infty dx x \ln[1 - \xi^2 x^2 \lambda_{mp}^2]. \tag{4.13}$$

As expected, this differs from conducting case (3.17) by the appearance of $\xi^2$ in front of $\lambda_{mp}$. The conducting case is obtained by setting $\xi=1$. All of this is just as for the circular cylinder case, which is obtained from the $p=1$ result by multiplying by a factor of 2.

Let us now extract both the $\xi=1$ (perfect conducting) and the small $\xi$ results for arbitrary $p$. A simple route is to follow the method given in [18] or in Chap. 7 of Ref. [47]. The point is simply that the uniform asymptotic expansion for the modified Bessel functions yields an asymptotic expansion for large $p$. Thus we can write (see the Appendix A for details)

$$2n\widetilde{\mathcal{E}} = \frac{\xi^2}{16\pi a^2} \ln(2\pi/p) + \overline{\mathcal{E}}_0 + 2\sum_{m=1}^{\infty} \overline{\mathcal{E}}_m, \tag{4.14}$$

where

$$\overline{\mathcal{E}}_0 = \frac{1}{4\pi a^2} \int_0^\infty dx x \left[ \ln(1 - \xi^2 x^2 \lambda_0^2(x)) + \frac{\xi^2}{4} \frac{x^4}{(1+x^2)^3} \right], \tag{4.15a}$$

$$\overline{\mathcal{E}}_m = \frac{1}{4\pi a^2} \int_0^\infty dx x \left[ \ln(1 - \xi^2 x^2 \lambda_{mp}^2(x)) + \frac{\xi^2}{4} \frac{x^4}{(m^2 p^2 + x^2)^3} \right]. \tag{4.15b}$$

(Further details are given in the cited references.) Because of the subtractions in the integrals, they are convergent.

Let us first consider $\xi$ as small, and keep only the terms of order $\xi^2$. Using the uniform asymptotic approximants, we find for large $mp$,

$$\overline{\mathcal{E}}_m \sim \frac{\xi^2}{4\pi a^2} \left( \frac{1}{96 m^2 p^2} - \frac{7}{3840 m^4 p^4} + \cdots \right), \tag{4.16}$$

while numerical integration gives

$$\overline{\mathcal{E}}_0 = \frac{\xi^2}{4\pi a^2} (-0.490\ 877\ 5). \tag{4.17}$$

Thus

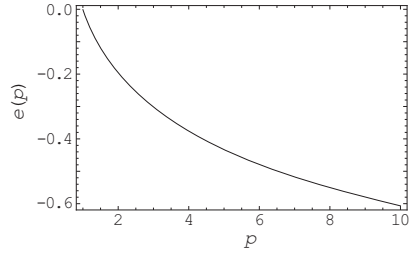


FIG. 3. Casimir energy for weak coupling, $\xi^2 \ll 1$, as a function of $p$ which is related to the dihedral angle $\alpha = \pi/p$. This graph shows the energy for $p > 1$.

$$\widetilde{\mathcal{E}} = \frac{\xi^2}{8\pi n a^2} \left( -0.490\ 877\ 5 + \frac{1}{4} \ln 2\pi/p + \frac{\pi^2}{288} \frac{1}{p^2} - \frac{7\pi^4}{172800} \frac{1}{p^4} + 2\sum_1^M [f(mp) - g(mp)] \right) \equiv \frac{\xi^2}{8\pi n a^2} e(p), \tag{4.18}$$

where we have added and subtracted the first two terms in the uniform asymptotic expansion,

$$g(\nu) = \frac{1}{96\nu^2} - \frac{7}{3840\nu^4}, \tag{4.19}$$

and $f$ is the integral appearing in $\overline{\mathcal{E}}_m$,

$$f(\nu) = \int_0^\infty dx x^3 \left[ -\lambda_\nu^2 + \frac{1}{4} \frac{x^2}{(x^2+\nu^2)^3} \right]. \tag{4.20}$$

In principle we are to take the $M \to \infty$ limit in Eq. (4.18). In practice, we may keep only a few terms in the $m$ sum. For example, keeping none of those corrections, that is setting $M=0$, we get for $p=1$, $e(1) \approx -0.001\ 084\ 7$. Keeping three terms is sufficient to find that $e(1)$ is less than $1 \times 10^{-6}$; indeed, the circular cylinder value is $e(1)=0$ [21–25]. This function $e(p)$ is plotted in Fig. 3, for $p > 1$, where it is sufficient to keep the leading asymptotic approximations; for $p$ between 1/2 and 1 ($\alpha$ between $\pi$ and $2\pi$) we must retain at least one correction, $M=1$, as shown in Fig. 4. (No observable change occurs with larger $M$.) Numerically, we see that

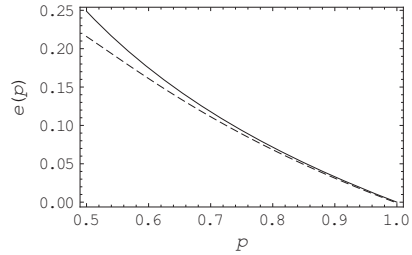


FIG. 4. Casimir energy for weak coupling, $\xi^2 \ll 1$, as a function of $p$ which is related to the dihedral angle $\alpha = \pi/p$. This graph shows the energy for $0.5 < p < 1$. The upper curve shows the exact energy, the lower the leading asymptotic approximation, obtained from Eq. (4.18) by setting $M=0$.

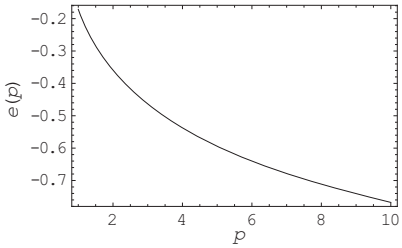


FIG. 5. Casimir energy for strong coupling, $\xi^2=1$, as a function of $p$, related to the dihedral angle by $\alpha=\pi/p$, for $p>1$. In this region $M=0$ in Eq. (4.22) is sufficient.

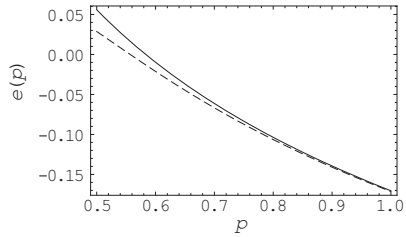


FIG. 6. Casimir energy for strong coupling, $\xi^2=1$, as a function of $p$, related to the dihedral angle by $\alpha=\pi/p$, for $0.5<p<1$. In this region $M=2$ in Eq. (4.22) is sufficient, and the comparison with the $M=0$ result (lower curve) is made.

the value for a cylinder with a conducting septum ($p=1/2$) is indistinguishable from $e(0.5)=1/4$.

Recall for periodic boundary conditions on the wedge (the "cone") $p=2\pi/\alpha\geq 1$, and an additional factor of two appears in the energy. Similarly, following the same references, we can obtain the strong coupling (perfect conductor) limit, $\xi=1$. This time the formula for the energy is

$$\tilde{\mathcal{E}}=\frac{1}{8\pi na^2}e(p), \tag{4.21}$$

where

$$e(p)=-0.651\,752+\frac{1}{4}\ln 2\pi/p+\frac{7\pi^2}{2880}\frac{1}{p^2}-\frac{\pi^4}{32256}\frac{1}{p^4}+2\sum_{m=1}^{M}[f(mp)-g(mp)], \tag{4.22}$$

where again the limit $M\to\infty$ is understood. Now $f$ is given by

$$f(\nu)=\int_0^\infty dx x\left[\ln(1-x^2\lambda_\nu^2)+\frac{1}{4}\frac{x^4}{(x^2+\nu^2)^3}\right], \tag{4.23}$$

and now the asymptotic terms are

$$g(\nu)=\frac{7}{960\nu^2}-\frac{5}{3584\nu^4}. \tag{4.24}$$

Keeping no correction terms is already very good at $p=1$, where with $M=0$ $e(1)/(4\pi)\approx -0.013\,633$, only slightly different from the exact answer of $-0.013\,56$ [17]. Keeping just $M=1$ gives exact coincidence to the indicated accuracy. This function $e(p)$ is plotted in Fig. 5 for $p>0$ where the asymptotic approximation is sufficient, while two correction terms are included in the region $0.5<p<1$, as shown in Fig. 6. It is curious that the energy vanishes now not at $p=1$, but at $p=0.583$.

(Again, recall only $p\geq 1$ is relevant for periodic boundary conditions on the wedge.)

### B. $n_1\neq n_2$, $\mu_1=\mu_2=1$

Finally, we can follow Ref. [21] to obtain the weak-coupling Casimir self-energy for a purely dielectric wedge, where $\mu_1=\mu_2=1$. We can only examine the coefficient of $(\epsilon_1-\epsilon_2)^2$ because the result is divergent in higher orders. It is hardly necessary to give details since all that is necessary is to replace $m$ by $mp$ in the analysis given in that reference. The energy per area in the wedge is

$$\tilde{\mathcal{E}}=\frac{(\epsilon_1-\epsilon_2)^2}{32\pi na^2}{\sum_{m=0}^{\infty}}'\int_0^\infty dy y^4 g_m(y), \tag{4.25}$$

where the exact form of $g_m$ is elaborate, but has the asymptotic form

$$g_m(y)\sim\frac{1}{2m^2p^2}\sum_{k=1}^{\infty}\frac{1}{(mp)^k}f_k(z),\quad mp\to\infty, \tag{4.26}$$

where $y=mpz$, and $f_k$ are rational functions of $z$, given in Ref. [21], about which all we need to know here is

$$p^2\lim_{s\to 0}\sum_{m=1}^{\infty}m^{2-s}\int_0^\infty dz z^{4-s}f_1(z)=-p^2\frac{\zeta(3)}{16\pi^2}, \tag{4.27a}$$

$$\int_0^\infty dz\left[z^4f_2(z)-\frac{1}{8}\right]=0, \tag{4.27b}$$

$$\lim_{s\to 0}{\sum_{m=0}^{\infty}}'(mp)^{-s}\int_0^\infty dz z^{4-s}f_3(z)=\frac{5}{32}\ln 2\pi/p, \tag{4.27c}$$

$$\int_0^\infty dz z^4 f_4(z)=0, \tag{4.27d}$$

$$\frac{1}{p^2}\sum_{m=1}^{\infty}\frac{1}{m^2}\int_0^\infty dz z^4 f_5(z)=\frac{19\pi^2}{7680}\frac{1}{p^2}, \tag{4.27e}$$

$$\int_0^\infty dz z^4 f_6(x)=0, \tag{4.27f}$$

$$\frac{1}{p^4}\sum_{m=1}^{\infty}\frac{1}{m^4}\int_0^\infty dz z^4 f_7(z)=-\frac{209\pi^4}{5\,806\,080}\frac{1}{p^4}. \tag{4.27g}$$

Here a contact term, which cannot contribute to any observable force, has been removed from Eq. (4.27b). Again, for

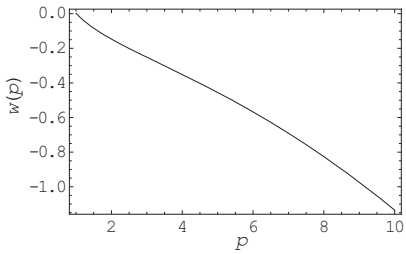


FIG. 7. Casimir energy for weak coupling, $|\epsilon_1-\epsilon_2|\ll 1$, as a function of $p$, which is related to the dihedral angle $\alpha=\pi/p$, for a purely dielectric wedge. Here, for $p>1$, only the leading asymptotic terms have been included.

the precise definition of Eq. (4.27c) see Appendix A. Then the Casimir energy per unit length of the dilute dielectric wedge is

$$\tilde{\mathcal{E}} \sim \frac{(\epsilon_1-\epsilon_2)^2}{64\pi n a^2} w(p), \tag{4.28}$$

where

$$w(p) \approx -p^2\frac{\zeta(3)}{16\pi^2}+\frac{5}{32}\ln(2\pi/p)+\frac{19\pi^2}{7680p^2}-0.301590 + \sum_{m=1}^{4} r(mp)-\frac{0.000\,012}{p^2}, \tag{4.29}$$

where

$$r(\nu)=2\int_0^\infty dy y^4\left[g_\nu(y)-\frac{1}{2\nu^2}\sum_{k=1}^{5}\frac{1}{\nu^k}f_k(y/\nu)\right], \tag{4.30}$$

and we have used the next term in the asymptotic series to estimate the contribution for $m\geq 5$. This, numerically, yields the correct value of zero for $p=1$. The values for the Casimir energy for larger values of $p$ are shown in Fig. 7, and for smaller values of $p$ in Fig. 8.

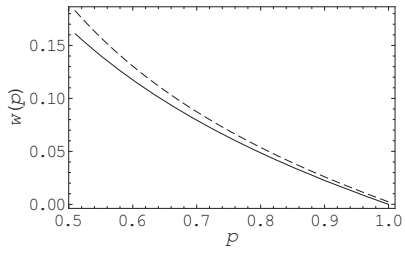


FIG. 8. Casimir energy for weak coupling, $|\epsilon_1-\epsilon_2|\ll 1$, as a function of $p$, which is related to the dihedral angle $\alpha=\pi/p$, for a purely dielectric wedge. Here, for $0.5<p<1$, the effect of the remainder is significant; the upper curve shows only the leading asymptotic terms, while the lower curve includes the remainder function $r$.

For the septum case, the numerical value of $w(0.5)=0.1666$, which seems likely to represent exactly 1/6. (Periodic boundary conditions restrict $p\geq 1$.)

## V. ENERGY PRODUCTION IN THE SUDDEN FORMATION OF A COSMIC STRING

As already mentioned, the electromagnetic theory of the wedge is related to the theory of cosmic strings. In general, cosmic strings are believed to be possible ingredients in the very early Universe; they are related to phase transitions. One particular aspect of this study is to estimate the energy production in the form of massless particles when a string is formed "suddenly" at some instant $t=t_0$, where $t_0$ is a characteristic time usually taken to be of order $1\times 10^{-40}$ s as is typical for grand unified theories (GUTs). One can calculate the number of particles associated with the formation of the string in terms of Bogoliubov coefficients relating the initial Minkowski metric to the (static) metric after the string has been formed. This approach was pioneered by Parker [51] for massless scalar fields, assuming the string radius to be zero. Analogous calculations were made in Ref. [52] in the electromagnetic case, still assuming the string radius to be zero, and in Ref. [53] for the case of a finite string radius. (See also Ref. [28].)

In the following we shall investigate the following model: Let a cosmic string of vanishing radius and large length $L$ be formed suddenly along the cusp line of the wedge, i.e., along the $z$ axis. The time of formation is $t=t_0$. In the interior region we assume that there is one single isotropic medium present, with refractive index $n=\sqrt{\epsilon\mu}$. The interior region is closed by a perfectly conducting arc with radius $r=a$. In the present context, $a$ plays the role of a "large" boundary; in connection with strings, $a$ is usually taken to be of the same order as $L$ [51]. The finiteness of $a$ will moreover make it possible to normalize the fundamental modes in a conventional way. As for the description of the electromagnetic fields, we have to distinguish between the Minkowski metric present for $t<t_0$ and the string metric for $t>t_0$.

### A. $t<t_0$ case

We shall consider the TM mode only, for which the central field component is $E_z$. For definiteness we reproduce the fields in the $m,k$ mode here, in a convenient notation (replacing the previous combination $2ia_m^i$ with the symbol $N$)

$$E_z = NJ_{mp}(\lambda r)F_0 \sin mp\theta, \tag{5.1}$$

$$E_r = \frac{ik}{\lambda}NJ'_{mp}(\lambda r)F_0 \sin mp\theta, \tag{5.2}$$

$$E_\theta = \frac{ikmp}{\lambda^2 r}NJ_{mp}(\lambda r)F_0 \cos mp\theta, \tag{5.3}$$

$$H_z = 0, \tag{5.4}$$

$$H_r = -\frac{imp\epsilon\omega}{\lambda^2 r}NJ_{mp}(\lambda r)F_0 \cos mp\theta, \tag{5.5}$$

$$H_\theta = \frac{i\omega\epsilon}{\lambda} N J'_{mp}(\lambda r) F_0 \sin mp\theta. \tag{5.6}$$

As before, $\lambda = \sqrt{n^2\omega^2 - k^2}$, $F_0 = \exp(ikz - i\omega t)$, and $m \geq 1$. The boundary condition on the arc is $J_{mp}(\lambda a) = 0$, giving the solutions $\lambda_{ms}$, $s = 1, 2, 3, \ldots$ for the transverse wave number $\lambda$.

It is now convenient as an intermediate step to make use of the formalism of scalar field theory. Define the scalar field mode $\psi_{msk}$, satisfying Dirichlet boundary conditions on all surfaces, as

$$\psi_{msk} = N J_{mp}(\lambda_{ms} r) F_0 \sin mp\theta. \tag{5.7}$$

It is seen to have the same form as the $m, s, k$ mode of the field component $E_z$. For reasons to become clear later, we choose the magnitude $|N|$ of the normalization constant $N$ to be

$$|N| = \frac{1}{n} \sqrt{\frac{2}{\alpha\epsilon\omega_{msk}}} \frac{\lambda_{ms}}{a |J_{mp+1}(\lambda_{ms} a)|}, \tag{5.8}$$

with $\omega_{msk} = (1/n)\sqrt{\lambda_{ms}^2 + k^2}$.

We define the Klein-Gordon product as

$$(\psi_{msk}, \psi_{m's'k'}) = \frac{-i\epsilon n^2}{\lambda_{ms}^2} \int \psi_{msk} \overleftrightarrow{\partial}_0 \psi^*_{m's'k'} r dr d\theta dz, \tag{5.9}$$

and then get by direct calculation

$$(\psi_{msk}, \psi_{m's'k'}) = 2\pi \delta(k - k') \delta_{mm'} \delta_{ss'}. \tag{5.10}$$

Consider now the electromagnetic energy $W$ in the wedge region. We may calculate it by integrating the energy density $w$ over the volume,

$$W = \int w dV = \frac{1}{4} \int [\epsilon |E|^2 + \mu |H|^2] r dr d\theta dz, \tag{5.11}$$

using the general recursion equation $[J_\nu = J_\nu(x)]$

$$(J'_\nu)^2 + \frac{\nu^2}{x^2} J_\nu^2 = \frac{1}{2}(J_{\nu-1}^2 + J_{\nu+1}^2), \tag{5.12}$$

as well as the integral formula

$$\int_0^a [J_{mp-1}^2(\lambda_{ms} r) + J_{mp+1}^2(\lambda_{ms} r)] r dr = a^2 J_{mp+1}^2(\lambda_{ms} a), \tag{5.13}$$

which holds when $J_{mp}(\lambda_{ms} a) = 0$. It is however simpler to go via the axial energy flux $P$, given as

$$P = \int S_z dA, \tag{5.14}$$

where $dA = r dr d\theta$ is the cross-sectional area element, and where

$$S_z = \frac{1}{2} \Re (E_r H_\theta^* - E_\theta H_r^*) \tag{5.15}$$

is the Poynting vector. As in any linear wave theory we can set [54]

$$P = \frac{W}{L} c_g, \tag{5.16}$$

where $c_g$ is the axial group velocity. From Eqs. (5.14) and (5.15) we then get

$$P = \frac{\alpha\epsilon k a^2 \omega_{mks}}{8\lambda_{ms}^2} |N|^2 J_{mp+1}^2(\lambda_{ms} a). \tag{5.17}$$

In geometric units $P$ has the dimension $\mathrm{cm}^{-2}$. As $c_g = d\omega/dk = k/(n^2\omega)$ we get for the energy per unit length

$$\frac{W}{L} = \frac{\alpha\epsilon n^2 a^2 \omega_{msk}^2}{8\lambda_{ms}^2} |N|^2 J_{mp+1}^2(\lambda_{ms} a). \tag{5.18}$$

We see that $W/L$ is expressible in terms of $|E_z|^2$ integrated over the cross section,

$$\frac{W}{L} = \frac{\epsilon n^2 \omega_{msk}^2}{2\lambda_{ms}^2} \int |E_z|^2 dA. \tag{5.19}$$

This relation will turn out to be useful in the following.

*Quantum theory.* We assume henceforth the real representation for the fields. The component $E_z(\mathbf{r}, t) \equiv E_z(x)$, considered quantum mechanically as a Hermitian operator, is expanded as

$$E_z(x) = \int_{-\infty}^{\infty} \frac{dk}{2\pi} \sum_{m=1}^{\infty} \sum_s [a_{msk} \psi_{msk}(x) + a_{msk}^\dagger \psi_{msk}^*(x)], \tag{5.20}$$

where $a_{msk}$ and $a_{msk}^\dagger$ are annihilation and creation operators satisfying the commutation relations

$$[a_{msk}, a_{m's'k'}^\dagger] = 2\pi \delta(k - k') \delta_{mm'} \delta_{ss'}. \tag{5.21}$$

We now go back to relation (5.19), and require that the total energy $W$ associated with the $m, k, s$ mode is equal to the occupation number $\langle a_{msk}^\dagger a_{msk} \rangle$ times the photon energy $\omega_{msk}$,

$$\frac{\epsilon n^2 \omega_{msk}^2}{\lambda_{ms}^2} \int \langle E_z^2 \rangle r dr d\theta dz = \left\langle a_{msk}^\dagger a_{msk} + \frac{1}{2} \right\rangle \omega_{msk}. \tag{5.22}$$

Here we insert expansion (5.20). Because of the orthogonality of Eq. (5.21), the various modes decouple so that the total energy is a sum over the mode energies. For the mode $\psi_{msk}$, written in the form of Eq. (5.7), we get from the condition above the expression for the normalization constant $|N|$ already given in Eq. (5.8). If $n = 1$ and $\alpha = 2\pi$, we recover the expression given in Ref. [52].

### B. $t > t_0$ case: The Bogoliubov transformation

After the sudden creation of the cosmic string along the cusp line (the $z$ axis) at the instant $t = t_0$, we assume that the string metric is static. All transient phenomena are intended to be taken care of via the use of the quantum mechanical sudden transformation below. We first have to establish the field expressions in the presence of the string metric. The central gravitational quantity appearing in the formalism will be

$$\beta = (1 - 4GM)^{-1}, \tag{5.23}$$

already introduced above in Eq. (1.2b). In a string context, $\beta$ is believed to be very close to unity. Writing the field component $E_z$ as $E_z(r)\exp(ikz - i\omega t)\sin mp\theta$ we obtain the following equation for the quantity $E_z(r)$:

$$\left(\frac{d^2}{dr^2} + \frac{1}{r}\frac{d}{dr} + \lambda^2 - \frac{\beta^2 m^2 p^2}{r^2}\right) E_z(r) = 0, \tag{5.24}$$

with $\lambda^2 = n^2\omega^2 - k^2$ as before. Introducing the symbol $\nu$ as

$$\nu = \beta m, \tag{5.25}$$

we can write the fundamental $\nu, s, k$ mode as

$$\psi_{\nu sk} = N_\nu J_{\nu p}(\lambda_{\nu s} r) F_0 \sin mp\theta, \tag{5.26}$$

with $F_0 = \exp(ikz - i\omega_{\nu sk} t)$. The boundary condition on $r = a$ is $J_{\nu p}(\lambda a) = 0$, giving solutions $\lambda_{\nu s}$, $s = 1, 2, 3\ldots$ for the transverse wave number.

The formalism now becomes quite similar to that given before in the nongravitational case. We list the main formulas. The normalization constant $|N_\nu|$ becomes

$$|N_\nu| = \frac{1}{n}\sqrt{\frac{2\beta}{\alpha\epsilon\omega_{\nu sk}}}\frac{\lambda_{\nu s}}{a|J_{\nu p+1}(\lambda_{\nu s} a)|}, \tag{5.27}$$

and the Klein-Gordon product, defined as

$$(\psi_{\nu sk}, \psi_{\nu' s' k'}) = \frac{-i\epsilon n^2}{\beta\lambda_{\nu s}^2}\int \psi_{\nu sk}\overleftrightarrow{\partial}_0 \psi^*_{\nu' s' k'} r dr d\theta dz, \tag{5.28}$$

leads to

$$(\psi_{\nu sk}, \psi_{\nu' s' k'}) = 2\pi\delta(k - k')\delta_{\nu\nu'}\delta_{ss'}. \tag{5.29}$$

The quantum-mechanical expansion for $E_z$ becomes

$$E_z(x) = \int_{-\infty}^{\infty}\frac{dk}{2\pi}\sum_{m=1}^{\infty}\sum_s [a_{\nu sk}\psi_{\nu sk}(x) + a^\dagger_{\nu sk}\psi^*_{\nu sk}(x)], \tag{5.30}$$

with associated commutation relations

$$[a_{\nu sk}, a^\dagger_{\nu' s' k'}] = 2\pi\delta(k - k')\delta_{\nu\nu'}\delta_{ss'}. \tag{5.31}$$

We have to specify the continuity conditions for the fields at the transition time $t_0$. The component $E_z$ will be required to be continuous,

$$E_z(x)|_{t_0^-} = E_z(x)|_{t_0^+}, \tag{5.32}$$

as well as the Klein-Gordon product,

$$\frac{-i}{\lambda_{ms}^2}\int [E_z\overleftrightarrow{\partial}_0 E_z^*]_{t_0^-} r dr d\theta dz = \frac{-i}{\beta\lambda_{\nu s}^2}\int [[E_z\overleftrightarrow{\partial}_0 E_z^*]]_{t_0^+} r dr d\theta dz, \tag{5.33}$$

from which we get

$$[\partial_0 E_z(x)]_{t_0^-} = \frac{\lambda_{ms}^2}{\beta\lambda_{\nu s}^2}[\partial_0 E_z(x)]_{t_0^+}. \tag{5.34}$$

*The Bogoliubov transformation*. We have now two kinds of basic modes, namely $\psi_{msk}$ for $t < t_0$, and $\psi_{\nu sk}$ for $t > t_0$. There are correspondingly two vacuum states, satisfying the relations $a_{msk}|0\rangle_{msk} = 0$ and $a_{\nu sk}|0\rangle_{\nu sk} = 0$. As in Refs. [52,53] we may expand the modes in terms of each other,

$$\psi_{\nu sk}(x) = \int_{-\infty}^{\infty}\frac{dk'}{2\pi}\sum_{m's'}[\gamma(\nu sk|m's'k')\psi_{m's'k'}(x) + \delta(\nu sk|m's'k')\psi^*_{m's'k'}(x)], \tag{5.35}$$

where $\gamma$ and $\delta$ are the Bogoliubov coefficients [55]. The corresponding expansions for the operators are

$$a_{\nu sk} = \int_{-\infty}^{\infty}\frac{dk'}{2\pi}\sum_{m's'}[\gamma(\nu sk|m's'k')a_{m's'k'} + \delta^*(\nu sk|m's'k')a^\dagger_{m's'k'}]. \tag{5.36}$$

It means that the average number of particles produced in the $m, s, k$ mode per unit $k$ space interval becomes

$$\frac{dN_{msk}}{dk} = \int_{-\infty}^{\infty}\frac{dk'}{2\pi}\sum_{m's'}|\delta(\nu sk|m's'k')|^2. \tag{5.37}$$

From Eq. (5.35) we obtain, when making use of the normalization of the scalar product corresponding to string space,

$$\delta(\nu sk|m's'k') = -(\psi_{\nu sk}, \psi^*_{m's'k'}) = \frac{i\epsilon n^2}{\beta\lambda_{\nu s}^2}\int \psi_{\nu sk}\overleftrightarrow{\partial}_0 \psi_{m's'k'} r dr d\theta dz. \tag{5.38}$$

Here we insert expressions (5.26) and (5.7) for $\psi_{\nu sk}$ and $\psi_{m's'k'}$, and for simplicity we put $t_0 = 0$. Defining the quantity $I_{ss'}$ as

$$I_{ss'} = \frac{\int_0^a J_{\nu p}(\lambda_{\nu s} r) J_{mp}(\lambda_{ms'} r) r dr}{a^2|J_{\nu p+1}(\lambda_{\nu s} r) J_{mp+1}(\lambda_{ms'} r)|}, \tag{5.39}$$

we then obtain after some calculation

$$\delta(\nu sk|m's'k') = -\frac{1}{\sqrt{\beta}}\frac{\lambda_{ms}}{\lambda_{\nu s}}2\pi\delta(k + k')\delta_{mm'} \times\left[\sqrt{\frac{\omega_{\nu sk}}{\omega_{msk}}} - \sqrt{\frac{\omega_{msk}}{\omega_{\nu sk}}}\right] I_{ss'}. \tag{5.40}$$

As the value of $\beta$ is very close to unity, we put $\beta = 1$ everywhere except in the difference between the square roots. With $J_{\nu p} \to J_{mp}$ and $\lambda_{\nu s'} \to \lambda_{ms'}$, the numerator in Eq. (5.39) reduces to $(a^2/2)J^2_{mp+1}(\lambda_{ms} a)\delta_{ss'}$, so that approximately

$$I_{ss'} = \frac{1}{2}\delta_{ss'}. \tag{5.41}$$

Moreover, by applying the integral operator $\int dk'/2\pi$ on $[2\pi(k + k')]^2$ we obtain effectively the length $L$ of the string. For the electromagnetic energy produced in the mode $m, s, k$, per unit wave-number interval, we then get

$$\frac{dW_{msk}}{dk} = \frac{\omega_{msk}}{L}\frac{dN_{msk}}{dk} = \frac{1}{4}\omega_{msk}\left(\frac{\omega_{\nu sk}}{\omega_{msk}} + \frac{\omega_{msk}}{\omega_{\nu sk}} - 2\right). \tag{5.42}$$

There are two properties of this expression worth noticing:

(1) It is independent of the opening angle $\alpha$. The physical reason for this appears to be related to the fact that our region of quantization is the interior wedge region only. All the produced energy is taken to be channeled into the wedge region (we are thus not cutting out a fraction $\alpha/2\pi$ of the total produced energy). This contrasts the behavior in the cylindrically symmetric case, where the produced energy is azimuthally symmetric in the whole region $0<\theta<2\pi$ [51].

(2) The produced energy, when expressed in terms of frequencies, does not contain the refractive index $n$ explicitly. Equation (5.42) is formally the same as Eq. (52) in Ref. [52].

We may process the expression further by making use of the asymptotic formula for the roots of the Bessel function,

$$\lambda_{ms}a = s\pi + \left(m - \frac{1}{2}\right)\frac{\pi}{2}. \tag{5.43}$$

Here it is of physical interest to consider the region around zero axial wave number, $k\approx 0$. Then $\omega_{\nu sk}\to\omega_{\nu s0}=\lambda_{\nu s}/n$, $\omega_{msk}\to\omega_{ms0}=\lambda_{ms}/n$, leading to

$$\sqrt{\frac{\omega_{\nu s0}}{\omega_{ms0}}} - \sqrt{\frac{\omega_{ms0}}{\omega_{\nu s0}}} = (\beta-1)\frac{m}{2s+m-\frac{1}{2}}, \tag{5.44}$$

where we have expanded in the small quantity $(\beta-1)$ to second order. Then,

$$\left.\frac{dW_{msk}}{dk}\right|_{k\approx 0} = \frac{\pi}{8na}(\beta-1)^2\frac{m^2}{2s+m-\frac{1}{2}}. \tag{5.45}$$

We thus see that finally the factor $n$ turns up in the denominator; this is a characteristic property of Casimir energy expressions for dielectrics [46].

The simplest possibility $m=s=1$ yields

$$\left.\frac{dW_{11k}}{dk}\right|_{k\approx 0} = \frac{\pi}{20na}(\beta-1)^2 = \frac{4\pi}{5na}(GM)^2. \tag{5.46}$$

The total energy $W$ produced per unit length follows by multiplying Eq. (5.46) with the wave-number width $\Delta k\sim 1/L\sim 1/a$ around $k=0$. We may take $a$ to be of the same order as the horizon size $\sim t$, $t$ being the time just after the Big Bang. We thus get, when leaving $n$ unspecified,

$$W \sim \frac{1}{n}\left(\frac{GM}{t}\right)^2. \tag{5.47}$$

This is a characteristic property of cosmic string theory.

## VI. CONCLUSIONS

We have computed the Casimir free energy for a wedge-shaped region bounded by perfectly conducting planes meeting in an angle. The wedge region is filled with an azimuthally symmetric material which is discontinuous at a radius $a$ from the intersection axis. In general the wedge geometry is plagued with divergence problems. Familiar is the divergence associated with the apex, which is not relevant to the force on the circular boundary. But there are also divergences associated with the corners where the circular arc meets the wedge boundary. These divergences are manifested only in the $m=0$ modes, which possess no dependence on the angular coordinate, and have here been isolated and disregarded in the calculational part of this paper. They will not be present if the perfectly conducting boundary conditions on the wedge are replaced by periodic boundary conditions, which restrict the parameter $p$ to be greater than unity. Then, if the speed of light is the same both inside and outside the radius $a$, the energy corresponding to changes in $a$ is finite. If the speed of light differs for $r<a$ and $r>a$, the Casimir energy is finite only through second order in the discontinuity of the speed of light. These results are seen to be straightforward generalizations of results holding for dielectric/diamagnetic circular cylinders, which are recovered if $p=1$. We also consider, in the "sudden" approximation, the electromagnetic radiation produced by the appearance of a cosmic string in this geometry.

## ACKNOWLEDGMENTS

The work of K.A.M. was supported in part by grants from the U.S. National Science Foundation and the U.S. Department of Energy. He thanks Jef Wagner and Prachi Parashar for helpful conversations. We thank Steve Fulling for very helpful comments on the first version of this paper, and especially an anonymous referee for pointing out our originally incorrect treatment of the zero modes.

## APPENDIX A: ANALYTIC REGULARIZATION OF LOGARITHMICALLY DIVERGENT TERM

The only subtlety in the numerical calculations in Sec. IV is how the superficially logarithmically divergent terms are regulated. Starting from Eq. (4.13) we have

$$\tilde{\mathcal{E}} = {\sum_{m=0}^{\infty}}' \tilde{\mathcal{E}}_m, \tag{A1}$$

where

$$n\tilde{\mathcal{E}}_0 = \bar{\mathcal{E}}_0 - \frac{\xi^2}{4\pi a^2}\int_0^\infty dx \frac{x^5}{4(1+x^2)^3}, \tag{A2a}$$

$$n\tilde{\mathcal{E}}_m = \bar{\mathcal{E}}_m - \frac{\xi^2}{4\pi a^2}\int_0^\infty dx \frac{x^5}{4(m^2p^2+x^2)^3}. \tag{A2b}$$

Here, it will be observed that the integrals over $x$ are logarithmically divergent. We will regulate them analytically by replacing in the numerator of both $x^5\to x^{5-s}$, where we will at the end take $s$ to zero through positive values. Thus we have

$$2n\bar{\mathcal{E}} - \bar{\mathcal{E}}_0 - 2\sum_{m=1}^{\infty} \bar{\mathcal{E}}_m = -\frac{\xi^2}{16\pi a^2}\int_0^\infty dx \frac{x^{5-s}}{(1+x^2)^3} \times\left(1 + 2\sum_{m=1}^{\infty} (mp)^{-s}\right), \tag{A3}$$

where we have let in the $m$ terms $x=mpz$. Now the last factor is, as $s\to 0$,

$$1 + 2\zeta(s)p^{-s} \to -s(\ln 2\pi - \ln p), \tag{A4}$$

while the integral diverges as $s\to 0$,

$$\int_0^\infty dx \frac{x^{5-s}}{(1+x^2)^3} = \frac{1}{s}. \tag{A5}$$

Result (4.14) follows immediately. An identical argument leads to Eq. (4.27c). This argument demonstrates the importance for achieving a finite result of including both TE and TM zero modes with half weight.

## APPENDIX B: CONVERGENCE CONDITION FOR ADDITIONAL ENERGY TERM ASSUMING HIGH FREQUENCY TRANSPARENCY

Energy expression (4.13),

$$\bar{\mathcal{E}} = \frac{1}{4\pi n a^2}{\sum_{m=0}^{\infty}}' \int_0^\infty dx x \ln[1 - \xi^2 x^2 \lambda_{mp}^2(x)], \tag{B1}$$

has an additional term consisting of one-half the $m=0$ term for the TE mode minus one-half times that of the TM mode. These modes are determined in the diaphanous case by $\Delta\tilde{\Delta}=0$, where $\Delta$ and $\tilde{\Delta}$ are the two factors in Eq. (4.8), which for the zero modes are proportional to

$$\Delta_0\tilde{\Delta}_0 \propto \left(\frac{1}{\varepsilon_1}\frac{I_0'}{I_0} - \frac{1}{\varepsilon_2}\frac{K_0'}{K_0}\right)\left(\varepsilon_1\frac{I_0'}{I_0} - \varepsilon_2\frac{K_0'}{K_0}\right). \tag{B2}$$

Then, using the Wronskian, we see that the residual zero-mode term is

$$\hat{\mathcal{E}} = -\frac{1}{16\pi n a^2}\int_0^\infty dx x^2 \frac{d}{dx}\ln\frac{1+\xi x\lambda_0(x)}{1-\xi x\lambda_0(x)}. \tag{B3}$$

(This just says that the reflection coefficients for the two modes are $\xi_{\mathrm{TM}}=\xi$ and $\xi_{\mathrm{TE}}=-\xi$.)

As in the perfectly conducting case, this is divergent, if $\xi$ is constant, because

$$[I_0(x)K_0(x)] \sim -\frac{1}{2x^2}, \quad x\to\infty, \tag{B4}$$

which means that the integral in Eq. (B3) is linearly divergent. However, if $\xi$ is frequency dependent so that

$$\xi \sim \zeta^{-\beta}, \quad \zeta\to\infty, \tag{B5}$$

it is apparent that the integral becomes finite if $\beta>1$.


[1] V. M. Mostepanenko and N. N. Trunov, *The Casimir Effect and Its Applications* (Oxford University Press, Oxford, 1997).
[2] J. S. Dowker and G. Kennedy, J. Phys. A **11**, 895 (1978).
[3] D. Deutsch and P. Candelas, Phys. Rev. D **20**, 3063 (1979).
[4] I. Brevik and M. Lygren, Ann. Phys. **251**, 157 (1996).
[5] I. Brevik, M. Lygren, and V. Marachevsky, Ann. Phys. **267**, 134 (1998).
[6] I. Brevik and K. Pettersen, Ann. Phys. **291**, 267 (2001).
[7] V. V. Nesterenko, G. Lambiase, and G. Scarpetta, Ann. Phys. **298**, 403 (2002).
[8] V. V. Nesterenko, G. Lambiase, and G. Scarpetta, J. Math. Phys. **42**, 1974 (2001).
[9] V. V. Nesterenko, I. G. Pirozhenko, and J. Dittrich, Class. Quantum Grav. **20**, 431 (2003).
[10] A. H. Rezaeian and A. A. Saharian, Class. Quantum Grav. **19**, 3625 (2002).
[11] A. A. Saharian, Eur. Phys. J. C **52**, 721 (2007).
[12] A. A. Saharian, in *The Casimir Effect and Cosomology (Volume in Honor of Professor Iver H. Brevik on the Occasion of His 70th Birthday)*, edited by S. D. Odinhov *et al.* (Tomsk State Pedagogical University Press, Tomsk, Russia, 2008), p 87.
[13] T. N. C. Mendes, F. S. S. Rosa, A. Tenório, and C. Farina, J. Phys. A **41**, 164029 (2008).
[14] F. S. S. Rosa, T. N. C. Mendes, A. Tenório, and C. Farina, Phys. Rev. A **78**, 012105 (2008).
[15] C. I. Sukenik, M. G. Boshier, D. Cho, V. Sandoghdar, and E. A. Hinds, Phys. Rev. Lett. **70**, 560 (1993).
[16] G. Barton, Proc. R. Soc. London **410**, 175 (1987).
[17] L. L. DeRaad Jr. and K. A. Milton, Ann. Phys. **136**, 229 (1981).
[18] K. A. Milton, A. V. Nesterenko, and V. V. Nesterenko, Phys. Rev. D **59**, 105009 (1999).
[19] P. Gosdzinsky and A. Romeo, Phys. Lett. B **441**, 265 (1998).
[20] G. Lambiase, V. V. Nesterenko, and M. Bordag, J. Math. Phys. **40**, 6254 (1999).
[21] I. Cavero-Peláez and K. A. Milton, Ann. Phys. (N.Y.) **320**, 108 (2005).
[22] I. Cavero-Peláez and K. A. Milton, J. Phys. A **39**, 6225 (2006).
[23] A. Romeo and K. A. Milton, Phys. Lett. B **621**, 309 (2005).
[24] A. Romeo and K. A. Milton, J. Phys. A **39**, 6703 (2006).
[25] I. Brevik and A. Romeo, Phys. Scr. **76**, 48 (2007).
[26] A. Vilenkin and E. P. S. Shellard, *Cosmic Strings and other Topological Defects* (Cambridge University Press, Cambridge, England, 1994), Sec. 7.
[27] V. P. Frolov and E. M. Serebriany, Phys. Rev. D **35**, 3779 (1987).
[28] N. R. Khusnutdinov and M. Bordag, Phys. Rev. D **59**, 064017 (1999).
[29] E. R. Bezerra de Mello, V. B. Bezerra, A. A. Saharian, and A. S. Tarloyan, Phys. Rev. D **78**, 105007 (2008).
[30] J. A. Stratton, *Electromagnetic Theory* (McGraw-Hill, New

York, 1941), p. 524.
[31] I. Brevik and H. Kolbenstvedt, Phys. Rev. D **25**, 1731 (1982).
[32] I. Brevik and H. Kolbenstvedt, Ann. Phys. (N.Y.) **143**, 179 (1982).
[33] I. Brevik and H. Kolbenstvedt, Ann. Phys. (N.Y.) **149**, 237 (1983).
[34] I. Brevik and H. Kolbenstvedt, Can. J. Phys. **62**, 805 (1984).
[35] I. Brevik and G. Einevoll, Phys. Rev. D **37**, 2977 (1988).
[36] I. Brevik and I. Clausen, Phys. Rev. D **39**, 603 (1989).
[37] O. Kenneth, I. Klich, A. Mann, and M. Revzen, Phys. Rev. Lett. **89**, 033001 (2002).
[38] I. Brevik and H. B. Nielsen, Phys. Rev. D **41**, 1185 (1990).
[39] I. Brevik and H. B. Nielsen, Phys. Rev. D **51**, 1869 (1995).
[40] X. Li, X. Shi, and J. Zhang, Phys. Rev. D **44**, 560 (1991).
[41] I. Brevik and E. Elizalde, Phys. Rev. D **49**, 5319 (1994).
[42] I. Brevik, A. A. Bytsenko, and H. B. Nielsen, Class. Quantum Grav. **15**, 3383 (1998).
[43] I. Brevik, A. A. Bytsenko, and B. M. Pimentel, in *Theoretical Physics 2002 (Horizons in World Physics)*, edited by T. F. George and H. F. Arnoldus (Nova Science, New York, 2002), Vol. 243, Pt. 2, pp. 117–139.
[44] I. Brevik, B. Jensen, and K. A. Milton, Phys. Rev. D **64**, 088701 (2001).
[45] V. V. Nesterenko, J. Phys. A **39**, 6609 (2006).
[46] I. Brevik and K. A. Milton, Phys. Rev. E **78**, 011124 (2008).
[47] K. A. Milton, *The Casimir Effect* (World Scientific, Singapore, 2001).
[48] J. Ambjørn and S. Wolfram, Ann. Phys. (N.Y.) **147**, 1 (1983).
[49] K. Okamoto, *Fundamentals of Optical Waveguides*, 2nd ed. (Elsevier, Amsterdam, 2000).
[50] V. V. Nesterenko, J. Phys. A: Math. Theor. **41**, 164005 (2008).
[51] L. Parker, Phys. Rev. Lett. **59**, 1369 (1987).
[52] I. Brevik and T. Toverud, Phys. Rev. D **51**, 691 (1995).
[53] I. Brevik and A. G. Frøseth, Phys. Rev. D **61**, 085011 (2000).
[54] K. A. Milton and J. Schwinger, *Electromagnetic Radiation: Variational Methods, Waveguides, and Accelerators* (Springer, Berlin, 2006).
[55] N. D. Birrell and P. C. W. Davies, *Quantum Fields in Curved Space* (Cambridge University Press, Cambridge, England, 1982).

# Article [j]

***Electrodynamic Casimir effect in a medium-filled wedge II***

S.Å. Ellingsen, I. Brevik, K.A. Milton

Physical Review E **80**, 021125 (2009)

# Electrodynamic Casimir effect in a medium-filled wedge. II

Simen Ådnøy Ellingsen* and Iver Brevik†
*Department of Energy and Process Engineering, Norwegian University of Science and Technology, N-7491 Trondheim, Norway*

Kimball A. Milton‡
*Oklahoma Center for High Energy Physics and H. L. Dodge Department of Physics and Astronomy,The University of Oklahoma, Norman, Oklahoma 73019, USA*

(Received 13 May 2009; published 27 August 2009)

We consider the Casimir energy in a geometry of an infinite magnetodielectric wedge closed by a circularly cylindrical, perfectly reflecting arc embedded in another magnetodielectric medium, under the condition that the speed of light be the same in both media. An expression for the Casimir energy corresponding to the arc is obtained and it is found that in the limit where the reflectivity of the wedge boundaries tends to unity the finite part of the Casimir energy of a perfectly conducting wedge-shaped sheet closed by a circular cylinder is regained. The energy of the latter geometry possesses divergences due to the presence of sharp corners. We argue how this is a pathology of the assumption of ideal conductor boundaries and that no analogous term enters in the present geometry.

DOI: 10.1103/PhysRevE.80.021125 PACS number(s): 05.30.−d, 42.50.Pq, 42.50.Lc, 11.10.Gh

## I. INTRODUCTION

The Casimir effect [1] may be understood as an effect of the fluctuations of the quantum vacuum. Casimir's original geometry involved two infinite and parallel ideal metal planes which were found to attract each other with a negative pressure scaling quartically with the inverse interplate separation. In a seminal paper, Lifshitz generalized Casimir's original calculation to imperfectly reflecting plates [2]. Since its feeble beginnings research on the Casimir effect has grown from being of peripheral interest to a few theorists to a bustling field of research both experimental and theoretical with publications numbering in the hundreds each year. Recent reviews include [3–6].

Progress on Casimir force calculations for other geometries has been slower in coming. Spherical and cylindrical geometries have naturally been objects of focus, the latter of direct interest to the effort reported herein. Only in 1981 was the Casimir energy of an infinitely long perfectly conducting cylindrical shell calculated [7] and the more physical but also significantly more involved case of a dielectric cylinder was considered only in recent years [8–14]. We might also mention recent work on the cylinder defined by a $\delta$-function potential, a so-called semitransparent cylinder [15]; for weak coupling, both the semitransparent cylinder and the dielectric cylinder have vanishing Casimir energy.

Closely related to the cylindrical geometry is the infinite wedge. The problem was first approached in the late 1970s [16,17] as part of the still ongoing debate about how to interpret various divergences in quantum field theory with sharp boundaries. Since, various embodiments of the wedge have been treated by Brevik and co-workers [18–20] and others [21,22]. A review may be found in [23]. A wedge intercut by a cylindrical shell was considered by Nesterenko and co-workers, first for a semicylinder [24], then for arbitrary opening angle [25], and the corresponding local stresses were studied by Saharian [26–28]. The group at Los Alamos studied the interaction of an atom with a wedge [29,30] previously investigated by Barton [31] and others [32,33], the geometry realized in an experiment by Sukenik *et al.* some years ago [34]. A recent calculation of the Casimir energy of a magnetodielectric cylinder intercut by a perfectly reflecting wedge filled with magnetodielectric material was recently reported by the current authors [35]. Common to all of these theoretical efforts is the assumption that the wedge be bounded by perfectly conducting walls.

While until recently relatively few treatments of the vacuum energy of the wedge existed, the problem of calculating the diffraction of electromagnetic fields by a dielectric wedge within classical eletromagnetics is an old one and several powerful methods have been developed within this field. The Green's function of the potential (Poisson) equation in the vicinity of a perfectly conducting wedge was found more than a century ago by Macdonald [36] and extended to the wave equation with a plane wave source by Sommerfeld [37]. Generalizing Sommerfeld's method, the first theoretical solution to the scattering problem involving a wedge of finite conductivity was found by Malyuzhinets in his Ph.D. work [38] (see [39] for a review; cf. also [40]).

A different method was proposed by Kontorovich and Lebedev in 1938 [41] and used by Oberhettinger to solve the Green's function problem some time later [42]. The method has been given attention in recent analytical and numerical studies of the diffraction problem [43–46].

In the present effort we study the Casimir energy in a magnetodielectric wedge of opening angle $\alpha$ inside and outside a perfectly conducting cylindrical shell of radius $a$—see Fig. 1. The interior and exterior of the wedge are both filled with magnetodielectric material under the restriction of isorefractivity (or diaphanousness), that is, the index of refraction $n^2(\omega)=\epsilon(\omega)\mu(\omega)$ is the same everywhere for a given frequency. This condition is adopted because without it the

*simen.a.ellingsen@ntnu.no
†iver.h.brevik@ntnu.no
‡milton@nhn.ou.edu

 

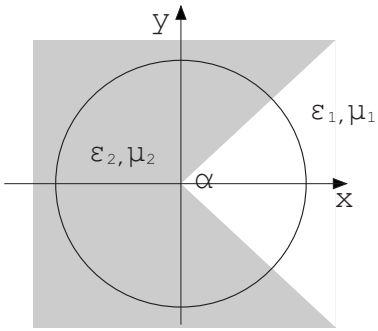


FIG. 1. The wedge geometry considered.

problem is no longer separable and not readily solvable. Moreover, we suspect that nondiaphanous media will lead to divergences, at least in the absence of dispersion.

As a natural extension of the considerations in [35] we derive an expression for the free energy of such a system by use of the argument principle [47]. (By free energy, we mean that bulk terms not referring to the circular arc boundary are subtracted.) The necessary dispersion relation provided by the electromagnetic boundary conditions at the wedge sides is derived in two different ways: by a standard route of expansion of the solutions in Bessel function partial waves and by use of the Kontorovich-Lebedev (KL) transform. (Still a third method, based on the Green's function formulation, is sketched in the Appendix.) The corresponding boundary condition equation at the cylindrical shell is well known. These together allow us to sum the energy of the eigenmodes of the geometry satisfying eigenvalue equations for the frequency and azimuthal wave number $\nu$ by means of the argument principle.

There are important differences between the diaphanous geometry considered herein and the standard geometry of a perfectly conducting wedge. Assuming diaphanous electromagnetic boundary conditions, the interior and exterior wedge sectors are coupled and remain so also in the limit where the reflectivity of the wedge boundaries tends to unity (for example, by letting $\epsilon\to\infty, \mu\to 0$ so that their product is constant). Assuming the wedge be perfectly conducting from the outset, however, the interior of the wedge is severed cleanly from its exterior at all frequencies, a significantly different situation.

The Casimir energy of the perfectly conducting wedge and magnetodielectric arc considered in [35] was found to possess an unremovable divergent term associated with the corners where the arc meets the wedge. This is a typical artifact of quantum field theory with nonflat boundary conditions (e.g., [21,24,25]). We will argue in Sec. III B that there is no such term present in the geometry considered herein and that the direct generalization of the finite part of the energy of the system considered in [35] to the present system is in fact the full regularized Casimir energy. The reason for this rests upon two unphysical effects of perfectly conducting boundary conditions at the wedge sides (the vanishing of the tangential components of the electric field there). Namely, such boundary conditions exclude the existence of an azimuthally constant TM mode and divide space cleanly into an interior and an exterior sector with no coupling allowed between modes in the two sectors. Moreover, for a wedge consisting of perfectly conducting thin sheets dividing space into two complementary wedges, the ideal conductor boundary conditions will count the azimuthally constant TE mode twice whereas with more realistic boundary conditions such as considered here, such a mode must be common to the *both sectors*, $0\le\theta<2\pi$. In these two respects the perfectly conducting wedge differs from the diaphanous one and put together these redefinitions provided by the diaphanous wedge exactly remove the divergent extra energy term found in [35] and previously in [25].

We show numerically that except for the singular term, the energy of a perfectly conducting wedge closed by a magnetodielectric cylinder whose reflectivity tends to unity is regained in the limit where we let the wedge boundaries become perfectly reflecting.

## II. BOUNDARY CONDITIONS AND DISPERSION RELATIONS

We begin by considering in general the form of an expression of the energy of a diaphanous wedge inside and outside a cylindrical shell such as depicted in Fig. 1. We assume the cylindrical shell to be perfectly reflecting. Let the interior sector $-\alpha/2<\theta<\alpha/2$ have permittivity and permeability $\epsilon_1$ and $\mu_1$ relative to vacuum and the corresponding values for the exterior sector $\pi\ge|\theta|>\alpha/2$ be $\epsilon_2$ and $\mu_2$ so that $\epsilon_1(\omega)\mu_1(\omega)=\epsilon_2(\omega)\mu_2(\omega)\equiv n^2(\omega)$. The cusp of the wedge is chosen to lie along the $z$ axis, which is also the center of the cylindrical shell, and the interfaces are found at $\theta=\pm\alpha/2$ and at $\rho=a$ ($\rho$ is the distance to the $z$ axis).

We will calculate the Casimir energy by "summing" over the eigenmodes of the geometry using the so-called argument principle, now a standard method in the Casimir literature. The eigenmodes of a given geometry are given by the solutions of the homogeneous Helmholtz equation,

$$(\nabla^2 - n^2\partial_t^2)u(\mathbf{r},t) = 0, \tag{2.1}$$

which also satisfy the system's boundary conditions. Here $u$ symbolizes a chosen field component of either the electric or magnetic field. We will choose $E_z$ and $H_z$ as the two independent field components from which the rest of the components can be derived by means of Maxwell's equations.

The translational symmetry with respect to $z$ and time makes it natural to introduce the Fourier transform,

$$E_z(\mathbf{r},t) = \int_{-\infty}^{\infty}\frac{d\omega}{2\pi}e^{-i\omega t}\int_{-\infty}^{\infty}\frac{dk_z}{2\pi}e^{ik_z z}E_z(\boldsymbol{\rho};\omega,k_z),$$

where $\boldsymbol{\rho}=(\rho,\theta)$ and $\rho=\sqrt{x^2+y^2}$. The Helmholtz equation now simplifies to the scalar Bessel equation,

$$(\nabla_\perp^2 + k_\perp^2)E_z(\boldsymbol{\rho};k_z,\omega) = 0, \tag{2.2}$$

where

$$\nabla_\perp^2 = \partial_\rho^2 + \frac{1}{\rho}\partial_\rho + \frac{1}{\rho^2}\partial_\theta^2 \tag{2.3}$$

and $k_\perp^2=\epsilon\mu\omega^2-k_z^2$.

We will define the quantity $\kappa$ as

$$\kappa = \sqrt{k_z^2 - \epsilon\mu\omega^2} = -ik_\perp, \tag{2.4}$$

where the root of $\kappa$ is to be taken in the fourth complex quadrant. When in the end we take frequencies to lie on the positive imaginary axis, $\kappa$ becomes real and positive, something we bear in mind in the subsequent calculations.

A general solution to Eq. (2.2) is of the form

$$E_z = [A_\nu H_\nu^{(1)}(k_\perp \rho) + B_\nu J_\nu(k_\perp \rho)](ae^{i\nu\theta} + be^{-i\nu\theta}), \tag{2.5}$$

where $A_\nu$, $B_\nu$, $a$, $b$, and $\nu$ are arbitrary. If, as in our case, $\nu$ is allowed to take noninteger values, we must restrict it to $\nu \geq 0$ because except at integers $J_\nu(z)$ and $J_{-\nu}(z)$ are linearly independent.

Solutions of the electromagnetic field in a wedge geometry are expressed as a sum over cylindrical partial waves whose kernels are Bessel and Hankel functions of argument $k_\perp \rho$. Thus it is clear that the boundary conditions on the wedge surfaces can only be solved for each partial wave if the speed of light is the same in both sectors since $k_\perp$ would otherwise take different values in the two media for given $k_z$ and $\omega$ and the kernel functions would be linearly independent functions of these. The diaphanous condition is thus prerequisite for the explicit solution of boundary conditions below. Without this condition the problem at hand is not analytically solvable with the methods used herein. We expect that even if we could solve the nondiaphanous problem we would encounter divergences that might or might not be curable by the inclusion of dispersion.

The presence of the wedge primarily has the role of dictating which values of $\nu$ are allowed. If one were to consider a cylinder (periodic boundary conditions), only integer values of $\nu$ (both positive and negative) would be acceptable and expressing the solution as a sum over these integer values would be appropriate. If one instead let the wedge be perfectly reflecting (Dirichlet and Neumann boundaries at $\pm\alpha/2$, where $\alpha$ is arbitrary) $\nu$ would be forced to take values that are non-negative integer multiples of $\pi/\alpha$. The diaphanous magnetodielectric boundaries present here also restrict $\nu$ to discrete values for given $\epsilon$'s and $\mu$'s, but explicitly determining these values is no longer immediate because modes existing in the exterior and interior sectors now couple to each other. For a given frequency we therefore make use of an appropriate dispersion function representing these boundaries in order to sum over the appropriate values of $\nu$ by means of the argument principle, whereupon we may sum over the eigenfrequencies of the modes inside and outside the cylindrical shell to obtain the energy.

The boundary condition dispersion relation pertaining to the circular boundary is known (e.g., Eq. (4.12) in [35], with $\xi^2 = 1$),

$$g_\nu(k_z, \omega) \equiv 1 - x^2 \lambda_\nu^2(x) = 0, \tag{2.6}$$

where $x = a\kappa$,

$$\lambda_\nu(x) = \frac{d}{dx}[I_\nu(x) K_\nu(x)], \tag{2.7}$$

and $I_\nu, K_\nu$ are the modified Bessel functions of the first and second kinds of order $\nu$. We can simply use this equation to sum modes satisfying the boundary condition on both sides because the wedge boundaries at $\pm\alpha/2$ impose the same discretization of $\nu$ inside and outside the cylindrical shell (if we were to have, e.g., a third medium in the sector $|\theta| < \alpha/2$, $\rho > a$ different from medium 1, this would no longer be the case as we will see: the field solutions would take different values of $\nu$ inside and outside the cylindrical boundary and the boundary conditions at the cylinder could no longer be solved for each eigenvalue of $\nu$). We now turn to a derivation of the dispersion relation pertaining to the interfaces at $\theta = \pm\alpha/2$.

In the following we shall use the term TE to denote electromagnetic modes whose **E** field has no component in the $z$ direction and TM denotes those modes whose **H** field has no $z$ component. This is not "transverse electric" and "transverse magnetic" with respect to the wedge boundaries at $\theta = \pm\alpha/2$, but this does not matter since we will find that the eigenequation of these boundaries is the same for all field components by virtue of the diaphanous condition.

### A. Kontorovich-Lebedev approach

We will first employ the technique of the KL transformation [41] and its inverse transform which may be written as

$$E_z(\boldsymbol{\rho}) = i\int_0^{i\infty} d\nu \nu e^{i\nu\pi/2} \sin(\pi\nu) K_\nu(\kappa\rho) \mathfrak{E}_z(\theta;\nu), \tag{2.8a}$$

$$\mathfrak{E}_z(\theta;\nu) = \frac{2}{\pi^2}\int_0^\infty \frac{d\rho}{\rho} e^{-i\nu\pi/2} K_\nu(\kappa\rho) E_z(\boldsymbol{\rho}) \tag{2.8b}$$

(dependence on $k_z$ and $\omega$ is implicit). While less extensively covered in the literature than most other integral transforms, some tables of KL transforms exist [48,49]. Numerical methods for evaluating such transforms were recently developed by Gautschi [50]. We will ignore the presence of the cylindrical shell in this section and only study how the presence of the walls of the wedge discretizes the spectrum of allowed values of the Bessel function order $\nu$.

With this, Eq. (2.2), after multiplying with $\rho^2$, transforms to

$$(\partial_\theta^2 + \nu^2)\mathfrak{E}_z(\theta;\nu,k_z,\omega) = 0. \tag{2.9}$$

Equation (2.9) is now in a form fully analogous to that encountered in a planar geometry (e.g., [51–53]). We follow now roughly the scheme in [53] and determine the dispersion relation [condition for eigensolutions of Eq. (2.2)] by means of summation over multiple reflection paths. By noting that the solutions to Eq. (2.9) have the form of propagating plane waves traveling clockwise or anticlockwise along the now formally straight $\theta$ axis ($\nu$ playing the role of a reciprocal azimuthal angle) the analogy to a plane parallel system is obvious.

We write the solution of Eq. (2.9) in the interior sector, $|\theta| < \alpha/2$, in the form

$$\mathfrak{E}_z = e^+ e^{i\nu\theta} + e^- e^{-i\nu\theta}, \tag{2.10}$$

where $e^\pm$ are undetermined integration coefficients which are field amplitudes at $\theta=0$ to be determined from boundary conditions at $\theta=\pm\alpha/2$.

Likewise the solutions in the exterior sector (the "complementary wedge") $\pi \geq |\theta| > \alpha/2$ may be written

$$\tilde{\mathfrak{E}}_z = \tilde{e}^+ e^{i\nu(\theta-\pi)} + \tilde{e}^- e^{-i\nu(\theta-\pi)}, \tag{2.11}$$

where the undetermined amplitudes $\tilde{e}^\pm$ are "measured" at $\theta=\pi$. The choice to measure the amplitudes in sectors 1 and 2 at $\theta=0$ and $\pi$, respectively, is arbitrary but makes for maximally symmetric boundary equations.

The homogeneous Helmholtz equation thus solves the scattered part of $\mathfrak{E}_z$ given some source field $\mathfrak{E}_z^0$. Let us assume there is a source field in the form of an infinitely thin phased line source parallel to the $z$ axis at some position $\theta_0$ in the interior sector. The direct field (which only propagates away from the source) may be written in the form

$$\mathfrak{E}_z^0 = \Theta(\theta-\theta_0) e_0^+ e^{i\nu\theta} + \Theta(\theta_0-\theta) e_0^- e^{-i\nu\theta}, \tag{2.12}$$

where $\Theta(x)$ is the unit step function and the field amplitudes are "measured" at $\theta=0$. We do not need to know the constants $e_0^\pm$ explicitly and take these to be known constants. The multiple reflection problem (or equivalently, boundary condition problem) is now a system of four equations for the four amplitudes $e^\pm, \tilde{e}^\pm$ as functions of $e_0^\pm$.

We define the reflection coefficients at the boundaries $\theta=\pm\alpha/2$ as the ratio of reflected vs incoming field amplitude, $r=\mathfrak{E}_{z,\mathrm{refl}}/\mathfrak{E}_{z,\mathrm{in}}$, as seen by a wave coming from and reflected back into sector 1 (a wave going the opposite way experiences a coefficient $-r$). With the assumption $\epsilon_1\mu_1=\epsilon_2\mu_2$ the reflection coefficients of the $s$ and $p$ modes differ only by a sign,

$$r_p = \frac{\epsilon_2-\epsilon_1}{\epsilon_2+\epsilon_1} = -r_s = -\frac{\mu_2-\mu_1}{\mu_2+\mu_1}. \tag{2.13}$$

We will simply use $r$ in the following, representing either of the modes. We also define the transmission coefficient, the ratio of the transmitted to the incoming amplitude, going from sector $i$ to sector $j$, $t_{ij}$, where $i,j=1,2$ denotes the sectors in Fig. 1,

$$t_{ij} \equiv t_{ij,s} = \frac{\mu_j}{\mu_i}\frac{2\epsilon_j}{\epsilon_j+\epsilon_i} = t_{ij,p} = \frac{2\mu_j}{\mu_j+\mu_i}. \tag{2.14}$$

Since these coefficients are invariant under KL transformation, they are the sought-after single interface reflection and transmission coefficients also in the KL regime. Note that with the diaphanous condition, reflection coefficients are independent of $\nu$, something which would not be true in general. If $r$ depended on $\nu$ this would give rise to corrections to the energy expression derived in Sec. III A. (See also the Appendix, where such $\nu$ dependence does occur.)

We formulate the electromagnetic boundary conditions in terms of reflection and transmission. In the KL domain the system looks and behaves analogously to the planar system (see [53] for details on this case), but with one important difference, namely, that a $\theta$ directed partial wave which is transmitted at a wedge boundary does not disappear from the system but is partly transmitted back into sector 1 again circularly. Thus we obtain four equations for the four amplitudes, $e^+$, $e^-$, $\tilde{e}^+$, and $\tilde{e}^-$, coupling to each other through paths reflected or transmitted at one interface,

$$e^+ = re_0^- e^{i\nu\alpha} + re^- e^{i\nu\alpha} + t_{21}\tilde{e}^+ e^{i\nu\pi}, \tag{2.15a}$$

$$e^- = re_0^+ e^{i\nu\alpha} + re^+ e^{i\nu\alpha} + t_{21}\tilde{e}^- e^{i\nu\pi}, \tag{2.15b}$$

$$\tilde{e}^+ = t_{12}e_0^+ e^{i\nu\pi} + t_{12}e^+ e^{i\nu\pi} - r\tilde{e}^- e^{i\nu(2\pi-\alpha)}, \tag{2.15c}$$

$$\tilde{e}^- = t_{12}e_0^- e^{i\nu\pi} + t_{12}e^- e^{i\nu\pi} - r\tilde{e}^+ e^{i\nu(2\pi-\alpha)}. \tag{2.15d}$$

Eigenvalues of $\nu$ for the wedge correspond to solutions of these boundary conditions, which exist when the secular equation of the set of linear equations for $e^\pm$ and $\tilde{e}^\pm$ is fulfilled. The characteristic matrix is

$$\mathbf{D} = \begin{pmatrix} 1 & -re^{i\nu\alpha} & -t_{21}e^{i\nu\pi} & 0 \\ -re^{i\nu\alpha} & 1 & 0 & -t_{21}e^{i\nu\pi} \\ -t_{12}e^{i\nu\pi} & 0 & 1 & re^{i\nu(2\pi-\alpha)} \\ 0 & -t_{12}e^{i\nu\pi} & re^{i\nu(2\pi-\alpha)} & 1 \end{pmatrix} \tag{2.16}$$

and the dispersion relation sought after is

$$D(\nu,\omega) \equiv \det \mathbf{D} = 0. \tag{2.17}$$

The matrix form [Eq. (2.16)] is rather instructive. Note that $\mathbf{D}$ is a block matrix of the form

$$\mathbf{D} = \begin{pmatrix} \mathbf{D}_1 & \mathbf{G}_{21} \\ \mathbf{G}_{12} & \mathbf{D}_2 \end{pmatrix},$$

where $\mathbf{D}_i$ describes multiple scattering within sector $i$ and $\mathbf{G}_{ij}$ describes coupling between the sectors by transmission from sector $i$ to $j$. Since the $\mathbf{G}$ matrices commute with the $\mathbf{D}$ matrices, $\det \mathbf{D}$ can be written as

$$\det \mathbf{D} = \det(\mathbf{D}_1\mathbf{D}_2 - \mathbf{G}_{21}\mathbf{G}_{12}). \tag{2.18}$$

We may use the energy conservation relation,

$$t_{12}t_{21} + r^2 = 1, \tag{2.19}$$

together with Eq. (2.18) to find the simple expression

$$\begin{aligned} D(\nu,\omega) &= (1-e^{2\pi i\nu})^2 - r^2[e^{i\nu(2\pi-\alpha)} - e^{i\nu\alpha}]^2 \\ &= -4e^{2\pi i\nu}\{\sin^2(\nu\pi) - r^2\sin^2[\nu(\pi-\alpha)]\}. \end{aligned} \tag{2.20}$$

It is noteworthy that this dispersion relation only has an implicit dependence on $\omega$ through the quantity $r^2(\omega)$. As an example we plot the solutions to Eq. (2.17) as a function of $\nu$ and $r$ in Fig. 2 for $\alpha=0.75$ rad.

Note at this point that whenever $r$ is real, all zeros of $D(\nu,\omega)$ in Eq. (2.20) are real. In the following we shall think of $r$ as well as the eigenvalues of $\nu$ as real quantities. For real frequencies $\omega$ reflection coefficients will in general be complex, while after a standard rotation of frequencies onto the imaginary frequency axis these coefficients are always real

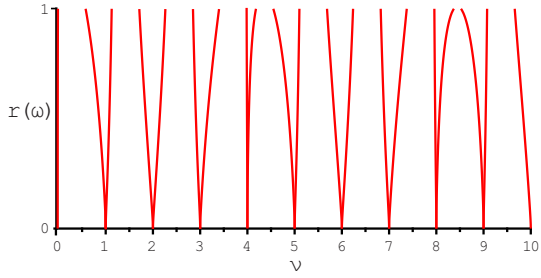


FIG. 2. (Color online) The solutions of dispersion relation (2.20) as a function of $r$ and $\nu$ for $\alpha=0.75$. The eigenvalues of $\nu$ for a given $r$ are marked; the energy is calculated by summing over these values and then integrating over all $\omega$.

as dictated by causality. Although zeros are complex the argument principle may still be used; the discussion of connected subtleties may be found in, e.g., [7,54,55].

It is easy to see that this dispersion relation generalizes that for a cylinder (of infinite radius) and a perfectly conducting wedge. In the latter limit, $r=1$, the determinant $\det \mathbf{D}$ has zeros where $\nu=m\pi/\alpha$ and at $\nu=m\pi/(2\pi-\alpha)$, where $m$ is an integer. This becomes obvious when noting that

$$D(\nu,\omega) \overset{r\to 1}{\to} -4e^{2\pi i\nu}\sin\nu\alpha\sin\nu(2\pi-\alpha). \tag{2.21}$$

This reproduces, in other words, the case where the wedge is made up of thin perfectly conducting sheets. For the perfectly conducting wedge it is customary to restrict $\nu$ to values that are integer multiples of $\pi/\alpha$ from the beginning.

Likewise when the two materials become equal,

$$D(\nu,\omega) \overset{r=0}{\to} -4e^{2\pi i\nu}\sin^2\nu\pi \equiv D_0(\nu), \tag{2.22}$$

which has double zeros where $\nu=m$, a positive integer, corresponding to a clockwise and an anticlockwise mode or, if the reader prefers, the sum over $\nu=+m$ and $-m$. This is just the cylinder case [7–14]. We see from Fig. 2 that except for $\nu=0$ which remains degenerate, the double zeroes split into two separate simple zeros for finite $r$. For special opening angles which are rational multiples of $\pi$ there will be other zeroes which remain degenerate as well.

One sees directly that if we were to solve Eq. (2.2) for $H_z$ instead of $E_z$ the dispersion relation would be identical to Eq. (2.17) since the only difference would be the sign of the reflection coefficient (we would employ $r_s$ rather than $r_p$), which only enters squared. One should note that the distinction between $r_s$ and $r_p$ here does not correspond to the distinction between TE and TM modes of the entire cavity, but this is of no consequence in the following because dispersion relation (2.17) is the same for all field components.

### B. Derivation by standard expansion

We will now sketch how result (2.20) may be derived by a more standard method similar to that made use of in [35]. The solutions of Eq. (2.5) that correspond to outgoing waves at $\rho\to\infty$ may be expanded following the scheme in [35] in an obvious generalization of those found in [56]. Due to criteria of outgoing-wave boundary conditions at $\rho\to\infty$ and nonsingularity at the origin the solution must consist purely of Hankel functions $H_\nu^{(1)}(k_\perp\rho)$ far from the origin and only of terms containing $J_\nu(k_\perp\rho)$ near $\rho=0$. Following the scheme in [35] we choose $H_\nu^{(1)}(k_\perp\rho)$ for $\rho\geq a$ and $J_\nu(k_\perp\rho)$ for $\rho\leq a$ both in the interior sector $-\alpha/2<\theta<\alpha/2$ and outside and couple the solutions across these straight boundaries. It will not matter which Bessel function we choose for the present purposes: the resulting solution expansions are identical but for the replacement of one Bessel function with another.

In a straightforward generalization of the expansion used in [35] we write down the following general solutions in sector 1 of Fig. 1 for $\rho>a$:

$$E_{r,1}=\int_0^\infty d\nu\left\{\left[\frac{ik_z}{k_\perp}H_\nu^{(1)\prime}\bar{a}_1-\frac{\nu\mu_1\omega}{k_\perp^2\rho}H_\nu^{(1)}\underline{b}_1\right]\cos\nu\theta+i\left[\frac{ik_z}{k_\perp}H_\nu^{(1)\prime}\underline{a}_1-\frac{\nu\mu_1\omega}{k_\perp^2\rho}H_\nu^{(1)}\bar{b}_1\right]\sin\nu\theta\right\}e^{i\pi\nu/2}, \tag{2.23a}$$

$$E_{\theta,1}=-\int_0^\infty d\nu\left\{\left[\frac{\nu k_z}{k_\perp^2\rho}H_\nu^{(1)}\underline{a}_1+\frac{i\mu_1\omega}{k_\perp}H_\nu^{(1)\prime}\bar{b}_1\right]\cos\nu\theta+i\left[\frac{\nu k_z}{k_\perp^2\rho}H_\nu^{(1)}\bar{a}_1+\frac{i\mu_1\omega}{k_\perp}H_\nu^{(1)\prime}\underline{b}_1\right]\sin\nu\theta\right\}e^{i\pi\nu/2}, \tag{2.23b}$$

$$E_{z,1}=\int_0^\infty d\nu H_\nu^{(1)}[\bar{a}_1\cos\nu\theta+i\underline{a}_1\sin\nu\theta]e^{i\pi\nu/2}, \tag{2.23c}$$

$$H_{r,1}=\int_0^\infty d\nu\left\{\left[\frac{\nu\omega\epsilon_1}{k_\perp^2\rho}H_\nu^{(1)}\underline{a}_1+\frac{ik_z}{k_\perp}H_\nu^{(1)\prime}\bar{b}_1\right]\cos\nu\theta+i\left[\frac{\nu\omega\epsilon_1}{k_\perp^2\rho}H_\nu^{(1)}\bar{a}_1+\frac{ik_z}{k_\perp}H_\nu^{(1)\prime}\underline{b}_1\right]\sin\nu\theta\right\}e^{i\pi\nu/2}, \tag{2.23d}$$

$$H_{\theta,1}=\int_0^\infty d\nu\left\{\left[\frac{i\omega\epsilon_1}{k_\perp}H_\nu^{(1)\prime}\bar{a}_1-\frac{\nu k_z}{k_\perp^2\rho}H_\nu^{(1)}\underline{b}_1\right]\cos\nu\theta+i\left[\frac{i\omega\epsilon_1}{k_\perp}H_\nu^{(1)\prime}\underline{a}_1-\frac{\nu k_z}{k_\perp^2\rho}H_\nu^{(1)}\bar{b}_1\right]\sin\nu\theta\right\}e^{i\pi\nu/2}, \tag{2.23e}$$

$$H_{z,1}=\int_0^\infty d\nu H_\nu^{(1)}[\bar{b}_1\cos\nu\theta+i\underline{b}_1\sin\nu\theta]e^{i\pi\nu/2}, \tag{2.23f}$$

where we have omitted the arguments of $H_\nu^{(1)}(k_\perp\rho)$ and its derivative, of $\bar{a}_1(\nu),\bar{b}_1(\nu)$, etc., the latter being undetermined coefficient functions of $\nu$.

We write the solution in sector 2 in exactly the same form but with the simple replacements $\theta \to \theta - \pi$, $\epsilon_1 \to \epsilon_2$, and $\mu_1 \to \mu_2$ and the same for the coefficient functions. With the isorefractive assumption $k_\perp$ is the same in both media for given $\omega$ and $k_z$, so the boundary conditions at the interfaces can be solved under the integral signs. In general there are eight unknown functions and eight equations, yet one finds that the $s$ and $p$ modes decouple into linear equation sets of $4 \times 4$ in the form

$$\tilde{\mathbf{D}} \cdot \mathbf{a} = 0, \tag{2.24}$$

where $\tilde{\mathbf{D}}$ equals

$$\begin{pmatrix} \cos\frac{\nu\alpha}{2} & 0 & -\cos\nu\left(\frac{\alpha}{2}-\pi\right) & 0 \\ 0 & \sin\frac{\nu\alpha}{2} & 0 & -\sin\nu\left(\frac{\alpha}{2}-\pi\right) \\ -\epsilon_1 \sin\frac{\nu\alpha}{2} & 0 & \epsilon_2 \sin\nu\left(\frac{\alpha}{2}-\pi\right) & 0 \\ 0 & -\epsilon_1\cos\frac{\nu\alpha}{2} & 0 & \epsilon_2\cos\nu\left(\frac{\alpha}{2}-\pi\right) \end{pmatrix}$$

and $\mathbf{a}$ is a vector, either $(\bar{a}_1, \underline{a}_1, \bar{a}_2, \underline{a}_2)$ or $(\bar{b}_1, \underline{b}_1, \bar{b}_2, \underline{b}_2)$.

As before the eigenmodes of the system solve the equation $\det \tilde{\mathbf{D}} = 0$. With some manipulation we find that the determinant can be written simply as

$$\det \tilde{\mathbf{D}} = \tfrac{1}{4}(\epsilon_2 - \epsilon_1)^2 \sin^2 \nu(\pi - \alpha) - \tfrac{1}{4}(\epsilon_2 + \epsilon_1)^2 \sin^2 \nu\pi. \tag{2.25}$$

Under the assumption that $\epsilon_2 + \epsilon_1 \neq 0$ the equation $\det \tilde{\mathbf{D}} = 0$ is equivalent to Eq. (2.17) with Eq. (2.20).

## III. CASIMIR ENERGY

In order to find the Casimir energy we shall employ the argument principle, introduced to the field of Casimir energy by van Kampen *et al.* [47] who rederived Lifshitz's result in a simple way. For a very readable review of the technique, see [57].

A similar system to that shown in Fig. 1 was considered in [35] where the plane sides of the wedge were instead made up of perfectly reflecting interfaces and the circular boundary was diaphanous. We will start from the result in [35] and generalize this step by step to approach the desired energy expression for the current situation. Except for the formally singular energy term associated with the sharp corners where the arc meets the wedge walls found in that paper (we shall regard this term separately below), the Casimir energy per unit length of that system in the limit of perfectly reflecting circular arc was [Eq. (4.11) in [35]]

$$\tilde{\mathcal{E}}_{\mathrm{id}} = \frac{1}{2\pi i}\int_{-\infty}^{\infty}\frac{dk_z}{2\pi}\sum_{m=0}^{\infty}{}'\oint_\Lambda d\omega\frac{\omega}{2}\frac{d}{d\omega}\ln g_{mp}(k_z,\omega), \tag{3.1}$$

with $g_\nu(k_z,\omega)$ given in Eq. (2.6) and we define the shorthand

$$p = \frac{\pi}{\alpha}. \tag{3.2}$$

The prime on the summation mark means that the $m=0$ term is taken with half-weight. The integration contour $\Lambda$ is chosen to follow the imaginary axis and is closed to the right by a large semicircle thus encircling the positive real axis. The roots of Eq. (2.6) are in general complex; the applicability of the argument principle for such situations was discussed in [7,54,55,58]. The energy $\tilde{\mathcal{E}}$ has been normalized so as to be zero when the circular arc is moved to infinity.

Each frequency satisfying $g_{mp}(k_z,\omega)=0$ gives a pole which adds the zero temperature energy $\frac{\omega}{2}$ of that mode through Cauchy's integral theorem. In the end there are sums over the eigenvalues of $\nu$, $mp$, the eigenvalues found when the sides of the wedge are assumed to be perfectly conducting. Employing such an assumption from the start completely decouples the interior sector $|\theta| < \alpha/2$ from the exterior. If we were to interpret the perfectly reflecting wedge as the *limit* of an isorefractive wedge such as that described by the dispersion relation Eq. (2.20) as $|r| \to 1$, however (for example, by letting $\epsilon_2 \to \infty$ and $\mu_2 \to 0$ so that their product is constant), the interior and exterior sectors remain coupled and we obtain an additional $m$ sum, namely, that over $\nu = mp'$ of the complementary wedge, where

$$p' = \frac{\pi}{2\pi - \alpha} = \frac{p}{2p-1}. \tag{3.3}$$

To obtain direct correspondence we therefore modify Eq. (3.1) by also including the energy of the modes of the complementary wedge, fulfilling $\nu = mp'$. Since we will soon generalize this result to the case where the wedge is diaphanous, it is reasonable to subtract the energy corresponding to the absence of the boundaries at $\pm\alpha/2$ by subtracting off the energy obtained if $\nu$ fulfilled periodic boundary conditions (i.e., a circular cylinder). The result is

$$\tilde{\mathcal{E}}_{\mathrm{id}} \to \frac{1}{4\pi i}\int_{-\infty}^{\infty}\frac{dk_z}{2\pi}\sum_{m=0}^{\infty}{}'\oint_\Lambda d\omega\omega\frac{d}{d\omega}\ln\frac{g_{mp}g_{mp'}}{g_m^2}. \tag{3.4}$$

The periodic function $g_m(k_z,\omega)$ is squared since both positive and negative integer orders contribute equally in the periodic case and the symmetry under $m \to -m$ makes for a factor of 2 except for $m=0$. The latter exception is automatically accounted for by the prime on the sum.

Note that employing $g_\nu(k_z,\omega)$ with the argument principle automatically takes care of the sum over the two polarizations since, by virtue of the diaphanous condition, $g_\nu$ is a product of boundary conditions for TE and TM modes (see, e.g., Appendix B in [35]).

Let us now perform the generalization of Eq. (3.4) to the present case. The sum over $\nu = mp$ and $mp'$ may be generalized to a sum over the solutions of Eq. (2.17) using the argument principle once more to count the zeros of Eq. (2.20), and the subtraction of the periodic modes in the absence of the boundary is performed by subtracting the solutions of $D_0(\nu)=0$ with $D_0$ from Eq. (2.22) (note that the zeros of $D_0$ are double, automatically giving the factor 2 manually introduced in Eq. (3.4) by taking the square of $g_m$). We obtain

$$\tilde{\mathcal{E}} = \frac{1}{2(2\pi i)^2}\int_{-\infty}^{\infty}\frac{dk_z}{2\pi}\oint_{\Lambda} d\omega\omega \times \oint_{\Lambda} d\nu\left[\frac{d}{d\omega}\ln g_{\nu}(k_z,\omega)\right]\frac{d}{d\nu}\ln\frac{D(\nu,\omega)}{D_0(\nu)}. \quad (3.5)$$

The contour of the $\nu$ integral is the same as that for the $\omega$ integral.

Neither of the contour integrals obtains contributions from the semicircular contour arcs so we are left with integrals over imaginary order and frequency. Performing substitutions $\omega = i\zeta$ and $\nu = i\eta$ we obtain

$$\tilde{\mathcal{E}} = \frac{1}{16\pi^3 i}\int_{-\infty}^{\infty} dk_z \int_{-\infty}^{\infty} d\zeta\zeta \times \int_{-\infty}^{\infty} d\eta\left[\frac{d}{d\zeta}\ln g_{i\eta}(k_z,i\zeta)\right]\frac{d}{d\eta}\ln\frac{D(i\eta,i\zeta)}{D_0(i\eta)}. \quad (3.6)$$

This is the general form of the Casimir energy of the system presented herein.

To be very explicit about the regularizations performed, Eq. (3.6) is the energy of the geometry of Fig. 1, minus the energy when the cylinder is pushed to infinity (the double wedge alone) and minus the renormalized energy of the cylinder relative to uniform space,

$$\tilde{\mathcal{E}} = (\mathcal{E}_{\circledcirc} - \mathcal{E}_{<}) - \tilde{\mathcal{E}}_{\circ}, \quad (3.7)$$

where $\tilde{\mathcal{E}}_{\circ}$ is the $\zeta$-renormalized energy of a cylindrical shell (relative to uniform space) considered in [10] and $\circledcirc, <$ symbolize the double wedge with and without the cylindrical shell. It is thus clear that the energy should vanish when either the cylindrical boundary tends to infinity ($\mathcal{E}_{\circledcirc} \to \mathcal{E}_{<}$ and $\tilde{\mathcal{E}}_{\circ} \to 0$) or when the wedge becomes completely transparent ($\mathcal{E}_{\circledcirc} - \mathcal{E}_{<} \to \tilde{\mathcal{E}}_{\circ}$).

The corresponding free energy at finite temperature $T$ is found by simply substituting the integral over $\zeta$ in Eq. (3.6) with the well known Matsubara sum over the frequencies $\zeta_k = 2\pi kT$, where $k \in \mathbb{Z}$,

$$\int_{-\infty}^{\infty} d\zeta f(i\zeta) \to 2\pi T\sum_{k=-\infty}^{\infty} f(i\zeta_k). \quad (3.8)$$

We will not consider finite temperature numerically in the present effort.

### A. Nondispersive approximation

In order to proceed to producing numerical results we make the simplifying assumption that $r$ be approximately constant with respect to $\zeta$ over the important range of $\zeta$ values: $dr/d\zeta \approx 0$. This a version of the constant reflection coefficient model which was previously found to be useful for the planar geometry [59]. While it is true that for any *real* material, reflectivity must tend to zero at infinite frequency, the nondispersive approximation is a useful one and allows a simpler expression to be derived. We will find below that the resulting Casimir energy expression is finite even when $r = 1$ for all frequencies except when $\alpha = 0$ or $2\pi$. There is therefore no need to assume high-frequency transparency for the sake of finiteness in this case.

With this assumption we can easily perform a partial integration in $\zeta$. We note that, when $r$ is independent of $\nu$ as in the diaphanous case (see the Appendix for a situation where this is not so),

$$\frac{d}{d\eta}\left[\ln\frac{D}{D_0}\right] = \frac{\alpha\sinh\eta(2\pi-\alpha) - (2\pi-\alpha)\sinh\eta\alpha}{\sinh^2\eta\pi - r^2\sinh^2\eta(\pi-\alpha)} \times \frac{r^2\sinh\eta(\pi-\alpha)}{\sinh\eta\pi}, \quad (3.9)$$

which is now approximated as independent of $\zeta$ and $k_z$. It is then opportune to perform a change in integration into the polar coordinates,

$$X = n\zeta = \kappa\cos\theta; \quad Y = k_z = \kappa\sin\theta, \quad (3.10)$$

so that $X^2 + Y^2 = \kappa^2$ and

$$\int_{-\infty}^{\infty} dk_z\int_{-\infty}^{\infty} d\zeta f(a\kappa) = \frac{2\pi}{na^2}\int_0^{\infty} dx x f(x), \quad (3.11)$$

where $x = a\kappa$ as before. We obtain after integrating by parts

$$\tilde{\mathcal{E}} = \frac{i}{8\pi^2 na^2}\int_{-\infty}^{\infty} d\eta\frac{r^2\sinh\eta(\pi-\alpha)[\alpha\sinh\eta(2\pi-\alpha) - (2\pi-\alpha)\sinh\eta\alpha]}{\sinh\eta\pi[\sinh^2\eta\pi - r^2\sinh^2\eta(\pi-\alpha)]}\int_0^{\infty} dx x\ln[1 - x^2\lambda_{i\eta}^2(x)]. \quad (3.12)$$

Despite appearances this expression is in fact real. This is because the dispersion function in the first integral is an odd function of $\eta$ while the real and imaginary parts of the logarithm are even and odd, respectively (provided the appropriate branch of the logarithm is taken), hence the imaginary part of $\tilde{\mathcal{E}}$ vanishes under symmetrical integration. It is straightforward to write down the correction terms containing $\frac{dr}{d\zeta}$ or $\frac{dr}{d\nu}$ should the reader wish to do so. Such is necessary if one were to study the role of dispersion on the energy; we shall not consider this herein—but see the Appendix for $dr/d\nu \neq 0$.

The energy expression (3.12) has the reasonable properties of being zero at $\alpha = \pi$ and symmetrical under the substitution $\alpha \leftrightarrow 2\pi - \alpha$. We will study Eq. (3.12) numerically in

Sec. IV. We argue in Sec. III B that Eq. (3.6) is the full Casimir energy of this system (after subtracting that of the cylinder alone). Thus the zero energy at $\alpha=\pi$ demonstrates a particular generalization of the theorem of Ambjørn and Wolfram ([60], stated in Eq. (2.49) in [3]): the energy of a semicircular compact diaphanous cylinder is half that of a full cylinder (there is an equal contribution from the exterior "half-cylinder" so the difference is zero).

For large $\eta$ the term proportional to $\alpha$ in the big fraction in Eq. (3.12) behaves for $\pi-\alpha>0$ as

$$\frac{d}{d\eta}\ln\frac{D}{D_0}\sim\frac{2\alpha r^2}{e^{2\alpha\eta}-r^2}, \tag{3.13}$$

with a similar behavior for the term proportional to $2\pi-\alpha$ and so is exponentially convergent. With perfect reflectivity Eq. (3.12) is finite except when $\alpha$ equals 0 or $2\pi$ when $|r|=1$.

### B. No additional corner term

In the geometry considered in [35], which differed from the present one primarily by the assumption that the wedge be perfectly conducting, the Casimir energy was found to possess a divergent term which could be associated with the corners where the arc meets the wedge sides. When the arc was instead made diaphanous it was shown that this term could be rendered finite by virtue of high-frequency transparency as displayed by any real material boundary.

The energy (3.6) is the direct generalization of the finite part of the energy of the system considered in [35]. We will argue that when the wedge is also diaphanous, this is indeed the full energy of the system, regularized by the subtraction of the energy of the cylinder alone (which in turn is regularized by subtracting the energy of uniform space).

Let us recapitulate how the divergent term in [35] came about. The zeta function regularized energy expression (Eq. (4.13) in [35]) adds the $m=0$ modes of both polarizations with half-weight. There should be no $m=0$ TM mode, however, because the perfectly conducting wedge forces any azimuthally constant electric field to have zero amplitude everywhere, thus the half-weight zero TM mode should be subtracted. Moreover, since for arbitrary opening angles only positive values of $m$ are allowed, the zero TE mode should be counted with full rather than half-weight, and thus the correction term equals one half the $m=0$ energy of the TE mode minus one half that of the TM mode.

In contrast we are here not considering perfectly conducting wedge boundaries so the TM $m=0$ mode should be included. The question becomes whether the $\nu=0$ TE and TM modes have been counted with only half the weight they should. In a system such as ours the interior and exterior sectors are coupled and all allowed modes are modes satisfying boundary conditions of the whole double wedge. Thus there can be only one azimuthally constant mode for all $\theta$ (not one for each sector as one obtains for a perfectly conducting wedge sheet) hence the zero mode should be counted once. This is exactly what is done in Eq. (3.6) because the dispersion function [Eq. (2.20)] has a double zero at $\nu=0$ canceling the factor 1/2. Hence no additional correction term is necessary and the use of dispersion relations with the argument principle automatically gives the full result.

In our numerical considerations reported in Sec. IV we find correspondence with the finite part of the energy reported in [35] when applied to two complementary wedges separated by a perfectly conducting sheet. Note how this correspondence is somewhat peculiar: in the energy expression of that reference the zero mode was counted with half-weight where it should have been accounted for fully, but in adding the energy of the complementary wedge as in Eq. (4.9) each of the complementary wedges contribute a half of the $m=0$ mode energy, amounting to the full energy when we insist that this mode be common to the whole system.

It is thus made clear how the divergent term found in [24,25,35] can be seen as a pathology of the ideal conductor boundary conditions at $\theta=\pm\alpha/2$ which (a) completely removes the azimuthally constant TM mode and (b) cleanly severs the connection between the interior and exterior of the wedge. Whether a similar term would appear—perhaps with a finite value—for a nondiaphanous wedge remains an open question since the diaphanous condition employed herein is also a special case.

## IV. NUMERICAL INVESTIGATION

It is useful to introduce the shorthand notation,

$$\tilde{\mathcal{E}}=-\frac{1}{4\pi^2na^2}\int_0^\infty d\eta\left[\frac{d}{d\eta}\ln\frac{D}{D_0}\right]Y(\eta), \tag{4.1}$$

where $Y$ is the imaginary part of the integral over the logarithm in Eq. (3.12),

$$Y(\eta)=\int_0^\infty dx\,x\arctan\frac{-x^2\,\mathrm{Im}\{\lambda_{i\eta}^2(x)\}}{1-x^2\,\mathrm{Re}\{\lambda_{i\eta}^2(x)\}}, \tag{4.2}$$

where we take the argument of the logarithm to lie in $[-\frac{\pi}{2},\frac{\pi}{2}]$.

Near $x=0$ this integrand [Eq. (4.2)] behaves like $x\sin(\ln x)$, oscillating increasingly fast. Techniques of rotating the integration path are restricted by the scarcity of methods for evaluating Bessel functions of general complex order and will anyway come at the cost of making $\frac{d}{d\eta}\ln D/D_0$ oscillatory. For numerical purposes it is more useful to perform the substitution $x=e^y$,

$$Y(\eta)=\int_{-\infty}^\infty dy e^{2y}\arctan\frac{-e^{2y}\,\mathrm{Im}\{\lambda_{i\eta}^2(e^y)\}}{1-e^{2y}\,\mathrm{Re}\{\lambda_{i\eta}^2(e^y)\}}. \tag{4.3}$$

For moderate values of $\eta$ this integrand is numerically manageable [there are $\mathcal{O}(4\eta)$ significant oscillations to integrate over], the remaining challenge being the evaluation of $\lambda_{i\eta}(x)$.

Rather than consider the complex function $I_{i\eta}(x)$ it is numerically useful to consider the real function

$$L_{i\eta}(x)=\tfrac{1}{2}[I_{i\eta}(x)+I_{-i\eta}(x)]. \tag{4.4}$$

When $\eta$ is real, $L_{i\eta}(x)=\mathrm{Re}\,I_{i\eta}(x)$. We find, using the Wronskian relation

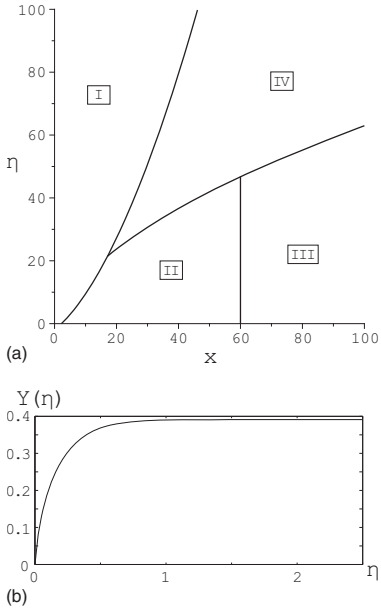


FIG. 3. (a) Different methods of calculation used in different areas of the $x,\eta$ plane (see text). (b) The function $Y(\eta)$.

$$\mathcal{W}[K_\nu, I_\nu](x) = 1/x \tag{4.5}$$

and relations between the two modified Bessel functions, that $\lambda_{i\eta}$ can be written as

$$\lambda_{i\eta}(x) = \frac{1}{x} + 2K'_{i\eta}(x)L_{i\eta}(x) - \frac{2i\sinh\eta\pi}{\pi}K'_{i\eta}(x)K_{i\eta}(x). \tag{4.6}$$

For obtaining the right limit of the integrand near $\eta=0$ one may notice that $Y(\eta)$ for small $\eta$ is

$$Y(\eta) \sim -\eta\int_0^\infty dx x^2 \frac{4K_0K_1(1-2xI_0K_1)}{x^2-(1-2xI_0K_1)^2} + \mathcal{O}(\eta^2)$$

plus higher orders. Numerically one finds

$$Y(\eta) \sim 0.874\,42\eta + \mathcal{O}(\eta^2). \tag{4.7}$$

A complete algorithm for evaluating $K$ and $L$ for imaginary order and real argument was developed by Gil *et al.* [61,62]. Since we are only calculating products of Bessel functions and the methods for calculating one is much like that for another, the code performance could be increased significantly by reprogramming (we used programming language C#).

Different calculation methods are appropriate in different areas of the $x,\eta$ plane as shown in Fig. 3(a). For $K$ and $K'$ we use Maclaurin-type series expansion in region I in the figure [bounded by $\eta > 0.044(x-3.1)^{1.9}+x-3.1$] and in regions II and III [bounded by $\eta < 380(\frac{x-3}{2300})^{0.572}$] a method of continued fractions is used [63] (the continued fraction method in [64] may be used for imaginary orders also). No continued fraction method is available for $L$, but series expansions turn out to be more robust than for $K,K'$; for $x<60$ (region II) Maclaurin series expansion is used, and asymptotic series expansion is used above this (region III). In the remaining area (region IV) Airy function-type asymptotic expansions were used [61,65,66]. In addition a fast method for evaluating complex gamma functions was necessary—we used that of Spouge [67]. The resulting algorithm was able to calculate $\lambda_{i\eta}(x)$ with at least eight significant digits on $x,\eta\in[0,100]$, more than sufficient for our purposes.

Because the calculation of $\lambda$ is rather elaborate we do not do the double integral [Eq. (4.1)] directly but calculate a number of discrete values of $Y(\eta)$ and use spline interpolation to represent $Y$ in the integration over $\eta$, which then converges rapidly. The function $Y(\eta)$ is zero at $\eta=0$ and increases smoothly thence to approach a positive constant, obtained already at modest values of $\eta$, as plotted in Fig. 3(b). The factor $[\ln D/D_0]'$ behaves as $e^{-2\eta\alpha}$ for large $\eta$ (assuming $\alpha<\pi$) assuring rapid convergence when $\alpha$ is not close to zero or $2\pi$.

In the limit $r^2\to 1$ we should obtain correspondence with [35] where the energy of a perfectly reflecting wedge closed by a diaphanous arc was considered. In this strong coupling case (the arc becoming perfectly reflecting) the energy of the sector inside the wedge only (modulo a singular term) was written on the form

$$\tilde{\mathcal{E}}_{\rm id} = \frac{1}{8\pi n a^2}e(p), \tag{4.8}$$

where the dimensionless function $e(p)$ is given in Eq. (4.22) in [35] and $p=\pi/\alpha$ as before. In the present case the modes in the interior and exterior sectors never decouple even in the limit $r\to 1$ and Eq. (3.12) thus calculates the energy of the whole system, regularized by subtracting the energy of free space, that is, by subtracting the result when the arc is moved to infinity [this is already implicitly subtracted by use of Eq. (2.6)] and the wedge boundaries become transparent. The energy to compare with is therefore on the form given in [35] where the energy of the complementary wedge is added and that of a cylinder is subtracted. We can therefore write Eq. (3.4) in the form $\tilde{\mathcal{E}}_{\rm id}=\tilde{e}_{\rm id}(p)/8\pi n a^2$ where

$$\tilde{e}_{\rm id}(p) = e(p) + e(p') - 2e(1) \tag{4.9}$$

and $p'$ was defined in Eq. (3.3).

For our system the corresponding function is

$$\tilde{e}(p) = -\frac{2}{\pi}\int_0^\infty d\eta\left[\ln\frac{D}{D_0}\right]' Y(i\eta;r). \tag{4.10}$$

We plot $\tilde{e}(p)$ as a function of $p$ and as a function of $\alpha$ in Fig. 4. When $r\to 1$ full agreement with $\tilde{e}_{\rm id}(p)$ of Eq. (4.9) is obtained.

## V. CONCLUSIONS

We have analyzed the Casimir energy of a magnetodielectric cylinder whose cross section is a wedge closed by a

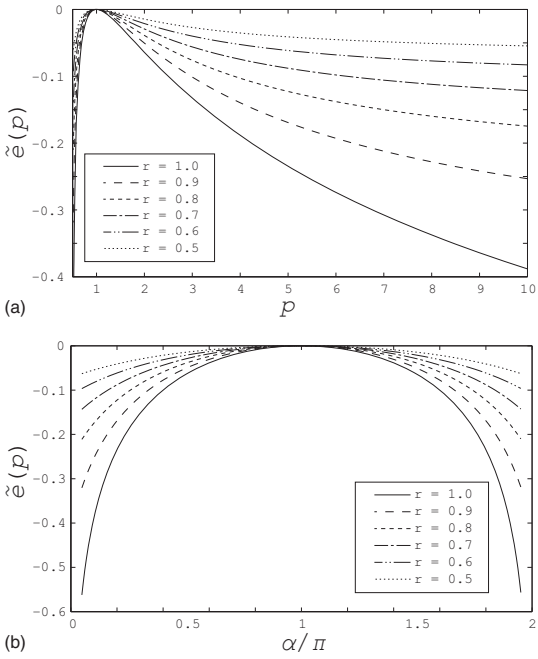


FIG. 4. Above: the function $\tilde{e}(p)$ calculated for different $r$. Below: same quantity, now plotted as a function of opening angle $\alpha$.

circular arc under the restriction that the cylinder be diaphanous, i.e., that the speed of light be spatially uniform. We obtain an expression for the Casimir energy per unit length of the cylinder, regularized by subtraction of the energy of the wedge alone and the cylinder alone. The energy is then zero when the opening angle of the wedge, $\alpha$, equals $\pi$, it is symmetrical under the substitution $\alpha \leftrightarrow 2\pi - \alpha$, and it remains finite as $\alpha$ tends to zero or $2\pi$ except when the absolute reflection coefficients of the wedge boundaries are equal to unity.

A numerical investigation confirms that this generalizes a previously known result for a perfectly conducting wedge closed by a diaphanous magnetodielectric arc in the limit where the arc becomes perfectly reflecting, except for a singular term present in that geometry which we argue does not present itself in the present configuration. This implies that the singular term found and discussed in [35] is an artifact of the use of ideal conductor boundary conditions and does not enter for a diaphanous wedge.

We mention finally that the diaphanous condition $\epsilon\mu$ =const is an important simplifying element in the analysis. If this condition were given up, the problem would be very difficult to solve. As mentioned also in [35], the effect is the same as that encountered in the Casimir theory of a solid ball: the condition of diaphanousness causes the divergent terms to *vanish* [68]. Analogously, when calculating the Casimir energy for a piecewise uniform string, the same effect turns up. If the velocity of sound (in this case sound replaces light) is the same (=$c$) in the different pieces of the string, then the theory works smoothly [69]. If this condition is relaxed, the problem becomes in practice intractable.

## ACKNOWLEDGMENTS

The work of K.A.M. was supported in part by grants from the (U.S.) National Science Foundation and the (U.S.) Department of Energy. S.Å.E. thanks Carsten Henkel and Francesco Intravaia for stimulating discussions on this topic. K.A.M. thanks Klaus Kirsten, Prachi Parashar, and Jef Wagner for collaboration. The authors are grateful to Vladimir Nesterenko for useful remarks on the paper.

## APPENDIX: SEMITRANSPARENT WEDGE

In this appendix we sketch another way of deriving the azimuthal dependence, based on an analogous scalar model, in which the wedge is described by a $\delta$-function potential,

$$V(\theta) = \lambda_1 \delta(\theta - \alpha/2) + \lambda_2 \delta(\theta + \alpha/2). \tag{A1}$$

This has the diaphanous property of preserving the speed of light both within and outside the wedge. We can solve this cylindrical problem in terms of the two-dimensional Green's function $G$, which satisfies

$$\left[ -\frac{1}{\rho}\frac{\partial}{\partial\rho}\rho\frac{\partial}{\partial\rho} + \kappa^2 - \frac{1}{\rho^2}\frac{\partial^2}{\partial\theta^2} + \frac{V(\theta)}{\rho^2} \right] G(\rho,\theta;\rho',\theta') = \frac{1}{\rho}\delta(\rho-\rho')\delta(\theta-\theta'). \tag{A2}$$

This separates into two equations, one for the angular eigenfunction $\Theta_\nu(\theta)$,

$$\left[ -\frac{\partial^2}{\partial\theta^2} + V(\theta) \right] \Theta_\nu(\theta) = \nu^2 \Theta_\nu(\theta), \tag{A3}$$

leaving us with the radial reduced Green's function equation,

$$\left[ -\frac{1}{\rho}\frac{\partial}{\partial\rho}\rho\frac{\partial}{\partial\rho} + \kappa^2 + \frac{\nu^2}{\rho^2} \right] g_\nu(\rho,\rho') = \frac{1}{\rho}\delta(\rho-\rho'). \tag{A4}$$

The latter, for a Dirichlet arc at $\rho = a$, has the familiar solution,

$$g_\nu(\rho,\rho') = I_\nu(\kappa\rho_<)K_\nu(\kappa\rho_>) - I_\nu(\kappa\rho)I_\nu(\kappa\rho')\frac{K_\nu(\kappa a)}{I_\nu(\kappa a)}, \qquad \rho,\rho' < a, \tag{A5a}$$

$$g_\nu(\rho,\rho') = I_\nu(\kappa\rho_<)K_\nu(\kappa\rho_>) - K_\nu(\kappa\rho)K_\nu(\kappa\rho')\frac{I_\nu(\kappa a)}{K_\nu(\kappa a)}, \qquad \rho,\rho' > a. \tag{A5b}$$

The azimuthal eigenvalue $\nu$ is determined by Eq. (A3). For the wedge $\delta$-function potential [Eq. (A1)] it is easy to determine $\nu$ by writing the solutions to Eq. (A3) as linear combinations of $e^{\pm i\nu\theta}$, with different coefficients in the sectors $|\theta| < \alpha/2$ and $\pi \geq |\theta| > \alpha/2$. Continuity of the function and discontinuity of its derivative are imposed at the wedge

boundaries. The four simultaneous linear homogeneous equations have a solution only if the secular equation is satisfied,

$$0 = D(\nu) = \sin^2 \nu(\alpha - \pi) - \left(1 - \frac{4\nu^2}{\lambda_1\lambda_2}\right)\sin^2 \pi\nu - \left(\frac{\nu}{\lambda_1} + \frac{\nu}{\lambda_2}\right)\sin 2\pi\nu. \tag{A6}$$

Because we recognize that the reflection coefficient for a single $\delta$-function interface is $r_i=(1+2i\nu/\lambda_i)^{-1}$, so,

$$\mathrm{Re}\, r_1^{-1}r_2^{-1} = 1 - \frac{4\nu^2}{\lambda_1\lambda_2}, \quad \mathrm{Im}\, r_1^{-1}r_2^{-1} = \frac{2\nu}{\lambda_1} + \frac{2\nu}{\lambda_2}, \tag{A7}$$

we see that this dispersion relation coincides with that in Eq. (2.20) when the reflection coefficient is purely real. Note that the $\nu=0$ root of Eq. (A6) is spurious and must be excluded; there are no $\nu=0$ modes for the semitransparent wedge.

Now the full Green's function can be constructed as

$$G(x,x') = \int \frac{d\omega}{2\pi} e^{-i\omega(t-t')} \int \frac{dk}{2\pi} e^{ik(z-z')} \times \frac{1}{2\pi}\sum_\nu \Theta_\nu(\theta)\Theta_\nu^*(\theta') g_\nu(\rho,\rho'), \tag{A8}$$

from which the Casimir energy per length can be computed from

$$\mathcal{E} = \frac{1}{2i}\int_{-\infty}^{\infty}\frac{d\omega}{2\pi}2\omega^2 \int_{-\infty}^{\infty}\frac{dk}{2\pi}\sum_\nu \int_0^\infty d\rho\rho g_\nu(\rho,\rho), \tag{A9}$$

where we have recognized that because the eigenvalue equation for $\nu$ is a Sturm-Liuoville problem, the integration over the $\theta$ eigenfunctions is $2\pi$. As above, we can enforce the eigenvalue condition by the argument principle, so we have the expression after again converting to polar coordinates as in Eq. (3.10),

$$\mathcal{E} = \frac{1}{8\pi^2 i}\int_0^\infty d\kappa\kappa^3 \int_{-\infty}^{\infty} d\eta \left(\frac{d}{d\eta}\ln D(i\eta)\right)\int_0^\infty d\rho\rho g_{i\eta}(\rho,\rho). \tag{A10}$$

Further, we must subtract off the free radial Green's function without the arc at $r=a$, which then implies

$$\int_0^\infty d\rho\rho g_{i\eta}(\rho,\rho) \to \frac{a}{2\kappa}\frac{d}{d\kappa a}\ln[I_{i\eta}(\kappa a)K_{i\eta}(\kappa a)], \tag{A11}$$

as well as remove the term present without the wedge potential,

$$D(\nu) \to \tilde{D}(\nu) = \frac{\lambda_1\lambda_2}{4\nu^2}\frac{D(\nu)}{\sin^2 \pi\nu}, \tag{A12}$$

leaving us with an expression for the Casimir energy analogous to Eq. (3.12). This can be further simplified by noting that $\frac{d}{d\eta}\ln \tilde{D}(i\eta)$ is odd, which then yields the expression

$$\mathcal{E} = -\frac{1}{4\pi^2 a^2}\int_0^\infty dx x \int_0^\infty d\eta \left(\frac{d}{d\eta}\ln \tilde{D}(i\eta)\right)\arctan\frac{K_{i\eta}(x)}{L_{i\eta}(x)}, \tag{A13}$$

where

$$K_\mu(x) = -\frac{\pi}{2\sin \pi\mu}[I_\mu(x) - I_{-\mu}(x)], \tag{A14a}$$

$$L_\mu(x) = \frac{i\pi}{2\sin \pi\mu}[I_\mu(x) + I_{-\mu}(x)], \tag{A14b}$$

where both $L_{i\eta}(x)$ and $K_{i\eta}(x)$ are real for real $\eta$ and $x$, and

$$I_{i\eta}(x) = \frac{\sinh \eta\pi}{\pi}[L_{i\eta}(x) - iK_{i\eta}(x)]. \tag{A15}$$

Details of the calculation of the Casimir energy for a semitransparent wedge will appear elsewhere.


[1] H. B. G. Casimir, Proc. K. Ned. Akad. Wet. **51**, 793 (1948).
[2] E. M. Lifshitz, Zh. Eksp. Teor. Fiz. **29**, 94 (1955) [Sov. Phys. JETP **2**, 73 (1956)].
[3] K. A. Milton, *The Casimir Effect: Physical Manifestations of the Zero-Point Energy* (World Scientific, Singapore, 2001).
[4] K. A. Milton, J. Phys. A **37**, R209 (2004).
[5] S. K. Lamoreaux, Rep. Prog. Phys. **68**, 201 (2005).
[6] S. Y. Buhmann and D.-G. Welsch, Prog. Quantum Electron. **31**, 51 (2007).
[7] L. L. DeRaad, Jr. and K. A. Milton, Ann. Phys. **136**, 229 (1981).
[8] I. Brevik and G. H. Nyland, Ann. Phys. **230**, 321 (1994).
[9] P. Gosdzinsky and A. Romeo, Phys. Lett. B **441**, 265 (1998).
[10] K. A. Milton, A. V. Nesterenko, and V. V. Nesterenko, Phys. Rev. D **59**, 105009 (1999).
[11] G. Lambiase, V. V. Nesterenko, and M. Bordag, J. Math. Phys. **40**, 6254 (1999).
[12] I. Cavero-Peláez and K. A. Milton, Ann. Phys. **320**, 108 (2005); J. Phys. A **39**, 6225 (2006).
[13] A. Romeo and K. A. Milton, Phys. Lett. B **621**, 309 (2005); J. Phys. A **39**, 6703 (2006).
[14] I. Brevik and A. Romeo, Phys. Scr. **76**, 48 (2007).
[15] I. Cavero-Peláez, K. A. Milton, and K. Kirsten, J. Phys. A **40**, 3607 (2007).
[16] J. S. Dowker and G. Kennedy, J. Phys. A **11**, 895 (1978).
[17] D. Deutsch and P. Candelas, Phys. Rev. D **20**, 3063 (1979).
[18] I. Brevik and M. Lygren, Ann. Phys. **251**, 157 (1996).
[19] I. Brevik, M. Lygren, and V. Marachevsky, Ann. Phys. **267**, 134 (1998).
[20] I. Brevik and K. Pettersen, Ann. Phys. **291**, 267 (2001).
[21] V. V. Nesterenko, G. Lambiase, and G. Scarpetta, Ann. Phys. **298**, 403 (2002).

[22] H. Razmi and S. M. Modarresi, Int. J. Theor. Phys. **44**, 229 (2005).
[23] V. M. Mostepanenko and N. N. Trunov, *The Casimir Effect and Its Applications* (Oxford University Press, Oxford, 1997).
[24] V. V. Nesterenko, G. Lambiase, and G. Scarpetta, J. Math. Phys. **42**, 1974 (2001).
[25] V. V. Nesterenko, I. G. Pirozhenko, and J. Dittrich, Class. Quantum Grav. **20**, 431 (2003).
[26] A. H. Rezaeian and A. A. Saharian, Class. Quantum Grav. **19**, 3625 (2002).
[27] A. A. Saharian, Eur. Phys. J. C **52**, 721 (2007).
[28] A. A. Saharian, in *The Casimir Effect and Cosmology: A Volume in Honour of Professor Iver H. Brevik on the Occasion of His 70th Birthday*, edited by S. Odintsov *et al.* (Tomsk State Pedagogical University Press, Tomsk, 2008), p. 87.
[29] T. N. C. Mendes, F. S. S. Rosa, A. Tenório, and C. Farina, J. Phys. A **41**, 164029 (2008).
[30] F. S. S. Rosa, T. N. C. Mendes, A. Tenório, and C. Farina, Phys. Rev. A **78**, 012105 (2008).
[31] G. Barton, Proc. R. Soc. London **410**, 175 (1987).
[32] S. C. Skipsey, G. Juzeliūnas, M. Al-Amri, and M. Babiker, Opt. Commun. **254**, 262 (2005).
[33] S. C. Skipsey, M. Al-Amri, M. Babiker, and G. Juzeliūnas, Phys. Rev. A **73**, 011803(R) (2006).
[34] C. I. Sukenik, M. G. Boshier, D. Cho, V. Sandoghdar, and E. A. Hinds, Phys. Rev. Lett. **70**, 560 (1993).
[35] I. Brevik, S. Å. Ellingsen, and K. A. Milton, Phys. Rev. E **79**, 041120 (2009).
[36] H. M. Macdonald, Proc. London Math. Soc. **s1-26**, 156 (1894).
[37] A. Sommerfeld, Math. Ann. **47**, 317 (1896).
[38] G. D. Malyuzhinets, Ph.D. thesis, P. N. Lebedev Physical Institute of the USSR Academy of Sciences, 1950.
[39] A. V. Osipov and A. N. Norris, Wave Motion **29**, 313 (1999).
[40] A. V. Osipov and K. Hongo, Electromagnetics **18**, 135 (1998).
[41] M. J. Kontorovich and N. N. Lebedev, Zh. Eksp. Teor. Fiz. **8**, 1192 (1938).
[42] F. Oberhettinger, Commun. Pure Appl. Math. **7**, 551 (1954).
[43] L. Knockaert, F. Olyslager, and D. De Zutter, IEEE Trans. Antennas Propag. **45**, 1374 (1997).
[44] A. D. Rawlins, Proc. R. Soc. London, Ser. A **455**, 2655 (1999).
[45] M. A. Salem, A. H. Kamel, and A. V. Osipov, Proc. R. Soc. London, Ser. A **462**, 2503 (2006).
[46] M. A. Salem and A. H. Kamel, Q. J. Mech. Appl. Math. **61**, 219 (2008).
[47] N. G. van Kampen, B. R. A. Nijboer, and K. Schram, Phys. Lett. A **26**, 307 (1968).
[48] V. A. Ditkin and A. P. Prudnikov, *Integral Transforms and Operational Calculus* (Pergamon Press, Oxford, 1965), Chap. 11.
[49] F. Oberhettinger, *Tables of Bessel Transforms* (Springer, Berlin, 1972), Chap. 5.
[50] W. Gautschi, BIT **46**, 21 (2006).
[51] J. Schwinger, L. L. DeRaad, Jr., and K. A. Milton, Ann. Phys. **115**, 1 (1978).
[52] S. A. Ellingsen and I. Brevik, J. Phys. A **40**, 3643 (2007).
[53] M. S. Tomaš, Phys. Rev. A **51**, 2545 (1995).
[54] I. Brevik, B. Jensen, and K. A. Milton, Phys. Rev. D **64**, 088701 (2001).
[55] V. V. Nesterenko, J. Phys. A **39**, 6609 (2006).
[56] J. A. Stratton, *Electromagnetic Theory* (McGraw Hill, New York, 1941) Sec. 9.15.
[57] V. A. Parsegian, *van der Waals Forces* (Cambridge University Press, Cambridge, 2006), Sec. L3.3.
[58] V. V. Nesterenko, J. Phys. A **41**, 164005 (2008).
[59] S. Å. Ellingsen, in *The Casimir Effect and Cosmology: A Volume in Honour of Professor Iver H. Brevik on the Occasion of His 70th Birthday*, edited by S. Odintsov *et al.* (Tomsk State Pedagogical University Press, Tomsk, 2008), p. 45; e-print arXiv:0811.4214.
[60] J. Ambjørn and S. Wolfram, Ann. Phys. **147**, 1 (1983).
[61] A. Gil, J. Segura, and N. M. Temme, ACM Trans. Math. Softw. **30**, 145 (2004).
[62] A. Gil, J. Segura, and N. M. Temme, ACM Trans. Math. Softw. **30**, 159 (2004).
[63] A. Gil, J. Segura, and N. M. Temme, J. Comput. Phys. **175**, 398 (2002).
[64] W. Press *et al.*, *Numerical Recipes*, 2nd ed. (Cambridge University Press, Cambridge, 1992), Sec. 6.6.
[65] N. M. Temme, Numer. Algorithms **15**, 207 (1997).
[66] A. Gil, J. Segura, and N. M. Temme, J. Comput. Appl. Math. **153**, 225 (2003).
[67] J. L. Spouge, SIAM (Soc. Ind. Appl. Math.) J. Numer. Anal. **31**, 931 (1994).
[68] I. Brevik and H. Kolbenstvedt, Ann. Phys. (N.Y.) **143**, 179 (1982); **149**, 237 (1983).
[69] To our knowledge the first paper in this direction was I. Brevik and H. B. Nielsen, Phys. Rev. D **41**, 1185 (1990); a survey is given by I. Brevik, A. A. Bytsenko, and B. M. Pimentel, in *Theoretical Physics 2002 (Horizons in World Physics)*, edited by T. F. George and H. F. Arnoldus (Nova Science, New York, 2002).

# Article [k]

***Casimir effect at nonzero temperature for wedges and cylinders***

S.Å. Ellingsen, I. Brevik, K.A. Milton

Physical Review D **81**, 065031 (2010)

PHYSICAL REVIEW D **81,** 065031 (2010)

# Casimir effect at nonzero temperature for wedges and cylinders

Simen Å. Ellingsen* and Iver Brevik†

*Department of Energy and Process Engineering, Norwegian University of Science and Technology, N-7491 Trondheim, Norway*

Kimball A. Milton‡

*Oklahoma Center for High Energy Physics and Homer L. Dodge Department of Physics and Astronomy, The University of Oklahoma, Norman, Oklahoma 73019, USA*

(Received 15 January 2010; published 26 March 2010)

We consider the Casimir-Helmholtz free energy at nonzero temperature $T$ for a circular cylinder and perfectly conducting wedge closed by a cylindrical arc, either perfectly conducting or isorefractive. The energy expression at nonzero temperature may be regularized to obtain a finite value, except for a singular corner term in the case of the wedge which is present also at zero temperature. Assuming the medium in the interior of the cylinder or wedge be nondispersive with refractive index $n$, the temperature dependence enters only through the nondimensional parameter $2\pi naT$, $a$ being the radius of the cylinder or cylindrical arc. We show explicitly that the known zero-temperature result is regained in the limit $aT \to 0$ and that previously derived high-temperature asymptotics for the cylindrical shell are reproduced exactly.

DOI: 10.1103/PhysRevD.81.065031 PACS numbers: 42.50.Lc, 11.10.Gh, 11.10.Wx, 42.50.Pq

## I. INTRODUCTION

The Casimir effect [1] is the name given to energies and forces due to field fluctuations in the presence of boundaries. Once a theoretical curiosity, the effect has gained enormous and still increasing attention since its first quantitative measurement a good decade ago [2]. Reviews of recent progress include Refs. [3–5].

The first geometry, considered in Casimir's classic paper [1] was that of two perfectly conducting plates, generalized to arbitrary dispersive materials by Lifshitz [6]. The force between parallel plates of any purely dielectric material is attractive, and it was therefore surprising when it was shown by Boyer that the Casimir stress on a perfectly conducting spherical shell is repulsive [7].

While it was clear from Boyer's result that the Casimir effect has a strong geometry dependence, results for new geometries were slow in coming for a long time, and it was only in 1981 that DeRaad and Milton calculated the Casimir energy for a circularly cylindrical shell [8]. Since then a number of analytical efforts have added to the knowledge of the Casimir effect in cylindrical cavities, both perfectly conducting [9–12] and (magneto)dielectric [13–18]. Most treatments of the cylindrical geometry have dealt with the zero-temperature situation, and only a few calculations have concerned finite temperature [19–21], and in these references only the high-temperature asymptotics were derived. No analytical expression valid for all temperatures exists for the cylindrical geometry to our knowledge.

A related geometry is the wedge. First considered with respect to the Casimir effect in the 1970s [22,23], it has been the subject of several treatments later [24–28]. The geometry is inviting in that it is analytically solvable and contains the geometries of parallel plates and a single semi-infinite plate as limiting cases. The geometry of a wedge intercut by a cylindrical shell was considered by Nesterenko and coworkers [29,30] and energy densities in the same geometry were calculated by Saharian and coworkers [31–33]. We are not aware of any previous efforts to tackle the Casimir energy problem for a wedge at nonzero temperature.

We recently revisited the latter geometry to calculate the energy, at zero temperature, of a perfectly conducting wedge closed by a cylindrical boundary, either perfectly conducting or magnetodielectric [34]. We showed how that energy could be written on the form (subscript 0 indicates zero-temperature)

$$\mathcal{E}_0 = \tilde{\mathcal{E}}_0(p) + \hat{\mathcal{E}}, \tag{1.1}$$

where $\tilde{\mathcal{E}}_0$ is a finite, regularizable energy closely analogous to that found for a cylinder [8,10], whereas $\hat{\mathcal{E}}$ is a divergent term associated with the corners where the arc meets the wedge.

Here and in the following we will make frequent use of the symbol

$$p = \pi/\alpha, \tag{1.2}$$

where the physical range is $p \in [\frac{1}{2}, \infty)$, but which we will in general allow to take any real positive value. Throughout our calculations we set $c = \hbar = k_B = 1$. It was shown [34] that $\hat{\mathcal{E}}$ could be rendered finite provided the arc become transparent at high frequencies.

*simen.a.ellingsen@ntnu.no
†iver.h.brevik@ntnu.no
‡milton@nhn.ou.edu

 

The calculations in [34] were extended to the first consideration of a wedge which is not perfectly conducting but instead assumed to be isorefractive (diaphanous), i.e., spatially uniform speed of light [35]. In that case the term $\hat{\mathcal{E}}$ is not present at all. The diaphanous wedge is analogous to the system of an annular region between two perfectly conducting cylinders, intercut by two semitransparent, radially directed interfaces [36,37]. Notably, while the energy expressions for a perfectly conducting wedge or circularly cylindrical shell require some regularization scheme in order to give numerical meaning, the energy expression obtained for the diaphanous wedge is immediately finite. A review of the Casimir wedge problem and an early exposition of the issue we elaborate herein are found in Ref. [38].

Naturally, for the geometry of a perfectly conducting cylinder there is no divergent term $\hat{\mathcal{E}}$ since there are no sharp corners. It turns out (c.f. the discussion in Section III of Ref. [34]) that the Casimir energy of a perfectly conducting cylindrical shell is

$$\tilde{\mathcal{E}}_{\mathrm{cyl}} = 2\tilde{\mathcal{E}}(p=1). \tag{1.3}$$

Thus, all of the calculations in the following sections, which are carried out for general $p$, are valid also for a cylindrical shell by letting $p \to 1$ and multiplying by an overall factor of 2.

In the following we derive an analytical expression for the Casimir energy of a perfectly conducting wedge (modulo a singular term as encountered in the past) and a perfectly conducting cylindrical shell, valid for arbitrary opening angles and all temperatures. This extends the calculations for the perfectly conducting wedge presented in Ref. [34], and simultaneously those for a circularly cylindrical conducting shell [8,10], to the case of finite temperature. We show how the energy expression, which for $T > 0$ is the Helmholtz free energy, may be regularized by a scheme of Epstein-zeta functions to obtain a numerically useful expression. We show explicitly that the expression thus obtained reduces to the previously derived zero-temperature limit, and that the two leading terms of the high-temperature asymptotic expansion, derived by Bordag, Nesterenko, and Pirozhenko [21], are reproduced exactly as a special case.

## II. CASIMIR-HELMHOLTZ FREE ENERGY OF WEDGE AND CYLINDER

We take as our starting point the zero-temperature energy derived in [34] for the geometry of a perfectly conducting wedge of opening angle $\alpha$ closed by a perfectly conducting cylindrical arc of radius $a$, shown on the left side of Fig. 1.

Henceforth we shall focus on the term $\tilde{\mathcal{E}}_0$, which may be written [34]

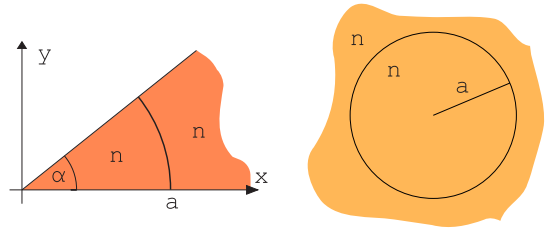


FIG. 1 (color online). The geometry considered: (left) a wedge of opening angle $\alpha$ closed by a cylindrical shell at radius $a$. The results are automatically applicable to a cylindrical shell of radius $a$ (right) when $\alpha = \pi$ [Eq. (1.3)].

$$\tilde{\mathcal{E}}_0 = {\sum_{m=0}^{\infty}}' \mathcal{E}_{m0} \tag{2.1}$$

with

$$\mathcal{E}_{m0} = -\frac{1}{8\pi^2}\int_{-\infty}^{\infty} dk \int_{-\infty}^{\infty} d\zeta\, \zeta \frac{d}{d\zeta} \times \ln[I_{mp}(x) I'_{mp}(x) K_{mp}(x) K'_{mp}(x)], \tag{2.2}$$

where we define the shorthand $x^2 = a^2(k^2 + n^2\zeta^2)$ where $n$ is the index of refraction of the medium inside the wedge. We assume $n$ to be constant with respect to $\zeta$ and uniform in space. Here $\omega = i\zeta$ is the reciprocal of imaginary (Euclidian) time. By means of partial integration with respect to $\zeta$, adding a trivial constant and noting that the integrand is symmetrical under $\zeta \to -\zeta$ and $k \to -k$, this may be written on the familiar form

$$\mathcal{E}_{m0} = \frac{1}{2\pi^2}\int_0^{\infty} dk \int_0^{\infty} d\zeta \ln[1 - x^2 \lambda_{mp}^2(x)], \tag{2.3}$$

wherein we use the shorthand

$$\lambda_\nu(x) = \frac{d}{dx}[I_\nu(x) K_\nu(x)]. \tag{2.4}$$

The Helmholtz free energy at $T > 0$ is obtained from the 'trace-log' formula (2.3) by compactifying the Euclidean time axis as is well known. Technically this amounts to the transition

$$\int_0^{\infty} d\zeta f(\zeta) \to 2\pi T {\sum_{j=0}^{\infty}}' f(\zeta_j), \tag{2.5}$$

where $\zeta_j = 2\pi j T$ are the Matsubara frequencies. Changing the integration variable from axial momentum $k$ to $x$, the resulting expression for the finite part of the free energy may be written

$$\tilde{\mathcal{E}} = \frac{T}{\pi a} {\sum_{m=0}^{\infty}}' {\sum_{j=0}^{\infty}}' e_{m,j}, \tag{2.6}$$

where

$$e_{m,j}(\tau, p) = \int_{j\tau}^{\infty} \frac{dxx}{\sqrt{x^2 - j^2\tau^2}} \ln[1 - x^2\lambda_{mp}^2(x)], \quad (2.7)$$

and where we have defined the dimensionless temperature

$$\tau = 2\pi naT. \quad (2.8)$$

Similarly to the case at zero-temperature this simple expression is in need of regularization in order to give numerical meaning since it is formally divergent.

## III. REGULARIZATION OF THE FREE ENERGY EXPRESSION

We here follow a scheme closely reminiscent of that of DeRaad and Milton [8], and particularly Milton, Nesterenko, and Nesterenko [10] (cf. also Appendix A of Ref. [34]).

As follows from the uniform asymptotic expansion of modified cylindrical Bessel functions, e.g. Sec. 9.7 of Ref. [39], the logarithmic factor in the integrand of (2.7) has the asymptotic behavior

$$\ln[1 - x^2\lambda_{mp}^2] \sim -\frac{x^4}{4(m^2p^2 + x^2)^3}, \qquad m, x \to \infty; \quad (3.1a)$$

$$\ln[1 - x^2\lambda_0^2] \sim -\frac{x^4}{4(1 + x^2)^3}, \qquad x \to \infty. \quad (3.1b)$$

To see how this behavior gives rise to a formal divergence, consider the case of large $m$ for which

$$e_{m,j} \sim -\frac{1}{4}\int_{j\tau}^{\infty} \frac{dxx^5}{\sqrt{x^2 - j^2\tau^2}(m^2p^2 + x^2)^3} = -\frac{1}{4}\int_0^{\infty} \frac{dy(y^4 + 2j^2\tau^2y^2 + j^4\tau^4)}{(m^2p^2 + j^2\tau^2 + y^2)^3} \quad (3.2a)$$

$$= -\frac{3\pi}{64\varphi} - \frac{\pi j^2\tau^2}{32\varphi^3} - \frac{3\pi j^4\tau^4}{64\varphi^5}, \quad (3.2b)$$

where we substituted $y^2 = x^2 - j^2\tau^2$ and defined the shorthand

$$\varphi = \sqrt{p^2m^2 + \tau^2j^2}. \quad (3.3)$$

The three terms of (3.2b) correspond to the three terms of the integrand of (3.2a). All of the terms of (3.2b) clearly diverge when summed over $j$ and $m$.

The first step in regularization is to add and subtract the asymptotic behavior (3.1) in the form (3.2a)

$$\tilde{\mathcal{E}} = \bar{\mathcal{E}} + \mathcal{E}_\infty \quad (3.4)$$

where we define the energy with the leading asymptotic term subtracted,

$$\bar{\mathcal{E}} = \frac{T}{\pi a}\sum_{m=0}^{\infty}{}'\sum_{j=0}^{\infty}{}' \tilde{e}_{m,j} \quad (3.5a)$$

$$\tilde{e}_{m,j} = \int_{j\tau}^{\infty} \frac{dxx}{\sqrt{x^2 - j^2\tau^2}} \times \left\{\ln[1 - x^2\lambda_{mp}^2(x)] + \frac{x^4}{4(m^2p^2 + x^2)^3}\right\}; \quad (3.5b)$$

$$\tilde{e}_{0,j} = \int_{j\tau}^{\infty} \frac{dxx}{\sqrt{x^2 - j^2\tau^2}} \times \left\{\ln[1 - x^2\lambda_0^2(x)] + \frac{x^4}{4(1 + x^2)^3}\right\}, \quad (3.5c)$$

and the additional, nonregularized energy

$$\mathcal{E}_\infty = -\frac{T}{4\pi a}\sum_{m=0}^{\infty}{}'\sum_{j=0}^{\infty}{}' \int_0^{\infty} \frac{dy(y^4 + 2j^2\tau^2y^2 + j^4\tau^4)}{(\tilde{\varphi}^2 + y^2)^3}. \quad (3.6)$$

wherein

$$\tilde{\varphi} = \begin{cases} \sqrt{1 + \tau^2j^2}, & m = 0 \\ \sqrt{p^2m^2 + \tau^2j^2}, & m \geq 1 \end{cases}. \quad (3.7)$$

To regularize $\mathcal{E}_\infty$ we introduce the small quantity $s$ and write

$$\mathcal{E}_\infty = -\frac{T}{4\pi a}\lim_{s\to 0^+}\sum_{m=0}^{\infty}{}'\sum_{j=0}^{\infty}{}' \int_0^{\infty} \frac{dyy^{-s}}{(\tilde{\varphi}^2 + y^2)^3} \times (y^4 + 2j^2\tau^2y^2 + j^4\tau^4) \sim -\frac{T}{64a}\lim_{s\to 0^+}\sum_{m=0}^{\infty}{}'\sum_{j=0}^{\infty}{}' \left\{\frac{3}{\tilde{\varphi}^{1+s}} + \frac{2j^2\tau^2}{\tilde{\varphi}^{3+s}} + \frac{3j^4\tau^4}{\tilde{\varphi}^{5+s}}\right\}, \quad (3.8)$$

where as in Eq. (3.2b) we have used the evaluation,

$$\int_0^{\infty} \frac{dyy^{4-s}}{(\tilde{\varphi}^2 + y^2)^3} = \frac{\pi(1 - s)(3 - s)}{16\tilde{\varphi}^{1+s}} \sec\frac{\pi s}{2}, \quad (3.9)$$

which is valid for $-1 < s < 5$, so it may be used for $s$ near 0, near 2, or near 4. We use the relations $[\partial_\tau = \partial/\partial\tau]$

$$\partial_\tau \frac{1}{\tilde{\varphi}^q} = -\frac{q\tau j^2}{\tilde{\varphi}^{q+2}}; \quad (3.10a)$$

$$\partial_\tau^2 \frac{1}{\tilde{\varphi}^q} = -\frac{qj^2}{\tilde{\varphi}^{q+2}} + \frac{q(q + 2)\tau^2j^4}{\tilde{\varphi}^{q+4}} \quad (3.10b)$$

to write

$$\mathcal{E}_\infty = -\frac{T}{64a}(3 - 3\tau\partial_\tau + \tau^2\partial_\tau^2)\lim_{s\to 0^+}\sum_{m=0}^{\infty}{}'\sum_{j=0}^{\infty}{}' \frac{1}{\tilde{\varphi}^{1+s}}. \quad (3.11)$$

The sum in (3.11) can be regularized by analytical continuation. We will write it in the following form, using symmetry properties with respect to $m \leftrightarrow -m$ and $j \leftrightarrow -j$:

$$\lim_{s\to 0^+}\sum_{m=0}^{\infty}{}'\sum_{j=0}^{\infty}{}'\frac{1}{\tilde{\varphi}^{1+s}}=\frac{1}{4}\lim_{s\to 0^+}\sum_{m,j\in\mathbb{Z}}\frac{1}{\tilde{\varphi}^{1+s}}$$
$$=\frac{1}{4}+\frac{1}{4}\mathcal{S}(\tau,p)+\frac{1}{2}\mathcal{K}(\tau). \quad (3.12)$$

Here we have defined

$$\mathcal{S}(\tau,p)=\lim_{s\to 0^+}\sum_{m,j\in\mathbb{Z}}{}''\frac{1}{\varphi^{1+s}}=\mathcal{S}(p,\tau), \quad (3.13)$$

wherein the double prime on the summation mark means that the term $m=j=0$ is explicitly excluded, and

$$\mathcal{K}(\tau)=\lim_{s\to 0^+}\sum_{j=1}^{\infty}\left[\frac{1}{\tilde{\varphi}^{1+s}}-\frac{1}{\varphi^{1+s}}\right]_{m=0}$$
$$=\sum_{j=1}^{\infty}\frac{j\tau-\sqrt{1+j^2\tau^2}}{j\tau\sqrt{1+j^2\tau^2}}. \quad (3.14)$$

Clearly, $\mathcal{K}(\tau)$ is finite for all $\tau>0$.

The function $\mathcal{S}(\tau,p)$ may be regularized by use of the Chowla-Selberg formula [see e.g. Eq. (4.33) of Ref. [40]]

$$\sum_{m,j\in\mathbb{Z}}{}''(am^2+bmj+cj^2)^{-q}$$
$$=2\zeta(2q)a^{-q}+\frac{2^{2q}\sqrt{\pi}a^{q-1}\Gamma(q-\frac{1}{2})\zeta(2q-1)}{\Gamma(q)\Delta^{q-(1/2)}}$$
$$+\frac{2^{q+(5/2)}\pi^q}{\Gamma(q)\Delta^{(1/2)(q-(1/2))}\sqrt{a}}\sum_{l=1}^{\infty}l^{q-(1/2)}\sigma_{1-2q}(l)$$
$$\times\cos(l\pi b/a)K_{q-(1/2)}(\pi l\sqrt{\Delta}/a), \quad (3.15)$$

where

$$\Delta=4ac-b^2, \quad (3.16)$$

$$\sigma_w(l)=\sum_{\nu|l}\nu^w, \quad (3.17)$$

where $\nu$ are summed over the divisors of $l$ and it is assumed that $\Delta>0$. $K$ is again the modified Bessel function of the second kind. The apparent pole as $q\to\frac{1}{2}$ now vanishes due to a cancellation between the first two terms of (3.15), and we find that letting $q=\frac{1}{2}+\frac{s}{2}$ and taking the limit $s\to 0^+$ (here $a=p^2$, $b=0$, $c=\tau^2$)

$$\mathcal{S}(\tau,p)=\frac{2}{p}\left(\gamma-\ln\frac{4\pi p}{\tau}\right)+\frac{8}{p}\sum_{l=1}^{\infty}\sigma_0(l)K_0(2\pi l\tau/p) \quad (3.18)$$

where $\gamma=0.577216\ldots$ is Euler's constant. Now $\sigma_0(l)$ is simply the number of positive divisors of $l$, $\sigma_0(1)=1$, $\sigma_0(2)=\sigma_0(3)=2$, $\sigma_0(4)=3$ etc. Note that Eq. (3.18) is valid for all $\tau$; although it appears most convenient for large $\tau$, it is, by the symmetry property seen in Eq. (3.13), equally useful for small $\tau$.

We finally write down the final, regularized energy of the wedge (and, simultaneously, cylinder) at finite $T$, using the convention used in Ref. [34]

$$\tilde{\mathcal{E}}(\tau,p,a)=\frac{1}{8\pi na^2}e(\tau,p), \quad (3.19)$$

in terms of

$$e(\tau,p)=\frac{4\tau}{\pi}\sum_{m=0}^{\infty}{}'\sum_{j=0}^{\infty}{}'\tilde{e}_{m,j}(\tau,p)-\frac{\tau}{64}(3-3\tau\partial_\tau+\tau^2\partial_\tau^2)$$
$$\times[1+2\mathcal{K}(\tau)+\mathcal{S}(\tau,p)]. \quad (3.20)$$

with $\tilde{e}_{m,j}$, $\mathcal{K}$, and $\mathcal{S}$ given in Eqs. (3.5), (3.14), and (3.18), respectively. The differentiations with respect to $\tau$ are now straightforward, should the full expanded expression be desirable.

In Fig. 2 we plot the three additional terms in the second line of Eq. (3.20) where we have defined the shorthand

$$\hat{\mathcal{T}}=(3-3\tau\partial_\tau+\tau^2\partial_\tau^2); \quad (3.21a)$$
$$E_S(\tau,p)=\frac{\tau}{64}\hat{\mathcal{T}}\mathcal{S}(\tau,p);$$
$$E_K(\tau,p)=\frac{\tau}{32}\hat{\mathcal{T}}\mathcal{K}(\tau). \quad (3.21b)$$

Figure 3 shows a numerical calculation of $e(\tau,p=3)$ as a function of $\tau$ along with its high and low $\tau$ asymptotes (see derivations in the following sections). The calculation was performed by "brute force" by truncating the sums after a number of terms, and has somewhat limited accu-

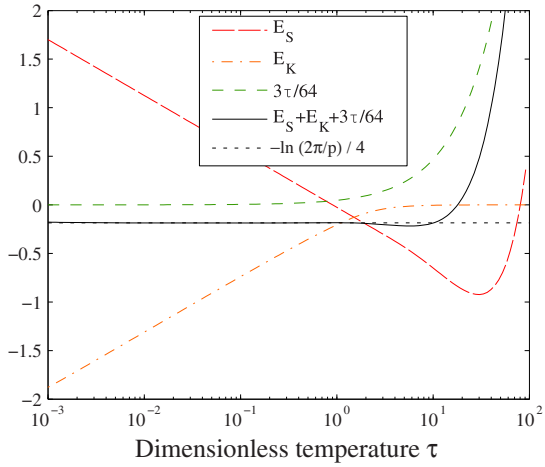


FIG. 2 (color online). The additional terms of the regularized energy in Eq. (3.20) which are subtracted from the double sum there in the case $p=3$. Shown also is the sum of the three additional terms and their low-temperature asymptotic value from Eq. (4.11).

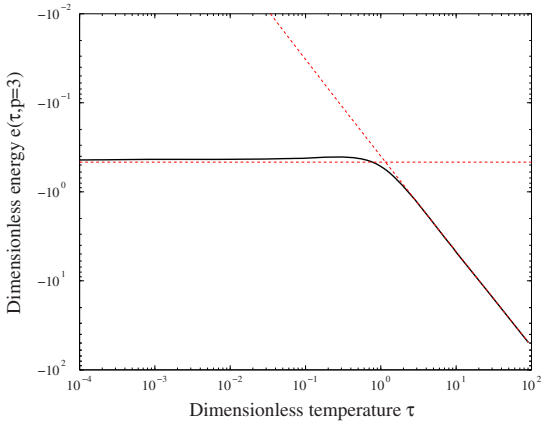


FIG. 3 (color online). Dimensionless energy $e(\tau, p)$ for the case $p = 3$, i.e. opening angle $\alpha = \pi/3$, approximated by a "brute force" calculation truncating the sums. The zero-temperature limit and high-$\tau$ asymptote are shown as dashed lines.

racy due to the large number of terms in the $j$ sum in Eq. (3.20) required for small $\tau$, scaling as $\tau^{-1}$.

## IV. REGAINING THE LIMIT OF ZERO TEMPERATURE

Comparing Eq. (3.20) with the zero-temperature result derived in Ref. [34], and previously known for the cylindrical shell [8,10], it is not obvious that our expression simplifies to the zero-temperature result as $\tau \to 0$. In this section we show that upon careful examination the correct limit is in fact obtained.

Let us write down the zero-temperature result $\tilde{\mathcal{E}}_0$ for general $p$ in its regularized form suitable for comparison[1] [c.f. Ref. [34], Eq. (4.14)]:

$$\tilde{\mathcal{E}}_0 = \frac{1}{2}\bar{\mathcal{E}}_0 + \sum_{m=1}^{\infty}\bar{\mathcal{E}}_m + \frac{1}{32\pi na^2}\ln(2\pi/p); \tag{4.1a}$$

$$\bar{\mathcal{E}}_0 = \frac{1}{4\pi na^2}\int_0^\infty dx x \times\left[\ln(1-x^2\lambda_0^2) + \frac{x^4}{4(1+x^2)^3}\right]; \tag{4.1b}$$

$$\bar{\mathcal{E}}_{m0} = \frac{1}{4\pi na^2}\int_0^\infty dx x \times\left[\ln(1-x^2\lambda_{mp}^2) + \frac{x^4}{4(m^2p^2+x^2)^3}\right]. \tag{4.1c}$$

[1]These definitions of $\bar{\mathcal{E}}_0$ and $\bar{\mathcal{E}}_{m0}$ differ from those of Ref. [34] by a prefactor $n$.

The finite temperature quantity $\bar{\mathcal{E}}$ of Eq. (3.5) is analytic as $\tau \to 0$ and inverse application of the transition (2.5) simply gives us

$$\bar{\mathcal{E}} \overset{\tau\to 0}{\to} \frac{1}{2}\bar{\mathcal{E}}_0 + \sum_{m=1}^{\infty}\bar{\mathcal{E}}_m. \tag{4.2}$$

What remains is essentially to determine the low $\tau$ behavior of $\mathcal{K}(\tau)$ and $\mathcal{S}(\tau, a)$ to check that the last term of Eq. (4.1a) may be regained.

To study the behavior of $\mathcal{S}$ it is convenient to employ the symmetry relation $\mathcal{S}(\tau, p) = \mathcal{S}(p, \tau)$ which gives

$$\mathcal{S}(\tau, p) = \frac{2}{\tau}\left(\gamma - \ln\frac{4\pi\tau}{p}\right) + \frac{8}{\tau}\sum_{l=1}^{\infty}\sigma_0(l)K_0(2\pi lp/\tau). \tag{4.3}$$

For large arguments $K_0(x) \propto \exp(-x)$, so the sum over $l$ is exponentially small as $\tau \to 0$. This immediately gives the asymptotic behavior:

$$\mathcal{S}(\tau, p) \sim \frac{2}{\tau}[\gamma - \ln(2\pi/p) - \ln 2 - \ln\tau], \qquad \tau \to 0. \tag{4.4}$$

Next we turn to $\mathcal{K}(\tau)$. Using the Euler-Maclaurin formula (e.g. Ref. [39], p. 806) we have

$$\begin{aligned}\mathcal{K}(\tau) &= \sum_{l=0}^{\infty}\varkappa(\tau + l\tau) \\ &= \frac{1}{\tau}\int_\tau^\infty dt\varkappa(t) + \frac{1}{2}\varkappa(\tau) - \sum_{l=1}^{\infty}\frac{\tau^{2l-1}B_{2l}}{(2l)!}\varkappa^{(2l-1)}(\tau)\end{aligned} \tag{4.5}$$

with

$$\varkappa(t) = \frac{t - \sqrt{1+t^2}}{t\sqrt{1+t^2}}. \tag{4.6}$$

The integral has the solution

$$\begin{aligned}\int_\tau^\infty dt\varkappa(t) &= \ln\frac{2\tau}{\tau + \sqrt{1+\tau^2}} \\ &= \ln\tau + \ln 2 - \tau + \frac{1}{6}\tau^3 + \ldots\end{aligned} \tag{4.7}$$

as $\tau \to 0$. Moreover, $\varkappa(\tau) = -1/\tau + 1 - \frac{1}{2}\tau^2 + \ldots$, and upon inspection we recognize that

$$\tau^{2l-1}\varkappa^{(2l-1)}(\tau) = \frac{(2l-1)!}{\tau} + (-1)^l\left[\frac{(2l)!}{2^l l!}\right]^2\tau^{2l} + \ldots \tag{4.8}$$

To leading order in $\tau$, thus, the sum in Eq. (4.5) reads $\frac{1}{\tau}\times\sum_{l=1}^{\infty}B_{2l}/2l$. As is typically the case for series expansions close to nonanalytical points, the series is formally divergent. It can, however, be regularized by means of Borel summation [41]. For a highly similar problem and details

on how to approach it, see Ref. [42]. We show in Appendix A that the Borel regularized sum evaluates to

$$\sum_{l=1}^{\infty} \frac{B_{2l}}{2l} = \gamma - \frac{1}{2}. \tag{4.9}$$

Thus we have found the low-$\tau$ expansion of $\mathcal{K}(\tau)$:

$$\mathcal{K}(\tau) \sim \frac{1}{\tau}(\ln\tau + \ln 2 - \gamma) - \frac{1}{2} + \ldots, \qquad \tau \to 0. \tag{4.10}$$

Further terms cancel at least to order $\tau^2$, the leading order correction being at least of order $\tau^4$.

Combining (4.4) and (4.10) we find, to leading order in $\tau$, the expression in square brackets in (3.20):

$$[1 + 2\mathcal{K} + \mathcal{S}] \sim -\frac{2}{\tau}\ln(2\pi/p) + \mathcal{O}(\tau^4), \qquad \tau \to 0 \tag{4.11}$$

and using

$$(3 - 3\tau\partial_\tau + \tau^2\partial_\tau^2)\frac{1}{\tau} = \frac{8}{\tau} \tag{4.12}$$

we regain exactly the zero-temperature result (4.1). As illustrated in Fig. 3 this limit is reached very rapidly as $\tau \to 0$. While we have ascertained in the above that the correction term in (4.11) is at least of order $\tau^4$, there is reason to suspect that the behavior is in fact exponential, as is the case for $\mathcal{S}$ as seen from Eq. (4.3).

## V. HIGH-$\tau$ ASYMPTOTICS: AGREEMENT WITH PREVIOUS RESULTS FOR CYLINDRICAL SHELL

We will finally determine the asymptotic behavior in the limit $\tau \gg 1$. Here the contribution from $\tilde{\mathcal{E}}$ is given by the zeroth Matsubara term only. Consider the reduced energy $e(\tau, p)$ of Eq. (3.20) in which

$$\frac{4\tau}{\pi}\sum_{m=0}^{\infty}{}'\sum_{j=0}^{\infty}{}' \tilde{e}_{m,j}(\tau, p) \sim \frac{2\tau}{\pi}C(p), \qquad \tau \to \infty, \tag{5.1}$$

with

$$C(p) = \frac{1}{2}\int_0^\infty dx\left[\ln(1 - x^2\lambda_0^2) + \frac{x^4}{4(1 + x^2)^3}\right] + \sum_{m=1}^{\infty}\int_0^\infty dx\left[\ln(1 - x^2\lambda_{mp}^2) + \frac{x^4}{4(m^2p^2 + x^2)^3}\right]. \tag{5.2}$$

Some numerical values are

$$C(1) = -0.75814; \tag{5.3a}$$

$$C(2) = -0.76558; \tag{5.3b}$$

$$C(3) = -0.76645. \tag{5.3c}$$

These values were obtained with Mathematica, including 100 terms in the sum while checking convergence.

The high-$\tau$ behavior of $\mathcal{S}$ is given immediately by Eq. (3.18):

$$\mathcal{S}(\tau, p) \sim \frac{2}{p}(\gamma - \ln 4\pi p + \ln\tau), \qquad \tau \to \infty \tag{5.4}$$

where the correction term is exponential, wherewith

$$\tau\partial_\tau\mathcal{S} \sim \frac{2}{p}; \qquad \tau^2\partial_\tau^2\mathcal{S} \sim -\frac{2}{p}.$$

To study the behavior of $\mathcal{K}(\tau)$ and its derivatives it is useful to define $\beta = 1/\tau$ and write $\mathcal{K}(\tau) = \beta\mathcal{H}(\beta)$ with

$$\mathcal{H}(\beta) = \sum_{j=1}^{\infty}\frac{j - \sqrt{j^2 + \beta^2}}{j\sqrt{j^2 + \beta^2}}. \tag{5.5}$$

With a little calculation one ascertains that

$$\tau(3 - 3\tau\partial_\tau + \tau^2\partial_\tau^2)\mathcal{K}(\tau) = (8 + 7\beta\partial_\beta + \beta^2\partial_\beta^2)\mathcal{H}(\beta). \tag{5.6}$$

When $\beta \to 0$ it is simple to see from

$$\mathcal{H}'(\beta) = -\beta\sum_{j=1}^{\infty}(j^2 + \beta^2)^{-(3/2)}; \tag{5.7a}$$

$$\mathcal{H}''(\beta) = \sum_{j=1}^{\infty}\frac{2\beta^2 - j^2}{(j^2 + \beta^2)^{5/2}}; \tag{5.7b}$$

that

$$\mathcal{H}(\beta) \sim \frac{1}{2}\beta\mathcal{H}'(\beta) \sim \frac{1}{2}\beta^2\mathcal{H}''(\beta) \sim -\frac{1}{2}\beta^2\zeta(3), \qquad \beta \to 0.$$

Hence we can safely ignore the term involving $\mathcal{K}$ at high $\tau$.

Combining this, the high-$\tau$ behavior of $e(\tau, p)$ is

$$e(\tau, p) \sim \tau\left[\frac{2C(p)}{\pi} - \frac{3p + 6(\gamma - \ln 4\pi p) - 8}{64p} - \frac{3}{32p}\ln\tau\right]. \tag{5.8}$$

The high-temperature asymptotics of perfectly conducting spherical and cylindrical shells with vacuum inside and outside were calculated by Bordag, Nesterenko, and Pirozhenko [20,21] using the method of heat kernel coefficients. They, like us, found that the two leading order terms were of order $T$ and $T\ln T$ as $T \to \infty$. The latter of these terms had been worked out some time previously by Balian and Duplantier [19], who also found an approximate (though not very accurate) value for the former.

The result of the calculations reported in [21] was, in our notation

$$\tilde{\mathcal{E}}_{\rm cyl} \sim -0.22924\frac{T}{a} - \frac{3T}{64a}\ln\frac{aT}{2} + \mathcal{O}(T^{-1}) = -\frac{\tau}{8\pi a^2}\left[0.44237 + \frac{3}{16}\ln\tau + \mathcal{O}(\tau^{-2})\right]. \tag{5.9}$$

As previously mentioned, $\tilde{\mathcal{E}}_{\rm cyl} = 2\tilde{\mathcal{E}}_{p=1}$. With the expansion (5.8) we find, using (5.3a),

$$2\tilde{\mathcal{E}}_{p=1} \sim -\frac{\tau}{8\pi a^2}\left[\frac{6\gamma - 5 - 6\ln 4\pi}{32} - \frac{4}{\pi}C(1) + \frac{3}{16}\ln\tau + \ldots\right] = -\frac{\tau}{8\pi a^2}\left[0.44270 + \frac{3}{16}\ln\tau + \ldots\right]. \quad (5.10)$$

The slight numerical difference we believe to be due to the approximate numerical method used in [21]. We show analytically in Appendix B that the correspondence is in fact exact.

One may note the absence in Eq. (5.8) of a specific term proportional to $T^2$ found for the non-closed wedge in Ref. [27]and attributed to the presence of the wedge apex. This term does not refer to the radius $a$, however, and has thus been subtracted from our free energy expression ab initio. Likewise, a Stefan-Boltzmann energy term proportional to $T^4$ is in general present, but is geometry independent and does not contribute to the free energy (c.f. Ref. [21] for a discussion)

## VI. WEDGE WITH DIAPHANOUS ARC

The above results can easily be extended to the case where the perfectly conducting arc is replaced by a diaphanous arc, that is, a magnetodielectric interface so that the product $n^2 = \varepsilon\mu$ is the same for radii both smaller than and greater than $a$ as shown in Fig. 4. This geometry was considered at zero temperature in Ref. [34]. The electromagnetic boundary conditions at the arc separate in a simple way in this case and the dependence on material properties enters only through the reflection coefficient

$$\xi = \frac{\varepsilon_2 - \varepsilon_1}{\varepsilon_2 + \varepsilon_1} = -\frac{\mu_2 - \mu_1}{\mu_2 + \mu_1}. \quad (6.1)$$

The change in geometry leaves the energy expression (2.3) unaltered but for the simple replacement

$$\ln[1 - x^2\lambda_{mp}^2(x)] \to \ln[1 - \xi^2 x^2 \lambda_{mp}^2(x)]. \quad (6.2)$$

This merely introduces a prefactor $\xi^2$ in all correction terms, and we can write down the result for the diaphanous wedge, and simultaneously cylinder (by letting $p = 1$ and multiplying by 2 as discussed above), as:

$$\tilde{\mathcal{E}}_\xi(\tau, p, a) = \frac{1}{8\pi n a^2} e_\xi(\tau, p); \quad (6.3a)$$

$$e_\xi(\tau, p) = \frac{4\tau}{\pi}{\sum_{m=0}^{\infty}}' {\sum_{j=0}^{\infty}}' \tilde{e}_{m,j}(\tau, p, \xi) - \frac{\tau\xi^2}{64}(3 - 3\tau\partial_\tau + \tau^2\partial_\tau^2) \times [1 + 2\mathcal{K}(\tau) + \mathcal{S}(\tau, p)], \quad (6.3b)$$

wherein

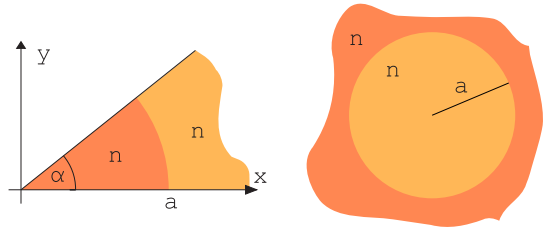


FIG. 4 (color online). Same geometry as in Fig. 1 but now with diaphanous instead of perfectly conducting arc, i.e., so that $n^2 = \varepsilon\mu$ is the same both sides of the interface. We still assume nondispersive media.

$$\tilde{e}_{m,j}(\tau, p, \xi) = \int_{j\tau}^{\infty} \frac{dxx}{\sqrt{x^2 - j^2\tau^2}}\left\{\ln[1 - \xi^2 x^2 \lambda_{mp}^2(x)] + \frac{\xi^2 x^4}{4(m^2p^2 + x^2)^3}\right\}; \quad (6.3c)$$

$$\tilde{e}_{0,j}(\tau, \xi) = \int_{j\tau}^{\infty} \frac{dxx}{\sqrt{x^2 - j^2\tau^2}}\left\{\ln[1 - \xi^2 x^2 \lambda_0^2(x)] + \frac{\xi^2 x^4}{4(1 + x^2)^3}\right\}. \quad (6.3d)$$

Since $\xi$ enters the correction terms from renormalization only through the prefactor, generalization of the weak-coupling expansions (to leading order in $\xi^2$) considered in [34] to nonzero $\tau$ is trivial.

## VII. CONCLUDING REMARKS

We have given for the first time results for the temperature dependence of the Casimir energy for a wedge, closed by a circular arc, all boundaries being perfectly conducting. This includes, as a special case, the perfectly conducting cylindrical shell case. (Except for that case, there is a divergent term, due to the corner where the circular arc meets the wedge boundaries, which we here simply omit.) The low-temperature result agrees with the zero-temperature result found previously, except for what is probably an exponentially small correction, while the high-temperature result agrees with that of Bordag, Nesterenko, and Pirozhenko for the case of a cylinder [21].

## ACKNOWLEDGMENTS

The work of K. A. M. was supported in part by grants from the U. S. National Science Foundation and the U. S. Department of Energy. We thank Professor Vladimir Nesterenko for several useful comments on the manuscript.

## APPENDIX A: EVALUATION OF EQ. (4.9) BY BOREL SUMMATION

To evaluate a (possibly divergent) series $Z = \sum_{l=1}^{\infty} a_l$ by Borel summation [41] we define the function

$$\phi(x) = \sum_{l=1}^{\infty} \frac{a_l}{l!} x^l. \tag{A1}$$

If $\phi(x)$ is finite for sufficiently small $x$, we define the Borel transform as

$$\mathcal{B}(x) = \int_0^\infty dt e^{-t} \phi(xt), \tag{A2}$$

from which the Borel regularized value of the sum $Z$ is $Z = \mathcal{B}(1)$. We consider the sum

$$\sum_{l=1}^{\infty} \frac{B_{2l}}{2l} = \frac{1}{2} + \sum_{l=1}^{\infty} \frac{B_l}{l}, \tag{A3}$$

since $B_1 = -1/2$ and $B_3 = B_5 = B_7 = \ldots = 0$. The Borel transform of the latter sum is thus

$$\mathcal{B}(x) = \int_0^\infty dt e^{-t} \sum_{l=1}^{\infty} \frac{B_l}{l \cdot l!} (xt)^l. \tag{A4}$$

The generating function of the Bernoulli numbers is

$$\sum_{l=1}^{\infty} \frac{B_l}{l!} y^l = \frac{y}{e^y - 1} - 1 \tag{A5}$$

which allows us to evaluate

$$\begin{aligned} \frac{d\mathcal{B}}{dx}(x) &= \frac{1}{x} \int_0^\infty dt e^{-t} \sum_{l=1}^{\infty} \frac{B_l}{l!} (xt)^l = \int_0^\infty \frac{dt t e^{-t}}{e^{xt} - 1} - \frac{1}{x} \\ &= x^{-2} \int_0^\infty \frac{du u e^{-u(x+1)/x}}{1 - e^{-u}} - \frac{1}{x} \\ &= x^{-2} \psi^{(1)}\left(\frac{x+1}{x}\right) - \frac{1}{x}, \end{aligned} \tag{A6}$$

where $\psi^{(n)}(x)$ is the polygamma function, whose integral representation was recognized (Ref. [39] Eq. 6.4.1) by making the substitution $u = xt$. Thus we evaluate the integral to

$$\begin{aligned} \mathcal{B}(x) + \ln x &= \int^x \frac{dy}{y^2} \psi^{(1)}\left(\frac{y+1}{y}\right) \\ &= -\int^{(x+1)/x} dv \psi^{(1)}(v) \\ &= -\psi\left(\frac{x+1}{x}\right) + \text{constant}, \end{aligned} \tag{A7}$$

where from the requirement that $\mathcal{B}(0) = 0$ we see that the integration constant is zero. Thus we find the Borel value of the sum (A3) to be

$$\sum_{l=1}^{\infty} \frac{B_{2l}}{2l} = \frac{1}{2} + \mathcal{B}(1) = \gamma - \frac{1}{2}, \tag{A8}$$

noting that $\psi(2) = 1 - \gamma$.

## APPENDIX B: CORRESPONDENCE WITH HIGH-$T$ ASYMPTOTICS FOR THE CYLINDER IN VACUUM

The heat kernel expansion for high temperatures calculated in Ref. [21] for the cylindrical shell in vacuum begins

$$\begin{aligned} \tilde{\mathcal{E}}_{\text{cyl}} &\sim -\frac{T}{2}\zeta'(0) - \frac{a_{3/2}}{(4\pi)^{3/2}} T \ln T + \ldots \\ &= -\frac{\tau}{8\pi a^2}\left[2a\zeta'(0) - \frac{3}{16}\ln 2\pi a + \frac{3}{16}\ln\tau + \ldots\right] \end{aligned} \tag{B1}$$

where the "zeta determinant" $\zeta'(0)$ is a constant defined in Ref. [21] and we have inserted their value [20,21]

$$\frac{a_{3/2}}{(4\pi)^{3/2}} = \frac{3}{64a}. \tag{B2}$$

The term proportional to $\tau \ln\tau$ is obviously identical to our expression in Eq. (5.10). We consider only the term linear in $\tau$. Comparison with (5.10) gives, with minimal manipulation, that the asymptotes correspond exactly according to $\tilde{\mathcal{E}}_{\text{cyl}} = 2\tilde{\mathcal{E}}_{p=1}$, provided

$$\pi a \zeta'(0) + 2C(1) = \frac{\pi}{64}\left[6\gamma - 5 + 6\ln\frac{a}{2}\right]. \tag{B3}$$

In Appendix B of [21] we find the following expression

$$\begin{aligned} \pi a \zeta'(0) = &\int_0^\infty dy y \frac{d}{dy} \ln[1 - y^2 \lambda_0^2(y)] + 2\sum_{m=1}^{\infty} m \int_0^\infty dy y \\ &\times \frac{d}{dy}\left\{\ln\left[1 - m^2 y^2 \lambda_m^2(my)\right] + \frac{y^4 t^6}{4m^2}\right\} \\ &+ \frac{\pi}{32}\left(3\gamma - 4 + 3\ln\frac{a}{2}\right) \end{aligned} \tag{B4}$$

with $t = 1/\sqrt{1+y^2}$. Let us call the two integrals in (B4) $X_0$ and $X_m$, where the latter is the integral inside the sum. After a partial integration and, in the case of $X_m$, a substitution $ym = x$, these can be written on the familiar form

$$X_0 = -\int_0^\infty dx \ln[1 - x^2 \lambda_0^2(x)] \tag{B5a}$$

$$X_m = -\frac{1}{m}\int_0^\infty dx \left\{\ln[1 - x^2 \lambda_m^2(x)] + \frac{z^4}{4(m^2 + x^2)^3}\right\}. \tag{B5b}$$

Comparing with (5.2) we see that

$$\begin{aligned} \pi a \zeta'(0) + 2C(1) &= \int_0^\infty \frac{dx x^4}{4(1+x^2)^3} + \frac{\pi}{32}\left(3\gamma - 4 + 3\ln\frac{a}{2}\right) \\ &= \frac{\pi}{64}\left[6\gamma - 5 + 6\ln\frac{a}{2}\right] \end{aligned} \tag{B6}$$

since $\frac{1}{4}\int_0^\infty dx x^4/(1+x^2)^3 = 3\pi/64$. We have thus shown the correspondence analytically.

[1] H. B. G. Casimir, Proc. K. Ned. Akad. Wet. **51**, 793 (1948).
[2] S. K. Lamoreaux, Phys. Rev. Lett. **78**, 5 (1997).
[3] M. Bordag, G. L. Klimchitskaya, U. Mohideen, and V. M. Mostepanenko, *Advances in The Casimir Effect* (Oxford University Press, Oxford, 2009).
[4] K. A. Milton, J. Phys. A **37**, R209 (2004).
[5] K. A. Milton, *The Casimir Effect: Physical Manifestations of the Zero-Point Energy* (World Scientific, Singapore, 2001).
[6] E. M. Lifshitz, Zh. Eksp. Teor. Fiz. **29**, 94 (1955) [Sov. Phys. JETP **2**, 73 (1956)].
[7] T. H. Boyer, Phys. Rev. **174**, 1764 (1968).
[8] L. L. DeRaad, Jr. and K. A. Milton, Ann. Phys. (N.Y.) **186**, 229 (1981).
[9] P. Gosdzinsky and A. Romeo, Phys. Lett. B **441**, 265 (1998).
[10] K. A. Milton, A. V. Nesterenko, and V. V. Nesterenko, Phys. Rev. D **59**, 105009 (1999).
[11] G. Lambiase, V. V. Nesterenko, and M. Bordag, J. Math. Phys. (N.Y.) **40**, 6254 (1999).
[12] H. Razmi and N. Fadaei, Nucl. Phys. B **814**, 582 (2009).
[13] I. Brevik and G. H. Nyland, Ann. Phys. (N.Y.) **230**, 321 (1994).
[14] V. V. Nesterenko and I. G. Pirozhenko, Phys. Rev. D **60**, 125007 (1999).
[15] I. Cavero-Peláez and K. A. Milton, Ann. Phys. (N.Y.) **320**, 108 (2005); J. Phys. A **39**, 6225 (2006).
[16] A. Romeo and K. A. Milton, Phys. Lett. B **621**, 309 (2005); J. Phys. A **39**, 6703 (2006).
[17] I. Cavero-Peláez, K. A. Milton, and K. Kirsten, J. Phys. A **40**, 3607 (2007).
[18] I. Brevik and A. Romeo, Phys. Scr. **76**, 48 (2007).
[19] R. Balian and B. Duplantier, Ann. Phys. (N.Y.) **112**, 165 (1978).
[20] M. Bordag, V. Nesterenko, and I. Pirozhenko, Nucl. Phys. B **104**, 228 (2002).
[21] M. Bordag, V. V. Nesterenko, and I. G. Pirozhenko, Phys. Rev. D **65**, 045011 (2002).
[22] J. S. Dowker and G. Kennedy, J. Phys. A **11**, 895 (1978).
[23] D. Deutsch and P. Candelas, Phys. Rev. D **20**, 3063 (1979).
[24] I. Brevik and M. Lygren, Ann. Phys. (N.Y.) **251**, 157 (1996).
[25] I. Brevik, M. Lygren, and V. Marachevsky, Ann. Phys. (N.Y.) **267**, 134 (1998).
[26] I. Brevik and K. Pettersen, Ann. Phys. (N.Y.) **291**, 267 (2001).
[27] V. V. Nesterenko, G. Lambiase, and G. Scarpetta, Ann. Phys. (N.Y.) **298**, 403 (2002).
[28] H. Razmi and S. M. Modarresi, Int. J. Theor. Phys. **44**, 229 (2005).
[29] V. V. Nesterenko, G. Lambiase, and G. Scarpetta, J. Math. Phys. (N.Y.) **42**, 1974 (2001).
[30] V. V. Nesterenko, I. G. Pirozhenko, and J. Dittrich, Classical Quantum Gravity **20**, 431 (2003).
[31] A. H. Rezaeian and A. A. Saharian, Classical Quantum Gravity **19**, 3625 (2002).
[32] A. A. Saharian, Eur. Phys. J. C **52**, 721 (2007).
[33] A. A. Saharian, in *The Casimir Effect and Cosmology: A volume in honour of Professor Iver H. Brevik on the occasion of his 70th birthday*, edited by S. Odintsov *et al.* (Tomsk State Pedagogical University Press, Tomsk, Russia, 2008), p. 87.
[34] I. Brevik, S. Å. Ellingsen, and K. A. Milton, Phys. Rev. E **79**, 041120 (2009).
[35] S. Å. Ellingsen, I. Brevik, and K. A. Milton, Phys. Rev. E **80**, 021125 (2009).
[36] K. A. Milton, J. Wagner, and K. Kirsten, Phys. Rev. D **80**, 125028 (2009).
[37] J. Wagner, K. A. Milton, and K. Kirsten, arXiv:0912.2374, to appear in the Proceedings of the 9th Conference on Quantum Field Theory Under the Influence of External Conditions (QFEXT09).
[38] I. Brevik, S. Å. Ellingsen, and K. A. Milton, arXiv:0911.2688, to appear in the Proceedings of the 9th Conference on Quantum Field Theory Under the Influence of External Conditions (QFEXT09).
[39] M. Abramowitz and I. A. Stegun, *Handbook of Mathematical Functions* (Dover, New York, 1964).
[40] E. Elizalde, *Ten Physical Applications of Spectral Zeta Functions* (Springer, Berlin, 1995).
[41] C. M. Bender and S. A. Orszag, *Advanced Mathematical Methods for Scientists and Engineers* (Springer, Berlin, 1999), Chap. 8.2.
[42] S. A. Ellingsen, I. Brevik, J. S. Høye, and K. A. Milton, Phys. Rev. E **78**, 021117 (2008).

# Part III

## Casimir-Polder effect out of thermal equilibrium

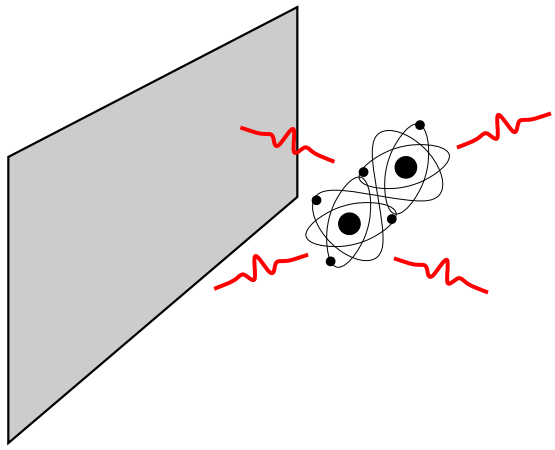

# Article [I]

***Dynamics of thermal Casimir-Polder forces on polar molecules***

S.Å. Ellingsen, S.Y. Buhmann, S. Scheel

Physical Review A **79**, 052903 (2009)

# Dynamics of thermal Casimir-Polder forces on polar molecules

Simen Ådnøy Ellingsen
*Department of Energy and Process Engineering, Norwegian University of Science and Technology, N-7491 Trondheim, Norway*

Stefan Yoshi Buhmann and Stefan Scheel
*Quantum Optics and Laser Science, Blackett Laboratory, Imperial College London, Prince Consort Road, London SW7 2AZ, United Kingdom*

(Received 10 December 2008; published 7 May 2009)

We study the influence of thermal Casimir-Polder forces on the near-surface trapping of cold polar molecules, with emphasis on LiH and YbF near a Au surface at room temperature. We show that even for a molecule initially prepared in its electronic and rovibrational ground state, the Casimir-Polder force oscillates with the molecule-wall separation. The nonresonant force and the evanescent part of the resonant force almost exactly cancel at high temperature which results in a saturation of the (attractive) force in this limit. This implies that the Casimir-Polder force on a fully thermalized molecule can differ dramatically from that obtained using a naive perturbative expansion of the Lifshitz formula based on the molecular ground-state polarizability. A dynamical calculation reveals how the spatial oscillations die out on a typical time scale of several seconds as thermalization of the molecule with its environment sets in.

DOI: 10.1103/PhysRevA.79.052903 PACS number(s): 34.35.+a, 12.20.−m, 42.50.Ct, 42.50.Nn

## I. INTRODUCTION

Cold ensembles of polar molecules such as YbF have recently received particular attention due to their potential use as ultrasensitive probes of the permanent electric dipole moment of the electron [1], measurements of which allow for investigating the possible existence of physics beyond the standard model [2]. The need for longer interrogation times has led to the development of Stark deceleration techniques for these heavy molecules [3,4], with a view to ultimately be able to trap molecules near microstructured surfaces (chips). Recently, trapping of light molecules such as metastable CO in traveling potential wells near a chip surface was achieved [5]. Another light diatomic molecule that has received considerable attention due to its large dipole moment is LiH, and the production of supersonic beams of cold LiH has been reported [6].

When attempting to trap polar molecules in close proximity to a surface, attractive Casimir-Polder (CP) forces [7]—effective electromagnetic forces between a neutral and polarizable particle and a macroscopic object—need to be taken into account as an important limiting factor. Thermal CP forces on atoms at thermal equilibrium with both the electromagnetic field and the present macroscopic bodies have been intensively studied in the past on the basis of Lifshitz theory [8–11], linear response theory [12,13], or normal-mode techniques [14,15]. At room temperature, the energies associated with atomic transitions are much larger than the thermal energy, $\hbar\omega_A \gg k_B T$, resulting in very low thermal photon numbers. A "high-temperature limit" is only accessible in a geometric sense when the atom-surface separation $z_A$ is much larger than the thermal wavelength, $z_A \gg \hbar c/(2\pi k_B T)$; in this case the thermal CP force on the atom can be approximated by [12,13]

$$\boldsymbol{F}(\boldsymbol{r}_A) \approx -\frac{|\boldsymbol{d}_A|^2}{8\pi\varepsilon_0 z_A^4}\frac{k_B T}{\hbar\omega_A}\boldsymbol{e}_z \tag{1}$$

for a two-level atom (transition frequency $\omega_A$, dipole matrix element $\boldsymbol{d}_A$) interacting with a perfectly conducting plate (unit normal $\boldsymbol{e}_z$).

The situation is different for molecules: whereas transition energies of atoms are typically much larger than attainable thermal energies, the energies associated with rotational and vibrational transitions of molecules, heavy molecules in particular, are often small compared to the thermal energy even at room temperature. A genuine high-temperature limit $\hbar\omega_A \ll k_B T$ is hence realized with an associated large number of thermal photons being present. An additional consequence of the long transition wavelengths is the fact that CP forces on molecules are expected to have a long range with the nonretarded regime $z_A \ll c/\omega_A$ extending quite far out from the surface. A naive application of above formula (1) for atoms beyond its scope to the high-temperature limit $\hbar\omega_A \ll k_B T$ would suggest that the force can get arbitrarily strong for molecules of smaller and smaller transition energies, which already indicates that CP forces on molecules must be treated with care.

Supersonic beam expansions typically produce cold molecules that are to a large fraction in their rovibrational ground states. For example, in the experiment reported in Ref. [6], 90% of the observed cold LiH molecules were in their electronic and rovibrational ground state $X\,^1\Sigma^+$. The cold molecule and the room-temperature surface are thus strongly out of equilibrium with respect to each other, so a study of the CP interaction necessitates that account be taken of the full nonequilibrium dynamics of the rotational and vibrational degrees of freedom of the cold molecule coupled to its thermal environment. In contrast, in the context of nonequilibrium forces on thermalized atoms in an environment of nonuniform temperature, as recently proposed [16]

 

and measured [17], a study of the full internal atomic dynamics was not necessary.

In this paper, we study the nonequilibrium thermal CP force on a polar molecule which is initially in its electronic and rovibrational ground state in the vicinity of a metal surface. A recently developed dynamical theory of forces on single atoms or molecules in arbitrary internal states and arbitrary uniform temperature environments [18] provides the necessary framework (note that a similar theory has been developed for two-atom van der Waals forces [19]). In particular, we will show that in contrast to the above intuitive expectation obtained from comparison with the atom case, the attractive CP force on a molecule saturates in the high-temperature limit.

## II. CASIMIR–POLDER FORCE FOR GIVEN MOLECULAR STATES

We consider a polar molecule (energy eigenstates $|n\rangle$, eigenenergies $\hbar\omega_n$, transition frequencies $\omega_{mn}=\omega_m-\omega_n$, and dipole matrix elements $\boldsymbol{d}_{mn}$) which is prepared in an incoherent superposition of its energy eigenstates with probabilities $p_n$. As shown in Ref. [18], the thermal CP force on such a molecule is given by

$$\boldsymbol{F}(\boldsymbol{r}_A)=\sum_n p_n \boldsymbol{F}_n(\boldsymbol{r}_A) \tag{2}$$

with perturbative force components

$$\begin{aligned}\boldsymbol{F}_n(\boldsymbol{r}_A)=&-\mu_0 k_B T\sum_{N=0}^{\infty}{}'\left(1-\frac{1}{2}\delta_{N0}\right)\xi_N^2\\&\times\boldsymbol{\nabla}_A\,\mathrm{Tr}[\boldsymbol{\alpha}_n(i\xi_N)\cdot\mathbf{G}^{(1)}(\boldsymbol{r}_A,\boldsymbol{r}_A,i\xi_N)]\\&+\mu_0\sum_k \omega_{nk}^2\{\Theta(\omega_{nk})[n(\omega_{nk})+1]-\Theta(\omega_{kn})n(\omega_{kn})\}\\&\times\boldsymbol{\nabla}_A\boldsymbol{d}_{nk}\cdot\mathrm{Re}\,\mathbf{G}^{(1)}(\boldsymbol{r}_A,\boldsymbol{r}_A,|\omega_{nk}|)\cdot\boldsymbol{d}_{kn}\end{aligned} \tag{3}$$

and molecular polarizability

$$\boldsymbol{\alpha}_n(\omega)=\lim_{\epsilon\to 0}\frac{1}{\hbar}\sum_k\left[\frac{\boldsymbol{d}_{kn}\boldsymbol{d}_{nk}}{\omega+\omega_{kn}+i\epsilon}-\frac{\boldsymbol{d}_{nk}\boldsymbol{d}_{kn}}{\omega-\omega_{kn}+i\epsilon}\right]. \tag{4}$$

Here, $\mathbf{G}^{(1)}$ is the scattering part of the classical Green tensor for the electromagnetic field in the given environment and $\xi_N=2\pi k_B TN/\hbar$ denotes the Matsubara frequencies. The CP force (3) contains both nonresonant contributions (first term) and resonant ones (second term), where the former would also follow from applying Lifshitz theory in conjunction with the ground-state polarizability (we refer to it as Lifshitz-type force in the following) and the latter are due to the absorption and emission of thermal photons with photon number

$$n(\omega)=\frac{1}{e^{\hbar\omega/(k_B T)}-1}. \tag{5}$$

Given a probability distribution $p_n$, Eq. (3) allows us to compute the thermal CP force. In particular, if the molecule is in an isotropic state such as the ground state or a thermal state (see below), the force simplifies to [18]

$$\begin{aligned}\boldsymbol{F}_n(\boldsymbol{r}_A)=&-\mu_0 k_B T\sum_{N=0}^{\infty}{}'\left(1-\frac{1}{2}\delta_{N0}\right)\xi_N^2\alpha_n(i\xi_N)\\&\times\boldsymbol{\nabla}_A\,\mathrm{Tr}[\mathbf{G}^{(1)}(\boldsymbol{r}_A,\boldsymbol{r}_A,i\xi_N)]\\&+\frac{\mu_0}{3}\sum_k \omega_{nk}^2\{\Theta(\omega_{nk})[n(\omega_{nk})+1]-\Theta(\omega_{kn})n(\omega_{kn})\}\\&\times|\boldsymbol{d}_{nk}|^2\boldsymbol{\nabla}_A\,\mathrm{Tr}\,\mathrm{Re}\,\mathbf{G}^{(1)}(\boldsymbol{r}_A,\boldsymbol{r}_A,|\omega_{nk}|)\end{aligned} \tag{6}$$

with

$$\alpha_n(\omega)=\lim_{\epsilon\to 0}\frac{1}{3\hbar}\sum_k\left[\frac{|\boldsymbol{d}_{nk}|^2}{\omega+\omega_{kn}+i\epsilon}-\frac{|\boldsymbol{d}_{nk}|^2}{\omega-\omega_{kn}+i\epsilon}\right]. \tag{7}$$

### A. Molecule near a plane surface

For example, let us consider a molecule at a distance $z_A$ from the planar surface of a (nonmagnetic) substrate. The respective scattering Green's tensor is given by [20]

$$\begin{aligned}\mathbf{G}^{(1)}(\boldsymbol{r},\boldsymbol{r},\omega)=&\frac{i}{8\pi}\int_0^{\infty}dq\frac{q}{\beta}e^{2i\beta z}\\&\times\left[\left(r_s-\frac{\beta^2c^2}{\omega^2}r_p\right)(\boldsymbol{e}_x\boldsymbol{e}_x+\boldsymbol{e}_y\boldsymbol{e}_y)+2\frac{q^2c^2}{\omega^2}r_p\boldsymbol{e}_z\boldsymbol{e}_z\right],\end{aligned} \tag{8}$$

where

$$r_s=\frac{\beta-\beta_1}{\beta+\beta_1},\quad r_p=\frac{\varepsilon(\omega)\beta-\beta_1}{\varepsilon(\omega)\beta+\beta_1} \tag{9}$$

with $\mathrm{Im}\,\beta,\ \mathrm{Im}\,\beta_1\geq 0$ are the Fresnel reflection coefficients for $s$- and $p$-polarized waves, $\beta=\sqrt{\omega^2/c^2-q^2}$ and $\beta_1=\sqrt{\varepsilon(\omega)\omega^2/c^2-q^2}$ are the $z$ components of the wave vectors in free space and inside the substrate, and $\varepsilon(\omega)$ is the (relative) permittivity of the substrate. Substitution of $\mathbf{G}^{(1)}(\boldsymbol{r},\boldsymbol{r},\omega)$ into Eq. (6) above leads to an explicit form for the CP force.

The results simplify in the nonretarded and retarded limits of small and large atom-surface separations. In the nonretarded limit $\max_i\{|\sqrt{\varepsilon(\omega_i)}|\omega_i\}z_A/c\ll 1$ ($\omega_i$: relevant molecular and medium frequencies), the approximation $\beta\simeq\beta_1\simeq iq$ leads to

$$\begin{aligned}\boldsymbol{F}_n(\boldsymbol{r}_A)=&-\frac{3k_BT}{8\pi\varepsilon_0 z_A^4}\sum_{N=0}^{\infty}{}'\left(1-\frac{1}{2}\delta_{N0}\right)\alpha_n(i\xi_N)\frac{\varepsilon(i\xi_N)-1}{\varepsilon(i\xi_N)+1}\boldsymbol{e}_z\\&-\frac{1}{8\pi\varepsilon_0 z_A^4}\sum_k|\boldsymbol{d}_{nk}|^2\left\{\Theta(\omega_{nk})[n(\omega_{nk})+1]\frac{|\varepsilon(\omega_{nk})|^2-1}{|\varepsilon(\omega_{nk})+1|^2}\right.\\&\left.-\Theta(\omega_{kn})n(\omega_{kn})\frac{|\varepsilon(\omega_{kn})|^2-1}{|\varepsilon(\omega_{kn})+1|^2}\right\}\boldsymbol{e}_z.\end{aligned} \tag{10}$$

Note that while applying well to dielectrics, the nonretarded limit often provides a very poor approximation for metals because the large factor $|\sqrt{\varepsilon(\omega_i)}|$ may restrict its range of applicability to extremely small distances.

In the retarded limit $\omega_{\min} z_A/c \gg 1$ ($\omega_{\min}$: minimum of the relevant molecular and medium frequencies), the resonant part of the force is well approximated by letting $q \simeq 0$, while the approximations $\alpha_n(i\xi_N) \simeq \alpha_n(0)$ and $\varepsilon(i\xi_N) \simeq \varepsilon(0)$ hold for those $\xi_N$ giving the main contribution to the nonresonant part. The $q$ integral for the $N=0$ term can then be carried out immediately, while those for the remaining part of the sum can be rewritten in a more convenient form by introducing the integration variable $v=\beta c/\xi_N$. Performing the sum according to

$$\sum_{N=1}^{\infty} N^4 y^N = \frac{y^4 + 11y^3 + 11y^2 + 1}{(1-y)^5}, \tag{11}$$

one finds

$$\begin{aligned}
\boldsymbol{F}_n(\boldsymbol{r}_A) = & -\frac{3k_B T \alpha_n(0)}{16\pi\varepsilon_0 z_A^4} \frac{\varepsilon(0)-1}{\varepsilon(0)+1} \boldsymbol{e}_z \\
& - \frac{k_B T \alpha_n(0)}{2\pi\varepsilon_0 z_A^4} \int_1^{\infty} dv v \left[ -\frac{v - \sqrt{\varepsilon(0)-1+v^2}}{v + \sqrt{\varepsilon(0)-1+v^2}} \right. \\
& \left. + (2v^2-1) \frac{\varepsilon(0) v - \sqrt{\varepsilon(0)-1+v^2}}{\varepsilon(0) v + \sqrt{\varepsilon(0)-1+v^2}} \right] \\
& \times \frac{x^4 (e^{-8vx} + 11e^{-6vx} + 11e^{-4vx} + e^{-2vx})}{(1-e^{-2vx})^5} \boldsymbol{e}_z \\
& + \frac{\mu_0}{6\pi c z_A} \sum_k |d_{nk}|^2 \left\{ \Theta(\omega_{nk}) \omega_{nk}^3 [n(\omega_{nk})+1] \right. \\
& \times \mathrm{Im}\left[ e^{2i\omega_{nk} z_A/c} \frac{\sqrt{\varepsilon(\omega_{nk})}-1}{\sqrt{\varepsilon(\omega_{nk})}+1} \right] \boldsymbol{e}_z - \Theta(\omega_{kn}) \omega_{kn}^3 \\
& \left. \times n(\omega_{kn}) \mathrm{Im}\left[ e^{2i\omega_{kn} z_A/c} \frac{\sqrt{\varepsilon(\omega_{kn})}-1}{\sqrt{\varepsilon(\omega_{kn})}+1} \right] \boldsymbol{e}_z \right\},
\end{aligned} \tag{12}$$

where $x=2\pi k_B T z_A/(\hbar c)$. In particular, for a conductor whose plasma frequency $\omega_P$ is large compared to $\omega_{nk}$ [cf. Eq. (14) below] one has $|\varepsilon| \gg 1$ and the retarded CP force is well approximated by

$$\begin{aligned}
\boldsymbol{F}_n(\boldsymbol{r}_A) \approx & -\frac{3k_B T \alpha_n(0)}{16\pi\varepsilon_0 z_A^4} \boldsymbol{e}_z - \frac{k_B T \alpha_n(0)}{8\pi\varepsilon_0 z_A^4} \frac{1}{(e^{2x}-1)^4} \\
& \times [(3+6x+6x^2+4x^3)e^{6x} - (9+12x-16x^3)e^{4x} \\
& + (9+6x-6x^2+4x^3)e^{2x} - 3] \boldsymbol{e}_z \\
& + \frac{\mu_0}{6\pi c z_A} \sum_k |\boldsymbol{d}_{nk}|^2 \{ \Theta(\omega_{nk}) \omega_{nk}^3 [n(\omega_{nk})+1] \\
& \times \sin(2\omega_{nk} z_A/c) \boldsymbol{e}_z - \Theta(\omega_{kn}) \omega_{kn}^3 n(\omega_{kn}) \\
& \times \sin(2\omega_{kn} z_A/c) \boldsymbol{e}_z \}.
\end{aligned} \tag{13}$$

Note that the retarded limit as given above holds for all distances which are sufficiently large with respect to the atomic and medium wavelengths, irrespective of the temperature. When in addition the distance is very large with respect to the thermal wavelength (such that $x \gg 1$), the contribution from the second terms in above Eqs. (12) and (13) vanishes and the nonresonant force approaches its well-known (geometric) high-temperature limit [cf. Eq. (1)]. In the opposite case of a distance which is much smaller than the thermal wavelength ($x \ll 1$), the first terms vanish and the nonresonant force reduces to its (retarded) zero-temperature form (cf. Ref. [21]). Our results, in particular those for the nonretarded limit, agree with the ones previously obtained in Ref. [15]. Note that resonant force components and their oscillatory behavior in the retarded regime were first discussed for excited atoms at zero temperature (cf., e.g., Refs. [22,23]).

The limits reveal that the CP force follows a $1/z_A^4$ power law for nonretarded distances. In the retarded regime, the nonresonant force components again follow an inverse power law whereas the resonant force components give rise to spatially oscillating forces whose amplitude is proportional to $1/z_A$. If present, the resonant force components are dominating over the nonresonant ones, in general. The magnitude of the contributions from various molecular transitions to the force (3) is determined by their dipole matrix elements and frequencies, where Eqs. (10) and (12) together with Eq. (7) imply that the strength of the nonresonant force is roughly proportional to $1/\omega_{kn}$, while that of the resonant force is governed by $n(\omega_{nk})+1$ or $n(\omega_{kn})$ in the nonretarded limit and by $\omega_{nk}^3[n(\omega_{nk})+1]$ or $\omega_{kn}^3 n(\omega_{kn})$ in the retarded regime. Equations (10) and (12) furthermore show that the force becomes larger for larger permittivity of the surface material and saturates in the high-conductivity limit.

The general results and discussion given above can be easily applied to various polar molecules interacting with different surface materials. The qualitative behavior of the forces will be similar for all molecules and materials, i.e., a power-law dependence for nonretarded distances will give way to an oscillating force in the retarded regime. The exact magnitude of the force as well as the length scale of the oscillations will depend on the dipole moments and frequencies associated with the specific molecular transitions involved and the electric response of the surface in the way indicated above. Tabulated data for a variety of molecules and metal surfaces can be found in Ref. [24]. In the following, we will consider two representative examples.

### B. Examples: LiH and YbF near a Au surface

We first consider a LiH molecule in its electronic, vibrational, and rotational ground states ($p_n=\delta_{n0}$) near a Au surface at room temperature $T=300$ K. With the help of the Green tensor [Eq. (8)], we are able to compute the force components according to Eq. (6) which are displayed in Fig. 1. For this molecule, the contribution from rotational transitions with $\omega_{kn}=2.79\times10^{12}$ rad/s and $d=1.96\times10^{-29}$ C m [24] ($\Sigma_k \boldsymbol{d}_{0k}\boldsymbol{d}_{k0}=d^2\mathbf{I}$, where $\mathbf{I}$ is the unit tensor) is strongly dominant over those of vibrational and electronic transitions with their considerably higher transition frequencies. Molecules with a similar behavior include NH, OH, OD, NaCs, and KCs. For the relative permittivity of the Au surface we have used a Drude model

$$\varepsilon(\omega) = 1 - \frac{\omega_P^2}{\omega(\omega + i\gamma)} \tag{14}$$

with $\omega_P=1.37\times10^{16}$ rad/s and $\gamma=5.32\times10^{13}$ rad/s [25]. In view of the current debate regarding the thermal Casimir

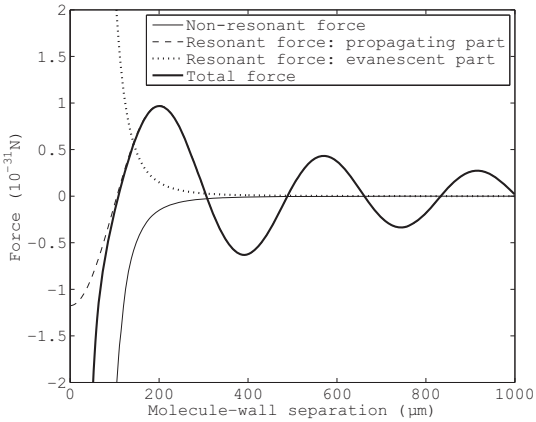


FIG. 1. Thermal CP force on a ground-state LiH molecule near a Au surface. For details, see text.

force (cf. [26,27] and references therein), we have also calculated the force using the alternative plasma model and found that the difference between the two models is of no importance in our case.

Figure 1 shows the contributions from the nonresonant force component (thin solid line) which is seen to be strictly attractive and the resonant force components (dashed and dotted lines). With regard to the latter, we have separately shown the propagating part [ $q \in [0, \omega/c$ ) in Eq. (8), dashed line] and the evanescent part ( $q \in [\omega/c, \infty$ ), dotted line). The rather astonishing result is that the evanescent part of the resonant force almost exactly cancels the nonresonant force component. Hence, in this highly nonequilibrium situation the largest contribution to the CP force arises from the propagating part of the resonant force. The total force (thick solid line in Fig. 1) thus closely follows the latter. Only at very small molecule-wall separation $z_A$ the force is given by its near-field part which, for a two-level isotropic molecule with $\hbar\omega_A \ll k_B T$, reads

$$\boldsymbol{F}(\boldsymbol{r}_A) = \frac{|\boldsymbol{d}_A|^2}{8\pi\varepsilon_0 z_A^4}\left[n(\omega_A)\frac{|\varepsilon(\omega_A)|^2 - 1}{|\varepsilon(\omega_A)+1|^2} - \frac{k_B T}{\hbar\omega_A}\frac{\varepsilon(0)-1}{\varepsilon(0)+1}\right]\boldsymbol{e}_z$$
$$\approx \frac{|\boldsymbol{d}_A|^2}{8\pi\varepsilon_0 z_A^4}\left[n(\omega_A) - \frac{k_B T}{\hbar\omega_A}\right]\boldsymbol{e}_z. \quad (15)$$

The approximation in the second line of Eq. (15) holds for good conductors. The force saturates in the high-temperature limit where the factor in square brackets approaches $-1/2$. In contrast, the nonresonant (Lifshitz-type) force alone would formally diverge. The predicted high-temperature saturation agrees with the previously found vanishing of the leading linear contribution in $k_B T/(\hbar\omega_A)$ in the good-conductor limit [15].

Let us next consider a molecule that is at thermal equilibrium with its environment, so that the probabilities $p_n$ are given by a Boltzmann distribution,

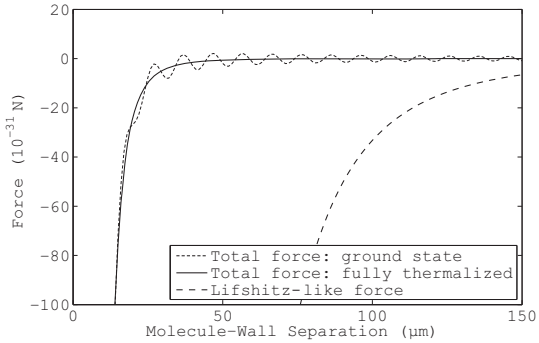


FIG. 2. Thermal CP force on a ground state vs fully thermalized YbF molecule near a Au surface. For details, see text.

$$p_n = \frac{e^{-\hbar\omega_n/(k_B T)}}{\sum_j e^{-\hbar\omega_j/(k_B T)}}. \quad (16)$$

Here, all resonant force components cancel and the force is given by a single nonresonant force contribution given by the first term in Eq. (6) where the molecular polarizability has to be replaced by its thermal counterpart [18],

$$\alpha_T(\omega) = \sum_n p_n \alpha_n(\omega). \quad (17)$$

In Fig. 2, we compare this equilibrium force on a thermalized molecule (solid line) with the nonequilibrium ground-state force (dotted line) for the case of YbF. In contrast to LiH, both rotational ($\omega_{kn}=9.05\times10^{10}$ rad/s, $d=1.31\times10^{-29}$ C m) and vibrational transitions ($\omega_{kn}=9.54\times10^{13}$ rad/s, $d=8.60\times10^{-31}$ C m) [24] give relevant contributions to the force because at room temperature the frequency of the latter is very close to the peak of the spectrum $\omega_{kn}^3 n(\omega_{kn})$ determining the resonant force contributions in the retarded limit. The results for YbF are thus representative of those to be expected for CaF, BaF, LiRb, NaRb, and LiCs, which also have considerable contributions from vibrational transitions at room temperature. Figure 2 shows that in contrast to the ground-state force, which oscillates as a function of molecule-wall separation (due to the influence of vibrational transitions), the force on a fully thermalized atom is monotonous and attractive (dominated by rotational transitions). We emphasize that the force at thermal equilibrium between the atom and its environment (solid line) is vastly overestimated by a Lifshitz-type macroscopic calculation (dashed line) that uses the ground-state polarizability $\alpha_0(\omega)$ as input parameter. The reduction factor in the near-field limit is approximately given in [18] as

$$\frac{|\boldsymbol{F}|}{|\boldsymbol{F}_{\text{Lifshitz}}|} \simeq \frac{1}{2n(\omega_{10})+1} \quad (18)$$

for all $z_A$. Its dependence on the relevant transition frequency clearly makes it species dependent. The potentially very large reduction factors ($\approx 1/870$ for YbF at room temperature) imply that these molecules can be brought much closer to metallic surfaces than previously thought.

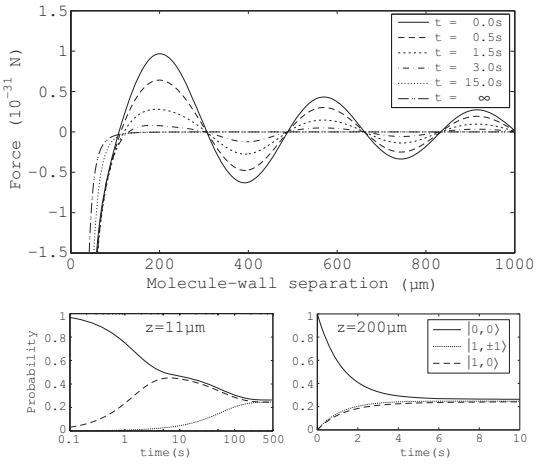


FIG. 3. Transient CP force and internal dynamics of a LiH molecule initially prepared in its ground state. For details, see text.

## III. DYNAMICAL CASIMIR-POLDER FORCE

In order to understand the transition between the nonequilibrium ground-state force and the fully thermalized one, we need to investigate the full internal molecular dynamics in the presence of the Au surface. The time-dependent probabilities $p_n=p_n(t)$ are governed by the rate equations

$$\dot{p}_n(t) = -\sum_k \Gamma_{nk} p_n(t) + \sum_k \Gamma_{kn} p_k(t), \tag{19}$$

where the transition rates are given by [24]

$$\Gamma_{nk} = \frac{2\mu_0}{\hbar}\omega_{nk}^2\{\Theta(\omega_{nk})[n(\omega_{nk})+1] + \Theta(\omega_{kn})n(\omega_{kn})\} \times \boldsymbol{d}_{nk}\cdot \mathrm{Im}\,\mathbf{G}(\boldsymbol{r}_A,\boldsymbol{r}_A,|\omega_{nk}|)\cdot\boldsymbol{d}_{kn}. \tag{20}$$

The transition rates for LiH near a Au surface can easily be calculated using the Green tensor [Eq. (8)]. The resulting time-dependent probabilities $p_n(t)$ are displayed for the ground state and the first manifold of rotationally excited states in the lower panels in Fig. 3, with the respective transition matrix elements being given by $\boldsymbol{d}_{|0,0\rangle\to|1,M\rangle}=d\boldsymbol{u}_M$, $\boldsymbol{u}_0=\boldsymbol{e}_z/\sqrt{3}$, and $\boldsymbol{u}_{\pm1}=(\mp\boldsymbol{e}_x+i\boldsymbol{e}_y)/\sqrt{6}$ [24]. For large molecule-wall separation the transition rates to the different substates of the first manifold are very similar and so are the resulting probabilities (lower right panel). When moving closer to the surface, the transition rates become affected by the evanescent and propagating parts of the reflected field. The contributions of the latter are strongly oscillating so that the rates $\Gamma_{|0,0\rangle\to|1,\pm1\rangle}$ exhibit a pronounced minimum at $z_A=11$ $\mu$m. This is not the case for the rate $\Gamma_{|0,0\rangle\to|1,0\rangle}$ due to the $1/z_A$ contribution from the evanescent fields (lower left panel in Fig. 3). Hence, at first only the occupation of the level $|1,0\rangle$ reaches equilibrium with the level $|0,0\rangle$, and full thermalization is realized only at a much later time.

The dynamics of the CP force is then governed by the internal molecular dynamics according to

$$\boldsymbol{F}(\boldsymbol{r}_A,t) = \sum_n p_n(t)\boldsymbol{F}_n(\boldsymbol{r}_A). \tag{21}$$

This time-dependent force is shown for a LiH molecule initially prepared in its ground state $p_n(t=0)=\delta_{n0}$ in the top panel of Fig. 3. We observe a gradual disappearance of the oscillating force components on a time scale of approximately 3 s. The attractive near-field force reaches its equilibrium value only much later due to the above-mentioned strongly reduced rate $\Gamma_{|0,0\rangle\to|1,\pm1\rangle}$. Note that during the thermalization the molecule is in an anisotropic state so that we have to use the general expression (3) for the force components rather than its isotropic special case (6).

## IV. CONCLUSIONS AND OUTLOOK

Studying the CP force on polar molecules near a planar surface at finite temperature, we have found that even ground-state molecules are subject to resonant spatially oscillating force components at finite temperature. They are due to the thermal nonequilibrium between the molecule and its environment. A full dynamical treatment has shown that these transient forces disappear in the course of thermalization of the molecule. The remaining equilibrium force can be vastly different from that calculated using a Lifshitz-type force expression for ground-state molecules.

In our numerical example of ground-state LiH, we have explicitly shown that the nonresonant force component and the evanescent part of the resonant force component cancel almost exactly, leaving a strongly reduced attractive force in the nonretarded limit which saturates at high temperatures. The force in the retarded limit is dominated by resonant contributions from rotational transitions. In contrast, the force on the heavier molecule YbF is dominated by resonant contributions from vibrational transitions. Moreover, in thermal equilibrium at room temperature the resulting force is a factor 1/870 smaller than would be expected from a Lifshitz-type calculation for the corresponding ground-state molecule.

Whereas the CP force on a fully thermalized molecule is always attractive, the nonequilibrium force on a ground-state molecule near a Au surface at room temperature has been found to show an oscillating behavior as a function of the molecule-wall separation $z_A$, with stable equilibrium positions away from the surface. Therefore, one might be tempted to use these (transient) minima for trapping purposes. It turns out, however, that for LiH the first potential well (with its minimum at $z_A=300$ $\mu$m) has a depth of approximately $10^{-12}$ K which is immeasurably small. In order to increase the trap depth, one might envisage a situation in which the molecule is embedded in a planar cavity of size $l$ consisting of two such Au surfaces. Then, the Fresnel reflection coefficients in Eq. (8) have to be replaced by $\tilde{r}_{s,p}=r_{s,p}/(1-r_{s,p}^2e^{2i\beta l})$. For very good conductors such as Au, one can set $|r_{s,p}|\approx 1-\eta$ with $\eta\ll 1$. Hence, for $\beta l=n\pi$ ($n\in\mathbb{N}$), the modified Fresnel coefficients increase as $|\tilde{r}_{s,p}|\propto 2/\eta$. Choosing $l$ close to a cavity resonance $n\pi c/\omega_A$, the contribution from propagating modes with small $q$ can thus be boosted by several orders of magnitude. Thus, if by use of

a cavity with a high $Q$ factor could increase the trap depth by a factor, e.g., $10^6$, the energy difference would be in the microkelvin regime which could be sufficiently deep to trap cold polar molecules with thermal photons. This question will be addressed in more detail in a future investigation.

**ACKNOWLEDGMENTS**

This work was supported by the Alexander von Humboldt Foundation and the Engineering and Physical Sciences Research Council (U.K.). S.Y.B. is grateful to M. R. Tarbutt for discussions.

[1] J. J. Hudson, B. E. Sauer, M. R. Tarbutt, and E. A. Hinds, Phys. Rev. Lett. **89**, 023003 (2002).
[2] E. D. Commins, Adv. At., Mol., Opt. Phys. **40**, 1 (1999).
[3] M. R. Tarbutt, H. L. Bethlem, J. J. Hudson, V. L. Ryabov, V. A. Ryzhov, B. E. Sauer, G. Meijer, and E. A. Hinds, Phys. Rev. Lett. **92**, 173002 (2004).
[4] S. Y. T. van de Meerakker, H. L. Bethlem, and G. Meijer, Nat. Phys. **4**, 595 (2008).
[5] S. A. Meek, H. L. Bethlem, H. Conrad, and G. Meijer, Phys. Rev. Lett. **100**, 153003 (2008).
[6] S. K. Tokunaga, J. O. Stack, J. J. Hudson, B. E. Sauer, E. A. Hinds, and M. R. Tarbutt, J. Chem. Phys. **126**, 124314 (2007).
[7] H. B. G. Casimir and D. Polder, Phys. Rev. **73**, 360 (1948).
[8] E. M. Lifshitz, Zh. Eksp. Teor. Fiz. **29**, 94 (1955) [Sov. Phys. JETP **2**, 73 (1956)].
[9] M. Boström and Bo E. Sernelius, Phys. Rev. A **61**, 052703 (2000).
[10] J. F. Babb, G. L. Klimchitskaya, and V. M. Mostepanenko, Phys. Rev. A **70**, 042901 (2004).
[11] K. A. Milton, J. Phys. A **37**, R209 (2004).
[12] A. D. McLachlan, Proc. R. Soc. London, Ser. A **274**, 80 (1963).
[13] C. Henkel, K. Joulain, J.-P. Mulet, and J.-J. Greffet, J. Opt. A, Pure Appl. Opt. **4**, S109 (2002).
[14] T. Nakajima, P. Lambropoulos, and H. Walther, Phys. Rev. A **56**, 5100 (1997).
[15] M.-P. Gorza and M. Ducloy, Eur. Phys. J. D **40**, 343 (2006).
[16] M. Antezza, L. P. Pitaevskii, and S. Stringari, Phys. Rev. Lett. **95**, 113202 (2005).
[17] J. M. Obrecht, R. J. Wild, M. Antezza, L. P. Pitaevskii, S. Stringari, and E. A. Cornell, Phys. Rev. Lett. **98**, 063201 (2007).
[18] S. Y. Buhmann and S. Scheel, Phys. Rev. Lett. **100**, 253201 (2008).
[19] Y. Sherkunov, Phys. Rev. A **79**, 032101 (2009).
[20] M. S. Tomaš, Phys. Rev. A **51**, 2545 (1995).
[21] S. Y. Buhmann, D.-G. Welsch, and T. Kampf, Phys. Rev. A **72**, 032112 (2005).
[22] G. Barton, Proc. R. Soc. London, Ser. A **320**, 251 (1970).
[23] J. M. Wylie and J. E. Sipe, Phys. Rev. A **32**, 2030 (1985).
[24] S. Y. Buhmann, M. R. Tarbutt, S. Scheel, and E. A. Hinds, Phys. Rev. A **78**, 052901 (2008).
[25] A. Lambrecht and S. Reynaud, Eur. Phys. J. D **8**, 309 (2000).
[26] I. Brevik, S. A. Ellingsen, and K. A. Milton, New J. Phys. **8**, 236 (2006).
[27] G. L. Klimchitskaya and V. M. Mostepanenko, Contemp. Phys. **47**, 131 (2006).

Article [m]

***Enhancement of thermal Casimir-Polder potentials of ground-state polar molecules in a planar cavity***

S.Å. Ellingsen, S.Y. Buhmann, S. Scheel

Physical Review A **80**, 022901 (2009)

# Enhancement of thermal Casimir-Polder potentials of ground-state polar molecules in a planar cavity

Simen Å. Ellingsen
*Department of Energy and Process Engineering, Norwegian University of Science and Technology, N-7491 Trondheim, Norway*

Stefan Yoshi Buhmann and Stefan Scheel
*Quantum Optics and Laser Science, Blackett Laboratory, Imperial College London, Prince Consort Road, London SW7 2AZ, United Kingdom*

(Received 12 June 2009; published 13 August 2009)

We analyze the thermal Casimir-Polder potential experienced by a ground-state molecule in a planar cavity and investigate the prospects for using such a setup for molecular guiding. The resonant atom-field interaction associated with this nonequilibrium situation manifests itself in oscillating standing-wave components of the potential. While the respective potential wells are normally too shallow to be useful, they may be amplified by a highly reflecting cavity whose width equals a half-integer multiple of a particular molecular transition frequency. We find that with an ideal choice of molecule and the use of a cavity bounded by Bragg mirrors of ultrahigh reflectivity, it may be possible to boost the potential by up to two orders of magnitude. We analytically derive the scaling of the potential depth as a function of reflectivity and analyze how it varies with temperature and molecular properties. It is also shown how the potential depth decreases for standing waves with a larger number of nodes. Finally, we investigate the lifetime of the molecular ground state in a thermal environment and find that it is not greatly influenced by the cavity and remains in the order of several seconds.

DOI: 10.1103/PhysRevA.80.022901 PACS number(s): 34.35.+a, 12.20.−m, 42.50.Ct, 42.50.Nn

## I. INTRODUCTION

Casimir-Polder (CP) forces are a particular example of dispersion forces, which arise due to the fluctuations of the quantized electromagnetic field [1]. These forces occur between polarizable atoms or molecules and metallic or dielectric bodies and can be intuitively understood as the dipole-dipole force that arises from spontaneous and mutually correlated polarization of the atom or molecule and the matter comprising the body. Casimir-Polder forces at thermal equilibrium have been commonly investigated in the linear-response formalism [2–4]. Studies of a wide range of geometries such as semi-infinite half-spaces [2–5], thin plates [6,7], planar cavities [8], spheres, and cylinders [9] as well as cylindrical shells [5,6,10] have revealed that thermal CP forces are typically attractive in the absence of magnetic effects.

Recent theoretical predictions [11] as well as experimental realizations [12] for CP forces in thermal nonequilibrium situations have pointed toward interesting effects which arise when an atom at equilibrium with its local environment interacts with a body held at different temperature. In particular, depending on the temperatures of the macroscopic body and the environment, the force can change its character from being attractive to repulsive and vice versa.

Nonequilibrium between atom and local environment can be investigated by means of normal-mode quantum electrodynamics (QED) [13,14] or macroscopic QED in absorbing and dispersing media [15,16]. In this case, thermal excitation and de-excitation processes lead to resonant contributions to the force. As discussed in a recent Letter by two of the present authors [17] (cf. similar findings reported in Ref. [18]), these resonant forces produce a different force from that obtained through the standard approach, a perturbative expansion of the Lifshitz formula using the ground-state polarizability of the atom. Only when the atom is fully thermalized, i.e., when it is in a superposition of energy states as given by the Boltzmann distribution, do the two approaches yield the same result, and only when the correct thermal polarizability is employed. For most atoms the resonant contribution is small because the respective excitation energies are much larger than the thermal energies; hence the atom is essentially always in its ground state.

For diatomic polar molecules such as LiH or YbF, however, whose lowest rovibrational eigenstates are typically separated by energies that are small on a thermal scale, the situation is changed, and the thermalized CP force can differ drastically from the standard "Lifshitz-like" expression. An investigation into these effects was undertaken in Ref. [19], where it was found that for a ground-state YbF molecule outside a metallic half-space at room temperature the fully thermalized CP force is smaller than the nonresonant force alone by a factor of 870. These results could be of importance for the trapping of Stark-decelerated polar molecules [20] near macroscopic bodies.

Equally interesting is the observation that even for an atom or a molecule in its ground state the resonant part of the Casimir-Polder force has a long-range and spatially oscillating contribution, due to propagating modes [14,19]. While this oscillatory behavior dies out as the system thermalizes, the thermalization time of a ground-state molecule can be quite long, often several seconds [21]. The oscillating propagating potential reported in [19], unfortunately, was found to be too small in amplitude to be useful for guiding purposes, but nonetheless points to interesting applications if a way could be found to enhance these oscillations.

In the present article we investigate the use of a planar cavity to enhance the amplitude of the potential oscillations.

 

This geometry has been discussed in detail in conjunction with excited atoms in a zero-temperature environment, where an oscillating standing-wave potential is known to occur [22–28]. For ground-state molecules in a cavity at finite temperature, an enhancement of up to two orders of magnitude will indeed be shown to be possible when the cavity width is fixed at the resonant length $a=\pi\hbar c/E_{10}$, where $E_{10}$ is the energy separation of the ground state and first-excited state of the molecule.

The paper is organized as follows: The general formalism of the CP force on a molecule in a cavity is developed in Sec. II, and numerical calculations for a gold cavity are undertaken in Sec. II A, where we also show how the potential is enhanced as the cavity approaches the resonant width. In Secs. II B and II C we investigate the strategies for further enhancing the potential by considering different cavity resonances and molecular species. The scaling of the potential with the reflectivity of the cavity is investigated numerically and analytically in Sec. II D, and we thereafter discuss how further enhancement can be achieved using a cavity of parallel Bragg mirrors tuned to frequency $\omega_{01}=E_{01}/\hbar$ and normal incidence (Sec. II E). Finally, in Sec. II F we investigate the effect of the cavity on the thermalization time of a molecule initially prepared in its ground state and find that this remains in the same order of magnitude as in free space, typically in the order of seconds. We summarize our result in Sec. III and provide a guide to further investigations.

## II. THERMAL CASIMIR-POLDER POTENTIAL IN A PLANAR CAVITY

We consider a polar molecule with energy eigenstates $|n\rangle$, eigenenergies $\hbar\omega_n$, transition frequencies $\omega_{mn}=\omega_m-\omega_n$, and dipole matrix elements $\mathbf{d}_{mn}$, which is prepared in an incoherent superposition of its energy eigenstates with probabilities $p_n$. As shown in Ref. [17], the CP force is conservative in the perturbative limit, $\mathbf{F}(\mathbf{r})=-\boldsymbol{\nabla}U(\mathbf{r})$, where the associated CP potential is given by

$$U(\mathbf{r}) = -\sum_n p_n U_n(\mathbf{r}), \tag{1}$$

and the potential components for an isotropic molecule read

$$\begin{aligned} U_n(\mathbf{r}) = {} & \mu_0 k_B T {\sum_{j=0}^{\infty}}' \xi_j^2 \alpha_n(i\xi_j) \mathrm{Re\ Tr}\, \mathbf{G}^{(1)}(\mathbf{r},\mathbf{r},i\xi_j) \\ & + \frac{\mu_0}{3}\sum_k \omega_{nk}^2 |\mathbf{d}_{nk}|^2 \\ & \times\{\Theta(\omega_{kn})n(\omega_{kn}) - \Theta(\omega_{nk})[n(\omega_{nk})+1]\} \\ & \times \mathrm{Re\ Tr}\, \mathbf{G}^{(1)}(\mathbf{r},\mathbf{r},|\omega_{nk}|), \end{aligned} \tag{2}$$

where $\mu_0$ is the free-space permeability, $k_B$ is Boltzmann's constant, $\xi_j=2\pi j k_B T/\hbar$ is the $j$th Matsubara frequency, and $\mathbf{G}^{(1)}(\mathbf{r},\mathbf{r}',\omega)$ is the scattering part of the classical Green tensor of the geometry the molecule is placed in. The prime on the Matsubara sum indicates that the $j=0$ term is to be taken with half weight. The molecular polarizability is given by

$$\alpha_n(\omega) = \lim_{\epsilon\to 0}\frac{1}{3\hbar}\sum_k \left[\frac{|\mathbf{d}_{nk}|^2}{\omega+\omega_{kn}+i\epsilon} - \frac{|\mathbf{d}_{nk}|^2}{\omega-\omega_{kn}+i\epsilon}\right]. \tag{3}$$

The photon number follows the Bose-Einstein distribution,

$$n(\omega) = \left[\exp\left(\frac{\hbar\omega}{k_B T}\right) - 1\right]^{-1}. \tag{4}$$

The first sum in Eq. (2) is the nonresonant force, reminiscent of that obtained by a dilute-gas expansion of the Lifshitz formula [2]. The second sum is the resonant contribution to the force. We will see how it splits naturally into a propagating plus an evanescent part.

We assume the molecule to be placed within an empty planar cavity bounded by two identical plates of infinite lateral extension with plane parallel surfaces, separated by a distance $a$. We choose the coordinate system such that the cavity walls are normal to the $z$ axis at $z=\pm a/2$ ($z=0$ being the center of the cavity) and denote directions in the $xy$ plane by the symbol $\perp$. The scattering Green tensor of the system is well known (cf., e.g., Ref. [29]), and the relevant diagonal elements inside the cavity are given by

$$G_{xx}^{(1)}(z,z,k_\perp,\omega) = -\frac{ic^2\beta}{\omega^2}\frac{r_p}{D_p}e^{i\beta a}\cos 2\beta z, \tag{5a}$$

$$G_{yy}^{(1)}(z,z,,k_\perp\omega) = \frac{i}{\beta}\frac{r_s}{D_s}e^{i\beta a}\cos 2\beta z, \tag{5b}$$

$$G_{zz}^{(1)}(z,z,,k_\perp\omega) = \frac{ic^2k_\perp^2}{\omega^2\beta}\frac{r_p}{D_p}e^{i\beta a}\cos 2\beta z, \tag{5c}$$

where we have performed a Weyl expansion,

$$\mathbf{G}^{(1)}(\mathbf{r},\mathbf{r}'\omega) = \int \frac{d^2k_\perp}{(2\pi)^2}\mathbf{G}^{(1)}(z,z',k_\perp,\omega)e^{i\mathbf{k}_\perp\cdot(\mathbf{r}-\mathbf{r}')_\perp}, \tag{6}$$

taken the coincidence limit $\mathbf{r}\to\mathbf{r}'$, and dropped all position-independent terms (which give rise to an irrelevant constant contribution to the CP potential). Here, $r_s, r_p$ are the reflection coefficients of the (identical) cavity walls for $s,p$ polarized waves and we have defined

$$D_\sigma = 1 - r_\sigma^2 e^{2i\beta a}, \tag{7}$$

$$\beta = \sqrt{\omega^2/c^2 - k_\perp^2}. \tag{8}$$

The square root is to be taken such that $\mathrm{Im}\,\beta\geq 0$. When the cavity walls are homogeneous semi-infinite half-spaces of an electric material of permittivity $\varepsilon(\omega)$, the reflection coefficients can be written simply as

$$r_s = \frac{\beta - \sqrt{\beta^2+(\varepsilon-1)\omega^2/c^2}}{\beta+\sqrt{\beta^2+(\varepsilon-1)\omega^2/c^2}}, \tag{9a}$$

$$r_p = \frac{\varepsilon\beta - \sqrt{\beta^2+(\varepsilon-1)\omega^2/c^2}}{\varepsilon\beta+\sqrt{\beta^2+(\varepsilon-1)\omega^2/c^2}}, \tag{9b}$$

where again the square roots are chosen such that their imaginary part is positive.

Adding Eqs. (5a)–(5c) and partially performing the Fourier integral by introducing polar coordinates in the $xy$ plane, the trace of the Green tensor of the cavity reads

$$\mathrm{Tr}\,\mathbf{G}^{(1)}(\mathbf{r},\mathbf{r},\omega) = \frac{1}{2\pi i}\int_0^\infty \frac{k_\perp dk_\perp}{\beta} \times\left[2\frac{c^2\beta^2}{\omega^2}\frac{r_p}{D_p} - \sum_{\sigma=s,p}\frac{r_\sigma}{D_\sigma}\right]e^{i\beta a}\cos 2\beta z. \tag{10}$$

This result can be substituted into Eq. (2) to obtain the thermal CP potential of a molecule in an arbitrary incoherent internal state. In the following, we will assume the molecule to be prepared in its ground state, so that the thermal CP potential is given by

$$U(\mathbf{r}) = \mu_0 k_B T {\sum_{j=0}^{\infty}}' \xi_j^2 \alpha(i\xi_j)\mathrm{Re}\,\mathrm{Tr}\,\mathbf{G}^{(1)}(\mathbf{r},\mathbf{r},i\xi_j) + \frac{\mu_0}{3}\sum_{k\neq 0}\omega_{0k}^2 n(\omega_{k0})|\mathbf{d}_{0k}|^2 \mathrm{Re}\,\mathrm{Tr}\,\mathbf{G}^{(1)}(\mathbf{r},\mathbf{r},\omega_{k0}), \tag{11}$$

$[\alpha(\omega)\equiv\alpha_0(\omega)$, ground-state polarizability] together with Eq. (10). The first term is the nonresonant part of the potential, it depends on the Green tensor taken at purely imaginary frequencies. Since $\beta$ is purely imaginary in this case, Green tensor (10) and hence the nonresonant potential is nonoscillating as a function of position. The second term in the CP potential is the resonant contribution, which depends on the Green tensor taken at real frequencies. The integral over $k_\perp$ in this case naturally splits into a region $0\leq k_\perp<\omega_{nk}$ of propagating waves in which $\beta$ is real and positive, and a region $\omega_{nk}\leq k_\perp$ of evanescent waves in which $\beta$ is purely imaginary. The contributions from propagating waves are oscillating as a function of position due to the term $\cos 2\beta z$, while those from evanescent waves are nonoscillating, just like the nonresonant part of the potential. The total potential (11) can thus be separated into nonresonant (first term), propagating (contributions to second term with $0\leq k_\perp<\omega_{nk}$), and evanescent components (contributions to second term with $\omega_{nk}\leq k_\perp$) according to

$$U(z) = U_{\mathrm{nr}}(z) + U_{\mathrm{pr}}(z) + U_{\mathrm{ev}}(z). \tag{12}$$

To illustrate the behavior of the total potential and its three components, we consider a LiH molecule in its electronic and rovibrational ground state placed inside a gold cavity. The permittivity of the (semi-infinite) cavity walls may be computed using the Drude model

$$\varepsilon(\omega) = 1 - \frac{\omega_p^2}{\omega(\omega+i\gamma)} \tag{13}$$

with $\omega_p=1.37\times10^{16}$ rad/s and $\gamma=5.32\times10^{13}$ rad/s [30]. As shown in Ref. [19], the CP potential of ground-state LiH is dominated by contributions from the rotational transitions to the first excited manifold, with the respective transition frequency and dipole matrix elements being given by $\omega_{0k}=2.78973\times10^{12}$ rad/s and $\Sigma_k|\mathbf{d}_{0k}|^2=3.847\times10^{-58}$ C$^2$ m$^2$, respectively [21]. Potential (11) and its three components [Eq. (12)] for a cavity of length $a=500$ $\mu$m at room temperature ($T=300$ K) is shown in Fig. 1 as the result of a numerical integration, where Eqs. (7), (8), (9a), (9b), and (10) have been used. For transparency, we have shifted all three components such that they vanish at the center of the cavity. It is seen that the nonresonant potential is attractive and has a maximum at the center of the cavity, while the evanescent potential is repulsive and has a minimum at the cavity center. As in the case of a single surface [19] these two contributions partially cancel, where the attractive nonresonant contribution is slightly larger and leads to an attractive total potential in the vicinity of the cavity walls. The propagating part of the potential is spatially oscillating and finite at the cavity walls, it dominates in the central region of the cavity where it gives rise to well-pronounced maxima and minima.

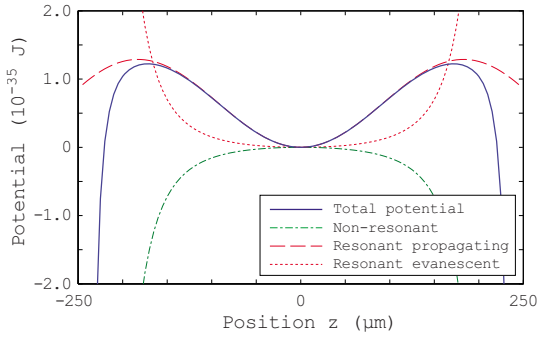


FIG. 1. (Color online) Casimir-Polder potential of a ground-state LiH molecule inside a gold cavity of width $a=500$ $\mu$m at room temperature ($T=300$ K). The nonresonant, propagating, and evanescent contributions to the total potential are shown separately.

It is natural to wonder whether these potential minima might be used for the purpose of guiding of polar molecules. With this in mind, we will in the following discuss strategies of enhancing the depth of the potential well by analyzing the dependence of the potential on the molecular species as well as the geometric and material parameters of the cavity.

### A. Cavity-induced enhancement of the potential

We begin our analysis by discussing the dependence of the potential on the cavity width. The one-dimensional confinement of the propagating modes in a cavity of highly reflecting mirrors leads to the formation of standing waves and associated cavity resonances. When the molecular transition frequency coincides with one of these resonances, the thermal CP potential can be strongly enhanced: When the squared reflection coefficient $r_\sigma^2$ is close to unity, the denominator $D_\sigma$ of Eq. (7), featuring in the Green tensor, becomes small if the exponential $\exp(2i\beta a)$ is equal to unity, resulting in a strong enhancement of the potential $U_{\mathrm{pr}}$. This happens for normal incidence ($k_\perp=0$) of the propagating waves, when the resonance condition $2\omega_{0k}a/c=2\pi\nu$, $\nu\in\mathbb{N}$ is fulfilled. In other words, the cavity length has to be equal to a

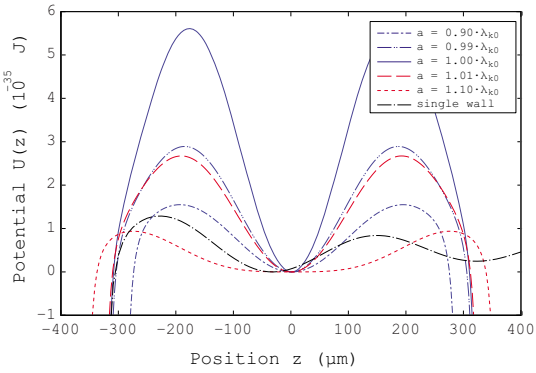


FIG. 2. (Color online) Cavity-induced enhancement of the thermal Casimir-Polder potential of a ground-state LiH molecule inside gold cavities of various widths close to the second resonance $a=\lambda_{k0}=673$ $\mu$m. The potential of a single plate at $z=-\lambda_{k0}/2$ is also displayed.

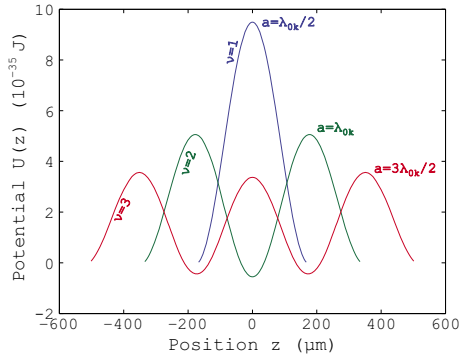


FIG. 3. (Color online) Propagating part of the thermal Casimir-Polder potentials of a ground-state LiH molecule inside gold cavities of widths $a=\nu\lambda_{k0}/2$ corresponding to resonances of different orders ($\nu=1,2,3$).

half-integer multiple of the molecular transition wavelength $\lambda_{k0}=2\pi c/\omega_{k0}$,

$$a=\nu\lambda_{k0}/2, \quad \nu\in\mathbb{N}. \tag{14}$$

We say that the molecular transition coincides with the $\nu$th cavity resonance.

The cavity-induced enhancement of the thermal CP potential is illustrated in Fig. 2, where we show the total thermal CP potential of a ground-state LiH molecule in gold cavities of widths such that the molecular transition is close to the second cavity resonance $\lambda_{k0}$. As seen, the amplitude of the spatial oscillations, associated with the propagating part of the potential $U_{\rm pr}$, sharply increases as the cavity width approaches $\lambda_{k0}$. For comparison, we have also displayed the potential of a single plate at $z=-\lambda_{k0}/2$, where Eq. (10) for the cavity Green tensor has been replaced with the single-plate result [19]

$$\mathrm{Tr}\,\mathbf{G}^{(1)}(\mathbf{r},\mathbf{r}',\omega)=\frac{i}{4\pi}\int_0^\infty\frac{k_\perp dk_\perp}{\beta}\sum_{\sigma=s,p}\left[r_\sigma-2\frac{c^2\beta^2}{\omega^2}r_p\right]e^{i\beta(a+2z)}. \tag{15}$$

The comparison shows that the amplitude of the oscillations, while hardly visible for the single plate, is strongly enhanced for a cavity. The depth of the potential minimum at the center of the cavity with respect to the neighboring maxima is increased by a factor 6.7 when using a resonant cavity rather than a single plate.

### B. Different cavity resonances

In the following, we are interested in the cavity-enhanced oscillations of the thermal potential. As seen from Fig. 2, they set in at some distance away from the cavity walls where the potential is well approximated by its propagating-wave contribution $U_{\rm pr}$. We can therefore restrict our attention to this part of the total CP potential. The (propagating-wave) potentials associated with different cavity resonances $\nu$ are shown in Fig. 3. It is seen that the order $\nu$ of the resonance corresponds to the number of maxima of the potential. Potentials associated with resonances of order $\nu\geq 2$ have minima. The amplitudes of the oscillations become generally smaller for higher resonance orders $\nu$. As seen from the case $\nu=3$, the minima and maxima are slightly more pronounced toward the cavity walls.

The scaling of the potential minima with the resonance order as observed in Fig. 3 can be confirmed by an analytical analysis. For each cavity order $\nu$, we define $\Delta U_\nu$ to be the depth of the deepest potential minimum with respect to the neighboring maxima. As suggested by Fig. 3, this deepest minimum will always be the one closest to the cavity walls. Cavity QED problems can often be solved analytically under the simplifying assumption that reflection coefficients are independent of the transverse wave number $k_\perp$ [31,32], and this method is also successful here. As shown in Appendix A, in the perfect conductor limit $r_p=-r_s\equiv r\to 1$, we have the simple scaling law

$$\Delta U_\nu\propto\frac{1}{\nu}. \tag{16}$$

For imperfect conductors, the $\Delta U_\nu$ will decrease somewhat less slowly with $\nu$.

The analytical scaling law obtained on the basis of simplifying assumptions supports the observation from the numerical results in Fig. 3 that the $\nu=2$ resonance provides the deepest potential minimum. In view of potential guiding, we can therefore restrict our attention to this case, $\Delta U\equiv\Delta U_2$.

### C. Different molecular species

The CP potential depends on the molecular transition in question via the respective transition frequencies and dipole matrix elements. Using the molecular data as listed in Ref. [21], we have calculated the depth of the $\nu=2$ potential minimum for both rotational and vibrational transitions of the polar molecules LiH, NH, OH, OD, CaF, BaF, YbF, LiRb, NaRb, KRb, LiCs, NaCs, KCs, and RbCs; the results are

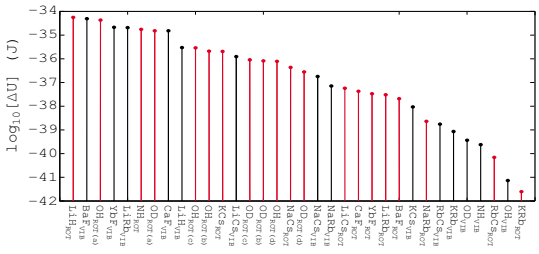


FIG. 4. (Color online) Depth $\Delta U$ of the $\nu=2$ potential minimum for rotational and vibrational transitions of various ground-state polar molecules inside gold cavities at $T=300$ K. The different nondegenerate transitions of OH and OD are labeled as (a)–(d) in order of ascending frequencies, cf. Ref. [21].

displayed in order of descending $\Delta U$ in Fig. 4. The figure shows that the deepest potential minima are realized when using the rotational transition of LiH, the vibrational transition of BaF or the dominant rotational transition of OH, followed by YbF (vibrational), LiRb (vibrational), NH (rotational), OD (dominant rotational transition), and CaF (vibrational).

The variation in the depth for different molecules is partly due to its dependence on the molecular transition frequency. As shown in Ref. [19], the resonant part of the CP potential of a single plate is proportional to $\omega_{k0}^2 n(\omega_{k0})$ for a good conductor with frequency–independent reflectivities. This remains true in the case of a cavity. In addition, the amplitude of the oscillations is inversely proportional to the molecule-wall separation. The largest potential maximum being situated at $z-a/2=\lambda_{k0}/4\propto 1/\omega_{k0}$, its height carries an additional $\omega_{k0}$ proportionality. The dependence of the potential-minimum depth on molecular transition frequency can thus be given as

$$\Delta U_\nu \propto \omega_{k0}^3 n(\omega_{k0}) \propto \begin{cases} \omega_{k0}^2, & \text{for } \hbar\omega_{k0} \ll k_B T \\ e^{-\hbar\omega_{k0}/k_B T}, & \text{for } \hbar\omega_{k0} \gg k_B T. \end{cases} \tag{17}$$

As shown in Sec. II D, this scaling becomes exact for cavities with frequency- and $k_\perp$-independent reflectivities. For real conductors, the decrease in $\Delta U_\nu$ for high frequencies will be stronger than given in Eq. (17) due to the decrease in the reflection coefficients. Note that Eq. (17) also shows that $\Delta U_\nu$ becomes larger for higher temperatures due to the increased thermal-photon number. Again, this only holds when disregarding the temperature dependence of the reflection coefficients, cf. also Sec. II E below.

The frequency dependence of $\Delta U_{\rm pr}$ is illustrated in Fig. 5 where we have plotted its values normalized by dividing by the transition-dipole moments $d^2$ ($d^2 \equiv \Sigma_k |\mathbf{d}_{0k}|^2$ with the sum running over the degenerate submanifold). The transition frequencies of some of the molecules investigated are indicated in the figure. In particular, the vibrational transitions of BaF and YbF, which have been seen in Fig. 4 to give rise to large potential-minimum depths, are very close to the peak of the function $\omega_{k0}^3 n(\omega_{k0})$, which is at $\omega_{k0}=1.11\times 10^{14}$ rad/s for room temperature.

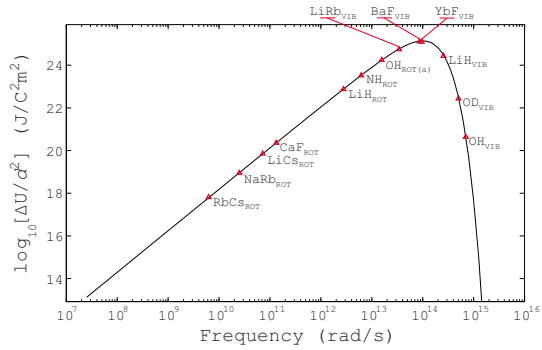


FIG. 5. (Color online) Frequency dependence of the depth $\Delta U$ of the $\nu=2$ potential minimum for polar molecules inside gold cavities at $T=300$ K.

The other main dependence of $\Delta U_\nu$ on the molecular species and transition is the proportionality to the modulus squared of the transition-dipole moments,

$$\Delta U_\nu \propto \sum_k |\mathbf{d}_{0k}|^2 = d^2. \tag{18}$$

The transition-dipole moments are typically larger for rotational transitions than for vibrational ones. For this reason, the rotational transition of LiH gives rise to the largest minimum depth although the vibrational transition frequencies of BaF and YbF are much closer to the peak frequency $1.11\times 10^{14}$ rad/s.

### D. Scaling with reflectivity

The cavity-induced enhancement of the thermal CP force strongly depends on the reflectivity of the cavity walls. To understand this dependence in more detail, let us for simplicity investigate how the height of the single maximum for a $\nu=1$ resonance depends on reflectivity. The scaling of the potential extrema with reflectivity is the same for all $\nu$ as is shown in Appendix A, so considering the simplest case will suffice.

We begin by writing the propagating part of the resonant CP potential associated with a single transition in the form

$$U_{\rm pr}(z) = \frac{1}{3\varepsilon_0} n(\omega_{k0}) |\mathbf{d}_{01}|^2 I(\phi), \tag{19}$$

where we have introduced the dimensionless position

$$\phi = \frac{z}{a} \tag{20}$$

and the integral

$$I(\phi) = \mathrm{Im} \int_0^{\omega_{k0}/c} \frac{dk_\perp k_\perp}{2\pi\beta} \left[ 2\beta^2 \frac{r_p}{D_p} - \frac{\omega_{k0}^2}{c^2} \sum_{\sigma=s,p} \frac{r_\sigma}{D_\sigma} \right] \times e^{i\beta a} \cos 2\beta a\phi. \tag{21}$$

As in Sec. II B, we consider the simple model case of frequency- and $k_\perp$-independent reflection coefficients $r_p=-r_s\equiv r$. With this assumption,

$$\sum_{\sigma=s,p} \frac{r_\sigma}{D_\sigma} = 0. \tag{22}$$

After introducing the dimensionless integration variable $x=2\beta a$ with $k_\perp dk_\perp = -4a^2 x dx$, the integral above takes the form

$$I(\phi) = \frac{r}{8\pi a^3} \mathrm{Im} \int_0^{x_0} dx \frac{x^2 e^{ix/2} \cos \phi x}{1 - r^2 e^{ix}}, \tag{23}$$

where $x_0 = 2\omega_{k0} a/c$. For the $\nu=1$ resonance, we have $a = \lambda_{0k}/2 = \pi c/\omega_{k0}$, so $x_0 = 2\pi$.

The required height of the potential maximum at the cavity center ($z=0$) with respect to the value of $U_{\mathrm{pr}}$ at the cavity walls $z = \pm a/2$ is proportional to the difference $I(0) - I(1/2)$. We have

$$\begin{aligned} I(1/2) &= \frac{r}{16\pi a^3} \mathrm{Im} \int_0^{2\pi} dx x^2 \frac{e^{ix} + 1}{1 - r^2 e^{ix}} \\ &= \frac{r}{16\pi a^3} \mathrm{Im} \int_0^{2\pi} dx x^2 [1 + (1 + r^{-2}) \mathrm{Li}_0(r^2 e^{ix})], \end{aligned} \tag{24}$$

where the polylogarithmic function is defined as

$$\mathrm{Li}_s(z) = \sum_{k=1}^{\infty} \frac{z^k}{k^s}. \tag{25}$$

The first term in Eq. (24) is real and does not contribute. The second one is easily calculated using the relation

$$\int dz \mathrm{Li}_s(A e^{bz}) = \frac{1}{b} \mathrm{Li}_{s+1}(A e^{bz}) + C, \tag{26}$$

valid for arbitrary constants $A, b$, where $|A| < 1$. Partially integrating this relation twice and substituting the result for $A = r^2$, $b = i$ into Eq. (24), one finds

$$\begin{aligned} I(1/2) &= \frac{r + r^{-1}}{16\pi a^3} \mathrm{Im} \left\{ \frac{4\pi^2}{i} \mathrm{Li}_1(r^2) + 4\pi \mathrm{Li}_2(r^2) \right\} \\ &= \frac{\pi(r + r^{-1})}{4a^3} \ln(1 - r^2), \end{aligned} \tag{27}$$

where we have noted that $\mathrm{Li}_1(z) = -\ln(1-z)$. In the limit of high reflectivity, $\delta \equiv 1 - r \to 0_+$ this exact result shows the asymptotic behavior

$$I(1/2) \sim \frac{\pi}{2a^3} (\ln \delta + \ln 2) \quad \text{for} \quad \delta \to 0_+, \tag{28}$$

with the first correction term being of order $\delta$.

The calculation of $I(0)$ is only slightly more involved. We have

$$\begin{aligned} I(0) &= \frac{r}{8\pi a^3} \mathrm{Im} \int_0^{2\pi} dx \frac{x^2 e^{ix/2}}{1 - r^2 e^{ix}} \\ &= \frac{r}{8\pi a^3} \sum_{l=0}^{\infty} r^{2k} \mathrm{Im} \int_0^{2\pi} dx x^2 e^{ix(l+1/2)}. \end{aligned} \tag{29}$$

By partial integration we obtain

$$\mathrm{Im} \int_0^{2\pi} dx x^2 e^{ix(l+1/2)} = \frac{4\pi^2}{\left(l + \frac{1}{2}\right)} - \frac{4}{\left(l + \frac{1}{2}\right)^3}. \tag{30}$$

After substitution of this result, the sum over $l$ can be performed by using the relations (cf. Sec. 1.513 in Ref. [33])

$$\sum_{l=0}^{\infty} \frac{r^{2l}}{l + \frac{1}{2}} = \frac{1}{r} \ln \frac{1 + r}{1 - r} \sim -\ln \delta + \ln 2 \quad \text{for} \quad \delta \to 0_+ \tag{31}$$

(leading corrections being of the order $\delta \ln \delta$) and

$$\sum_{l=0}^{\infty} \frac{r^{2l}}{\left(l + \frac{1}{2}\right)^3} \sim 8 \left[ \sum_{l=1}^{\infty} \frac{1}{l^3} - \sum_{l=1}^{\infty} \frac{1}{(2l)^3} \right] = 7\zeta(3) \quad \text{for} \quad \delta \to 0_+,$$

where $\zeta(z)$ is the Riemann zeta function. We thus find

$$I(0) \sim -\frac{\pi}{2a^3} \left[ \ln \delta - \ln 2 + \frac{7}{\pi^2} \zeta(3) \right] \quad \text{for} \quad \delta \to 0_+, \tag{32}$$

with the first correction again being of order $\delta \ln \delta$.

Substituting results (28) and (32) into Eq. (19), the difference between the maximum and minimum values of the $\nu=1$ propagating potential reads

$$U_{\mathrm{pr}}(0) - U_{\mathrm{pr}}(a/2) \sim -\frac{\pi \Sigma_k |\mathbf{d}_{0k}|^2 n(\omega_{k0})}{3\varepsilon_0 a^3} \left[ \ln \delta + \frac{7\zeta(3)}{2\pi^2} \right] \quad \text{for} \quad \delta \to 0_+. \tag{33}$$

This result being representative of the case of arbitrary $\nu$, we can conclude that

$$\Delta U_\nu \propto \ln(1 - r) \tag{34}$$

in the limit $r \to 1$. In the case where the reflection coefficients are not the same for both polarizations but still assumed constant, the coefficient of the term $\propto \ln \delta$ in Eq. (33) will change, leading to a slight quantitative but no qualitative difference to the scaling of the potential-minimum depth. Note that Eq. (33) immediately implies scaling law (17) for the frequency dependence of $\Delta U_\nu$.

The fact that the potential depth diverges only logarithmically as reflectivity tends to unity poses severe restrictions on the potential which is obtainable using a planar cavity. The mathematical reason for the relative weakness of the resonance is that the integrand of the $k_\perp$ integral only becomes large at a single point, at $k_\perp = 0$. The physical reason is that the photonic modes in the cavity are only confined in one out of three spatial dimensions. We conjecture that the potential due to the resonant CP force on a ground-state molecule can

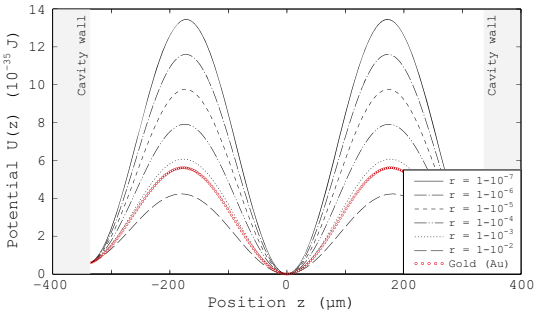


FIG. 6. (Color online) Propagating part of the thermal CP potential for a ground-state LiH molecule inside different cavities with constant reflection coefficients. The rotational transition of LiH is assumed to coincide with the $\nu=2$ resonance of the cavities. For comparison, the exact result for a gold cavity is also shown.

be much increased by a resonant cavity if confinement is imposed in two or even three dimensions, i.e., in a cylindrical or spherical cavity.

The logarithmic scaling law of the potential-minimum depth $\Delta U_\nu$ for the case $\nu=2$ is confirmed by a numerical calculation in which reflection coefficients are set constant, $r_p=-r_s\equiv r$ and close to unity. The result for the rotational transition of LiH is shown in Fig. 6 where the exact result for a gold cavity is also included. By comparing the latter curve to the potentials for constant reflection coefficients, one can read off the relatively small "effective" reflectivity of gold between $1-10^{-2}$ and $1-10^{-3}$ at the respective transition frequency of LiH. For a molecule with a smaller eigenfrequency $\omega_{k0}$ the gold cavity does slightly better because the permittivity is larger. Consider the vibrational transition of YbF with $\omega_{k0}\approx 9\times 10^{10}$ rad/s as an example, for which the effective reflectivity of the gold cavity (in the sense of Fig. 6) increases to about $1-10^{-3.5}$.

### E. Enhanced reflectivity using Bragg mirrors

In contrast with the nonresonant CP force which depends on a very broad band of frequencies, the resonant part of the ground-state force on a two-level molecule depends on the reflection properties of the cavity at a single frequency, $\omega=\omega_{k0}$. In addition, the resonance of the cavity is also associated with a single value of the wave vector $\mathbf{k}_\perp$, namely, normal incidence. An enhancement of the propagating potential hence does not require a good conductor like gold which is a good reflector for a broad range of frequencies and all angles of incidence; instead, cavity walls whose reflectivity has a sharp peak at normal incidence and the single frequency $\omega_{k0}$ are sufficient. The obvious candidate is to use multilayer Bragg mirrors, which consist of alternating layers of two different materials, each layer of thickness being equal to one quarter of the wavelength $\lambda_{10}=2\pi/n\omega_{k0}$ in that layer, where $n$ is the respective refractive index.

The reflection coefficient of a stack of layers with permittivities $\varepsilon_j$ and thicknesses $d_j$ is found by recursive use of the formula

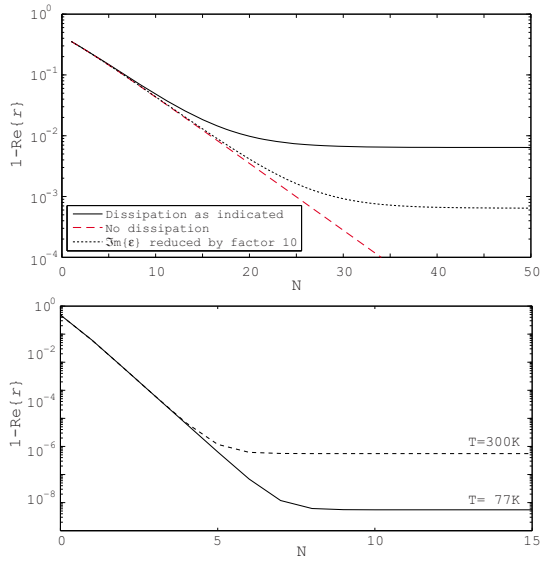


FIG. 7. (Color online) Reflection coefficients of Bragg mirrors for normal incidence at the rotational transition frequency of LiH vs the number of double layers $N$. *Above:* GaAs/AlAs mirror, where the results for reduced and vanishing absorption are also displayed for comparison. *Below:* Vacuum/sapphire mirror at two different temperatures $T=77$ and 300 K.

$$r_{ijk\cdots}=\frac{r_{ij}+r_{jk(l\cdots)}e^{2i\beta_j d_j}}{1+r_{ij}r_{jk(l\cdots)}e^{2i\beta_j d_j}} \tag{35}$$

($\beta_j=\sqrt{n_j^2\omega^2/c^2-k_\perp^2}$), which relates the reflection coefficient of a set of three adjacent layers $ijk\cdots$ (and all the layers behind) to the respective result for the next set of adjacent layers $jkl\cdots$. If the $k$th layer is the last one of the stack, the coefficients $r_{jk(l\cdots)}$ reduce to the two-layer coefficients $r_{jk}$. In straightforward generalization of Eqs. (9a) and (9b), the two-layer coefficients read

$$r_{ij}^s=\frac{\beta_i-\beta_j}{\beta_i+\beta_j}, \tag{36a}$$

$$r_{ij}^p=\frac{\varepsilon_j\beta_i-\varepsilon_i\beta_j}{\varepsilon_j\beta_i+\varepsilon_i\beta_j} \tag{36b}$$

for $s$- and $p$-polarized waves, respectively. The Casimir effect for such multilayer stacks has been extensively studied in the past [34–37].

A very common pair of materials to use for Bragg mirrors is GaAs and AlAs. At the rotational transition frequency of LiH, the permittivity of the two materials can be roughly given as $\varepsilon_{\mathrm{GaAs}}=12.96+0.02i$ [38,39] and $\varepsilon_{\mathrm{AlAs}}=10.96+0.02i$ [40]. The reflection coefficient of a GaAs/AlAs Bragg mirror is plotted as a function of the number of (double) layers $N$ in the upper panel of Fig. 7. For a given $N$, the Bragg mirror consists of $2N+1$ layers in total, i.e., $N$ pairs of GaAs and AlAs layers of thickness $\lambda_{10}/4$ (beginning with

GaAs) and a terminating GaAs layer of infinite thickness. As Fig. 7 shows, the reflectivity initially increases for increasing $N$ and then eventually saturates for $N \gtrsim 30$ to some finite value where $1-\mathrm{Re}\, r \simeq 10^{-2}$. This saturation is due to absorption, as is illustrated by the other two curves, where we have given the results that would be obtained for a reduced or vanishing imaginary part of the permittivities. For a reduced imaginary part, the saturation sets in for higher $N$, and consequently to a lower $\delta$. In the absence of absorption, the reflectivity could be brought arbitrarily close to unity by adding more and more layers.

A higher reflectivity could hence be obtained by using materials with very small dielectric loss. One example of such a Bragg mirror could be alternating layers of vacuum and sapphire, which can have an extremely low loss tangent ($\mathrm{Im}\,\varepsilon/\mathrm{Re}\,\varepsilon \simeq 10^{-5}$ and $10^{-7}$ at room temperature and 77 K, respectively [41]) combined with a refractive index considerably larger than unity ($\mathrm{Re}\,\varepsilon \simeq 10$ [42]). Using the approximative values $\varepsilon_{\mathrm{sapph}} = 10 + 10^{-4} i$ at 300 K and $\varepsilon_{\mathrm{sapph}} = 10 + 10^{-6} i$ at 77 K, we have computed the reflection coefficients of the vacuum/sapphire mirror as displayed in the lower panel of Fig. 7. At room temperature, the coefficient saturates at $N \gtrsim 6$ to $\delta = 5.5 \times 10^{-6}$. At $T = 77$ K, the reflection coefficient saturates at $N \gtrsim 8$ to $\delta = 5.5 \times 10^{-8}$, the increase in reflectivity is obviously due to the reduction in material absorption for the lower temperature. Note that in comparison to the GaAs/AlAs mirror, the number of layers required for saturation is significantly lower because of the larger dielectric contrast; and the room-temperature reflectivity at saturation is increased by about four orders of magnitude.

The resulting propagating part of the resonant CP potential at resonant-cavity width using the sapphire/vacuum Bragg mirror at $T = 77$ K and 300 K are shown in Fig. 8, where the corresponding graphs at various constant reflection coefficients have also been displayed for reference. The effective reflection coefficients achieved at the two temperatures are around $\delta = 10^{-4.8}$ and $\delta = 10^{-6.7}$, respectively, and the potential depths approximately a factor 2.45 and 1.77 greater than that of the gold cavity at the same temperatures. Note, however, that the effect of the enhanced reflectivity at 77 K is counteracted by the overall decrease of the potential due to the lower photon number.

### F. Lifetime of the ground state in the cavity

Resonant CP potentials are only present for molecules which are not at equilibrium with their thermal environment, i.e., on a time scale given by the inverse heating rate [19]. When enhancing the thermal CP potential via a resonant cavity, it is necessary to ascertain that the simultaneous cavity enhancement of heating rates does not reduce the lifetime of the resonant potential by so much as to render it experimentally inaccessible. We show in the following that the lifetime of the molecular ground state is not radically changed even by the presence of a resonant planar cavity.

The total heating rate of an isotropic molecule out of its ground state may be written as [17] $\Gamma = \Gamma_0 + \Gamma_{\mathrm{cav}}$, where

$$\Gamma_0 = \frac{\Sigma_k |\mathbf{d}_{0k}|^2 \omega_{k0}^3 n(\omega_{k0})}{3\pi\hbar c^3 \varepsilon_0} \tag{37}$$

is the heating rate in free space and

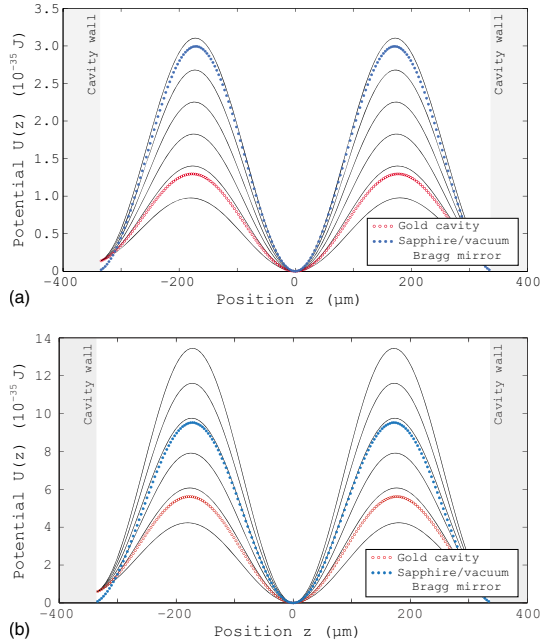


FIG. 8. (Color online) Resonant part of the thermal CP potential associated with the rotational transitions of a ground-state LiH molecule at $\nu = 2$ resonance with a gold cavity and a cavity bounded by vacuum/sapphire Bragg mirrors at two different temperatures: 77 K above, 300 K below. The solid black lines represent calculations at constant reflection coefficients as in Fig. 6; the corresponding values of $1-r$ decrease in powers of 10 from $10^{-2}$ (lowest curve) to $10^{-7}$ (highest curve). The same permittivity is used for gold for both temperatures.

$$\Gamma_{\mathrm{cav}} = \frac{2\mu_0}{3\hbar} \sum_k |\mathbf{d}_{0k}|^2 \omega_{k0}^2 n(\omega_{k0}) \mathrm{Im\ Tr}\, \mathbf{G}^{(1)}(\mathbf{r}, \mathbf{r}, \omega_{k0}) \tag{38}$$

is its change due to the presence of the cavity. Apart from the prefactor, this additional term has the same form as the expression for the potential, except that the imaginary part of the Green tensor is taken rather than the real part.

In Sec. II D, we had shown that for real and constant reflection coefficients, the Green tensor exhibits a logarithmic divergence as $r \to 1$ with a purely real coefficient, whereas all other contributions remain finite. This shows that the imaginary part of the Green tensor responsible for the decay rate can be expected to remain finite even for strongly increased reflectivity. It follows that the presence of the cavity does not drastically change the lifetime of the ground state of the molecule, which will typically be in the order of seconds. This is confirmed in Fig. 9 where we display the ground-state heating rate of a LiH molecule inside a $\nu = 1$ gold cavity and near a gold half-space. The lifetime is reduced by only a factor 2 at the center of the cavity, remaining in the order of seconds.

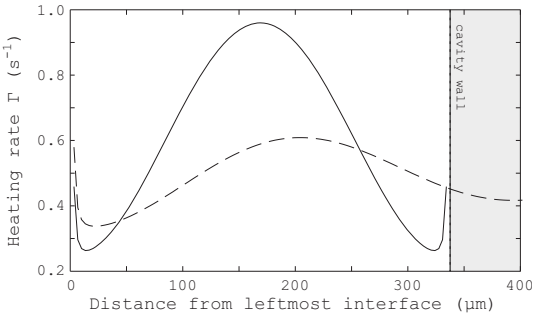


FIG. 9. Ground-state rotational heating rate of a LiH molecule in a gold cavity at $\nu=1$ resonance $a=\pi c/\omega_{k0}$ (solid line) and to the right of a gold half-space (dashed line) at room temperature ($T=300$ K).

## III. CONCLUSIONS AND OUTLOOK

We have studied the thermal Casimir-Polder potential of ground-state polar molecules placed within a planar cavity at room temperature. As was previously found in Ref. [19], the resonant absorption of thermal photons by a molecule gives rise to spatial oscillations of that potential. Our results demonstrate that the amplitude of these oscillations is enhanced when placing the molecule inside a suitable cavity such that a molecular transition frequency coincides with a cavity resonance. We have analyzed the dependence of this oscillating potential on the parameters of the molecule and the cavity by both analytical and numerical means and found that the depth of potential minima

(i) (Cavity resonance) decreases with increasing order of the cavity resonance approximately as $1/\nu$;

(ii) (Molecular eigenfrequency) is proportional to $\omega_{k0}^3 n(\omega_{k0})$ for good conductors, where $n(\omega_{k0})$ is the thermal-photon number;

(iii) (Molecular dipole moments) is proportional to the modulus squared $\Sigma_k|\mathbf{d}_{0k}|^2=d^2$ of the respective transition-dipole moment;

(iv) (Temperature) increases with temperature due to an increase of the thermal-photon number $n(\omega_{k0})$;

(v) (Reflectivity of cavity walls) scales as $\ln(1-r)$ for high reflectivity $r$.

In view of observing this potential and possibly utilizing it for the guiding of cold polar molecules, these observations imply the following strategies for enhancing the depth of the potential minima:

(i) *Cavity resonance.* The $\nu=2$ resonance is most suitable since it gives the deepest minimum.

(ii) *Molecular species.* At room temperature, the deepest minima are realized for molecules whose transitions are not too far from the peak frequency $1.11\times10^{14}$ rad/s and which at the same time feature suitably large transition-dipole moments. Good candidates are, e.g., LiH (rotational transitions), BaF (vibrational transitions), or OH (rotational transitions).

(iii) *Cavity walls.* Highly reflecting cavities are required in order to enhance the potential. Bragg mirrors consisting of materials with small absorption such as sapphire are favorable to single layers of good conductors like gold.

(iv) *Temperature.* Temperatures should be in the range of room temperature or even higher in order to achieve large photon numbers. This should be balanced, however, against the adverse reduction of reflectivity of most materials with increasing temperature.

With an optimum choice of all these parameters, the planar cavity can be used to enhance the resonant potential by one or at most two orders of magnitude with respect to the single-plate case. However, the thermal potentials achievable with planar cavities are in all likelihood still too small to facilitate the guiding of polar molecules.

The limitations of the enhancement of the potential in a planar cavity are ultimately due to the weak (logarithmic) scaling with reflectivity. A stronger scaling may be expected in geometries providing mode confinement in more than just one dimension such as cylindrical or spherical cavities. This will be investigated in a future publication. Note that apart from the different expected scaling with reflectivity, all other conclusions regarding the dependence of the potential on the relevant molecular and material parameters as given above hold irrespective of the geometry under consideration. The strategies for the enhancement of thermal CP potentials developed in this work will thus present a valuable basis when considering more complicated cavity geometries.

## ACKNOWLEDGMENTS

This work was supported by the Alexander von Humboldt Foundation, the U.K. Engineering and Physical Sciences Research Council, and the SCALA program of the European Commission. S.Å.E. acknowledges financial support from the European Science Foundation under the program "New Trends and Applications of the Casimir Effect."

## APPENDIX A: SCALING OF POTENTIAL DEPTH WITH RESONANCE ORDER

For a cavity of width $a=\nu\lambda_{k0}/2$ the potential has $\nu$ peaks, roughly located at $z=-\nu\lambda_{k0}/4+(\mu-1/2)\lambda_{k0}/2$ $(\mu=1,\ldots,\nu)$ and $\nu-1$ minima at $z=-\nu\lambda_{k0}/4+\mu\lambda_{k0}/2$ $(\mu=1,\ldots,\nu-1)$. For a given resonance order $\nu$, the deepest minima are the ones closest to the cavity walls (and which have a maximum on both sides), for example the rightmost one at $z=(\nu-2)\lambda_{k0}/4$. It has to be compared with the lower of the two adjacent maxima, i.e., the one immediately to the right at $z=(\nu-3)\lambda_{k0}/4$. The required depth of the deepest minimum is hence given by

$$\Delta U_\nu = U[(\nu-3)\lambda_{k0}/4]-U[(\nu-2)\lambda_{k0}/4]. \tag{A1}$$

We calculate this depth for a cavity whose reflection coefficients are independent of the transverse wave number $k_\perp$, $r_p=-r_s\equiv r$, and close to unity, $\delta=1-r\ll1$. Noting that the oscillating part of the potential is determined by $U_{\mathrm{pr}}$ and introducing definition (21), cf. Sec. II D, we thus have

$$\Delta U_\nu \propto I\left(\frac{1}{2}-\frac{3}{2\nu}\right)-I\left(\frac{1}{2}-\frac{1}{\nu}\right). \tag{A2}$$

We consider in the following only the terms which do not vanish as $\delta \to 0_+$. For arbitrary $\phi$, we have

$$I(\phi) = \frac{r}{2\pi\nu^3\lambda_{0k}^3}\mathrm{Im}\int_0^{2\pi\nu} dx \frac{x^2 e^{ix/2}\cos\phi x}{1-r^2e^{ix}}, \tag{A3}$$

which, after expanding the fraction in powers of $r^2$, solving the integral over $x$, and taking the imaginary part, can be written as

$$I(\phi) = \frac{r}{2\pi\nu^3\lambda_{0k}^3}\sum_{j=0}^{\infty}\left[y\left(j+\frac{1}{2}+\phi\right)+y\left(j+\frac{1}{2}-\phi\right)\right] \tag{A4}$$

with

$$y(p) = -\frac{2}{p^3}+\left(\frac{2}{p^3}-\frac{4\nu^2\pi^2}{p}\right)\cos(2\pi\nu p)+\frac{4\nu\pi}{p^2}\sin(2\pi\nu p). \tag{A5}$$

In particular, this implies

$$I\left(\frac{1}{2}-\frac{3}{2\nu}\right) = \frac{2r}{\pi\nu^3\lambda_{0k}^3}\sum_{j=0}^{\infty} r^{2j}\left[\frac{\nu^2\pi^2}{j+1-\frac{3}{2\nu}}+\frac{\nu^2\pi^2}{j+\frac{3}{2\nu}} - \frac{1}{\left(j+1-\frac{3}{2\nu}\right)^3}-\frac{1}{\left(j+\frac{3}{2\nu}\right)^3}\right], \tag{A6a}$$

$$I\left(\frac{1}{2}-\frac{1}{\nu}\right) = -\frac{2r\pi}{\nu\lambda_{0k}^3}\sum_{j=0}^{\infty}\left[\frac{r^{2j}}{j+1-\frac{1}{\nu}}+\frac{r^{2j}}{j+\frac{1}{\nu}}\right]. \tag{A6b}$$

The evaluation of sums with simple denominators can be performed by using the relation (formula 9.559 in Ref. [33])

$$\sum_{j=0}^{\infty}\frac{r^{2j}}{j+b} = \frac{1}{b}F(1,b;1+b;r^2), \tag{A7}$$

valid for any $b \neq 0,-1,-2,\ldots$ Here, $F(a,b;c;z) \equiv {}_2F_1(a,b;c;z)$ is a hypergeometric function which in turn has the following expansion in powers of $\delta = 1-r$ (formula 15.3.10 in Ref. [43]):

$$\frac{1}{b}F(1,b;1+b;r^2) \sim -\ln\delta - \ln 2 - \gamma - \psi(b) \tag{A8}$$

as $\delta \to 0_+$, the correction terms being of order $\delta\ln\delta$. Here, $\psi(x)$ is the logarithmic derivative of the gamma function and $\psi(1) = -\gamma$, where $\gamma = 0.577\,216$ is Euler's constant.

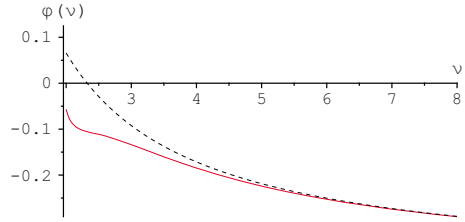


FIG. 10. (Color online) Graph of $\varphi(\nu)/\nu$ (solid line) and its asymptote (dashed line) as given by Eq. (A13).

For the sums in Eq. (A6) with cubic denominators, one can set $r=1$ with an error of order $\delta$. The sums are then simply Hurwitz zeta functions $\zeta(3,b)$,

$$\sum_{l=0}^{\infty}\frac{1}{(l+b)^3} \equiv \zeta(3,b). \tag{A9}$$

We thus find

$$I\left(\frac{1}{2}-\frac{3}{2\nu}\right)-I\left(\frac{1}{2}-\frac{1}{\nu}\right) = -\frac{8\pi}{\nu\lambda_{0k}^3}[\ln\delta+\varphi(\nu)]+\cdots \tag{A10}$$

as $\delta \to 0_+$ with corrections being of order $\delta\ln\delta$ and

$$\varphi(\nu) \equiv \ln 2+\gamma+\frac{1}{4}\psi\left(1-\frac{3}{2\nu}\right)+\frac{1}{4}\psi\left(\frac{3}{2\nu}\right)+\frac{1}{4}\psi\left(1-\frac{1}{\nu}\right) + \frac{1}{4}\psi\left(\frac{1}{\nu}\right)+\frac{1}{4\pi^2\nu^2}\left[\zeta\left(3,1-\frac{3}{2\nu}\right)+\zeta\left(3,\frac{3}{2\nu}\right)\right]. \tag{A11}$$

Some numerical values of $\varphi(\nu)$ are

$$\varphi(2) = -0.113\,442\,372\,4, \tag{A12a}$$

$$\varphi(3) = -0.401\,594\,950\,3, \tag{A12b}$$

$$\varphi(4) = -0.738\,447\,947\,0. \tag{A12c}$$

We give a plot of $\varphi(\nu)/\nu$ in Fig. 10. For large $\nu$, one obviously has

$$\varphi(\nu) \sim -\left(\frac{5}{12}-\frac{2}{27\pi^2}\right)\nu+\ln(2)+\frac{1}{4}+\ldots \approx -0.409\,161\,393\,8\,\nu+0.943\,147\,180\,6+\cdots \tag{A13}$$

plus terms of order $\nu^{-1}$ and smaller. Already at $\nu=4$ this is a fairly good approximation to Eq. (A11) as shown in Fig. 10.

[1] H. B. G. Casimir and D. Polder, Phys. Rev. **73**, 360 (1948).
[2] E. M. Lifshitz, Zh. Eksp. Teor. Fiz. **29**, 94 (1955) [Sov. Phys. JETP **2**, 73 (1956)].
[3] A. D. McLachlan, Proc. R. Soc. London, Ser. A **274**, 80 (1963).
[4] C. Henkel, K. Joulain, J. P. Mulet, and J.-J. Greffet, J. Opt. A, Pure Appl. Opt. **4**, S109 (2002).
[5] G. L. Klimchitskaya, E. V. Blagov, and V. M. Mostepanenko, J. Phys. A **39**, 6481 (2006).
[6] E. V. Blagov, G. L. Klimchitskaya, and V. M. Mostepanenko, Phys. Rev. B **71**, 235401 (2005).
[7] M. Bordag, B. Geyer, G. L. Klimchitskaya, and V. M. Mostepanenko, Phys. Rev. B **74**, 205431 (2006).
[8] M. Boström and B. E. Sernelius, Phys. Rev. A **61**, 052703 (2000).
[9] V. M. Nabutovskiĭ, V. R. Belosludov, and A. M. Korotkikh, Sov. Phys. JETP **50**, 352 (1979).
[10] E. V. Blagov, G. L. Klimchitskaya, and V. M. Mostepanenko, Phys. Rev. B **75**, 235413 (2007).
[11] M. Antezza, L. P. Pitaevskii, and S. Stringari, Phys. Rev. Lett. **95**, 113202 (2005).
[12] J. M. Obrecht, R. J. Wild, M. Antezza, L. P. Pitaevskii, S. Stringari, and E. A. Cornell, Phys. Rev. Lett. **98**, 063201 (2007).
[13] T. Nakajima, P. Lambropoulos, and H. Walther, Phys. Rev. A **56**, 5100 (1997).
[14] S.-T. Wu and C. Eberlein, Proc. R. Soc. London, Ser. A **456**, 1931 (2000).
[15] S. Y. Buhmann and D.-G. Welsch, Prog. Quantum Electron. **31**, 51 (2007).
[16] S. Scheel and S. Y. Buhmann, Acta Phys. Slov. **58**, 675 (2008).
[17] S. Y. Buhmann and S. Scheel, Phys. Rev. Lett. **100**, 253201 (2008).
[18] M.-P. Gorza and M. Ducloy, Eur. Phys. J. D **40**, 343 (2006).
[19] S. Å. Ellingsen, S. Y. Buhmann, and S. Scheel, Phys. Rev. A **79**, 052903 (2009).
[20] S. Y. T. van de Meerakker, H. L. Bethlem, and G. Meijer, Nat. Phys. **4**, 595 (2008).
[21] S. Y. Buhmann, M. R. Tarbutt, S. Scheel, and E. A. Hinds, Phys. Rev. A **78**, 052901 (2008).
[22] G. Barton, Proc. R. Soc. London, Ser. A **320**, 251 (1970).
[23] G. Barton, Proc. R. Soc. London, Ser. A **367**, 117 (1979).
[24] G. Barton, Proc. R. Soc. London, Ser. A **410**, 141 (1987).
[25] W. Jhe, Phys. Rev. A **43**, 5795 (1991).
[26] W. Jhe, Phys. Rev. A **44**, 5932 (1991).
[27] E. A. Hinds, Adv. At. Mol. Opt. Phys. **28**, 237 (1991).
[28] E. A. Hinds, Adv. At. Mol. Opt. Phys. Suppl. **2**, 1 (1994).
[29] M. S. Tomaš, Phys. Rev. A **51**, 2545 (1995).
[30] A. Lambrecht and S. Reynaud, Eur. Phys. J. D **8**, 309 (2000).
[31] S. Å. Ellingsen, EPL **82**, 53001 (2008).
[32] S. Å. Ellingsen, in *The Casimir Effect and Cosmology: A Volume in Honour of Professor Iver H. Brevik on the Occasion of His 70th Birthday*, edited by S. Odintsov *et al.* (Tomsk State Pedagogical University Press, Tomsk, Russia, 2008), p. 45.
[33] I. S. Gradshteyn and I. M. Ryzhik, *Table of Integrals, Series and Products*, 4th ed. (Academic Press, New York, 1980).
[34] R. Esquivel-Sirvent, C. Villarreal, and G. H. Cocoletzi, Phys. Rev. A **64**, 052108 (2001).
[35] C. Raabe, L. Knöll, and D.-G. Welsch, Phys. Rev. A **68**, 033810 (2003).
[36] M. S. Tomaš, Phys. Lett. A **342**, 381 (2005).
[37] S. Å. Ellingsen, J. Phys. A **40**, 1951 (2007).
[38] C. J. Johnson, G. H. Sherman, and R. Weil, Appl. Opt. **8**, 1667 (1969).
[39] W. E. Courtney, IEEE Trans. Microwave Theory Tech. **25**, 697 (1977).
[40] S. Adachi, J. Appl. Phys. **58**, R1 (1985).
[41] M. M. Driscoll, J. T. Haynes, R. A. Jelen, R. W. Weinert, J. R. Gavaler, J. Talvacchio, G. R. Wagner, K. A. Zaki, and X. P. Liang, IEEE Trans. Ultrason. Ferroelectr. Freq. Control **39**, 405 (1992).
[42] G. G. Wang, M. F. Zhang, J. C. Han, X. D. He, H. B. Zuo, and X. H. Yang, Cryst. Res. Technol. **43**, 531 (2008).
[43] M. Abramowitz and I. A. Stegun, *Handbook of Mathematical Functions* (Dover, New York, 1964).

# Article [n]

***Temperature-Independent Casimir-Polder Forces Despite Large Thermal Photon Numbers***

S.Å. Ellingsen, S.Y. Buhmann, S. Scheel

Physical Review Letters **104**, 223003 (2010)

# Temperature-Independent Casimir-Polder Forces Despite Large Thermal Photon Numbers

Simen Å. Ellingsen,[1,*] Stefan Yoshi Buhmann,[2] and Stefan Scheel[2]

[1]*Department of Energy and Process Engineering, Norwegian University of Science and Technology, N-7491 Trondheim, Norway*
[2]*Quantum Optics and Laser Science, Blackett Laboratory, Imperial College London, Prince Consort Road, London SW7 2AZ, United Kingdom*

(Received 2 March 2010; published 2 June 2010)

We demonstrate that Casimir-Polder potentials can be entirely independent of temperature even when allowing for the relevant thermal photon numbers to become large. This statement holds for potentials that are due to low-energy transitions of a molecule placed near a plane metal surface whose plasma frequency is much larger than any atomic resonance frequencies. For a molecule in an energy eigenstate, the temperature independence is a consequence of strong cancellations between nonresonant potential components and those due to evanescent waves. For a molecule with a single dominant transition in a thermal state, upward and downward transitions combine to form a temperature-independent potential. The results are contrasted with the case of an atom whose potential exhibits a regime of linear temperature dependence. Contact with the Casimir force between a weakly dielectric and a metallic plate is made.

DOI: 10.1103/PhysRevLett.104.223003 PACS numbers: 31.30.jh, 12.20.−m, 34.35.+a, 42.50.Nn

Dispersion forces between polarizable objects were originally predicted by Casimir and Polder as a consequence of quantum zero-point fluctuations [1]. Recent measurements of both Casimir-Polder (CP) forces between atoms and surfaces [2] and Casimir forces between macroscopic bodies [3,4] typically operate at room temperature, where thermal fluctuations also come into play [5–8]. The temperature dependence of dispersion forces is of relevance for both fundamental and practical reasons.

On the theoretical side, the correct description of the Casimir force between metals at finite temperature is subject to an ongoing debate [4,9]. To wit, predictions differ for the high-temperature behavior of the Casimir force between metals, for which employing a standard dissipative description of the surfaces fails to reproduce the experimental observations [10]. This suggests that progress can be made by directly observing the variation of the Casimir force with temperature.

On the practical side, CP forces become increasingly relevant when trying to trap and coherently manipulate cold atoms near surfaces [11]. Current endeavours aim at extending these techniques to more complex systems such as polar molecules [12]. Such systems typically exhibit long-wavelength transitions so that CP forces become increasingly long-ranged. This raises the question of whether they can be controlled by lowering the ambient temperature and hence suppressing thermal force components.

Thermal contributions to the CP potential are governed by the photon number $n(\omega) = [e^{\hbar\omega/(k_B T)} - 1]^{-1}$. A noticeable deviation of the potential from its zero-temperature value is to be expected when $n(\omega) \gtrsim 1$ in the relevant frequency range. This is the case, for instance, for molecules with small transition frequencies, $|\omega_{kn}| \lesssim k_B T/\hbar = 3.93 \times 10^{13}$ rad/s at room temperature (300 K). The associated wavelengths are much larger than typical experimental molecule-surface separations in the nanometer to micrometer range [2], $z_A \ll c/|\omega_{kn}|$. Furthermore, experimental realizations typically involve metal surfaces with $|\varepsilon(\omega_{kn})| \gg 1$ which act like perfect reflectors.

As we will show in this Letter, the above three conditions combined result in potentials which are independent of temperature over the entire range from zero to room temperature and beyond. We will first discuss the case of a molecule prepared in an energy eigenstate and then consider molecules at thermal equilibrium with their environment, comparing our results with those for atoms whose transitions involve higher energies.

*Molecule vs atom in an eigenstate.*—As shown in Ref. [13], the CP potential of a molecule prepared in an isotropic energy eigenstate $|n\rangle$ at distance $z_A$ from the plane surface of a metal,

$$U_n(z_A) = U_n^{\mathrm{nr}}(z_A) + U_n^{\mathrm{ev}}(z_A) + U_n^{\mathrm{pr}}(z_A), \tag{1}$$

may be separated into three contributions: a nonresonant term $U_n^{\mathrm{nr}}$ due to virtual photons that is formally similar to that produced by the Lifshitz theory [5], and a resonant contribution due to real photons which may be further split into contributions from evanescent ($U_n^{\mathrm{ev}}$) and propagating ($U_n^{\mathrm{pr}}$) waves. The nonresonant potential is given by [13]

$$U_n^{\mathrm{nr}}(z_A) = -\frac{\mu_0 k_B T}{6\pi\hbar} \sum_k |\boldsymbol{d}_{nk}|^2 {\sum_{j=0}^{\infty}}' \frac{\omega_{kn}}{\omega_{kn}^2 + \xi_j^2} \int_{\xi_j/c}^{\infty} db \times e^{-2bz_A} \{2b^2 c^2 r_p(i\xi_j) - \xi_j^2 [r_s(i\xi_j) + r_p(i\xi_j)]\} \tag{2}$$

[$\omega_{kn} = (E_k - E_n)/\hbar$, transition frequencies; $\boldsymbol{d}_{nk}$, dipole matrix elements; $\xi_j = j\xi$ with $\xi = 2\pi k_B T/\hbar$, Matsubara frequencies; and the primed summation indicates half-weight for the term $j = 0$] and the evanescent one reads

$$U_n^{\mathrm{ev}}(z_A) = \frac{\mu_0}{12\pi} \sum_k n(\omega_{kn}) |\boldsymbol{d}_{nk}|^2 \int_0^{\infty} db e^{-2bz_A} \times \{2b^2 c^2 \mathrm{Re}[r_p(\omega_{kn})] + \omega_{nk}^2 \mathrm{Re}[r_s(\omega_{kn}) + r_p(\omega_{kn})]\}; \tag{3}$$

note that $n(\omega_{kn}) = -[n(\omega_{nk}) + 1]$ for downward transi-

 

tions. These two contributions dominate in the region $z_A|\omega_{kn}|/c \ll 1$ that we are interested in, while the spatially oscillating $U_n^{pr}$ becomes relevant only in the far-field range $z_A|\omega_{kn}|/c \gg 1$. The reflection coefficients of the surface for $s$- and $p$-polarized waves are given by $r_s(\omega) = (b - b_1)/(b + b_1)$ and $r_p(\omega) = [\varepsilon(\omega)b - b_1]/[\varepsilon(\omega)b + b_1]$ with $b_1 = \sqrt{b^2 - [\varepsilon(\omega) - 1]\omega^2/c^2}$, $\mathrm{Re}(b_1) > 0$.

For our analytical investigations, we will model the metal surface by a perfect reflector with frequency-independent reflection coefficients $r_s \approx -1$ and $r_p \approx 1$. This is well justified, as the plasma frequency is typically much larger than the molecular transition frequency $\omega_{kn}$, and hence $|\varepsilon(\omega)| \gg 1$ in the relevant frequency range. The $b$ integrals can then be performed to give

$$U_n^{nr}(z_A) = -\frac{k_B T}{12\pi\varepsilon_0\hbar z_A^3}\sum_k |\boldsymbol{d}_{nk}|^2 {\sum_{j=0}^{\infty}}' \frac{\omega_{kn} e^{-2jz_A\xi/c}}{\omega_{kn}^2 + j^2\xi^2} \times\left[1 + 2j\frac{z_A\xi}{c} + 2j^2\frac{z_A^2\xi^2}{c^2}\right], \quad (4)$$

$$U_n^{ev}(z_A) = \frac{1}{24\pi\varepsilon_0 z_A^3}\sum_k n(\omega_{kn})|\boldsymbol{d}_{nk}|^2. \quad (5)$$

The asymptotic temperature dependence of the potential for a given distance $z_A$ is governed by two characteristic temperatures: The molecular transition frequency defines a spectroscopic temperature $T_\omega = \hbar|\omega_{kn}|/k_B$, which is roughly the temperature required to noticeably populate the upper level. Similarly, the distance introduces a geometric temperature $T_z = \hbar c/(z_A k_B)$, i.e., the temperature of radiation whose wavelength is of the order $z_A$.

We will now show that the total potential becomes independent of temperature in both the geometric low-temperature limit $T \ll T_z$ and the spectroscopic high-temperature limit $T \gg T_\omega$. For a typical molecule with its long-wavelength transitions, the potential is nonretarded for typical molecule-surface distances, $z_A|\omega_{kn}|/c \ll 1$. As depicted in Fig. 1 (i), this implies $T_\omega \ll T_z$; hence, the two regions of constant potential overlap and the potential is constant for all temperatures. For an atom, on the contrary, the transition wavelengths are much shorter, so that we may have $z_A|\omega_{kn}|/c \gg 1$. In this case, an intermediate regime $T_z \ll T \ll T_\omega$ exists where the potential increases linearly with temperature, cf. Fig. 1 (ii).

We begin with a typical molecule with $z_A|\omega_{kn}|/c \ll 1$. In the geometric low-temperature limit $T \ll T_z$, we have $z_A\xi/c \ll 1$; hence, the sum in Eq. (4) is densely spaced. The factor $1/(\omega_{kn}^2 + j^2\xi^2)$ restricts it to values where $jz_A\xi/c \leq z_A|\omega_{kn}|/c \ll 1$. With this approximation, the summation can be performed as

$${\sum_{j=0}^{\infty}}' \frac{1}{a^2 + j^2} = \frac{\pi}{2a}\coth(\pi a) \quad (6)$$

and we find

$$U_n^{nr}(z_A) \overset{T\ll T_z}{=} -\frac{1}{24\pi\varepsilon_0 z_A^3}\sum_k\left[n(\omega_{kn}) + \frac{1}{2}\right]|\boldsymbol{d}_{nk}|^2, \quad (7)$$

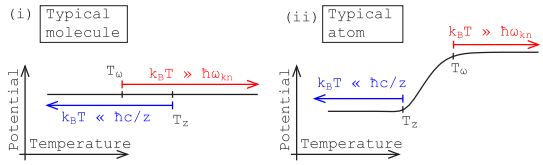


FIG. 1 (color online). Sketch of the temperature dependence of the CP potential for a typical molecule vs a typical atom.

noting that $\coth[\hbar\omega_{kn}/(2k_BT)] = 2n(\omega_{kn}) + 1$. Adding the evanescent contribution (5), we find the temperature-independent total potential

$$U_n(z_A) \overset{T\ll T_z}{=} -\frac{\sum_k |\boldsymbol{d}_{nk}|^2}{48\pi\varepsilon_0 z_A^3} = -\frac{\langle\hat{\boldsymbol{d}}^2\rangle_n}{48\pi\varepsilon_0 z_A^3}, \quad (8)$$

in agreement with the well-known nonretarded zero-temperature result [1].

In the spectroscopic high-temperature limit $T \gg T_\omega$, we have $\xi/|\omega_{kn}| \gg 1$. Because of the denominator $\omega_{kn}^2 + j^2\xi^2$, the $j = 0$ term strongly dominates the sum in Eq. (4) and we find

$$U_n^{nr}(z_A) \overset{T\gg T_\omega}{=} -\frac{1}{24\pi\varepsilon_0 z_A^3}\sum_k \frac{k_B T}{\hbar\omega_{kn}}|\boldsymbol{d}_{nk}|^2. \quad (9)$$

Under the condition $T \gg T_\omega$, i.e., $k_BT \gg \hbar|\omega_{kn}|$, the evanescent contribution (5) reduces to

$$U_n^{ev}(z_A) \overset{T\gg T_\omega}{=} \frac{1}{24\pi\varepsilon_0 z_A^3}\sum_k\left(\frac{k_B T}{\hbar\omega_{kn}} - \frac{1}{2}\right)|\boldsymbol{d}_{nk}|^2. \quad (10)$$

Adding the two results, the total potential is again temperature independent and given by Eq. (8). This limit is just the high-temperature saturation found in Refs. [7,13].

The thermal CP potential of a typical molecule with its long-wavelength transitions has thus been found to be temperature independent in the geometric low-temperature and spectroscopic high-temperature regimes. Because of the condition $z_A|\omega_{kn}|/c \ll 1$, at least one of the conditions $T \ll T_z$ or $T \gg T_\omega$ always holds, implying that the potential is constant for all temperatures and it agrees with its zero-temperature value. The independence of the total potential in both regimes is a result of cancellations between nonresonant and evanescent potential components, which both strongly depend on temperature. This is illustrated in Fig. 2, where we display the total temperature-independent potential as well as its nonresonant and evanescent parts for a ground-state LiH molecule in front of a Au surface for various temperatures. It is seen that very strong cancellations occur, especially at high temperatures. Note that, while our theoretical arguments are based on the perfect-conductor limit, all numerical examples use the reflectivities of real metals.

We now turn to the case of atoms, whose electronic wavelengths are short compared to typical experimental separations: $z_A|\omega_{kn}|/c \gg 1$. The exponential restricts the sum in Eq. (4) to terms with $j\xi \lesssim c/z_A \ll |\omega_{kn}|$, so the

term $j^2\xi^2$ in the denominator may be neglected. The sum can then be performed according to

$$\sum_{j=0}^{\infty}{}' e^{-2ja}(1+2ja+2j^2a^2) \to \begin{cases} 3/(2a) & a \ll 1 \\ 1/2 & a \gg 1. \end{cases} \quad (11)$$

In the geometric low-temperature regime $T \ll T_z$, we further have $z_A\xi/c \ll 1$, i.e., $a \ll 1$ in Eq. (11); hence

$$U_n^{\mathrm{nr}}(z_A) \overset{T\ll T_z}{=} -\frac{c}{16\pi^2\varepsilon_0 z_A^4}\sum_k \frac{|\boldsymbol{d}_{nk}|^2}{\omega_{kn}}, \quad (12)$$

in agreement with the famous zero-temperature result of Casimir and Polder [1]. Moreover, the condition $z_A|\omega_{kn}|/c \gg 1$ implies that $T \ll T_z \ll T_\omega$: The geometric low-temperature regime is also a spectroscopic one, and hence the evanescent potential reduces to

$$U_n^{\mathrm{ev}}(z_A) \overset{T\ll T_z}{=} -\frac{1}{24\pi\varepsilon_0 z_A^3}\sum_k \Theta(\omega_{nk})|\boldsymbol{d}_{nk}|^2. \quad (13)$$

[$\Theta(x)$ is the unit step function.] Adding the two contributions, we find the temperature-independent total potential

$$U_n(z_A) \overset{T\ll T_z}{=} -\frac{1}{24\pi\varepsilon_0 z_A^3}\sum_k \left[\frac{3c}{2z_A\omega_{kn}} + \Theta(\omega_{nk})\right]|\boldsymbol{d}_{nk}|^2 \quad (14)$$

in the geometric low-temperature regime.

For intermediate temperatures $T_z \ll T \ll T_\omega$, we have $z_A\xi/c \gg 1$, so using $a \gg 1$ in the sum (11), the nonresonant potential (4) is found to read as in Eq. (9). The evanescent contribution is still given by Eq. (13), so the total potential varies linearly with temperature,

$$U_n(z_A) \overset{T_z\ll T\ll T_\omega}{=} -\frac{1}{24\pi\varepsilon_0 z_A^3}\sum_k \left[\frac{k_BT}{\hbar\omega_{kn}} + \Theta(\omega_{nk})\right]|\boldsymbol{d}_{nk}|^2. \quad (15)$$

In the spectroscopic high-temperature limit $T \gg T_\omega$, the evanescent contribution is given by Eq. (10) as already shown. It cancels with the nonresonant contribution, still agreeing with Eq. (9), to give a saturated potential of the form (8). However, with, e.g., $T_\omega \approx 18.000$ K for Rb, this saturation is unobservable. Moreover, as the electronic transition frequencies can be comparable to the plasma frequency of the metal, the assumptions $r_s \approx -1$ and $r_p \approx 1$ do not hold. As a consequence, the cancellations required to achieve saturation do not occur for atoms near realistic metal surfaces.

We have thus seen that for an atom with $z_A|\omega_{kn}|/c \gg 1$, separate geometric low-temperature and spectroscopic high-temperature regimes exist, with the potential exhibiting a linear temperature dependence between these two regions. The difference between the thermal CP potentials of typical atoms vs molecules is illustrated in Fig. 3, where we show the temperature dependence of the potential at fixed distance from a Au surface for different species. The potentials associated with the long-wavelength, rotational transitions of LiH and OH are virtually temperature independent, while the short-wavelength electronic transition of Rb shows a linear increase over a large range of temperatures. YbF, with its dominant vibrational transition, lies in between the two extremes of typical long-wavelength molecular and short-wavelength atomic transitions; its potential increases by about 30% in the displayed temperature range. In contrast to the other examples, the potential of YbF noticeably deviates from the corresponding ideal conductor result due to imperfect reflection. Note that contributions to the molecular CP potentials due to electronic transitions are smaller than the rotational and vibrational ones (8) by factors $c/(z_A\omega_{kn}) \ll 1$ (14) or $k_BT/(\hbar\omega_{kn}) \ll 1$ (15) within the displayed temperature range and are hence negligible.

*Molecule at thermal equilibrium.*—The proven temperature independence immediately generalizes to molecules in incoherent superpositions of energy eigenstates with temperature-independent probabilities $p_n \neq p_n(T)$ and total potential $U(z_A) = \sum_n p_n U_n(z_A)$. The situation is different for a molecule at thermal equilibrium with its environment because the respective probabilities $p_n(T) = \exp[-E_n/(k_BT)]/\sum_k \exp[-E_k/(k_BT)]$ do depend on $T$. At thermal equilibrium, all resonant potential components

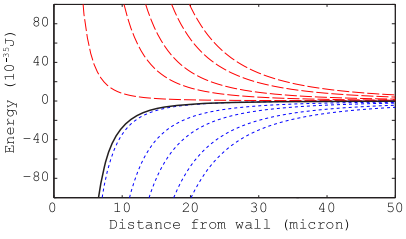


FIG. 2 (color online). CP potential of a ground-state LiH molecule in front of a Au surface. We show the total potential (solid line) as well as its evanescent (dashed line) and nonresonant (dotted line) contributions for temperatures 10 K, 50 K, 100 K, 200 K, 300 K (left to right).

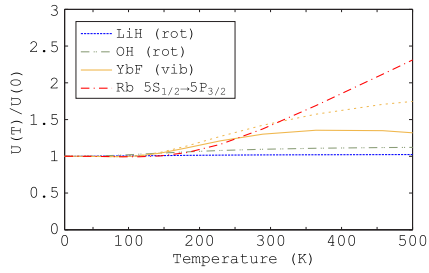


FIG. 3 (color online). Temperature dependence of the CP potential of various ground-state atoms and molecules at distance $z_A = 5$ $\mu$m from a Au surface. The transition frequencies of these species are such that $z_A\omega_{kn}/c = 0.046$ (LiH), 0.26 (OH), 1.59 (YbF), 40.2 (Rb). For comparison, the perfect-conductor result for YbF is also shown (dotted line).

cancel pairwise [8]. Introducing potential components $U_{nk}$ due to a particular transition $n \leftrightarrow k$ (such that $U_n = \sum_k U_{nk}$) and the associated statistical weights $p_{nk} = p_n + p_k$, and exploiting the fact that $U_{kn} = -U_{nk}$, we can write the total potential in the form

$$U(z_A) = \sum_{n<k} (p_n - p_k) U^{\mathrm{nr}}_{nk}(z_A) = \sum_{n<k} p_{nk} \tanh\left(\frac{\hbar\omega_{kn}}{2k_B T}\right) U^{\mathrm{nr}}_{nk}(z_A). \quad (16)$$

The behavior of this potential in the two limits relevant for a molecule with $z_A|\omega_{kn}|/c \ll 1$ follows immediately from the asymptotes given in the previous section. For $T \ll T_z$, $U^{\mathrm{nr}}_{nk}$ from Eq. (7) leads to

$$U(z_A) \overset{T \ll T_z}{=} -\frac{1}{48\pi\varepsilon_0 z_A^3} \sum_{n<k} p_{nk} |\boldsymbol{d}_{nk}|^2, \quad (17)$$

where $n(\omega_{kn}) + 1/2 = \coth[\hbar\omega_{kn}/(2k_B T)]/2$ has been used once more. For $T \gg T_\omega$, we recall $U^{\mathrm{nr}}_{nk}$ from Eq. (9) and note that $\tanh[\hbar\omega_{kn}/(2k_B T)] \approx \hbar\omega_{kn}/(2k_B T)$ to again find the potential (17).

Combining the two results, we may use the main argument of the previous section to conclude that the potential components $U_{nk}$ associated with a particular transition $n \leftrightarrow k$ are independent of temperature for all temperatures. The independence is a result of cancellations between the purely nonresonant contributions from lower state $n$ and upper state $k$. Note, however, that the statistical weights $p_{nk}$ introduce a weak temperature dependence, in general: The total potential is only strictly temperature independent when dominated by a single transition. For instance, when accounting for the presence of the first vibrational transition in LiH (labeled as 2), the weight $p_{01}$ for the dominant rotational transition varies from its zero-temperature value unity to $p_{01}(T) = (1 + e^{-\hbar\omega_{10}/k_B T})/(1 + e^{-\hbar\omega_{10}/k_B T} + e^{-\hbar\omega_{20}/k_B T}) = 0.9994$ at room temperature.

*Relevance to Casimir forces.*—To illustrate the relevance of the demonstrated temperature independence to the Casimir force, let us consider an infinite dielectric half-space filled with molecules of number density $\eta$ at a distance $z$ from a metal plane. For a weakly dielectric medium, the Casimir energy per unit area is given by $E(z) = \int_z^\infty dz_A \eta U(z_A)$ [14]. Using Eq. (17), we find that

$$E(z) = \frac{\eta}{96\pi\varepsilon_0 z^2} \sum_{n<k} p_{nk} |\boldsymbol{d}_{nk}|^2, \quad (18)$$

which is temperature independent under the conditions mentioned above. Note that Lifshitz's expression only agrees with this statement if the correct thermal permittivity is used [8]. If the ground-state permittivity is used, one describes a system out of equilibrium, and the Lifshitz formula does not apply.

For dielectrics with a stronger response (such that $\varepsilon - 1 \ll 1$ does not hold), many-body effects will lead to temperature-dependent corrections of higher order in the molecular polarizability. They are suppressed in the spectroscopic high-temperature limit $T \gg T_\omega$, since they are of higher order in $\tanh[\hbar\omega_{kn}/(2k_B T)] \ll 1$. Our results hence remain valid in this latter limit even for moderately strong dielectrics. On the contrary, they do not immediately generalize to the force between two metals.

*Summary.*—The temperature independence encountered for molecules with long-wavelength transitions shows that CP forces on such systems cannot be altered via the ambient temperature. Instead, the original zero-temperature results of Casimir and Polder apply universally across the whole temperature range. It is worth emphasizing that a "classical" regime of linear temperature dependence is never reached. Our results further indicate that when accounting for the thermal excitation of the media, the temperature dependence of Casimir forces involving dielectrics may be weaker than previously thought.

We have benefited from discussions with I. Brevik, A. Lambrecht, and S. Reynaud. This work was supported by the U.K. Engineering and Physical Sciences Research Council. Support from the European Science Foundation within the activity "New Trends and Applications of the Casimir Effect" is gratefully acknowledged.

*simen.a.ellingsen@ntnu.no

[1] H. B. G. Casimir and D. Polder, Phys. Rev. **73**, 360 (1948).
[2] C. I. Sukenik *et al.*, Phys. Rev. Lett. **70**, 560 (1993); M. Marrocco *et al.*, Phys. Rev. Lett. **81**, 5784 (1998); H. Failache *et al.*, Phys. Rev. Lett. **83**, 5467 (1999); V. Druzhinina and M. DeKieviet, Phys. Rev. Lett. **91**, 193202 (2003); H. Kübler *et al.*, Nat. Photon. **4**, 112 (2010).
[3] S. de Man *et al.*, Phys. Rev. Lett. **103**, 040402 (2009); F. Capasso *et al.*, IEEE J. Sel. Top. Quantum Electron. **13**, 400 (2007) and references therein.
[4] M. Bordag *et al.*, *Advances in the Casimir Effect* (Oxford University Press, Oxford, 2009).
[5] E. M. Lifshitz, Sov. Phys. JETP **2**, 73 (1956).
[6] T. Nakajima, P. Lambropoulos, and H. Walther, Phys. Rev. A **56**, 5100 (1997); S.-T. Wu and C. Eberlein, Proc. R. Soc. A **456**, 1931 (2000); Y. Sherkunov, Phys. Rev. A **79**, 032101 (2009).
[7] M.-P. Gorza and M. Ducloy, Eur. Phys. J. D **40**, 343 (2006).
[8] S. Y. Buhmann and S. Scheel, Phys. Rev. Lett. **100**, 253201 (2008).
[9] I. Brevik *et al.*, New J. Phys. **8**, 236 (2006).
[10] R. S. Decca *et al.*, Ann. Phys. (N.Y.) **318**, 37 (2005).
[11] Y. J. Lin *et al.*, Phys. Rev. Lett. **92**, 050404 (2004).
[12] J. van Veldhoven, H. L. Bethlem, and G. Meijer, Phys. Rev. Lett. **94**, 083001 (2005).
[13] S. Å. Ellingsen, S. Y. Buhmann, and S. Scheel, Phys. Rev. A **79**, 052903 (2009).
[14] C. Raabe and D.-G. Welsch, Phys. Rev. A **73**, 063822 (2006).

# Article [o]

***Thermal Casimir-Polder shifts in Rydberg atoms near metallic surfaces***

J.A. Crosse, S.Å. Ellingsen, K. Clements, S.Y. Buhmann, S. Scheel

Physical Review A **82**, 010901(R) (2010)
Physical Review A **82**, 029902(E) (2010)

PHYSICAL REVIEW A **82**, 010901(R) (2010)

# Thermal Casimir-Polder shifts in Rydberg atoms near metallic surfaces

J. A. Crosse,[1,*] Simen Å. Ellingsen,[2] Kate Clements,[1] Stefan Y. Buhmann,[1] and Stefan Scheel[1]
[1]*Quantum Optics and Laser Science, Blackett Laboratory, Imperial College London, Prince Consort Road, London SW7 2AZ, United Kingdom*
[2]*Department of Energy and Process Engineering, Norwegian University of Science and Technology, N-7491 Trondheim, Norway*
(Received 10 May 2010; published 8 July 2010)

The Casimir-Polder (CP) potential and transition rates of a Rydberg atom above a plane metal surface at finite temperature are discussed. As an example, the CP potential and transition rates of a rubidium atom above a copper surface at 300 K are computed. Close to the surface we show that the quadrupole correction to the force is significant and increases with increasing principal quantum number $n$. For both the CP potential and decay rates one finds that the dominant contribution comes from the longest wavelength transition and the potential is independent of temperature. We provide explicit scaling laws for potential and decay rates as functions of atom-surface distance and principal quantum number of the initial Rydberg state.

DOI: 10.1103/PhysRevA.82.010901 PACS number(s): 34.35.+a, 32.80.Ee, 42.50.Ct, 42.50.Nn

Rydberg atoms—atoms excited to large principal quantum numbers $n$—have attracted much attention in recent decades [1,2]. Aside from the inherent interest of studying such extreme states, the exaggerated properties of these highly excited atoms make them ideal for examining the properties of a variety of systems that would be awkward to probe by other means. The large cross sections and weakly bound outer electrons associated with Rydberg atoms make them extremely sensitive to small-scale perturbations and dispersion potentials, such as the van der Waals (vdW) and Casimir–Polder (CP) potentials [3].

For example, the strong scaling of the free-space vdW potential between two Rydberg atoms with $n$ ($\propto n^{11}$) leads to the Rydberg blockade mechanism which has been put forward as a candidate for implementing controlled gate operations between isolated atoms [4,5]. The effect relies on the massive level shift that one Rydberg atom experiences in close proximity to another.

Level shifts of similar origin arise if the atoms are brought into the vicinity of a macroscopic body. With the increasing ability to trap and manipulate atoms close to macroscopic bodies, the effects of these surface (CP) potentials have become a subject of great interest. Applications range from novel atom trapping methods [6] to atom chip physics [7]. Thus, it is of both fundamental and practical interest to understand the interplay between atoms in highly excited states and field fluctuations emanating from macroscopic bodies.

In this Rapid Communication we provide evidence that dispersion forces have a sizable effect on the energy levels of highly excited Rydberg atoms when brought close to metallic surfaces, with shifts on the order of several GHz expected at micrometer distances. Due to the large atom size, next-to-leading order terms in the multipole expansion of the radiation field give additional contributions in the MHz range. Despite the existence of large numbers of thermal photons at 300 K at the relevant atomic transition frequencies, the level shifts are in fact temperature independent [8].

For a given atom-field coupling $\hat{H}_{\rm int}$, the CP potential for an atom in state $|n\rangle$ and the radiation field in state $|q\rangle$ is given by the position-dependent part of the energy shift which, to second order in perturbation theory, reads

$$\delta E_n = \langle n,q|\hat{H}_{\rm int}|n,q\rangle + \sum_{n',q'\neq n,q} \frac{|\langle n,q|\hat{H}_{\rm int}|n',q'\rangle|^2}{E_{n+q} - E_{n'+q'}}, \quad (1)$$

where $E_{n+q}$ are the unperturbed energy eigenvalues of the atom-field system. In the long-wavelength approximation, the electric field couples to the atomic dipole moment $\hat{\mathbf{d}}$ via the interaction Hamiltonian,

$$\hat{H}_{\rm int} = -\hat{\mathbf{d}}\cdot\hat{\mathbf{E}}(\mathbf{r}_A), \quad (2)$$

with the electric field given in terms of the classical Green tensor (for a recent review see, e.g., [9]),

$$\hat{\mathbf{E}}(\mathbf{r}) = \sum_{\lambda=e,m}\int d^3r'\int d\omega\, \boldsymbol{G}_\lambda(\mathbf{r},\mathbf{r}',\omega)\cdot\hat{\mathbf{f}}_\lambda(\mathbf{r}',\omega) + \text{h.c.}, \quad (3)$$

with

$$\boldsymbol{G}_e(\mathbf{r},\mathbf{r}',\omega) = i\frac{\omega^2}{c^2}\sqrt{\frac{\hbar}{\pi\varepsilon_0}\text{Im}\varepsilon(\mathbf{r}',\omega)}\boldsymbol{G}(\mathbf{r},\mathbf{r}',\omega), \quad (4)$$

$$\boldsymbol{G}_m(\mathbf{r},\mathbf{r}',\omega) = -i\frac{\omega}{c}\sqrt{\frac{\hbar}{\pi\varepsilon_0}\frac{\text{Im}\mu(\mathbf{r}',\omega)}{|\mu(\mathbf{r}',\omega)|^2}}[\boldsymbol{G}(\mathbf{r},\mathbf{r}',\omega)\times\overleftarrow{\nabla}']. \quad (5)$$

The Green tensor $\boldsymbol{G}(\mathbf{r},\mathbf{r}',\omega)$ solves the Helmholtz equation for a point source and contains all the information about the geometry of the system. The bosonic vector fields $\hat{\mathbf{f}}_\lambda(\mathbf{r},\omega)$ describe collective excitations of the electromagnetic field and the linearly absorbing dielectric matter.

The CP potential at temperature $T$ acting on an atom in state $|n\rangle$ via a dipole interaction (2) is given by [10]

$$\begin{aligned} U_{\rm CP}^{\rm dip}(\mathbf{r}_A) &= \mu_0 k_B T {\sum_{j=0}^{\infty}}' \xi_j^2 \left[\boldsymbol{\alpha}(i\xi_j)\bullet\boldsymbol{G}^{(1)}(\mathbf{r}_A,\mathbf{r}_A,i\xi_j)\right] \\ &\quad + \mu_0\sum_{k\neq n}\omega_{kn}^2 n(\omega_{kn})(\mathbf{d}_{nk}\otimes\mathbf{d}_{kn})\bullet\text{Re}\boldsymbol{G}^{(1)}(\mathbf{r}_A,\mathbf{r}_A,\omega_{kn}), \end{aligned} \quad (6)$$

where $\bullet$ denotes the Frobenius inner product ($\boldsymbol{A}\bullet\boldsymbol{B} = \sum_{i_1\ldots i_k} A_{i_1\ldots i_k}B_{i_1\ldots i_k}$) and the primed summation means that

*jac00@imperial.ac.uk

 

the term with $j = 0$ contributes only with half-weight. Here $\boldsymbol{G}^{(1)}(\mathbf{r}_A,\mathbf{r}_A,\omega)$ is the scattering part of the Green tensor. The atomic polarizability is defined as

$$\boldsymbol{\alpha}(\omega) = \left[\frac{1}{\hbar}\sum_{k\neq n}\frac{\mathbf{d}_{nk}\otimes\mathbf{d}_{kn}}{(\omega_{kn}+\omega)} + \frac{\mathbf{d}_{nk}\otimes\mathbf{d}_{kn}}{(\omega_{kn}-\omega)}\right], \tag{7}$$

with $\omega_{kn} = (E_k - E_n)/\hbar$ denoting the atomic transition frequencies. The frequencies $\xi_j = 2\pi k_B T j/\hbar$, $j \in \mathbb{N}$ are the Matsubara frequencies and $n(\omega) = [e^{\hbar\omega/k_BT} - 1]^{-1}$ is the thermal photon number distribution.

The reflective part of the scattering Green tensor of an infinitely extended planar metal that fills the lower half-space $z < 0$ is given by [11]

$$\boldsymbol{G}^{(1)}(\mathbf{r},\mathbf{r}',\omega) = \int\frac{d^2k_\parallel}{(2\pi)^2}\boldsymbol{R}(\mathbf{k}_\parallel,z,z',\omega)e^{i\mathbf{k}_\parallel\cdot(\mathbf{r}_\parallel-\mathbf{r}'_\parallel)}, \tag{8}$$

with $\mathbf{r}_\parallel = (x,y,0)$, $\mathbf{k}_\parallel = (k_x,k_y,0)$, and $k_\parallel = |\mathbf{k}_\parallel|$. The reflection tensor $\boldsymbol{R}(\mathbf{k}_\parallel,z,z',\omega)$ has the form,

$$\boldsymbol{R}(\mathbf{k}_\parallel,z,z',\omega) = \frac{-i}{8\pi^2\beta_+}\sum_{\sigma=s,p}r_\sigma e^{i\beta_+(z+z')}\mathbf{e}_\sigma^+\otimes\mathbf{e}_\sigma^-. \tag{9}$$

Here, the unit vectors for $s$-polarized and $p$-polarized waves are $\mathbf{e}_s^\pm = \mathbf{e}_{k_\parallel}\times\mathbf{e}_z$ and $\mathbf{e}_p^\pm = (k_\parallel\mathbf{e}_z \mp \beta_+\mathbf{e}_{k_\parallel})/q$. The functions $r_s = [\varepsilon(\omega)\beta_+ - \beta_-]/[\varepsilon(\omega)\beta_+ + \beta_-]$ and $r_p = [\beta_+ - \beta_-]/[\beta_+ + \beta_-]$ are the usual Fresnel reflection coefficients for those waves with wave numbers $\beta_- = \sqrt{q^2\varepsilon(\omega) - k_\parallel^2}$ and $\beta_+ = \sqrt{q^2 - k_\parallel^2}$, and $q = \omega/c$. The permittivity of the metal surface is modeled by the Drude relation, $\varepsilon(\omega) = 1 - \omega_p/\omega(\omega + i\gamma)$, where $\omega_p$ and $\gamma$ are the plasma frequency and the relaxation rate of the metal, respectively. Magnetic effects will be neglected.

Matrix elements of the dipole operator $\hat{\mathbf{d}} = e\hat{\mathbf{r}} = e\hat{r}\mathbf{e}_r$ for the transition between two electronic states $|n,l,j,m\rangle$ ($n$, principal quantum number; $l,j,m$, quantum numbers for orbital and total angular momentum and $z$ component of the latter) and $|n',l',j',m'\rangle$ factor into a radial and an angular part according to

$$\langle n',l',j,m'|\hat{\mathbf{d}}|n,l,j,m\rangle = e\langle R_{n',l',j'}|\hat{r}|R_{n,l,j}\rangle\langle l'j'm'|\mathbf{e}_r|ljm\rangle, \tag{10}$$

where $|R_{n,l,j}\rangle$ are the radial wave functions. The radial matrix elements are computed numerically using the Numerov method [12,13] in which the suitably scaled radial Schrödinger equation is integrated inward until an inner cutoff point (commonly the radius of the rump ion). The eigenenergies are computed as $E_{n,l,j} = -\mathcal{R}/n^{*2}$ ($\mathcal{R}$ is the Rydberg constant) where $n^* = n - \delta_{n,l,j}$ is the effective quantum number and $\delta_{n,l,j}$ the quantum defect [14] whose values are tabulated in the literature [15].

To evaluate the angular part, we first convert from the $jm$ basis to a $m_l m_s$ basis ($m_l$, $m_s$ are the $z$ components of orbital angular momentum and spin) by summing over the relevant Clebsch-Gordan coefficients,

$$\langle l'j'm'|\mathbf{e}_r|ljm\rangle = \sum_{\substack{m_l m'_l\\ m_s}} C^{j,l,1/2}_{m,m_l,m_s}C^{j',l',1/2}_{m',m'_l,m_s}\langle Y_{l',m'_l}|\mathbf{e}_r|Y_{l,m_l}\rangle, \tag{11}$$

with the orbital-angular momentum eigenstates $|Y_{l,m_l}\rangle$ being spherical harmonics. Matrix elements in the $m_l m_s$ basis are computed by rewriting the radial unit vector in terms of spherical harmonics [$Y_{lm} \equiv Y_{lm}(\vartheta,\varphi)$],

$$\mathbf{e}_r = \sqrt{\frac{2\pi}{3}}\begin{pmatrix} Y_{1,-1} - Y_{1,1}\\ i(Y_{1,-1} + Y_{1,1})\\ \sqrt{2}Y_{1,0}\end{pmatrix}, \tag{12}$$

and using the integral relation [$d\Omega \equiv \sin\vartheta\, d\vartheta\, d\varphi$],

$$\int d\Omega\, Y_{l_1,m_1}Y_{l_2,m_2}Y_{l_3,m_3} = \sqrt{\frac{1}{4\pi}\prod_{v=1}^{3}(2l_v+1)}\begin{pmatrix} l_1 & l_2 & l_3\\ 0 & 0 & 0\end{pmatrix}\begin{pmatrix} l_1 & l_2 & l_3\\ m_{l_1} & m_{l_2} & m_{l_3}\end{pmatrix} \tag{13}$$

that expresses the angular integral over three spherical harmonics in terms of Wigner $3j$ symbols.

When Rydberg atoms are held sufficiently close to a surface, their effective radius $\langle r\rangle \simeq a_0 n^2$ ($a_0$ is the Bohr radius) can be on the order of micrometers and therefore a significant fraction of the surface distance. The dipole approximation is then no longer appropriate. In other words, the atom cannot be viewed as a point-like particle, and its non-negligible size requires the inclusion of contributions from higher-order multipoles. This correction can be found via a similar method as described previously, with the dipole interaction Hamiltonian replaced by the quadrupole interaction Hamiltonian [16],

$$\hat{H}_{\rm int} = -\hat{\mathbf{Q}}\bullet[\boldsymbol{\nabla}\otimes\hat{\mathbf{E}}(\mathbf{r}_A)]. \tag{14}$$

In close analogy to the dipole case the CP potential for a quadrupole interaction is found to be

$$U_{\rm CP}^{\rm quad}(\mathbf{r}_A) = \mu_0 k_B T{\sum_{j=0}^{\infty}}'\xi_j^2\boldsymbol{\alpha}^{(4)}(i\xi_j) \bullet[\boldsymbol{\nabla}\otimes\boldsymbol{G}(\mathbf{r}_A,\mathbf{r}_A,i\xi_j)\otimes\overleftarrow{\boldsymbol{\nabla}}] + \mu_0\sum_{k\neq n}\omega_{kn}^2 n(\omega_{kn}) \times(\mathbf{Q}_{nk}\otimes\mathbf{Q}_{kn})\bullet[\boldsymbol{\nabla}\otimes{\rm Re}\boldsymbol{G}(\mathbf{r}_A,\mathbf{r}_A,\omega_{kn})\otimes\overleftarrow{\boldsymbol{\nabla}}], \tag{15}$$

with the quadrupole moment operator $\hat{\mathbf{Q}} = e(\hat{\mathbf{r}}\otimes\hat{\mathbf{r}})/2$ and the atomic quadrupole polarizability defined as

$$\boldsymbol{\alpha}^{(4)}(\omega) = \frac{1}{\hbar}\sum_{k\neq n}\left[\frac{\mathbf{Q}_{nk}\otimes\mathbf{Q}_{kn}}{(\omega_{kn}+\omega)} + \frac{\mathbf{Q}_{nk}\otimes\mathbf{Q}_{kn}}{(\omega_{kn}-\omega)}\right]. \tag{16}$$

The matrix elements for the quadrupole transitions can again be evaluated by factoring $\hat{\mathbf{Q}} = (e/2)\hat{r}^2\mathbf{e}_r\otimes\mathbf{e}_r$ and computing the matrix elements between the radial and angular parts of the wave functions separately. Evaluation of the radial integral is again performed numerically. The tensor product of unit vectors in spherical harmonic form reads $\mathbf{e}_r\otimes\mathbf{e}_r = \sqrt{\frac{2\pi}{15}}\mathrm{A}$ with

$$A_{\substack{xx\\yy}} = \pm Y_{2,-2} \pm Y_{2,2} - \sqrt{\frac{2}{3}}Y_{2,0} + \sqrt{\frac{10}{3}}Y_{0,0}, \tag{17a}$$

$$A_{xy} = A_{yx} = i(Y_{2,-2} - Y_{2,2}), \tag{17b}$$

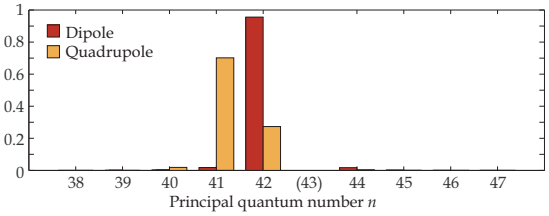


FIG. 1. (Color online) Relative contributions from different transitions to the CP dipole and quadrupole level shift of the state $43s$ of $^{87}$Rb.

$$A_{xz} = A_{zx} = Y_{2,-1} - Y_{2,1}, \tag{17c}$$

$$A_{yz} = A_{zy} = i(Y_{2,-1} + Y_{2,1}), \tag{17d}$$

$$A_{zz} = \sqrt{\frac{8}{3}}Y_{2,0} + \sqrt{\frac{10}{3}}Y_{0,0}. \tag{17e}$$

The angular matrix elements can then be evaluated using Eq. (13).

As can be seen from Eqs. (6) and (15), the CP potential is comprised of a pair of sums, one over the Matsubara frequencies and one over all available atomic transitions. It turns out, however, that due to the finite-temperature environment only a limited number of dipole and quadrupole transitions contribute significantly to the total level shift. This effect is depicted in Fig. 1, where we show the relative contributions of the dipole transitions $43s \to np$ and quadrupole transitions $43s \to nd$ to the total level shift of the $43s$ state of $^{87}$Rb. Note that the dominant transitions are different for dipole and quadrupole shifts. This is due to the differing quantum defects for the respective target $p$ and $d$ states. Moreover, for each of these individual (long-wavelength) transitions the first term in the Matsubara sum (with $j = 0$) dominates at the micrometer atom-surface distances envisaged here, and all other terms can be safely neglected. Remarkably, we observe that the CP potential is independent of temperature from $T = 0 - 300$ K and beyond. As was recently shown [8], this is due to the dominance of contributions from transitions whose wavelengths far exceed atom-surface separations.

Figure 2(a) shows the total CP potential (and hence level shifts) $U_{\rm CP} = U_{\rm CP}^{\rm dip} + U_{\rm CP}^{\rm quad}$ for various $ns$ states (with $n =$ 32,43,54) of $^{87}$Rb near a copper surface at 300 K. As we are not interested in a particular transition channel, the weighted sum over all possible final states has been taken.

One observes that for very small (yet experimentally achievable and indeed desirable) distances of less than 2 $\mu$m the expected level shifts rapidly grow to GHz sizes. At these distances, we also observe significant deviations of the total shift from the dipole contribution (6) alone due to the increasingly important quadrupole shifts [Eq. (15)] which themselves can be as large as several MHz [inset in Fig. 2(a)].

Related to the energy level shift is a line broadening effect (i.e., an increased rate of spontaneous decay due to strong nonradiative processes) as the atom approaches the surface [9,16]. This strongly enhanced body-induced spontaneous decay partially counteracts the expected increase in lifetime as a function of the principal quantum number $n$ in free space ($\Gamma_0 \propto n^{-3}$) [1].

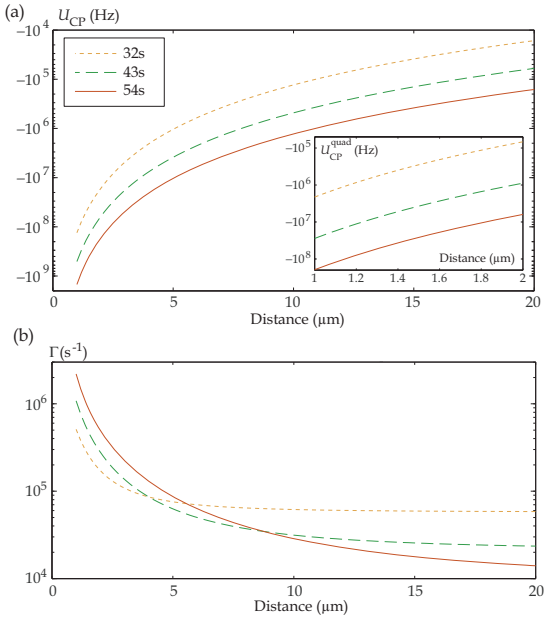


FIG. 2. (Color online) (a) Casimir-Polder level shifts of the states $32s$ (dotted line), $43s$ (dashed line), and $54s$ (solid line) of $^{87}$Rb near a copper surface at 300 K; total shift and quadrupole contribution alone (inset). (b) Spontaneous decay rate near a copper surface at 300 K for the initial states $32s$ (dotted line), $43s$ (dashed line), and $54s$ (solid line) of $^{87}$Rb.

In Fig. 2(b) we show the total decay rates of the Rydberg states $ns$ ($n = 32,43,54$) of $^{87}$Rb as a function of atom-surface distance. The body-induced decay rates for electric dipole and quadrupole transitions are calculated from Ref. [16] as [$\Gamma_{nk} = \Gamma_{nk}^{\rm dip} + \Gamma_{nk}^{\rm quad}$]

$$\Gamma_{nk}^{\rm dip}(\mathbf{r}_A) = \frac{\omega_{nk}^2}{\hbar\varepsilon_0 c^2}(\mathbf{d}_{nk} \otimes \mathbf{d}_{kn}) \bullet \mathrm{Im}\, \boldsymbol{G}(\mathbf{r}_A, \mathbf{r}_A, |\omega_{nk}|) \times \{\Theta(\omega_{nk})[n(\omega_{nk}) + 1] + \Theta(\omega_{kn})n(\omega_{kn})\}, \tag{18}$$

$$\Gamma_{nk}^{\rm quad}(\mathbf{r}_A) = \frac{\omega_{nk}^2}{\hbar\varepsilon_0 c^2}(\mathbf{Q}_{nk} \otimes \mathbf{Q}_{kn}) \bullet [\nabla \otimes \mathrm{Im}\, \boldsymbol{G}(\mathbf{r}_A, \mathbf{r}_A, |\omega_{nk}|) \otimes \overleftarrow{\nabla}] \times \{\Theta(\omega_{nk})[n(\omega_{nk}) + 1] + \Theta(\omega_{kn})n(\omega_{kn})\}. \tag{19}$$

Note that, unlike the CP potential, the decay rates are always temperature dependent. One observes a strong increase of the decay rates near the surface ($z \lesssim 10$ $\mu$m) which becomes more pronounced for states with higher principal quantum number $n$. This translates into a relative line broadening of more than three orders of magnitude that potentially limits trapping and manipulation times of high-lying states near surfaces. For larger distances ($z \gtrsim 15$ $\mu$m) the rates quickly approach their free-space values and show the expected suppression with increasing $n$.

Finally, we will briefly consider how the CP potential and transition rates scale with atom-surface distance $z$ and the principal quantum number $n$. For metal surfaces, the reflection

coefficients are nearly independent of $\omega$ at infrared frequencies and below. In the low-temperature limit, when the thermal photon number is negligible, there is no $\omega$ dependence for either the CP potential or the transition rates. The dipole and quadrupole moments for the dominant $ns \to (n-1)p$ and $ns \to (n-1)d$ transitions scale as $n^2$ and $n^4$, respectively, for large $n$. In the nonretarded limit (valid for surface distances beyond even 100 $\mu$m), the body-induced rates and the CP potential scale as $z^{-3}$ and $z^{-5}$ for the dipole and quadrupole contributions, respectively [16]. Combining these results leads to a scaling behavior of

$$\left|U_{\mathrm{CP}}^{\mathrm{dip}}\right|, \quad \Gamma_{nk}^{\mathrm{dip}} \propto \frac{n^4}{z^3}, \quad \left|U_{\mathrm{CP}}^{\mathrm{quad}}\right|, \quad \Gamma_{nk}^{\mathrm{quad}} \propto \frac{n^8}{z^5}, \qquad (20)$$

for the dipole and quadrupole components of the CP potential $U_{\mathrm{CP}}$ and the decay rate $\Gamma_{nk}$.

In the high-temperature limit, the scaling of the CP shifts remains the same due to the temperature independence demonstrated in Ref. [8], whereas the transition rates become proportional to the mean photon number $n(\omega) \approx k_B T/(\hbar\omega)$. For the dominant dipole and quadrupole transitions (Fig. 1), one finds $\omega \propto n^{-3}$, and the transition rates scale as $\Gamma_{nk}^{\mathrm{dip}} \propto n^7/z^3$ and $\Gamma_{nk}^{\mathrm{quad}} \propto n^{11}/z^5$, respectively.

We have shown in this Rapid Communication that the interaction between highly excited atoms and macroscopic surfaces leads to energy level shifts that can be as large as several GHz. This implies that any scheme that relies on the manipulation of (trapped) Rydberg atoms near surfaces has to account for this major adjustment. Moreover, some of the advantages of using highly excited Rydberg atoms, in particular their rapidly decreasing Einstein coefficients with increasing principal quantum number $n$, are counteracted by the atom-surface interactions.

## ACKNOWLEDGMENTS

We thank D. Cano and J. Fortágh for helpful discussions. This work was supported by the UK Engineering and Physical Sciences Research Council. Support from the European Science Foundation (ESF) within the activity "New Trends and Applications of the Casimir Effect" is gratefully acknowledged.

[1] T. F. Gallagher, *Rydberg Atoms* (Cambridge University Press, Cambridge, 1994).
[2] T. Nakajima, P. Lambropoulos, and H. Walther, Phys. Rev. A **56**, 5100 (1997).
[3] H. B. G. Casimir and D. Polder, Phys. Rev. **73**, 360 (1948).
[4] M. D. Lukin *et al.*, Phys. Rev. Lett. **87**, 037901 (2001).
[5] H. Kübler *et al.*, Nature Photonics **4**, 112 (2010).
[6] H. Bender, P. Courteille, C. Zimmermann, and S. Slama, Appl. Phys. B **96**, 275 (2009).
[7] J. Fortágh and C. Zimmermann, Rev. Mod. Phys. **79**, 235 (2007).
[8] S. Å. Ellingsen, S. Y. Buhmann, and S. Scheel, Phys. Rev. Lett. **104**, 223003 (2010).
[9] S. Scheel and S. Y. Buhmann, Acta Phys. Slov. **58**, 675 (2008).
[10] S. Y. Buhmann and S. Scheel, Phys. Rev. Lett. **100**, 253201 (2008).
[11] W. C. Chew, *Waves and Fields in Inhomogeneous Media* (IEEE Press, New York, 1995).
[12] J. M. Blatt, J. Comput. Phys. **1**, 382 (1967).
[13] S. A. Bhatti, C. L. Cromer, and W. E. Cooke, Phys. Rev. A **24**, 161 (1981).
[14] M. Seaton, Rep. Prog. Phys. **46**, 167 (1993).
[15] W. Li, I. Mourachko, M. W. Noel, and T. F. Gallagher, Phys. Rev. A **67**, 052502 (2003); C.-J. Lorenzen and K. Niemax, Phys. Scr. **27**, 300 (1983).
[16] J. A. Crosse and S. Scheel, Phys. Rev. A **79**, 062902 (2009).

# Erratum: Thermal Casimir-Polder shifts in Rydberg atoms near metallic surfaces [Phys. Rev. A 82, 010901(R) (2010)]

J. A. Crosse,* Simen Å. Ellingsen, Kate Clements, Stefan Y. Buhmann, and Stefan Scheel

(Received 21 July 2010; published 11 August 2010)

DOI: 10.1103/PhysRevA.82.029902 PACS number(s): 34.35.+a, 32.80.Ee, 42.50.Ct, 42.50.Nn, 99.10.Cd

An error occurred in the numerical examples presented in the original article, as the contribution from the $ns \rightarrow np$ transition was neglected in the calculation of the dipole Casimir-Polder (CP) shift and transition rates. This transition is relevant for rubidium as a result of differing quantum defects for the $ns$ and $np$ states. As seen in the corrected Fig. 1, the $43s \rightarrow 43p$ transition contributes about 50% to the total level shift. As a result, the CP shifts of rubidium in Rydberg states are even larger than stated in the original article, roughly by a factor of 2, as can be seen from the corrected Fig. 2(a). The decay rates are affected in a similar way [cf. the corrected Fig. 2(b)]. Note that these quantitative changes do not affect any of the conclusions made in the original article regarding the physics of Rydberg atoms near surfaces.

Also, in the text following Eq. (9), the Drude relation for the permittivity of a metal should read $\varepsilon(\omega) = 1 - \omega_p^2/\omega(\omega + i\gamma)$.

We thank R. Fermani for bringing these issues to our attention.

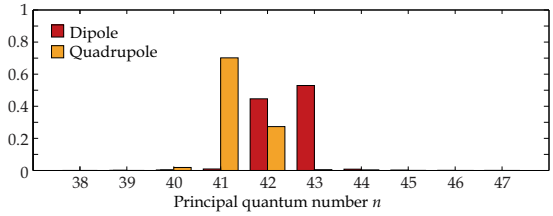


FIG. 1. (Color online) Relative contributions from different transitions to the CP dipole and quadrupole level shift of the state $43s$ of $^{87}$Rb.

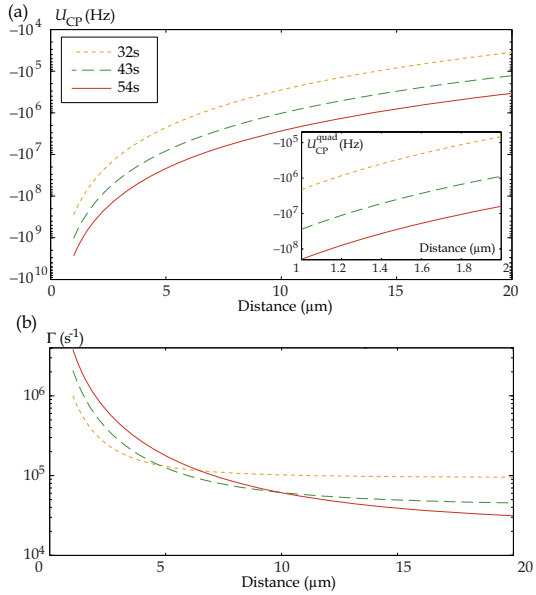


FIG. 2. (Color online) (a) Casimir-Polder level shifts of the states $32s$ (short-dashed line), $43s$ (long-dashed line), and $54s$ (solid line) of $^{87}$Rb near a copper surface at 300 K. Total shift and quadrupole contribution alone (inset). (b) Spontaneous decay rate near a copper surface at 300 K for the initial states $32s$ (short-dashed line), $43s$ (long-dashed line), and $54s$ (solid line) of $^{87}$Rb.

*jac00@imperial.ac.uk

 

Article [p]

***Casimir-Polder potential and transition rate in resonating cylindrical cavities***

S.Å. Ellingsen, S.Y. Buhmann, S. Scheel

Physical Review A **82**, 032516 (2010)

PHYSICAL REVIEW A **82**, 032516 (2010)

# Casimir-Polder potential and transition rate in resonating cylindrical cavities

Simen Å. Ellingsen
*Department of Energy and Process Engineering, Norwegian University of Science and Technology, N-7491 Trondheim, Norway*

Stefan Yoshi Buhmann and Stefan Scheel
*Quantum Optics and Laser Science, Blackett Laboratory, Imperial College London, Prince Consort Road, London SW7 2AZ, United Kingdom*

(Received 7 July 2010; published 29 September 2010)

We consider the Casimir-Polder potential of particles placed inside a metallic cylindrical cavity at finite temperatures, taking account of thermal nonequilibrium effects. In particular, we study how the resonant (thermal nonequilibrium) potential and transition rates can be enhanced by fine tuning the radius of the cavity to match the transition wavelength of the dominant transitions of the particle. Numerical calculations show that the cavity-induced energy-level shift of atoms prepared in low-lying Rydberg states can be enhanced beyond 30 kHz, which is within the range of observability of modern experiments. Because the magnitude of the resonance peaks depends sensitively on the low-frequency dissipation of the cavity metal, experiments in this setup could be a critical test of the disputed thermal correction to the Casimir force between metal plates.

DOI: 10.1103/PhysRevA.82.032516 PACS number(s): 31.30.jh, 34.35.+a, 42.50.Ct, 42.50.Nn

## I. INTRODUCTION

Casimir-Polder (CP) forces [1] belong to the group of of dispersion forces, which arise due to the fluctuations of the quantized electromagnetic field. They occur between polarizable atoms or molecules and metallic or dielectric macroscopic bodies and can be intuitively thought of as the dipole-dipole force caused by spontaneous and mutually correlated polarization of the atom or molecule and the matter comprising the body. Under the assumption of thermal equilibrium, CP forces have been commonly investigated in the linear-response formalism [2–4].

Recent theoretical predictions [5] as well as experimental realizations [6] for CP forces in thermal nonequilibrium situations have pointed toward interesting effects which arise when an atom at equilibrium with its local environment interacts with a body held at a different temperature. In particular, depending on the temperatures of the macroscopic body and the environment, the force can change its character from being attractive to repulsive and vice versa.

Nonequilibrium situations between atom and local environment can be investigated by means of normal-mode QED [7,8] or macroscopic QED in absorbing and dispersing media [9,10]. In this case, thermal excitation and de-excitation processes lead to resonant contributions to the force [11] (cf. similar findings reported in Ref. [12]). At particle-body separations that are larger than the wavelengths associated with the dominating atomic transitions (retarded regime), the interaction potential becomes spatially oscillating [13]. Similar behavior has been observed for the transition rate of molecules in the past [14,15].

The spatially oscillating nonequilibrium forces on ground-state atoms or molecules are proportional to the thermal photon number. In order to observe them, it is necessary to make use of atomic systems whose internal eigenstates exhibit energy separations of order $k_{\mathrm{B}}T$ or less ($T$, temperature; $k_{\mathrm{B}}$, Boltzmann constant). We have investigated polar molecules with their low-energy rotational and vibrational transitions as possible candidates [13]. However, the large photon numbers obtained using molecules with small excitation energies come at a cost: Due to the large wavelengths associated with such molecular transitions, the retarded regime where oscillations might be observed sets in at very large distances, typically of the order of tens to hundreds of micrometers. As the CP potential decays away rapidly from the body surface, it is very small at such distances.

As already discussed in conjunction with excited atoms in a zero-temperature environment, resonant forces can be enhanced in a planar cavity whose width is fine tuned to match the wavelength of the transition [16–22]. Note that resonating cavities have been employed experimentally for enhancement and inhibition of spontaneous emission rates for excited systems for a long time (cf. e.g., [23–26]). We have previously investigated the potential of such a setup to enhance the predicted spatial oscillations of the thermal force on ground-state molecules [27]. Unfortunately, the cavity enhancement factor turns out to scale logarithmically with the cavity $Q$ factor, which strongly limits the possibilities of the scheme. As we have shown, it is unlikely to achieve more than an order of magnitude's enhancement of the force amplitudes, which is still insufficient for detection using polar molecules.

In the present article, we present a scheme by which oscillations of the resonant thermal CP force can be brought into the measurable regime. This is achieved by replacing the planar cavity with a cylindrical cavity [28] and employing Rydberg atoms rather than polar molecules [29]. The geometry is shown in Fig. 1. The limited cavity enhancement in a planar setup is due to the insufficient, purely one-dimensional confinement of the electromagnetic modes. A cylindrical cavity is therefore an obvious candidate for improvement: It confines the modes in two of the three spatial dimensions so that a stronger resonant enhancement may be expected. At the same time, it is a practical geometry for experimental and guiding purposes, allowing particles to travel freely along the axial direction (we will only consider particles at rest

 

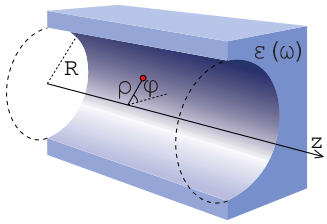


FIG. 1. (Color online) Cross section of the geometry considered: a particle in a vacuum-filled circularly cylindrical cavity.

herein, leaving moving atoms [30] in this geometry for future study). As a caveat, one has to bear in mind that a cylindrical cavity will simultaneously enhance both the CP potential and the relaxation rates; thus reducing the time scales on which nonequilibrium effects can be observed. A similar geometry, that is, an (anisotropic) particle above a spherical hole in a thin metal plate, has recently been suggested as a candidate for observing repulsive Casimir forces [31].

Rydberg atoms are ideal candidates for observing resonant thermal CP potentials. Their valence electrons are excited to relatively stable states with very large principal quantum numbers $n$, typically in the range 30–60. The spatial extent of such highly excited atoms is then enormous on an atomic scale, exceeding 1 $\mu$m in diameter, and the transition dipole moments consequently orders of magnitude larger than those of ground-state atoms or polar molecules. Resonant CP interactions being proportional to the respective transition dipole moment squared, a strong enhancement follows. Moreover, an atom excited to a particular eigenstate with large $n$ is necessarily out of thermal equilibrium with its environment, and the energy difference to neighboring states is typically small compared to $k_B T$ at room temperature, hence fulfilling the condition for observing an oscillating potential.

The structure of the article is as follows. In Sec. II we present the general formalism of the thermal CP interaction and transition rates in a cylindrical cavity, including the necessary Green tensor. Thereafter, in Sec. III we derive the cylinder radii which resonate with the atomic transition frequency. We begin with the simplest case of a perfectly conducting cavity and then discuss how the optimal radii deviate from the perfect conductor results when realistic metallic permittivity functions are employed. We provide simple formulas for the optimal radii when the permittivity of the cylinder medium is large. In Sec. IV, we discuss how the potential and heating rate enhancements scale with the relevant atomic and cavity parameters, with emphasis on the dependence on the cavity permittivity. Finally we undertake numerical calculations of resonant CP potential and heating rates for two example cases: the $32s_{1/2} \rightarrow 31p_{3/2}$ transition of Rydberg Rb in a cylindrical Au cavity at temperature $T = 300$ K and a ground-state LiH molecule in a similar cavity.

## II. GENERAL FORMALISM

We consider an atomic system (in what follows we study the cases of Rydberg atoms and polar molecules) with internal energy eigenstates $|n\rangle$, eigenenergies $\hbar\omega_n$, transition frequencies $\omega_{mn} = \omega_m - \omega_n$, and dipole matrix elements $\mathbf{d}_{mn} = \langle m|\hat{\mathbf{d}}|n\rangle$, which is prepared in an incoherent superposition of its energy eigenstates with probabilities $p_n$.

### A. Thermal Casimir-Polder potential

The thermal CP force on such a system in an environment of uniform temperature $T$ was derived in detail in Ref. [11]. As shown, it is conservative in the perturbative limit, $\mathbf{F}(\mathbf{r}) = -\nabla U(\mathbf{r})$, where the associated CP potential is given by

$$U(\mathbf{r}) = \sum_n p_n U_n(\mathbf{r}). \tag{2.1}$$

The potential components associated with a given eigenstate $n$ splits naturally into a nonresonant contribution $U_n^{\rm nr}$ and a resonant one $U_n^{\rm res}$,

$$U_n(\mathbf{r}) = U_n^{\rm nr}(\mathbf{r}) + U_n^{\rm res}(\mathbf{r}). \tag{2.2}$$

The nonresonant potential $U_n^{\rm nr}$ is due to virtual photons and is reminiscent of that obtained by a dilute-gas expansion of Lifshitz' formula [2]. The resonant contribution $U_n^{\rm res}$ is due to absorption and emission of thermal photons; it is present because the particle in its ground state is out of thermal equilibrium with its environment.

The nonresonant potential reads

$$U_n^{\rm nr}(\mathbf{r}) = \frac{k_B T}{\varepsilon_0} {\sum_{j=0}^{\infty}}' \frac{\xi_j^2}{c^2} {\rm Tr}[\boldsymbol{\alpha}_n(i\xi_j)\cdot\mathbf{G}^{(1)}(\mathbf{r},\mathbf{r},i\xi_j)], \tag{2.3}$$

where $\mu_0$ is the free-space permeability, $\xi_j = 2\pi j k_B T/\hbar$ is the $j$th Matsubara frequency, and the prime on the Matsubara sum indicates that the $j = 0$ term is to be taken with half weight. The atomic or molecular polarizability is given by

$$\boldsymbol{\alpha}_n(\omega) = \lim_{\epsilon\rightarrow 0} \frac{1}{\hbar} \sum_k \left( \frac{\mathbf{d}_{kn}\mathbf{d}_{nk}}{\omega + \omega_{kn} + i\epsilon} - \frac{\mathbf{d}_{nk}\mathbf{d}_{kn}}{\omega - \omega_{kn} + i\epsilon} \right) \tag{2.4}$$

and $\mathbf{G}^{(1)}(\mathbf{r},\mathbf{r}',\omega)$ is the scattering part of the classical Green tensor of the geometry the particle is placed in. Note that dyadic multiplication is implied for products of vectors without multiplication symbol: $\mathbf{AB} \equiv \mathbf{A}\otimes\mathbf{B}$. For an isotropic particle, the nonresonant potential components may be simplified to

$$U_n^{\rm nr}(\mathbf{r}) = \frac{k_B T}{\varepsilon_0} {\sum_{j=0}^{\infty}}' \frac{\xi_j^2}{c^2} \alpha_n(i\xi_j) {\rm Tr}\mathbf{G}^{(1)}(\mathbf{r},\mathbf{r},i\xi_j), \tag{2.5}$$

with

$$\alpha_n(\omega) = \lim_{\epsilon\rightarrow 0} \frac{2}{3\hbar} \sum_k \frac{|\mathbf{d}_{nk}|^2 \omega_{kn}}{\omega_{kn}^2 - \omega^2 - i\epsilon\omega}. \tag{2.6}$$

The resonant potential reads

$$U_n^{\rm res}(\mathbf{r}) = \mu_0 \sum_k \omega_{kn}^2 \mathbf{d}_{nk}\cdot {\rm Re}\,\mathbf{G}^{(1)}(\mathbf{r},\mathbf{r},|\omega_{kn}|)\cdot\mathbf{d}_{kn} \times\{\Theta(\omega_{kn})n(\omega_{kn}) - \Theta(\omega_{nk})[n(\omega_{nk})+1]\}, \tag{2.7}$$

where $\mu_0$ is the free-space permeability and $\Theta(x)$ denotes the Heaviside step function. The photon number follows the Bose-Einstein distribution

$$n(\omega) = \left[\exp\left(\frac{\hbar\omega}{k_B T}\right) - 1\right]^{-1}. \tag{2.8}$$

For an isotropic particle, the resonant potential components reduce to

$$U_n^{\rm res}(\mathbf{r}) = \frac{\mu_0}{3}\sum_k \omega_{kn}^2 |\mathbf{d}_{nk}|^2 {\rm Tr}\,{\rm Re}\,\mathbf{G}^{(1)}(\mathbf{r},\mathbf{r},|\omega_{kn}|) \times \{\Theta(\omega_{kn})n(\omega_{kn}) - \Theta(\omega_{nk})[n(\omega_{nk})+1]\}. \quad (2.9)$$

### B. Environment-assisted transition rates

An atomic system initially prepared in a given energy eigenstate $|n\rangle$ and placed in an environment of uniform temperature $T$ will undergo transitions to different eigenstates due to absorption and emission of thermal photons. As shown in Ref. [32], the total rate

$$\Gamma_n(\mathbf{r}) = \Gamma_n^{(0)} + \Gamma_n^{(1)}(\mathbf{r}) \quad (2.10)$$

for transitions out of state $|n\rangle$ consists of a free-space part $\Gamma_n^{(0)}$ and an environment-induced part $\Gamma_n^{(1)}$. In the perturbative limit, these are given as

$$\Gamma_n^{(0)} = \sum_k \frac{|\omega_{kn}|^3 |\mathbf{d}_{nk}|^2}{3\pi\hbar\varepsilon_0\hbar}\{\Theta(\omega_{nk})[n(\omega_{nk})+1] + \Theta(\omega_{kn})n(\omega_{kn})\} \quad (2.11a)$$

and

$$\Gamma_n^{(1)}(\mathbf{r}) = \frac{2}{\varepsilon_0\hbar}\sum_k \frac{\omega_{kn}^2}{c^2}\mathbf{d}_{nk}\cdot {\rm Im}\,\mathbf{G}^{(1)}(\mathbf{r},\mathbf{r},|\omega_{kn}|)\cdot\mathbf{d}_{kn} \times \{\Theta(\omega_{nk})[n(\omega_{nk})+1] + \Theta(\omega_{kn})n(\omega_{kn})\}. \quad (2.11b)$$

The environment-induced rate simplifies for an isotropic particle to

$$\Gamma_n^{(1)}(\mathbf{r}) = \frac{2}{3\varepsilon_0\hbar}\sum_k \frac{\omega_{kn}^2}{c^2}|\mathbf{d}_{nk}|^2 {\rm Tr}\,{\rm Im}\,\mathbf{G}^{(1)}(\mathbf{r},\mathbf{r},|\omega_{kn}|) \times \{\Theta(\omega_{nk})[n(\omega_{nk})+1] + \Theta(\omega_{kn})n(\omega_{kn})\}. \quad (2.12)$$

### C. The Green tensor in a cylindrical cavity

We are going to study atomic systems placed at position $\mathbf{r} = (\rho,\varphi,z)$ inside a circularly cylindrical free-space cavity of radius $R$ in a bulk nonmagnetic medium with permittivity $\varepsilon = \varepsilon(\omega)$ as shown in Fig. 1. The respective scattering Green tensor can be found in Ref. [33] (see also Appendix A4.2 of [10]):

$$\mathbf{G}^{(1)}(\mathbf{r},\mathbf{r},\omega) = \frac{i}{4\pi}\int_{-\infty}^{\infty} dq \sum_{m=0}^{\infty}{}' \eta^{-2}\left[r_{\rm MM}\mathbf{M}_{\substack{o\\e}m\eta}(q)\mathbf{M}_{\substack{e\\o}m\eta}(-q) \pm r_{\rm NM}\mathbf{N}_{\substack{o\\e}m\eta}(q)\mathbf{M}_{\substack{e\\o}m\eta}(-q) \pm r_{\rm MN}\mathbf{M}_{\substack{e\\o}m\eta}(q) \times \mathbf{N}_{\substack{o\\e}m\eta}(-q) + r_{\rm NN}\mathbf{N}_{\substack{e\\o}m\eta}(q)\mathbf{N}_{\substack{e\\o}m\eta}(-q)\right], \quad (2.13)$$

where $\eta = \sqrt{k^2 - q^2}$ and $k = \omega/c$. The cylindrical vector wave functions inside the cavity are [10,33,34]

$$\mathbf{M}_{\substack{o\\e}m\eta}(q) = \left[\mp\frac{m}{\rho}J_m(\eta\rho)\begin{matrix}\sin\\\cos\end{matrix} m\varphi\hat{\boldsymbol{\varrho}} \; -\eta J_m'(\eta\rho)\begin{matrix}\cos\\\sin\end{matrix} n\varphi\hat{\boldsymbol{\varphi}}\right]e^{iqz}, \quad (2.14a)$$

$$\mathbf{N}_{\substack{e\\o}m\eta}(q) = \left(\frac{iq\eta}{k}J_m'(\eta\rho)\begin{matrix}\cos\\\sin\end{matrix} m\varphi\hat{\boldsymbol{\varrho}} \mp \frac{iqm}{k\rho}J_m(\eta\rho)\begin{matrix}\sin\\\cos\end{matrix} m\varphi\hat{\boldsymbol{\varphi}} + \frac{\eta^2}{k}J(\eta\rho)\begin{matrix}\cos\\\sin\end{matrix} m\varphi\hat{\mathbf{z}}\right)e^{iqz}. \quad (2.14b)$$

The compact wave vector notation used here implies $\mathbf{A}_{\substack{o\\e}}\mathbf{B}_{\substack{e\\o}} = \mathbf{A}_e\mathbf{B}_e + \mathbf{A}_o\mathbf{B}_o$, etc., and the upper (lower) sign in (2.13) corresponds to upper (lower) index $e,o$ of the vector wave functions. $J_m$ are cylindrical Bessel functions of the first kind. The reflection coefficients $r$ can be found from a system of linear equations as described in Ref. [33]. For the single-interface cylindrical cavity in a bulk medium as considered here, the result for the diagonal coefficients $r_M \equiv r_{\rm MM}$ and $r_N \equiv r_{\rm NN}$ may be written as

$$r_{M,N} = -\frac{H_m^{(1)}(x)}{J_m(x)}\tilde{r}_{M,N}, \quad (2.15)$$

with

$$\tilde{r}_\sigma = \frac{A + B_\sigma}{A + B_D}, \quad \sigma = M,N, \quad (2.16)$$

and 2.17

$$A = -m^2(kR)^2(qR)^2(\varepsilon-1)^2, \quad (2.17a)$$

$$B_M = x_1^2x^2\left[\varepsilon\tilde{h}_1^2x^2 - (\tilde{h}_1\tilde{\jmath} + \varepsilon\tilde{h}_1\tilde{h})x_1x + \tilde{h}\tilde{\jmath}x_1^2\right], \quad (2.17b)$$

$$B_N = x_1^2x^2\left[\varepsilon\tilde{h}_1^2x^2 - (\varepsilon\tilde{h}_1\tilde{\jmath} + \tilde{h}_1\tilde{h})x_1x + \tilde{h}\tilde{\jmath}x_1^2\right], \quad (2.17c)$$

$$B_D = x_1^2x^2\left[\varepsilon\tilde{h}_1^2x^2 - (\varepsilon+1)\tilde{h}_1\tilde{\jmath}x_1x + \tilde{\jmath}^2x_1^2\right]. \quad (2.17d)$$

Here, $x = \eta R$, $x_1 = \eta_1 R$, $\eta_1 = \sqrt{\varepsilon(\omega)\omega^2/c^2 - q^2}$, $\varepsilon = \varepsilon(\omega)$ is the permittivity of the cylinder, $H_m^{(1)}$ are Hankel functions of the first kind, and we have defined the shorthand quantities

$$\tilde{h} = \tilde{h}(x), \quad \tilde{h}_1 = \tilde{h}(x_1), \quad \tilde{\jmath} = \tilde{\jmath}(x), \quad \tilde{\jmath}_1 = \tilde{\jmath}(x_1), \quad (2.18)$$

where the reduced Bessel functions denoted $\tilde{h}(x)$ and $\tilde{\jmath}(x)$ are 2.19

$$\tilde{h}(x) = \frac{H_m^{(1)\prime}(x)}{H_m^{(1)}(x)} = \frac{d}{dx}\ln H_m^{(1)}(x); \quad (2.19a)$$

$$\tilde{\jmath}(x) = \frac{J_m'(x)}{J_m(x)} = \frac{d}{dx}\ln J_m(x). \quad (2.19b)$$

Note that $\tilde{\jmath}$ is a real function for real arguments, whereas $\tilde{h}$ is complex for real arguments. Explicit knowledge of the off-diagonal reflection coefficients is not required; for our purposes, it is sufficient to note that $r_{\rm MN} = r_{\rm NM}$ (cf. Refs. [10,33] for details).

Substituting the vector wave functions (2.14a) and (2.14b) into Eq. (2.13), making use of $r_{\rm MN} = r_{\rm NM}$ and the fact that odd functions of $q$ do not contribute to the integral, the Green tensor is found to take the diagonal form

$$\mathbf{G}^{(1)}(\mathbf{r},\mathbf{r},\omega) = \frac{i}{2\pi}\int_0^\infty dq \sum_{m=0}^{\infty}{}'\left[\left(\frac{m^2}{\eta^2\rho^2}J_m^2(\eta\rho)r_M + \frac{q^2}{k^2}J_m'^2(\eta\rho)r_N\right)\hat{\boldsymbol{\varrho}}\hat{\boldsymbol{\varrho}} + \left(J_m'^2(\eta\rho)r_M + \frac{m^2q^2}{k^2\eta^2\rho^2}J_m^2(\eta\rho)r_N\right)\hat{\boldsymbol{\varphi}}\hat{\boldsymbol{\varphi}} + \frac{\eta^2}{k^2}J_m^2(\eta\rho)r_N\hat{\mathbf{z}}\hat{\mathbf{z}}\right]. \quad (2.20)$$

The trace of the Green tensor required for isotropic molecules hence reads

$$\begin{aligned}&\mathrm{Tr}\,\mathbf{G}^{(1)}(\mathbf{r},\mathbf{r},\omega)\\&= \frac{i}{2\pi}\int_0^\infty dq \sum_{m=0}^{\infty}{}'\left\{\left(r_M+\frac{q^2}{k^2}r_N\right)\right.\\&\left.\times\left[\frac{m^2}{\eta^2\rho^2}J_m^2(\eta\rho)+J_m'^2(\eta\rho)\right]+r_N\frac{\eta^2}{k^2}J_m^2(\eta\rho)\right\}.\end{aligned}\tag{2.21}$$

It should be noted that the terms containing $m^2/\eta^2\rho^2$ exhibit third-order poles at $q=k$, where $\eta$ vanishes. The physically correct treatment of such poles consists of adding a small imaginary part to the free-space wave vector $k=\omega/c+i\delta$ and performing the limit $\delta\to 0$. In this way, the pole is circumvented from below as $q$ is integrated along the positive real axis [see Fig. 2(a)]. Correspondingly, $\eta$ is integrated along a part of the real axis, around the singularity at the origin and along the positive imaginary axis [Fig. 2(c)]. Recall that in planar geometries the Green tensor at real frequencies may be separated into a propagating part ($q<k$), which exhibits an oscillating behavior due to interference of incoming and reflected photons and an evanescent part ($q>k$), which falls off monotonously away from a surface [13]. In the present case, however, such a distinction cannot be made in a straightforward manner due to the pole at the separation point $q=k$; the individual propagating and evanescent parts would diverge.

For numerical purposes, the original integration contour is unfavorable since it involves subtraction of almost equal numbers, associated with a considerable loss of accuracy. Instead, we rotate the contour of the integral over the variable $q$ to lie along a line at a small negative angle $\theta$, below the real axis as shown in Fig. 2(b). As shown in Fig. 2(d), the corresponding path for $\eta$ is slightly shifted with respect to the original one but still contained within the first quadrant: When $\theta\ll 1$, the point of closest approach to the pole at $\eta=0$ is approximately $\theta(1+i)$ and the integration path thence approaches an asymptote at an angle $\pi/2-\theta$.

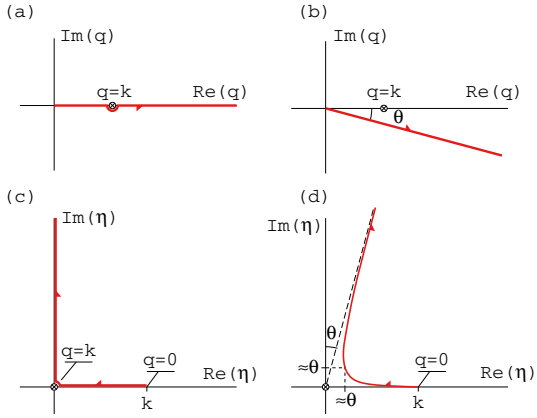


FIG. 2. (Color online) (a, b) Rotation of the $q$-integration path by an angle $\theta$. (c, d) Resulting paths for $\eta$.

We show in Sec. III B that all the poles of the reflection coefficients lie below the real $\eta$ axis when $|\varepsilon|<\infty$, approaching the real axis from below in the perfect conductor limit. There are no other possible singularities in the integrands in Eqs. (2.20) and (2.21), so the area contained between the original and deformed integration contours for $\eta$ is free of poles. As the integrands vanish along a path at imaginary infinity connecting the two paths, they are equivalent by virtue of Cauchy's theorem as long as $\theta<\pi/2$; we typically choose $\theta=0.1$ rad. An additional benifit of the rotated integration path is the fact that the integral becomes exponentially convergent.

The Green tensor becomes particularly simple on the cavity axis, $\rho=0$ where only a few of the functions $J_m(\eta\rho)$, $J_m'(\eta\rho)$ are different from zero. We have for $m=0,1,2,\ldots$

$$\frac{m^2}{\eta^2\rho^2}J_m^2(\eta\rho)\to 0,\tfrac{1}{4},0,0,\ldots,\tag{2.22a}$$

$$J_m'^2(\eta\rho)\to 0,\tfrac{1}{4},0,0,\ldots,\tag{2.22b}$$

$$J_m^2(\eta\rho)\to 1,0,0,0,\ldots,\tag{2.22c}$$

so that

$$\begin{aligned}\mathbf{G}^{(1)}(\mathbf{r},\mathbf{r},\omega)|_{\rho=0}=\frac{i}{8\pi}\int_0^\infty dq\left[\frac{2\eta^2}{k^2}r_N^{m=0}\hat{\mathbf{z}}\hat{\mathbf{z}}\right.\\\left.+\left(r_M^{m=1}+\frac{q^2}{k^2}r_N^{m=1}\right)(\hat{\boldsymbol{\varrho}}\hat{\boldsymbol{\varrho}}+\hat{\boldsymbol{\varphi}}\hat{\boldsymbol{\varphi}})\right]\end{aligned}\tag{2.23}$$

and

$$\begin{aligned}&\mathrm{Tr}\,\mathbf{G}^{(1)}(\mathbf{r},\mathbf{r},\omega)_{\rho=0}\\&=\frac{i}{4\pi}\int_0^\infty dq\left(\frac{\eta^2}{k^2}r_N^{m=0}+r_M^{m=1}+\frac{q^2}{k^2}r_N^{m=1}\right).\end{aligned}\tag{2.24}$$

Finally, let us briefly discuss the Green tensor at purely imaginary frequencies $\omega=i\xi$ as required for the nonresonant potentials (2.3) and (2.5). We have $\eta=i\sqrt{\xi^2/c^2+q^2}\equiv i\zeta$, so the arguments of the cylindrical Bessel and Hankel functions appearing in the reflection coefficients (2.15)–(2.17) become purely imaginary. One has

$$J_m(iy)=i^m I_m(y),\tag{2.25a}$$

$$J_m'(iy)=i^{m-1}I_m'(y),\tag{2.25b}$$

$$H_m^{(1)}(iy)=\frac{2}{\pi}i^{-(m+1)}K_m(y),\tag{2.25c}$$

$$H_m^{(1)\prime}(iy)=\frac{2}{\pi}i^{-m}K_m'(y);\tag{2.25d}$$

hence, the reflection coefficients become ($\sigma=M,N$),

$$r_\sigma(i\xi)=\frac{2i}{\pi}(-1)^m\frac{K_m(y)}{I_m(y)}\tilde{r}_\sigma(i\xi).\tag{2.26}$$

The reduced reflection coefficients are found from (2.16) with the substitutions $x\to iy=i\zeta R$, $x_1\to iy_1=i\zeta_1 R$ with $\zeta_1=\sqrt{\varepsilon(i\xi)\xi^2/c^2+q^2}$, and $\tilde{\jmath}\to\tilde{\imath}/i,\tilde{h}\to\tilde{k}/i$ with reduced modified Bessel functions analogous to (2.19):

$$\tilde{\imath}(y)=\frac{I_n'(y)}{I_n(y)};\quad \tilde{k}(y)=\frac{K_n'(y)}{K_n(y)}.$$

Using the reflection coefficients (2.26), the Green tensor (2.20) at purely imaginary frequencies is seen to be purely real and given by ($\kappa = \xi/c$)

$$\mathbf{G}^{(1)}(\mathbf{r},\mathbf{r},i\xi) = \frac{1}{\pi^2}\int_0^\infty dq \sum_{m=0}^{\infty}{}' \frac{K_m(\zeta R)}{I_m(\zeta R)} \times\Bigg[\left(\frac{m^2}{\zeta^2\rho^2} I_m^2(\zeta\rho)\tilde{r}_M - \frac{q^2}{\kappa^2} I_m'^2(\zeta\rho)\tilde{r}_N\right)\hat{\boldsymbol{\varrho}}\hat{\boldsymbol{\varrho}} + \left(I_m'^2(\zeta\rho)\tilde{r}_M - \frac{m^2q^2}{\kappa^2\zeta^2\rho^2} I_m^2(\zeta\rho)\tilde{r}_N\right)\hat{\boldsymbol{\varphi}}\hat{\boldsymbol{\varphi}} - \frac{\zeta^2}{\kappa^2} I_m^2(\zeta\rho)\tilde{r}_N\hat{\mathbf{z}}\hat{\mathbf{z}}\Bigg]. \tag{2.27}$$

Correspondingly, its trace reads

$$\mathrm{Tr}\,\mathbf{G}^{(1)}(\rho,\rho,i\xi) = \frac{1}{\pi^2}\int_0^\infty dq \sum_{m=0}^{\infty}{}' \Bigg[\left(\tilde{r}_M - \frac{q^2}{\kappa^2}\tilde{r}_N\right) \times\left(\frac{m^2}{\zeta^2\rho^2} I_m^2(\zeta\rho) + I_m'^2(\zeta\rho)\right) - \frac{\zeta^2}{\kappa^2}\tilde{r}_N I_m^2(\zeta\rho)\Bigg]\frac{K_m(\zeta R)}{I_m(\zeta R)}. \tag{2.28}$$

Note that for purely imaginary frequencies, the $q$ integration in the Green tensor is unproblematic as the integrand remains finite along the real $q$ axis.

## III. RESONANT RADII

Combining the general expressions for the CP potential given in Sec. II A with the Green tensor of the cylindrical cavity as laid out in Sec. II C, we can explicitly calculate the full potential of any particular atom or molecule in a given state placed in a cavity of given size and material. Such examples, which require a numerical analysis, will be given in Sec. V.

Our main intention is to enhance the resonant potential by means of the cavity. To that end, it is worth recalling the case of the planar cavity: The resonant CP potential of an atom placed between two plane surfaces is enhanced for certain interplate separations [27]. For a given transition frequency there exists a series of such resonant separations corresponding to integer multiples of the atomic transition wavelength. In such a case, the transition is (near-)resonant with a standing-wave mode of the planar cavity. Mathematically speaking, the enhancement results from a closest matching of the transition frequency with a pole of the scattering Green tensor.

Similarly, for the cylindrical cavity we find that for a given transition frequency there exists a series of discrete radii such that the transition is near-resonant with one of the cavity modes. In this section, we explore analytically the structure of these resonances.

### A. Perfect reflector

Let us begin with the limit $|\varepsilon| \to \infty$ of a perfectly conducting cavity. For large $|\varepsilon|$, the leading order terms of the coefficients $A$ and $B_{M,N,D}$ in Eqs. (2.17) read

$$A \sim -m^2(kR)^2(qR)^2\varepsilon^2 + O(\varepsilon), \tag{3.1a}$$

$$B_M \sim -(kR)^3(\eta R)^3\tilde{h}_1\tilde{h}\varepsilon^{5/2} + O(\varepsilon^2), \tag{3.1b}$$

$$B_N \sim B_D \sim -(kR)^3(\eta R)^3\tilde{h}_1\tilde{j}\varepsilon^{5/2} + O(\varepsilon^2). \tag{3.1c}$$

Hence, in the limit $|\varepsilon| \to \infty$, Eq. (2.16) simplifies to

$$\tilde{r}_M \overset{|\varepsilon|\to\infty}{\longrightarrow} \frac{\tilde{h}}{\tilde{j}}; \quad \tilde{r}_N \overset{|\varepsilon|\to\infty}{\longrightarrow} 1, \tag{3.2}$$

and so the reflection coefficients (2.15) become [34]

$$r_M \overset{|\varepsilon|\to\infty}{\longrightarrow} -\frac{H_m^{(1)\prime}(x)}{J_m'(x)}; \quad r_N \overset{|\varepsilon|\to\infty}{\longrightarrow} -\frac{H_m^{(1)}(x)}{J_m(x)}. \tag{3.3}$$

The potential (2.2) diverges, and is thus truly resonant, when at least one of these coefficients has a pole at $q = 0$. Since $x = \eta R = kR$ for $h = 0$, it is clear that resonances occur in the perfectly reflecting limit when either $J_m(kR) = 0$ or $J_m'(kR) = 0$, that is, when the radius equals one of the radii given as

$$R_{mj}^{(\prime)} = \frac{c}{\omega} j_{mj}^{(\prime)}, \tag{3.4}$$

where $j_{mj}$ and $j_{mj}'$ are the $j$th zero of $J_m(x)$ and $J_m'(x)$, respectively (only zeros $j_{mj}^{(\prime)} > 0$ are considered).

For each mode $m$ and each polarization, there is hence a number of possible radii $R_{mj}$ leading to a resonant enhancement of the CP potential. The strongest resonance is that corresponding to the smallest resonant radius, which is $R_{11}'$, corresponding to the first zero of $J_1'$, $j_{11}' \approx 1.841\,183\,8$. If the dominant transition $|n\rangle \to |k\rangle$ is a downward one, that is, $\omega_{kn} < 0$, this resonance corresponds to a potential minimum which can act as a guiding potential. For an upward transition (such as will be the case, e.g., for a ground-state molecule), the strongest resonance which corresponds to a potential minimum in the cylinder center is $R = R_{11} = R_{01}'$, which happens to be a double resonance since $j_{11} = j_{01}' \approx 3.831\,706\,0$. We will analyze these examples further in Sec. V.

### B. Good conductor

In reality, any metal has a finite conductivity so that $|\varepsilon| < \infty$. As we now show, this results in a shifting of the values of $kR$ which give poles at $q = 0$ away from the zeros of the Bessel functions. As a consequence, the optimal radii for enhancing the CP potential or transition rates deviate from their perfect-conductor values as given by Eq. (3.4). We derive approximate formulas for the new optimal radii, valid for good conductors.

In the following we consider a metal described by the Drude model,

$$\varepsilon(\omega) = 1 - \frac{\omega_p^2}{\omega(\omega + i\gamma)} = 1 - \frac{\omega_p^2}{\omega^2+\gamma^2} + i\frac{\gamma}{\omega}\frac{\omega_p^2}{\omega^2+\gamma^2}, \tag{3.5}$$

where $\omega_p$ is the plasma frequency and $\gamma$ is the relaxation frequency. For good conductors one has $\omega_p \gg \gamma$, and we

assume this is true in the following. Since we are considering transitions in Rydberg atoms or molecules, we will restrict our interest to low frequencies and therefore also assume $\omega \ll \omega_p$. Under these assumptions, the following is true:

$$\mathrm{Re}\,\varepsilon < 0; \quad \mathrm{Im}\,\varepsilon > 0; \quad |\mathrm{Re}\,\varepsilon|, \mathrm{Im}\,\varepsilon \gg 1. \tag{3.6}$$

Let us consider the reflection coefficients $r_{M,N}$ as given by Eqs. (2.15)–(2.17) once more. We are looking for the complex resonant value of $kR$ which corresponds to a zero of the denominator of $r_{M,N}$ when $q = 0$. The coefficient $A$ vanishes quadratically for small $q$, so we can set $A = 0$ in the following and consider the coefficients $B_{M,N,D}$. The sought value of $kR$ is hence the solution of the equation $B_D|_{q=0} = 0$,[1] which may be written as

$$\frac{\tilde{h}(\sqrt{\varepsilon}kR)}{\tilde{\jmath}(kR)} + \frac{\tilde{\jmath}(kR)}{\tilde{h}(\sqrt{\varepsilon}kR)} = \sqrt{\varepsilon} + \frac{1}{\sqrt{\varepsilon}}. \tag{3.7}$$

The two roots of this second-order equation in $\tilde{\jmath}(kR)$ give all the resonances since $B_D$ is the denominator of both reduced reflection coefficients for $q = 0$. The perfect conductor limit $|\varepsilon| \to \infty$ is easily recovered from this equation, in which case the solutions $\tilde{\jmath}(kR) = \infty$ and $\tilde{\jmath}(kR) = 0$ are just the solutions (3.4), that is, $kR = j_{mn}$ and $kR = j'_{mn}$.

Approximate solutions to (3.7) when $|\varepsilon|$ is large but finite are straightforward to find. We write

$$kR = j_{mj}^{(\prime)} + \delta^{(\prime)}, \tag{3.8}$$

where $\delta^{(\prime)}$ are small complex numbers. The prime corresponds to solutions close to a zero of $J'_m$. Solving Eq. (3.7) to leading order in $\varepsilon^{-1}$ then gives

$$\delta \approx -\frac{i}{\sqrt{\varepsilon}}; \tag{3.9a}$$

$$\delta' = \delta'_{mj} \approx \frac{J_m(j'_{mj})}{J''_m(j'_{mj})}\frac{i}{\sqrt{\varepsilon}}; \tag{3.9b}$$

note that $\tilde{h}(z) \sim i + O(z^{-1}), |z| \to \infty$ (cf. e.g., [35], Sec. 9.2). The fraction $J_m(j'_{mj})/J''_m(j'_{mj})$ is a real and negative number of order unity which tends asymptotically to $-1$ for large arguments. For a good conductor (3.6), $\varepsilon$ is in the second quadrant of the complex plane, so $\sqrt{\varepsilon}$ is in the first quadrant for an absorbing medium, and $i/\sqrt{\varepsilon}$ is in the first complex quadrant. The shifts $\delta$ and $\delta'$ to the poles at $q = 0$ lie in the third quadrant.

Similarly, one can show that all poles of the integrand of the scattering Green tensor of a well conducting surface are displaced from the Bessel zeros $\eta R = j_{mj}$ and $\eta R = j'_{mj}$ by small quantities which lie in the third complex quadrant. This means that the poles of the reflection coefficients all lie in the lower half of the complex $\eta$ plane when $|\varepsilon| < \infty$, justifying the rotation of $q$-integral path mentioned in Sec. II C and shown in Fig. 2.

[1] One may note here that the original pole due to the zero of $J_m(x)$ in the prefactor (2.15) is canceled by the presence of $\tilde{\jmath}^2$ in the denominator, whereas $\tilde{\jmath}$ only enters to linear order in the numerator. This is how the pole is moved to the value of $kR$ which solves Eq. (3.7).

For real frequencies, the cavity radius can never be chosen such that it lies exactly on one of the complex-valued resonances. Instead, we will derive optimal real radii close to the resonances that maximize the real or imaginary parts of the Green tensor. As these optimal radii turn out to be different for the real vs imaginary parts, we have to distinguish between radii which maximize the resonant potential (2.7) and those which maximize the transition rate (2.11b).

### C. Optimal radii for enhancing the potential

Consider first a resonance associated with a pole of $r_N$. We represent the pole in the form (3.8) and let $q$ and $\delta$ be small so that

$$x = \eta R \approx j_{nj} + \delta - \frac{1}{2} j_{nj} \frac{q^2}{k^2}.$$

Keeping only leading orders in the small quantities $\delta$, $q^2$, and $1/\sqrt{\varepsilon}$, that is, using Eqs. (3.1a)–(3.1c) with

$$B_N \sim -(kR)^3(\eta R)^3 \tilde{h}_1 \tilde{\jmath} \varepsilon^{5/2} + (kR)^4(\eta R)^2 \tilde{\jmath}^2 \varepsilon^2 + O(\varepsilon^{3/2}), \tag{3.10}$$

the reflection coefficient as given by (2.15)–(2.17) becomes

$$\begin{aligned} r_N &\approx \frac{i\sqrt{\varepsilon} H_m^{(1)}(x)}{i\sqrt{\varepsilon} J_m(x) - J'_m(x)} \\ &\approx -\frac{i Y_m(j_{mj})}{J'_m(j_{mj})} \frac{1}{q^2 j_{mj}/(2k^2) - \zeta}, \end{aligned} \tag{3.11}$$

with

$$\zeta = \delta + i/\sqrt{\varepsilon}. \tag{3.12}$$

We have used that $\tilde{h}_1 \approx i$ because of its argument being large with positive imaginary part (see the asymptotic expansions, Sec. 9.2 of [35]) and noted that $H_m^{(1)}(x) \approx i Y_n(x)$.

Now we note that in the integrand of the integral (2.20), the term which resonates is the last one, which does not have a prefactor $q^2$. For this term there is no other resonating structures in the integrand, and we can simply conclude that close to a strong resonance

$$\begin{aligned} U_n^{\mathrm{res}}(\mathbf{r}) &\propto \mathrm{Re}\,\mathbf{G}(\mathbf{r},\mathbf{r},\omega) \propto \mathrm{Im}\int_0^\infty dq r_N \\ &\propto \mathrm{Re}\int_0^\infty \frac{dq}{q^2 - \zeta} \propto \mathrm{Re}\sqrt{\frac{1}{-\zeta}} \propto \mathrm{Im}\sqrt{\frac{1}{\zeta}}, \end{aligned} \tag{3.13}$$

where we have made the substitution $q \to \sqrt{2/j_{mj}}q/k$ at the beginning of the second line. Explicitly, we have

$$\begin{aligned} \mathrm{Im}\sqrt{\frac{1}{\zeta}} &= -|\zeta|^{-1/2} \sin\left(\frac{1}{2}\arctan\frac{\mathrm{Im}\,\zeta}{\mathrm{Re}\,\zeta}\right) \\ &= \frac{-1}{\sqrt{2}\sqrt[4]{\mathrm{Re}^2\zeta + \mathrm{Im}^2\zeta}} \sqrt{1 - \frac{\mathrm{Re}\,\zeta}{\sqrt{\mathrm{Re}^2\zeta + \mathrm{Im}^2\zeta}}}. \end{aligned} \tag{3.14}$$

where $\mathrm{Re}\,\zeta = \delta - \mathrm{Im}\{\varepsilon^{-1/2}\}$ and $\mathrm{Im}\zeta = \mathrm{Re}\{\varepsilon^{-1/2}\}$. Differentiating this result with respect to $\delta$, we find that the maximum

lies at

$$\mathrm{Re}\,\zeta = -\mathrm{Im}\,\zeta/\sqrt{3}, \tag{3.15}$$

so that

$$\delta \approx \mathrm{Im}\{\varepsilon^{-1/2}\} - \frac{1}{\sqrt{3}}\mathrm{Re}\{\varepsilon^{-1/2}\}. \tag{3.16}$$

Note that $\delta$ is independent of $m$ and $j$ to leading order in the large parameter $\varepsilon$. The resonant radii associated with resonances of $r_N$ are hence given by

$$kR \approx j_{mj} + \mathrm{Im}\{\varepsilon^{-1/2}\} - \frac{1}{\sqrt{3}}\mathrm{Re}\{\varepsilon^{-1/2}\}. \tag{3.17}$$

For resonances due to $r_M$, we present the poles of $J'_m(x)$ in the form (3.8). A virtually identical procedure then leads to

$$\delta' = \delta'_{mj} \approx -\frac{J_m(j'_{mj})}{J''_m(j'_{mj})}\delta. \tag{3.18}$$

Consequently, the respective resonant radii read

$$kR \approx j'_{jm} - \frac{J_m(j'_{mj})}{J''_m(j'_{mj})}\left(\mathrm{Im}\{\varepsilon^{-1/2}\} - \frac{1}{\sqrt{3}}\mathrm{Re}\{\varepsilon^{-1/2}\}\right). \tag{3.19}$$

As a numerical example, take Rb in its $32s_{1/2}$ Rydberg state whose strongest downward $|n\rangle = 32s_{1/2} \to |k\rangle = 31p_{3/2}$ transition has frequency $\omega_{kn} \approx -9.013 \times 10^{11}$ rad/s and a cylinder made of Au using $\omega_p \approx 1.4 \times 10^{16}$, $\gamma \approx 5.4 \times 10^{13}$ [36]. In this case, the shifts of the maxima away from the Bessel zero for for resonances due to $r_N$ are found to be $\delta \approx -0.00056$.

In Fig. 3, we show the potential as a function of radius close to the resonance at $kR_{01} \approx j_{01}$, resonating with the downward transition to $31p_{3/2}$. More details on the specifics of CP potentials on Rydberg atoms are found in Ref. [29] and summarized in Sec. V. It is interesting to note that even though gold is a good conductor whose permittivity is much greater than unity as assumed previously, the shift of the resonant radius away from the perfect-conductor result is not negligible. We see in Fig. 3 that the potential at the optimal radius is about a factor 2.5 greater than its value for $kR_{01} = j_{01}$. The resonant radius is given with excellent approximation by Eq. (3.17), which for this example predicts the maximum at $R - R_{01} \approx -187$ nm.

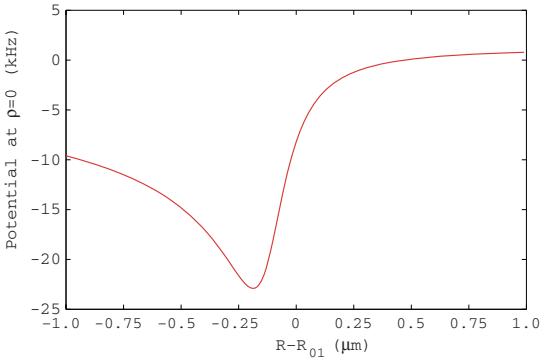


FIG. 3. (Color online) The potential of Rydberg Rb in its $32s_{1/2}$ state at the center ($\rho = 0$) of a Au cavity as a function of radius close to the resonance corresponding to the first zero $j_{01} \approx 2.4$ of $J_0$. The cavity resonantly enhances the contribution from the $32s_{1/2} \to 31p_{3/2}$ transition. $R_{01} = 799.9$ $\mu$m as given by Eq. (3.4) is the corresponding perfect conductor resonant radius.

We note furthermore that the width of the radius resonances is on the order of 500 nm, which is expected to be well within the accuracy obtainable for production of pipes with diameters on the order of hundreds of micrometers. It is also much wider than surface roughness amplitudes of good metal surfaces, indicating that the associated diminishing of the CP-potential enhancement is not expected to be important. The narrowness of the peaks are thus on the order of 1/3000th of the cylinder radius, and we do not expect observation and utilization of the resonant behavior to be hampered by issues of production accuracy.

### D. Optimal radii for enhancing transition rates

Optimal radii for resonantly enhancing transition rates in a conducting cavity can be derived in close analogy to the previous section. We again start with resonances of $r_N$ as approximated by Eq. (3.11). The transition rates (2.11b) close to a resonance are found just as in (3.13) to be proportional to

$$\Gamma_n^{(1)}(\mathbf{r}) \propto \mathrm{Im}\,\mathbf{G}(\mathbf{r},\mathbf{r},\omega) \propto \mathrm{Re}\sqrt{\frac{1}{\zeta}}, \tag{3.20}$$

where

$$\mathrm{Re}\sqrt{\frac{1}{\zeta}} = |\zeta|^{-1/2}\cos\left(\frac{1}{2}\arctan\frac{\mathrm{Im}\,\zeta}{\mathrm{Re}\,\zeta}\right) = \frac{1}{\sqrt{2}\sqrt[4]{\mathrm{Re}^2\zeta + \mathrm{Im}^2\zeta}}\sqrt{1 + \frac{\mathrm{Re}\,\zeta}{\sqrt{\mathrm{Re}^2\zeta + \mathrm{Im}^2\zeta}}}. \tag{3.21}$$

The maximum of the preceding function is again found by differentiation with respect to $\delta$. It now lies at $\mathrm{Re}\,\zeta = \mathrm{Im}\,\zeta/\sqrt{3}$, so that

$$\delta \approx \mathrm{Im}\{\varepsilon^{-1/2}\} + \frac{1}{\sqrt{3}}\mathrm{Re}\{\varepsilon^{-1/2}\} \tag{3.22}$$

is again independent of $m$ and $j$ to leading order in $\varepsilon$. The resonant radii associated with resonances of $r_N$ for enhancing transition rates

$$kR \approx j_{mj} + \mathrm{Im}\{\varepsilon^{-1/2}\} + \frac{1}{\sqrt{3}}\mathrm{Re}\{\varepsilon^{-1/2}\} \tag{3.23}$$

are thus different from the corresponding radii (3.17) for enhancing the CP potential.

As for the potential, the resonances due to $r_M$ are found to be maximal at

$$\delta'_{mj} \approx -\frac{J_m(j'_{mj})}{J''_m(j'_{mj})}\delta; \tag{3.24}$$

that is,

$$kR \approx j'_{jm} - \frac{J_m(j'_{mj})}{J''_m(j'_{mj})}\left(\mathrm{Im}\{\varepsilon^{-1/2}\} + \frac{1}{\sqrt{3}}\mathrm{Re}\{\varepsilon^{-1/2}\}\right). \tag{3.25}$$

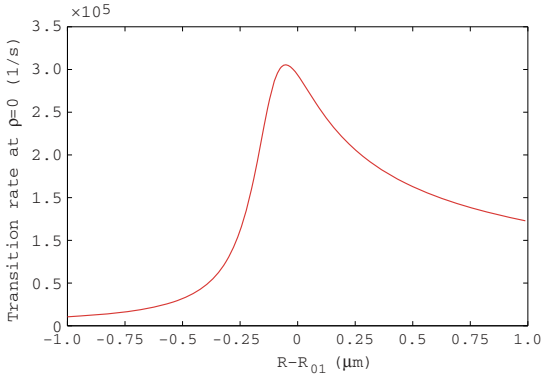


FIG. 4. (Color online) Same setup as Fig. 3, but for the cavity-assisted transition rate from state $32s_{1/2}$ to $32p_{3/2}$.

The resonant enhancement of the transition rate $32s_{1/2} \to 32p_{3/2}$ of a Rydberg Rb atom placed at the center of a Au cavity is shown in Fig. 4, again for the $j_{01}$ resonance of $r_N$. The true optimal radius is seen to be well approximated by Eq. (3.23); it is smaller than the perfect-conductor value by 0.006%, with $\delta \approx -0.000\,15$. The optimal radii for enhancing potential vs rate thus differ notably, by about 135 nm.

## IV. GENERAL SCALING PROPERTIES

In this section we discuss the scaling properties of resonant thermal CP forces, that is, their dependencies on the relevant molecular, material, thermal, and geometric parameters. These were discussed in detail for the case of a planar cavity in Ref. [27], and many of the results remain valid also in the cylindrical geometry. The resonant potential corresponding to a dipole transition from state $n$ to state $k$ is proportional to the absolute square of the transition dipole moment, $|\mathbf{d}_{kn}|^2$.

We recently showed that the monotonously decaying, short-distance part of the CP potential on a Rydberg atom is virtually independent of temperature from room temperature down to absolute zero [37]. This is not so for the oscillatory part considered herein, however, which is proportional to the photon number $n(|\omega_{kn}|)$ just as was found in the planar case. For temperatures larger than the transition frequency the temperature dependence is thus approximately linear, $U^{\mathrm{res}}(\rho) \propto T, k_{\mathrm{B}}T \gg \hbar\omega_{kn}$. In the opposite limit the resonant potential is exponentially suppressed: $U^{\mathrm{res}}(\rho) \propto \exp(-\hbar\omega_{kn}/k_{\mathrm{B}}T)$, $k_{\mathrm{B}}T \ll \hbar\omega_{kn}$. For a Rydberg atom at room temperature, the former limit applies.

On the contrary, the scaling of the potential with the permittivity of the cavity walls depends strongly on the geometry. For the cylindrical cavity, this scaling follows immediately from the discussion of the resonant radii in Sec. III C. As shown by Eq. (3.13), the resonant potential is proportional to $\sqrt{1/\zeta}$. This function (3.14) has its maximum at $\mathrm{Re}\,\zeta = -\mathrm{Im}\,\zeta/\sqrt{3}$, where it takes the value $\sqrt[4]{3}/(2\sqrt{2\mathrm{Im}\,\zeta})$ with $\mathrm{Im}\,\zeta = \mathrm{Re}\{\varepsilon^{-1/2}\}$. To leading order in the large quantity $\varepsilon$, the potential for near-resonant radius hence

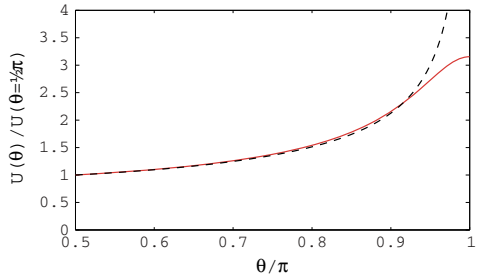


FIG. 5. (Color online) The dependence of the peak potential at resonance on $\theta = \arg(\varepsilon)$. The solid graph is $U^{\mathrm{res}}$ calculated for a $32s$ Rydberg atom whose $32s_{1/2} \to 31p_{3/2}$ transition is in resonance with the $j_{01}$ zero of $J_0(x)$, varying the phase of $\varepsilon$ throughout the physical range but keeping $|\varepsilon|$ constant and equal to its value using Eq. (3.5). The dashed graph is the theoretical curve based on the approximate scaling of Eq. (4.1). Both functions have been normalized by their values at $\arg\varepsilon = \pi/2$.

scales as

$$U_n^{\mathrm{res}}(\mathbf{r}) \propto \frac{|\varepsilon|^{1/4}}{\sqrt{\cos\left[\frac{1}{2}\arg(\varepsilon)\right]}}. \tag{4.1}$$

Note that this scaling is an improvement with respect to the enhancement achievable in a planar cavity for which we found the potential to be proportional to $\ln\varepsilon$ [27]. The resonant enhancement in the preceding approximation diverges as $\arg(\varepsilon) \to \pi$. A full numerical investigation shows that the potential in fact remains finite in this limit (cf. Fig. 5). In the displayed example for the $\arg(\varepsilon)$ dependence of the potential of Rydberg Rb in its $32s_{1/2}$ state, the value of the potential changes by more than a factor of three as the phase of $\varepsilon$ is varied from $\pi/2$ (purely imaginary permittivity) to $\pi$ (purely real permittivity). This implies that decreasing the dissipation rate of the cavity material can increase the enhancement significantly. Note that with $\gamma \approx 5.4 \times 10^{13}$ [36], the actual phase of Au at the relevant transition frequency is close to $\pi/2$.

The shown dependence of the resonant potential on the phase of the permittivity is also interesting in light of the thermal anomaly of the Casimir effect for metals [38,39]. This dispute centers in an essential way on the description of the dissipation of the metal: Employing the standard Drude model (3.5) with measured optical dissipation data gives a different prediction of the force at high temperature than that using a nondissipative plasma model in which one sets $\gamma = 0$ at the outset. Experiments appear to favor the latter approach [39,40]. The cavity enhancement of the CP potential as a related quantum vacuum effect is good system for investigating the thermal anomaly further: As Eq. (4.1) shows, the potential at resonance using a plasma model predicts a signal more than three times that calculated for the Drude model (note that $|\varepsilon|$ is also larger using a plasma model, adding to the relative difference in prediction).

Finally, let us consider the scaling of the potential with the transition frequency. The frequency influences the potential (2.7) in three ways: First, there is a prefactor $\omega_{kn}^2 n(|\omega_{kn}|)$,

independent of the particular cavity geometry considered. Second, there is an additional factor of $\omega_{nk}$ because the magnitude of oscillations fall off as $J_m^2, J_m'^2 \sim 1/(R-\rho)$ away from the cavity walls and the resonant cavity radius is in turn proportional to $\omega_{kn}$. This geometric frequency-dependence is closely similar to that found for a planar cavity [27]; it is a consequence of the general scaling law for the Green tensor as established in Ref. [41]. Third, the $\varepsilon$ scaling introduces an additional frequency dependence. For $\omega_{kn} \ll \gamma$, Eq. (4.1) leads to a $\sqrt[4]{1/\omega_{kn}}$ scaling. Combining these three effects, the peak resonant potentials scale as $\omega_{kn}^{2.75} n(|\omega_{kn}|)$. For comparison, the scaling $\omega_{kn}^3 n(|\omega_{kn}|)$ for a planar cavity is slightly stronger due to the much weaker $\varepsilon$ dependence.

For atoms in highly excited Rydberg states (cf. Sec. V), the CP potential is dominated by transitions to neighboring states. For these transitions, the frequencies and dipole matrix elements depend in a simple way on the principal quantum number $n$ of the initial atomic Rydberg state: For sufficiently large $n$, the transition frequencies can be given as $\omega_{kn} = 2\mathrm{Ry}/(\hbar n^3)$ (Ry, Rydberg energy), while the dipole moments scale as $n^2$. Combining this with the dependencies discussed previously, one finds that the CP potential of a Rydberg atom scales as

$$\begin{aligned} U_n^{\mathrm{res}} &\propto n^{-4.25} n(\omega_{kn}) \\ &\propto \begin{cases} n^{-1.25}, & n \gg n_T; \\ \exp[-(n_T/n)^3], & n \ll n_T, \end{cases} \end{aligned} \tag{4.2}$$

where we have introduced a characteristic thermal principal quantum number

$$n_T = \left( \frac{2\mathrm{Ry}}{k_{\mathrm{B}} T} \right)^{\frac{1}{3}}. \tag{4.3}$$

The maximum potential is found for states with a principal quantum number around $n \sim n_T$. At $T = 300\,\mathrm{K}$ we have $n_T \approx 10.2$; hence, the maximum potential is found for principal quantum numbers below the Rydberg range. For this reason we have chosen a low Rydberg state, $32s$, for our preceding numerical examples and in the following.

## V. NUMERICAL RESULTS

We now present numerical studies of the CP potential inside a cylindrical cavity based on the exact formulas presented in Sec. II. Due to the complexity of the formulaic apparatus for the case of the cylinder, it is necessary to first ascertain the correctness of the numerical calculations. As a numerical benchmark, we verified that for positions sufficiently close to the cylinder wall ($R - \rho \ll R$) the potential tends asymptotically to that outside a half space (cf. e.g., [13]).

We are interested in an observable resonant enhancement of the potential predicted for the radii derived in Sec. III. As is clear from Sec. IV, this requires a cavity made of a good conductor and an atomic system whose transition frequencies lie close to the peak of the thermal spectrum $\omega_{kn}^{11/4} n(|\omega_{kn}|)$ at room temperature and whose respective dipole matrix elements are large. Rydberg atoms with their enormous matrix elements and relatively small transition frequencies fulfill both of these requirements.

In practice, Rydberg states with principal quantum number $n$ in the range 30–50 can readily be prepared using standard Rydberg lasers. As shown at the end of Sec. IV, the optimal choice of $n$ for measuring the resonant enhancement is smaller than the standard Rydberg regime, around $n = 10$: While transition dipole moments increase with higher $n$, transition frequencies of the dominant transitions decrease further away from the optimal frequency value $\sim k_{\mathrm{B}} T$, resulting together in a low optimum $n$. As a compromise, we use the value $n = 32$ for our numerical examples, being a level in the lower part of the Rydberg spectrum while still being readily available with standard equipment. In all calculations the temperature was 300 K.

The resonant potential is calculated only for the strongest downward transition to $31p_{3/2}$. The transition to $32p$ states are approximately the same strength, but being upward transitions they correspond to potential maxima on the axis at the strongest cavity resonances, and we find it preferable to consider a downward transition whose maximally enhanced potential has a minimum, potentially useful for guiding purposes. Transitions to higher and lower $n$ contribute significantly only in the nonretarded regime close to the cylinder walls which we are not interested in in the present investigation (but see [29] for details). Results are shown in Fig. 6 for the first eight resonances of the coefficient $r_N$ [corresponding to zeros of $J_m(x)$] and $r_M$ [corresponding to zeros of $J_m'(x)$]. Note how some radii resonate both with $r_M$ and $r_N$ since $J_0'(x) = -J_1(x)$.

For the considered case of a resonantly enhanced downward transition, we observe that a potential at the resonant radius corresponding to $j_{mj}^{(\prime)}$ has $j$ local minima. Potentials for $j_{mj}$ have minima on the cylinder axis for even $m$ and maxima for odd $m$. For the $j_{mj}'$ resonances, the situation is reversed. The double resonances are dominated by the $j_{mj}$ contribution, so the first of the two rules applies. For a given $m$, the maximum potential depth decreases with $j$.

One might expect that smaller radii give the deeper potential minima, based on the fact that the amplitude of oscillations decrease away from a boundary (outside a planar half space the oscillation amplitude decreases proportional to inverse distance [13]). Unlike the planar case [27], however, this is not true in general. The lowest Bessel zeros are $j_{11}' \approx 1.8412$, $j_{01} \approx 2.4048$, $j_{21}' \approx 3.0542$, and $j_{01}' = j_{11} \approx 3.8317$. The first two on this list indeed correspond to the two largest potential extrema in the same order, but $j_{21}'$ in fact represents the shallowest of the eight enhanced potentials considered in Fig. 6. Compared to the situation outside a half space, spatial energy level oscillation amplitudes are enhanced by two orders of magnitude.

The corresponding enhancement of the transition rate from $32s_{1/2}$ to $31p_{3/2}$ is shown in Fig. 7, where the cylinder radii are picked according to Eqs. (3.23) and (3.25) as appropriate. The figure thus shows the maximally enhanced transition rate between these two levels. The transition rate is increased by about a factor 5.0 for the smallest cavity corresponding to $j_{11}'$ compared to the transition rate in free space, which for the $32s$ state is about 105 kHz. In comparison, the transition rate outside a half space oscillates about its free-space value within

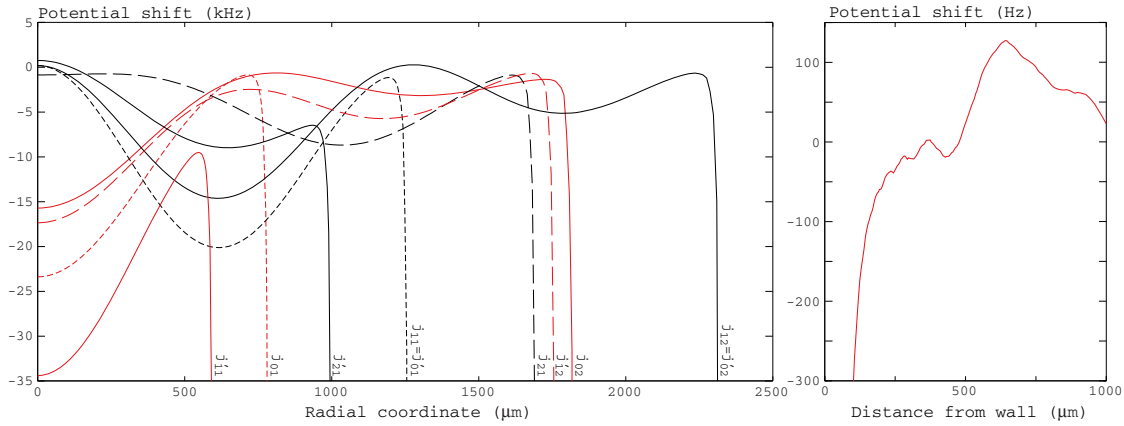


FIG. 6. (Color online) (Left) Casimir-Polder potential at the eight smallest resonant radii acting on isotropic Rb in the state $32s_{1/2}$, whose transition to $31p_{3/2}$ resonates with various modes of a gold cavity described by Eq. (3.5). The radii are chosen according to Eq. (3.17) ($j_{01}$, $j_{02}$, $j_{11} = j'_{01}$, $j_{12} = j'_{02}$, and $j_{21}$) and Eq. (3.19) ($j'_{11}$, $j'_{12}$, $j'_{21}$). (Right) The potential outside a plane half space.

variations of about 10 kHz in the far zone, hence showing that the cavity can enhance the oscillating contribution to the rate alone by about a factor 50. The lifetime of the initial state against spontaneous and stimulated decay is thus reduced from its free-space value of 9.5–1.9 $\mu$s inside the cylindrical cavity for the $j'_{11}$ resonance. Recall from Sec. III that the potentials and transition rates peak at different radii. In Fig. 7, we have chosen the optimal radii for enhancing the rates. By contrast, the transition rates at the optimal radii for enhancing potentials (not displayed) are smaller by about a factor 2.

For comparison, we consider the case of the polar molecule LiH. Polar molecules also exhibit transitions in the frequency regime ideal for enhancement, but with the respective dipole matrix elements being much smaller than those of Rydberg atoms. LiH has a lowest transition frequency (rotational) of $\omega_{10} = 2.79 \times 10^{12}$ rad/s and corresponding transition dipole moment $|\mathbf{d}_{10}|^2 = 3.85 \times 10^{-58}$ C$^2$ m$^2$. As a result of the smaller dipole moment, the CP potential of polar molecules is much smaller than that of Rydberg atoms. In spite of a relative enhancement of about a factor 50–100 in a cylindrical cavity, the achievable potential depth is still less than 1 Hz, which is insufficient for molecular guiding purposes.

While a cavity enhancement of two orders of magnitude is modest for the CP potential of a polar molecule, it is of interest when regarding the ground-state heating rates. As Fig. 8 shows, the transition to a particular state (in this case the lowest rotational state) can be enhanced by a factor of about 30, considerably reducing the lifetime of the rotational ground state against heating from 2.1 to 0.064 s.

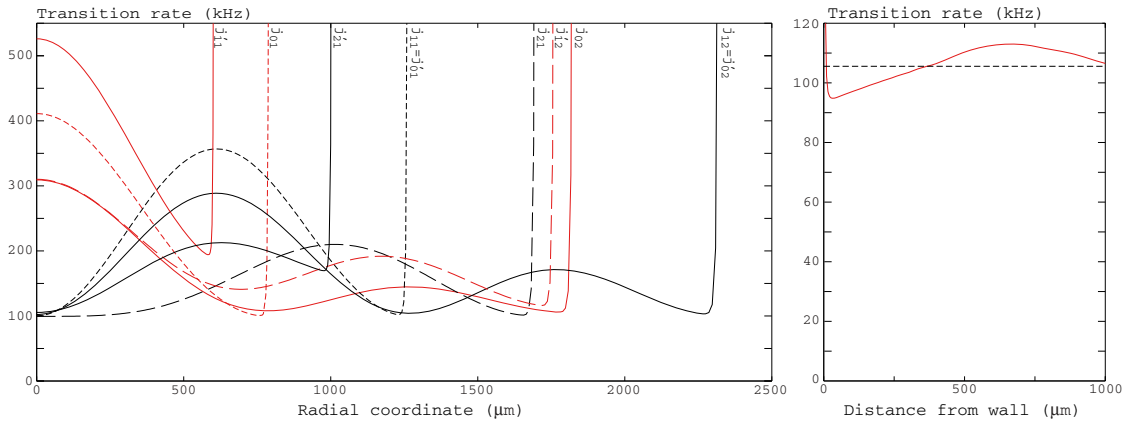


FIG. 7. (Color online) (Left) Enhanced transition rates at the eight smallest resonant radii acting on isotropic Rb in the state $32s_{1/2}$, whose transition to $31p_{3/2}$ resonates with various modes of in a gold cavity described by Eq. (3.5). The radii are chosen according to Eq. (3.23) ($j_{01}$, $j_{02}$, $j_{11} = j'_{01}$, $j_{12} = j'_{02}$, and $j_{21}$) and Eq. (3.25) ($j'_{11}$, $j'_{12}$, $j'_{21}$). (Right) The shift outside a plane half space.

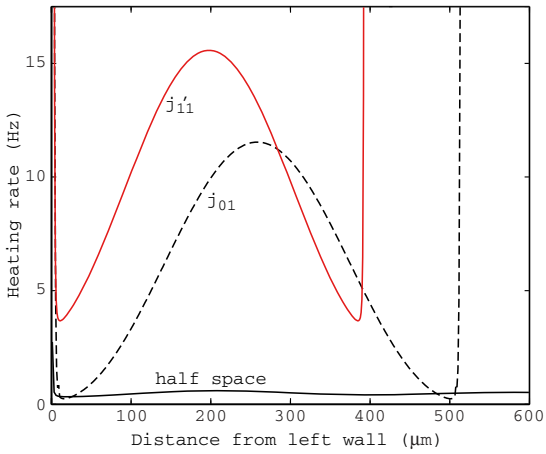


FIG. 8. (Color online) Comparison of enhanced and nonenhanced heating rate of ground-state LiH. The heating rate outside a half space [32] shown together with the two highest cylinder resonances [radii from (3.23) and (3.25)] along a central cylinder cross section.

## VI. CONCLUSIONS

We have presented the detailed theory for a particle (atom or molecule) in an eigenstate inside a cylindrical cavity carved out of a homogeneous and nonmagnetic material. A particle out of thermal equilibrium with its environment is subject to spatially oscillating CP forces near surfaces, and we have focused particularly on a scheme to enhance the oscillating force components by fine tuning the cavity radius to resonate with the particle's internal transition wavelength. A similar oscillating behavior is observed for the transition rates between eigenstates.

Formulas for calculating appropriate radii for maximal enhancement of potential and rates have been derived. For a perfectly conducting cylinder, the resonant radii are exactly given as the zeros of the Bessel function $J_m$ and its derivatives divided by the wave number of the resonating transition. The optimal radii are slightly shifted when the cavity is not perfectly conducting, and simple expressions for the correction have been derived for good conductors. The corrected optimal radii for enhancing potential vs transition rates are now slightly different.

We have shown how the cavity enhancement scales with the relevant paramaters of the setup. In particular, we have paid attention to the dependence of the enhancement on the permittivity $\varepsilon(\omega_{kn})$ of the cavity material. We have shown that the potential at resonance scales as $U \propto |\varepsilon(\omega_{kn})|^{1/4}$, which is a noticeable improvement over the planar geometry, for which the scaling was found to be logarithmic, $U \propto \ln \varepsilon(\omega_{kn})$ [27]. A strong dependence is also found on the phase $\arg \varepsilon(\omega_{kn})$ of the permittivity. This is interesting in light of the controversy surrounding the temperature correction to the Casimir force between metals, for which the complex phase of $\varepsilon$ for the metal in question is of the essence. A precision experiment of the potential enhancement in a cylindrical cavity could be a critical experiment in this respect.

The cases of a Rydberg atom and a ground-state LiH molecule have been studied numerically, both of which are of experimental and technological interest. We have found that the deepest potential minima for Rydberg atoms can be obtained for quantum numbers in the lower end of the Rydberg regime. With the smallest cavity enhancement [corresponding to the first zero of $J_1'(x)$], a guiding potential depth in excess of 25 kHz is obtainable, which is within the region of observability of modern experiments. The enhancement factor obtained is more than 100, at least an order of magnitude better than what we obtained for a planar gold cavity [27]. For the polar molecule LiH, the cavity enhancement was found to be insufficient to bring the potential into the observable regime. Instead, a considerable enhancement of ground-state heating rates can be achieved.

## ACKNOWLEDGMENTS

We have benefited from discussions with J. Fortágh, and thank R. Messina for pointing out some misprints in the original manuscript. This work was supported by the UK Engineering and Physical Sciences Research Council. Support from the European Science Foundation (ESF) within the program "New Trends and Applications of the Casimir Effect" (www.casimir-network.com) is gratefully acknowledged.

[1] H. B. G. Casimir and D. Polder, Phys. Rev. **73**, 360 (1948).
[2] E. M. Lifshitz, Zh. Eksp. Teor. Fiz. **29**, 94 (1955) [Sov. Phys. JETP **2**, 73 (1956)].
[3] A. D. McLachlan, Proc. R. Soc. Lond. A **274**, 80 (1963).
[4] C. Henkel, K. Joulain, J. P. Mulet, and J.-J. Greffet, J. Opt. A **4**, S109 (2002).
[5] M. Antezza, L. P. Pitaevskii, and S. Stringari, Phys. Rev. Lett. **95**, 113202 (2005).
[6] J. M. Obrecht, R. J. Wild, M. Antezza, L. P. Pitaevskii, S. Stringari, and E. A. Cornell, Phys. Rev. Lett. **98**, 063201 (2007).
[7] T. Nakajima, P. Lambropoulos, and H. Walther, Phys. Rev. A **56**, 5100 (1997).
[8] S.-T. Wu and C. Eberlein, Proc. R. Soc. London A **456**, 1931 (2000).
[9] S. Y. Buhmann and D.-G. Welsch, Prog. Quantum Electron. **31**, 51 (2007).
[10] S. Scheel and S. Y. Buhmann, Acta Phys. Slov. **58**, 675 (2008).
[11] S. Y. Buhmann and S. Scheel, Phys. Rev. Lett. **100**, 253201 (2008).
[12] M.-P. Gorza and M. Ducloy, Eur. Phys. J. D **40**, 343 (2006).
[13] S. Å. Ellingsen, S. Y. Buhmann, and S. Scheel, Phys. Rev. A **79**, 052903 (2009).
[14] K. H. Drexhage, in *Progress in Optics XII*, edited by E. Wolf (North-Holland, Amsterdam, 1974), p. 163.

[15] R. R. Chance, A. Prock, and R. Silbey, in *Advances in Chemical Physics XXXVII*, edited by I. Prigogine and S. A. Rice (Wiley, New York, 1978), p. 1.
[16] G. Barton, Proc. R. Soc. London A **320**, 251 (1970).
[17] G. Barton, Proc. R. Soc. London A **367**, 117 (1979).
[18] G. Barton, Proc. R. Soc. London A **410**, 141 (1987).
[19] W. Jhe, Phys. Rev. A **43**, 5795 (1991).
[20] W. Jhe, Phys. Rev. A **44**, 5932 (1991).
[21] E. A. Hinds, Adv. At. Mol. Opt. Phys. **28**, 237 (1991).
[22] E. A. Hinds, Adv. At. Mol. Opt. Phys. Suppl. **2**, 1 (1994).
[23] D. Kleppner, Phys. Rev. Lett. **47**, 233 (1981).
[24] P. Goy, J. M. Raimond, M. Gross, and S. Haroche, Phys. Rev. Lett. **50**, 1903 (1983).
[25] M. S. Ünlü and S. Strite, J. Appl. Phys. **78**, 607 (1995).
[26] H. Walther, B. T. H. Varcoe, B.-G. Englert, and T. Becker, Rep. Prog. Phys. **69**, 1325 (2006).
[27] S. Å. Ellingsen, S. Y. Buhmann, and S. Scheel, Phys. Rev. A **80**, 022901 (2009).
[28] S. Å. Ellingsen, Y. Sherkunov, S. Y. Buhmann, and S. Scheel, in *Proceedings of the Ninth Conference on Quantum Field Theory Under the Influence of External Conditions (QFEXT09)*, edited by M. Bordag and K. A. Milton (World Scientific, Singapore, 2010), p. 168.
[29] J. A. Crosse, S. Å. Ellingsen, K. Clements, S. Y. Buhmann, and S. Scheel, Phys. Rev. A **82**, 010901(R) (2010); cf. also **82**, 029902(E) (2010).
[30] S. Scheel and S. Y. Buhmann, Phys. Rev. A **80**, 042902 (2009).
[31] M. Levin, A. P. McCauley, A. W. Rodriguez, M. T. H. Reid, and S. G. Johnson, Phys. Rev. Lett. **105**, 090403 (2010).
[32] S. Y. Buhmann, M. R. Tarbutt, S. Scheel, and E. A. Hinds, Phys. Rev. A **78**, 052901 (2008).
[33] L.-W. Li, M.-S. Leong, T.-S. Yeo, and P.-S. Kooi, J. Electromagn. Waves Appl. **14**, 961 (2000).
[34] C.-T. Tai, *Dyadic Green's Functions in Electromagnetic Theory* (Intext Educational, Scranton, 1971), Chap. 6.
[35] M. Abramowitz and I. A. Stegun, *Handbook of Mathematical Functions* (Dover, New York, 1964).
[36] A. Lambrecht and S. Reynaud, Eur. Phys. J. D **8**, 309 (2000).
[37] S. Å. Ellingsen, S. Y. Buhmann, and S. Scheel, Phys. Rev. Lett. **104**, 223003 (2010).
[38] I. Brevik, S. A. Ellingsen, and K. A. Milton, New J. Phys. **8**, 236 (2006).
[39] M. Bordag, G. L. Klimchitskaya, U. Mohideen, and V. M. Mostepanenko, *Advances in the Casimir Effect* (Oxford University Press, Oxford, 2009).
[40] R. S. Decca, D. López, E. Fischbach, G. L. Klimchitskaya, D. E. Krause, and V. M. Mostepanenko, Ann. Phys. **318**, 37 (2005).
[41] S. Y. Buhmann, S. Scheel, and J. Babington, Phys. Rev. Lett. **104**, 070404 (2010).

# Addendum

# Other publications (selected)

The following articles are appended to the printed dissertation for completeness and are not to be considered part of the thesis.

- I. Brevik, K.A. Milton and S.A. Ellingsen "Thermal corrections to the Casimir effect" *New Journal of Physics* **8**, 236 (2006)
- S.A. Ellingsen "Casimir attraction in multilayered plane parallel magneto-dielectric systems" *Journal of Physics A* **40**, 1951 (2007)
- S.A. Ellingsen and I. Brevik "Casimir force on real materials - the slab and cavity geometry" *Journal of Physics A* **40**, 3643 (2007)
- S.Å. Ellingsen, Y. Sherkunov, S.Y. Buhmann and S. Scheel "Casimir-Polder potential in thermal non-equilibrium" in *Proceedings of QFEXT09* edited by K.A. Milton and M. Bordag (World Scientific, 2010)
- I. Brevik and S.Å. Ellingsen "Transverse radiation force in a tailored optical fiber" *Physical Review A* **81**, 011806(R) (2010)
- I. Brevik and S.Å. Ellingsen "Possibility of measuring the Abraham force using whispering gallery modes" *Physical Review A* **81**, 063830 (2010)
- I. Brevik and S.Å. Ellingsen "Electromagnetic momentum conservation in media" *Annals of Physics (N.Y.)* in press (2010)
- S.Å. Ellingsen, K.S. Gjerden, M. Grøva and A. Hansen "Model for density waves in gravity-driven granular flow in narrow pipes" *Physical Review E* **81**, 061302 (2010)

Publications in the Addendum



**These articles are not included due to copyright**

**Ellingsen, Simen Andreas Ådnøy; Sherkunov, Yury; Buhmann, Stefan Yoshi; Scheel, Stefan.**
Casimir-Polder Potential in Thermal Non-equilibrium. I: Proceedings of the Ninth Conference on Quantum Field Theory Under the Influence of External Conditions (QFEXT09). World Scientific 2010 ISBN 978-981-4289-85-6. s. 168-177

**I. Brevik and S.Å Ellilngsen** "Electromagnetic momentum conservation in media" Annals of Physics (N.Y.) in press 2010

New Journal of Physics
The open-access journal for physics

# Thermal corrections to the Casimir effect

**Iver Brevik**[1], **Simen A Ellingsen**[1] **and Kimball A Milton**[2,3]

[1] Department of Energy and Process Engineering,
Norwegian University of Science and Technology, N-7491,
Trondheim, Norway
[2] Department of Physics, Washington University, St. Louis,
MO 63130, USA
E-mail: iver.h.brevik@ntnu.no, simenand@stud.ntnu.no and
milton@nhn.ou.edu

*New Journal of Physics* **8** (2006) 236
Received 2 May 2006
Published 20 October 2006
Online at http://www.njp.org/
doi:10.1088/1367-2630/8/10/236

**Abstract.** The Casimir effect, reflecting quantum vacuum fluctuations in the electromagnetic field in a region with material boundaries, has been studied both theoretically and experimentally since 1948. The forces between dielectric and metallic surfaces both plane and curved have been measured at the 10–1% level in a variety of room temperature experiments, and remarkable agreement with the zero-temperature theory has been achieved. In fitting the data various corrections due to surface roughness, patch potentials, curvature, and temperature have been incorporated. It is the latter that is the subject of the present paper. We point out that, in fact, no temperature dependence has yet been detected, and that the experimental situation is still too fluid to permit conclusions about thermal corrections to the Casimir effect. Theoretically, there are subtle issues concerning thermodynamics and electrodynamics which have resulted in disparate predictions concerning the nature of these corrections. However, a general consensus has seemed to emerge that suggests that the temperature correction to the Casimir effect is relatively large, and should be observable in future experiments involving surfaces separated at the few micrometre scale.

[3] Permanent address: Oklahoma Center for High Energy Physics and Homer L. Dodge Department of Physics and Astronomy, The University of Oklahoma, Norman, OK 73019, USA. Author to whom any correspondence should be addressed.


PII: S1367-2630(06)23709-1

**Contents**



## 1. Introduction

About the same time that Schwinger and Feynman were inventing renormalized quantum electrodynamics, Casimir discovered that quantum electrodynamic fluctuations resulted in macroscopic forces between conductors and dielectrics [1]. The theory was a natural outgrowth of the Casimir–Polder theory of the retarded dispersion force between molecules [2]. The general theory for the forces between parallel dielectrics was worked out by Lifshitz *et al* [3], who also included temperature corrections, which were considered further by Sauer [4] and Mehra [5]. Some years later, the whole theory was rederived by Schwinger *et al* [6].

The early experiments on Casimir forces were rather inconclusive—for a review see [7]. However, the corresponding Lifshitz theory was verified rather impressively by Sabisky and Anderson [8], so there could hardly be any doubt of the validity of the essential ideas. Starting about a decade ago, modern experiments by Lamoreaux [9]–[12], Mohideen *et al* [13]–[15], and by Ederth [16] brought the experimental measurement of the Casimir force between curved metal surfaces (mapped to the plane geometry by the proximity approximation [17, 18]) into the percent accuracy region. (Exact results have now apparently rendered the use of the proximity approximation, which cannot be extended beyond leading order, unnecessary. See, for example, [19]–[21].) Application of such Casimir forces to nanoelectromechanical devices have been suggested by experiments at Bell Labs and Harvard [22]–[24]. Only one experiment so far, of limited accuracy ($\sim$15%), has employed parallel plates [25]. The difficulty of maintaining parallelism in that geometry limits the accuracy of the experiment, but the forces are much larger than those between a sphere and a plate, so the forces can, in principle, be determined at much larger separations. Proposals to perform measurements of the force between a cylinder and a plane [26] and between eccentric cylinders [27] have advantages because the forces are stronger than between a sphere and a plane, yet the difficulties in assuring parallelism are not so severe as with two plane surfaces. The most precise experiments so far, based on both static and dynamical procedures between a plate and a spherical surface, have been performed at Purdue [28]–[30], where the accuracy is claimed to be better than 1% at separations down to less than 100 nm.

All present experiments agree well with the zero-temperature Casimir theory when surface roughness and finite conductivity corrections are included [31, 32]. The issue about which controversy has recently erupted is the temperature dependence. (For recent statements of both sides of the controversy, see [30], [33]–[36].) All experiments reported to date have been conducted at room temperature, so there is no direct evidence for or against any particular model of the temperature dependence. Indirect evidence for this dependence has been inferred based on the nonzero shift in the theoretical Casimir force between the surfaces due to the difference between the force at zero temperature and at 300 K. Surprisingly, this temperature shift is not so straightforwardly computed as one would have at first suspected.

It is the purpose of the present paper to frame the question of the temperature dependence of the Casimir force in the context of the history of the subject and the present experimental constraints, as well as to point out ways of reconciling the ambiguities both from the theoretical and experimental sides. In the following section, we review the standard approach given in [6] for both dielectric and metal surfaces. Then, in section 3, we give the arguments why the transverse electric (TE) zero mode should not be included, and how this impacts the temperature dependence of the force, and the resulting impact on the free energy and entropy. Other theoretical arguments for and against this point of view are discussed in section 4. The status of the experimental situation, and the possibility of dedicated experiments to search for the temperature dependence of the Casimir effect, will be reviewed in section 5. Some new calculations are presented in section 6 in the hope of providing signatures to help resolve the controversy. Finally, concluding remarks are offered in section 7.

## 2. Conventional temperature approach

The zero-temperature Casimir effect between parallel conducting plates, or between parallel dielectrics, is very well understood, and is not controversial. The formula for the latter, which includes the former as a singular limit, may be derived by a multitude of formalisms, which will not be reviewed here [6, 31], [37]–[39]. For a system of parallel dielectric media, characterized by a permittivity

$$\varepsilon(z) = \begin{cases} \varepsilon_1, & z < 0, \\ \varepsilon_3, & 0 < z < a, \\ \varepsilon_2, & a < z, \end{cases} \tag{2.1}$$

where the various permittivities are functions of frequency, the Lifshitz force per unit area on one of the surfaces is at zero temperature

$$P^{T=0} = -\frac{1}{4\pi^2} \int_0^\infty \mathrm{d}\zeta \int_0^\infty \mathrm{d}k_\perp^2 \, \kappa_3 (d^{-1} + d'^{-1}), \tag{2.2}$$

where $\zeta$ is the imaginary frequency, $\zeta = -\mathrm{i}\omega$, and the longitudinal wavenumber is

$$\kappa_i = \sqrt{k_\perp^2 + \zeta^2 \varepsilon_i(\mathrm{i}\zeta)}, \tag{2.3}$$

while the TE and transverse magnetic (TM) Green's functions are characterized by the denominators

$$d = \frac{\kappa_3 + \kappa_1}{\kappa_3 - \kappa_1}\frac{\kappa_3 + \kappa_2}{\kappa_3 - \kappa_2}e^{2\kappa_3 a} - 1, \qquad d' = \frac{\kappa_3' + \kappa_1'}{\kappa_3' - \kappa_1'}\frac{\kappa_3' + \kappa_2'}{\kappa_3' - \kappa_2'}e^{2\kappa_3 a} - 1, \tag{2.4}$$

respectively, where $\kappa_i' = \kappa_i/\varepsilon_i$.

The attractive Casimir pressure between parallel perfectly conducting planes separated by a vacuum space of thickness $a$ is obtained by setting $\varepsilon_{1,2} \to \infty$ and $\epsilon_3 = 1$. In that case the TE and TM contributions are equal, and we have

$$P_C = -\frac{1}{8\pi^2}\int_0^\infty d\zeta \int_{\zeta^2}^\infty d\kappa^2 \frac{4\kappa}{e^{2\kappa a} - 1} = -\frac{1}{\pi^2}\int_0^\infty d\zeta \frac{\zeta^3}{e^{2\zeta a} - 1} = -\frac{\pi^2 \hbar c}{240 a^4}, \tag{2.5}$$

which is Casimir's celebrated result [1].

The controversy surrounds the question of how to incorporate thermal corrections into the latter result. At first glance, the procedure to do this seems straightforward. It is well-known that thermal Green's functions must be periodic in imaginary time, with period $\beta = 1/T$ [40]. This implies a Fourier series decomposition, rather than a Fourier transform, where in place of the imaginary frequency integral in (2.5), we have a sum over Matsubara frequencies

$$\zeta_m^2 = \frac{4\pi^2 m^2}{\beta^2}, \tag{2.6}$$

that is, the replacement

$$\int_0^\infty \frac{d\zeta}{2\pi} \to \frac{1}{\beta}\sum_{m=0}^{\infty\prime}, \tag{2.7}$$

the prime being an instruction to count the $m = 0$ term in the sum with half weight. This prescription leads to the following formula for the Casimir pressure between perfect conductors at temperature $T$,

$$P^T = -\frac{1}{4\pi\beta a^3}\sum_{m=0}^{\infty\prime}\int_{mt}^\infty y^2\, dy \frac{1}{e^y - 1}, \tag{2.8}$$

where

$$t = \frac{4\pi a}{\beta}. \tag{2.9}$$

From this, it is straightforward to find the high and low temperature limits,

$$P^T \sim -\frac{1}{4\pi\beta a^3}\zeta(3) - \frac{1}{2\pi\beta a^3}\left(1 + t + \frac{t^2}{2}\right)e^{-t}, \quad \beta \ll 4\pi a, \tag{2.10a}$$

$$P^T \sim -\frac{\pi^2}{240 a^4}\left[1 + \frac{16}{3}\frac{a^4}{\beta^4} - \frac{240}{\pi}\frac{a}{\beta}e^{-\pi\beta/a}\right], \quad \beta \gg 4\pi a. \tag{2.10b}$$

These are the results found by Sauer [4] and Mehra [5], and by Lifshitz [3]. The two limits are connected by the duality symmetry found by Brown and Maclay [41]. The pressure may be obtained by differentiating the free energy,

$$P = -\frac{\partial}{\partial a} F, \tag{2.11}$$

which takes the following form for low temperature (now omitting the exponentially small terms)

$$F \sim -\frac{\pi^2}{720a^3} - \frac{\zeta(3)}{2\pi} T^3 + \frac{\pi^2}{45} T^4 a, \quad aT \ll 1, \tag{2.12}$$

from which the entropy follows,

$$S \sim -\frac{\partial}{\partial T} F \sim \frac{3\zeta(3)}{2\pi} T^2 - \frac{4\pi^2}{45} T^3 a, \quad aT \ll 1, \tag{2.13}$$

which vanishes as $T$ goes to zero, in accordance with the third law of thermodynamics, the Nernst heat theorem.

## 3. Exclusion of TE zero mode

However, there is something peculiar about the procedure adopted above for a perfect metal. (This seems first to have been appreciated by Boström and Sernelius [42].) It has to do with the TE mode of zero frequency, which we shall refer to as the TE zero mode. If we examine the zero frequency behaviour of the reflection coefficients for a dielectric appearing in (2.4), we see that providing $\zeta^2 \varepsilon(\mathrm{i}\zeta) \to 0$ as $\zeta \to 0$, the longitudinal wavenumber $\kappa_i \to k$ as $\zeta \to 0$, and hence $d \to \infty$ as $\zeta \to 0$. This means that there is no TE zero mode for a dielectric. This statement does not appear to be controversial [43]. However, if a metal is modelled as the $\varepsilon \to \infty$ limit of a dielectric, the same conclusion would apply. Because that would spoil the concordance with the third law noted in the previous section, the prescription was promulgated in [6] that the $\varepsilon \to \infty$ limit be taken before the $\zeta \to 0$ limit. But, of course, a real metal is not described by such a mathematical limit, so we must examine the physics carefully.

A simple model for the dielectric function is the plasma dispersion relation,

$$\varepsilon(\omega) = 1 - \frac{\omega_\mathrm{p}^2}{\omega^2}, \tag{3.1}$$

where $\omega_\mathrm{p}$ is the plasma frequency. For this dispersion relation, the condition $\zeta^2 \varepsilon(\mathrm{i}\zeta) \to 0$ fails to hold as $\zeta \to 0$, and the idealized prescription result, namely the contribution of the TE zero mode, holds. However, real metals are not well described by this dispersion relation. Rather, the Drude model,

$$\varepsilon(\mathrm{i}\zeta) = 1 + \frac{\omega_\mathrm{p}^2}{\zeta(\zeta + \gamma)}, \tag{3.2}$$

where the relaxation frequency $\gamma$ represents dissipation, very accurately fits optical experimental data for the permittivity for $\zeta < 2 \times 10^{15}\,\mathrm{rad\,s^{-1}}$ [44, 45]. For example, for gold, appropriate

values of the parameters are [46]

$$\omega_{\rm p} = 9.03\,{\rm eV}, \qquad \gamma = 0.0345\,{\rm eV}. \tag{3.3}$$

In this case, the arguments given above for the exclusion of the TE zero mode apply.

The arguments are somewhat subtle [38, 39], so we review and extend them here. Let us write the Lifshitz formula at finite temperature in the form

$$P^T = \sum_{m=0}^{\infty}{}' f_m = \int_0^\infty {\rm d}m f(m) - \sum_{k=0}^{\infty} \frac{B_{2k}}{(2k)!} f^{(2k-1)}(0), \tag{3.4}$$

where the second equality uses the Euler–Maclaurin sum formula, in terms of

$$f(m) = -\frac{1}{2\pi\beta}\int_0^\infty {\rm d}k_\perp^2 \kappa(\zeta_m)\left(d_m^{-1} + d_m'^{-1}\right), \tag{3.5}$$

according to (2.2) and (2.7), where we assume that vacuum separates the two plates so $\kappa_3(\zeta_m) = \kappa(\zeta_m) = \sqrt{k_\perp^2 + \zeta_m^2}$. Here, the denominators (2.4) are functions of $\zeta_m$. By changing the integration variable from $m$ to $\zeta_m$, we immediately see that the integral term in the Euler–Maclaurin sum formula corresponds precisely to the zero-temperature result (2.2).

One must, however, be careful in computing the low temperature corrections to this. One cannot directly expand the denominator $d$ in powers of $\zeta$ because the $k_\perp$ integral in (3.5) ranges down to zero. Let us rewrite the TE term there as follows:

$$f^{({\rm TE})}(m) = -\frac{1}{\pi\beta}\int_{2m\pi/\beta}^\infty {\rm d}\kappa\,\kappa^2 \left\{\left[\frac{1+\sqrt{1+\zeta_m^2(\varepsilon({\rm i}\zeta_m)-1)/\kappa^2}}{1-\sqrt{1+\zeta_m^2(\varepsilon({\rm i}\zeta_m)-1)/\kappa^2}}\right]^2 {\rm e}^{2\kappa a} - 1\right\}^{-1}. \tag{3.6}$$

Evidently, for the Drude model, or more generally, whenever

$$\lim_{\zeta\to 0}\zeta^2[\varepsilon({\rm i}\zeta) - 1] = 0, \tag{3.7}$$

$f^{({\rm TE})}(0) = 0$. However, it is important to appreciate the physical discontinuity between $m = 0$ and $m = 1$ for room temperature. At 300 K, while $\zeta_0 = 0$, $\zeta_1 = 2\pi T = 0.16\,{\rm eV}$, large compared the relaxation frequency $\gamma$. Therefore, for $m > 0$,

$$f^{({\rm TE})}(m) \approx -\frac{1}{\pi\beta}\int_{\zeta_m}^\infty {\rm d}\kappa\,\kappa^2 \left[\left(\frac{\sqrt{1+\omega_{\rm p}^2/\kappa^2}+1}{\sqrt{1+\omega_{\rm p}^2/\kappa^2}-1}\right)^2 {\rm e}^{2\kappa a} - 1\right]^{-1} \approx -\frac{1}{\pi\beta}\int_{\zeta_m}^\infty {\rm d}\kappa\,\kappa^2 \frac{1}{{\rm e}^{2\kappa a}-1}, \tag{3.8}$$

provided the significant values of $\zeta_m$ and $\kappa$ are small compared to the plasma frequency $\omega_{\rm p}$. This is just the ideal metal result contained in (2.8). Insofar as this is accurate, this expression yields the low- and high-temperature corrections seen in (2.10*b*) and (2.10*a*). However, there is now a discontinuity in the function $f^{({\rm TE})}$. As $\zeta_m \to 0$,

$$f^{({\rm TE})}(m) \to -\frac{1}{\pi\beta}\int_0^\infty {\rm d}\kappa \frac{\kappa^2}{{\rm e}^{2\kappa a}-1} = -\frac{\zeta(3)}{4\pi\beta a^3}, \tag{3.9}$$

rather than zero. This implies an additional linear term in the pressure at low temperatures

$$P^T \sim P^{T=0} + \frac{\zeta(3)}{8\pi a^3} T, \quad aT \ll 1. \tag{3.10}$$

Exclusion of the TE zero mode will also reduce the linear temperature dependence expected at high temperatures,

$$P^T \sim -\frac{\zeta(3)}{8\pi a^3} T, \quad aT \gg 1, \tag{3.11}$$

one-half the usual ideal metal result seen in (2.10*a*), and this is indeed predicted in numerical results (see figure 4 of [38] for $a > 5\,\mu$m, for example).

Most experiments are carried out between a sphere (of radius $R$) and a plane. In this circumstance, if $R \gg a$, $a$ being the separation between the sphere and the plate at the closest point, the force may be obtained from the proximity force approximation,

$$\mathcal{F} = 2\pi R F(a), \tag{3.12}$$

$F(a)$ being the free energy for the case of parallel plates separated by a distance $a$. Thus in the idealized description, the low temperature dependence including our linear term is

$$\mathcal{F} \sim -\frac{\pi^3 R}{360 a^3}\left[1 - \frac{45}{\pi^3}\zeta(3)aT + \frac{360}{\pi^3}\zeta(3)(aT)^3 - 16(aT)^4\right], \quad aT \ll 1. \tag{3.13}$$

Since this conversion is trivial, in the following we will restrict attention to the straightforward parallel plate situation.

These results are only approximate, because they assume the metal is ideal except for the exclusion of the TE zero. Elsewhere, we have referred to this model as the Modified Ideal Metal (MIM) model [38, 39]. Evidently, for sufficiently low temperatures the approximation used here, that $\zeta_1 \gg \gamma$, breaks down, the function $f(m)$ becomes continuous, and the linear term disappears. Indeed, numerical calculations based on real optical data for the permittivity show this transition. An example of such a calculation is presented in section 6. There, in figure 1, we see a negative slope in the quantity $P/P_C$ as a function of the plate separation $a$ in the region between 1 and 2 $\mu$m. This slope is approximately $-0.1\,\mu\text{m}^{-1}$. Here $P$ is the pressure between the plates at 300 K, while $P_C$ is the ideal Casimir pressure (2.5). If we compare this to our approximate prediction (3.10),

$$\frac{P^{T=300\,\text{K}}}{P_C} \approx 1 - \frac{30}{7.62}\frac{\zeta(3)}{\pi^3}\frac{a}{\mu\text{m}} = 1 - 0.15\frac{a}{\mu\text{m}}, \tag{3.14}$$

the slope and intercepts agree at the 20% level. Accurate numerical results between real metal plates and spheres are given in [33].

Because this linear behaviour does not persist at arbitrarily small temperatures, it is clear that the conflict with the third law anticipated in the arguments in the previous section do not apply. In fact, as we shall now see, the entropy does go to zero at zero temperature.

## 4. Arguments in favour of and against the TE zero mode

As noted above, there are strong thermodynamic and electrodynamic arguments in favour of the exclusion of the TE zero mode. Essentially, the point is that a realistic physical system can have only one state of lowest energy. Electrodynamically, one can start from the Kramers–Kronig relation that relates the real and imaginary part of the permittivity, required by causality, which can be written in the form of a dispersion relation for the electric susceptibility [47]

$$\chi(\omega) = \frac{\omega_{\mathrm{p}}^2}{4\pi}\int_0^\infty \mathrm{d}\omega' \frac{p(\omega')}{\omega'^2 - (\omega + \mathrm{i}\epsilon)^2}. \tag{4.1}$$

If the spectral function $p(\omega') \geqslant 0$ is nonsingular at the origin, it is easily seen that $\omega^2\chi(\omega) \to 0$ as $\omega \to 0$, which as shown in the previous section implies the absence of the TE zero mode. Conversely, $p(\omega')$ must have a $\delta$-function singularity at the origin to negate this conclusion. This would seem implausible for any but an overly idealized model. In contrast, in the Drude model

$$p(\omega') = \frac{2}{\pi}\frac{\gamma}{\omega'^2 + \gamma^2} \to 2\delta(\omega') \qquad \gamma \to 0. \tag{4.2}$$

It has been objected that rather than employing bulk permittivities as done in the usual expression for the Lifshitz formula, one should use surface impedances instead [30, 34, 48, 49]. Indeed this may be done, but it leads to identical results. The surface impedance merely expresses the linear relation between tangential components of the electric and magnetic fields at the interface between the two media,

$$\mathbf{E}_\perp = Z(\omega, \mathbf{k}_\perp)\mathbf{B}_\perp \times \mathbf{n}, \qquad \mathbf{n} \times \mathbf{E}_\perp = Z(\omega, \mathbf{k}_\perp)\mathbf{B}_\perp, \tag{4.3}$$

where $\mathbf{n}$ is the normal to the interface at the point in question. From Maxwell's equations we deduce [39, 47] for the reflection coefficient for the TE modes

$$r^{\mathrm{TE}} = -\frac{\zeta + Z\kappa}{\zeta - Z\kappa}, \quad \kappa^2 = \zeta^2 + k_\perp^2, \tag{4.4}$$

and the surface impedance is [4]

$$Z = -\frac{\zeta}{\sqrt{\zeta^2[\varepsilon(\mathrm{i}\zeta) - 1] + \kappa^2}}. \tag{4.5}$$

From this reflection coefficient, the Lifshitz formula is constructed according to $d = (r^{\mathrm{TE}})^{-2}\mathrm{e}^{2\kappa a} - 1$. Evidently the resultant expression for the Lifshitz pressure coincides with that found from the permittivity, seen for example in (3.6). This coincidence has been well recognized by previous authors [51, 52]. The reason why Mostepanenko and co-workers obtain a different result is that they omit the transverse momentum dependence in (4.5) and thereby argue that

[4] Here we have assumed that the permittivity is independent of transverse momentum. In principle this is incorrect, although optical data suggest that the transverse momentum dependence of $\varepsilon$ is rather small. See also [50].

at zero frequency $Z$ vanishes,

$$Z \to -\frac{1}{\sqrt{\varepsilon(\mathrm{i}\zeta)}} \sim \frac{\sqrt{\gamma}}{\omega_{\mathrm{p}}}\sqrt{\zeta}, \tag{4.6}$$

which is the content of the normal skin effect formula

$$Z(\omega) = -(1-\mathrm{i})\sqrt{\frac{\omega}{8\pi\sigma}}, \tag{4.7}$$

where $\sigma$ is the conductivity. (These two formulae are seen to be identical if we replace $\omega = \mathrm{i}\zeta$ and recognize that $\gamma = \omega_{\mathrm{p}}^2/(4\pi\sigma)$.) These formulae apply when we have the restriction appropriate to real photons $k_\perp^2 \leqslant \omega^2$. However, no such mass-shell condition applies to the virtual or evanescent photons involved in the thermal Casimir effect. The same sort of error seems to be made by Torgerson and Lamoreaux [53, 54], and by Bimonte [55, 56].

As noted above, use of the plasma model in the reflection coefficients would lead to the conventional temperature dependence, but this dispersion relation is inconsistent with real data. However, it has been argued that in the ideal Bloch–Grüneisen model [57], the relaxation parameter goes to zero at zero temperature. However, real metals exhibit scattering by impurities; in any case, at sufficiently low temperatures the residual value of the relaxation parameter does not play a role, as the frequency characteristic of the anomalous skin effect becomes dominant [58]. Moreover, the authors of [30, 34] also extrapolate the plasma formula from the infrared region down to zero frequency, whereas in fact frequencies very small compared to the frequency corresponding to the separation distance play a dominant role in the temperature dependence [58]. Finally, we emphasize that all present experiments are carried out at room temperature, where the known room temperature data are relevant.

The principal reason for the theoretical controversy has to do with the purported violation of the third law of thermodynamics if the TE zero mode is not included. If ideal metal reflection coefficients are used otherwise (the MIM model) such a violation indeed occurs, because the free energy per unit area for small temperature then behaves like

$$F = F_0 + T\frac{\zeta(3)}{16\pi a^2}. \tag{4.8}$$

However, we and others have shown [39], [58]–[60] that for real metals, the free energy per area has a vanishing slope at the origin. Indeed, in the Drude model we have

$$F = F_0 + T^2\frac{\omega_{\mathrm{p}}^2}{48\gamma}(2\ln 2 - 1), \tag{4.9}$$

for sufficiently low temperatures. There is, however, an intermediate range of temperatures where it is expected that the entropy is negative. We do not believe that this presents a thermodynamic difficulty, and reflects the fact that the electrodynamic fluctuations being considered represent only part of the complete physical system [33, 38, 59], although this is not a universal opinion [58]. (See also the further remarks in section 7.) New calculations are underway, showing explicitly the zero slope of the curve for the free energy near $T = 0$, thus corresponding to zero entropy [61].

Two other recent papers also lend support to our point of view. Jancovici and Šamaj [62] and Buenzli and Martin [63] have examined the Casimir force between ideal-conductor walls with emphasis on the high-temperature limit. Not surprisingly, ideal inert boundary conditions are shown to be inadequate, and fluctuations within the walls, modelled by the classical Debye–Hückel theory, determine the high temperature behaviour. The linear in temperature behaviour of the Casimir force is found to be reduced by a factor of two from the behaviour predicted by an ideal metal, just as in (3.11). This is precisely the signal of the omission of the $m = 0$ TE mode. Thus, it is very hard to see how the corresponding modification of the low-temperature behaviour can be avoided.

Further support for our conclusions can be found in the recent paper of Sernelius [64], who calculates the van der Waals–Casimir force between gold plates using the Lindhard or random phase approximation dielectric function. The central theme of his work is to describe the thermal Casimir effect in terms of *spatial dispersion*. Physically, spatially nonlocal effects play a role at low frequencies because charge carriers can move freely over large distances. Deviations from standard local electromagnetic theory can then be expected. Spatial dispersion implies that the standard Fresnel equations no longer apply. Moreover, because of lack of experimental data, one has to rely on theoretical model-dielectric functions.

Sernelius finds [64] that for large separations the force is one-half that of the ideal metal, just as in the calculation in [62, 63]. This agreement is not quite trivial; it means that the thermal Casimir effect can be explained in two, apparently unrelated ways: one way is to include spatial dispersion in the formalism from the beginning, omitting dissipation. The other way is the conventional one, namely to describe the thermal effect in terms of dissipation alone, by introducing the relaxation frequency $\gamma$ as we have done above. Sernelius shows that, for arbitrary separation between the plates, the spatial-dispersion results nearly exactly coincide with the local dissipation-based results [42, 65].

## 5. Experimental constraints

We have marshaled theoretical arguments that seem to us quite overwhelming in favour of the absence of the TE zero mode in the temperature dependence of the Casimir force between real metal plates, which seem to imply unambiguously that there should be large ($\sim$15%) thermal corrections to the Casimir force at separations of order 1 $\mu$m. New detailed calculations based on this theory, and using real optical data for aluminum, are discussed in the following section. The difficulty is that, experimentally, it is not easy to perform Casimir force measurements at other than room temperature, so current constraints on the theory all come from room temperature experiments. Then all one can do is compare the theory at room temperature with the experimental results, which must be corrected for a variety of effects, such as surface roughness, finite conductivity and patch potentials. A deviation between the corrected zero temperature theory and the room temperature observations then is taken as a measure of the temperature correction.

The temperature correction is evidently relatively largest at the largest separations, where, unfortunately, the total Casimir force is weakest. Lamoreaux's early experiments [9] were conducted at the 1 $\mu$m scale, so if they were accurate to 10% they would have seen the effect our theory predicts, but probably, in spite of Lamoreaux's assertion, they were not so accurate, because few essential corrections were included [66]. The experiments of Mohideen *et al* [13]–[15] were much more accurate, but because they were conducted at much smaller distances, even our

rather large temperature correction would have remained inaccessible. It is the most recent experiments of the Purdue group [29, 30] that claim the extraordinarily high precision to be able to see our effect at distances as small as 100 nm. Indeed, they see no deviation from the corrected zero-temperature Lifshitz theory using optical permittivities, and hence assert that our theory is decisively ruled out. The effect we predict for the temperature correction is only 1.5% at a distance of 160 nm [35], so the measurement must be performed at the 1% level to see the effect there. (For the usually employed sphere-plate configuration, $\Delta\mathcal{F}/\mathcal{F} \approx 2.5\%$ at $a = 160\,\mathrm{nm}$.) Although they claim this degree of accuracy, it is doubtful that they have achieved it, because, for example, to achieve 1% accuracy, the separation would have to be determined to better than 0.3%, or 0.5 nm at $a = 160\,\mathrm{nm}$. Since the roughness in the surfaces involved is much larger than this (see also [67]), and other corrections (such as the fact that the metallic surfaces are actually thin films, and the effects of surface plasmons [68, 69]) have not been included, we have reason to be skeptical of such claims [70].

In any case, it would seem imperative to perform experiments at different temperatures in order to provide evidence for or against temperature dependence of Casimir forces. We understand such experiments are in progress. We encourage experimentalists to redouble their efforts to determine the presence or absence of such an effect in an unbiased manner, for the issues involved touch at the heart of our fundamental theoretical understanding of electrodynamics, statistical mechanics and quantum field theory.

## 6. New calculations

To aid in the experimental disentanglement of this effect, we have carried out new calculations of the Casimir force between two infinite half-spaces made of aluminum, separated by a vacuum space of width $a$. (Other recent calculations appear in [35, 46, 71].) The results are shown in figure 1. (Figures 1–9 are taken from the Master's Thesis of SAE [72].) Formulae made use of are read off from (2.2) and are now given in usual dimensional units

$$P_{T=0}(a) = -\frac{\hbar}{2\pi^2}\int_0^\infty \mathrm{d}\zeta \int_0^\infty \mathrm{d}k_\perp k_\perp \kappa_0 \left(\frac{\Delta_{\mathrm{TE}}^2 \mathrm{e}^{-2\kappa_0 a}}{1-\Delta_{\mathrm{TE}}^2 \mathrm{e}^{-2\kappa_0 a}} + \frac{\Delta_{\mathrm{TM}}^2 \mathrm{e}^{-2\kappa_0 a}}{1-\Delta_{\mathrm{TM}}^2 \mathrm{e}^{-2\kappa_0 a}}\right), \tag{6.1a}$$

$$P_{T>0}(a) = -\frac{k_{\mathrm{B}}T}{\pi}{\sum_{m=0}^{\infty}}' \int_0^\infty \mathrm{d}k_\perp k_\perp \kappa_0 \left(\frac{\Delta_{\mathrm{TE}}^2 \mathrm{e}^{-2\kappa_0 a}}{1-\Delta_{\mathrm{TE}}^2 \mathrm{e}^{-2\kappa_0 a}} + \frac{\Delta_{\mathrm{TM}}^2 \mathrm{e}^{-2\kappa_0 a}}{1-\Delta_{\mathrm{TM}}^2 \mathrm{e}^{-2\kappa_0 a}}\right), \tag{6.1b}$$

where $a$ is the separation between plates (of infinite thickness), and

$$\Delta_{\mathrm{TE}} = \frac{\kappa - \kappa_0}{\kappa + \kappa_0}, \tag{6.2a}$$

$$\Delta_{\mathrm{TM}} = \frac{\kappa - \varepsilon(\mathrm{i}\zeta)\kappa_0}{\kappa + \varepsilon(\mathrm{i}\zeta)\kappa_0}, \tag{6.2b}$$

$$\kappa = \sqrt{k_\perp^2 + \varepsilon(\mathrm{i}\zeta)\frac{\zeta^2}{c^2}}, \tag{6.2c}$$

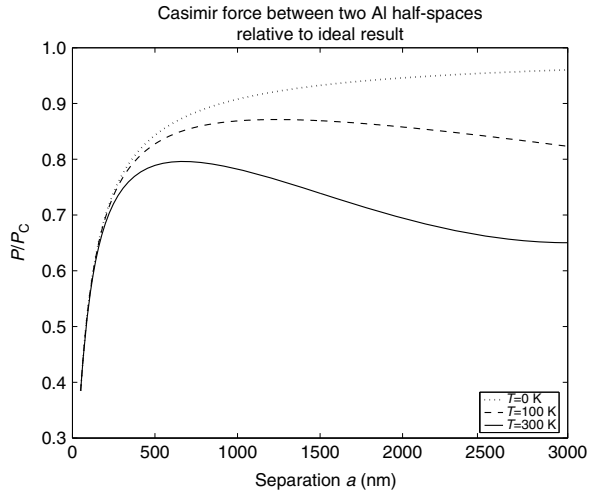


**Figure 1.** Temperature dependence of the Casimir force between aluminum plates.

$$\kappa_0 = \sqrt{k_\perp^2 + \frac{\zeta^2}{c^2}}. \tag{6.2d}$$

Here, $\varepsilon(\mathrm{i}\zeta) = \epsilon(\mathrm{i}\zeta)/\epsilon_0$ is the usual permittivity relative to the vacuum. In the case of finite temperatures, $\zeta = \zeta_m = 2\pi m k_B T/\hbar$, and a standard Lifshitz substitution of integration variables was made during calculations (see for example (3.2b) of [38]). The results are plotted relative to the standard Casimir pressure $P_C$ in (2.5). Calculations have been carried to a relative accuracy of better than $10^{-4}$. Even at $T = 0$, there are large deviations from the ideal Casimir result at all distance scales.

To illustrate the contributions of the TE and TM modes, figures 2–4 depict the TE and TM integrands of a Casimir pressure expression of the type

$$P_{T=0} = \int_0^\infty \mathrm{d}\zeta \int_0^\infty \mathrm{d}k_\perp [I_{\mathrm{TE}}(\mathrm{i}\zeta, k_\perp) + I_{\mathrm{TM}}(\mathrm{i}\zeta, k_\perp)]. \tag{6.3}$$

It is clear that the TE term in the integrand falls off rapidly to zero as $\zeta \to 0$ whereas the TM term remains finite. The relative contributions to the pressure by the TE and TM modes are illustrated in figures 5 and 6. Evidently, the contribution of the TE mode rapidly decreases with increasing temperature and increasing plate separation.

### *6.1. Results for a five-layer model*

Because many experiments have been carried out with a conducting surface between parallel capacitor plates it is useful to consider the five layer geometry which has been treated repeatedly by Tomaš in recent years [73]. The geometry is defined by figure 7. All three slabs are assumed to be made of aluminum. We assume one intermediate plate of width $b$, immersed in a cavity of total width $c = a + a' + b$. Between the central plate and the two outer semi-infinite media,

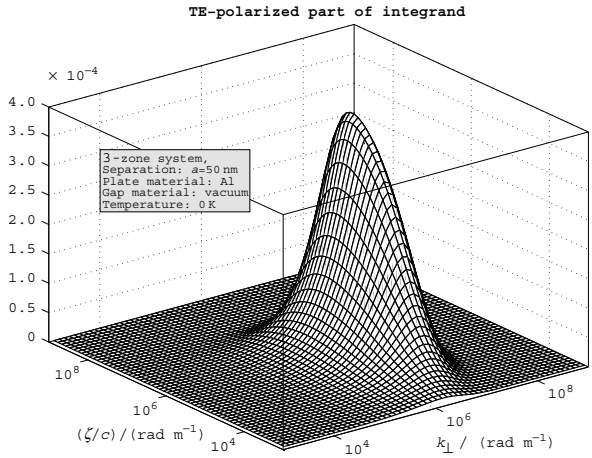


**Figure 2.** TE part of the integrand in (6.3).

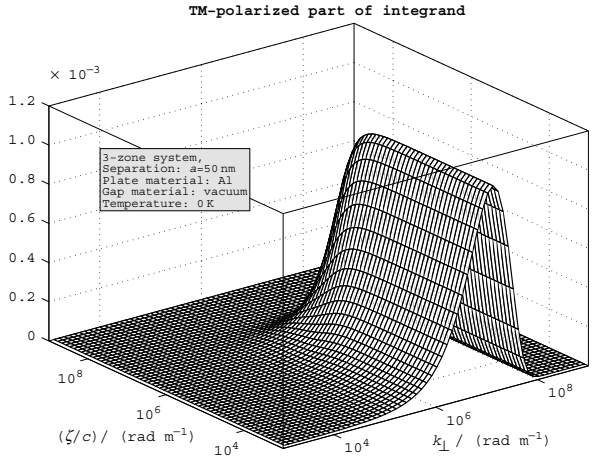


**Figure 3.** TM part of the integrand in (6.3).

we assume a vacuum ($\varepsilon_g = 1$). The quantity $h$ is defined as $h = c - b$. The quantity $\delta$ is the deviation of the centre of the plate from the midline of the cavity. The Casimir pressure at zero and finite temperature is given by

$$P_{T=0}(\delta; b, c) = \frac{\hbar}{2\pi^2} \int_0^\infty \mathrm{d}\zeta \int_0^\infty \mathrm{d}k_\perp \sum_{q=\mathrm{TE}}^{\mathrm{TM}} I_q(\mathrm{i}\zeta, k_\perp; \delta, b, c), \tag{6.4a}$$

$$P_{T>0}(\delta; b, c) = \frac{k_B T}{\pi} {\sum_{m=0}^{\infty}}' \int_0^\infty \mathrm{d}k_\perp \sum_{q=\mathrm{TE}}^{\mathrm{TM}} I_q(\mathrm{i}\zeta_m, k_\perp; \delta, b, c). \tag{6.4b}$$

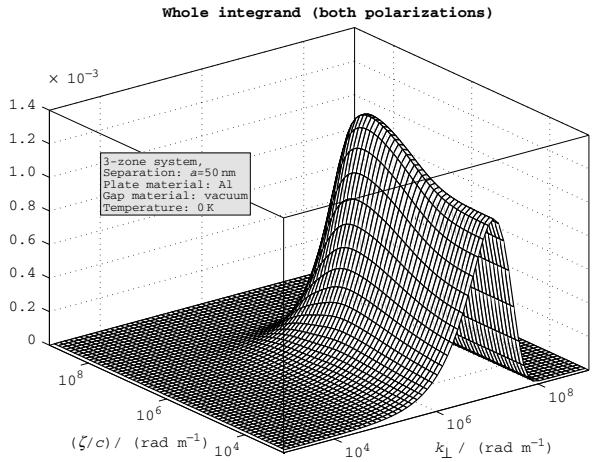


**Figure 4.** Total integrand in (6.3).

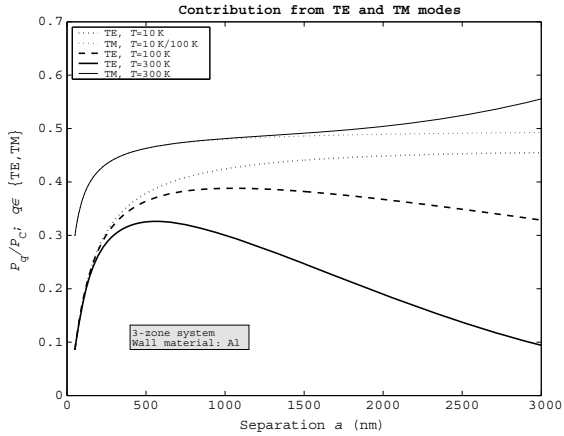


**Figure 5.** TE and TM contributions to the pressure shown in figure 1.

Here, the integrand is

$$I_q(\mathrm{i}\zeta, k_\perp; \delta, b, c) = k_\perp \kappa_0 2\Delta_{1q}\Delta_{2q}(1-\mathrm{e}^{-2\kappa_2 b})\mathrm{e}^{-\kappa_0 h}\sinh 2\kappa_0\delta\Big[-\Delta_{2q}^2\mathrm{e}^{-2\kappa_2 b}+1 \\ -\Delta_{1q}^2\mathrm{e}^{-2\kappa_0 h}(\mathrm{e}^{-2\kappa_2 b}-\Delta_{2q}^2)-2\Delta_{1q}\Delta_{2q}(1-\mathrm{e}^{-2\kappa_2 b})\mathrm{e}^{-\kappa_0 h}\cosh 2\kappa_0\delta\Big]^{-1}. \quad (6.5)$$

The Casimir force is positive for positive $\delta$, and is antisymmetric around the cavity centre $\delta = 0$. The index $q$ in the $\Delta$'s in the formulae runs over the polarizations TE and TM, which are given by equations (6.2*a*) and (6.2*b*). These results are equivalent to those found earlier by Tomaš [74], but presented in a more illustrative form.

Numerically, we choose $c = 3\,\mu$m and $b = 500\,$nm. The pressure $P(\delta)$, calculated from $\delta = 0$ to $\delta = (c-b)/2 - 50\,$nm, is shown in figure 8. All calculations are done with an accuracy

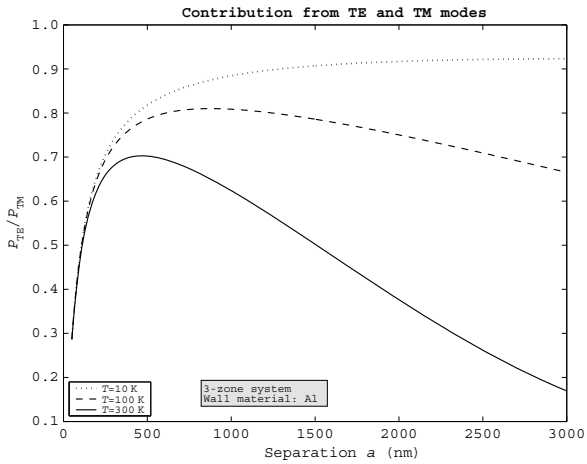


**Figure 6.** Ratio of the TE and TM mode pressures contributing to the pressure shown in figure 1.

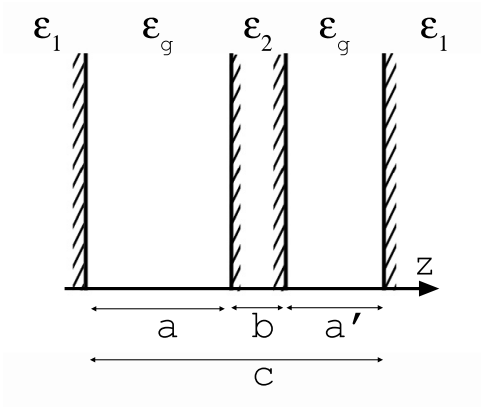


**Figure 7.** The 5-zone geometry. Here, we have set $\varepsilon_g = 1$.

of better that $10^{-4}$ in the final result, which should be sufficient for practical purposes. Figure 9 shows the pressure relative to Casimir's result for ideal conductors,

$$P_{\mathrm{C}} = -\frac{\pi^2\hbar c}{240}\left(\frac{1}{(h/2+\delta)^4} - \frac{1}{(h/2-\delta)^4}\right). \tag{6.6}$$

As for the finite temperature calculations, it has been checked that all terms in the sum (except for the zero mode) lie within the frequency domain covered by Lambrecht's data. There is thus no extra assumption made in the calculation, such as the property $\varepsilon\zeta^2/c^2 \to 0$ as $\zeta \to 0$, following from the Drude relation, except to ensure that there is no contribution from the TE

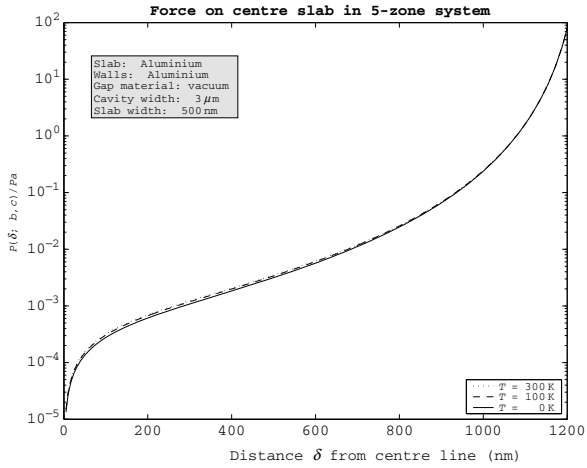


**Figure 8.** Pressure on the plate at a distance $\delta$ from the cavity centre. If $\delta < 0$, one gets the antisymmetric prolongation about the position $\delta = 0$.

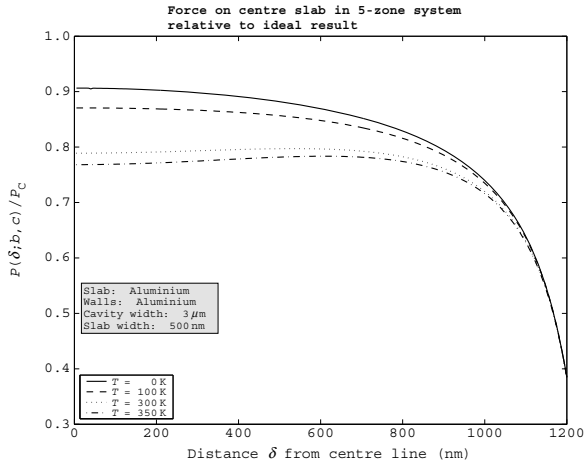


**Figure 9.** Pressure on the plate at a distance $\delta$ from the cavity centre relative to Casimir's result (6.6) for ideal conductors. For $\delta < 0$, one gets the symmetric prolongation of the curve about the position $\delta = 0$.

zero mode. In the $T = 0$ case, the Drude relation is used for low frequencies. The contribution to the force coming from frequencies outside the Lambrecht region is very small, smaller than the accuracy of the calculation. Again, we see large deviations from the ideal Casimir result at all temperatures, as well as relatively large temperature corrections, which we hope will be readily detectable in future experiments.

It would be very interesting to conduct experiments which are sensitive to the 5-zone geometry we have considered, namely a slab in a cavity. In particular, one could study the case of a slab oscillating about the centre of a cavity, detecting how the oscillation frequency varies with temperature. Using a cavity of width 2–4 $\mu$m, say, one finds that the temperature corrections are largest for slab-wall separations on the order of 1 $\mu$m.

## 7. Conclusions

We have shown how the Casimir pressure between parallel plates can be calculated with the inclusion, as well as with the exclusion, of the TE zero mode. We emphasized (section 4) that there are strong thermodynamic and electrodynamic arguments in favour of the latter option. As is known in general, instead of employing bulk permittivities, it is possible to use surface impedances instead. We pointed out that in such a case it becomes necessary to take into account also the transverse momentum dependence in the expression (4.5) for the surface impedance. Otherwise, if one leaves out the transverse momentum, one will obtain erroneous results as has often been the case in the literature [30, 34, 48, 49], [53]–[56].

We advocate the use of Drude's dispersion relation (3.2) throughout. The alternative plasma relation (3.1) is inconsistent with real dispersive data. One peculiar effect arising from use of the Drude relation is the appearance of negative Casimir entropy in a finite frequency interval. The physical reason for this kind of behaviour is the following: it reflects the fact that we are dealing with only a part of the complete physical system. The effect may appear counterintuitive, but is not so uncommon in physics after all. One cannot apply usual thermodynamic restrictions such as positiveness of entropy to a 'subsystem' formed by the induced interaction part of the free energy of the full system. This issue was discussed in detail in a previous paper [38]. In section 4 of that paper we introduced, as an illustrative mechanical model, a system of two harmonic oscillators interacting via a third one. Such oscillators represent a simplified picture of two parallel plates interacting via the electromagnetic field. We calculated the classical as well as the quantum free energy of this mechanical system, and found there to be a finite temperature interval for which the interaction free energy increases with increasing temperature, thus leading to a negative interaction entropy term $S = -\partial F/\partial T$. In this way, a mechanical analogy with the Casimir interaction energy (and corresponding interaction entropy) was demonstrated.

The new developments of our paper are the establishment of the complete mathematical formalism necessary to calculate the temperature correction to the Casimir force. We assumed infinite, parallel, plates, with no surface roughness included, and assumed in all calculations the tabulated dispersive data for bulk materials. Then, we showed calculated results in figures 1–9 which are all new. They all assume aluminum plates. We gave results for three-layer geometry, and also some for a five-layer geometry. Our general suggestion for experimentally measuring the influence from finite temperature is to keep the geometry of the setup as constant as possible (by using an invar material, for instance), and then measure the force at two accessible temperatures in the laboratory, for instance 300 and 350 K. It would be even better if experiments could be carried out at liquid He temperatures; we understand such experiments are underway.

## Acknowledgments

KAM thanks the Physics Department of Washington University for its hospitality. His work has been supported in part by the US Department of Energy. We are grateful to Bernard Jancovici, Umar Mohideen and Roberto Onofrio for helpful conversations and correspondence, and Astrid Lambrecht and Serge Reynaud for making their data available to us.

## References

[1] Casimir H B G 1948 *Proc. K. Ned. Akad. Wet.* **51** 793
[2] Casimir H B G and Polder D 1948 *Phys. Rev.* **73** 360
[3] Lifshitz E M 1956 *Zh. Eksp. Teor. Fiz.* **29** 94
Lifshitz E M 1956 *Sov. Phys.—JETP* **2** 73 (Engl. Transl.)
Dzyaloshinskii I D, Lifshitz E M and Pitaevskii L P 1961 *Usp. Fiz. Nauk* **73** 381
Dzyaloshinskii I D, Lifshitz E M and Pitaevskii L P 1961 *Sov. Phys.—Usp.* **4** 153 (Engl. Trans.)
Lifshitz E M and Pitaevskii L P 1980 *Statistical Physics, Part 2* (Oxford: Pergamon) section 81
[4] Sauer F 1962 *PhD Thesis* Göttingen
[5] Mehra J 1967 *Physica* **37** 145
[6] Schwinger J, DeRaad L L Jr and Milton K A 1978 *Ann. Phys. (NY)* **115** 1
[7] Sparnaay M J 1989 *Physics in the Making: Essays on the Development in 20th Century Physics in Honour of H.B.G. Casimir on the Occasion of his 80th Birthday* ed A Sarlemijn and M J Sparnaay (Amsterdam: North-Holland) p 235
[8] Sabisky E S and Anderson C H 1973 *Phys. Rev.* A **7** 790
[9] Lamoreaux S K 1997 *Phys. Rev. Lett.* **78** 5
[10] Lamoreaux S K 1998 *Phys. Rev. Lett.* **81** 5475 (E)
[11] Lamoreaux S K 1999 *Phys. Rev.* A **59** R3149
[12] Lamoreaux S K 2000 *Phys. Rev. Lett.* **84** 5673
[13] Mohideen U and Roy A 1998 *Phys. Rev. Lett.* **81** 4549
[14] Roy A, Lin C-Y and Mohideen U 1999 *Phys. Rev.* D **60** R111101
[15] Harris B W, Chen F and Mohideen U 2000 *Phys. Rev.* A **62** 052109
[16] Ederth T 2000 *Phys. Rev.* A **62** 062104
[17] Blocki J, Randrup J, Świątecki W J and Tsang C F 1977 *Ann. Phys. (NY)* **105** 427
[18] Abrikosova I I and Deriagin B V 1953 *Dokl. Akad. Nauk SSSR* **90** 1055
Deriagin B V and Abrikosova I I 1956 *Zh. Eksp. Teor. Fiz.* **30** 993
Deriagin B V and Abrikosova I I 1957 *Sov. Phys.—JETP* **3** 819 (Engl. Transl.)
Derjaguin B V, Abrikosova I I and Lifshitz E M 1956 *Q. Rev.* **10** 295
Deryagin B V 1934 *Kolloidn. Zh.* **69** 155
Deryagin B V *et al* 1975 *J. Colloid Interface Sci.* **53** 314
[19] Emig T, Jaffe R L, Kardar M and Scardichio A 2006 *Phys. Rev. Lett.* **96** 080403 (*Preprint* cond-mat/0601055)
[20] Gies H and Klingmüller K 2006 *Preprint* quant-ph/0601094
[21] Bordag M 2006 *Phys. Rev.* D **73** 125018 (*Preprint* hep-th/0602295)
[22] Chan H B, Aksyuk V A, Kleiman R N, Bishop D J and Capasso F 2001 *Science* **291** 1941
[23] Chan H B, Aksyuk V A, Kleiman R N, Bishop D J and Capasso F 2001 *Phys. Rev. Lett.* **87** 211801
[24] Iannuzzi D, Lisanti M and Capasso F 2004 *Proc. Natl Acad. Sci. USA* **101** 4019
[25] Bressi G, Carugno G, Onofrio R and Ruoso G 2002 *Phys. Rev. Lett.* **88** 041804
[26] Brown-Hayes M, Dalvit D A R, Mazzitelli F D, Kim W J and Onofrio R 2005 *Phys. Rev.* A **72** 052102
[27] Dalvit D A R, Lombardo F C, Mazzitelli F D and Onofrio R 2004 *Europhys. Lett.* **67** 517
[28] Decca R S, López D, Fischbach E and Krause D E 2000 *Phys. Rev. Lett.* **62** 050402
[29] Decca R S, Fischbach E, Klimchitskaya G L, López D and Mostepanenko V M 2003 *Phys. Rev.* D **68** 116003

[30] Decca R S, López D, Fischbach E, Klimchitskaya G L, Krause D E and Mostepanenko V M 2005 *Ann. Phys. (NY)* **318** 37 (*Preprint* quant-ph/0503105v1)
[31] Bordag M, Mohideen U and Mostepanenko V M 2001 *Phys. Rep.* (*Preprint* quant-ph/0106045)
[32] Lamoreaux S K 2005 *Rep. Prog. Phys.* **68** 201
[33] Brevik I, Aarseth J B, Høye J S and Milton K A 2005 *Phys. Rev.* E **71** 056101 (*Preprint* quant-ph/0410231)
[34] Bezerra V B, Decca R S, Fischbach E, Geyer B, Klimchitskaya G L, Krause D E, López D, Mostepanenko V M and Romero C 2006 *Phys. Rev.* E **73** 028101 (*Preprint* quant-ph/0503134)
[35] Høye J S, Brevik I, Aarseth J B and Milton K A 2006 *J. Phys. A: Math. Gen.* **39** 6031 (*Preprint* quant-ph/0506025 v4)
[36] Mostepanenko V M, Bezerra V B, Decca R, Geyer B, Fischbach E, Klimchitskaya G L, Krause D E, Lopez D and Romero C 2006 *J. Phys. A: Math. Gen.* **39** 6589 (*Preprint* quant-ph/0512134)
[37] Milton K A 2001 *The Casimir Effect: Physical Manifestations of Zero-Point Energy* (Singapore: World Scientific)
[38] Høye J S, Brevik I, Aarseth J B and Milton K A 2003 *Phys. Rev.* E **67** 056116 (*Preprint* quant-ph/0212125)
[39] Milton K A 2004 *J. Phys. A: Math. Gen.* **37** R209 (*Preprint* hep-th/0406024)
[40] Martin P C and Schwinger J 1959 *Phys. Rev.* **115** 1342
[41] Brown L S and Maclay G J 1969 *Phys. Rev.* **184** 1272
[42] Boström M and Sernelius Bo E 2000 *Phys. Rev. Lett.* **84** 4757
[43] Geyer B, Klimchitskaya G L and Mostepanenko V M 2005 *Phys. Rev.* D **72** 085009 (*Preprint* quant-ph/0510054)
[44] Lambrecht A and Reynaud S 2000 *Eur. Phys. J.* D **8** 309 (*Preprint* quant-ph/9907105)
[45] Lambrecht A and Reynaud S 2000 *Phys. Rev. Lett.* **84** 5672 (*Preprint* quant-ph/9912085)
[46] Brevik I and Aarseth J B 2006 *J. Phys. A: Math. Gen.* **39** 6187 (*Preprint* quant-ph/0511037)
[47] Schwinger J, DeRaad L L Jr, Milton K A and Tsai W-y 1998 *Classical Electrodynamics* (New York: Perseus/Westview) chapter 41
[48] Geyer B, Klimchitskaya G L and Mostepanenko V M 2003 *Phys. Rev.* A **67** 062102 (*Preprint* quant-ph/0202018)
[49] Bezerra V B, Klimchitskaya G L, Mostepanenko V M and Romero C 2004 *Phys. Rev.* A **69** 022119 (*Preprint* quant-ph/0401138)
[50] Esquivel-Sirvent R, Villarreal C, Mochán W L, Contreras-Reyes A M and Svetovoy V B 2006 *J. Phys. A: Math. Gen.* **39** 6323 (*Preprint* quant-ph/0512243)
[51] Boström M and Sernelius Bo E 2000 *Phys. Rev.* A **61** 052703
[52] Mochán W L, Villareal C and Esquivel-Sirvent R 2002 *Rev. Mex. Fiz.* **48** 339 (*Preprint* quant-ph/0206119)
[53] Torgerson J R and Lamoreaux S K 2003 *Preprint* quant-ph/0309153
[54] Torgerson J R and Lamoreaux S K 2002 *Preprint* quant-ph/0208042
[55] Bimonte G 2006 *Phys. Rev. Lett.* **96** 160401 (*Preprint* quant-ph/0511248)
[56] Bimonte G 2006 *Phys. Rev.* E **73** 048101 (*Preprint* quant-ph/0603003)
[57] Condon E U and Odishaw H (ed) 1967 *Handbook of Physics* (New York: McGraw-Hill) equation 6.12
[58] Svetovoy V B and Esquivel R 2005 *Phys. Rev.* E **72** 036113 (*Preprint* quant-ph/0508068)
[59] Brevik I, Aarseth J B, Høye J S and Milton K A 2004 *Proc. 6th Workshop on Quantum Field Theory Under the Influence of External Conditions (QFEXT03) (Norman, OK, 15–19 September 2003)* ed K A Milton (Princeton, NJ: Rinton) (*Preprint* quant-ph/0311094)
[60] Sernelius Bo E 2005 *Phys. Rev.* B **71** 235114
[61] Brevik I, Høye J S and Aarseth J B, in preparation
[62] Jancovici B and šamaj L 2005 *Europhys. Lett.* **72** 35 (*Preprint* cond-mat/0506363)
[63] Buenzli P R and Martin Ph D 2005 *Europhys. Lett.* **72** 42
[64] Sernelius Bo E 2005 Spatial dispersion has dramatic effects on the Casimir effects between two metal plates *Europhys. Lett.* submitted (*Preprint*)
[65] Sernelius Bo E 2001 *Surface Modes in Physics* (Berlin: Wiley-VCH)

[66] Mohideen U and Roy A 1999 *Phys. Rev. Lett.* **83** 3341
[67] Maia Neto P A, Lambrecht A and Reynaud S 2005 *Europhys. Lett.* **69** 924
[68] Intravaia F and Lambrecht A 2005 *Phys. Rev. Lett.* **94** 110404
[69] Bordag M 2006 *J. Phys. A: Math. Gen.* **39** 6173 (*Preprint* hep-th/0511269)
[70] Iannuzzi D, Gelfand I, Lisanti M and Capasso F 2004 *Proc. 6th Workshop on Quantum Field Theory Under the Influence of External Conditions (QFEXT03) (Norman, OK, 15–19 September 2003)* ed K A Milton (Princeton, NJ: Rinton)
[71] Bentsen V S, Herikstad R, Skriudalen S, Brevik I and Høye J S 2005 *J. Phys. A: Math. Gen.* **38** 9575 (*Preprint* quant-ph/0505136)
[72] Ellingsen S A 2006 *Master's Thesis* Department of Physics, Norwegian University of Science and Engineering, Trondheim
[73] Tomaš M S 2005 *Phys. Rev.* A **72** 034104 (*Preprint* quant-ph/0505127)
[74] Tomaš M S 2002 *Phys. Rev.* A **66** 052103

J. Phys. A: Math. Theor. **40** (2007) 1951–1961 doi:10.1088/1751-8113/40/9/003

# Casimir attraction in multilayered plane parallel magnetodielectric systems

**Simen A Ellingsen**[1]

Department of Energy and Process Engineering, Norwegian University of Science and Technology, N-7491, Trondheim, Norway

E-mail: simen.ellingsen@kcl.ac.uk

Received 23 July 2006, in final form 12 November 2006
Published 14 February 2007
Online at stacks.iop.org/JPhysA/40/1951

**Abstract**

A powerful procedure is presented for calculating the Casimir attraction between plane parallel multilayers made up of homogeneous regions with arbitrary magnetic and dielectric properties by the use of the Minkowski energy–momentum tensor. The theory is applied to numerous geometries and shown to reproduce a number of results obtained by other authors. Although the various pieces of theory drawn upon are well known, the relative ease with which the Casimir force density in even complex planar structures may be calculated, appears not to be widely appreciated, and no single paper to the author's knowledge renders explicitly the procedure demonstrated herein. Results may be seen as an important building block in the settling of issues of fundamental interest, such as the long-standing dispute over the thermal behaviour of the Casimir force or the question of what is the correct stress tensor to apply, a discussion requickened by the newly suggested alternative theory due to Raabe and Welsch.

PACS numbers: 05.30.−d, 12.20.Ds, 32.80.Lg, 41.20.Jb, 42.50.Nn

## 1. Introduction

Over the last decade or so enormous progress has been made in experimental tests of the Casimir effect [1]. This macroscopic manifestation of quantum electrodynamics, once something of a curiosity subject mainly to the scrutiny of a few theorists, has been measured with high precision and is now spoken of as possibly exploitable in nanoelectromechanical applications [2].

[1] Current address: Department of War Studies, King's College London, Strand, London WC2R 2LS, UK.

Although only a single modern experiment has so far employed parallel plates and with moderate accuracy [3][2], experiments employing other geometries (typically a sphere and a plate) have normally had to resort to planar geometries for theoretical support, accompanied by the necessary corrections to account for curved surfaces (see e.g. [5]).

The individual pieces of theory assembled in this paper are not in themselves new; the paper draws heavily on several references, many of which more than a decade old. The theory of Green's functions in a dielectric multilayer was treated by Tomaš 11 years ago [6], building in turn on previous work by Mills and Maradudin [7] two decades earlier. Companioned by the now classical theory by Lifshitz and co-workers [8] and standard optical theory of reflection it provides all the necessary tools. Despite this fact however, the ease with which the Casimir forces in plane parallel systems may be expressed appears not to be commonly recognized, although it has been implicitly employed by Tomaš ([9] and later papers). Furthermore, no publication exists to the author's knowledge, explaining explicitly the procedure derived and demonstrated herein.

This paper provides background theory to aid the settlement of at least two ongoing disputes in the Casimir branch. First, the as yet unsettled disagreement over the temperature effect of the Casimir force (for a recent discussion see [10] and references therein); numerical and theoretical treatment of the expressions obtained, e.g., in chapter 4 using dispersion data for real materials provide predictions to settle experimentally the existence or non-existence of the large thermal variations of the force upheld by many. Second, doubts have been raised recently about the applicability of the Minkowski stress tensor and an alternative, Lorentz force-based tensor was suggested [11], in turn disputed by Pitaevskii [12]. A procedure similar to that presented here seems to have been employed by Tomaš in his calculations of the effects of the Lorentz-type tensors [13, 14]. The discussion of the applicability or indeed correctness of their theory, however, is not within the scope of this paper.

We have structured the paper as follows. In chapters 2 to 4 the background theory of Green's function calculation of the Casimir attraction is derived briefly, arriving at equation (15), the main result of the paper. In chapter 5 we demonstrate the strength of the procedure by using it to readily reproduce an array of previous results in various configurations: two half-spaces, a plate and a wall, a plate in a cavity and two plates.

Many detailed calculations which are straightforward in principle have been omitted. For details, the reader may refer to [15].

## 2. Background theory: force on an interface

When electro- and magnetostrictive contributions are neglected, forces acting inside magnetodielectric media assuming no net external charge or currents are present, may in general be expressed through space components of the Minkowski energy–momentum tensor [16]. Assuming isotropic, homogeneous and linear media the electromagnetic force density acting at position $\boldsymbol{r}$ is

$$f_i(\boldsymbol{r}) = \partial_k T_{ik} = -\tfrac{1}{2}\epsilon_0 \boldsymbol{E}^2 \partial_i \epsilon(\boldsymbol{r}) - \tfrac{1}{2}\mu_0 \boldsymbol{H}^2 \partial_i \mu(\boldsymbol{r}), \tag{1}$$

where $T_{ik}$ is the Maxwell stress tensor,

$$T_{ik} = E_i D_k + H_i B_k - \tfrac{1}{2}\delta_{ik}(\boldsymbol{E}\cdot\boldsymbol{D} + \boldsymbol{H}\cdot\boldsymbol{B}), \tag{2}$$

where indices $i, k \in \{x, y, z\}$ denote Cartesian vector components. We have suppressed the frequency dependence of the permittivity and permeability, respectively $\epsilon$ and $\mu$, both defined relative to vacuum so that $D_i = \epsilon_0 \epsilon E_i$ and $B_i = \mu_0 \mu H_i$.

[2] The first experimental demonstration of the Casimir force by Sparnaay in 1958 also employed parallel plates [4] with low accuracy by today's standards.

We introduce the classical Green's dyadic $\Gamma_{ik}$ according to the convention of Schwinger and co-workers [17] defined according to

$$\boldsymbol{E}(x) = \frac{1}{\epsilon_0}\int \mathrm{d}^4x' \overleftrightarrow{\boldsymbol{\Gamma}}(x,x')\cdot\boldsymbol{P}(x') \tag{3}$$

where $x = (\boldsymbol{r}, t)$. Due to causality, $t'$ is only integrated over the region $t' \leqslant t$: the polarization at a time $t'$ cannot influence the resulting electric field at time $t$ prior to $t'$. The definition (3) ensures that $\Gamma$ is a generalized susceptibility. It is well known that according to Maxwell's equations, $\Gamma$ satisfies

$$\nabla\times\nabla\times\overleftrightarrow{\boldsymbol{\Gamma}}(\boldsymbol{r},\boldsymbol{r}';\omega) - \frac{\epsilon(\boldsymbol{r})\mu(\boldsymbol{r})\omega^2}{c^2}\overleftrightarrow{\boldsymbol{\Gamma}}(\boldsymbol{r},\boldsymbol{r}';\omega) = \frac{\mu(\boldsymbol{r})\omega^2}{c^2}\delta(\boldsymbol{r}-\boldsymbol{r}')\overleftrightarrow{\mathbf{1}}, \tag{4}$$

where we have performed a Fourier transformation according to

$$\overleftrightarrow{\boldsymbol{\Gamma}}(x,x') = \int_{-\infty}^{\infty}\frac{\mathrm{d}\omega}{2\pi}\,\mathrm{e}^{-\mathrm{i}\omega\tau}\overleftrightarrow{\boldsymbol{\Gamma}}(\boldsymbol{r},\boldsymbol{r}';\omega), \tag{5}$$

with $\tau \equiv t - t'$.

Invoking the fluctuation-dissipation theorem in a standard manner (e.g. [8]) yields[3]

$$\mathrm{i}\langle E_i(\boldsymbol{r})E_k(\boldsymbol{r}')\rangle_\omega = \frac{\hbar}{\epsilon_0}\coth\left(\frac{\hbar\omega}{2k_BT}\right)\mathrm{Im}\{\Gamma_{ik}(\boldsymbol{r},\boldsymbol{r}';\omega)\} \tag{6a}$$

$$\mathrm{i}\langle H_i(\boldsymbol{r})H_k(\boldsymbol{r}')\rangle_\omega = \frac{\hbar}{\mu_0}\coth\left(\frac{\hbar\omega}{2k_BT}\right)\frac{c^2}{\mu\mu'\omega^2}\,\mathrm{Curl}_{ij}\,\mathrm{Curl}'_{kl}\,\mathrm{Im}\{\Gamma_{jl}(\boldsymbol{r},\boldsymbol{r}';\omega)\}, \tag{6b}$$

where we have used the notation $\mathrm{Curl}_{ik} \equiv \epsilon_{ijk}\partial_j$ ($\epsilon_{ijk}$ being the Levi-Civita symbol and summation over identical indices is implied), $\mathrm{Curl}'_{ik} \equiv \epsilon_{ijk}\partial'_j$ where $\partial'_j$ is differentiation with respect to component $j$ of $\boldsymbol{r}'$, and $\mu' \equiv \mu(\boldsymbol{r}')$. The brackets denote the mean value of the $\omega$ Fourier component of the field component products with respect to fluctuations. For now let us assume $T = 0$ for simplicity.

Following the Lifshitz procedure we introduce the useful quantities

$$\Gamma^E_{ik}(\boldsymbol{r},\boldsymbol{r}';\omega) \equiv \Gamma_{ik}(\boldsymbol{r},\boldsymbol{r}';\omega), \tag{7a}$$

$$\Gamma^H_{ik}(\boldsymbol{r},\boldsymbol{r}';\omega) \equiv \frac{c^2}{\omega^2}\,\mathrm{Curl}_{il}\,\mathrm{Curl}'_{km}\,\Gamma_{lm}(\boldsymbol{r},\boldsymbol{r}';\omega), \tag{7b}$$

and replace the (fluctuation averaged) field components contained in $T_{ik}$ with their Green's function equivalents.

Consider now a sharp interface between two different magnetodielectric media such as described above. The force density acting on the interface equals the net $zz$-component of $T_{ik}$ when $\boldsymbol{r} \to \boldsymbol{r}'$ at the surface, averaged with respect to fluctuations, that is the net flow of momentum through the interface when all unphysical contributions have been subtracted, i.e. all that flowing in equal amounts both ways across the interface. The resulting force expression is [8] (the original expression has been generalized to allow $\mu \neq 1$)

$$\langle\mathcal{F}_z\rangle = \hbar\int_0^\infty\frac{\mathrm{d}\zeta}{2\pi}\left[\epsilon\left(\Gamma^{E,\mathrm{h}-}_{xx}+\Gamma^{E,\mathrm{h}-}_{yy}-\Gamma^{E,\mathrm{h}-}_{zz}\right)+\frac{1}{\mu}\left(\Gamma^{H,\mathrm{h}-}_{xx}+\Gamma^{H,\mathrm{h}-}_{yy}-\Gamma^{H,\mathrm{h}-}_{zz}\right)\right]_{\boldsymbol{r}=\boldsymbol{r}'}, \tag{8}$$

where a standard frequency rotation to $\omega = \mathrm{i}\zeta$ has been performed. The dependence of the components of $\Gamma$ on $\boldsymbol{r}$, $\boldsymbol{r}'$ and $\omega$ has been suppressed and superscript h indicates that only

[3] Compared to [8], $\Gamma = -\frac{\omega^2}{\hbar c^2}D$.

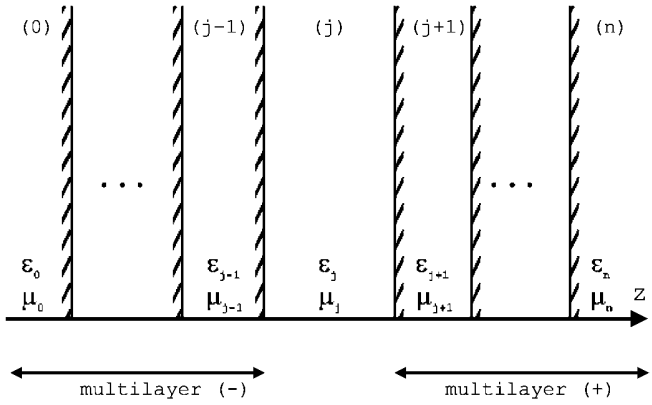


**Figure 1.** The multilayer geometry as discussed. We need to calculate the homogeneous part of Green's function in layer $(j)$.

the homogeneous solution of (4) is included. A solution of (4) generally takes the form $f(z-z')+g(z+z')$ and the superscript '$-$' denotes that terms of $\Gamma$ dependent on $z+z'$ are discarded[4]. The limit $\boldsymbol{r}\to\boldsymbol{r}'$ is taken so that (8) is evaluated entirely on one side of the interface.

Prior to solving (4) explicitly in some planar geometry, we introduce one further Fourier transformation:

$$\overleftrightarrow{\boldsymbol{\Gamma}}(\boldsymbol{r},\boldsymbol{r}';\omega)=\int\frac{\mathrm{d}^2k_\perp}{(2\pi)^2}\,\mathrm{e}^{\mathrm{i}\boldsymbol{k}_\perp\cdot(\boldsymbol{r}_\perp-\boldsymbol{r}'_\perp)}\overleftrightarrow{\boldsymbol{\Gamma}}(z,z';\boldsymbol{k}_\perp,\omega), \tag{9}$$

where the subscript $\perp$ denotes a direction perpendicular to the longitudinal or $z$-axis, i.e. in the $xy$-plane.

## 3. Green's functions in a multilayer geometry

We regard a multilayered geometry with a total of $n+1$ layers such as depicted in figure 1. Each layer is assumed homogeneous, isotropic and of infinite transverse size. The thickness of some layer $(l)$ is denoted $a_l$. The Casimir attractive force per unit transverse area between multilayers (+) and (−) bordering on either side of some (not arbitrarily chosen) layer $(j)$ so that $0<j<n$ may be calculated using (8) by evaluating Green's function near any of the boundaries of layer $(j)$. In a real setting, layers (0) and $(n)$ will both typically be vacuum or air, and it should be obvious that the two multilayers exert forces on each other in a reciprocal manner (there is a subtlety when material 0 does not equal material $n$ as discussed below).

Tomaš shows [6] how the homogeneous solution of (4) in layer $(j)$ is found in the $(\boldsymbol{k}_\perp,\omega)$ Fourier domain (now treating $z$ and $z'$ as parameters and $\boldsymbol{k}_\perp$ and $\omega$ as variables, not the other

[4] The terms of $\Gamma$ omitted from (8) are non-physical in our formalism. The particular solution of (4) equals the Green function in an infinitely large and homogeneous magnetodielectric, and is thus geometry independent. The $z+z'$-terms, argues Lifshitz, make no contribution to the net flux of momentum inside a single homogeneous medium, and it is straightforward to show formally that they make zero contribution to (8) if included [15]. These terms may be understood as a constant background of radiation contributing to what Milton in his book refers to as 'bulk energy' [17], generally of different values in different materials. Notably, if one followed the procedure Schwinger, Milton *et al* used to include the stress tensor, all terms of the homogeneous solution must be included since Green's function is evaluated on both sides of an interface, i.e. in two different media. Both approaches yield the same end result as they should.

way around)[5]. We have repeated his procedure allowing $\mu(\boldsymbol{r}) \neq 1$, yielding

$$\overleftrightarrow{\boldsymbol{\Gamma}}^{\mathrm{h}}_j(\boldsymbol{k}_\perp, \omega; z, z') = \frac{\mu_j}{2\kappa_j}\frac{\omega^2}{c^2}\sum_{q=\mathrm{TE}}^{\mathrm{TM}}\frac{\mathrm{e}^{-\kappa_j a_j}}{D_{qj}}\xi_q\big[\hat{\boldsymbol{e}}^+_{qj}(\boldsymbol{k}_\perp)\,\mathrm{e}^{-\kappa_j z}r^-_{qj}\boldsymbol{\mathcal{E}}^>_{qj}(-\boldsymbol{k}_\perp, \omega; z') + \hat{\boldsymbol{e}}^-_{qj}(\boldsymbol{k}_\perp)\,\mathrm{e}^{\kappa_j z}r^+_{qj}\,\mathrm{e}^{-\kappa_j a_j}\boldsymbol{\mathcal{E}}^<_{qj}(-\boldsymbol{k}_\perp, \omega; z')\big].$$

Here $z, z' \in (j)$ and we use the notation $\boldsymbol{AB} \equiv \boldsymbol{A} \otimes \boldsymbol{B}$. The vectors

$$\boldsymbol{\mathcal{E}}^>_{qj}(\boldsymbol{k}_\perp, \omega; z) \equiv \hat{\boldsymbol{e}}^+_{qj}(\boldsymbol{k}_\perp)\,\mathrm{e}^{-\kappa_j(z-a_j)} + r^+_{qj}\hat{\boldsymbol{e}}^-_{qj}(\boldsymbol{k}_\perp)\,\mathrm{e}^{\kappa_j(z-a_j)}, \tag{10}$$

$$\boldsymbol{\mathcal{E}}^<_{qj}(\boldsymbol{k}_\perp, \omega; z) \equiv \hat{\boldsymbol{e}}^-_{qj}(\boldsymbol{k}_\perp)\,\mathrm{e}^{\kappa_j z} + r^-_{qj}\hat{\boldsymbol{e}}^+_{qj}(\boldsymbol{k}_\perp)\,\mathrm{e}^{-\kappa_j z} \tag{11}$$

describe waves propagating in layer $(j)$ towards right and left respectively and which are reflected off the bordering interfaces. Here

$$\hat{\boldsymbol{e}}^\pm_{\mathrm{TM},j}(\boldsymbol{k}_\perp) = \frac{1}{k_j}(k_\perp\hat{\boldsymbol{z}} \mp \mathrm{i}\kappa_j\hat{\boldsymbol{k}}_\perp) = \hat{\boldsymbol{e}}^\mp_{\mathrm{TM},j}(-\boldsymbol{k}_\perp)$$

$$\hat{\boldsymbol{e}}^\pm_{\mathrm{TE},j}(\boldsymbol{k}_\perp) = \hat{\boldsymbol{k}}_\perp \times \hat{\boldsymbol{z}} = -\hat{\boldsymbol{e}}^\mp_{\mathrm{TE},j}(-\boldsymbol{k}_\perp)$$

are direction vectors in a Cartesian coordinate system $(\hat{\boldsymbol{k}}_\perp, \hat{\boldsymbol{z}}, \hat{\boldsymbol{k}}_\perp \times \hat{\boldsymbol{z}})$ defined relative to the wave vector: $\boldsymbol{k} = k_\perp\hat{\boldsymbol{k}}_\perp + k_\parallel\hat{\boldsymbol{z}}$. Furthermore one has introduced the quantities

$$\kappa_j = \sqrt{k_\perp^2 - \epsilon_j\mu_j\omega^2/c^2}, \qquad k_j = \sqrt{\epsilon_j\mu_j\omega^2/c^2},$$

$$D_{qj} = 1 - r^+_{qj}r^-_{qj}\,\mathrm{e}^{-2\kappa_j a_j}, \qquad \xi_q = \delta_{q,\mathrm{TM}} - \delta_{q,\mathrm{TE}}.$$

For physical reasons, recognizing that $k_\parallel(z)|_{z\in(j)} = \mathrm{i}\kappa_j$ we must choose $\mathrm{Im}\{\kappa_j\} < 0$. The polarization mode $q$ runs over the polarizations TE and TM and the Fresnel coefficients $r^\pm_{qj}$ are the relative reflected amplitudes of a $q$-polarized field from the entire stack of layers to the left $(-)$ or right $(+)$ of layer $(j)$.

We may thus write the attraction between multilayers on either side of $(j)$ as (it is sufficient to regard an interface on one side of $(j)$ since attraction is reciprocal)

$$\langle\mathcal{F}^0_z\rangle = \hbar\int_0^\infty\frac{\mathrm{d}\zeta}{2\pi}\int\frac{\mathrm{d}^2k_\perp}{(2\pi)^2}\left[\epsilon_j\big(\Gamma^{E,\mathrm{h}-}_{xx,j} + \Gamma^{E,\mathrm{h}-}_{yy,j} - \Gamma^{E,\mathrm{h}-}_{zz,j}\big) + \frac{1}{\mu_j}\big(\Gamma^{H,\mathrm{h}-}_{xx,j} + \Gamma^{H,\mathrm{h}-}_{yy,j} - \Gamma^{H,\mathrm{h}-}_{zz,j}\big)\right] \tag{12}$$

where Green's function components are taken in the limit $z \to z' \in (j)$ close to either of the interfaces bounding on $(j)$. We assume in this expression that $a_j$ may be varied whereas the thicknesses of other layers are treated as parameters.

The rather complicated expression for $\Gamma^{\mathrm{h}}_{ik,j}$ above may be vastly simplified for our purposes. We introduce ordinary co-ordinates according to the convention of Schwinger *et al* [17] by choosing $\hat{\boldsymbol{x}} = \hat{\boldsymbol{k}}_\perp$ so that $(\hat{\boldsymbol{k}}_\perp, \hat{\boldsymbol{z}}, \hat{\boldsymbol{k}}_\perp \times \hat{\boldsymbol{z}}) \to (\hat{\boldsymbol{x}}, \hat{\boldsymbol{z}}, -\hat{\boldsymbol{y}})$. Introducing the important quantity

$$\frac{1}{d_{qj}} = \frac{r^-_{qj}r^+_{qj}\,\mathrm{e}^{-2\kappa_j a_j}}{1 - r^-_{qj}r^+_{qj}\,\mathrm{e}^{-2\kappa_j a_j}}, \tag{13}$$

and keeping only terms dependent on $z - z'$ we show with some lengthy but straightforward manipulation that Green's function may be written very elegantly as

$$\overleftrightarrow{\boldsymbol{\Gamma}}^{h-}_j(\boldsymbol{k}_\perp, \omega; z, z') = \left[\frac{k_\perp^2}{\epsilon_j\kappa_j}\frac{1}{d_{\mathrm{TM},j}}\hat{\boldsymbol{z}}\hat{\boldsymbol{z}} - \frac{\kappa_j}{\epsilon_j}\frac{1}{d_{\mathrm{TM},j}}\hat{\boldsymbol{x}}\hat{\boldsymbol{x}} + \frac{\mu_j\omega^2}{\kappa_j c^2}\frac{1}{d_{\mathrm{TE},j}}\hat{\boldsymbol{y}}\hat{\boldsymbol{y}}\right]\cosh(z - z') + \frac{\mathrm{i}k_\perp}{\epsilon_j}\frac{1}{d_{\mathrm{TM},j}}(\hat{\boldsymbol{z}}\hat{\boldsymbol{x}} + \hat{\boldsymbol{x}}\hat{\boldsymbol{z}})\sinh(z - z'). \tag{14}$$

[5] For the sake of comparison, [6] makes use of the quantity $G_{ik} = \frac{4\pi c^2}{\omega^2}\Gamma_{ik}$

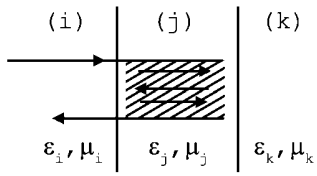


**Figure 2.** Multiple reflections between interfaces. The scrambled area represents all possible paths originating and ending in layer $(i)$.

It is now simple matter to calculate $\Gamma^E_{ik}$ and $\Gamma^H_{ik}$ and take the limit $z \to z'$ to find that our final result at zero temperature becomes beautifully simple:

$$\langle \mathcal{F}^0(a_j)\rangle = -\frac{\hbar}{2\pi^2}\int_0^\infty \mathrm{d}\zeta \int_0^\infty \mathrm{d}k_\perp \cdot k_\perp \kappa_j \sum_{q=\mathrm{TE}}^{\mathrm{TM}} \frac{1}{d_{qj}}. \tag{15}$$

At finite temperatures, the integral over all positive imaginary frequencies in (1) becomes the sum of the residues of the coth factors of (6*a*) and (6*b*), the Matsubara frequencies $\mathrm{i}\zeta_m = 2\pi \mathrm{i} k_B T m/\hbar$,

$$\langle \mathcal{F}^T(a_j)\rangle = -\frac{k_B T}{\pi}{\sum_{m=0}^{\infty}}' \int_0^\infty \mathrm{d}k_\perp \cdot k_\perp \kappa_j \sum_{q=\mathrm{TE}}^{\mathrm{TM}} \frac{1}{d_{qj}}, \tag{16}$$

where the prime on the summation indicates that the $m = 0$ term is given half weight.

## 4. Generalized reflection coefficients

The task remaining is to evaluate the generalized Fresnel reflection coefficients $r_q^{\pm}$ of a stack of magnetodielectric layers.

For a single interface between media $(i)$ and $(j)$, the reflected amplitude ratio of a $q$-polarized wave arriving from $(i)$ and is partly reflected back into $(i)$ is found from Maxwell's equations to be [18]

$$r_{q,ij} \equiv \Delta_{q,ij} = \frac{\kappa_i - \gamma_{q,ij}\kappa_j}{\kappa_i + \gamma_{q,ij}\kappa_j} \tag{17}$$

with $\kappa$ as defined above and

$$\gamma_{q,ij} = \begin{cases} \mu_i/\mu_j; & q = \mathrm{TE} \\ \epsilon_i/\epsilon_j; & q = \mathrm{TM}. \end{cases}$$

Second, the reflection coefficient of a system of two interfaces such as depicted in figure 2 may be calculated as the sum of coefficients pertaining to each of the infinitely many optical paths originating and ending in $(i)$. We let the transmission coefficient of a wave transmitted from $(i)$ to $(j)$ be $t_{ij}$ (omitting for now polarization $q$) and recognize the longitudinal wave vector in $(j)$ to be $k_{\parallel,j} = \sqrt{\epsilon_j \mu_j \omega^2/c^2 - k_\perp^2} = \mathrm{i}\kappa_j$ so that a wave travelling a distance $a_j$ must be multiplied by $\exp(\mathrm{i}k_{\parallel,j}a_j) = \exp(-\kappa_j a_j)$; a phase shift if $\kappa_j$ is imaginary (propagating wave) or attenuation if $\kappa_j$ is real (evanescent wave). Thus,

$$r_{ijk} = r_{ij} + t_{ij}\,\mathrm{e}^{-\kappa_j a_j} r_{jk}\,\mathrm{e}^{-\kappa_j a_j} t_{ji} + \cdots = r_{ij} + t_{ij}t_{ji}r_{jk}\,\mathrm{e}^{-2\kappa_j a_j}\sum_{n=0}^{\infty}(r_{jk}r_{ji}\,\mathrm{e}^{-2\kappa_j a_j})^n$$

$$= \frac{r_{ij} + r_{jk}\,\mathrm{e}^{-2\kappa_j a_j}}{1 + r_{ij}r_{jk}\,\mathrm{e}^{-2\kappa_j a_j}} \tag{18}$$

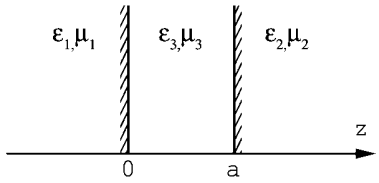


**Figure 3.** The trizone configuration of two half-spaces separated by a gap region.

where we have made use of the properties $t_{ij}t_{ji} - r_{ij}r_{ji} = 1$ and $r_{ij} = -r_{ji}$. Equation (18) is valid for either polarization, respectively.

This provides a simple procedure for calculating the reflection coefficient of a multilayer containing any finite number of interfaces. To calculate $r^-_{qj}$, say, as it appears in figure 1, we start with the leftmost interface between zones (1) and (0) and find $r_{q,10} = \Delta_{q,10}$ and invoke (18) recursively to find the reflection coefficient of the two leftmost interfaces, then the three leftmost and so on until the closest interface, between $(j)$ and $(j-1)$, is reached.

## 5. The Casimir attraction calculated in various configurations

We go on to demonstrate the strength of the above procedure by calculating the Casimir force in an array of different plane parallel configurations so as to reproduce the results of several references.

### *5.1. Two half-spaces*

Consider first the simplest system of two half-spaces of some magnetodielectric material separated by a gap of width $a$, generally made of some other material. We denote the half-spaces 1 and 2 (see figure 3) and the gap 3.

There is now only one interface on either side of the gap and obtaining the force expression is almost trivial. The reflection coefficients to the right and left are

$$r^+_q = \Delta_{q,32} \qquad \text{and} \qquad r^-_q = \Delta_{q,31}$$

as defined in (17). We get the force density expression (suppressing the averaging notation henceforth)

$$\mathcal{F}^0(a) = -\frac{\hbar}{2\pi^2}\int_0^\infty \mathrm{d}\zeta \int_0^\infty \mathrm{d}k_\perp \cdot k_\perp \kappa_3 \sum_{q=\mathrm{TE}}^{\mathrm{TM}} \frac{\Delta_{q,32}\Delta_{q,31}\,\mathrm{e}^{-2\kappa_3 a}}{1-\Delta_{q,32}\Delta_{q,31}\,\mathrm{e}^{-2\kappa_3 a}}, \tag{19}$$

which is the classical Lifshitz result quoted in numerous references, e.g. [8, 17] (this expression, notably, is a generalization of both references since it allows for $\mu \neq 1$).

### *5.2. A plate outside a wall*

We consider a plate of finite thickness $b$ and material denoted 2 separated by a distance $a$ from an infinitely thick wall of material 1 as depicted in figure 4. Such a system has recently been considered by Tomaš [14] for the sake of discussing the consequences of using an alternative Lorentz force stress tensor, and his results using the Minkowski tensor for comparison agrees with ours. The gap material, denoted with subscript g is allowed to be different from the material of the exterior, denoted with subscript e. Green's function is calculated in the gap

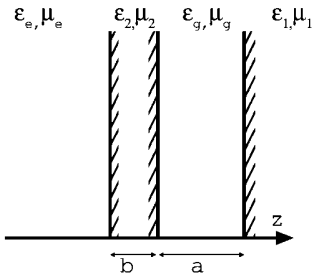


**Figure 4.** The four-layered configuration of a plate and a wall.

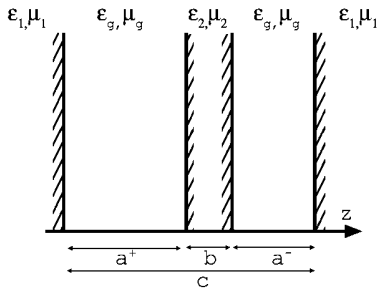


**Figure 5.** The system of a slab in a cavity.

region, and $r_q^-$ and $r_q^+$ are the relative reflected amplitude of a wave originating in the gap and propagating towards the left and right, respectively.

We see immediately that $r_q^+ = (\kappa_\mathrm{g} - \gamma_{q,\mathrm{g}1}\kappa_1)/(\kappa_\mathrm{g} + \gamma_{q,\mathrm{g}1}\kappa_1) = -\Delta_{q,1\mathrm{g}}$ and combining (17) and (18) readily yields

$$r_q^- = \frac{-\Delta_{q,2\mathrm{g}} + \Delta_{q,2\mathrm{e}}\,\mathrm{e}^{-2\kappa_2 b}}{1 - \Delta_{q,2\mathrm{g}}\Delta_{q,2\mathrm{e}}\,\mathrm{e}^{-2\kappa_2 b}},$$

so that

$$\frac{1}{d_{qj}} = \frac{(\Delta_{q,1\mathrm{g}}\Delta_{q,2\mathrm{g}} - \Delta_{q,1\mathrm{g}}\Delta_{q,2\mathrm{e}}\,\mathrm{e}^{-2\kappa_2 b})\,\mathrm{e}^{-2\kappa_\mathrm{g} a}}{1 - \Delta_{q,1\mathrm{g}}\Delta_{q,2\mathrm{g}}\,\mathrm{e}^{-2\kappa_2 b} - (\Delta_{q,1\mathrm{g}}\Delta_{q,2\mathrm{g}} - \Delta_{q,1\mathrm{g}}\Delta_{q,2\mathrm{e}}\,\mathrm{e}^{-2\kappa_2 b})\,\mathrm{e}^{-2\kappa_\mathrm{g} a}},$$

from which Green's function and the Casimir attraction per unit area between plate and wall follow neatly from (14) and (15).

### *5.3. A slab in a cavity*

We go on to study the five-layered system of a slab between two walls as defined in figure 5. A general system of five layers was first considered by Zhou and Spruch [19] and the special case of a slab in a cavity was treated, apparently using the method presented here, by Tomaš [9]. Some manipulation shows that our result coincide with the finds of both references. We calculate the attraction with respect to each of the gaps in turn and subsequently find the force acting on the slab as the difference between these. The procedure is identical to that above so the details of the somewhat more lengthy but in principle uncomplicated calculations are left out.

We denote the left- and right-hand gaps with superscript + and − respectively for reasons which will become obvious and for simplicity we assume both walls to be made of the same material, denoted 1, whereas the slab is made of a material indexed 2. Furthermore, we use the simplifying notation $\Delta_{iq} \equiv \Delta_{q,i\mathrm{g}}$ with $i = 1, 2$. With this we find for the left- and right-hand gaps

$$\frac{1}{d_q^{\pm}} = \frac{U_q^{\mp}\,\mathrm{e}^{-2\kappa_{\mathrm{g}}a^{\pm}}}{V_q^{\mp} - U_q^{\mp}\,\mathrm{e}^{-2\kappa_{\mathrm{g}}a^{\pm}}},$$

where

$$U_q^{\pm} = \Delta_{1q}\Delta_{2q}\bigl(1 - \Delta_{1q}\Delta_{2q}\,\mathrm{e}^{-2\kappa_{\mathrm{g}}a^{\pm}}\bigr) - \Delta_{1q}\bigl(\Delta_{2q} - \Delta_{1q}\,\mathrm{e}^{-2\kappa_{\mathrm{g}}a^{\pm}}\bigr)\,\mathrm{e}^{-2\kappa_2 b},$$
$$V_q^{\pm} = 1 - \Delta_{1q}\Delta_{2q}\,\mathrm{e}^{-2\kappa_{\mathrm{g}}a^{\pm}} - \Delta_{2q}\bigl(\Delta_{2q} - \Delta_{1q}\,\mathrm{e}^{-2\kappa_{\mathrm{g}}a^{\pm}}\bigr)\,\mathrm{e}^{-2\kappa_2 b},$$

and the resulting force on the centre slab is accordingly (a function of *either* $a^+$ or $a^-$ when $b$ and $c$ are assumed constant parameters)

$$\mathcal{F}^0(a^{\pm}; b, c) = \frac{\hbar}{2\pi^2}\int_0^{\infty}\mathrm{d}\zeta\int_0^{\infty}\mathrm{d}k_{\perp}\cdot k_{\perp}\kappa_{\mathrm{g}}\sum_{q=\mathrm{TE}}^{\mathrm{TM}}\left(\frac{1}{d_q^-} - \frac{1}{d_q^+}\right). \tag{20}$$

Notice how, if we let the gap be either very wide ($b \to \infty$) or the slab perfectly reflecting ($\kappa_2 \to \infty$), the terms containing the factor $\exp(-2\kappa_2 b)$ vanish, and we get back Lifshitz' expression for two separate gaps as we should.

A rather more instructive expression is obtained if the position of the slab is given not by $a^+$ and $a^-$, but the deviation $\delta$ of the centre of the slab from the midline of the cavity. Introducing the quantity $h = c - b = a^+ + a^-$, we write $a^{\pm} = h/2 \pm \delta$ and the force density expression becomes after some shuffling of symbols

$$\mathcal{F}^0(\delta; b, c) = \frac{\hbar}{2\pi^2}\int_0^{\infty}\mathrm{d}\zeta\int_0^{\infty}\mathrm{d}k_{\perp}\cdot k_{\perp}\kappa_{\mathrm{g}}\sum_{q=\mathrm{TE}}^{\mathrm{TM}}\frac{A_q\sinh 2\kappa_{\mathrm{g}}\delta}{B_q - A_q\cosh 2\kappa_{\mathrm{g}}\delta} \tag{21}$$

with

$$A_q = 2\Delta_{1q}\Delta_{2q}(1 - \mathrm{e}^{-2\kappa_2 b})\,\mathrm{e}^{-\kappa_{\mathrm{g}}h},$$
$$B_q = 1 - \Delta_{2q}^2\,\mathrm{e}^{-2\kappa_2 b} + \Delta_{1q}^2\bigl(\Delta_{2q}^2 - \mathrm{e}^{-2\kappa_2 b}\bigr)\,\mathrm{e}^{-2\kappa_{\mathrm{g}}h}.$$

One should note in this context that this is the geometry treated by Raabe and Welsch [11] and later by Tomaš [13], making use of their alternative, Lorentz-type stress tensor.

### *5.4. Two plates of finite thickness*

The system of two plates each of finite thickness has been treated by numerous authors. First to do so was Kupiszewska [20], who employed an effectively one-dimensional model by insisting that waves be reflected at normal incidence, as have several authors after her. A three-dimensional geometry, allowing nonzero values of $k_{\perp}$, appears first to have been considered by Jaekel and Reynaud in 1991 [21] whose result is found to be smaller than ours by a factor 1/2 (it should be noted that comparison is not trivial due to formal differences). A number of other references [19, 22, 23], however, obtain results agreeing perfectly with that found by using the above procedure. The in principle identical system of two semispaces each covered with a thin layer of a different substance was considered by Klimchitskaya and co-workers [24], again in agreement with the below.

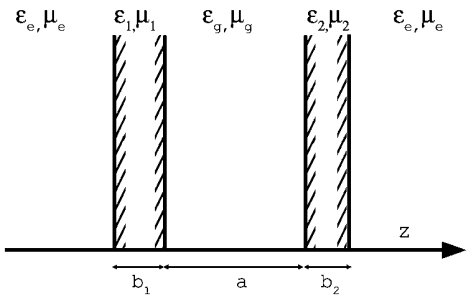


**Figure 6.** A system of two plates of finite thickness.

The geometry is defined in figure 6. Just as before we determine the reflection coefficients of either slab as seen from the gap,

$$r_q^+ = \frac{-\Delta_{q,2\mathrm{g}} + \Delta_{q,2\mathrm{e}}\,\mathrm{e}^{-2\kappa_2 b_2}}{1 - \Delta_{q,2\mathrm{g}}\Delta_{q,2\mathrm{e}}\,\mathrm{e}^{-2\kappa_2 b_2}} \qquad r_q^- = \frac{-\Delta_{q,1\mathrm{g}} + \Delta_{q,1\mathrm{e}}\,\mathrm{e}^{-2\kappa_1 b_1}}{1 - \Delta_{q,1\mathrm{g}}\Delta_{q,1\mathrm{e}}\,\mathrm{e}^{-2\kappa_1 b_1}}, \tag{22}$$

and the Casimir attractive force per unit area of the plates is found neatly from (13) and (15).

## 6. The neglected bulk force

In the case that materials 0 and $n$ in figure 1 are different, a second force appears in addition to the Casimir force. It is a force acting on the entire multilayer system and we shall refer to it as a bulk force. Quantitatively the electromagnetic force density was found to be $\boldsymbol{f} = \overleftrightarrow{\mathbf{T}} \cdot \overleftarrow{\nabla}$ and the force acting on some volume $\mathcal{V}$ is

$$\boldsymbol{F} = \int_{\mathcal{V}} \mathrm{d}^3 r\, \boldsymbol{f} = \oint_{\partial\mathcal{V}} \overleftrightarrow{\mathbf{T}} \cdot \mathrm{d}\boldsymbol{S}$$

where the divergence theorem has been invoked and $\mathrm{d}\boldsymbol{S}$ points normally out of $\mathcal{V}$, enclosed by the surface $\partial\mathcal{V}$. Let $\mathcal{V}$ be a box enclosing all interfaces of the multilayer system so that its $z$-boundaries lie at $z^- \in (0)$ and $z^+ \in (n)$. Only the sides of $\mathcal{V}$ parallel to the $xy$-plane contribute to the bulk force, which is evaluated per unit transverse area as (averaging with respect to fluctuations is understood)

$$\begin{aligned}\boldsymbol{\mathcal{F}}_{\mathrm{bulk}} &= [T_{zz}(z^+) - T_{zz}(z^-)] \cdot \hat{\boldsymbol{z}} \\ &= -\frac{\hat{\boldsymbol{z}}\epsilon_0}{2}\big[\epsilon(z^+)\big(E_z^2 - E_x^2 - E_y^2\big)\big|_{z=z^+} - \epsilon(z^-)\big(E_z^2 - E_x^2 - E_y^2\big)\big|_{z=z^-}\big] \\ &\quad - \frac{\hat{\boldsymbol{z}}\mu_0}{2}\big[\mu(z^+)\big(H_z^2 - H_x^2 - H_y^2\big)\big|_{z=z^+} - \mu(z^-)\big(H_z^2 - H_x^2 - H_y^2\big)\big|_{z=z^-}\big].\end{aligned} \tag{23}$$

If now media (0) and $(n)$ are the same, the mean squared fluctuating fields will be the same on either side of the multilayer, and the bulk force is zero, otherwise $\mathcal{F}_{\mathrm{bulk}}$ is generally nonzero.

This force is typically neglected, and an argument in favour of doing so is surely that in a real system, layers are not infinitely thick. The outmost layers of a multiple configuration should realistically be air or vacuum, and if they are not, it simply means that $\mathcal{V}$ does not contain the entire system and the bulk force is identically cancelled by reflections at surfaces (not necessarily parallel with the system, or even plane) outside $\mathcal{V}$, as it should be according to Newton's third law.

## 7. Conclusion

With the above procedure, the calculation of Casimir forces in even complex multilayered geometries is both quick and straightforward and shown able to reproduce the results of a number of previous works. Various configurations may thus be considered theoretically and numerically with ease to study the various dependences, e.g., on material properties and temperatures. The procedure may furthermore be repeated to reveal differences between various electromagnetic stress tensors, a subject of dispute for decades [16, 25].

## Acknowledgment

The author thanks professor Iver Brevik for helpful comments and many rewarding discussions on the subject.

## References

[1] Casimir H B G 1948 *Proc. K. Ned. Akad. Wet.* **51** 793
[2] Chan H B, Aksyuk V A, Kleiman R N, Bishop D J and Capasso F 2001 *Science* **291** 1941
[3] Bressi G, Carugno G, Onofrio R and Ruoso G 2002 *Phys. Rev. Lett.* **88** 041804
[4] Sparnaay M J 1958 *Physica* **24** 751
[5] Lamoreaux S 2005 *Rep. Prog. Phys.* **68** 201
[6] Tomaš M S 1995 *Phys. Rev.* A **51** 2545
[7] Mills D L and Maradudin A A 1975 *Phys. Rev.* B **12** 2943
[8] Dzyaloshinskii I E, Lifshitz E M and Pitaevskii L P 1961 *Sov. Phys.—Usp.* **73** 153
Lifshitz E M and Pitaevskii L P 1980 *Statistical Physics:* Part 2 (Oxford: Elsevier/Butterworth-Heinemann)
[9] Tomaš M S 2002 *Phys. Rev.* A **66** 052103
[10] Brevik I, Ellingsen S A and Milton K A 2006 *New J. Phys.* **8** 236
[11] Welsch D-G and Raabe Ch 2005 *Phys. Rev.* A **71** 013814
[12] Pitaevskii L P 2006 *Phys. Rev.* A **73** 047801
[13] Tomaš M S 2005 *Phys. Rev.* A **71** 060101
Tomaš M S 2005 *Phys. Rev.* A **72** 034104
Tomaš M S 2005 *Fizika* A **14** 29
[14] Tomaš M S 2006 *J. Phys. A: Math. Gen.* **39** 6785
[15] Ellingsen S A 2006 Master's *Thesis,* Norwegian University of Science and Technology, Department of Physics
[16] Brevik I 1979 *Phys. Rep.* **52** 133
[17] Schwinger J, DeRaad L L and Milton K A 1978 *Ann. Phys.* **115** 1
Milton K A 2001 *The Casimir Effect: Physical Manifestations of Zero-Point Energy* (Singapore: World Scientific)
[18] Ford G W and Weber W H 1984 *Phys. Rep.* **113** 195
[19] Zhou F and Spruch L 1995 *Phys. Rev.* A **52** 297
[20] Kupiszewska D and Mostowski J 1990 *Phys. Rev.* A **41** 4636
Kupiszewska D 1992 *Phys. Rev.* A **46** 2286
[21] Jaekel M T and Reynaud S 1991 *J. Phys.* I (France) **1** 1395
[22] Matloob R and Falinejad H 2001 *Phys. Rev.* A **64** 042102
[23] Mochán W L, Villarreal C and Esquivel-Sirvent R 2002 *Rev. Mex. Fis.* **48** 339 (*Preprint* quant-ph/0206119v1)
[24] Klimchitskaya G L, Mohideen U and Mostepanenko V M 2000 *Phys. Rev.* A **61** 062107
[25] Stallinga S 2006 *Opt. Exp.* **14** 1286

J. Phys. A: Math. Theor. **40** (2007) 3643–3664 doi:10.1088/1751-8113/40/13/021

# Casimir force on real materials—the slab and cavity geometry

**Simen A Ellingsen**[1] **and Iver Brevik**

Department of Energy and Process Engineering, Norwegian University of Science and Technology, N-7491 Trondheim, Norway

E-mail: iver.h.brevik@ntnu.no

Received 3 November 2006, in final form 12 February 2007
Published 14 March 2007
Online at stacks.iop.org/JPhysA/40/3643

**Abstract**

We analyse the potential of the geometry of a slab in a planar cavity for the purpose of Casimir force experiments. The force and its dependence on temperature, material properties and finite slab thickness are investigated both analytically and numerically for the slab and walls made of aluminium and teflon FEP respectively. We conclude that such a setup is ideal for measurements of the temperature dependence of the Casimir force. By numerical calculation it is shown that temperature effects are dramatically larger for dielectrics, suggesting that a dielectric such as teflon FEP whose properties vary little within a moderate temperature range, should be considered for experimental purposes. We finally discuss the subtle but fundamental matter of the various Green's two-point function approaches present in the literature and show how they are different formulations describing the same phenomenon.

PACS numbers: 05.30.−d, 12.20.Ds, 32.80.Lg, 41.20.Jb, 42.50.Nn

## 1. Introduction

The Casimir effect [1] can be seen as an effect of the zero-point energy of vacuum which emerges due to the non-commutativity of quantum operators upon quantization of the electromagnetic (EM) field. Although formally infinite in magnitude, the EM field density in bulk undergoes finite alterations when dielectric or metal boundaries are introduced in the system, giving rise to finite and measurable forces. As is well known, at nanometre to micrometre separations the Casimir attraction between bodies becomes significant, and the effect has attracted much attention during the last decade in the wake of the rapid advances in nanotechnology. The existence of the Casimir force was shown experimentally as early as 1958 by Spaarnay [2], yet only recently new and much more precise measurements of Lamoreaux and others (see the review [3]) have boosted the interest in the effect from a much broader

[1] Present address: Department of War Studies, King's College London, Strand, London WC2R 2LS, UK.

audience. Experiments like that of Mohideen and Roy [4], and the very recent one of Harber *et al* [5], making use of the oscillations of a magnetically trapped Bose–Einstein condensate, were subject to widespread regard. The same was true for the nonlinear micromechanical Casimir oscillator experiment of Chan *et al* [6, 7].

Recent reviews on the Casimir effect are given in [3, 8–11]. Much information about recent developments can also be found in the special issues of *J. Phys. A: Math. Gen.* (May 2006) [12] and of *New J. Phys.* (October 2006) [13].

Actual calculations of Casimir forces are usually performed via two different routes [8]; either by summation of the energy of discrete quantum modes of the EM field (cf, for instance, [14]), or via a Green's function method first developed by Lifshitz [15]. Mode summation, despite its advantage of a simpler and more transparent formalism, is usually far inferior. In practice it is only in systems where quantum energy states are known that energy summation can be carried out explicitly. This requires the system to be highly symmetric, and favour assumptions such as perfectly conducting walls like in the original Casimir problem. Geometries in which quantum states are known exactly, unfortunately, are few.

The method of calculating the force through Green's functions avoids some but not all of these problems; exact solutions are still only known in highly symmetrical systems such as infinitely large parallel plates or concentric spheres. Via the fluctuation–dissipation theorem, the EM field energy density is linked directly to the photonic Green's function, and the force surface density acting on boundaries can be calculated, at least in principle. The theory of Green's functions and the application of them will be central in the present paper.

The purpose of the present work is twofold. First, we intend to explore some of the delicate issues that occur in the Green's function formalism in typical settings involving dielectric boundaries. Upon relating the two-point functions to Green's function one may choose to calculate the Green function in full [8, 16]. The method is complete but may appear cumbersome, at least so in the presence of several dielectric surfaces. It is possible to reduce the calculational burden somewhat by simplifying the Green function expressions, by omitting those parts that do not contribute to the Casimir force. This means that one works with 'effective' Green functions. This method is employed and briefly discussed by Lifshitz and co-workers; cf e.g. [17]. The connections between the different kinds of Green's functions are in our opinion far from trivial, and we therefore believe it of interest to present some of the formulae that we have compiled and which have turned out to be useful in practice.

As for the calculational technique for the Casimir force in a multilayer system, there exists a powerful formalism worked out, in particular, by Tomaš [18]. In turn, this formalism was based on work by Mills and Maradudin two decades earlier [19]. One of us recently made a review of this technique, with various applications [20]. We shall make use of this technique in the following. In company with the by now classic theory of Lifshitz and co-workers [15, 21] and the standard Fresnel theory in optics, the necessary set of tools is provided.

Our second purpose is to apply the formalism to concrete calculations of the Casimir pressure on a dielectric plate in a multilayer setting. Especially, we will consider the pressure on a plate situated in a cavity (five-zone system). We work out force expressions and eigenfrequency changes when the plate is acted upon by a harmonic-oscillator mechanical force (spring constant $k$) in addition to the Casimir force, and is brought to oscillate horizontally. To our knowledge, explicit calculations of this sort have not been made before. A chief motivation for this kind of calculation is that we wish to evaluate the magnitudes of thermal corrections to the Casimir pressure. In recent years there have been lively discussions in the literature about the thermal corrections; for some statements of both sides of the controversy; see [16, 22–29]. We hope that the consideration of planar multilayer systems may provide additional insight into the temperature problem.

We will be considering uniformly heated systems only. The recent experiment of Harber *et al* [5] investigated the surface-atom force at thermal equilibrium at room temperature, the goal being to measure the surface-atom force at very large distances, taking into account the peculiar properties of a Bose–Einstein condensate gas. Later, the same group investigated the non-equilibrium effect [30]. This paper seems to have reported the first accurate measurement of the thermal effect (of any kind) of the Casimir force, in good agreement with earlier theoretical predictions [31] (cf also the prior theory of Pitaevskii on the non-equilibrium dynamics of EM fluctuations [32]). Consideration of such systems lies, however, outside the scope of the present paper.

The following point ought also to be commented upon, although it is not a chief ingredient of the present paper: Our problem bears a relationship to the famous Abraham–Minkowski controversy, or more generally the question of how one should construct the correct form of the EM energy–momentum tensor in a medium. This problem has been discussed more and less intensely ever since Abraham and Minkowski proposed their energy–momentum expressions around 1910. The advent of accurate experiments, in particular, has aided a better insight into this complicated aspect of field–matter interacting systems. Some years ago, one of the present authors wrote a review of the experimental status in the field [33] (cf also [34]). There is by now a rather extensive literature in this field; some papers are listed in [35–42]. In the present case, where the EM surface force on a dielectric boundary results from integration of the volume force density across the boundary region, the Abraham and Minkowski predictions actually become equal. Recently, in a series of papers Raabe and Welsch have expressed the opinion that the Abraham–Minkowski theory is inadequate and that a different form of the EM energy–momentum tensor has to be employed [43–46]. We cannot agree with this statement, however. All the experiments in optics that we are aware of can be explained in terms of the Abraham–Minkowski theory in a straightforward way. One typical example is provided, for instance, by the oscillations of a water droplet illuminated by a laser pulse. Some years ago, Zhang and Chang made an experiment in which the oscillations of the droplet surface were clearly detectable [47]. It was later shown theoretically how the use of the Abraham–Minkowski theory could reproduce the observed results to a reasonable accuracy [48, 49]. In our theory below, we will use the Abraham–Minkowski theory throughout.

SI units are used throughout the calculations, and permittivity $\epsilon$ and permeability $\mu$ are defined as relative (nondimensional) quantities. We thus write $\mathbf{D} = \epsilon_0 \epsilon \mathbf{E}$, $\mathbf{B} = \mu_0 \mu \mathbf{H}$.

The outline of the paper is as follows. In the next section we analyse the 5-layered magnetodielectric system (figure 1), presenting the full Green's function as well as its effective (or reduced) counterpart. We here aim at elucidating some points in the formalism that in our opinion are rather delicate. Section 3 is devoted to a study of an oscillating slab in a Casimir cavity, permitting, in principle at least, how the change in the eigenfrequency of the slab with respect to the temperature can give us information about the temperature dependence of the Casimir force. Section 4 discusses more extensively the relationships between the Green's two-point functions as introduced by Lifshitz *et al* and by Schwinger *et al*. In section 5 we present results of numerical Casimir force calculations for selected substances, taking Al as example of a metal, and teflon FEP as example of a dielectric[2]. In section 6 we consider the effect of finite slab thickness, i.e. the 'leakage' of vacuum radiation from one gap to the other.

[2] As a word of caution, we mention here that our permittivity data for metals are intended to hold in the bulk, whereas in practice the real and imaginary parts of the index of refraction for metals come from ellipsometry measurements, and are thus really *surface* measurements. There is an inherent uncertainty in the calculated results coming from this circumstance, of unknown magnitude, although in our opinion the corrections will hardly exceed the 1% level due to the general robustness of the force expression against permittivity variations. Ideally, information about the permittivity versus imaginary frequency would be desirable, for a metallic film. We thank Steve Lamoreaux for comments on this point.

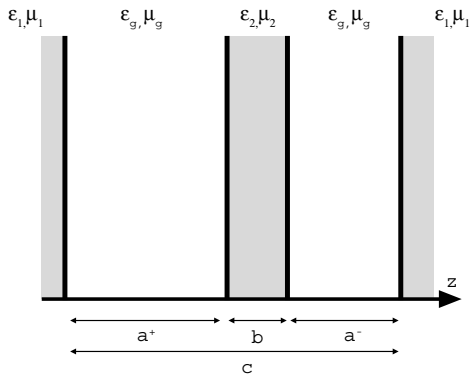


**Figure 1.** The five-zone geometry of a slab in a cavity. We have chosen $z = 0$ at the left-hand cavity wall.

We find the striking result that for dielectrics the relative finite thickness correction is much larger than for metals. For teflon FEP versus Al the relative correction is almost two orders in magnitude higher.

A word is called for, as regards the permeability $\mu$. As anticipated above, we allow $\mu$ to be different from 1. This is motivated chiefly by completeness, and is physically an idealization. It is known that the permeability for most materials is lossy at high frequencies, corresponding to imaginary values for $\mu$. That phenomenon is limited to a restricted frequency interval, however, (10–100 GHz), and loses effect at the higher frequencies.

## 2. Casimir force on a slab in a cavity

We shall consider a five-layered magnetodielectric system such as depicted in figure 1. The analytical calculation of the Casimir force density acting on the slab in such a geometry is well known; it may be calculated, quite simply, by a straightforward generalization of the famous calculation by Lifshitz and co-workers used for the simpler, three-layered system of two half-spaces separated by a gap [17, 21].

Rather than starting from the photonic Green's function as a propagator as known from quantum electrodynamics, we introduce classical and macroscopic two-point (Green's) function according to the convention of Schwinger *et al* [52] as

$$\boldsymbol{E}(x) = \frac{1}{\epsilon_0}\int \mathrm{d}^4x'\,\overleftrightarrow{\boldsymbol{\Gamma}}(x,x')\cdot\boldsymbol{P}(x'), \tag{1}$$

where $x = (\boldsymbol{r}, t)$. Due to causality, $t'$ is only integrated over the region $t' \leqslant t$. It follows from Maxwell's equations that $\Gamma$ obeys the relation

$$\nabla\times\nabla\times\overleftrightarrow{\boldsymbol{\Gamma}}(\boldsymbol{r},\boldsymbol{r}';\omega) - \frac{\epsilon(\boldsymbol{r})\mu(\boldsymbol{r})\omega^2}{c^2}\overleftrightarrow{\boldsymbol{\Gamma}}(\boldsymbol{r},\boldsymbol{r}';\omega) = \frac{\mu(\boldsymbol{r})\omega^2}{c^2}\delta(\boldsymbol{r}-\boldsymbol{r}')\overleftrightarrow{\mathbf{1}}, \tag{2}$$

where we have performed a Fourier transformation according to

$$\overleftrightarrow{\boldsymbol{\Gamma}}(x,x') = \int_{-\infty}^{\infty}\frac{\mathrm{d}\omega}{2\pi}\,\mathrm{e}^{-\mathrm{i}\omega\tau}\overleftrightarrow{\boldsymbol{\Gamma}}(\boldsymbol{r},\boldsymbol{r}';\omega), \tag{3}$$

with $\tau \equiv t - t'$.

A comparison of (2) with the corresponding equation in [17, 21] shows formally that $\Gamma$ is essentially equivalent with the retarded photonic Green's function in a medium[3]. The physical connection is not entirely trivial, however. As motivation we note that (1) expresses the linear relation between the dipole density at $x'$ and the resulting electric field at $x$, in essence the extent to which an EM field is able to *propagate* from $x'$ to $x$. This is exactly the classical analogy of the quantum definition of a Green's function propagator, in accordance with the correspondence principle as introduced by Niels Bohr in 1923. We note furthermore that insisting that $t' \leqslant t$ ensures that account is taken of retardation, corresponding to the Lifshitz definition of the retarded photonic Green's function (e.g. [17, section 75]) which is 0 for $t < t'$.

We make use of the fluctuation–dissipation theorem at zero temperature, rendered conveniently as

$$\mathrm{i}\langle E_i(\boldsymbol{r})E_k(\boldsymbol{r}')\rangle_\omega = \frac{\hbar}{\epsilon_0}\,\Im\mathrm{m}\{\Gamma_{ik}(\boldsymbol{r},\boldsymbol{r}';\omega)\} \tag{4a}$$

$$\mathrm{i}\langle H_i(\boldsymbol{r})H_k(\boldsymbol{r}')\rangle_\omega = \frac{\hbar}{\mu_0}\frac{c^2}{\mu\mu'\omega^2}\,\mathrm{Curl}_{ij}\,\mathrm{Curl}'_{kl}\,\Im\mathrm{m}\{\Gamma_{jl}(\boldsymbol{r},\boldsymbol{r}';\omega)\}, \tag{4b}$$

with the notation $\mathrm{Curl}_{ik} \equiv \epsilon_{ijk}\partial_j$ ($\epsilon_{ijk}$ being the Levi-Civita symbol and summation over identical indices is implied), $\mathrm{Curl}'_{ik} \equiv \epsilon_{ijk}\partial'_j$ where $\partial'_j$ is differentiation with respect to component $j$ of $\boldsymbol{r}'$, and $\mu' \equiv \mu(\boldsymbol{r}')$. The brackets denote the mean value with respect to fluctuations. The Casimir pressure acting on some surface is now given by the $zz$-component of the Abraham–Minkowski stress tensor, found by simple insertion to become [17, 21][4]

$$\mathcal{F}_z = \hbar\int_0^\infty \frac{\mathrm{d}\zeta}{2\pi}\left[\epsilon\left(\Gamma^E_{xx}+\Gamma^E_{yy}-\Gamma^E_{zz}\right)+\frac{1}{\mu}\left(\Gamma^H_{xx}+\Gamma^H_{yy}-\Gamma^H_{zz}\right)\right]_{\boldsymbol{r}=\boldsymbol{r}'}, \tag{5}$$

where a standard frequency rotation $\omega = \mathrm{i}\zeta$ has been performed and the convenient quantities $\Gamma^E$ and $\Gamma^H$ have been defined according to

$$\Gamma^E_{ik}(\boldsymbol{r},\boldsymbol{r}';\omega) \equiv \Gamma_{ik}(\boldsymbol{r},\boldsymbol{r}';\omega), \tag{6a}$$

$$\Gamma^H_{ik}(\boldsymbol{r},\boldsymbol{r}';\omega) \equiv \frac{c^2}{\omega^2}\,\mathrm{Curl}_{il}\,\mathrm{Curl}'_{km}\,\Gamma_{lm}(\boldsymbol{r},\boldsymbol{r}';\omega). \tag{6b}$$

In (5) only the homogeneous (geometry dependent) solution of (2) is included; the inhomogeneous solution pertaining to the delta function represents the solution inside a homogeneous medium filling all of space. This term is geometry independent, and cannot contribute to any physically observable quantity. Importantly, however, any such simplification from the full Green's function to its 'effective' counterpart must only be made subsequent to all other calculations.

The system is symmetrical with respect to translation and rotation in the $xy$-plane and we transform the Green's function once more:

$$\overleftrightarrow{\boldsymbol{\Gamma}}(\boldsymbol{r},\boldsymbol{r}';\omega) = \int\frac{\mathrm{d}^2k_\perp}{(2\pi)^2}\,\mathrm{e}^{\mathrm{i}\boldsymbol{k}_\perp\cdot(\boldsymbol{r}_\perp-\boldsymbol{r}'_\perp)}\overleftrightarrow{\mathbf{g}}(z,z';\boldsymbol{k}_\perp,\omega). \tag{7}$$

Here and henceforth, the subscript $\perp$ refers to a direction in the $xy$-plane. In the $\boldsymbol{k}_\perp, \omega$ Fourier domain one finds [8, 52] that the component equations (2) combine to (among others) the equations

$$\left(\partial_z^2-\kappa^2\right)g_{xx}(z,z';\boldsymbol{k}_\perp,\omega) = \frac{\kappa^2}{\epsilon\mu}\delta(z-z') \tag{8}$$

[3] Compared to Lifshitz *et al* $\mathcal{D} = -\hbar c^2\Gamma/\omega^2$, which is only a matter of definition.

[4] The expression is generalized compared to the original reference to allow $\mu \neq 1$.

and

$$\left(\partial_z^2 - \kappa^2\right) g_{yy}(z, z'; \boldsymbol{k}_\perp, \omega) = -\frac{\mu\omega^2}{c^2}\delta(z - z'), \tag{9}$$

which readily give us these two components in each homogeneous zone. We have defined the quantity $\kappa \equiv \left(k_\perp^2 - \epsilon\mu\omega^2/c^2\right)^{1/2}$. The final diagonal component is found by means of the relations

$$g_{zz}(z, z'; \boldsymbol{k}_\perp, \omega) = -\frac{\mathrm{i}k_\perp}{\kappa^2}\partial_z g_{xz}(z, z'; \boldsymbol{k}_\perp, \omega) + \frac{1}{\kappa^2}\frac{\mu\omega^2}{c^2}\delta(z - z') \tag{10a}$$

$$g_{zx}(z, z'; \boldsymbol{k}_\perp, \omega) = -\frac{\mathrm{i}k_\perp}{\kappa^2}\partial_z g_{xx}(z, z'; \boldsymbol{k}_\perp, \omega) \tag{10b}$$

$$g_{xz}(z, z'; \boldsymbol{k}_\perp, \omega) = g_{zx}(z', z; -\boldsymbol{k}_\perp, \omega), \tag{10c}$$

of which the first two are components of (2) and the last was shown by Lifshitz (e.g. [17]).

We return to the geometry of figure 1. An important point to emphasize is that unlike certain authors in the past (e.g. [53]) we make no principal difference between the walls of the cavity and the slab; they are both made of real materials with finite permittivity and conductivity at all frequencies as is the case in any real experimental setting. The net force density per unit transverse area acting on the slab is found by first placing the source (i.e. $z'$) in one of the gaps and calculate the resulting Green's function in this gap. This yields the attraction the stack of layers to the left and right of this gap exert upon each other. The procedure is then repeated with respect to the other gap region and the net force on the slab found as the difference between the two.

The solution of (8) may be written down directly, yielding in the case where $z'$ lies in the gap region to the left of the slab

$$g_{xx} = \begin{cases} A\,\mathrm{e}^{\kappa_1 z} & z < 0 \\ C_1\,\mathrm{e}^{\kappa_g z} + C_2\,\mathrm{e}^{-\kappa_g z} + G\,\mathrm{e}^{-\kappa_g |z - z'|} & 0 < z < a^+ \\ E_1\,\mathrm{e}^{\kappa_2 z} + E_2\,\mathrm{e}^{-\kappa_2 z} & a^+ < z < a^+ + b \\ D_1\,\mathrm{e}^{\kappa_g z} + D_2\,\mathrm{e}^{-\kappa_g z} & a^+ + b < z < c \\ B\,\mathrm{e}^{-\kappa_1 z} & z > c \end{cases} \tag{11}$$

with $G = -\kappa_g/(2\epsilon_g\mu_g)$. The 'constants' $A$ to $E$ are $z'$-dependent. From standard conditions of EM field continuity and (4*a*) and (4*b*) one may show that $g_{xx}$ and $(\epsilon/\kappa^2)\partial_z g_{xx}$ are continuous across interfaces, giving a total of eight equations which are solved with respect to $C_1$ and $C_2$ yielding after lengthy but straightforward calculation (for details, cf [54]) the solution in the left hand gap ($0 < z < a^+$, denoted by superscript +)

$$g_{xx}(+) = -\frac{\kappa_g}{2\epsilon_g}\left\{\frac{1}{d_{\mathrm{TM}}^+}\left[2\cosh\kappa_g(z - z') + \frac{\mathrm{e}^{\kappa_g(z+z')}}{\Delta_1^{\mathrm{TM}}} + \Delta_1^{\mathrm{TM}}\,\mathrm{e}^{-\kappa_g(z+z')}\right] + \Delta_1^{\mathrm{TM}}\,\mathrm{e}^{-\kappa_g(z+z')}\right\}.$$

Here and henceforth the inhomogeneous $|z - z'|$-term has been omitted subsequent to other calculation as argued above. Foreknowingly, we have defined the key quantities

$$\frac{1}{d_q^\pm} = \frac{U_q^\mp\,\mathrm{e}^{-2\kappa_g a^\pm}}{V_q^\mp - U_q^\mp\,\mathrm{e}^{-2\kappa_g a^\pm}}, \qquad q = \{\mathrm{TE}, \mathrm{TM}\} \tag{12}$$

where

$$U_q^\pm = \Delta_{1q}\Delta_{2q}\left(1 - \Delta_{1q}\Delta_{2q}\,\mathrm{e}^{-2\kappa_g a^\pm}\right) - \Delta_{1q}\left(\Delta_{2q} - \Delta_{1q}\,\mathrm{e}^{-2\kappa_g a^\pm}\right)\mathrm{e}^{-2\kappa_2 b},$$
$$V_q^\pm = 1 - \Delta_{1q}\Delta_{2q}\,\mathrm{e}^{-2\kappa_g a^\pm} - \Delta_{2q}\left(\Delta_{2q} - \Delta_{1q}\,\mathrm{e}^{-2\kappa_g a^\pm}\right)\mathrm{e}^{-2\kappa_2 b},$$

using the single-interface Fresnel reflection coefficients

$$\Delta_{i,q} = \frac{\kappa_i - \gamma_{i,q}\kappa_g}{\kappa_i + \gamma_{i,q}\kappa_g}, \qquad \gamma_{i,q} = \begin{cases} \mu_i/\mu_g, & q = \text{TE} \\ \epsilon_i/\epsilon_g, & q = \text{TM}, \end{cases} \qquad i = 1, 2. \tag{13}$$

Note already how the quantity $(d^{\pm})^{-1}$ is a generalization of the quantity $d^{-1}$ as it was defined for the three-layer system by Schwinger *et al* [8, 52] (dubbed $\Delta$ in the Lifshitz *et al* literature). In the limit $\kappa_2 \to \kappa_g$ we immediately get $\left(d_q^{\pm}\right)^{-1} \to \left(\Delta_{1q}^{-2}\,\mathrm{e}^{2\kappa_g c} - 1\right)^{-1}$, i.e. the three-layer standard result for a cavity of width $c$ with no slab.

Following the above described procedure we get

$$g_{zz}(+) = \frac{k_\perp^2}{2\kappa_g\epsilon_g}\left\{\frac{1}{d_{\text{TM}}^+}\left[2\cosh\kappa_g(z-z') - \frac{\mathrm{e}^{\kappa_g(z+z')}}{\Delta_1^{\text{TM}}} - \Delta_1^{\text{TM}}\,\mathrm{e}^{-\kappa_g(z+z')}\right] + \Delta_1^{\text{TM}}\,\mathrm{e}^{-\kappa_g(z+z')}\right\}.$$

Exactly the same procedure as for $g_{xx}$ is followed to obtain the $yy$-component. One finds that $g_{yy}$ and $\mu^{-1}\partial_z g_{yy}$ are continuous across boundaries, giving eight new equations solved as above to yield:

$$g_{yy}(+) = \frac{\mu_g}{2\kappa_g}\frac{\omega^2}{c^2}\left\{\frac{1}{d_{\text{TE}}^+}\left[2\cosh\kappa_g(z-z') - \frac{\mathrm{e}^{\kappa_g(z+z')}}{\Delta_1^{\text{TE}}} - \Delta_1^{\text{TE}}\,\mathrm{e}^{-\kappa_g(z+z')}\right] - \Delta_1^{\text{TE}}\,\mathrm{e}^{-\kappa_g(z+z')}\right\}.$$

The results for the right-hand $(-)$ gap is found by transforming the above results according to $a^{\pm} \to a^{\mp}$ and $z \to c - z, z' \to c - z'$.

To obtain the force density on each side of the slab, the solutions are now inserted into (5). One may show [54] that the terms depending on $z + z'$ do not contribute to the force density (this is a subtle point which will be discussed further below). Upon omitting these terms, the right-hand expressions are simply given by swapping + and − indices everywhere and we are left with the *effective* Green's function solution in the $\omega, k_\perp$-domain:

$$g_{xx}(\pm) = -\frac{\kappa_g}{\epsilon_g}\frac{1}{d_{\text{TM}}^{\pm}}\cosh\kappa_g(z-z') \tag{14a}$$

$$g_{yy}(\pm) = \frac{\omega^2\mu_g}{c^2\kappa_g}\frac{1}{d_{\text{TE}}^{\pm}}\cosh\kappa_g(z-z') \tag{14b}$$

$$g_{zz}(\pm) = \frac{k_\perp^2}{\kappa_g\epsilon_g}\frac{1}{d_{\text{TM}}^{\pm}}\cosh\kappa_g(z-z'). \tag{14c}$$

Upon insertion into (5) we find the force on either side of the slab yielding the net Casimir pressure acting on the slab towards the right as

$$\mathcal{F}^0(a^+, a^-; b, c) = \frac{\hbar}{2\pi^2}\int_0^\infty \mathrm{d}\zeta \int_0^\infty \mathrm{d}k_\perp \cdot k_\perp\kappa_g \sum_{q=\text{TE}}^{\text{TM}}\left(\frac{1}{d_q^-} - \frac{1}{d_q^+}\right). \tag{15}$$

Naturally, the force will always point away from the centre position. Superscript 0 here denotes that the expression is taken at zero temperature. The finite temperature expression, as is well known, is found by replacing the frequency integral by a sum over Matsubara frequencies according to the transition

$$\hbar\int_0^\infty \frac{\mathrm{d}\zeta}{2\pi} f(\mathrm{i}\zeta) \to k_B T \sum_{m=0}^{\infty\,\prime} f(\mathrm{i}\zeta_m), \qquad \mathrm{i}\zeta_m = \mathrm{i}(2\pi k_B T/\hbar)\cdot m$$

yielding

$$\mathcal{F}^T(a^+, a^-; b, c) = \frac{k_B T}{\pi}\sum_{m=0}^{\infty\,\prime}\int_0^\infty \mathrm{d}k_\perp \cdot k_\perp\kappa_g \sum_{q=\text{TE}}^{\text{TM}}\left(\frac{1}{d_q^-} - \frac{1}{d_q^+}\right). \tag{16}$$

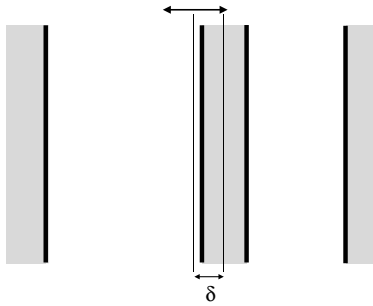


**Figure 2.** The slab oscillates about the cavity midline. We imagine a spring is attached to the slab exercising a Hooke-force towards the equilibrium position.

The prime on the summation mark denotes that the zeroth term is given half weight as is conventional.

Rather than painstakingly solving the eight continuity equations to obtain the Green's function as above, the result (15) is found much more readily using a powerful procedure following Tomaš as presented recently by one of us [20]. The above result was obtained by Tomaš [55] presumably using this procedure. It was worth going through the above calculations, however, for the sake of shedding light on some in our opinion non-trivial details which are often tacitly bypassed.

## 3. Casimir measurement by means of an oscillating slab

Equation (16) may be written on a more handy form in terms of the distance $\delta$ from the centre of the slab to the midline of the cavity as depicted in figure 2. We introduce the system parameter $h = c - b = a^+ + a^-$ and substitute according to $a^\pm = h/2 \pm \delta$. With some straightforward manipulation we are able to write (16) as

$$\mathcal{F}^T(\delta; b, c) = \frac{k_B T}{\pi} {\sum_{m=0}^{\infty}}' \int_0^\infty \mathrm{d}k_\perp \cdot k_\perp \kappa_g \sum_{q=\mathrm{TE}}^{\mathrm{TM}} \frac{A_q \sinh 2\kappa_g \delta}{B_q - A_q \cosh 2\kappa_g \delta} \tag{17}$$

with

$$A_q = 2\Delta_{1q}\Delta_{2q}(1 - \mathrm{e}^{-2\kappa_2 b})\,\mathrm{e}^{-\kappa_g h},$$
$$B_q = 1 - \Delta_{2q}^2\,\mathrm{e}^{-2\kappa_2 b} + \Delta_{1q}^2\left(\Delta_{2q}^2 - \mathrm{e}^{-2\kappa_2 b}\right)\mathrm{e}^{-2\kappa_g h}.$$

We write the force on the slab at finite temperatures as a Taylor expansion to first order in $\delta$ as

$$\mathcal{F}^T(\delta; b, c) = a_1 \delta + \mathcal{O}(\delta^3) \tag{18}$$

with

$$a_1(T; b, c) = \frac{2k_B T}{\pi} {\sum_{m=0}^{\infty}}' \int_0^\infty \mathrm{d}k_\perp \cdot k_\perp \kappa_g^2 \sum_{q=\mathrm{TE}}^{\mathrm{TM}} \frac{A_q}{B_q - A_q}. \tag{19}$$

Assume now the slab is attached to a spring with spring constant $k$ per unit transverse area. For small $\delta$ we may assume the slab to oscillate in a harmonic fashion (assuming $k > a_1$ now) with frequency given by Newton's second law as

$$\Omega = \Omega_0 - \Delta\Omega(T) = \sqrt{\frac{k - a_1(T)}{m}},$$

where $\Omega_0 = \sqrt{k/m}$ and $m$ is the mass of the slab per unit transverse area. In the case that $k \gg a_1$ we get

$$\Delta\Omega(T) \approx \frac{a_1(T)}{2\sqrt{km}} = \Omega_0 \frac{a_1(T)}{2k}.$$

We show by numerical calculation in section 5 how the Taylor coefficient $a_1(T)$ varies significantly with $T$ rendering an oscillating slab-in-cavity setup possibly suitable for future experimental investigation of the true temperature dependence of the Casimir force.

The setup as described is somewhat reminiscent of the setup currently employed by Onofrio and co-workers in Grenoble [50] where plates mounted on a double torsion balance are attracted to a pair of fixed plates. In their planned experiment, the distance from plate to wall will however kept constant during force measurements. Indeed, a double torsion balance might be one way of envisioning an experimental realization essentially equivalent to the system described (if thickness corrections are neglected) if the plates are mounted such that when one pair of plates approach each other, separation is increased between the pair on the opposite side of the pendulum. An even closer relative might be the recent experiments in Colorado where perturbations of the eigenfrequency of a magnetically trapped Bose–Einstein substrate in the vicinity of a surface provides a sensitive force measurement technique [5, 30, 51]. Both of these experiments involve a plate (in the widest sense) attracted to a wall on only *one* side; an 'open cavity'.

While a one-sided configuration is possibly experimentally simpler, there are two physical advantages of the sandwich geometry as presented here: the frequency shift $\Delta\Omega(T)$ is essentially twice as large using a closed cavity and, perhaps more importantly, in a symmetrical geometry the harmonical approximation ($\mathcal{F}^T \propto \delta$) is accurate for larger deviations $\delta$ from the equilibrium position than is the case for an open geometry. These points are elaborated further in appendix.

## 4. Fundamental discussion: two-point functions and Green's functions

In the standard Casimir literature there are two famous and somewhat different derivations of the classical Lifshitz expression[5], namely that of Lifshitz and co-workers in 1956–1961 [15, 17] and that of Schwinger and co-workers some years later [8, 52]. The two both make use of a Green's two-point function but in two different ways which upon comparison seem somewhat contradictory at first glance. Understanding how they relate to each other is not trivial in our opinion.

In order to calculate the force acting on an interface between two different media, both schools calculate what in our coordinates is the $zz$ component of the Abraham–Minkowski energy–momentum tensor as described above using the Green's function through the fluctuation–dissipation theorem as in (4*a*) and (4*b*). Lifshitz argues as recited above that in his formalism some terms of the Green's function (those dependent on $z + z'$) make no contribution to the force[6]. These are consequently omitted, leaving an *effective* Green's function. Schwinger *et al*, however, make use of the *entire* Green's function ultimately arriving at an expression similar to (5) in which the $z + z'$ terms *are* included and indeed necessary in order to reproduce Lifshitz' result. The $|z - z'|$-dependent source term is geometry independent and eventually omitted in both references.

[5] By 'Lifshitz force' is henceforth meant the Casimir force between two plane parallel (magneto) dielectric half-spaces separated by a medium different from both. By the 'Lifshitz expression' is meant the mathematical expression for this force as derived by Lifshitz and co-workers [21].

[6] This is shown formally in [54].

To solve the paradox we recognize one important difference between the two procedures: Lifshitz takes the limit $\boldsymbol{r} \to \boldsymbol{r}'$ so that $\boldsymbol{r}$ and $\boldsymbol{r}'$ are both on the same side of one of the sharp interfaces, whereas in Schwinger's method, $\boldsymbol{r}$ is on one side whilst $\boldsymbol{r}'$ is on the other. By using continuity conditions for the EM field, calculations can be carried out with analytic knowledge of the Green's function only on one side of the interface in both cases, thus masking this principal difference. Remembering that $T_{zz}$ is the density of momentum flux in the $z$-direction, the physical difference between the methods is that whilst Lifshitz calculates the force density as the *net* stream of momentum into one side of the interface, Schwinger *et al*'s expression represents the *entire* stream into one side minus the entire stream out of the other side. Due to conservation of momentum, the procedures are physically equivalent.

The question remains how to interpret the terms dependent on $z + z'$. Arguably, the absolute value of such terms must be arbitrary, since they will depend on the position of an arbitrarily placed origin[7]. Furthermore, since these terms cancel each other perfectly in (5), one may think of them as representing an isotropic flux of photonic momentum, flowing in equal amounts in both directions along the $z$-axis, giving rise to no measurable effect *inside a homogeneous medium*.

Schwinger, however, insists $\boldsymbol{r}$ and $\boldsymbol{r}'$ lie infinitesimally close to *either side* of an interface. While the $z + z'$ terms cancel each other when all calculated in the same medium, their values depend on $\epsilon$ and $\mu$, so when $\epsilon \neq \epsilon'$ or $\mu \neq \mu'$, their net contribution is finite.

This is exactly made up for in Lifshitz' approach by the fact that a sudden change in permittivity and permeability (such as at an interface between a dilute and an opaque medium) causes some of the radiation to be reflected off the interface in accordance with Fresnel's theory. Thus although $z$ and $z'$ both lie inside the same medium, there is a net flow of momentum either out of (attractive) or into (repulsive) the gap giving rise to a Casimir force. Such an analysis of the use of Green's functions gives way for an understanding of how three different representations of the Casimir effect come together; the derivation by Lifshitz starting from photonic propagators in quantum electrodynamics, that by Schwinger *et al* based on Green's function calculations from classical electrodynamics and a third approach based on Fresnel theory which we may refer to as the 'optical approach' (originally in form of non-retarded Van der Waals theory [56, 57], recently revisited by Scardicchio and Jaffe; see [58] and references therein).

We showed that the factors $\left(d_q^{\pm}\right)^{-1}$ were generalized versions of the factors denoted by $d^{-1}$ and $(d')^{-1}$ in Schwinger *et al*'s theory for the three-layer model. These are both special cases of a more general quantity

$$\frac{1}{d_q} = \frac{r_{q\mathrm{L}} r_{q\mathrm{R}}\, \mathrm{e}^{-2\kappa_g a}}{1 - r_{q\mathrm{L}} r_{q\mathrm{R}}\, \mathrm{e}^{-2\kappa_g a}}$$

pertaining to a gap of width $a$ separating planar bodies to the left (L) and right (R) of it whose Fresnel reflection coefficients are $r_{q\mathrm{L}}$ and $r_{q\mathrm{R}}$ respectively. If the media are infinitely large and homogeneous media indexed 1 and 2 respectively, say, $r_{q\mathrm{L}}$ and $r_{q\mathrm{R}}$ are simply $-\Delta_{1q}$ and $-\Delta_{2q}$ from (13); if the bodies are more complex, e.g. has a multilayered structure, their corresponding Fresnel coefficients will be more complicated. This is discussed in detail in [20]. An EM plane wave with momentum $\hbar\mathbf{k}$ is described as $\mathrm{e}^{\mathrm{i}(\mathbf{k}_\perp \cdot \mathbf{r}_\perp + k_z z)}$. In medium $g$, furthermore, $k_z = \mathrm{i}\kappa_g$ according to Maxwell's equations, i.e. the wave is evanescent in the $z$-direction if $k_\perp^2 > \epsilon_g \mu_g \omega^2/c^2$ (otherwise propagating). After frequency rotation $\omega^2 \to -\zeta^2$

[7] The notion of arbitrarily large energy densities, of course, is not foreign to Casimir calculations; Casimir's original calculation involved the difference between the apparently infinite energy density of the zero-point photon field in the absence and presence of perfectly conducting interfaces.

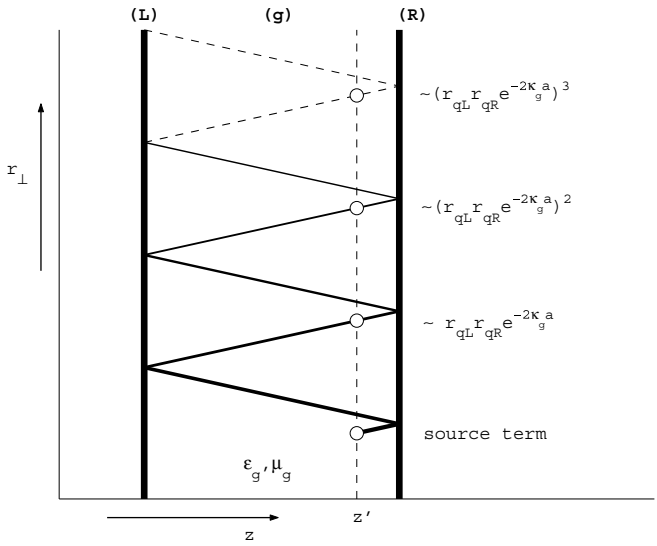


**Figure 3.** Contributions to $\overleftrightarrow{\mathbf{g}}$ in a gap between two bodies in the optical visualization. The distance between the bodies is $a$. Each term has a weight factor as shown on the right-hand side. The sum of the infinitely many reflections of a $q$-polarized wave is $d_q^{-1}$.

this is always true ($k_\perp$ is assumed real), so *every* wave is described as an evanescent wave. The attenuation of an EM field of frequency $i\zeta$ propagating a distance $l$ along the $z$-axis in medium $g$ is $\exp(-\kappa_g l)$, so one readily shows that $d_q^{-1}$ is the sum of *relative amplitudes* of the electric fields having travelled all paths starting and ending at the same $z$-coordinate and with the same direction:

$$\frac{1}{d_q} = r_{q\mathrm{L}} r_{q\mathrm{R}}\, \mathrm{e}^{-2\kappa_g a} + (r_{q\mathrm{L}} r_{q\mathrm{R}}\, \mathrm{e}^{-2\kappa_g a})^2 + \cdots = \sum_{n=1}^{\infty} (r_{q\mathrm{L}} r_{q\mathrm{R}}\, \mathrm{e}^{-2\kappa_g a})^n.$$

An illustration of this is found in figure 3. Since the phase shift from propagation in the $\perp$ direction is disregarded in this respect, one might think of $d_q^{-1}$ as a sum over all *closed* paths, parallel to the $z$-axis and starting and ending in the same point.

Considering again the expressions for the complete Green's functions $g_{xx}$, $g_{yy}$ and $g_{zz}$ in section 2, we see that the last terms of all three components are the only ones not multiplied by a factor $d_q^{-1}$ (indices $\pm$ suppressed). Since this factor is the only part of $\overleftrightarrow{\mathbf{g}}$ containing geometry information, the last term is geometry independent, and can obviously make no contribution to a physical force. Hence, all contributing terms are proportional with $d_q^{-1}$ which leads us to the conclusion that the Casimir attraction between bodies on either side of a gap region at a given temperature depends solely on the extent to which some EM field originating in the gap, stays in the gap.

To sum it all up, we argued that Schwinger's classical Green's function as introduced is the exact macroscopic analogy of Lifshitz' QED propagator according to Bohr's correspondence principle. In its Fourier transformed form it expresses the probability amplitude that an electric field which has transverse momentum $\hbar\mathbf{k}_\perp$, energy $\hbar\omega$ and coordinate $z'$ will give rise to a field of the same energy and momentum at $z$. When then $z$ and $z'$ are only infinitesimally different, the only way this can happen by classical reasoning is that the two are in fact exactly the same

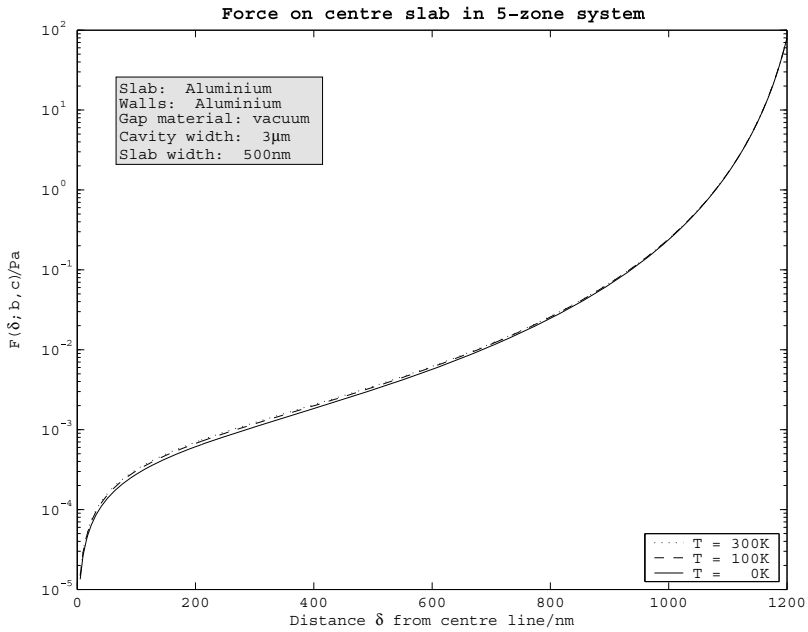


**Figure 4.** The force on an Al slab in a vacuum-filled cavity between Al walls. $\delta$ is the distance from the centre of the slab to the midline of the cavity. For negative $\delta$ one gets the antisymmetrical extension of the graph.

(corresponding to the $|z - z'|$-dependent source term) or that the field has been reflected off both walls once or more. This is what figure 3 demonstrates.

## 5. Numerical investigation and temperature effects

For our numerical calculations, we have used permittivity data for aluminium, gold and copper supplied by Astrid Lambrecht (personal communication). For ease of comparison, aluminium is used in figures throughout; all variations acquired by replacing one metal by another are of a quantitative, not qualitative nature, and are not included here. In all our numerical investigations, we have assumed non-magnetic media, i.e. $\mu_1 = \mu_2 = \mu_g = 1$.

As an example of a dielectric, we have chosen teflon-fluorinated ethylene propylene (teflon FEP) because its chemical and physical properties are remarkably invariant with respect to temperature. Permittivity data for teflon FEP are taken from [59].

Figure 4 shows the Casimir force acting on a relatively thick aluminium slab in a cavity as a function of $\delta$. For negative values of $\delta$ the situation is identical but the force has the opposite direction. We have chosen a gap width of 3 $\mu$m and a slab thickness of 500 nm. These values are not arbitrary: first, the relative temperature corrections of the Casimir force are predicted to be large at plate separations of 1–3 $\mu$m, so a slab-to-wall distance in this region is desirable (here $h/2 = 1250$ nm). Secondly, choosing the slab significantly thicker than the penetration depth of the EM field makes the five-zone geometry instantly comparable to the well-known three-zone Lifshitz geometry of two half-spaces; for slabs of a good metal thicker than $\sim$50 nm there is virtually no difference between the five-zone expression as derived above and that

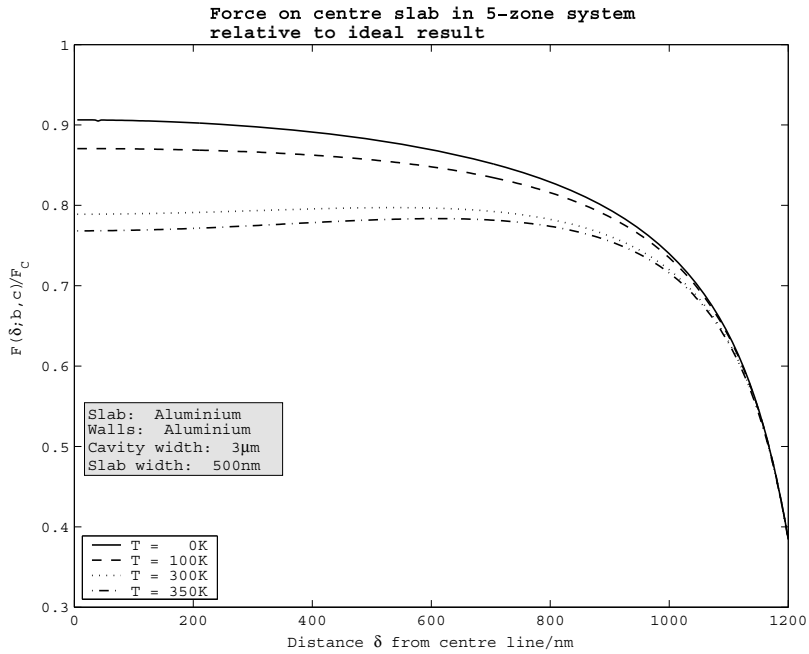


**Figure 5.** The force on an Al slab in a vacuum-filled cavity between Al walls relative to its value for ideally conducting slab and walls, equation (20). $\delta$ is the distance from the centre of the slab to the midline of the cavity. For negative $\delta$ one gets the symmetrical extension of the graph.

which one would acquire applying the standard Lifshitz expression to each gap in turn and finding the net force density on the slab as the difference between the two.

Figure 5 shows the net vacuum pressure acting on the slab relative to Casimir's result for ideal conductors,

$$\mathcal{F}_{\mathrm{C}} = \frac{\hbar c \pi^2}{240}\left[\frac{1}{(h/2-\delta)^4} - \frac{1}{(h/2+\delta)^4}\right]. \tag{20}$$

In such a plot we see clearly how a slab and cavity set-up might be suitable for measurements of temperature effects; whereas such effects are small for very small separations, they grow most considerable near the centre position where slab-to-wall distance is in the order of a micrometre.

An altogether different result is obtained upon replacing metal with a dielectric in both walls and slab. In figure 6 the same calculation as in figure 5 has been performed with both slab and walls of teflon FEP. Casimir experiments using dielectrics were proposed by Torgerson and Lamoreaux [60] where the use of diamond was suggested.

It is important to note here that we have not taken into account variations of the dielectric properties of teflon FEP with temperature; much as teflon FEP is renowned for its constancy in electrical and chemical properties over a large temperature range and is used in space technology for this very reason, one must assume there are corrections at extremely low temperatures. We shall not enter into a discussion on material properties here; the point to take on board is rather that temperature effects are found to be very large indeed near the centre position, a fact that does not change should the calculated values be several percent off.

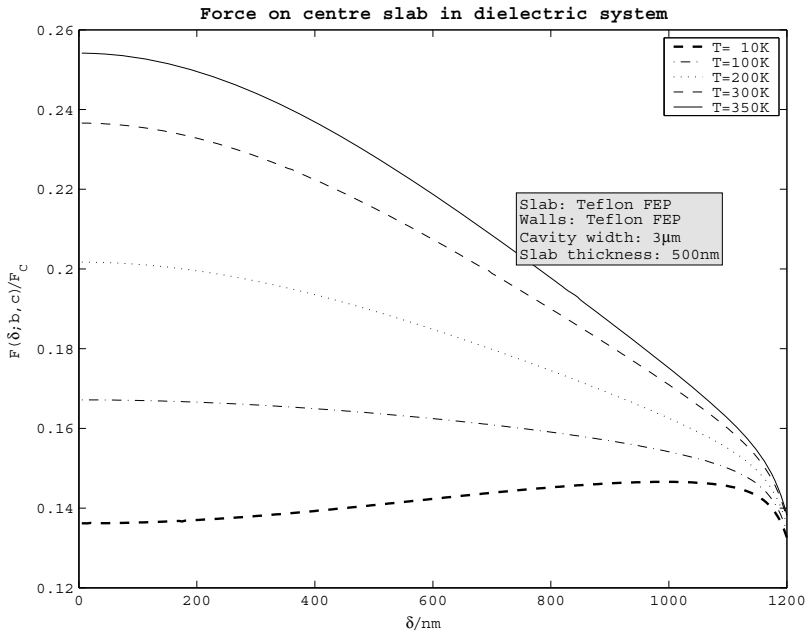


**Figure 6.** The force on a teflon FEP slab in a vacuum-filled cavity between teflon FEP walls relative to the result for ideally conducting slab and walls, equation (20). Note that dielectric properties are assumed constant with temperature.

This strongly indicates that the use of dielectrics in Casimir experiments could be an excellent means of measuring the still controversial temperature dependence of the force.

We note furthermore that whilst for metals the force decreases with rising temperatures, the opposite is the case for the dielectric. Mathematically this is readily explained from e.g. (16). Temperature enters into the expression in two ways; first, each term of the Matsubara sum has a prefactor $T$, secondly the distancing of the discrete imaginary frequencies increases linearly with $T$. The first dependence tends to increase the force with respect to $T$ whilst the other decreases it (bearing in mind that the integrand, which is proportional with $\exp(-\kappa_g h)$, decreases rapidly with respect to $\zeta$ for $\zeta$ larger than roughly the $m = 1$ Matsubara frequency at room temperature). As temperature rises, thus, the higher order terms of the sum quickly become negligible, leaving the first few terms to dominate[8]. In the high temperature limit, $m = 0$ becomes the sole significant term and the force becomes proportional[9] to $T$. This is true for metals and dielectrics alike, but while the trend is seen at low temperatures for dielectrics, for metals the $T$-linear trend typically becomes visible only at temperatures much higher than room temperature. In metals the low (nonzero) frequency terms are boosted since $\epsilon_i \gg \epsilon_g$ for $\zeta$ much smaller than the plasma frequency, in which case reflection coefficients $|\Delta_{iq}|$ approximately equal unity. The first few Matsubara terms thus remain significant as temperature rises, countering the $T$-proportionality effect, at the same time as each $m > 0$ term decreases in value as the Matsubara frequencies take higher values, allowing the resulting force to decrease with increasing temperature.

[8] The same phenomenon for increasing distances rather than temperatures is treated in [62].

[9] For the three-layer Lifshitz set-up, the zero term and thus the force becomes proportional to $T/a^3$ where $a$ is the gap width, as shown formally in [11].

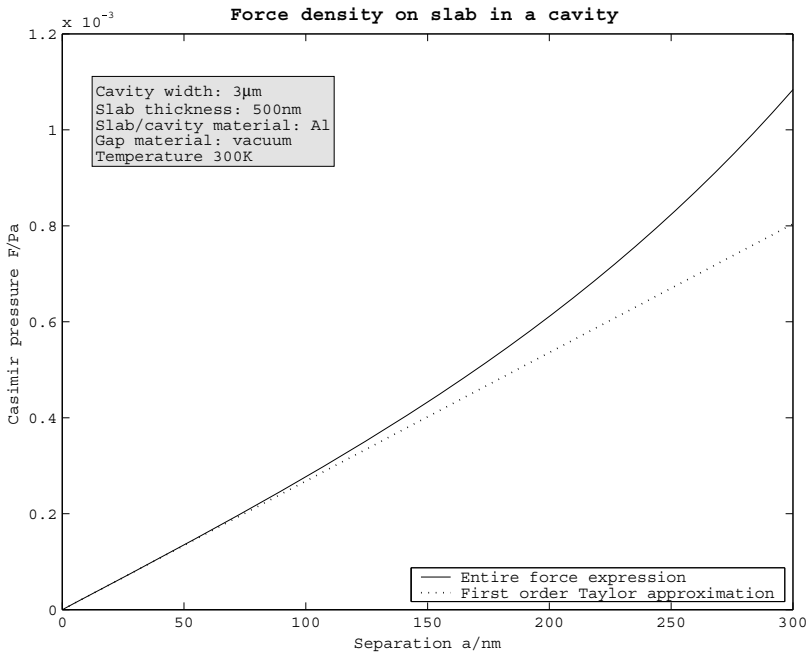


**Figure 7.** The Casimir force density on the slab of figure 1 as a function of the distance $\delta$ from the centre of the slab to the cavity midline as compared to its first-order Taylor expansion, equation (18) at temperature 300 K.

Figure 7 shows the force acting on the slab in the previously described geometry (such as plotted in figure 4) as well the first-order Taylor expansion. The figure gives a rough idea as to the size of the central cavity region in which one may regard the force density as linear with respect to $\delta$. With the system parameters as chosen we see that, depending on precision one may allow oscillation amplitudes $\delta$ of several tens of nanometres, a length which is not small relative to the system.

The first-order Taylor coefficient itself has been calculated and plotted in figure 8 for aluminium and teflon FEP slabs in an aluminium cavity. These are furthermore compared to Casimir's ideal result (20) whose first-order Taylor coefficient is readily found to be

$$a_{1\mathrm{C}} = \frac{16\hbar c\pi^2}{15} h^{-5} \approx 3.3283 \times 10^{-25}\ \mathrm{N\,m^2}\ h^{-5}. \tag{21}$$

## 6. The effect of finite slab thickness

As measurements of the Casimir force have become drastically more accurate over the last few years, with researchers claiming to reproduce theoretical results to within 1% [3, 22], it is well worth asking whether any *theoretical* calculation may rightly claim such an accuracy. A point of particular interest in this respect is the strong dependence of the Casimir force on the permittivity of the media involved. The permittivity data for aluminium, copper and gold supplied by Lambrecht and Reynaud were calculated by using experimental values for the susceptibility at a wide range of real frequencies (approx. $1.5 \times 10^{14}$ rad s$^{-1}$ $< \omega <$ $1.5 \times 10^{19}$ rad s$^{-1}$), extrapolating towards zero frequency by means of the Drude relation (for small

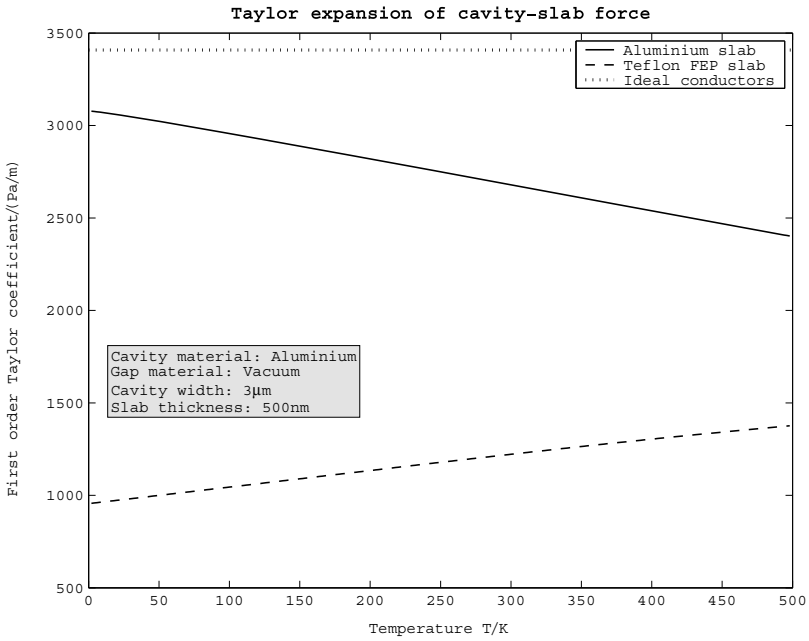


**Figure 8.** The first-order Taylor coefficient of equation (18) for aluminium and teflon FEP slabs in an Al cavity. The horizontal dotted line is the coefficient pertaining to the Casimir result for ideal conductors (both slab and walls), equation (21). One should note that the dielectric properties of the materials at extremely low temperatures are not known.

$\omega <$ approx $1.5 \times 10^{14}$ rad s$^{-1}$). $\epsilon(\omega)$ was subsequently mapped onto the imaginary frequency axis invoking Kramers–Kronig relations numerically. Thus, although matching theoretical values (Drude mode l) excellently for imaginary frequencies up to about $10^{15}$ rad s$^{-1}$ [24], the data have intrinsic uncertainties. Recently, Lambrecht and co-workers addressed the question of the uncertainty related to calculation of the Casimir force due to uncertainty in the Drude parameters used for extrapolation, found to add up to as much as 5%, considerably more than the accuracy claimed for the best experiments to date [61].

The effect of the 'leakage' of vacuum radiation from one gap region to the other in our five-zone geometry is worth a brief investigation in this context. Excepting the zero frequency term, it is unambiguous from e.g. the definition of $\kappa$ that when the slab is metallic, the factor $\exp(-2\kappa_2 b)$ is small compared to unity for sufficiently large values of $b$, due to the large values of $\epsilon_2$ for all important frequencies $i\zeta$ [10]. Let us regard one of the gap regions, of index $\pm$. With some manipulation one may expand (12) to first order in the factor $\exp(-2\kappa_2 b)$ to find the pertaining quantity

$$\frac{1}{d_q^{\pm}} = \frac{\Delta_{1q}\Delta_{2q}\,\mathrm{e}^{-2\kappa_g a^{\pm}}}{1-\Delta_{1q}\Delta_{2q}\,\mathrm{e}^{-2\kappa_g a^{\pm}}} - \mathrm{e}^{-2\kappa_2 b}\frac{\Delta_{1q}\left(1-\Delta_{2q}^2\right)\mathrm{e}^{-2\kappa_g a^{\pm}}}{\left(1-\Delta_{1q}\Delta_{2q}\,\mathrm{e}^{-2\kappa_g a^{\pm}}\right)^2} \cdot \frac{\Delta_{2q}-\Delta_{1q}\,\mathrm{e}^{-2\kappa_g a^{\mp}}}{1-\Delta_{1q}\Delta_{2q}\,\mathrm{e}^{-2\kappa_g a^{\mp}}} + \mathcal{O}(\mathrm{e}^{-4\kappa_2 b}). \tag{22}$$

[10] The $m = 0$ term is a subtle matter we shall not enter into here. For a recent review, see e.g. [29] and references therein.

The first term is immediately recognized as giving the Lifshitz expression for the Casimir attraction between two half-spaces of materials 1 and 2 separated by a gap of width $a^{\pm}$ and material $g$, and the second term is the first-order correction due to penetration of radiation through the slab.

In terms of $\delta$ we may write in the case where $\exp(-2\kappa_2 b) \ll 1$ for all relevant frequencies (again subsequent to some manipulation) the force on the slab as $\mathcal{F}^T(\delta) \approx \mathcal{F}^T_{\mathrm{L}} + \Delta\mathcal{F}^T$ where

$$\mathcal{F}^T_{\mathrm{L}}(\delta; h) = \frac{k_B T}{\pi} {\sum_{m=0}^{\infty}}' \int_0^{\infty} \mathrm{d}k_\perp k_\perp \kappa_g \sum_{q=\mathrm{TE}}^{\mathrm{TM}} \frac{A_{q\mathrm{L}} \sinh 2\kappa_g \delta}{B_{q\mathrm{L}} - A_{q\mathrm{L}} \cosh 2\kappa_g \delta}$$

is the result using the Lifshitz expression on both gaps and taking the difference; here

$$A_{q\mathrm{L}} \equiv 2\Delta_{1q}\Delta_{2q}\,\mathrm{e}^{-\kappa_g h} \qquad \text{and} \qquad B_{q\mathrm{L}} \equiv 1 + \Delta_{1q}^2\Delta_{2q}^2\,\mathrm{e}^{-2\kappa_g h}, \tag{23}$$

and

$$\Delta\mathcal{F}^T(\delta; h, b) = -\frac{k_B T}{\pi} {\sum_{m=0}^{\infty}}' \int_0^{\infty} \mathrm{d}k_\perp k_\perp \kappa_g \sum_{q=\mathrm{TE}}^{\mathrm{TM}} \mathrm{e}^{-2\kappa_2 b} \times \frac{A_{q\mathrm{L}}\left(B_{q\mathrm{L}} - \Delta_{2q}^2 - \Delta_{1q}^2\,\mathrm{e}^{-2\kappa_g h}\right) \sinh 2\kappa_g \delta}{(B_{q\mathrm{L}} - A_{q\mathrm{L}} \cosh 2\kappa_g \delta)^2}. \tag{24}$$

The factor $\exp(-2\kappa_2 b)$ and consequently the first-order correction is very sensitive with respect to even small changes in $\epsilon_2(\mathrm{i}\zeta)$. For very thin slabs ($b < 50$ nm) and small cavities, the correction could be in the order of magnitude of the currently claimed measurement accuracy. Furthermore, we see that the integrand of (24) depends on $\epsilon_2$ in an exponential way. In conclusion: to the extent that the thickness correction is of significance in an experimental measurement, exact knowledge of the permittivity as a function of imaginary frequency is of the essence. In such a scenario, approximate knowledge of the dispersion function could effectively limit our ability to even *calculate* the force with the precision that recent experiments claim to reproduce theory [22]. A calculation of the thickness correction for aluminium slab and walls is shown in figure 9.

In the case of dielectrics, as shown in figure 10, the correction is almost two orders of magnitude larger and should be readily measurable. Experiments in a geometry involving dielectric plates of finite thickness might even be a possible means of evaluating the correctness of the dielectric function employed.

## 7. Conclusion and final remarks

The main conclusion from the work presented is that from a theoretical point of view the five-zone setup (figure 1) as discussed could be ideal for detection of the temperature dependence of the Casimir force when the wall-to-slab distance is in the order of 1 $\mu$m. One method as suggested is a measurement of the difference in the eigenfrequency of an oscillating slab in the absence and presence of a cavity.

When metal is replaced by a dielectric in slab and walls, relative temperature corrections become much larger, suggesting that using dielectrics whose dielectric properties vary little with respect to temperature be excellent for such measurements.

Our treatment of the effect of finite slab thickness shows that the effect of finite thickness varies dramatically with respect to the properties of the materials involved, specifically $\epsilon$ and $\mu$. Much as the effect is generally quite small for metals, to the extent such effects do play a role

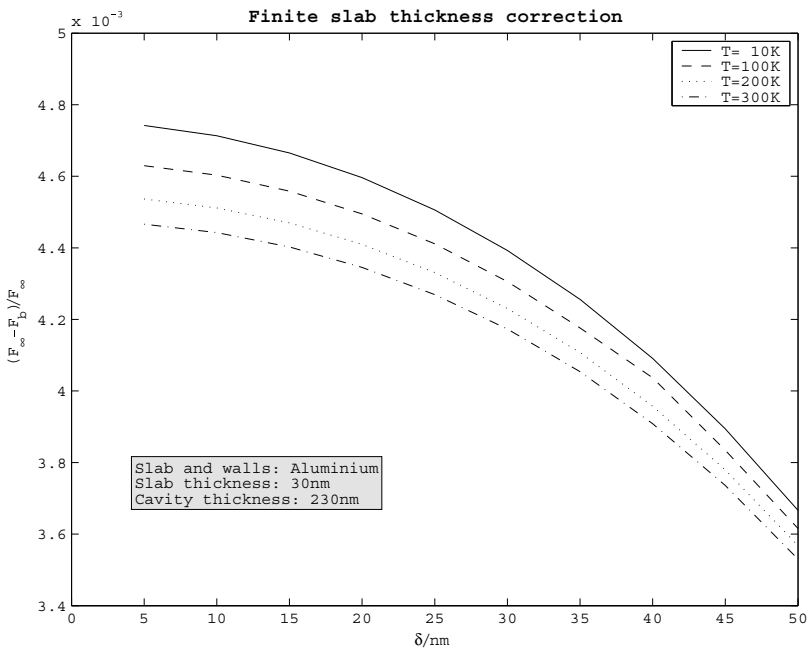


**Figure 9.** Thickness correction due to 'leakage' of radiation through a thin slab in a small cavity. The absolute value of the correction is approximately exponentially decreasing with the thickness $b$.

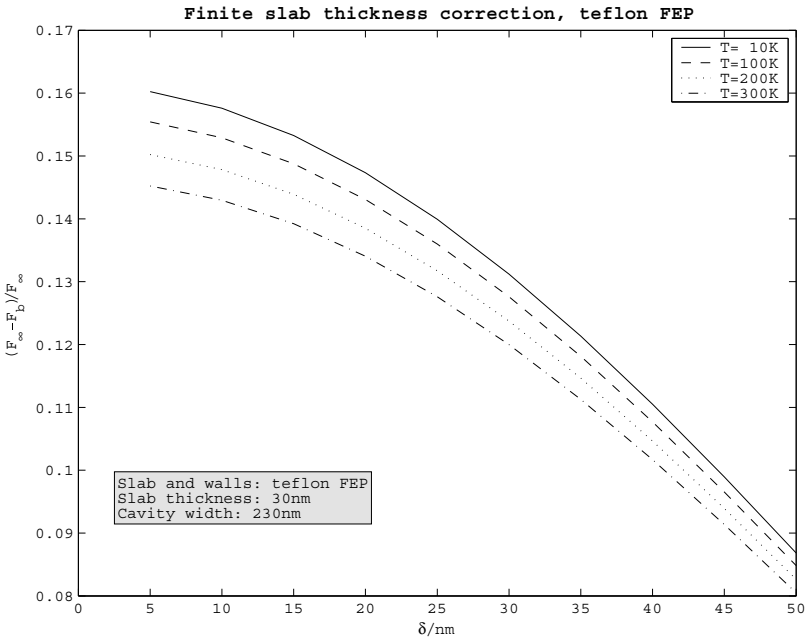


**Figure 10.** Thickness correction due for teflon FEP.

even a moderately good estimate of their exact magnitude requires very accurate dielectricity data for the material in question. This is but one example of the more general point that the still considerable uncertainties associated with the best available permittivity data for real materials call for soberness in any assessment of our ability to numerically calculate Casimir forces with great precision.

Finally, a couple of remarks: it ought to be pointed out that our proposed method of investigating the thermal Casimir force via observing the oscillations of a slab in a cavity, can be classified as belonging to the subfield usually called the 'dynamic Casimir effect'. The use of mechanical microlevers has turned out to be very effective components for high sensitivity position measurements, of interest even in the context of gravitational waves detection. As for the basic principles of the method see, for instance Jaekel *et al* [63] with further references therein, especially [64]. For more recent papers on microlevers, see [65–68].

Moreover, we note the connection between our approach and the statistical mechanical approach of Buenzli and Martin [69]. These authors computed the force between two quantum plasma slabs within the framework of non-relativistic quantum electrodynamics including quantum and thermal fluctuations of both matter and field. It was found that the difference in the predictions for the temperature dependence of the Casimir effect is satisfactorily explained by taking into account the fluctuations *inside* the material. Their predictions for the force are in agreement with ours.

**Acknowledgments**

Permittivity data for aluminium, gold and copper used in our calculations were kindly made available to us by Astrid Lambrecht and Serge Reynaud. We furthermore thank Valery Marachevsky for stimulating discussions and input, and Mauro Antezza for valuable correspondence.

## Appendix. Closed geometry versus open configuration

We will demonstrate briefly the two physical properties favouring a closed cavity configuration (figure 1) as compared to an open configuration in which a similarly oscillating plate is held in equilibrium by an external spring system. For the purpose of comparison we will disregard effects due to finite plate thickness, so that the net force experienced by a slab in a cavity is the difference between standard Lifshitz forces on both sides, whist that between plate and wall in a one-sided geometry (like figure 1 but with the right-hand wall removed) is simply the Lifshitz force. For separations of some hundred nanometres or more, the Lifshitz force varies as $\mathcal{F}_{\rm L}(d) \propto d^{-4}$. Thus the net force on the slab in the sandwich geometry attached to a spring of spring constant $k$ per unit transverse area is (we assume $k > \mathcal{F}(a)/\delta$ as before)

$$\begin{aligned}\mathcal{F}_{\rm sandwich} &= \mathcal{F}_{\rm L}(a+\delta) - \mathcal{F}_{\rm L}(a-\delta) - k\delta \\ &= \frac{\mathcal{F}_{\rm L}(a)}{(1+\delta/a)^4} - \frac{\mathcal{F}_{\rm L}(a)}{(1-\delta/a)^4} - k\delta \\ &= -\left[ka - 8\,|\mathcal{F}_{\rm L}(a)|\right]\frac{\delta}{a} + 40\,|\mathcal{F}_{\rm L}(a)|\,\frac{\delta^3}{a^3} + \cdots \end{aligned} \tag{A.1}$$

where $a = h/2$ is here the distance from slab to wall in equilibrium position ($\mathcal{F}_{\rm L}(d) < 0$).

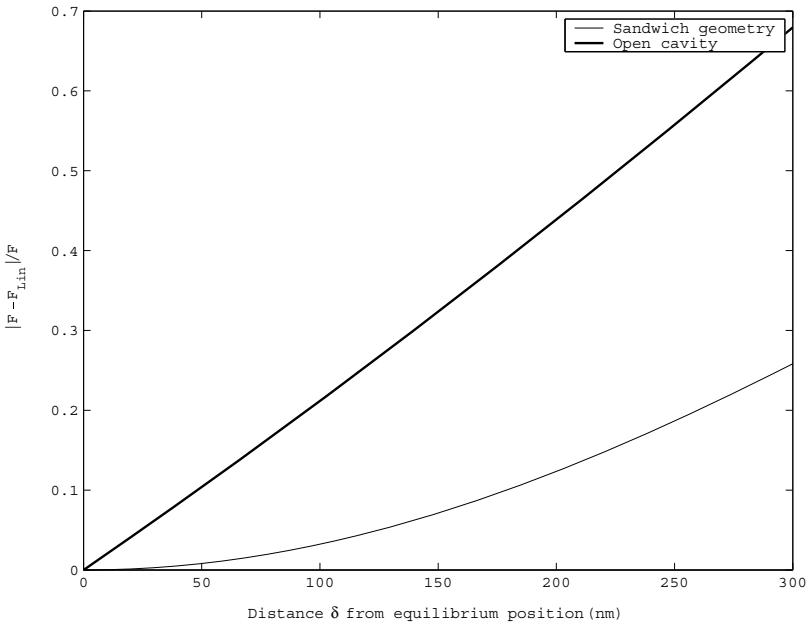


**Figure A1.** The relative correction to the linear Taylor expansion, $\mathcal{F}_{\rm Lin}$, of the Casimir force near equilibrium position for the open and closed geometries plotted for positive $\delta$. Calculations assume aluminium plate and walls, equilibrium plate-to-wall separation of $a = 1250$ nm in both configurations and temperature 300 K. For the sandwich geometry, $\mathcal{F}$ is given by (16) whilst in the open geometry $\mathcal{F} = \mathcal{F}_{\rm L}(a+\delta) - \mathcal{F}_{\rm L}(a)$ with $\mathcal{F}_{\rm L}$ the standard Lifshitz expression for the attraction between two half-spaces.

Now consider an open configuration in which a plate is held in equilibrium by an external spring, also of spring constant $k$ per unit transverse area. Assume that the forces are in equilibrium when the plate is a distance $a$ from the cavity wall. The net force on the plate is

$$\begin{aligned}\mathcal{F}_{\rm open} &= \mathcal{F}_{\rm L}(a+\delta) - \mathcal{F}_{\rm L}(a) - k\delta \\ &= -[ka - 4|\mathcal{F}_{\rm L}(a)|]\frac{\delta}{a} - 10|\mathcal{F}_{\rm L}(a)|\frac{\delta^2}{a^2} + \cdots . \end{aligned} \tag{A.2}$$

There are thus two properties that favour the closed geometry. First, the first-order perturbation of the spring constant is twice as large and second, that the leading-order correction to the harmonical approximation ($\mathcal{F}^T \propto \delta/a$) is cubical whist it is quadratic for the open configuration[11]. The closed geometry thus allows considerably larger deviations from equilibrium position at a given accuracy without taking non-harmonic effects into account. In figure A1 this is demonstrated by plotting the relative nonharmonic correction as a function of $\delta$ at a separation 1250 nm. In accordance with our results, the relative correction $(\mathcal{F} - \mathcal{F}_{\rm Lin})/\mathcal{F}$ is approximately linear for an open geometry $\left(\approx -\frac{5}{2}\frac{\delta}{a}\right)$ and approximately quadratic for a sandwich $\left(\approx 5\frac{\delta^2}{a^2}\right)$.

[11] Note that the specific assumption $\mathcal{F}_{\rm L}(d) \propto d^{-4}$ is not necessary for either of these results; they pertain almost exclusively to geometry. A more general power $\mathcal{F}_{\rm L}(d) \propto d^{-\sigma}$, $\sigma > 0$, say, gives the same properties.

## References


[1] Casimir H B G 1948 *Proc. K. Ned. Akad. Wet.* **51** 793
[2] Spaarnay M J 1958 *Physica* **24** 751
[3] Lamoreaux S K 2005 *Rep. Prog. Phys.* **68** 201
[4] Mohideen U and Roy A 1998 *Phys. Rev. Lett.* **81** 4549
[5] Harber D M, Obrecht J M, McGuirk J M and Cornell E A 2005 *Phys. Rev.* A **72** 033610
[6] Chan H B, Aksyuk V A, Kleinman R N, Bishop D J and Capasso F 2001 *Phys. Rev. Lett.* **87** 211801
[7] Chan H B, Aksyuk V A, Kleinman R N, Bishop D J and Capasso F 2001 *Science* **291** 1941
[8] Milton K A 2001 *The Casimir Effect: Physical Manifestation of Zero-Point Energy* (Singapore: World Scientific)
[9] Bordag M, Mohideen U and Mostepanenko V M 2001 *Phys. Rep.* **353** 1
[10] Milton K A 2004 *J. Phys. A: Math. Gen.* **37** R209
[11] Nesterenko V V, Lambiase G and Scarpetta G 2004 *Riv. Nuovo Cimento* **27** (6) 1
[12] 2006 *J. Phys. A: Math. Gen.* **39** (21) (Special issue: Papers Presented at the *7th Workshop on Quantum Field Theory under the Influence of External Conditions (QFEXT05) (Barcelona, Spain, 5–9 Sept. 2005)*
[13] 2006 *New J. Phys.* **8** (234) (Focus issue on Casimir Forces)
[14] Plunien G, Müller B and Greiner W 1986 *Phys. Rep.* **134** 87
[15] Lifshitz E M 1956 *Zh. Eksp. Teor. Fiz.* **29** 94
Lifshitz E M 1956 *Sov. Phys.—JETP* **2** 73 (Engl. Transl.)
[16] Høye J S, Brevik I, Aarseth J B and Milton K A 2003 *Phys. Rev.* E **67** 056116
[17] Lifshitz E M and Pitaevskii L P 1980 *Statistical Physics* Part 2 (Oxford: Pergamon)
[18] Tomaš M S 1995 *Phys. Rev.* A **51** 2545
[19] Mills D L and Maradudin A A 1975 *Phys. Rev.* B **12** 2943
[20] Ellingsen S A 2007 *J. Phys. A: Math. Theor.* **40** 1951 (*Preprint* quant-ph/0607157)
[21] Dzyaloshinskii I E, Lifshitz E M and Pitaevskii L P 1961 *Usp. Fiz. Nauk.* **73** 381
Dzyaloshinskii I E, Lifshitz E M and Pitaevskii L P 1961 *Sov. Phys. Usp.* **4** 153 (Engl. Transl.)
[22] Decca R S, López D, Fischbach E, Klimchitskaya G L, Krause D E and Mostepanenko V M 2005 *Ann. Phys. NY* **318** 37
[23] Brevik I, Aarseth J B, Høye J S and Milton K A 2005 *Phys. Rev.* E **71** 056101
[24] Bentsen V S, Herikstad R, Skriudalen S, Brevik I and Høye J S 2005 *J. Phys. A: Math. Gen.* **38** 9575
[25] Bezerra V B, Decca R S, Fischbach E, Geyer B, Klimchitskaya G L, Krause D E, López D, Mostepananko M and Romero C 2006 *Phys. Rev.* E **73** 028101
[26] Høye J S, Brevik I, Aarseth J B and Milton K A 2006 *J. Phys. A: Math. Gen.* **39** 6031
[27] Mostepanenko V M, Bezerra V B, Decca R, Geyer B, Fischbach E, Klimchitskaya G L, Krause D E, López D and Romero C 2006 *J. Phys. A: Math. Gen.* **39** 6589
[28] Brevik I and Aarseth J B 2006 *J. Phys. A: Math. Gen.* **39** 6187
[29] Brevik I, Ellingsen S A and Milton K A 2006 *New J. Phys.* **8** 236
[30] Obrecht J M, Wild R J, Antezza M, Pitaevskii L P, Stringari S and Cornell E A 2007 *Phys. Rev. Lett.* **98** 063201
[31] Antezza M, Pitaevskii L P and Stringari S 2005 *Phys. Rev. Lett.* **95** 113202
[32] Pitaevskii L P 2000 *Comments At. Mol. Phys.* **1** 363
[33] Brevik I 1979 *Phys. Rep.* **52** 133
[34] Brevik I 1986 *Phys. Rev.* B **33** 1058
[35] Møller C 1972 *The Theory of Relativity* 2nd edn (Oxford: Clarendon) section 7.7
[36] Kentwell G W and Jones D A 1987 *Phys. Rep.* **145** 319
[37] Antoci S and Mihich L 1998 *Eur. Phys. J.* **3** 205
[38] Obukhov Y N and Hehl F W 2003 *Phys. Lett.* A **311** 277
[39] Loudon R, Allen L and Nelson D F 1997 *Phys. Rev.* E **55** 1071
[40] Garrison J C and Chiao R Y 2004 *Phys. Rev.* A **70** 053826
[41] Feigel A 2004 *Phys. Rev. Lett.* **92** 020404
[42] Leonhardt U 2006 *Phys. Rev.* A **73** 032108
[43] Raabe C and Welsch D-G 2005 *Phys. Rev.* A **71** 013814
[44] Welsch D-G and Raabe C 2005 *Phys. Rev.* A **72** 034104
[45] Raabe C and Welsch D-G 2005 *J. Opt. B: Quantum Semiclass.* **7** 610
[46] Raabe C and Welsch D-G 2006 *Preprint* quant-ph/0602059
[47] Zhang J Z and Chang R K 1988 *Opt. Lett.* **13** 916
[48] Lai H M, Leung P T, Poon K L and Young K 1989 *J. Opt. Soc. Am.* B **6** 2430
[49] Brevik I and Kluge R 1999 *J. Opt. Soc. Am.* B **16** 976
[50] Lambrecht A, Nesvizhevsky V V, Onofrio R and Reynaud S 2005 *Class. Quantum. Grav.* **22** 5397

[51] McGuirk J M, Harber D M, Obrecht J M and Cornell E A 2004 *Phys. Rev.* A **69** 062905
[52] Schwinger J, DeRaad L L and Milton K A 1978 *Ann. Phys.* **115** 1
[53] Matloob R and Falinejad H 2001 *Phys. Rev.* A **64** 042102
[54] Ellingsen S A 2006 *Master's Thesis* Department of Physics, Norwegian University of Science and Technology
[55] Tomaš M S 2002 *Phys. Rev.* A **66** 052103
[56] Langbein D 1974 *Theory of Van der Waals Attraction (Springer Tracts in Modern Physics* vol 72*)* (Berlin: Springer)
[57] Parsegian V A 2006 *Van der Waals Forces* (Cambridge: Cambridge University Press)
[58] Scardicchio A and Jaffe R L 2004 *Nucl. Phys.* B **704** 552
[59] Chaudhury M K 1984 Short-range and long-range forces in colloidal and macroscopic systems *PhD Thesis* Faculty of the Graduate School, State University of New Yourk on Buffalo
[60] Torgerson J R and Lamoreaux S 2004 *Phys. Rev.* E **70** 047102
[61] Pirozhenko I, Lambrecht A and Svetovoy V B 2006 *New J. Phys.* **8** 238
[62] Brevik I, Aarseth J B, Høye J S and Milton K A 2004 *Proc. 6th Workshop on Quantum Field Theory under the Influence of External Conditions* ed K A Milton (Paramus, NJ: Rinton Press) p 54 (*Preprint* quant-ph/0311094)
[63] Jaekel M-T, Lambrecht A and Reynaud S 2002 *New Astron. Rev.* **46** 727
[64] Jaekel M-T and Reynaud S 1992 *J. Phys. I France* **2** 149
[65] Milonni P W and Chernobrod B M 2004 *Nature* **432** 965
[66] Karrai K 2006 *Nature* **444** 41
[67] Arcizet O, Cohadon P-F, Briant T, Pinard M and Heidmann A 2006 *Nature* **444** 71
[68] Kleckner D and Bouwmeester D 2006 *Nature* **444** 75
[69] Buenzli P R and Martin Ph A 2005 *Europhys. Lett.* **72** 42

**Ellingsen, Simen Andreas Ådnøy; Sherkunov, Yury; Buhmann, Stefan Yoshi; Scheel, Stefan.** Casimir-Polder Potential in Thermal Non-equilibrium. I: Proceedings of the Ninth Conference on Quantum Field Theory Under the Influence of External Conditions (QFEXT09). World Scientific 2010 ISBN 978-981-4289-85-6. s. 168-177

PHYSICAL REVIEW A **81**, 011806(R) (2010)

# Transverse radiation force in a tailored optical fiber

Iver Brevik and Simen Å. Ellingsen*
*Department of Energy and Process Engineering, Norwegian University of Science and Technology, N-7491 Trondheim, Norway*
(Received 31 August 2009; published 27 January 2010)

We show, by means of simple model calculations, how a weak laser beam sent though an optical fiber exerts a transverse radiation force if there is an azimuthal asymmetry present in the fiber such that one side has a slightly different refractive index than the other. The refractive index difference $\Delta n$ needs only to be very low, of order $10^{-3}$, to produce an appreciable transverse displacement of order 10 $\mu$m. We argue that the effect has probably already been seen in a recent experiment by W. She *et al.* [Phys. Rev. Lett. **101**, 243601 (2008)], and we discuss the correspondence between these observations and the theory presented. The effect could be used to bend optical fibers in a predictable and controlled manner and we propose that it could be useful for micron-scale devices.

DOI: 10.1103/PhysRevA.81.011806 PACS number(s): 42.50.Wk, 03.50.De

Recent years have seen increased interest in radiation forces in optics. Optical tweezers, atom traps, and optical manipulation of soft materials such as interfaces between liquids—especially near the critical point, where surface tension is low—are typical examples. This trend will, in all probability, continue in the near-future.

Our objective in the present Rapid Communication is to point toward the possibility of creating a tailored transverse optical force in a fiber transmitted by a laser beam. The beam may be pulsed, or it may be continuous. The gist of the principle is to introduce an accurate mechanical imbalance in the fiber, implying a slight asymmetry in the refractive index $n$. (In practice, such a deviation from axisymmetry may easily result inadvertently, during the mechanical drawing of the fiber.) If one side of the fiber is harder than the other, there may be a slight refractive index difference $\Delta n$ between the two sides, resulting in a transverse optical force. As fibers of micron-scale cross sections are very light and bend easily, a sideways motion may easily occur. The effect, besides being of basic interest, may be of practical utility. We describe the effect, making use of simple models for the fiber, and thereafter compare the theory with a recent experiment which, in our opinion, has most likely already observed this effect.

The problem is to some extent related to the 100-year-old Abraham-Minkowski debate on the correct electromagnetic energy-momentum tensor in dielectric media. From a physical point of view the key issue is that one is dealing with a *nonclosed* system, matter and field. Macroscopic or phenomenological electromagnetic theory, implying the use of a permittivity $\varepsilon$ and permeability $\mu$, means that one is dealing with a complicated interaction system involving external fields, internal fields, and constituent molecules, by using only simple material parameters. The solution to the problem lies in extracting the energy-momentum form that leads to a theoretical description of observable effects in a clean and simple manner. For an overview of the Abraham-Minkowski debate, see, for example, Ref. [1]. At present there are a great number of papers discussing the Abraham-Minkowski problem, for instance, the recent Ref. [2] and the review Ref. [3].

Assume now, for definiteness, that the fiber is hanging vertically and that a laser pulse is transmitted through it. The general expression for the electromagnetic force density in the medium, assumed hereafter to be nonmagnetic, is derived from a given stress tensor $\sigma_{ik}$ as $f_i = \partial_k \sigma_{ik}$. For the Abraham and Minkowski tensors this implies (see Refs. [1,4] for details)

$$\mathbf{f} = \mathbf{f}^{\mathrm{AM}} + \frac{n^2 - 1}{c^2} \frac{\partial}{\partial t} (\tilde{\mathbf{E}} \times \tilde{\mathbf{H}}). \tag{1}$$

Here $\mathbf{f}^{\mathrm{AM}} = -(\varepsilon_0/2)\tilde{E}^2 \nabla n^2$ is nonvanishing in any region where $n$ varies, especially in surface regions. We use the notation $\tilde{\mathbf{E}}(\mathbf{r}, t) = \mathrm{Re}\{\mathbf{E}(x) e^{i(\omega t - \beta z)}\}$ and skip the exponential factor in the following (see Ref. [5], Chap. 1.3, for notational details). As this force is common for the Abraham and Minkowski tensors, it may appropriately be denoted $\mathbf{f}^{\mathrm{AM}}$. The Abraham momentum density $\mathbf{g}^A = (1/c^2)\tilde{\mathbf{E}} \times \tilde{\mathbf{H}}$ occurs in the second term. We henceforth ignore it, for the following two reasons: (i) for a stationary beam the term fluctuates out when averaged over an optical period; (ii) under perfectly axisymmetric conditions the force exerted on the fiber during the transient entrance and exit periods necessarily has to be vertical, thus being unable to initiate any sideways motion.

In the following we investigate the effect of the force $\mathbf{f}^{\mathrm{AM}}$ when the refractive index contrast $\Delta n$ is assumed to be known from the mechanical production process. Two simple planar models are considered, in order of increasing complexity. Finally, we compare the theory with a recent experiment by She *et al.* [6] and demonstrate how the deflection observed could very plausibly be a demonstration of the effect mentioned.

We henceforth limit ourselves to planar geometries for the fiber. This is mathematically simplifying, but the model is nevertheless expected to incorporate the essentials of the imbalance effect. Probably the simplest arrangement is to consider a uniform slab, infinite in the horizontal $y$ direction, having a finite width $2a$ in the horizontal $x$ direction.

The setup is sketched in Fig. 1(a); it is essentially the same as Fig. 2.1 in Ref. [5]. The beam is propagating into the plane, in the $z$ direction. On the lower side of the slab ($x < -a$) we assume vacuum (or air), with refractive index $n_0 = 1$. On the upper side ($x > a$), we assume that there is a dilute medium, extending to $x = \infty$, with refractive index $n_2 = 1 + \Delta n$, $\Delta n \ll 1$. When light propagates through the fiber, there will thus be an imbalance in the surface force

*simen.a.ellingsen@ntnu.no

 

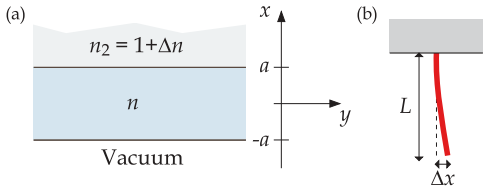


FIG. 1. (Color online) (a) The simplest model, a slab waveguide with a slight difference in refractive index above and below. (b) The geometry of a vertically hanging optical fiber subject to sideways motion.

densities on the lower and upper surfaces. Let us choose a TE mode (following the notation in Ref. [5]). This means that the electric field has only a $y$ component different from zero, $\mathbf{E} = (0, E_y, 0)$. In the dielectric boundary layers located around $x = -a$ and $x = a$, the transverse force component is $f_x^{\mathrm{AM}} = -(\varepsilon_0/4)E_y^2\, d(n^2)/dx$, yielding the respective surface force densities,

$$\sigma_x(-a) = -\tfrac{1}{4}\varepsilon_0 E_y^2(-a)(n^2 - 1), \tag{2}$$

$$\sigma_x(a) = -\tfrac{1}{4}\varepsilon_0 E_y^2(a)\left(n_2^2 - n^2\right). \tag{3}$$

We have taken into account here that the longitudinal component $E_y$ is continuous across the surfaces and that $\langle \tilde{E}_y^2 \rangle = \frac{1}{2}E_y^2$, where $\langle\,\rangle$ is averaged over oscillations in time and the $z$ direction.

The net transverse surface force density is $\sigma_x = \sigma_x(-a) + \sigma_x(a)$. As $\Delta n$ is small, we can make use of the expression for $E_y^2$ corresponding to a symmetric fiber, thus with the assumption $n_2 = 1$. Accordingly we get to first order in $\Delta n$,

$$\sigma_x = -\tfrac{1}{2}\varepsilon_0 E_y^2(a) \cdot \Delta n, \tag{4}$$

where now $E_y^2(a)$ refers to the symmetric situation. We see that for positive $\Delta n$, the surface force is directed downward in Fig. 1(a), that is, in the negative $x$ direction. This is as it should be, as surface forces are always directed toward the optically thinner region at a dielectric surface.

The presence of $\sigma_x$ makes it possible to regard the fiber as an elastic rod exposed to a constant transverse load. Let us first, however, relate $\sigma_x$ to the total power $P$ in the fiber. For the TE mode we have, using the same notation as in Ref. [5],

$$E_y = \begin{cases} A\cos(\kappa a - \phi)e^{-\xi(x-a)}, & x > a, \\ A\cos(\kappa x - \phi), & -a \leqslant x \leqslant a, \\ A\cos(\kappa a + \phi)e^{\xi(x+a)}, & x < -a. \end{cases} \tag{5}$$

Here $\kappa = \sqrt{(n^2\omega^2/c^2) - \beta^2}$ and $\xi = \sqrt{\beta^2 - (\omega^2/c^2)}$, where $\beta$, lying in the interval $\omega/c \leqslant \beta \leqslant n\omega/c$, is the wave-number component in the $z$ direction. The corresponding nondimensional transverse wave vectors are $u = \kappa a$ and $w = \xi a$.

The electromagnetic boundary conditions, requiring that $dE_y/dx$ be continuous, yield the following equations:

$$u = \tfrac{1}{2}m\pi + \arctan(w/u), \quad \phi = \tfrac{1}{2}m\pi, \tag{6}$$

with $m = 0, 1, 2, \ldots$, while $u$ and $w$ are related via

$$u^2 + w^2 = \frac{\omega^2 a^2}{c^2}(n^2 - 1). \tag{7}$$

From these two equations $\beta$ and $w$ can be calculated, and we can find the relationship between $P$ and the constant $A$ in Eq. (5) using formula (2.34) of Ref. [5]:

$$A^2 = \frac{2\omega\mu_0 P}{\beta ab[1 + (1/w)]}. \tag{8}$$

Recall that $P$ refers to the total power transmitted by the fiber. In the planar model, we let $b$ denote the fiber width in the $y$ direction. The cross-sectional area of the model fiber is thus $2ab$, and the power per unit length in the $y$ direction is $P/b$. Edge effects because of the finite value of $b$ are ignored. The transverse surface force density can now be expressed as

$$\sigma_x = -\frac{P}{abn_e c[1 + (1/w)]}\frac{n^2 - n_e^2}{n^2 - 1}\Delta n, \tag{9}$$

where we have defined

$$n_e = \beta c/\omega \tag{10}$$

and used that the continuity of $dE_y/dx$ across the interface at $x = a$ implies that

$$\cos^2(u - \phi) = \cos^2(u + \phi) = \frac{\kappa^2}{\xi^2 + \kappa^2} = \frac{n^2 - n_e^2}{n^2 - 1}. \tag{11}$$

For practical purposes it may be convenient to express $\Delta n$ in Eq. (9) in terms of the corresponding increase in material density $\Delta\rho$. We can make use of the Clausius-Mossotti relation, which is a good approximation, at least for nonpolar materials. Then we get

$$\Delta n^2 = \frac{1}{3\rho}(n^2 - 1)(n^2 + 2)\Delta\rho. \tag{12}$$

Consider next the fiber as an elastic rod of rectangular cross section, clamped at one end ($z = 0$) and free at the other end ($z = L$). For convenience we let the $z$ axis be horizontal. We choose $b = 2a$, implying a square cross section of the fiber. The transverse load per unit length in the longitudinal direction is $\sigma_x b$ acting downward in the negative $x$ direction. The governing equation for the elastic deflection is (ignoring gravity) $x''''(z) = \sigma_x b/(EI)$, where $E$ is Young's modulus and $I = b^4/12$ is the moment of inertia of the cross-sectional area about its centroidal axis [7]. The solution of the governing equation is

$$x(z) = -\frac{\sigma_x b}{24EI}z^2(z^2 - 4Lz + 6L^2). \tag{13}$$

The deflection at the tip, termed simply $\Delta x$, is thus

$$\Delta x = -\frac{\sigma_x b L^4}{8EI}. \tag{14}$$

We can now calculate the perturbation $\Delta n$ required to produce a relative deflection $\Delta x/L$ at the tip:

$$|\Delta n| = \frac{8EI}{L^3 P}n_e ac\left(1 + \frac{1}{w}\right)\frac{n^2 - 1}{n^2 - n_e^2}\frac{|\Delta x|}{L}. \tag{15}$$

To obtain an order-of-magnitude estimate for the required difference in $n$ to yield a prescribed value for $\Delta x$, we insert numerical values that are appropriate for a low-intensity laser beam in a fiber (the values are typical and the same as used in Ref. [6]): $\lambda = 650$ nm, $P = 6.4$ mW, $L = 1.5$ mm, and $b = 2a = 450$ nm.

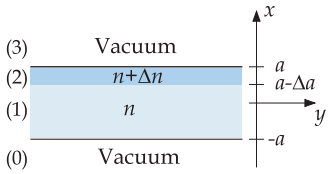


FIG. 2. (Color online) A two-layered model.

For the eigenvalues of the transverse wave number $\beta$ (or, equivalently, $n_e$), corresponding to the guiding modes of the planar fiber, we again use the solutions for the symmetrical situations, as corrections to this enter beyond leading order only in $\Delta n$. Following [5], the eigenvalue of index $m = 0, 1, 2, \ldots,$ solves

$$f(b) = v\sqrt{1-b} - \arctan\sqrt{\frac{b}{1-b}} - \frac{m\pi}{2} = 0, \qquad (16)$$

where $v = (\omega a/c)\sqrt{n^2 - 1}$ and $b = (n_e^2 - 1)/(n^2 - 1)$. With the current numbers there are only two modes, $n_{e,0} = 1.3635$ and $n_{e,1} = 1.1072$.

As an example, assume now that we desire a lateral displacement $\Delta x = 15\ \mu$m. With the preceding numbers we find that the required $\Delta n$ is only $5.5 \times 10^{-4}$ for $m = 0$ and $1.6 \times 10^{-4}$ for $m = 1$. Minor mechanical defects from production could easily give rise to changes of this magnitude in the reflective index. While the planar model is likely to slightly underestimate the required $\Delta n$ compared to a circular fiber, as an order-of-magnitude estimate it demonstrates the feasibility of the scheme.

Regard now a slightly more realistic model where the slab has a layer of slightly higher refractive index on one side. The geometry is as considered in Fig. 2, where the slab, still of width $2a$ and refractive index $n$, has a refractive index increased by $\Delta n$ in a layer of thickness $\Delta a$. Again, we consider the TE mode, whose solution for the electric field component $E_y$ is written [in layers (3) to (0) from top to bottom]

$$E_y = A \times \begin{cases} \cos(u - \Delta u - \phi)\cos(\Delta v - \psi)e^{-\xi(x-a)}, \\ \cos(u - \Delta u - \phi)\cos[\kappa'(x - a + \Delta a) - \psi], \\ \cos(\kappa x - \phi)\cos\psi, \\ \cos(u + \phi)\cos\psi \cdot e^{\xi(x+a)}, \end{cases} \qquad (17)$$

where $\Delta u = \kappa\Delta a$, $\Delta v = \kappa'\Delta a$, $\phi$, and $\psi$ are unknown phase angles and $\kappa'^2 = (n + \Delta n)^2 k^2 - \beta^2 \approx \kappa^2 + 2nk^2\Delta n$. The net surface force per unit area is now given by $\sigma_x = -(\varepsilon_0/4)E_y^2(x)|_{x=-a}^{x=a}$.

$$\sigma_x = -\tfrac{1}{4}\varepsilon_0 A^2[\cos^2(u - \Delta u - \phi)\cos^2(\Delta v - \psi) - \cos^2(u + \phi)\cos^2\psi]. \qquad (18)$$

To leading order in $\Delta n$ we may again use relation (8) for $A$, and $\cos^2(u + \phi)$ is again given by Eq. (11).

From the continuity of $dE_y/dx$ at $x = a$, it follows that $\cos^2(\Delta v - \psi) = \kappa'^2/(\xi^2 + \kappa'^2)$, that is,

$$\cos^2(\Delta v - \psi) \approx \cos^2(u + \phi)\left(1 - \frac{2n\Delta n}{n^2 - 1}\right) + \frac{2n\Delta n}{n^2 - 1}.$$

Similarly, from the condition of continuity of $dE_y/dx$ at $x = a - \Delta a$, we derive that, to linear order in $\Delta n$, we have

$$\cos^2(u - \Delta u - \phi) \approx \cos^2\psi\left(1 - \frac{2n\Delta n}{n^2 - n_e^2}\sin^2\psi\right).$$

Thus we find with some calculation that the surface force per unit area may be written as

$$\sigma_x \approx \frac{1}{2}\varepsilon_0 A^2 \frac{n\Delta n}{n^2 - 1}\cos^2\psi\left(\frac{n^2 - n_e^2}{n^2 - 1} - \cos^2\psi\right). \qquad (19)$$

We can express $\cos^2\psi$ by means of the parameter $\Delta u$ by using the equation of continuity of $dE_y/dx$ at $x = a$, which can be written $\psi = -\arctan(\xi/\kappa) + \Delta v - m\pi, m = 0, 1, \ldots,$ to derive the relation, valid to leading order in $\Delta n$,

$$\cos^2\psi \approx \frac{n^2 - n_e^2}{n^2 - 1}\left(\cos\Delta u + \frac{w}{u}\sin\Delta u\right)^2. \qquad (20)$$

When $\Delta n$ is small we may use the same eigenvalues of $n_e$ as before.

Assuming once again that a displacement of $\Delta x = 15\ \mu$m is sought, Fig. 3(a) shows how the required $\Delta n$ changes with varying values of $\Delta a/a$. For the $m = 0$ mode values of $\Delta n$ are somewhat larger when $\Delta a/a$ is low. This is because $\sigma_x \propto \Delta n\Delta a$ as $\Delta a \to 0$. The required $\Delta n$ remains small, however, as long as the layer of slightly increased $n$ is nonvanishing. For $\Delta n > 1\%$, for example, $\Delta a/a$ must be less than $\sim$0.035 to achieve the observed deflection.

The surface force density $\sigma_x/\Delta n$ to leading order is plotted as a function of $\Delta a/a$ in Fig. 3(b). As in the simplest model in Fig. 1 the force is directed downward when $\Delta a/a$ is lower than approximately unity. In the present example it is reasonable to assume that it is a small number compared to 1. We also performed the calculation using different laser wavelengths, in which case the graph in Fig. 3(b) looks qualitatively similar,

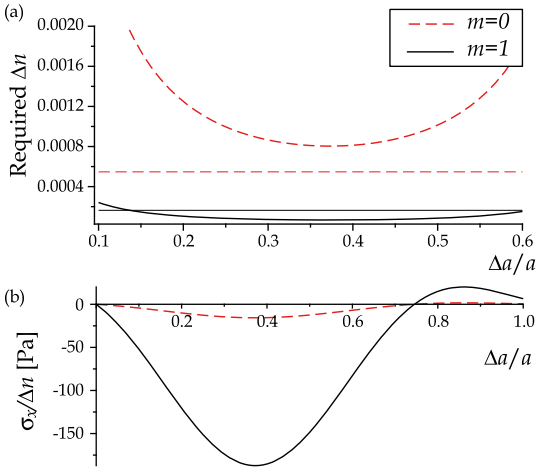


FIG. 3. (Color online) (a) Required $\Delta n$ as a function of $\Delta a/a$ to obtain $\Delta x = 15\ \mu$m with parameters as given in the text. The dashed and solid horizontal lines show the corresponding values for the simple model in Fig. 1. (b) Surface force per unit area divided by $\Delta n$ as a function of $\Delta a/a$.

but the abscissa is rescaled. Because the point where the force density changes sign [about $\Delta a/a = 0.75$ in Fig. 3(b)] then moves along the abscissa, it is possible to change the sign of the force by changing the optical frequency, provided $\Delta a/a$ is chosen carefully.

The recent experiment by She *et al.* [6] appears to be a natural example of application of the present theory. This experiment tested precisely the sideways motion of a vertical fiber when transmitted by a laser beam. Whereas the authors actually related their observations to the Abraham-Minkowski problem mentioned previously, we do not think that such a conclusion is right, and one of us has discussed this issue in more detail elsewhere [8]. In the experiment [6] one side of the fiber was slightly harder than the other from fabrication [9], and it is natural to suggest that this could have given rise to an appreciable $\Delta n$.

Noting how even a very small $\Delta n$ can cause deflections of the magnitude observed, and how the surface force depends on the geometry of the hardened layer in a nontrivial way, it is much more likely, in our opinion, that all the observed transverse deviations reported in [6] were due to the force $\mathbf{f}^{\mathrm{AM}}$. As such the experiment is a striking demonstration of the theory presented here. For ease of comparison, our preceding numerical examples use data taken from the experiment [6], including a deflection of the order of 15 $\mu$m. A change in the refractive index on one side of the fiber of the order of $<1\%$ is shown to be sufficient to produce deflections of such magnitude.

In conclusion, even a minute change in the refractive index, $\sim 10^{-3}$, in a layer on one side of an optical fiber of centimeter length and micron-scale cross section is sufficient to produce an appreciable transverse deflection of the fiber. A tailored fiber of this kind, where $\Delta n$ is prescribed accurately, should provide the possibility of bending fibers in a controlled and predictable way. Because the lateral force acting on the fiber depends on the laser frequency in a nontrivial way, it would, moreover, be possible to design a fiber which bends one way at one frequency and changes direction of movement when a different frequency is used. The force can be used to carry a small load, and one can envisage uses within micro- and nanorobotics.

I.B. thanks Weilong She for correspondence.

[1] I. Brevik, Phys. Rep. **52**, 133 (1979); Phys. Rev. B **33**, 1058 (1986).
[2] E. A. Hinds and S. M. Barnett, Phys. Rev. Lett. **102**, 050403 (2009).
[3] R. N. C. Pfeifer *et al.*, Rev. Mod. Phys. **79**, 1197 (2007).
[4] C. Møller, *The Theory of Relativity*, 2nd ed. (Clarendon Press, Oxford, 1972), Chap. 7.
[5] K. Okamoto, *Fundamentals of Optical Waveguides* (Academic Press, London, 2000).
[6] W. She, J. Yu, and R. Feng, Phys. Rev. Lett. **101**, 243601 (2008); Physical Review Focus[online] **22**(10 December):story 20 (2008).
[7] L. D. Landau and E. M. Lifshitz, *Theory of Elasticity* (Pergamon Press, Oxford, 1970).
[8] I. Brevik, Phys. Rev. Lett. **103**, 219301 (2009); W. She, J. Yu, and R. Feng, *ibid* **103**, 219302 (2009).
[9] W. She (personal communication).

PHYSICAL REVIEW A **81**, 063830 (2010)

# Possibility of measuring the Abraham force using whispering gallery modes

I. Brevik* and S. Å. Ellingsen
*Department of Energy and Process Engineering, Norwegian University of Science and Technology, N-7491 Trondheim, Norway*
(Received 25 March 2010; published 28 June 2010)

Critical experimental tests of the time-dependent Abraham force in phenomenological electrodynamics are scarce. In this paper, we analyze the possibility of making use of intensity-modulated whispering gallery modes in a microresonator for this purpose. Systems of this kind appear attractive, as the strong concentration of electromagnetic fields near the rim of the resonator serves to enhance the Abraham torque exerted by the field. We analyze mainly spherical resonators, although as an introductory step we consider also the cylinder geometry. The orders of magnitude of the Abraham torques are estimated by inserting reasonable and common values for the various input parameters. As expected, the predicted torques turn out to be very small, although probably not beyond reach experimentally. Our main idea is essentially a generalization of the method used by G. B. Walker *et al.* [Can. J. Phys. **53**, 2577 (1975)] for low-frequency fields, to the optical case.

DOI: 10.1103/PhysRevA.81.063830 PACS number(s): 42.50.Wk, 42.50.Tx, 03.50.−z

## I. INTRODUCTION

The 100-year-old Abraham-Minkowski energy-momentum problem in phenomenological electrodynamics [1,2] has recently attracted considerable interest. Assume henceforth for simplicity that the medium is nonmagnetic and nondispersive, with refractive index $n$. In our opinion—as expressed in the review article some years ago by one of the present authors [3]—the most physical expression for the electromagnetic force density is the Abraham expression (International System (SI) of units assumed)

$$\mathbf{f}^{\mathrm{A}} = \mathbf{f}^{\mathrm{AM}} + \frac{n^2-1}{c^2}\frac{\partial}{\partial t}(\mathbf{E}\times\mathbf{H}). \tag{1.1}$$

Here the first term $\mathbf{f}^{\mathrm{AM}} = -(\epsilon_0/2)E^2\nabla n^2$ is different from zero in regions where $n$ varies with position, especially in the surface regions of dielectrics. This term is common for the Abraham and Minkowski tensors, and may appropriately be called the Abraham-Minkowski term. The second, time-dependent term in Eq. (1.1) is the Abraham term. It may be noted that the expression (1.1) is in agreement with Ginzburg [4], as well as with Landau and Lifshitz [5].

One may ask the question: Is it possible to detect the Abraham term in an experiment? The answer is yes, but the task has proven to be surprisingly difficult. The magnitude of the electromagnetic frequency is a significant factor in this context. Let us give a brief account of three important experimental cases:

(1) The first case is the quasistationary torque experiment of Walker *et al.* [6,7]. Strong, time-varying, orthogonal electric and magnetic fields were applied across a dielectric shell of high permittivity, making it possible to detect the *oscillations themselves.* In this way the Abraham term was measured quantitatively.

(2) When considering instead high-frequency fields such as in optics, the Abraham term fluctuates out when averaged over a period. One can thus no longer detect this force directly. The physical effect of this force is, however, to produce an accompanying mechanical momentum propagating together with the Abraham momentum. The resulting total momentum is the Minkowski momentum, corresponding to the divergence-free Minkowski energy-momentum tensor. This tensor has the particular property of being spacelike, corresponding to the possibility of getting negative field energy in certain inertial frames. An authoritative experiment measuring the Minkowski momentum is that of Jones *et al.* [8,9], measuring the radiation pressure on a mirror immersed in a dielectric liquid. Both cases (1) and (2) are discussed in some detail in Ref. [3].

(3) The third example to be mentioned is the photon recoil experiment of Campbell *et al.* [10], where the photon momentum in a medium (in this case a Bose-Einstein condensate) was found to be equal to the Minkowski value $\hbar\mathbf{k}$.

Most other experiments are measuring not the Abraham term but rather the surface force $\mathbf{f}^{\mathrm{AM}}$, although claims are sometimes made to the contrary. In our opinion this is the case also for the interesting new fiber optical experiment of She *et al.* [11]; see the remarks in Refs. [12,13].

Our main purpose in the present paper is, however, not to interpret already existing experiments, but instead to propose the idea of using *whispering gallery modes* as a convenient experimental tool to detect the Abraham term in optics. Whispering gallery modes are commonly produced in microspheres; they have a large circulating power, about 100 W typically, and the field energy is concentrated along the rim of the sphere. That means, if such a sphere is suspended in the gravitational field and fed with an appropriate intensity modulated field, the sphere becomes exposed to a vertical torque according to Eq. (1.1). With the field energy essentially concentrated along the rim, the arm in the torque calculation is essentially the same as the radius, thus maximizing the torque. In effect, this is the idea of the experiment of Walker *et al.* [6,7], generalized to optical frequencies. We have actually suggested this idea qualitatively before, in Refs. [12,13].

The next two sections give quantitative estimates for performing such an experiment. The torque turns out to be small, as expected, but not beyond any possibility for experimental detection. Spherical geometry, as mentioned, is most typical for the whispering gallery setup. In the next section, however, we consider as an introductory step the somewhat more simple geometry of a cylindrical shell.

*iver.h.brevik@ntnu.no

 

Before closing this section, let us give a few more references to the Abraham-Minkowski problem, in addition to the references given above. A nice introduction can be found in Møller's book [14]. A review, up to 2007, is given by Pfeifer *et al.* [15]. Some more recent papers are Refs. [16–18].

## II. CYLINDRICAL GEOMETRY

Consider first as the simplest case a compact cylinder of length $L$ and radius $a$. On the inside, $r < a$, the permittivity is $\epsilon$ and the permeability $\mu$. On the outside, $r > a$, a vacuum is assumed. The dispersion relation for stationary modes is known to be [19]

$$\left[\frac{\mu}{u}\frac{J_m'(u)}{J_m(u)} - \frac{1}{v}\frac{H_m^{(1)\prime}(v)}{H_m^{(1)}(v)}\right]\left[\frac{\epsilon\,\omega^2}{u}\frac{J_m'(u)}{J_m(u)} - \frac{\omega^2}{v}\frac{H_m^{(1)\prime}(v)}{H_m^{(1)}(v)}\right] = m^2k^2\left(\frac{1}{v^2}-\frac{1}{u^2}\right)^2. \tag{2.1}$$

We are working with SI units and let $\epsilon$ and $\mu$ be dimensional, so that $\mathbf{D} = \epsilon\mathbf{E}$, $\mathbf{B} = \mu\mathbf{H}$. The transverse wave vectors on the inside and the outside are

$$\lambda_1 = n\omega/c, \quad \lambda_2 = \omega/c, \tag{2.2}$$

respectively, while their nondimensional counterparts are

$$u = \lambda_1 a, \quad v = \lambda_2 a. \tag{2.3}$$

An important property of this equation is that when the axial wave vector $k = 0$—as is of interest here since we consider azimuthal modes only—the right-hand side vanishes and the problem becomes separable into TE and TM modes.

We write the mode expansions for the fields in the inner region [19] as

$$E_r = -\frac{\mu\omega}{\lambda_1^2 r}\sum_{m=-\infty}^{\infty} m J_m(\lambda_1 r)\, b_m F_m, \tag{2.4a}$$

$$E_\theta = -\frac{i\mu\omega}{\lambda_1}\sum_{m=-\infty}^{\infty} J_m'(\lambda_1 r)\, b_m F_m, \tag{2.4b}$$

$$E_z = \sum_{m=-\infty}^{\infty} J_m(\lambda_1 r)\, a_m F_m, \tag{2.4c}$$

and

$$H_r = \frac{\epsilon\omega}{\lambda_1^2 r}\sum_{m=-\infty}^{\infty} m J_m(\lambda_1 r)\, a_m F_m, \tag{2.5a}$$

$$H_\theta = \frac{i\epsilon\omega}{\lambda_1}\sum_{m=-\infty}^{\infty} J_m'(\lambda_1 r)\, a_m F_m, \tag{2.5b}$$

$$H_z = \sum_{m=-\infty}^{\infty} J_m(\lambda_1 r)\, b_m F_m, \tag{2.5c}$$

where

$$F_m = e^{im\theta - i\omega t}. \tag{2.6}$$

The coefficients $a_m$ and $b_m$, corresponding to the transverse magnetic (TM) and the transverse electric (TE) modes, give the weight of each mode.

In our considerations below, we will for simplicity extract one single TE mode of high order $m$, such that there is an azimuthally moving momentum concentrated in the vicinity of the boundary $r = a$. (In reality, the incident power may be distributed over a band of neighboring $m$ modes, but this does not influence the essence of our argument.) We first need to determine the magnitude of the radial argument $\lambda_1 r \approx u$. Let us take

$$m = 100, \quad n = 1.5, \quad a = 100\,\mu\text{m}. \tag{2.7}$$

It is known that for a large value of the order $m$ the first maximum of the function $J_m(x)$ occurs when $x$ is very close to $m$. This maximum is the one of interest here. Thus the lowest resonance frequency $\omega$ is determined by the equation

$$na\omega/c = m. \tag{2.8}$$

With the numbers given above,

$$\omega = 2\times 10^{16}\ \text{s}^{-1}. \tag{2.9}$$

In this manner, we manage to make the beam strongly concentrated near the rim, as desired. One has in this case $E_z = 0$, $H_r = 0$, while the nonvanishing field components of interest are

$$E_r = -\frac{\mu\omega}{\lambda_1^2 r}\, m J_m(\lambda_1 r)\, b_m F_m, \tag{2.10}$$

$$H_z = J_m(\lambda_1 r) b_m F_m. \tag{2.11}$$

The azimuthal component of the Poynting vector $\mathbf{S}(r)$ in the interior is

$$S_\theta(r) = -\frac{1}{2}\text{Re}[E_r H_z^*] = \frac{\mu\omega m}{2\lambda_1^2 r} J_m^2(\lambda_1 r)|b_m|^2, \tag{2.12}$$

corresponding to the azimuthal power

$$P = L\int_0^a S_\theta\, dr = \frac{\mu\omega m L}{2\lambda_1^2}|b_m|^2\int_0^u \frac{dx}{x} J_m^2(x). \tag{2.13}$$

In our case the factor $1/x$ can be extracted outside the integral, so that

$$P = \frac{\mu\omega m L}{2\lambda_1^2 u}|b_m|^2\int_0^u dx\, J_m^2(x). \tag{2.14}$$

Assume now that the beam is intensity modulated with a frequency $\omega_0$ ($\omega_0$ is low compared with optical frequencies),

$$P = P_0\cos\omega_0 t, \quad S_\theta = S_0\cos\omega_0 t. \tag{2.15}$$

Then the azimuthal Abraham force density $f_\phi^{\text{A}}$ is

$$f_\phi^{\text{A}} = \frac{n^2-1}{c^2}\frac{\partial S_\theta}{\partial t} = -\frac{n^2-1}{c^2}\omega_0 S_0 \sin\omega_0 t, \tag{2.16}$$

giving rise to the following Abraham torque $N_z^{\text{A}}$ around the vertical symmetry axis:

$$N_z^{\text{A}} = 2\pi L\int_0^a r^2 f_\phi^{\text{A}}\, dr \approx 2\pi L a^2\int_0^a f_\phi^{\text{A}}\, dr. \tag{2.17}$$

Defining the quantity $K$ as

$$K = -\frac{n^2-1}{c^2}2\pi a^2 P_0, \tag{2.18}$$

we thus see that the torque can be written as

$$N_z^{\mathrm{A}} = K\omega_0 \sin\omega_0 t. \tag{2.19}$$

As expected, the torque becomes very small. As order of magnitude we get

$$K \sim \frac{2\pi a^2}{c^2} P_0 \sim (0.7\times 10^{-24}\ \mathrm{s}^2) P_0, \tag{2.20}$$

and the Abraham torque is estimated as

$$N_z^{\mathrm{A}} \sim (0.7\times 10^{-24}\ \mathrm{s}^2)\omega_0 P_0. \tag{2.21}$$

Insert first the very low value of $\omega_0 \sim 1\ \mathrm{s}^{-1}$, and take $P_0 \sim 100$ W. We get $N_z \sim 0.7\times 10^{-22}$ N m, which is much less than the value $10^{-16}$ N m obtained in the classic Beth experiment [20], for example, in which the angular momentum of light was measured. It is, however, possible to improve the situation by exploiting the fact that the buildup and ringdown times for this kind of resonator are known to be very small, in the order of tens to hundreds of *n*s (see discussion below). It is thus realistic to insert a much higher value for $\omega_0$. Inserting tentatively $\omega_0 = 1000\ \mathrm{s}^{-1}$, we get $N_z \sim 0.7\times 10^{-19}$ N m, which is perhaps not so unrealistic after all.

It is physically instructive to look at the system in another way, by considering the angular deflection $\phi$ of the cylinder instead of the magnitude of the torque. Let the cylinder be hanging vertically in the gravitational field, suspended by a thin wire of known torsion constant $\kappa$. Denoting the eigenfrequency of the cylinder in the absence of any torque by $\Omega$, and denoting the damping coefficient by $\gamma$, we have as the equation of motion

$$\ddot{\phi} + \gamma\dot{\phi} + \Omega^2\phi = \frac{K}{I}\omega_0 \sin\omega_0 t. \tag{2.22}$$

Here $I = \frac{1}{2}Ma^2$ is the moment of inertia about the $z$ axis, $M = \rho a^2 L$ being the cylinder mass with $\rho$ the material density. In our notation, $\kappa = I\Omega^2$. With $a = 100\ \mu$m as above we obtain, when choosing $L = 1$ mm and assuming $\rho \sim 10^3\ \mathrm{kg/m}^3$,

$$\Omega = \sqrt{\kappa/I} \sim 10^8\sqrt{\kappa}. \tag{2.23}$$

For the magnitude of $\kappa$ we may choose a typical value characteristic of torsion experiments testing the equivalence principle, $\kappa \sim 10^{-9}$ N m/rad [21,22]. Then,

$$\Omega \sim 10^3\ \mathrm{rad\,s}^{-1}. \tag{2.24}$$

The magnitude of $\Omega$ is large because $a$ is assumed small.

The largest oscillations occur at resonance, when $\omega_0$ is chosen equal to $\Omega$. Then,

$$\phi = -\frac{K}{I\gamma}\cos\Omega t. \tag{2.25}$$

The maximum value, when $P_0 \sim 100$ W, is

$$\phi_{\max} = \frac{n^2-1}{c^2}\frac{4}{M}\frac{P_0}{\gamma} \sim \frac{10^{-7}}{\gamma}\ \mathrm{rad\,s}^{-1}. \tag{2.26}$$

It would be of interest to make an estimate of the damping constant $\gamma$ here, but we postpone that until the next section.

Notice that the very existence of a oscillatory movement would be enough to make the experiment critical with respect to the Abraham force. The Minkowski tensor does not predict an azimuthal movement at all.

## III. SPHERICAL GEOMETRY

As mentioned above, whispering gallery modes are usually associated with microspheres. Let the radius of the sphere be denoted by $a$. As above, we look for the eigenmodes, and we will for simplicity focus on the TE modes only. (The meaning of the symbol TE is here that the electric field is transverse to the radius vector $\mathbf{r}$.) We introduce quantities $\alpha$ and $\tilde{r}$ defined by

$$\alpha = \omega a/c, \quad \tilde{r} = r/a. \tag{3.1}$$

Thus $\alpha$ is the magnitude of the nondimensional wave vector in the exterior region (vacuum), whereas $\tilde{r} = 1$ at the boundary. Making use of the Riccati-Bessel function

$$\psi_l(x) = x j_l(x), \tag{3.2}$$

the basic TE modes in the interior can conveniently be written as

$$E_r = 0, \tag{3.3a}$$

$$E_\theta = -\frac{imA_{lm}}{n\alpha\tilde{r}}\frac{P_l^m(\cos\theta)}{\sin\theta}\psi_l(n\alpha\tilde{r})\,F_m, \tag{3.3b}$$

$$E_\phi = \frac{A_{lm}}{n\alpha\tilde{r}}\frac{dP_l^m(\cos\theta)}{d\theta}\psi_l(n\alpha\tilde{r})\,F_m, \tag{3.3c}$$

and

$$H_r = -\frac{l(l+1)}{i\omega\mu}\frac{A_{lm}}{n\alpha\tilde{r}^2}\frac{1}{a}P_l^m(\cos\theta)\psi_l(n\alpha\tilde{r})\,F_m, \tag{3.4a}$$

$$H_\theta = -\frac{1}{i\omega\mu}\frac{A_{lm}}{\tilde{r}}\frac{1}{a}\frac{dP_l^m(\cos\theta)}{d\theta}\psi_l'(n\alpha\tilde{r})F_m, \tag{3.4b}$$

$$H_\phi = -\frac{m}{\omega\mu\sin\theta}\frac{A_{lm}}{\tilde{r}}\frac{1}{a}P_l^m(\cos\theta)\,\psi_l'(n\alpha\tilde{r})F_m, \tag{3.4c}$$

where $A_{lm}$ are constants, and

$$F_m = e^{im\phi - i\omega t}. \tag{3.5}$$

The mode expansions above essentially follow Stratton [19].

The components of Poynting's vector are, when averaged over an optical period,

$$S_r = \tfrac{1}{2}\mathrm{Re}[E_\theta H_\phi^* - E_\phi H_\theta^*], \tag{3.6a}$$

$$S_\theta = \tfrac{1}{2}\mathrm{Re}[E_\phi H_r^*], \tag{3.6b}$$

$$S_\phi = -\tfrac{1}{2}\mathrm{Re}[E_\theta H_r^*]. \tag{3.6c}$$

Assume that the sphere is fed by an incident flux from the outside such that only the component $S_\phi$ of $\mathbf{S}$ in the interior is different from zero. With an intensity modulated energy flux such as above, $S_\phi = S_0\cos\omega_0 t$, we thus get for the azimuthally directed Abraham force density in the interior

$$f_\phi^{\mathrm{A}} = -\frac{n^2-1}{c^2}\omega_0 S_0 \sin\omega_0 t. \tag{3.7}$$

From the above expressions,

$$S_0 = \frac{m}{2(n\alpha)^2\tilde{r}^3}\frac{l(l+1)}{\omega\mu}\frac{|A_{lm}|^2}{a}\frac{\left[P_l^m(\cos\theta)\right]^2}{\sin\theta}\psi_l^2. \tag{3.8}$$

The Abraham torque, directed along the $z$ axis, then becomes

$$N_z^{\mathrm{A}} = \int (\mathbf{r} \times \mathbf{f}^{\mathrm{A}})_z dV = \int r f_\phi^{\mathrm{A}} \sin\theta \, dV, \tag{3.9}$$

where the integration is over the sphere, with $dV = r^2 \sin\theta \, dr \, d\theta \, d\phi$. Making use of Eqs. (3.7) and (3.8), we obtain

$$N_z^{\mathrm{A}} = -\frac{n^2-1}{c^2} \frac{\pi m a^3}{(n\alpha)^2} \frac{l(l+1)}{\omega\mu} |A_{lm}|^2 \omega_0 \, K_{\mathrm{I}} K_{\mathrm{II}} \sin\omega_0 t, \tag{3.10}$$

where $K_{\mathrm{I}}$ and $K_{\mathrm{II}}$ are the integrals

$$K_{\mathrm{I}} = \int_0^1 \psi_l^2(n\alpha\tilde{r}) d\tilde{r} = \frac{1}{2}\left[\psi_l^2(n\alpha) - \psi_{l-1}(n\alpha)\psi_{l+1}(n\alpha)\right], \tag{3.11a}$$

$$K_{\mathrm{II}} = \int_0^\pi \left[P_l^m(\cos\theta)\right]^2 \sin\theta \, d\theta = \frac{2}{2l+1}\frac{(l+m)!}{(l-m)!}. \tag{3.11b}$$

We want to relate this to the total power $P$ flowing in the azimuthal direction in the sphere. We calculate $P$ by integrating $S_\phi$ over the area of a semicircle with radius $a$,

$$P = \int_0^\pi d\theta \int_0^a r \, dr S_\phi = \frac{ma}{2(n\alpha)^2} \frac{l(l+1)}{\omega\mu} |A_{lm}|^2 K_{\mathrm{III}} K_{\mathrm{IV}} \cos\omega_0 t, \tag{3.12}$$

where

$$K_{\mathrm{III}} = \int_0^1 \frac{d\tilde{r}}{\tilde{r}^2} \psi_l^2(n\alpha\tilde{r}), \tag{3.13a}$$

$$K_{\mathrm{IV}} = \int_0^\pi \frac{\left[P_l^m(\cos\theta)\right]^2}{\sin\theta} d\theta. \tag{3.13b}$$

As before, it is assumed that the supplied power is intensity modulated, $P = P_0 \cos\omega_0 t$.

The two last integrals can be processed further, at least approximatively. First, we can rewrite $K_{\mathrm{III}}$ as

$$K_{\mathrm{III}} = \frac{1}{2}\pi n\alpha \int_0^{n\alpha} \frac{dx}{x} J_\nu^2(x), \tag{3.14}$$

with $\nu = l + 1/2$. For actual physical values, $n\alpha \gg 1$. We can thus replace the upper limit with infinity, and make use of formula 6.574.2 in Ref. [23] to get

$$K_{\mathrm{III}} \approx \frac{\pi n\alpha}{2(2l+1)}. \tag{3.15}$$

Finally, the integral $K_{\mathrm{IV}}$ is simply (cf. formula 8.14.14 in Ref. [24])

$$K_{\mathrm{IV}} = \frac{(l+m)!}{m(l-m)!}. \tag{3.16}$$

We are now able to relate the torque $N_z^{\mathrm{A}}$ to the power $P$. The result becomes quite simple:

$$N_z^{\mathrm{A}} = -\frac{n^2-1}{c^2} \frac{4ma^2\omega_0}{n\alpha} P_0 \sin\omega_0 t \times \left[\psi_l^2(n\alpha) - \psi_{l-1}(n\alpha)\psi_{l+1}(n\alpha)\right]. \tag{3.17}$$

The radius of the sphere is seen to appear in the prefactor $a^2$, as well as in the nondimensional parameter $\alpha = \omega a/c$. The parameter $l$ occurs only as an order parameter in the function $\psi_l$. We see that the torque is proportional to $m$. This is as we would expect, because the whispering gallery modes are associated with $m = l$, i.e., the maximum value of $m$. It should correspond to a maximum angular momentum and accordingly a maximum torque.

To proceed quantitatively, the value of $\alpha$ has to be determined. For the TE modes it is determined by the dispersion relation [19]

$$\frac{n\mu_0}{\mu} \frac{\psi_l'(n\alpha)}{\psi_l(n\alpha)} = \frac{\xi_l^{(1)\prime}(\alpha)}{\xi_l^{(1)}(\alpha)}, \tag{3.18}$$

where $\xi_l^{(1)}(x) = x h_l^{(1)}(x)$ is another member of the Riccati-Bessel functions. The equation (3.18) is complex and does not in general have real solutions, but approximate solutions with only a small imaginary inequality are found close to $\alpha \approx l$ for $l \gg 1$.

As at the end of the previous section, we focus attention now on the magnitude of the angular deflection $\phi$, as this is most likely the quantity of main experimental interest. Without changing the notation, we write the Abraham torque in the form $N_z^{\mathrm{A}} = K\omega_0 \sin\omega_0 t$ as before, where now

$$K = -\frac{n^2-1}{c^2} \frac{4ma^2}{n\alpha} \times \left[\psi_l^2(n\alpha) - \psi_{l-1}(n\alpha)\psi_{l+1}(n\alpha)\right] P_0. \tag{3.19}$$

The equation of motion for $\phi$ takes the same form (2.22) as before, where now the moment of inertia is

$$I = \frac{2}{5}Ma^2 = \frac{8\pi}{15}\rho a^5, \tag{3.20}$$

$M$ being the mass of the sphere. For definiteness let us take $a = 100$ $\mu$m. Then, with $\rho \sim 10^3$ kg/m$^3$, we get $M \approx 4$ $\mu$g and so, with $\kappa \sim 10^{-9}$ N m/rad as before,

$$\Omega \sim 10^8 \sqrt{\kappa} \sim 10^3 \text{ rad s}^{-1}. \tag{3.21}$$

With these numerical choices, the value of $\Omega$ becomes of the same order as in the cylinder case. The magnitude $\phi_{\max}$ of the maximum deflection at resonance $\omega_0 = \Omega$ is now

$$\phi_{\max} = \frac{10m}{Mn\alpha} \frac{n^2-1}{c^2} \times \left[\psi_l^2(n\alpha) - \psi_{l-1}(n\alpha)\psi_{l+1}(n\alpha)\right] \frac{P_0}{\gamma}. \tag{3.22}$$

As we have assumed $l \gg 1$ and $n\alpha \gg 1$ but otherwise left the ratio of these quantities unspecified, the $\psi_l$ functions ought to be calculated numerically.

Let us finally make an estimate of the magnitude of the damping coefficient $\gamma$, assuming for definiteness that the damping is due to the viscosity of air only. We then need

to know the viscous torque on a sphere executing rotary oscillations about its symmetry axis. The solution of this problem is shown in Ref. [25]. An important parameter in this context is the penetration depth $\delta = \sqrt{2\nu/\Omega}$, where $\nu$ is the kinematic viscosity of the surrounding medium. For air, $\nu = 1.5 \times 10^{-5}\ \mathrm{m^2\,s^{-1}}$. Thus with $\Omega \sim 10^3\ \mathrm{rad\,s^{-1}}$ we get $\delta \sim 170\ \mu$m, which is of the same order as $a$. Strictly speaking we should therefore have to use the complete expression for the viscous torque, which is somewhat complicated. For our order-of-magnitude considerations, however, it is sufficient to use the simple expression

$$(N_z)_{\mathrm{viscous}} \approx 8\pi\eta a^3\Omega \tag{3.23}$$

(corresponding mathematically to the $a/\delta \ll 1$ limit), where $\eta = 1.8 \times 10^{-5}$ Pa s is the dynamic viscosity for air. Identifying $(N_z)_{\mathrm{viscous}}$ with $I\gamma\,\Omega$ in accordance with Eq. (2.22), we get for the damping coefficient

$$\gamma = \frac{8\pi\eta}{I}a^3 \sim 30\ \mathrm{s^{-1}}, \tag{3.24}$$

and the expression (3.22) for the maximum deflection can finally be written as

$$\phi_{\max} = \frac{m}{2\pi n\alpha\eta a}\frac{n^2-1}{c^2} \times \left[\psi_l^2(n\alpha) - \psi_{l-1}(n\alpha)\psi_{l+1}(n\alpha)\right] P_0. \tag{3.25}$$

As expected, the deflection is very small. Whereas numerical evaluation of the $\psi_l$ functions in general is called for, as mentioned, we may note that in cases where $l \ll n\alpha$ the approximation $\psi_l(n\alpha) \approx \sin(n\alpha - \frac{l\pi}{2})$ is useful. Moreover, one can obtain a simple estimate of the magnitude in the cylinder case by inserting $\gamma$ from Eq. (3.24) into Eq. (2.26), whereby one finds $\phi_{\max} \sim 10^{-8}$ rad. Careful adjustments of input parameters are obviously needed if the effect is to be verified experimentally.

## IV. MAGNITUDE OF TORQUES IN EXISTING EXPERIMENTS

We close this investigation by making some estimates of radiation torques on spheres, as well as on ring resonators (a closely related geometry), for already existing experiments. As a first example, we take the setup reported in Ref. [26], where an infrared laser of wavelength $\lambda = 1500$ nm was used. Two different sphere radii were investigated, $a = 40\ \mu$m and $a = 70\ \mu$m, corresponding to values of $\alpha \approx l = m$ equal to 162 and 283, respectively. Although the feeding laser had a power on the order of tens of microwatts to milliwatts, the extremely high $Q$ factor of the silica sphere meant the buildup of circulating modes in the sphere grew enormous. Circulating powers in excess of 100 W are routinely reported in such systems (e.g., [27]) (although this quantity was not explicitly given in Ref. [26]). The refractive index of materials used for ultrahigh-$Q$ spherical resonators, such as fused silica [26,28] and quartz [29], are about $n = 1.5$. With these values as input for $P_0$ we obtain the torques $[N_z^{\mathrm{A}} = N_0 \sin\omega_0 t]$

$$N_0 \approx \begin{cases} (4\times10^{-24}\ \mathrm{N\,m\,s})\,\omega_0, \\ (1\times10^{-23}\ \mathrm{N\,m\,s})\,\omega_0, \end{cases} \quad \text{for} \quad a = \begin{cases} 40\ \mu\mathrm{m}, \\ 70\ \mu\mathrm{m}. \end{cases} \tag{4.1}$$

Note in general that for a sphere, $N_z^{\mathrm{A}} \propto a$ according to Eq. (3.17), whereas $\phi_{\max} \propto a^{-2}$ according to Eq. (3.25) when the viscous damping is accounted for.

The geometry of Ref. [27], which reports circulating powers in excess of 100 W, employs the toroidal ring resonator. This geometry has the benefit of having smaller mass and therefore smaller moment of inertia than a sphere of the same radius, allowing for larger angular deflections. For a thin ring, the moment of inertia is

$$I_{\mathrm{toroid}} \approx 2\pi\rho A a^3, \tag{4.2}$$

where $A$ is the area of cross section. The torque on such a toroid would be roughly similar to that on a sphere, so it is reasonable to assume the angular deflection to be larger and scale as $a^{-1}$. This could allow larger radii, which could be beneficial for detection. See also the review article [30].

We wish finally to reemphasize the possibility of using quite high frequencies $\omega_0$ in order to produce measurable values for the Abraham torque. We assumed above the strong field inside the microcavity to react instantaneously to the sinusoidal variations of the input signal, an approximation which is good provided the buildup and ringdown time ($\tau$) of the resonator is small compared to $2\pi/\omega_0$. For the 45 $\mu$m radius toroidal resonator in Ref. [31], for example, a ringdown time of about 43 ns was measured. For cavities of even higher $Q$ factor, ringdown times are somewhat longer, yet this implies that we may choose tuning frequencies $\omega_0$ as high as $10^6$ without invalidating the theory. Due to the proportionality of the torque with $\omega_0$, going close to the megahertz regime could increase the torque to perhaps $10^{-17}$ N m for a sphere with radius of some tens of micrometers.

## ACKNOWLEDGMENTS

I.B. thanks Giovanni Carugno for correspondence concerning measurement accuracies.

[1] M. Abraham, Rend. Circ. Matem. Palermo **28**, 1 (1909); **30**, 33 (1910).
[2] H. Minkowski, Nachr. Königl. Ges. Wiss. Göttingen, p. 53 (1908) [reprinted as Math. Ann. **68**, 472 (1910)].
[3] I. Brevik, Phys. Rep. **52**, 133 (1979).
[4] V. L. Ginzburg, *Applications of Electrodynamics in Theoretical Physics and Astrophysics* (Gordon and Breach, New York, 1989).
[5] L. D. Landau and E. M. Lifshitz, *Electrodynamics of Continuous Media*, 2nd ed. (Butterworth-Heinemann, Oxford, 1984).
[6] G. B. Walker, D. G. Lahoz, and G. Walker, Can. J. Phys. **53**, 2577 (1975).
[7] G. B. Walker and D. G. Lahoz, Nature (London) **253**, 339 (1975).
[8] R. V. Jones and J. C. Richards, Proc. R. Soc. A **221**, 480 (1954).
[9] R. V. Jones and B. Leslie, Proc. R. Soc. A **360**, 347 (1978).

[10] G. K. Campbell, A. E. Leanhardt, J. Mun, M. Boyd, E. W. Streed, W. Ketterle, and D. E. Pritchard, Phys. Rev. Lett. **94**, 170403 (2005).
[11] W. She, J. Yu, and R. Feng, Phys. Rev. Lett. **101**, 243601 (2008).
[12] I. Brevik, Phys. Rev. Lett. **103**, 219301 (2009).
[13] I. Brevik and S. Å. Ellingsen, Phys. Rev. A **81**, 011806(R) (2010).
[14] C. Møller, *The Theory of Relativity*, 2nd ed. (Clarendon, Oxford, 1972).
[15] R. N. C. Pfeifer, T. A. Nieminen, N. R. Heckenberg, and H. Rubinsztein-Dunlop, Rev. Mod. Phys. **79**, 1197 (2007).
[16] I. Brevik and S. A. Ellingsen, Phys. Rev. A **79**, 027801 (2009).
[17] S. M. Barnett and R. Loudon, Philos. Trans. R. Soc. A **368**, 927 (2010).
[18] S. M. Barnett, Phys. Rev. Lett. **104**, 070401 (2010).
[19] J. A. Stratton, *Electromagnetic Theory* (McGraw-Hill, New York, 1941).
[20] R. A. Beth, Phys. Rev. **50**, 115 (1936).
[21] L.-S. Hou, W.-T. Ni, and Y.-C. M. Li, Phys. Rev. Lett. **90**, 201101 (2003).
[22] S. Schlamminger, K.-Y. Choi, T. A. Wagner, J. H. Gundlach, and E. G. Adelberger, Phys. Rev. Lett. **100**, 041101 (2008).
[23] I. S. Gradshteyn and I. M. Ryzhik, *Table of Integrals, Series and Products*, 4th ed. (Academic, New York, 1980).
[24] M. Abramowitz and I. A. Stegun, *Handbook of Mathematical Functions* (Dover, New York, 1972).
[25] L. D. Landau and E. M. Lifshitz, *Fluid Mechanics*, 2nd ed. (Pergamon, Oxford, 1987), Sec. 24, Problem 10.
[26] S. M. Spillane, T. J. Kippenberg, and K. J. Vahala, Nature (London) **415**, 621 (2002).
[27] H. Rokshari, T. J. Kippenberg, T. Carmon, and K. J. Vahala, Opt. Express **13**, 5293 (2005).
[28] M. L. Gorodetsky, A. A. Savchenko, and V. S. Ilchenko, Opt. Lett. **21**, 453 (1998).
[29] D. W. Vernooy, V. S. Ilchenko, H. Mabuchi, E. W. Streed, and H. J. Kimble, Opt. Lett. **23**, 247 (1998).
[30] K. J. Vahala, Nature (London) **424**, 839 (2002).
[31] D. K. Armani, T. J. Kippenberg, S. M. Spillane, and K. J. Vahala, Nature (London) **421**, 925 (2003).

**I. Brevik and S.Å Ellilngsen** "Electromagnetic momentum conservation in media" Annals of Physics (N.Y.) in press 2010
doi:10.1016/j.aop.2010.08.003

# Model for density waves in gravity-driven granular flow in narrow pipes

Simen Å. Ellingsen
*Department of Energy and Process Engineering, Norwegian University of Science and Technology, N-7491 Trondheim, Norway*

Knut S. Gjerden, Morten Grøva, and Alex Hansen
*Department of Physics, Norwegian University of Science and Technology, N-7491 Trondheim, Norway*
(Received 5 January 2010; revised manuscript received 15 March 2010; published 10 June 2010)

A gravity-driven flow of grains through a narrow pipe in vacuum is studied by means of a one-dimensional model with two coefficients of restitution. Numerical simulations show clearly how density waves form when a strikingly simple criterion is fulfilled: that dissipation due to collisions between the grains and the walls of the pipe is greater per collision than that which stems from collisions between particles. Counterintuitively, the highest flow rate is observed when the number of grains per density wave grows large. We find strong indication that the number of grains per density wave always approaches a constant as the particle number tends to infinity, and that collapse to a single wave, which was often observed also in previous simulations, occurs because the number of grains is insufficient for multiple wave formation.

DOI: 10.1103/PhysRevE.81.061302 PACS number(s): 45.70.Mg, 47.11.Mn, 47.57.Gc

## I. INTRODUCTION

Transport of dry granular media through pipes and channels is a problem of fundamental interest which is of considerable industrial importance [1], and it has been studied intensely both experimentally and theoretically in recent decades [2–5]. Granular media behave radically different from both liquids and solids [3] and in granular pipe flow driven either by gravity or pressurized gas, nonlinear dynamical phenomena such as clogging (density waves) are observed, but not yet well understood.

We consider dry grains falling inside a pipe. In this system, encountered industrially, e.g., in emptying of silos and transportation of sand or powder, there are three main mechanisms of interaction: (a) collisions between grains, (b) collisions between grains and walls, and (c) interaction of the grains with air in the system. Assuming the pipe is narrow, we approach this problem by means of a simple one-dimensional model with periodic boundary conditions in which collisions are modeled by means of two coefficients of restitution $\mu$ and $\nu$, corresponding to the collisions of mechanisms (a) and (b), respectively. We demonstrate that this is sufficient to observe the formation of density waves.

Granular media has frequently been investigated by means of numerical simulations. Features such as clustering through dissipative collisions [6,7] and inelastic collapse [8,9] are among those reported. Various driving mechanisms have been considered, which can roughly be divided into two categories: vibrating walls [10–12] and interior heating [13–18]. The case of an emptying hopper has been studied, see e.g. [19,20], as has the decompaction transient associated with the release of an initially dense packing [21].

The particular case of gravity-driven granular flow through channels and pipes has been studied for some time, both experimentally and theoretically. In previous experimental investigations [22–28], the importance of the presence of air in the flow has been emphasized and the formation of density waves in falling sand has been explained with primary reference to the air-grain interaction. Although clearly of importance in real systems, we demonstrate that the introduction of air in the model is not necessary to observe density waves. Our simulation suggests that such flocculent behavior, while certainly influenced by the presence of air, can occur also in evacuated pipes, provided dissipation from collisions between grains and walls is faster than dissipation from grain-grain collisions.

Previous simulations of granular pipe flow have also reported density waves [6,29–34]. Several mechanisms for velocity dissipation through inelastic collisions, damping and static friction have been employed, see, e.g. [35]. Early papers [6,29] were unable to study sufficiently large numbers of grains and collisions to reach a state independent of initial conditions. The model used by Lee [30] was a 2+1-dimensional time-driven molecular dynamics (MD) simulation, with at least eight significant parameters. In the model of Peng and Herrmann [31,32], a 2+1-dimensional lattice gas automaton is used in which various events are assigned probabilistic collision rules. Another model was proposed by Liss, Conway and Glasser [33]. Again, this is a 2+1-dimensional model with more complicated collision rules than ours. In their simulation, the grain-wall coefficient of restitution was found to be of little importance. In all these models stable density waves were seen.

Our model is one-dimensional and much simpler, yet reproduces similar qualitative phenomena, dictated essentially by two coefficients of restitution whose interpretation is physically transparent. We present our model and the results of our simulations and demonstrate that the model has two clearly distinct regimes in the parameter plane, one in which density waves form (flocculent regime) and one where no such are present (gaseous regime). Average number of grains per density wave and flow rate as functions of the two coefficients of restitution are studied.

## II. MODEL

The pipe of our model is sufficiently narrow to prevent grains from passing each other, and sufficiently wide to allow them to fall approximately freely between collisions. As

 

a consequence, grain-wall collisions are triggered by, and occur immediately subsequent to, grain-grain collisions. The pipe is therefore assumed to be too narrow for arching effects to play a role. We thus propose that the system is essentially one-dimensional in behavior and may be captured qualitatively by a one-dimensional model where collisions with walls are incorporated into the grain-grain collision rules themselves.

The setup is the following. Let $N$ grains move in one dimension so that grain $i$ has position $x_i$ and velocity $v_i$. We use periodic boundary conditions, with grains falling beneath $x=0$ reinserted at $x=L$, where $L$ is the length of the pipe. The grains are accelerated by a constant gravity $g$ toward $x=0$. In the dilute limit $dN \ll L$, where $d$ is the diameter of a single grain, we find that the behavior is independent of $d$, and we set $d=0$ for simplicity.

As mentioned, the collision rules employed are based on the idea that the falling grains lose energy due to two different types of collisions, with the walls and with each other. Grain-grain collisions are modeled by reducing the relative velocity of the colliding grains through a coefficient of restitution $\mu \in [0,1]$. Thus, $v^+_{\mathrm{R,ab}}=-\mu v^-_{\mathrm{R,ab}}$ where $v_{\mathrm{R,ab}}=v_{\mathrm{a}}-v_{\mathrm{b}}$, grain "a" is directly above grain "b," and we use superscripts "–" and "+" to denote times just before and after a collision, respectively.

Grain-wall collisions tend to decrease the average velocity of the system, $v_{\mathrm{av}}=N^{-1}\sum_{i=1}^{N} v_i$, which would otherwise diverge in time. Instead, $v_{\mathrm{av}}$ eventually reaches and fluctuates around a constant value at which dissipated energy is in equilibrium with energy gained from the gravitational field. We model the interaction with the walls at each collision by a coefficient of restitution $\nu \in [0,1]$ which dissipates grain energy by reducing the center of mass (CM) velocity of the two colliding grains according to $v^+_{\mathrm{CM,ab}}=\nu v^-_{\mathrm{CM,ab}}$, where the CM velocity of the pair is $v_{\mathrm{CM,ab}}=\frac{1}{2}(v_{\mathrm{a}}+v_{\mathrm{b}})$. These rules combine to

$$v^+_{\mathrm{a}} = \frac{1}{2}(\nu-\mu)v^-_{\mathrm{a}} + \frac{1}{2}(\nu+\mu)v^-_{\mathrm{b}}, \tag{1a}$$

$$v^+_{\mathrm{b}} = \frac{1}{2}(\nu+\mu)v^-_{\mathrm{a}} + \frac{1}{2}(\nu-\mu)v^-_{\mathrm{b}}. \tag{1b}$$

Note that introducing a restitution of $v_{\mathrm{CM}}$, momentum is transferred for each collision from the grains to the (infinitely massive) pipe, and the momentum of the grains alone is not conserved. This causes the flow to approach a constant flow rate as observed in experiments.

While a collision changes the velocities of just two grains, the relative and CM velocities of three *pairs* of grains are affected: the colliding pair plus the neighboring pairs above and below. In particular, a collision increases the relative velocity of the pair above the collision in proportion to the lost CM velocity of the colliding pair. Thus, relative velocities are constantly regenerated, and the phenomenon of inelastic collapse [8,9] is avoided for $\mu>0$ and $\nu<1$.

## III. SIMULATION AND RESULTS

We use event-driven molecular dynamics for our simulations. Each grain is given an initial velocity which is assigned randomly according to various initialization schemes. The grains are also given equidistant starting positions between 0 and $L$.

Simulations are run for different grain numbers $N$ at constant grain density $\rho=N/L$. After a "thermalization" time the system reaches a steady state where the flow rate of the whole system fluctuates about a mean value. Initializing the simulations with different initial conditions yields the same dynamic steady state, characterized by average flow rate, collision frequency and the average number of density waves.

In Fig. 1, we plot grain trajectories in space and time. In these plots we have used, in arbitrary units, $L=1$, $g=0.01$, and $N=100$. In these simulations initial velocities between 0 and 1 were drawn randomly from a uniform distribution.

We observe two distinct regimes in the $\mu,\nu$ plane. When $\nu<\mu$, dense regions tend to spread out. In this "gaseous" regime, shown in Fig. 1(a), no steady density waves are observed. Whenever $\nu>\mu$, density waves are observed, and the transition from gaseous to flocculent behavior at $\mu=\nu$ is sudden.

For the special case $\mu=\nu$ seen in Fig. 1(b), the Eq. (1) simplify to $v^+_{\mathrm{a}}=\mu v^-_{\mathrm{b}}$ and $v^+_{\mathrm{b}}=\mu v^-_{\mathrm{a}}$. Now the velocity of grain "a" after a collision is only a function of the velocity of grain "b" before the collision, and vice versa. After "thermalization," we observe that the grain velocities are organized about two values: a lower velocity for the grains whose last collision was with the grain below it and a higher velocity for those which last collided with the grain above it.

While the qualitative behavior in the gaseous regime, $\mu>\nu$, is insensitive to the values of $\mu$ and $\nu$, the situation in the flocculent regime is quite different. As exemplified for the parameter pairs in Fig. 1, the wave patterns vary strongly in this half of the parameter plane. Both the magnitude and velocity of the density waves depend sensitively on the values of $\mu$ and $\nu$. Moreover, the qualitative picture varies from a few large and stable waves with approximately constant velocity to many small and volatile waves which emerge, merge and dissolve and vary greatly in velocity even for a single set of parameters. Two examples are shown in Figs. 1(c) and 1(d), but a multitude of different multiwave patterns may be observed.

Beyond rescaling the time axis, the values of $L$ and $g$ do not affect the wave patterns, so long as the grain number $N$ is large compared to the average number of grains per density wave. For $N$ below some $(\mu,\nu)$-dependent threshold, the grains will gather in one or a few stable or metastable waves, as exemplified in panels (e) and (f) of Fig. 1.

When $N$ is increased beyond this threshold, however, we find that the number of density waves increases linearly, while the number of grains per density wave remain constant. Average flow rate and the average velocity of density waves also remain independent of $N$ in the limit of large $N$. This represents the asymptotic limit of our system, where there is no dependence on density $\rho$, which we illustrate for three pairs of coefficients in Fig. 2. Due to limitations of computer time we have not investigated this limit when $N_w$

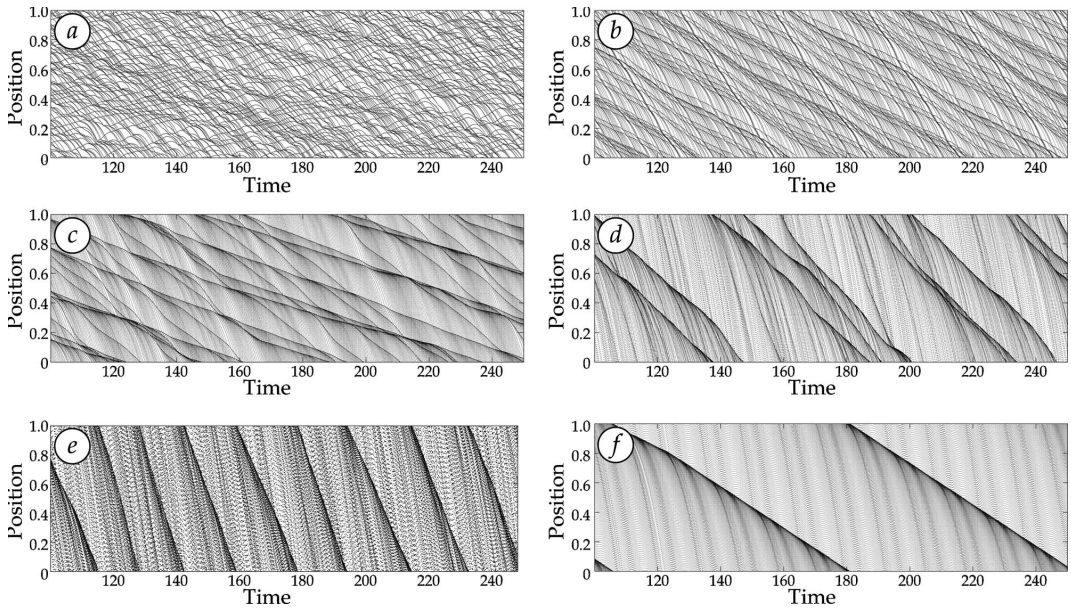


FIG. 1. Spatiotemporal plots of grain trajectories. (a) Gaseous regime $\mu=0.8$, $\nu=0.3$. (b) Split velocity transition point $\mu=\nu=0.55$. (c) and (d): Different multiwave patterns, $(\mu,\nu)=(0.55,0.65)$ and $(0.30,0.85)$, respectively. (e) and (f): Collapse to a single wave; $(\mu,\nu)=(0.70,0.95)$ and $(0.15, 0.85)$, respectively. Further details in text.

grows beyond $\approx 400$, which happens in the limit of either small $\mu$, or $\nu \approx 1$, but we conjecture that such an asymptotic regime always exists when $\mu$ and $\nu$ are both on the open interval $\langle 0,1\rangle$. Single-wave pictures such as panels (e) and (f) of Fig. 1, seen also in various other simulations [30–33], thus appear in our model simply because there are not enough particles in the system to form more than one wave [36].

In Fig. 3(a), we estimate the number of grains per wave in the flocculent regime, $N_w$, after "thermalization" (calculated as $N$ divided by the number of density waves) in the asymptotic (large $N$) regime. In practice, we choose $N$ large enough that the observed value of $N_w$ is constant with increasing $N$. We have used $N$ ranging from 500 to 4000 in different areas of the plotted region. $N_w$ varies nonmonotonously and spans several orders of magnitude. Indeed, when $\mu$ decreases below 0.2 or $\nu$ approaches 1, both $N_w$ and "thermalization" time diverge rapidly, making calculation in this region expensive.

In Fig. 3(b), the average flow rate is given for all values of $\mu$ and $\nu$. In the gaseous regime we see a monotonous variation supporting our observation that there is no significant parameter dependency on the structures formed in this region. Within the flocculent regime the pattern is similar to that observed for the number of grains per density wave.

Counterintuitively, flow rate is highest in areas of the $\mu,\nu$ plane in which the density waves are large, and conversely, smaller waves correspond to a low flow rate. Since wave velocity is always lower than the flow rate, each grain will approach a density wave from above, collide its way through it, and fall into a low-density area beneath it once more be-

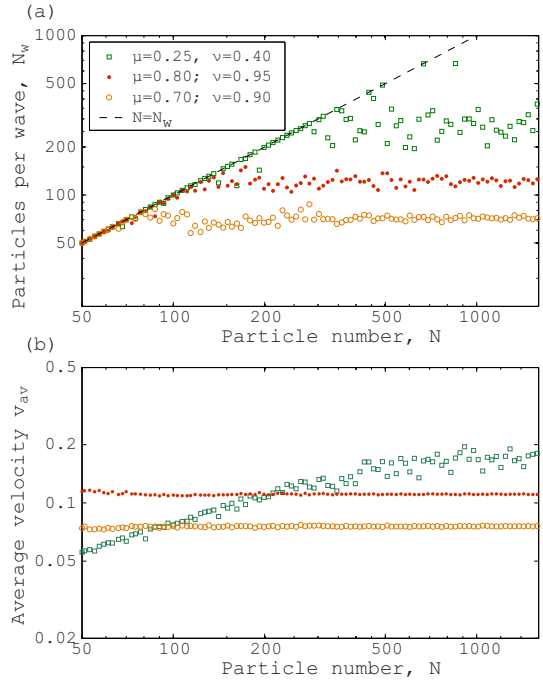


FIG. 2. (Color online) (a) Number of grains per waves and (b) average grain velocity as functions of particle number $N$ for three sets of parameters (same in both panels). The dashed line in the above panel is $N=N_w$, i.e., a single density wave is present.

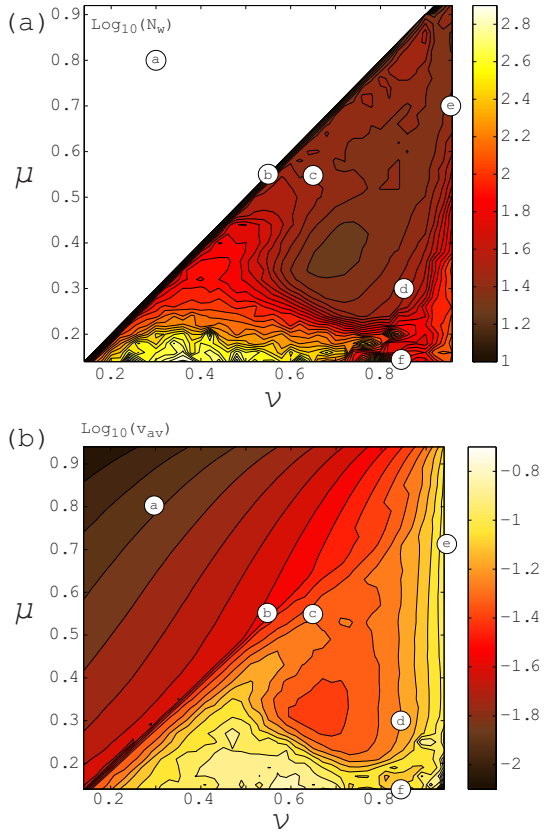


FIG. 3. (Color online) (a): Plot of log $N_w$ where $N_w$ is number of grains per density wave as a function of $\mu$ and $\nu$ in the asymptotic limit. (b): Plot of average flow rate as a function of $\mu$ and $\nu$ in the asymptotic limit. In both panels, encircled letters refer to parameter pairs in Fig. 1.

fore meeting another wave. Although large waves move more slowly than smaller waves, we find that this is more than compensated by the presence of large low density areas between waves in which the grains can fall freely. Hence the total flow rate is governed by the length of these acceleration stretches whereas we find no clear connection between flow rate and wave velocity.

We have analyzed the power spectrum of a typical wave pattern [that of Fig. 1(d)] shown in Fig. 4. The analysis was performed by recording density in a region of length $L/10$ as a function of time. With sampling frequency 10 per time unit, about $10^7$ data points were recorded. The series was then divided into subsamples which were Fourier transformed individually, and the average of the power for all

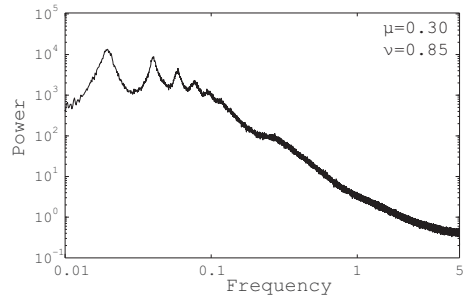


FIG. 4. Frequency spectrum of the wave pattern of Fig. 1(d). The graph is the average over the power spectra of 200 subsamples of a long time series of $\approx 10^7$ data points.

subsamples were then taken (different number of subsamples were used for comparison; 200 subsamples are used in Fig. 4). The spectrum is peaked at a few frequencies, demonstrating how the wave pattern has a number of preferred wave-front velocities. This is not obvious from studying spatiotemporal diagrams such as Fig. 1(d). In the high-frequency regime the power dies off in a manner consistent with a power law with exponent −2, consistent with the wave-fronts undergoing Brownian fluctuations.

## IV. CONCLUSIONS

We have studied granular pipe flow by means of a one-dimensional two-parameter model. The two parameters are the coefficients of restitution for collisions between grains and collisions between grains and walls. The very simple collision rules are contrasted by the amount of structure exhibited by the model, and formation of density waves varying greatly in magnitude and qualitative behavior is observed. We find a criterion for the formation of density waves: that the dissipation from collisions with walls be greater than that from grain-grain collision. Under this criterion our model predicts that density waves can form also in the absence of any interstitial gas.

Contrary to intuition, the flow rate is largest when density waves are large, slow and far between. This indicates that in some circumstances, the flow rate in gravity-driven granular pipe flow can be increased by softening or roughening the pipe walls. For example, with soft grains described by $\mu = 0.3$, a "rough" pipe with $\nu = 0.5$ gives a flow rate two to three times faster than a "smoother" pipe for which $\nu = 0.7$.

## ACKNOWLEDGMENTS

We have benefited from discussions with J. P. Hulin and the Granular Media Group at FAST laboratory, Orsay.

[1] R. Jackson, *The Dynamics of Fluidized Particles* (Cambridge University Press, Cambridge, England, 2000).
[2] M. A. Goodman and S. C. Cowin, J. Fluid Mech. **45**, 321 (1971).
[3] H. M. Jaeger, S. R. Nagel, and R. P. Behringer, Rev. Mod. Phys. **68**, 1259 (1996).
[4] H. Jaeger and S. Nagel, Science **255**, 1523 (1992).
[5] I. Goldhirsch, Annu. Rev. Fluid Mech. **35**, 267 (2003).
[6] M. A. Hopkins and M. Y. Louge, Phys. Fluids A **3**, 47 (1991).
[7] I. Goldhirsch and G. Zanetti, Phys. Rev. Lett. **70**, 1619 (1993).
[8] S. McNamara and W. R. Young, Phys. Fluids **4**, 496 (1992).
[9] S. McNamara and W. R. Young, Phys. Rev. E **50**, R28 (1994).
[10] S. Luding, E. Clément, A. Blumen, J. Rajchenbach, and J. Duran, Phys. Rev. E **49**, 1634 (1994).
[11] O. Herbst, P. Müller, M. Otto, and A. Zippelius, Phys. Rev. E **70**, 051313 (2004).
[12] O. Herbst, P. Müller, and A. Zippelius, Phys. Rev. E **72**, 041303 (2005).
[13] R. Cafiero, S. Luding, and H. J. Herrmann, Phys. Rev. Lett. **84**, 6014 (2000).
[14] D. R. M. Williams and F. C. MacKintosh, Phys. Rev. E **54**, R9 (1996).
[15] G. Peng and T. Ohta, Phys. Rev. E **58**, 4737 (1998).
[16] J. S. van Zon and F. C. MacKintosh, Phys. Rev. Lett. **93**, 038001 (2004).
[17] J. S. van Zon and F. C. MacKintosh, Phys. Rev. E **72**, 051301 (2005).
[18] D. J. Bray, M. R. Swift, and P. J. King, Phys. Rev. E **75**, 062301 (2007).
[19] G. W. Baxter, R. P. Behringer, T. Fagert, and G. A. Johnson, Phys. Rev. Lett. **62**, 2825 (1989).
[20] G. H. Ristow and H. J. Herrmann, Phys. Rev. E **50**, R5 (1994).
[21] L. Conrath and J. M. Salazar, Granular Matter **2**, 47 (2000).
[22] O. Moriyama, N. Kuroiwa, M. Matsushita, and H. Hayakawa, Phys. Rev. Lett. **80**, 2833 (1998).
[23] G. Reydellet, F. Rioual, and E. Clement, EPL **51**, 27 (2000).
[24] Y. Bertho, F. Giorgiutti-Dauphiné, and J.-P. Hulin, Phys. Fluids **15**, 3358 (2003).
[25] J.-L. Aider, N. Sommier, T. Raafat, and J.-P. Hulin, Phys. Rev. E **59**, 778 (1999).
[26] S. Horikawa, T. Isoda, T. Nakayama, A. Nakahara, and M. Matsushita, Physica A **233**, 699 (1996).
[27] T. Raafat, J. P. Hulin, and H. J. Herrmann, Phys. Rev. E **53**, 4345 (1996).
[28] Y. Bertho, F. Giorgiutti-Dauphiné, T. Raafat, E. J. Hinch, H. J. Herrmann, and J. P. Hulin, J. Fluid Mech. **459**, 317 (2002).
[29] T. Pöschel, J. Phys. I **4**, 499 (1994).
[30] J. Lee, Phys. Rev. E **49**, 281 (1994).
[31] G. Peng and H. J. Herrmann, Phys. Rev. E **49**, R1796 (1994).
[32] G. Peng and H. J. Herrmann, Phys. Rev. E **51**, 1745 (1995).
[33] E. D. Liss, S. L. Conway, and B. J. Glasser, Phys. Fluids **14**, 3309 (2002).
[34] C. Becco, H. Caps, S. Dorbolo, C. Bodson, and N. Vandewalle, in *Traffic and Granular Flow '03*, edited by S. P. Hoogendorn *et al.* (Springer, Berlin, 2005), pp. 543–551.
[35] J. Lee and H. J. Herrmann, J. Phys. A **26**, 373 (1993).
[36] Naturally we cannot conclude that the same is necessarily true for the simulations of Refs. [30–33].